A COMPREHENSIVE GEOLOGICAL, PETROLOGICAL, AND GEOCHEMICAL EVALUATION OF THE VOISEY'S BAY NI-CU-CO SULFIDE DEPOSIT: AN INTEGRATION OF EMPIRICAL DATA AND PROCESS MECHANICS

MICHELLE A.E. HUMINICKI

A COMPREHENSIVE GEOLOGICAL, PETROLOGICAL, AND GEOCHEMICAL EVALUATION OF THE VOISEY'S BAY NI-CU-CO SULFIDE DEPOSIT: AN INTEGRATION OF EMPIRICAL DATA AND PROCESS MECHANICS

by

© Michelle A.E. Humininicki

A thesis submitted to the

School of Graduate Studies

in partial fulfillment of the

requirements for the degree of

Doctorate of Philosophy

Department of Earth Sciences

Memorial University of Newfoundland

October, 2007

St. John's Newfoundland

ABSTRACT

This thesis consists of three manuscripts, which report results on: 1) methodologies for systematic ore characterization utilizing the Voisey's Bay Ni-Cu-Co magmatic sulfide Ovoid deposit of northern Labrador as an example; 2) genesis of Voisey's Bay ores, focusing on the Ovoid deposit; and 3) discovery of a platinum-group element (PGE) occurrence in the vicinity of the Southeast Extension of the Voisey's Bay Ovoid deposit.

The first manuscript defines, describes, and characterizes mineralogical and geochemical zonation of the Voisey's Bay massive sulfide Ovoid deposit to determine relationships between macroscopic ore textures, mineralogy, and chemical compositions of the sulfides. The emphasis is on development of algorithms to predict ore mineralogy derived from bulk chemical assays. A comparison to results from mineral liberation analysis indicates that the algorithms are very robust. The results show that the Ovoid deposit is strongly zoned from pyrrhotite-rich margins to a chalcopyrite-pentlandite-rich transitional zone and a magnetite-rich core. The TYPE I inner magnetite-rich ore has elevated Pb, Pt, and Pd relative to the remainder of the Ovoid (which correlate with high magnetite and moderate chalcopyrite) with the exception of a very central zone that has high chalcopyrite and Zn but lower Pb, Pt, and Pd relative to the remainder of the Ovoid. TYPE II ore is elevated in Pd and Zn, which corresponds to the chalcopyrite-pentlandite-rich zone. Lead, Zn, Pt, and Pd are not enriched in the pyrrhotite-rich TYPE III outer ore zone relative to the remainder of the Ovoid.

The second manuscript integrates mineralogical data and bulk assay data to quantitatively describe and model the emplacement (including physical/mechanical controls/processes) and crystallization history of the sulfide parent magmas of the Ovoid deposit and associated mineralized zones. Various models for ore upgrading (R, N, L factors) and crystallization (equilibrium, fractional, and partial fractional crystallization) were evaluated to determine which was involved in producing observed Ni and Cu tenors. Parental and derivative silicate magma compositions that may have been responsible for the ores were evaluated. The major conclusion is that the Ovoid deposit formed at an R factor of ~150 from common basalt parent magmas and differentiated by partial fractional crystallization, trapping 30-40% residual liquid, mainly in the core of the ore body. Some of the residual liquid escaped to form disseminated mineralization.

The third manuscript reports the first occurrence of platinum group-minerals (PGM) at Voisey's Bay, with grades of 1.95g/t Pt, 1.41g/t Pd, and 6.59g/t Au. Most of the PGE are present as discrete minerals hosted by disseminated base-metal sulfides in a hornblende gabbro dyke near the Southeast Extension of the Ovoid deposit. The PGM were determined to have a primary magmatic origin. Geological and geochemical relationships suggest that the dyke is associated with the main troctolite rocks that host the Ovoid, indicating a similar magma source. The PGM are related to a highly differentiated sulfide liquid that formed intermediate solid solution (ISS), which was derived by crystallization of monosulfide solid solution (MSS) from a sulfide melt. The sulfide melt was similar to that which formed the Ovoid deposit. The depletion of Pb and Pt in the center of the Ovoid may indicate loss of this material to the surroundings,

ACKNOWLEDGEMENTS

This project would not have been possible without the support and guidance of my supervisor Dr. P.J. Sylvester (Memorial University of Newfoundland - Inco Innovation Center). My co-supervisor Dr. Louis Cabri (Memorial University of Newfoundland - Cabri Consulting Limited) was also integral in this project. It was an honor to be able to work with the excellent personnel (Dawn Evans-Lamswood, Robert Wheeler, Dan Lee, and Brain Bengert at Voisey's Bay Nickel Company Limited) as well as Dr. Larry Cochrane (previously of Inco Limited). The level of enthusiasm, logistical, and technical support I received was a rare and treasured gift. I would also like to thank my committee members Dr. Derek Wilton, Dr. Alison Leitch, and Dr. Mark Wilson for their guidance and meaningful contributions at various stages along the way.

Funding for this study was provided by Inco Limited, Voisey's Bay Nickel Limited, and a Natural Science and Engineering Research Council (NSERC) grant held by Dr. P.J. Sylvester. This project was also supported by a Dennis R. Prince Memorial Scholarship (2006-2007), an Atlantic Innovation Fund – Inco Innovation Centre student scholarship (2005-2006), a Memorial University of Newfoundland fellowship (2005-2006), two Northern Scientific Training Program scholarships (2004-2005 and 2005-2006), a Society of Economic Geology student research grant (2005), an NSERC postgraduate scholarship (2003-2005), and two Alfred Snelgrove awards (2003 and 2004) held by M.A.E. Huminicki.

Analytical work was carried out in the Earth Science laboratories and the Inco Innovation Center (IIC) at Memorial University of Newfoundland with the assistance of

Michael Shaffer, Michael Tubrett, and Pam King and at CANMET with the assistance of Dr. Rolando Lastra. The many hours on the laser were made enjoyable with the thanks to Michael Tubrett; his teaching and kindness is a rare find. The dedication and willingness to follow through on projects and ideas made collaborating with Michael Shaffer a privilege; but the greatest honor was becoming friends. M. Poujol carried out the first lead isotope measurements at the Inco Innovation Center – Memorial University of Newfoundland. I gratefully appreciate the assistance of Gerri Starkes and Joanne Samson and all the faculty, staff, and students in the Department of Earth Sciences and the Inco Innovation Center at Memorial University of Newfoundland. Especially my first Newfoundland friend, Sheldon Huelin; my dear Turkish friends Ayse Idil Cakiroglu, Oznur Yasar, and Cagri Diner; the one who hung out on the other side of the office, a Mr. Pat Collins; the one who kept things interesting, Dr. Ron Voordouw; the one who had insight, our Tanya Tettelaar; and Cassandra Marion and Marc Beauchamp. There are many more of you who are too numerous to list, but you know who you are.

Thanks Mom and Dad for your friendship, love, and support. Thanks to my family Lisa Huminicki, Paige Lauer, Cassidy Lauer, Conrad Lauer, and Patricia Tennescoe for staying so close when I was so far. Thanks to my best friend Mandie Dionne Sellar who has stuck by me through so many years. Thanks to my brother-in-law David Benson who is a brother and friend to me. My darling Twin A, Twin B is done at last.

DEDICATION

This thesis is dedicated to my Supervisor, Dr. Paul J. Sylvester. He inspired me and let me inspire. He let me have my independence yet was always there for me when I needed him. The journey we went through was one of a kind and remembering to live the journey while it was happening is what made memories that will last forever.

Paul, you are truly an amazing person and I hope you take these words with you in your own life and know that you have made a special difference in my life. I truly could not have done this without you, nor would I have wanted to. In the end, I got more than I bargained for…..

…a lifelong friend!

TABLE OF CONTENTS

LIST OF TABLES

CHAPTER 1

CHAPTER 2

CHAPTER 3

CHAPTER 4

LIST OF FIGURES

CHAPTER 1

CHAPTER 2

CHAPTER 3

CHAPTER 4

CO-AUTHORSHIP STATEMENT

In regards to collaborative research involved in the manuscripts regarded as chapters in this thesis, Michelle A.E. Huminicki is the primary author and researcher on all manuscripts (chapters) including the proposals and outlines of projects, analytical work, synthesis and interpretation of data, and preparation of manuscripts. Specific contributions of co-authors are outlined below for each manuscript.

Chapter 2 benefited from the contribution of P.J. Sylvester in the context of data interpretation and significant editorial handling; from the contribution of M. Shaffer in the context of mineral liberation analysis (MLA) assistance and ideas on methodology; from the contribution of D.H.C. Wilton in the context of discussions on economic geology and manuscript review; from the contributions of D. Evans-Lamswood in the context of discussions on the Voisey's Bay deposit and industry perspective on economic research; and from the contributions of R.I. Wheeler in the context of assistance to implement the designed algorithm into 3D software utilized in industry.

Chapter 3 benefited from the contribution of P.J. Sylvester in the context of assistance in data interpretation.

Chapter 4 benefited from the contribution of P.J. Sylvester in the context of assistance in data interpretation and input on geological modeling; from the contributions of R. Lastra in performing automated precious mineral searches in the CANMET facilities, Ottawa; from the contributions of L.J. Cabri in the context of discussions and reviews in the area of his expertise (precious minerals); from the contributions of D.

Evans-Lamswood in the context of discussions on the Voisey's Bay deposit and industry perspective on economic research; and from the contribution of D.H.C. Wilton in the context of discussions on economic geology and manuscript review.

CHAPTER 1: INTRODUCTION

This thesis is a study of a magmatic sulfide ore deposit. The desire to study the Voisey's Bay Ni-Cu-Co Ovoid deposit stems from the fact that it is a relatively new massive sulfide discovery (discovered in 1993) and that during the course this study, open pit mining began on the deposit. Voisey's Bay Nickel Company (VBNC) Limited provided access to their entire drill core assay database, including access to samples, as part of the development of the Inco Innovation Centre (IIC) at Memorial University of Newfoundland (MUN).

The project proposed here will capitalize on the opportunity to study the ore petrology and genesis of the Voisey's Bay deposit in some detail. Since production (i.e., mining and processing) has already begun on the deposit, it is important to know: 1) the full economic potential of the ore deposit in order to plan future mining strategies; 2) the mineral and metal distributions in order to focus and guide advanced exploration; and 3) the best means to economically extract the metals (i.e., improve metal recoveries during extraction). This thesis contributes to these issues.

This thesis is a compilation of three manuscripts. The first manuscript (Chapter 2) develops a method to systematically characterize an ore deposit in its mineralogy utilizing the Voisey's Bay Ni-Cu-(Co) massive sulfide Ovoid deposit as an example. The second manuscript (Chapter 3) focuses on ore genesis by addressing processes responsible for the various compositions of the ores (ore tenors). The third manuscript (Chapter 4) describes a new style of platinum-group element (PGE) mineralization

identified in a dyke near the Southeast Extension Zone of the Voisey's Bay Ovoid and the origin of this mineralization including its relationship to the genesis of the major Ni-Cu-(Co) sulfide deposits. The manuscripts in the thesis are preceded by an introduction, which gives a general review of magmatic sulfide and PGE deposits and outlines the main objectives of the thesis. The manuscripts are followed by a summary chapter that outlines the major findings of the thesis and discusses the relevance of these findings.

1.1 BACKGROUND

1.1.1 Overview of magmatic Ni-Cu-(Co) sulfide deposits

There are several ways to classify magmatic sulfide deposits, one of which is whether they are sulfide-rich base-metal or sulfide-poor PGE deposits. The sulfide-rich base-metal (Ni-Cu) deposits can further be classified into six types based on magma associations as follows (Naldrett, 2004):

1) Deposits related to komatiite magmatism of Archean age (i.e., Abitibi, Canada; Zimbabwe; and Kambalda, Australia) and komatiite related magmatism of Proterozoic age (i.e., Thompson, Canada and Raglan, Canada);
2) Deposits related to feeders associated with flood basalt magmatism including continental rift/triple junction (i.e., Noril'sk, Russia; Duluth, USA; and Muskox, Canada), rifted continental margin magmatism (i.e., Insizwa, South Africa), and oceanic flood basalt magmatism (i.e. Wrangelia, Canada);

3) Deposits related to ferropicritic magmatism thought to have formed at rifted margins (i.e., Pechenga, Russia);
4) Deposits related to incipient rifting possibly involving mantle plumes and produced by anorthosite-granite-troctolite magmatism (i.e., Voisey's Bay, Canada);
5) Miscellaneous deposits associated with picritic to tholeiitic magmatism in a variety of tectonic settings (i.e., Montcalm, Canada; Yinchuan, China; Niquelandia, Brazil; Moxie, USA; Aberdeenshire gabbros, UK; Rona, Norway; and Acoje, Philippines);
6) Mineralization associated with an impact melt sheet (i.e., Sudbury, Canada).

The sulfide-poor PGE deposits can also be divided into six types based on petro-tectonic setting or magmatism association as follows:

1) Deposits related to mixing of boninitic (U-type) magma with lesser tholeiitic magma in intracratonic settings (i.e., Stillwater, USA; and the Great Dyke, Zimbabwe) or crustally contaminated high-Mg tholeiite magma in intracratonic settings (i.e., Bushveld; Wilson and Chunnett, 2006);
2) Deposits related to mixing of tholeiitic magma with lesser proportions of U-type magma at rifted continental margins (i.e., Pennikat, Finland; Portimo, Finland; and Munni Munni, Australia);
3) Deposits related to tholeiitic magmatism formed at a rifted continental margin/triple junction (i.e., East Bull Lake, Canada; River Valley, Canada; Sonju Lake, USA; Coldwell Complex, Canada; Lac Des Illes, Canada; and Skaergaard, Greenland);

4) Deposits related to calc-alkaline orogenic (island arc) related magmatism (i.e., Platinum belt in Ural Mountains, Russia and the Longwoods Intrusive Complex, New Zealand);
5) Deposits related to ultramafic intrusive Ural-Alaskan type magmatism with the primary magma having an alkaline affinity produced in a orogenic (island arc) setting (i.e., Soloview Hills, Russia; Kondyor massif, Siberia; and Seynav-Galmoznav massif, Russia);
6) Deposits related to carbonate-bearing alkaline mafic/ultramafic rift related intrusive magmatism (i.e., Guli intrusion, Siberia).

Some of the larger magmatic base-metal sulfide and PGE deposits are compared in Table 1.1 based on their key characteristics. The manner in which the Voisey's Bay base-metal sulfide deposit fits into the sulfide classifications is discussed in more detail in section 1.1.3. This thesis describes the first reported occurrence of platinum-group minerals in the Voisey's Bay deposit, therefore a more detailed review of various types of major platinum-group element deposits is also outlined in section 1.1.2 in order to place the Voisey's Bay occurrence into context.

1.1.2 Types of platinum-group element (PGE) deposits

Chapter 4 of this thesis discusses the discovery and origin of a troctolitic dyke elevated in PGE located near the Southeast Extension Zone of the Voisey's Bay Ovoid

deposit. As such, this section provides background on PGE deposits to put the mineralized dyke in the Southeast Extension Zone occurrence into context of other known deposits. A list of known magmatic and hydrothermal as well as more unconventional PGE deposits are listed in Table 1.2, however, this section will only discuss the magmatic related PGE deposits. The magmatic associated PGE deposits can be classified into two main groups: 1) low sulfur PGE (LSPGE) associated deposits, and 2) high sulfur base-metal (HSBM) associated deposits. The sulfide-poor PGE deposits can be further classified based on whether they are stratabound, contact related, or associated with sulfide or chromitite (Table 1.2).

Although each deposit is unique, platinum-group element deposits can often be classified under more than one group (Table 1.2) and may not fit into a single model. However, it is still important to classify PGE deposits and occurrences in terms of the "key criteria" (i.e., sulfide content, mineralization style, age, form, geological setting, size of magmatic system, magma composition such as high Mg olivine-rich rocks, local S source, flow through system, brecciation, and structural traps; Table 1.1) to place the occurrence in context with other producing PGE deposits. Figure 1.1 is a schematic summary of some of the main types of PGE deposits associated with mafic intrusions.

Table 1.1. List of "key criteria" in the formation of some large magmatic base-metal (Ni-Cu) and PGE sulfide deposits.

Host Body	Location	Deposit or Zones	LSPGE or HSBM	*Style	*Age Ma	*Form	*Tectonic Setting	*Magmatic System Size (km)	*Thickness (m)	Magma Pulses	Magma Type	Host rocks (High-Mg)	Local S Source - Country Rocks	Interaction with Country Rocks	Flow-Through System	Breccias	Traps	*PGE Resource (106 oz)
Bushveld Igneous Complex	South Africa	Merensky Reef; Platreef; UG2; Lower Chromitites; Dunite Pipes	LSPGE	Merensky Reef (sulfide reef); Platreef (contact-type); UG2 (chromitite reef)	2060	Batholith	Intracratonic rift	350 x 250	5250	Multiple (Naldrett, 2004)	U-Type (high MgO); T-Type (tholeiitic) (Naldrett, 2004)	Melanorite, pyroxenite-leuconorite contact (Naldrett, 2004)	Transvaal Supergroup (quartzites, argillites, and dolomites) (Naldrett, 2004)	Geochemistry (isotopes) (Barnes and Maier, 2002)	?	Dolomite inclusions in Platreef (Naldrett, 2004)	Potholes (Naldrett, 2004)	1969
Great Dyke	Zimbabwe	Main Sulfide Zone, Lower Sulfide Zone	LSPGE	Main Sulfide Zone (sulfide reef)	2570	Batholith	Intracratonic rift	550 x 11	3500	Multiple (Naldrett, 2004)	U-Type (high MgO) (Naldrett, 2004)	Pyroxenite, gabbro, and olivine gabbro (Naldrett, 2004)	Archean granites and greenstones of Zimbabwe craton (Naldrett, 2004)	?	?	?	?	448
Stillwater Igneous Complex	USA	JM Reef, Picket Pin	LSPGE	JM Reef (sulfide reef)	2705	Interconnected lopitliths	Intracratonic rift	42 x 10	5500	Multiple (Todd *et al.*, 1982)	U-Type (high MgO); T-Type (tholeiitic) (Naldrett, 2004)	Peridotite, troctolite, norite, gabbro, and anorthosite (Naldrett, 2004)	M-UM and clastic seds of Wyoming Province (Naldrett, 2004)	Geochemistry (Os isotopes) (Lambert *et al.*, 1989)	No	No	"Ballroom" structures (Naldrett, 2004)	89.3
Duluth Complex	USA	Dunka Road, Babbit	LSPGE	Contact-type	1107	Irregular sills	Continental flood basalt province	200 x 50	<1500	Multiple (Foose and Weiblen, 1986)	Flood basalt (Naldrett, 2004)	Troctolite, gabbro, and anothosite (Naldrett, 2004)	Virginia Formation (Severson and Hauck, 1990)	Only local SiO_2 contamination indicating not whole-rock assimilation (Ripley, 1986)	Feeder sills (Logan sills?) (Severson and Hauck, 1990)	Virginia Formation inclusions in contaminated norite (Naldrett, 2004)	No	84
Noril'sk-Talnakh	Russia	Massive, disseminated, and Cu-rich ores	HSBM	Magmatic Ni-Cu sulfide, PGE by-product	252	Chonolith/irregular sills	Continental flood basalt province	<20 x 5, variable	500	Multiple (Naldrett, 2004)	Picrite (Naldrett, 2004)	Olivine gabbro dolerite (Naldrett, 2004)	Evaporites (Naldrett, 2004)	Taxitic gabbro, geochemistry (isotopes) (Naldrett, 2004)	Feeder sills (Naldrett, 2004)	Yes (Naldrett, 2004)	No	383
Sudbury Igneous Complex	Canada	Offset dykes, Cu-footwall veins, and Sublayer	HSBM	Magmatic Ni-Cu sulfide, PGE by-product	1850	Lopilith/batholith	Meteorite impact at craton margin	60 x 30	>2500	Single (Naldrett, 2004)	Impact melt sheet (Naldrett, 2004)	Norite (Naldrett, 2004)	Target rocks	Xenoliths, geochemistry (isotopes) (Naldrett, 2004)	No	Footwall breccias and Sublayer (Pattison, 1979)	Embayments	62
Voisey's Bay Intrusion (Nain Plutonic Suite)	Canada	Ovoid, Mini Ovoid, Reid Brook, Eastern Deeps, Discovery Hill, and Southeast Extension Zones	HSBM	Magmatic Ni-Cu sulfide, (PGE by-product?)	1334 (Ryan, 2000)	"Stitching" Batholith	Incipient rifting	19000 km2 (Funck et el., 2000)	8-11km (Funck *et al.*, 2000)	Multiple (Scoates and Mitchell, 2000)	Basaltic (Li *et al.*, 2000)	Troctolite and olivine gabbro (Li and Naldrett, 1999)	Tasiuyak Gneiss (Ryan, 2000)	Geochemistry (isotopes indicate minor contamination from Tasiuyak) (Amelin *et al.*, 2000)	Conduit (Evans-Lamswood *et al.*, 2000)	Basal Breccia Sequence (Li and Naldrett, 1999)	Throat, inflections in conduit (Evans-Lamswood *et al.*, 2000)	?

*Green and Peck (2005) and references therein unless otherwise noted

LSPGE = low sulfur platinum-group element; HSBM = high sulfur base metal

M = mafic; UM = ultramafic

Table 1.2. Simple classification of PGE deposits (modified from Green and Peck, 2005).

1. Low S layered intrusion hosted PGE deposits
    (a) Stratabound sulfide-bearing layers, i.e., Bushveld, Stillwater, Great Dyke
    (b) Contact (non-stratabound sulfide-bearing), i.e., Platreef (Bushveld), River Valley, Lac Des Iles
    (c) Stratabound chromitite layers, i.e., UG-2 (Bushveld)
    (d) Hydrothermal remobilization, i.e., Lac Des Iles, Duluth, Bushveld dunite pipes, Rambler
2. High S magmatic Ni-sulfide associated PGE deposits, i.e., Noril'sk, Sudbury, Raglan
3. Placers PGE deposits, i.e., Urals
4. Unconventional PGE deposits
    (a) Ophiolites, i.e., Shetlands (Unst), Troodos, Ray-Iz, Kempirsay, Acoje
    (b) Alaskan type intrusions, i.e., Fifield, Urals, Wellgreen, Tulameen, Duke Island
    (c) Porphyries, i.e., Mamut, Skouries
    (d) Sedimentary (Cu-Au) black shale-hosted, i.e., Kupferschiefer, Sukhoi Log
    (e) Unconformity related (U-Au-PGE), i.e., Rottenstone, Alligator River, Nicholson Bay, Shinkolobwe
    (f) Laterites, i.e., Weld Ridge, Fifield, Syerston, Yubdo, Freetown, Gilgarnia
    (g) Marine ferromanganese crusts, i.e., Ivalojoki and Lemmenjoki rivers, Finnish Lapland (Kojonen *et al.*, 2005)
    (h) Mine tailings, i.e., Sudbury, Noril'sk, Kambalda

A key criterion for PGE deposits is the age of the associated intrusion since it is known that there were large episodes of magma generation that occurred during specific time intervals. During these episodic periods (~250Ma Noril'sk; ~2000Ma Bushveld, Ungava, and Povungnituk; ~2500Ma Great Dyke and Stillwater) magmatic activity generated large igneous bodies at active tectonic zones (rifting centers). The size of an intrusion is another important criterion for base-metal deposits and may also be important in the formation of the large economic PGE deposits. This is because the larger a system is, the greater the potential for it to: 1) carry more source metal, 2) become more fractionated causing S saturation, 3) interact with a host rock and incorporate a S source or cause silicification of the magma, both of which can induce S saturation, 4) have a higher R factor (mass ratio of silicate magma to sulfide melt), which will be favorable for

higher tenor deposits, 5) have a dynamic environment (conduits, feeder dykes), which increases chances of multiple pulses of magma injection and magma mixing that can introduce more metal and invoke S saturation, and 6) create traps in a dynamic system (embayments may be scoured out by previous magma pulses and act as ground preparation for deposits). It is important to keep in mind that the biggest PGE producers are associated with large mafic-ultramafic intrusions (Naldrett, 2004); it is also important to clarify whether the PGE are a deposit or resource versus just a property or occurrence. A deposit or resource would indicate extraction of the metals for economic profit, whereas a property or occurrence infers some degree of mineralization has been identified but its economic potential has not yet been established. The rest of this section discusses the major PGE deposits in terms of their key criteria with a comparison to the PGE occurrence near the Southeast Extension Zone of the Voisey's Bay Ovoid deposit.

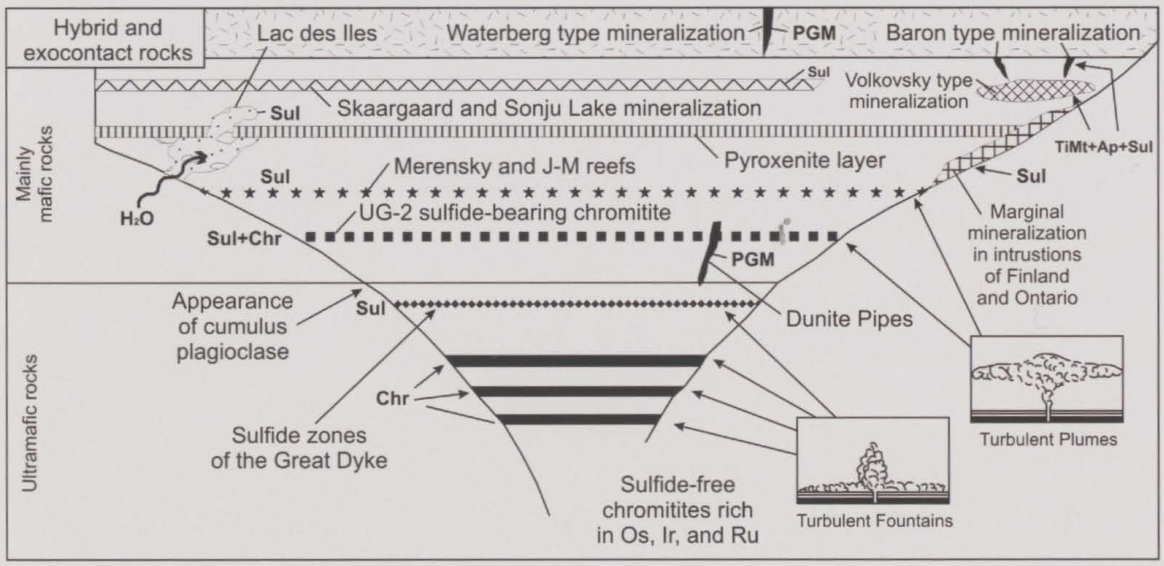

Figure 1.1. Schematic diagram of various types of PGE deposits (after Naldrett, 2004). Sul = sulfide; Chr = chromite; TiMt = titanomagnetite; Ap = apatite; PGM = platinum-group minerals.

1.1.2.1 Summary of different PGE deposits with respect to key criteria

The largest PGE producing deposits (i.e., "The Big Three": Bushveld, Stillwater, and the Great Dyke; Naldrett, 2004) are summarized in Table 1.1 in terms of their deposit style and other key criteria. The large PGE deposits (Bushveld, Stillwater, and Great Dyke) and high S base-metal deposits (Noril'sk and Sudbury) that contain PGE as by-product are discussed in more detail below in terms of their key criteria. Besides the criteria outlined in Table 1.1, other factors that may play an important role in deposit formation are crustal scale faults, structural intersections, deformation, and fluid involvement.

Bushveld Igneous Complex

The Bushveld Igneous Complex is the largest known mafic intrusion (~350 x 250km) with an age of 2060Ma (Green and Peck, 2005). There is evidence of multiple injections of magma, country rock interaction, and cumulus processes forming olivine-rich rocks in the Bushveld Complex (Naldrett, 2004). The parent magmas intruded quartzites, argillites, and conglomerates of the Transvaal Supergroup (Naldrett, 2004). The Bushveld contains: i) sulfide-poor PGE reef style mineralization (i.e., Merensky Reef), ii) sulfide-poor PGE chromitite associated reef style PGE mineralization (i.e., UG1 and UG2), iii) sulfide-poor PGE contact style deposits (i.e., Platreef), and iv) discordant dunite pipes.

The Merensky Reef is a sulfide-poor stratiform PGE deposit. The main reef style mineralization was thought to have formed in the presence of two magmas, an early boninitic, U-type magma (high MgO, SiO_2, and Cr) and a later tholeiitic magma, both which contain different PGE and S contents and crystallized in a different manner (Naldrett, 2004). However, more recently, the U-type magma has been shown to be a crustally contaminated high-Mg tholeiite magma (Wilson and Chunnett, 2006). The Merensky Reef occurs in the Upper Critical Zone of the Bushveld Complex and is a highly productive mineralized zone. The Upper Critical Zone consists of an upper part of chromite-harzburgite-bronzitite-norite-anorthosite in an ordered succession and a lower part that is not as orderly as the upper part but consists of pyroxenite, norite, and anorthosite layers. Although, the mineralization is generally stratiform, the reef horizon does cut down into stratigraphy and scour out "potholes" that further act as traps for mineralization (Naldrett, 2004).

The Platreef also occurs in the Upper Critical Zone but unlike the Merensky Reef it is stratabound and not strictly stratiform (Naldrett, 2004). The Platreef is often overlain by anorthosite and in general can be divided into an upper part (C Reef) of unmineralized pyroxenite, underlain by a highly mineralized coarse pyroxenite (B Reef), and a lower inhomogeneous feldspathic pyroxenite (A Reef) with common blebs of base metal sulfide (Naldrett, 2004). PGE mineralization can be highly variable in the Platreef between different locations (Naldrett, 2004).

The UG1 Chromitite occurs at the base of the upper Critical Zone beginning the layered succession of chromite-harzburgite-bronzitite-norite-anorthosite (Naldrett, 2004).

The UG2 Chromitite occurs at the base of UG2 cyclic unit where the footwall is often a coarse pegmatitic feldspathic pyroxenite (Cawthorn, 2002). The UG2 chromitite consists of 60-90% chromite with plagioclase and orthopyroxene and ranges from 70-130cm thick (Naldrett, 2004). Similar to the Merensky Reef, the UG2 can contain potholes (Naldrett, 2004).

The platiniferous dunite pipes (i.e., Onverwacht, Mooihoek, Driekop, and Maandagshoek) contain some of the highest PGE grades in the Bushveld Complex but are small in size. They consist of discordant pipe-like dunite bodies surrounded by olivine-bronzite-plagioclase pegmatoids. The Onverwacht (Wagner, 1929; Cameron and Desborough, 1964) is a typical ~100m diameter dunite pipe that consists of a low forsterite core surrounded by a high forsterite margin and narrows at its base while crosscutting the layered bronzitite.

Stillwater Igneous Complex

The Stillwater Complex is a large (42 x 10km) differentiated, stratiform intrusion with an age of 2705Ma (Naldrett, 2004). It intrudes older mafic-ultramafic rocks and clastic Mg- and Fe-enriched sediments of the Archean Wyoming Province. The rock units are composed of: 1) the Basal Series, 2) the Ultramafic Series, and 3) the Banded Series. The Ultramafic Series contains the chromitite-bearing Peridotite Zone with overlying Bronzite Zone. The Banded Series consists of the Lower, Middle, and Upper Banded Series of repeated cyclic units comprising olivine bearing rocks, norite, and

gabbro. The main PGE mineralization at Stillwater is sulfide-poor, stratiform reef style mineralization (J-M Reef).

Similar to the Bushveld's Merensky Reef, the J-M Reef at Stillwater is co-incident with the influx of a new tholeiitic (high Al_2O_3) magma following the injection of the initial high MgO magma. This is evidenced by the changes in cumulus mineralogy from orthopyroxene to olivine followed by plagioclase (Todd *et al.*, 1982). The J-M Reef is contained within the "Reef Package", which consists of predominantly troctolite with lesser anorthosite, peridotite-dunite, and norite with olivine-rich pegmatoidal pyroxenites (Naldrett, 2004). PGE mineralization can be contained within any of these rock types.

In some locations the mineralization can be contained in what are termed "ballroom" features, which are defined as either: 1) thickened zones of mineralization extending from the hanging wall into the footwall, 2) thickened mineralization in thickened portions of the reef package, and 3) mineralization in footwall rocks separate from the reef package (Naldrett, 2004).

The Great Dyke

The Great Dyke is 550 x 11km with an age of 2579Ma (Armstrong and Wilson, 2000). It intrudes Archean granites and greenstones of the Zimbabwe craton and consists of narrow magma chambers with the layers dipping toward the center of the dyke (Naldrett, 2004). There is evidence for multiple pulses of a high-Mg (15% MgO) basalt (Naldrett, 2004). The mineralization occurs in the Middle Sulfide Zone and the Lower

Sulfide Zone, which are located within massive bronzitite. The Middle Sulfide Zone and Lower Sulfide Zone occur below the gabbro and olivine gabbro cap, which represents the first appearance of cumulus plagioclase (Naldrett, 2004). PGE tenor is also higher in the center of the dyke (Naldrett and Wilson, 1990).

Noril'sk-Talnakh

The Noril'sk feeder sills cover an area <20 x 5km and have an age of 252 Ma. The Noril'sk region is characterized by the Siberian Flood Basalt plain, is related to major crustal scale faults (Kharaelakh and Imangda faults), contains olivine-rich rocks, and the feeders intrude the Paleozoic sedimentary rocks containing thick deposits of $CaSO_4$ overlain by coal measures (which act as an available S source). An important feature of the Noril'sk region in terms of mineralization is the chalcophile element depletion of the thick overlying volcanic package, which is was thought to be an available source of the metals. The flood basalts formed from relatively primitive, high temperature magmas, which were able to assimilate country rocks. The main bodies have well-developed metamorphic aureoles indicative of large masses of magma flowing through the conduits (Naldrett, 2004). The PGE mineralization at Noril'sk is associated with the sulfide-rich base-metal deposits.

Sudbury Igneous Complex

The Sudbury Igneous Complex is a large (60 x 30km) differentiated melt sheet with an age of 1850 Ma. It is thought to have formed during a single meteorite impact event or single igneous event. It consists of olivine-poor rocks. The Sudbury Structure occurs near the intersection of three provinces of the Canadian Shield: the Superior Province (Archean) to the north, the Southern Province (Early Proterozoic) to the south, and the Grenville Province (Early and Middle Proterozoic) to the east. The complex consists of mafic norites, felsic norites, quartz diorite, and granophyre. The PGE mineralization at Sudbury is sulfide-rich base-metal related where the 3 dominant styles of mineralization are: 1) Ni-rich contact sublayer norite hosted sulfides, 2) Cu-rich footwall veins, and 3) offset-style quartz diorite hosted sulfide deposits. The PGE mineralization is predominantly associated with Cu-rich massive sulfide veins and offset-style quartz diorite hosted sulfide mineralization.

Voisey's Bay Southeast Extension PGE Occurrence

The PGE occurrence near the Southeast Extension of the Voisey's Bay Ovoid is described for the first time in this thesis. The PGE exist as an elevated occurrence within Voisey's Bay troctolitic rocks (Huminicki *et al.*, 2008). The Nain Plutonic Suite, which hosts the Voisey's Bay troctolites, is a much larger system than those that host any of the other PGE deposits or occurrences (Table 1.1). The age of the Nain Plutonic Suite ranges

from 1350 to 1290Ma with the Voisey's Bay intrusion ~1334Ma (Ryan, 2000). This age is dissimilar to other better known PGE deposits or occurrences (Table 1.1). The PGE at Voisey's Bay are related to a sulfide-rich base-metal deposit (i.e., Ovoid deposit) similar to Sudbury and Noril'sk; however, the PGE mineralization itself is locally hosted in trace to disseminated sulfides and not in the massive sulfides. There is evidence for multiple magmatic pulses in the Voisey's ore system similar to Bushveld, the Great Dyke, Stillwater, Duluth, and Noril'sk (Table 1.1). The host rocks to the base-metal massive sulfide mineralization at Voisey's Bay are olivine-bearing troctolites similar to Duluth (and some Stillwater rocks) and the trace to disseminated sulfide and PGE are hosted by a hornblende gabbro dyke that likely had a troctolite to olivine gabbro protolith (Table 1.1). There is a local S source (Tasiuyak Gneiss) and evidence of interaction of the magma with this host source (partially digested country rock xenoliths in the Basal Breccia Sequence) similar to Noril'sk, Sudbury, and Duluth (Table 1.1). The Voisey's Bay intrusion formed in a dynamic environment consisting of breccia, conduits, and failed feeder dykes or splays to the main dyke. The Voisey's Bay Intrusion contains favorable traps such as inflections in the feeder dyke, the base of an upper chamber, and structural intersections (Evans-Lamswood *et al.*, 2000).

In light of the above, the Voisey's Bay intrusion may have the potential to contain associated by-product PGE to a primarily base metal sulfide deposit. Whether there is potential to host by-product PGE at the scale of Noril'sk and Sudbury, which is very significant, is not presently determined. At this stage the PGE present are only an occurrence and any comparison to other deposits should be considered in this context.

Voisey's Bay is a large rift-related, crustal scale intrusion with olivine-rich rocks, a dynamic system with a S source and country rock interaction, and structural traps. All of which are favorable for genesis of base-metal sulfide and PGE deposits.

1.1.2.2 PGE mineralization in various PGE deposits

A direct comparison of PGE mineral compositions in different deposits is not a simple task. Mineral compositions do not appear to be unique to specific deposit types but rather seem to be associated with the factors responsible for generating the source mineralizing melts or fluids (source environment, contaminants on transport, and fluid evolution). However, there are still some important similarities between various deposits and below is a summary of the composition and occurrence of PGE and associated sulfide mineralization in some major PGE deposits and a comparison to the Southeast Extension PGE occurrence at Voisey's Bay.

Bushveld Igneous Complex

The PGM reported in the Merensky Reef of the Bushveld Igneous Complex are atokite (Pd_3Sn), braggite [(Pt,Pd)S], cooperite (PtS), genkinite [$(Pt,Pd)_4Sb_3$], geversite ($PdSb_2$), hollingworthite (RhAsS), irarsite (IrAsS), merenskyite (PdTe2), platarsite (PtAsS), rustenburgite (Pt_3Sn), stibiopalladinite ($Pd_{5+x}Sb_{2-x}$), stumpflite (PtSb), and tetraferroplatinum (PtFe). The dominant phases are the laurite (RuS_2) – erlichmanite

(OsS_2) series and the Pt-Pd-(Ni)-sulfides vysotskite (PdS), braggite [(Pt,Pd)S], and cooperite (PtS) (Cawthorn *et al.*, 2002 and references therein). The dominant sulfide minerals and their average abundances are pyrrhotite (1.09 wt%), pentlandite (0.61 wt%), chalcopyrite (0.45 wt%), and pyrite (0.60 wt%). There also exist other trace sulfides that are not well documented (Cawthorn *et al.*, 2002). Although, the PGE exist predominantly as discrete PGM, a simple mass balance will not account for all the PGE; Pd exists in solid solution in pentlandite (Cabri, 1981; Peyerl, 1983; Paktunc *et al.*, 1990; Cabri, 1992).

The UG2 Chromitite contains millerite (NiS) in the base-metal assemblage, which forms due to the replacement or breakdown of pentlandite (Verryn and Merkle, 1994; Peyerl, 1982; Penberthy and Merkle, 1999) and likely represents an overprint of the ore from secondary processes (Cawthorn *et al.*, 2002).

It should be noted that there are lateral and vertical variations in the PGM assemblages in the Merensky and UG2 Chromitite reefs of the Bushveld Complex that may be related to proximity to potholes, replacement bodies, faults, pegmatites, and changes in host rock lithologies. Although there have been little quantitative correlations between these regional differences and PGM composition, there are some general trends that have been noted. For instance, Cawthorn *et al.* (2002) attribute the increase in Pt-Fe alloys and phases with As and Sb in the UG2 reef to the proximity of replacement bodies.

In the Platreef of Bushveld, the PGM are dominantly sulfides, tellurides, and arsenides (Schouwstra *et al.*, 2000). Variation in PGM assemblages in the Platreef have also been attributed to a function of host rock lithology. For example, in the upper

pyroxenites, PGE sulfides are more abundant than alloys and at the base the alloys are more abundant than PGE sulfides (Schouwstra *et al.*, 2000); serpentinites are associated with an increase in sperrylite (Wagner, 1929); and PGM proximal to the sedimentary sequence are predominantly sulfides, whereas the PGM proximal to basement granite are predominantly tellurides and arsenides (Lee, 1996).

Other chromitite related PGM occurrences (i.e., UG1, MG1, MG2, MG3, and MG4) tend to be dominated by laurite (often hosted by chromite) with a general upward increase in Pt, Pd, and Rh reflecting the increase in influence of sulfide collection over the chromite association (von Gruenewaldt and Merkle, 1995; Cawthorn *et al.*, 2002). PGE-tellurides and sperrylite have been documented by Harney and Merkle (1990) in anorthositic footwall and magnetite layers in the Upper Zone of the Bushveld Complex, which are hosted by altered silicate phases even in the presence of minor chalcopyrite and pyrrhotite (Cawthorn *et al.*, 2002). The PGM in the Fe-rich ultramafic discordant pegmatite pipes at Bushveld are dominated by Pt-Fe alloy > sperrylite > hollingworthite > irarsite > rare PGM (Lee, 1996; Cawthorn *et al.*, 2002). The near surface material of the Waterberg quartz veins are mainly Fe-free native Pt alloyed with minor Pd (McDonald *et al.*, 1995; Cawthorn *et al.*, 2002).

The PGM in the Bushveld Complex are associated with base-metal sulfides, chromite, and silicates; however, there is a great degree of variability between the PGM and their host phases at the mine scale and the regional scale, making it difficult to do a quantitative evaluation (Cawthorn at al., 2002). Surface alteration may also affect the

composition of the base-metal sulfides and PGM, remobilizing the PGE and dispersing them as new phases in silicate minerals (Hey, 1999; Cawthorn *et al.*, 2002).

Stillwater Igneous Complex

The dominant PGM in the Stillwater Igneous Complex are braggite [(Pt,Pd)S], cooperite (PtS), moncheite ($PtTe_2$), vysotskite (PdS), and isoferroplatinum (Pt_3Fe). The majority of the Pt occurs as discrete PGM, whereas the majority of Pd occurs in solid solution in pentlandite and other sulfide minerals. Other rare PGM include rustenburgite (Pd_3Sn), hollingworthite (RhAsS), mertieite II [$Pd(Sb,As)_3$], arsenopalladinite ($Pd_8As_{2.5}Sb_{0.5}$), palladobismutharsenide ($Pd_2As_{0.8}Bi_{0.2}$) and several undefined PGM (Zientek *et al.*, 2002).

The PGE at Stillwater are hosted by or associated with disseminated base-metal sulfides that are intercumulus to the early cumulus silicates. The high temperature sulfide minerals that are associated with or host the PGM in the JM Reef are pyrrhotite, pentlandite, and chalcopyrite. The PGM are Pd-, Pt-, and Ru-sulfides; Pt- and Pd-telluride and arsenides; and Pt-Fe, Pt-Pd-S, Pd-Pb, Pd-Hg, Au-Pt-Pd, and Rh-Pt alloys (Zientek *et al.*, 2002).

Texturally, the PGM are: 1) hosted by base-metal sulfide often at the silicate-sulfide grain boundary (i.e., monchiete and Pt-Fe alloy), 2) as inclusions in silicate minerals, or 3) as discontinuous stringers or veinlets without base-metal sulfide (Zientek *et al.*, 2002). The last occurrence is of interest because it is thought that this occurrence

may represent the end-product crystallization of a PGE-enriched immiscible sulfide liquid. Serpentinization and associated veining postdate these veinlets (Zientek *et al.*, 2002).

The Great Dyke

The PGE mineralization in the Great Dyke is associated with the Main Sulfide Zone (MSZ). The PGM are (Pt,Pd)-sulfides and PGE-sulfarsenides. The PGM consist of, on average, 50.1% (Pt,Pd)-bismuthotellurides moncheite ($PtTe_2$), maslovite (PtBiTe), merenskyite ($PdTe_2$), michenerite (PdBiTe); 19% sperrylite ($PtAs_2$); 8.5% (Pt,Pd)-sulfides cooperite (PtS), braggite [(Pt,Pd)S]; 11.9% PGE-sulfarsenides hollingworthite (RhAsS), platarsite (PtAsS), irarsite (IrAsS), ruarsite (RuAsS); 5.0% laurite (RuS_2); 2.4% Pt-Fe alloy; and rare insizwaite ($PtBi_2$), froodite ($PdBi_2$), kotulskite (PdTe), sobolovskite (PdBi), malanite ($CuPt_2S_4$), unnamed (PtSnS), menshikovite (RuAsS), atheneite [$(Pd,Hg)_3As$], isomertieite [$Pd_{11}(Sb,As)_4$], stibiopalladinite (Pt_5Sb_2), and rustenburgite (Pt_3Sn) (Oberthür, 2002). Texturally, the PGM are: 1) mostly hosted by pyrrhotite or chalcopyrite, 2) along sulfide grains boundaries, 3) along sulfide-silicate grain boundaries, or 4) rarely hosted by silicates, pentlandite, and pyrite (Oberthür, 2002). The PGE-sulfarsenides tend to be zoned in Rh, Pt, Ir, and Ru (Oberthür, 2002). The PGM also vary in modal proportions and grain size regionally (i.e., higher PGE-arsenides and sulfarsenides in the South Chamber versus the North Chamber). The increased levels of

arsenic are attributed to contamination of the magma by country rock assimilation causing an increase in arsenic fugacities (Oberthür, 2002).

The PGE mineralization in the Great Dyke in the Main Sulfide Zone (MSZ) is associated with 0.5-10% magmatic intercumulus base-metal sulfide hosted in cumulate pyroxenites. The main sulfides consist of pyrrhotite, pentlandite, chalcopyrite, and pyrite with lesser amounts of mackinawite, cubanite, and cobaltite (common in the South Chamber) and rare galena (occasionally Se-bearing), sphalerite, molybdenite, argentopentlandite, graphite and various Ni-, Ag-, Pb-, and Bi-tellurides. The secondary oxidation minerals consist of pyrite, marcasite, covellite, and violarite; oxide minerals consist of magnetite, rutile, ilmentite, chromite, and loveringite (Oberthür, 2002). Other trace minerals include the tellurides, Pd-bearing melonite ($NiTe_2$), Ni-bearing merenskyite ($PdTe_2$), altaite (PbTe), Pd-bearing empressite (AgTe), tsumoite (BiTe), tellurobismutite (Bi_2Te_3), and rucklideite [$(Pb,Bi)_3Te_4$], which mostly occur as overgrowths on sulfides and along silicate grain boundaries. The electrum and Au are mostly intergrown with or associated with chalcopyrite (Oberthür, 2002).

The PGE in solid solution in sulfides include Pd (max = 2236ppm) and Rh (max = 259ppm) homogeneously distributed in pentlandite and Pt (ave = 35.5ppm) in pyrite; the Pd content varies in pentlandite with whole rock Pd values (Oberthür, 2002).

Noril'sk Talnakh

The ores at Noril'sk-Talnakh occur as: 1) massive ores at the base of intrusions with >70% sulfide, 2) disseminated footwall ore, and 3) stringer-disseminated ore in intrusive rocks (Kozyrev *et al.*, 2002).

The massive ores at the base of intrusions are divided into pyrrhotite dominant ores and chalcopyrite dominant ores. The pyrrhotite dominant ores consist of pyrrhotite ore, chalcopyrite-pyrrhotite ore, and cubanite-chalcopyrite-pyrrhotite ore comprising a combination of hexagonal pyrrhotite (± troilite), pentlandite, chalcopyrite (± cubanite) with minor or rare mackinawite, sphalerite, galena, ± argentopentlandite, ± pyrite, ± marcasite, ± Ag- and Au-minerals, ± valleriite, ± djerfisherite, and PGM. The chalcopyrite dominant ores consist of chalcopyrite-group minerals (mooihoeckite, talnakhite, and putoranite), pentlandite, and troilite with minor valleriite, mackinawite, sphalerite, galena, shadlunite, djerfisherite, argentopentlandite, parkerite, native Cu, PGM, Au-minerals, and Ag-minerals (Kozyrev *et al.*, 2002). The PGM present in the different massive ores are isoferroplatinum, sperrylite, cooperite, rustenburgite, kotulskite, merenskyite, arsenopalladinite, atokite, froodite, geversite, hollingworthite, insizwaite, isomertieite, maslovite, moncheite, mertieite I, mertieite II, michenerite, niggliite, palladoarsenide, paolovite, antimonian paolovite, platinum, sobolevskite, stibiopalladinite, taimyrite, tellurpalladinite, tetraferroplatinum, urvantsevite, zvyagintsevite, $(Pd,Ni)_5As_3$, $Pd_2(Sb,Sn)$, and native Au (Kozyrev *et al.*, 2002). The

pyrrhotite ores are dominated by the Pt-mineral isoferroplatinum and chalcopyrite ores are dominated by more abundant and diverse Pd-minerals (Kozyrev *et al.*, 2002).

Disseminated mineralization is restricted to the lower portions of the intrusions in association with picritic gabbro-dolerites and taxitic gabbro-dolerites with up to 10-15% sulfides (Kozyrev *et al.*, 2002). The disseminated mineralization consists of pyrrhotite ore, cubanite ore, and chalcopyrite ore. The pyrrhotite ore comprises pyrrhotite, chalcopyrite, pentlandite, cubanite, and pyrite with minor argentopentlandite, mackinawite, valleriite, and rare marcasite, galena, sphalerite, Au-Ag alloys, and PGM. The cubanite ore comprises cubanite, chalcopyrite, pyrrhotite, and pentlandite, minor mackinawite, sphalerite, galena, Cu-pentlandite, Au- and Ag-minerals, and PGM. The chalcopyrite ore comprises talnakhite, mooihoekite, and tetragonal chalcopyrite, pentlandite, troilite, hexagonal pyrrhotite, cubanite, with minor valleriite, mackinawite, sphalerite, Cu-pentlandite, Au-Ag alloys, and PGM (Kozyrev *et al.*, 2002). The PGM consist of isoferroplatinum, sperrylite, cooperite, rustenburgite, kotulskite, arsenopalladinite, atokite, braggite, cabriite, froodite, geversite, hollingworthite, insizwaite, isomertieite, kharaelakhite, majakite, maslovite, moncheite, mertieite I, mertieite II, niggliite, osmium, osmium rhenium, palarstanide, palladoarsenide, antimonian palladoarsenide, paolovite, antimonian paolovite, arsenian paolovite, plumbopalladinite, polarite, sobolevskite, sopcheite, stillwaterite, sudburyite, stannopalladinite, stibiopalladinite, taimyrite, telargpalite, tetraferroplatinum, tulameenite, urvantsevite, vysotskite, zvyagintsevite, $(Pd,Ni)_5As_3$, $Pd_2(Sb,Sn)$, $(Pd,Pt)_3(As,Sn)_2$, Pd_2Ge, $(Fe,Pt)_2S$, and Fe-Ni-Pt alloy (Kozyrev *et al.*, 2002).

The stringer-disseminated mineralization occurs in country rocks adjacent to the upper intrusive contact overlying massive ore. The stringer mineralization is fault-controlled where ore-bearing fluids were channelized through altered metasediments (Kozyrev *et al.*, 2002). The mineralization includes breccia-matrix, disseminated, and stringer-disseminated structures with three mineral assemblages: chalcopyrite-pyrrhotite, pyrrhotite-chalcopyrite, and pentlandite-millerite-chalcopyrite (Kozyrev *et al.*, 2002). Ores of chalcocite, bornite, and millerite are less abundant and contain secondary assemblages of pyrite, magnetite, marcasite, vaalleriite, djerfisherite, violarite, cobaltite, and polydymite (Kozyrev *et al.*, 2002). The main sulfides are chalcopyrite, pyrrhotite, and pentlandite with minor sphalerite, galena, clausthalite, hawleyite, argentopentlandite, hessite, native Au, and PGM (Kozyrev *et al.*, 2002). The PGM are atokite, braggite, cabriite, cooperite, froodite, gerversite, insizwaite, isoferroplatinum, kotulskite, laurite, majakite, merenskyite, mertieite II, michenerite, moncheite, palastanide, palladoarsenide, paolovite, platinum, polarite, rustenburgite, sobolevskite, sopcheite, sperrylite, stibiopalladinite, taimyrite, telarpalite, tetraferroplatinum, vysotskite, and $Pd_2(Sb,Sn)$ (Kozyrev *et al.*, 2002).

Sudbury Igneous Complex

The PGM at Sudbury are dominated by tellurides, bismuth-tellurides, and arsenides. Unlike reef-style PGE mineralization (i.e., Bushveld and Stillwater) and other

low sulfide PGE deposits (i.e., Lac des Iles), there are no Pt-Fe, PGE-metal alloys, or PGE-sulfides at Sudbury (Farrow and Lightfoot, 2002).

The palladium minerals identified in Sudbury in order of decreasing abundance are michenerite (PdBiTe), froodite ($PdBi_2$), merenskyite ($PdTe_2$), sudburyite (PdSb), sobolevskite (PdBi), kotulskite (PdTe), mertieite II (Pd_8Sb_3), and sopcheite ($Ag_4Pd_3Te_4$). Paolovite (Pd_2Sn), palladian melonite [$(Ni,Pd)(Te,Bi)_2$], stannopalladinite (Pd_3Sn_2), unidentified [$(Pd,Pt)_3Bi_2Te_2$], and unidentified [$(Ni,Pd)_4(Te,Sb)_5$] are less common or rare phases. The palladium minerals in the South Range are more Sb-rich than the North Range containing the minerals sudburyite and michenerite with Sb (Farrow and Lightfoot, 2002). Palladium minerals are hosted by sulfides and silicates most often forming composite grains with hessite ($AgTe_2$) or other telluride and bismuthide PGM and trace minerals (Farrow and Lightfoot, 2002). The dominant platinum mineral is sperrylite ($PtAs_2$) in the South Range and occurs by itself or associated with cobaltite-gersdorffite. Moncheite ($PtTe_2$) is the dominant phase in the North Range and is associated with hessite or other telluride and bismuthide PGM and trace minerals (Farrow and Lightfoot, 2002). Other Pt minerals identified are geversite ($PtSb_2$), hongshiite (PtCu), insizwaite ($PtBi_2$), maslovite (PtBiTe), moncheite ($PtTe_2$), niggliite (PtSn), and platinian melonite [$(Ni,Pt)(Te,Bi)_2$]. Niggliite has only been noted in the North and East Range, which is thought to be due to the incorporation of Sn from local host rock sources (Farrow and Lightfoot, 2002). The Ir-, Rh-, and Ru-minerals reported are hollingworthite (RhAsS), irarsite (IrAsS), rhodarsenide (Rh_2As), ruarsite (RuAsS), and ruthenium (Ru) (Farrow and Lightfoot, 2002). Several occurrences of the Rh- and Ir-

minerals, hollingworthite (RhAsS) and irarsite (IrAsS) have been described in the South Range and are associated with or hosted by cobaltite-gersdorffite most commonly in ores with low Cu/Ni ratio (Farrow and Lightfoot, 2002) (i.e., more primitive magmatic sulfide). The presence of native Ru and rhodarsenide (Rh_2As) have also been reported by Cabri and Laflamme (1984).

Other precious minerals associated with Sudbury ores are electrum, the Ag-telluride hessite (Ag_2Te), which is often associated with other bismuthides and tellurides, native Ag, which is often hosted by bornite in Cu-rich footwall deposits in the North Range, and volynskite ($AgBiTe_2$), which has only been observed in the South Range occurs with other bismuthides and tellurides (Farrow and Lightfoot, 2002). Other trace minerals associated with PGM in the Sudbury ores include altaite (PbTe), argentopentlandite [$(Ag(Fe,Ni)_8S_8)$], melonite ($NiTe_2$), parkerite ($Ni_3Bi_2S_2$), hauchecornite (Ni_9BiTeS_8), bismuth-telluride minerals, cobaltite-gersdorffite, nikeline (NiAs), and maucherite ($Ni_{11}As_8$) (Farrow and Lightfoot, 2002). The Sn-oxide, casseterite (SnO_2) has only been observed in the North Range (Farrow and Lightfoot, 2002).

Texturally, the Pt- and Pd-minerals are most often hosted by sulfides and silicates along grain boundaries; the Pt-mineral, sperrylite, can also be hosted entirely by pyrrhotite (Huminicki, 2003). They are often spatially associated with chalcopyrite and silicate alteration minerals such as actinolite and quartz in Cu-rich footwall and offset environments (Farrow and Lightfoot, 2002). The Ru- and Ir-minerals are most often hosted within sulfide or sulfarsenides minerals (Farrow and Lightfoot, 2002).

By far, the majority of PGE at Sudbury occur as discrete PGM, however, minor amounts of Pd (2088ppb; Li *et al.*, 1992) can substitute in solid solution in pentlandite and still greater quantities of PGE can reside as solid solution in the sulfarsenides gersdorffite-cobaltite (NiAsS-CoAsS) (up to 1.95 wt% Pd, 4.5 wt% Pt, 23.3 wt% Pd, and 41.2 wt% Rh; Farrow and Lightfoot, 2002 and references therein)

Similar to the Bushveld, the PGM at Sudbury appear to have different compositions loosely correlated to the regional setting (i.e., whether they are hosted by the Huronian metasediments of the South Range or Archean gneisses of North Range; Farrow and Lightfoot, 2002).

Voisey's Bay Southeast Extension PGE Occurrence

PGM in this newly discovered occurrence are associated with a sulfide-poor hornblende gabbro dyke. The sulfide assemblage contains a typical magmatic pyrrhotite, pentlandite, and chalcopyrite assemblage in the outer (marginal) portions of the dyke with low PGE values, and a metal-rich pyrrhotite, pentlandite, chalcopyrite, bornite, galena, millerite, parkerite, makinawite, and volfsonite sulfide assemblage in the inner (central) portion of the dyke associated with high PGE values. The majority of the PGE occur as PGM consisting of sperrylite, paolivite, froodite, Pd-Bi-Te-Sb, Sn-stibiopalladinite, maslovite, gerversite, sobolevskite, insizwaite, niggliite, and Pt-Sn-Te assemblage. Other minerals associated with the PGE mineralization are stützite, matildite, electrum, native Ag, and tsumoite. The PGE can also occur in minor amounts

in solid solution in pentlandite (ave = 2ppm; n = 37) and galena (ave = 1.9ppm; n = 17) indicating that these minerals formed contemporaneously with the PGE mineralizing event.

1.1.3 Previous work on the Voisey's Bay Ni-Cu-(Co) deposit

Much of the previous research on the Voisey's Bay discovery was presented in an Economic Geology Special Issue on the Voisey's Bay Ni-Cu-Co Deposit (2000).

1.1.3.1 Key characteristics of the Voisey's Bay deposits

Some of the key characteristics of the Voisey's Bay deposit are outlined in Table 1.1. The Voisey's Bay deposit is a sulfide-rich base-metal (Ni-Cu-Co) magmatic deposit. The deposit is hosted by troctolitic rocks of the 1334Ma Nain Plutonic Suite (NPS). Tasiuyak gneiss is a metasedimentary host rock unit that was a sulfur contamination source in the troctolites, triggering sulfide precipitation (Ryan, 2000). The NPS is thought to be a "stitching" batholith bridging the suture between the Archean Nain Province to the east and the Paleoproterozoic Churchill Province to the west. Genetically, the sulfides are related to multiple pulses of magma injection into a conduit dyke, whereby the sulfides are now located in inflections and the throat of the conduit (Evans-Lamswood *et al.*, 2000). Li and Naldrett (1999) proposed that the conduit dyke connected a deep, lower magma chamber to a shallower, upper magma chamber.

1.1.3.2 Geology and mineralogy

The regional setting of the Voisey's Bay Ni-Cu-Co deposit has been described by Emslie *et al.* (1994) and Ryan (2000) and references therein. Rock types and components of the Voisey's Bay intrusion have been described by Li and Naldrett (1999). The composition and mineralogy of Voisey's Bay Ni-Cu-Co sulfide deposit has been previously described by Naldrett *et al.* (2000a) and Naldrett *et al.* (2000b), respectively. The salient geological and mineralogical features of the deposit are described in more detail in subsequent chapters of this thesis.

1.1.3.3 Isotope geochemistry and source magma

Isotopic studies have been done on the Voisey's Bay deposit related to ore genesis. They have emphasized the source of the parent magma(s) using stable and radiogenic isotope systems (Amelin *et al.*, 2000; Ripley *et al.*, 2000; Lambert *et al.*, 2000).

Previous work on O isotopes carried out by Ripley *et al.* (2000) has focused on assessing the role of magma contamination in producing sulfide mineralization. The Tasiuyak paragneiss has $\delta^{18}O$ values between 8.3-16.1‰, the enderbitic orthogneiss has $\delta^{18}O$ values between 5.7-8.7‰, and the main units of the Voisey's Bay intrusion have $\delta^{18}O$ values between 5.4-7.7‰. From the bulk isotopic data, it is difficult to assess whether contamination occurred from the enderbitic orthogneiss since the $\delta^{18}O$ values are

nearly similar to the intrusive rocks and there appears to be little indication that contamination occurred from the Tasiuyak paragneiss since the Voisey's Bay intrusion values remain near mantle values (5.7 ± 0.3‰: Rollinson, 1993). However, there is other evidence from paragneiss xenoliths in the basal breccia sequence that indicate some contamination of the mafic magma occurred, depleting the fragments ($\delta^{18}O$ = 4.7-10.6‰) relative to the surrounding parental Tasiuyak paragneiss, leaving residual plagioclase and hercynite (low $\delta^{18}O$) assemblages (Ripley *et al.* 2000). High $\delta^{18}O$ values (up to 9.3‰) occur within the troctolitic and noritic matrix of the breccia but only at the cm-scale (Ripley *et al.* 2000). This was interpreted by Ripley *et al.* (2000) to be a product of isotope exchange produced during subsolidus cooling. There is still a large amount of ^{18}O lost from the gneissic fragments that has not been accounted for. Ripley *et al.* (2000) proposed that the majority of the ^{18}O lost from the paragneiss fragment was transported from the lower to upper magma chambers by fresh influxes of magma now preserved as hosts to the fragments. The loss of ^{18}O from gneiss fragments is consistent with expulsion of a siliceous-rich phase to the magma. Therefore felsification may have worked in conjunction with S-assimilation (from the Tasiuyak gneiss) as a trigger for sulfide saturation.

Ripley *et al.* (2000) also evaluated S isotope data pertaining to the Voisey's Bay mineralization. The main conclusions from their results are: (1) The Reid Brook Zone has $\delta^{34}S$ values of -2.5 to -4.1‰ in the massive sulfides, the Eastern Deeps and Ovoid Zones have values of -2.5 to +1.5‰ in the massive sulfides, the normal troctolite has values of +0.5 to +1.8‰ in disseminated sulfides, the Tasiuyak gneiss has values of -6 to -7‰ in

pyrrhotite, and enderbitic gneiss has values of -4.6 to +3.3‰ in trace sulfides, (2) A decrease in $\delta^{34}S$ to the west reflects a progressive increasing influence of the Tasiuyak gneiss. However, to the east it is difficult to determine degree of crustal component since the host orthogneisses have similar $\delta^{34}S$ values as the mafic magma, (3) It is not possible to conclusively assess the overall isotope composition of the Tasiuyak gneiss from available samples because the spread in $\delta^{34}S$ values range from -17 to +18‰.

Amelin *et al.* (2000) used Nd-Pb-Sr isotopes of plagioclase and apatite to evaluate amount and type of crustal contamination. Results indicated that the Voisey's Bay intrusion has the most mantle-like, least contaminated initial isotopic compositions of the Nain Plutonic Suite (ε_{Nd} = -1 to -2, $^{87}Sr/^{86}Sr$ = 0.7034-0.7038, $^{206}Pb/^{204}Pb$ = 15.34-15.54, $^{207}Pb/^{204}Pb$ = 15.10-15.18, and $^{205}Pb/^{204}Pb$ = 35.24-35.56), which are consistent in all parts of the intrusion. The isotope data indicate that primary magmas were derived from either an enriched continental magma or contaminated by a small amount of crustal material on ascent through the lower-middle crust, then contaminated (8-13%) by the Tasiuyak gneiss in the upper crust. Amelin *et al.* (2000) suggested that little contamination occurred during magma ascent and that early sulfide separation did not likely occur.

1.1.3.4 Mechanical transport of sulfides within the Voisey's Bay intrusion

Ideas on physical processes of magma transport, entrainment, and deposition of sulfide deposits has been described by Evans-Lamswood *et al.* (2000). Mineralization at

Voisey's Bay is described as occurring within a subvertical conduit dike system between the Reid Brook lower chamber and the Eastern Deeps upper chamber. The mineralization occurs as magmatic-textured sulfides within fragment-bearing troctolites and olivine gabbros related to the conduit dikes, as opposed to occurring as basal accumulations in the chambers. Sulfides reside in physical irregularities, particularly where changes in the conduit morphology (inflections) acted as traps for the precipitation, capture, and preservation of sulfides due to changing velocity and viscosity of the magma. Sulfide textures within the different locations of the conduit environment are consistent with formation by magmatic processes and unlikely to have been disturbed by later remobilization. Evans-Lamswood *et al.* (2000) argued that dike geometry (thickness and orientation) and fluid dynamics of the magma in a conduit (density, viscosity, and amount of fragments) play key roles in the present location of particular deposits. For instance, the Ovoid fills a bulge in the dike conduit, the Reid Brook deposit occurs at the axis of an inflection, and the Eastern Deeps occur at the opening of a feeder into a magma chamber. High Ni tenor sulfide trapped between silicates is evidence that gravitational settling did not play the major role in location of the deposits; instead Evans-Lamswood *et al.* (2000) thought that sulfide saturation occurred at depth and sulfide melts were emplaced upwards by multiple pulses of magma in a dynamic conduit system. Although it is implied that the lower and upper chambers are connected by the conduit dyke, there is no definitive geological evidence that this is the case and it may be that the dyke and the chambers are solely coincident (Evans-Lamswood, pers. comm., 2003).

1.1.3.5 Chemical exchange reactions

Key data that need to be explained at Voisey's Bay are: i) the variation of Ni versus forsterite content of the olivines, ii) the low Ni content at a given forsterite content of some of the rocks, and iii) the high Ni content of the ores. It has been proposed by Li and Naldrett (1999) that the distribution of Ni versus forsterite content of the olivines in the rocks in the Voisey's Bay troctolite complex resulted from a combination of: i) initial fractional crystallization of a troctolite magma, ii) trapped silicate liquid causing a shift in forsterite content ("trapped liquid shift"), and iii) re-equilibration between sulfide and olivine.

1.2 THESIS OBJECTIVES

1.2.1 Ore characterization

The main objective of the first paper in this thesis (Chapter 2) was to develop a method to systematically characterize an ore deposit with respect to mineralogy and textures. This was accomplished by developing an algorithm to calculate the modal abundance of each individual sulfide mineral. This algorithm can then be utilized as a predictive model to determine mineral distributions within ore deposits. These types of algorithms have been discussed by others (i.e., Naldrett *et al.*, 2000a). However, this study goes a step further by utilizing the extensive Voisey's Bay Nickel Company

Limited Mine Exploration Borehole System whole rock geochemical database and integrating the mineral data with three dimensional models. The advantage of this approach is that spatial variations in mineralogy can be visualized, providing a more complete picture of the ore deposit. The algorithm requires: i) the identity of the major and minor sulfide phases present in the deposit, ii) whole rock geochemical data for the main sulfide mineral-forming elements, and iii) the mineral chemistry, in order to determine modal abundances of each mineral. Each algorithm is specific to a particular sulfide mineral assemblage, but can be tailored to apply to a range of ore deposits. In this instance, the Voisey's Bay massive sulfide Ovoid deposit was used as a type example.

It has been previously suggested that it is of little advantage to account for individual sulfide minerals in ores (Kerr, 2003) because the sulfide mineral chemistry must be known for each deposit type before these calculations can be applied. Here, the sulfide mineral chemistry has been well established for much of the Voisey's Bay deposit and therefore we can account for the individual sulfide minerals. Accounting for individual minerals is important and subsequent objectives of the paper were to determine mineral zonation and characterize mineral domains of a deposit based on the systematic characterization of the each mineral phase determined by the algorithm. This is important in both determining the economic value of a deposit and aiding in processing of the deposit since mineralogical domains (based on the individual mineral abundances) can be predicted.

In characterizing an ore deposit, it is also desirable to integrate textural information. However, textural zonations are more difficult to determine than

mineralogical zonations because they require sample by sample assessment, which is time-consuming, as opposed calculations utilizing the geochemical database, which can be made almost instantaneously. Nonetheless, a textural classification scheme that can be applied to deposit in a systematic manner can provide useful information when it is based on representative samples.

A final component of this paper is a robust check of accuracy of the algorithm method for determining mineral abundances using image analysis, particularly that provided by automated mineral liberation analysis (MLA) software on a scanning electron microscope (SEM). A check of the accuracy of the algorithm method can be carried out by a comparison of the modal sulfide abundances determined by both the algorithm and by MLA on representative samples.

1.2.2 Ore genesis

Other work has been done on the Voisey's Bay deposit related to ore genesis. This has emphasized the conditions under which the deposit formed, such as: i) source of the parent magma(s) using stable and radiogenic isotope systems (Amelin *et al.*, 2000; Ripley *et al.*, 2000; Lambert *et al.*, 2000), ii) chemical exchange reactions during cooling and crystallization (Li and Naldrett, 1999), and iii) physical/mechanical transport, entrainment/separation, and deposition mechanisms (Evans-Lamswood *et al.*, 2000).

One of the major objectives of the second thesis paper (Chapter 3) was to describe and model the composition of parent source magma(s) and derivative silicate liquid(s)

that the sulfide deposits were produced from. This was accomplished by modeling the initial sulfide compositions and R factors responsible for the observed bulk compositions of the different ore deposits using published partition coefficients between the sulfide and silicate liquids for Ni and Cu. Another objective was to compare the observed rocks present in the ore system to determine if they represent the modeled parental or derivative magmas that formed after sulfide precipitation.

The paper in Chapter 3 also expands on the quantitative mineralogical zonations in the Ovoid (outlined in Chapter 2), focusing on the genetic implications. More specifically, Chapter 3 attempts to define the nature of zonation of metals and minerals within the Ovoid deposit in order to: 1) determine whether it formed by fractional, equilibrium, or partial fractional crystallization, and 2) whether massive and disseminated ores represent cumulates and residual liquids, respectively.

1.2.3 Platinum-group element mineralization

The third paper (Chapter 4) of this thesis reports the first documented occurrence of platinum group-minerals (PGM) associated with the Voisey's Bay magma system. The PGM are present in a sulfide poor, hornblende gabbro dyke located between the Southeast Extension Zone of the massive sulfide Ovoid deposit and the Eastern Deeps Zone. This discovery is of interest as it was previously thought that the Voisey's Bay Ovoid did not contain significant amounts of Au, Pt, and Pd (Naldrett *et al.*, 2000a) and

therefore the potential for the Voisey's Bay deposit to contain economic amounts of PGE (platinum-group-elements) has likely been underestimated.

Since this is a new mineralization style at Voisey's Bay, one of the main objectives was to characterize the abundance, association, distribution, composition, and the significance of PGE mineralization by petrographic, mineralogical, and geochemical analysis to determine if it occurs as solid solution in other minerals (sulfides) or as discrete platinum-group minerals (PGM); to determine what rock types host the mineralization and are associated with it; to determine whether there is lateral continuity of the "PGE-enriched zone"; and to determine if there are any geochemical parameters that can help to "vector" toward the "PGE-enriched zone".

The paper (Chapter 4) provides detailed data on the mineralogy, geology, and geochemistry of the PGM occurrence and the data are used to assess magmatic and hydrothermal origins for the precious metal mineralogy.

The origin of the PGM mineralization is important since it serves to determine if the PGM mineralization is related to the major Ni-Cu-Co sulfide mineralization at Voisey's Bay that is described in Chapter 2. Some geological and geochemical evidence presents possible links of the PGE mineralization to the massive Ni-Cu-Co deposits as a late Cu-rich residual sulfide liquid. If the PGM mineralization is related to the major sulfide mineralization at Voisey's Bay, this implies that there may be more PGE mineralization present in the ore system. There are also implications for the Ovoid sulfide melts (or possibly the Eastern Deeps) behaving as an open magmatic system, as described in Chapter 3.

1.3 ANALYTICAL TECHNIQUES

Analytical methods and techniques included in the thesis are: 1) sampling and sample preparation, 2) petrographic analyses, 3) X-ray fluorescence for whole-rock major and trace element geochemistry, 4) solution ICP-MS for whole-rock trace element geochemistry, 5) NiS fire assay for whole-rock PGE geochemistry, 6) electron probe microanalysis to determine major and trace element mineral chemistry, 7) laser ablation – inductively coupled plasma – mass spectrometry for *in situ* trace element and isotope analyses, 8) a hydroseparation technique to concentrate platinum-group minerals (PGM), 9) automated precious metal mineral searches by mineral liberation analysis, 10) optical image analysis, 11) lead isotope analyses, and 12) 3D computer modeling using Voisey's Bay Nickel Limited's Mine Exploration Borehole System (MEBS) containing geological and geochemical information on over 60,000 samples. Detailed discussions of the various methods are outlined in each of the following chapters where appropriate.

1.4 SUMMARY OF MAJOR RESULTS

The major results of each of the three papers is briefly summarized below and are discussed in detail in each chapter and revisited in the final summary chapter.

1.4.1 Ore characterization

A main result from the ore characterization paper (Chapter 2) is that the most efficient method in determining sulfide mineral modes is to derive a series of calculations (algorithm) using whole-rock geochemistry and representative mineral chemistry. Another result of the ore characterization paper is the successful validation of the algorithm employing image analysis techniques (in particular mineral liberation analysis).

Three-dimensional computer modeling revealed that the Voisey's Bay Ni-Cu-Co massive sulfide Ovoid deposit is quantitatively zoned into three main mineral domains: 1) a magnetite-rich, pyrrhotite-poor central zone with moderate chalcopyrite and pentlandite (TYPE I ore), surrounded by 2) a pentlandite-rich, chalcopyrite-rich zone with moderate pyrrhotite and low magnetite (TYPE II ore), followed by 3) an outer pyrrhotite-rich zone with low chalcopyrite, moderate pentlandite and low to moderate magnetite (TYPE III ore). Concentrations of Zn correlate to chalcopyrite-rich zones and Pt and Pb show a marked decrease in the very central zone of the Ovoid. The Pt and Pb depletion is thought to indicate escape of late stage enriched sulfide liquid from the Ovoid center to its surroundings.

1.4.2 Ore genesis

Major conclusions of quantitative modeling of Ni and Cu in the various ores at Voisey's Bay indicate that the ores could have formed from silicate parent magma(s)

with broadly basaltic Ni and Cu compositions. A picritic parent magma is not required. It is also shown that the disseminated sulfide hosted by the ultramafic inclusions and the massive sulfide hosted by troctolite can be explained by a single basaltic parent magma or a composition similar to the variable troctolite related by a single "upgrading" process (R, N, or R_L) with values of ~150 and ~300-500, respectively. These sulfides could have formed from the same magma but the sulfides in the ultramafic inclusions would have been upgraded in metal tenor due to slightly higher R, N, or R_L factors indicating they reacted with more silicate magma than the massive sulfides. Simple upgrading processes (R, N, or R_L) alone cannot explain the trend between massive sulfides to semi-massive sulfides to disseminated sulfides. However, the compositional trend can be explained by partial fractional crystallization. The increasing Cu-content from massive to semi-massive to disseminated mineralization is consistent with increasing fractionation.

1.4.3 Platinum-group element mineralization

The major results of the third paper in Chapter 4 indicate that the PGM occurrence in the hornblende gabbro dyke in the Southeast Extension Zone of the Voisey's Bay Ovoid deposit has a primary magmatic origin and is likely the product of crystallization from a highly differentiated Cu-rich intermediate solid solution enriched sulfide melt. The PGE-bearing dyke formed from a mafic silicate magma and geological relationships indicate that the dyke is spatially connected as a splay off the main troctolite conduit dyke and is also geochemically related to the main conduit troctolites, which host

the Ovoid massive sulfide deposit. This is an important link as it implies the PGM mineralization may be related to the major sulfide mineralization at Voisey's Bay. Following crystallization of the PGM from magmatic sulfide, an external hydrothermal fluid was introduced to the system. However, no direct evidence was found that the PGE were disturbed by this later hydrothermal fluid.

1.5 REFERENCES

Amelin, Y., Li, C., Valayev, O., and Naldrett, A.J., 2000, Nd-Pb-Sr Isotope Systematics of Crustal Assimilation in the Voisey's Bay and Mushuau Intrusions, Labrador, Canada: Economic Geology, v. 95, p. 815-830.

Armstrong, R., and Wilson, A.H., 2000, A SHRIMP U-Pb study of zircons from the layered sequence of the Great Dyke Zimbabwe and a granitoid anataectic dyke: Earth and Planetary Science Letter 180, p. 1-12.

Barnes, S-J., and Maier, W.D., 2002, Platinum-group element distributions in the Rustenburg Layered Suite of the Bushveld Complex, South Africa, *in* Cabri, L.J., ed., The Geology, Geochemistry, Mineralogy, and Mineral Beneficiation of Platinum-Group Elements: Canadian Institute of Mining, Metallurgy, and Petroleum, Special Volume 54, p. 431-458.

Cabri, L.J., 1981, Relationship of mineralogy to the recovery of platinum-group elements from ores, *in* Cabri, L.J., ed., Platinum-group elements: Mineralogy, Geology, Recovery: Canadian Institute of Mining and Metallurgy, Special Volume 23, p. 233-250.

Cabri, L.J., 1992, The distribution of trace precious metals in minerals and mineral products: Mineralogical Magazine, v. 56, p. 289-308.

Cabri, L.J., and Laflamme, J.H.G., 1984, Mineralogy and distribution of platinum-group elements in mill products from Sudbury, *in* Park, W., Hausen, D.M., and Hagni, R., eds., Applied Mineralogy: Proceedings of the 2nd International Congress on Applied Mineralogy, The Mineral Society AIME, p. 911-922.

Cameron, E.N., and Desborough, G.A., 1964, Origin of certain magnetite-bearing pegmatites in the eastern part of the Bushveld Complex, South Africa: Economic Geology, v. 59, p. 197-225.

Cawthorn, R.G., 2002, The role of magma mixing in the genesis of PGE mineralization in the Bushveld Complex. Thermodynamic calculations and new interpretations – a discussion: Economic Geology, v. 97, p. 663-666.

Cawthorn, R.G., Merkle, R.K., Viljoen, M.J., 2002, Platinum-Group element deposits in the Bushveld Complex, South Africa, *in* Cabri, L.J., ed., The Geology, Geochemistry,

Mineralogy, and Mineral Beneficiation of Platinum-Group Elements: Canadian Institute of Mining, Metallurgy, and Petroleum, Special Volume 54, p. 389-429.

Emslie, R.F., Hamilton, M.A., and Theriault, R.J, 1994, Petrogenesis of a Mid-Proterozoic Anorthosite-Mangerite-Charnockite-Granite (AMCG) Complex: Isotopic and Chemical Evidence from the Nain Plutonic Suite: Journal of Geology, v. 102, p. 539-558.

Evans-Lamswood, D.M., Butt, D.P., Jackson, R.S., Lee, D.V., Muggridge, M.G., Wheeler R.I., and Wilton, D.H.C., 2000, Physical Controls Associated with the Distribution of Sulfides in the Voisey's Bay Ni-Cu-Co Deposit, Labrador: Economic Geology, v. 95, p. 749-770.

Farrow, C.E.G., and Lightfoot, P.C., 2002, Sudbury PGE Revisited: Toward an Integrated Model, *in* Cabri, L.J., ed., The Geology, Geochemistry, Mineralogy and Beneficiation of Platinum-Group Elements: Canadian Institute of Mining, Metallurgy, and Petroleum, Special Volume 54, p. 579-617.

Foose, M., and Wieblen, P., 1986, The physical and petrologic setting and textural and compositional characteristics of sulfides from the South Kawishiwi intrusion, Duluth Complex, Minnesota, USA, *in* Freidrich, G.H., Genkin, A.D., Naldrett, A.J., Ridge, J.D., Sillitoe, R.H., and Vokes, F.M., eds., Geology and metallogeny of copper deposits: Springer-Verlag, Heidelberg, p. 8-24.

Funck, T., K.E., Louden, R.J., Wardle, J., Hall, J.W., Hobro, M.H., Salisbury, and A.M., Muzzatti, 2000, Three-dimensional structure of the Torngat Orogen (NE Canada) from active seismic tomography: Journal of Geophysical Research, v. 105, p. 23403-23420.

Green, T., and Peck, D., 2005, Platinum-group elements exploration: economic considerations and geological criteria, *in* Mungall, J.E., ed., Exploration for Platinum-Group Element Deposits: Mineralogical Association of Canada Short Course Volume 35, p. 247-274.

Grimbeek, J.C., 1996, The effect of the Vaalkop replacement pegmatoid on the sulfide mineralogy at Western Platinum Mine in the Mooinooi district: Unpublished M.Sc. thesis, Hillcrest, University of Pretoria, 111p.

Harney, D.M.W., and Merkle, R.K.W., 1990, Pt Pd minerals from the Upper Zone of the eastern Bushveld Complex, South Africa: Canadian Mineralogist, v. 28, p. 619-624.

Hey, P.V., 1999, The effects of weathering on the UG2 chromitite reef of the Bushveld Complex, with special reference to platinum-group minerals: South African Journal of Geology, v. 102, p. 251-260.

Huminicki, M.A.E., 2003, Geology, Mineralogy, and Geochemistry of the Kelly Lake Ni-Cu-PGE Deposit, Sudbury, Ontario: Unpublished M.Sc. thesis, Sudbury, Ontario, Laurentian University, 219p.

Huminicki, M.A.E., Sylvester, P.J., Lastra, R., Cabri, L.J., Evans-Lamswood, D., Wilton, D.H.C., 2008, First report of platinum-group minerals from a hornblende gabbro dyke in the vicinity of the Southeast Extension Zone of the Voisey's Bay Ni-Cu-Co deposit, Labrador: Mineralogy and Petrology, v. 92, p. 129-164.

Kerr, A., 2003, Guidelines for the calculation and use of sulfide metal contents in research and mineral exploration: Newfoundland Department of Mines and Energy, Geological Survey, Report 03-1, p. 223-229.

Kozyrev, S.M., Komarova, M.Z., Emelina, L.N., Oleshkevich, O.I., Yakovleva, O.A., Lyalinov, D.V., and Maximov, V.I., 2002, The mineralogy and behavior of PGM during processing of the Noril'sk-Talnakh PGE-Cu-Ni ores, *in* Cabri, L.J., ed., The Geology, Geochemistry, Mineralogy and Beneficiation of Platinum-Group Elements: Canadian Institute of Mining, Metallurgy, and Petroleum, Special Volume 54, p. 579-617.

Lambert, D.D., Morgan, J.W., Walker, R.J., Shirey, S.B., Carlson, R.W., Zientek, M.L., Koski, M.S., 1989, Re-Os, Sm-Nd, and Rb-Sr isotope systematics of the Stillwater

Complex, Montana: Evidence for the origin of platinum-group element deposits in mafic layered intrusions: Science, v. 244, p. 1169-1174.

Lambert, D.D., Frick, L.R., Foster, J.G., Li, C., and Naldrett, A.J., 2000, Re-Os Isotope Systematics of the Voisey's Bay Ni-Cu-Co Magmatic Sulfide System, Labrador, Canada: II. Implications for Parental Magma Chemistry, Ore Genesis, and Metal Redistribution: Economic Geology, v. 95, p. 867-888.

Lee, C.A., 1996, A review of mineralization in the Bushveld Complex and some other layered intrusions, *in* Cawthorn, R.G., ed., Layered Intrusions, Elsevier, Amsterdam, p. 103-145.

Li, C., Coats, A.J., and Johannessen, P., 1992, Platinum, palladium, gold, and copper-rich stringers at Strathcona Mine, Sudbury: Their enrichment by fractionation of a sulfide liquid: Economic Geology, v. 87, p. 1584-1596.

Li, C., and Naldrett, A.J., 1999, Geology and petrology of the Voisey's Bay intrusion: reaction of olivine with sulfide and silicate liquids: Lithos, v. 47, p. 1-31.

Li, C., Lightfoot, P.C., Amelin, Y., and Naldrett, A.J., 2000, Contrasting Petrological and Geochemical Relationships in the Voisey's Bay and Mushuau Intrusions, Labrador, Canada: Implications for Ore Genesis: Economic Geology, v. 95, p. 771-799.

Lightfoot, P.C., and Naldrett, A.J., 1999, Geological and geochemical relationships in the Voisey's Bay intrusion, Nain Plutonic Suite, Labrador, Canada: Geological Association of Canada Short Course Notes Volume 13, p. 1-30.

McDonald, I., Vaughan, D.J., and Tredoux, M., 1995, Platinum mineralization in quartz veins near Naboomspruit, central Transvaal: South African Journal of Geology, v. 98, p. 168-175.

Naldrett, A.J., 2004, Magmatic Sulfide Deposits: Geology, Geochemistry, and Exploration: Springer, 727p.

Naldrett, A.J., and Wilson, A.H., 1990, Horizontal and vertical variations in noble metals in the Great Dyke of Zimbabwe: A model for the origin of the PGE mineralization by fractional segregation: Chemical Geology, v. 88, p. 279-300.

Naldrett, A.J., Asif, M., Krstic, S., and Li, C., 2000a, The Composition of Mineralization at the Voisey's Bay Ni-Cu Sulfide Deposit, with Special Reference to Platinum-Group Elements: Economic Geology, v. 95 , p. 845-866.

Naldrett, A.J., Singh, J., Krstic, S., and Li, C., 2000b, The Mineralogy of the Voisey's Bay Ni-Cu-Co Deposit, Northern Labrador, Canada: Influence of Oxidation State on Textures and Mineral Compositions: Economic Geology, v. 95, p. 889-900.

Oberthür, T., 2002, Platinum-group element mineralization of the Great Dyke, *in* Cabri, L.J., ed., The Geology, Geochemistry, Mineralogy and Beneficiation of Platinum-Group Elements: Canadian Institute of Mining, Metallurgy, and Petroleum, Special Volume 54, p. 483-506.

Paktunc, A.D., Hulbert, L.J., and Harris, D.C., 1990, Partitioning of the platinum-group and other trace elements in sulfides from the Bushveld Complex and Canadian occurrences of nickel-copper sulfides: Canadian Mineralogist, v. 28, p. 475-488.

Pattison, E., 1979, The Sudbury Sublayer: Canadian Mineralogist, v. 17, p. 257-274.

Penberthy, C.J., and Merkle, R.K.W., 1999. Lateral variations in the platinum-group element content and mineralogy of the UG2 chromitite layer, Bushveld Complex: South African Journal of Geology, v. 102, p. 240-250.

Peyerl, W., 1982, The influence of the Driekop dunite pipe on the platinum-group mineralogy of the UG2 chromitite in its vicinity: Economic Geology, v. 77, p. 1432-1438.

Peyerl, W., 1983, The metallurgical implications of the mode of occurrence of platinum-group metals in the Merensky Reef and UG2 chromitite of the Bushveld Complex, *in* de Villiers, J.P.R., and Cawthorn, P.A., eds., Applied Mineralogy: Proceedings of the 1st

International Congress on Applied Mineralogy, Special Publication 7, Geological Society of South Africa, p. 295-300.

Ripley, E.M., 1986, Applications of stable isotope studies to problems of magmatic sulfide ore genesis with special reference to the Duluth Complex, Minnesota, *in* Freidrich, G.H., Genkin, A.D., Naldrett, A.J., Ridge, J.D., Sillitoe, R.H., and Vokes, F.M., eds., Geology and metallogeny of copper deposits, Springer-Verlag, Heidelberg, Berlin, p. 25-42.

Ripley, E., Park, Y-R, Li, C., and Naldrett, A.J., 2000, Oxygen Isotope Studies of the Voisey's Bay Ni-Cu-Co Deposit, Labrador, Canada: Economic Geology, v. 95, p. 831-844.

Rollinson, H., 1993, Using geochemical data. Longman Group, 352p.

Ryan, B., 2000, The Nain-Churchill Boundary and the Nain Plutonic Suite: A Regional Perspective on the Geologic Setting of the Voisey's Bay Ni-Cu-Co Deposit: Economic Geology, v. 95, p. 703-724.

Schouwstra, R.P., Kinloch, E.D., and Lee, C.A., 2000, A short review of the Bushveld Complex,: Platinum Minerals Review, v. 44, p.33-39.

Scoates, J.S., and Mitchell, J.N., 2000, The evolution of troctolitic and high Al basaltic magmas in Proterozoic anorthositic plutonic suites and implications for the Voisey's Bay massive Ni-Cu sulfide deposit: Economic Geology, v. 95, p. 677-702.

Severson, M.J., and Hauck, S., 1990, Geology, geochemistry, and stratigraphy of a portion of the Partridge River intrusion: A progress report (Technical Report NRRI/GMIN-TR-89-11), Natural Resources Research Institute, University of Minnesota, Duluth, 230p.

Todt, S.G., Keith, D.W., Le Roy, L.W., Schissel, D.J., Mann, E.L., and Irvine, T.N., 1982, The J-M Platinum-Palladium Reef of the Stillwater Complex, Montana. 1. Stratigraphy and Petrology: Economic Geology, v. 77, p. 1454-1480.

Verryn, S.M.C., and Merkle, R.K.W., 1994, Compositional variation of cooperate, braggite, and vysotskite from the Bushveld Complex: Mineralogical Magazine, v. 58, p. 223-234.

von Gruenewaldt, G., and Merkle, R.K.W.,1995, Platinum group element proportions in chromitites of the Bushveld Complex: Implications for fractionation and magma mixing models: Journal of African Earth Sciences, v. 21, p. 615-632.

Wagner, P.A., 1929, The platinum deposits and mines of South Africa. C. Struik (Pty) Ltd., Capetown, 356p.

Wilson, A., and Chunnett, G., 2006, Trace Element and Platinum Group Element Distributions and the Genesis of the Merensky Reef, Western Bushveld Complex, South Africa: Journal of Petrology, v. 47, no. 12, p. 2369-2403.

Zientek, M.L., Cooper, R.W., Corson, S.R., and Geraghty, E.P., 2002, Platinum-Group Element Mineralization in the Stillwater Complex, *in* Cabri, L.J., ed., The Geology, Geochemistry, Mineralogy and Beneficiation of Platinum-Group Elements: Canadian Institute of Mining, Metallurgy, and Petroleum, Special Volume 54, p. 459-481.

CHAPTER 2: SYSTEMATIC AND INTEGRATIVE ORE CHARACTERIZATION OF MASSIVE SULFIDE DEPOSITS: AN EXAMPLE FROM THE VOISEY'S BAY OVOID DEPOSIT, LABRADOR

M. A. E. HUMINICKI, P. J. SYLVESTER, M. SHAFFER,

D.H.C. WILTON,

Inco Innovation Centre and Department of Earth Sciences, Memorial University of Newfoundland, St. John's, Newfoundland, Canada A1B 3X5, e-mail: g26mah@mun.ca

D. EVANS-LAMSWOOD, and R.I. WHEELER,

Voisey's Bay Nickel Company Limited, Suite 700, Baine Johnston Centre, 10 Fort William Place, St. John's, NL Canada A1C 1K4

2.1 ABSTRACT

A series of systematic calculations (an algorithm) was developed for quantitative determination of normative mineral abundances in massive sulfide ores using whole-rock geochemistry. The algorithm was applied to 3175 massive Ni-Cu-Co sulfide samples from the Voisey's Bay Ovoid deposit and integrated into a 3D block model to define and describe mineralogical zones within the ore body. Three principal mineralogical domains were defined in the Ovoid deposit: TYPE I ore occurs in the center of the deposit and is magnetite-rich, pyrrhotite-poor with moderate pentlandite and chalcopyrite. TYPE II ore surrounds TYPE I ore and is pentlandite- and chalcopyrite-rich with moderate pyrrhotite and low magnetite. TYPE III ore occurs at the base and outer peripheries of the deposit; it is pyrrhotite-rich with low chalcopyrite, moderate pentlandite, and low to moderate magnetite. All ore zones contain trace (<0.05 wt%) amounts of sphalerite and galena. Concentrations of Zn correlate to chalcopyrite-rich zones and Pt and Pb show a marked decrease in the very central zone of the Ovoid. The Pt and Pb depletion is thought to indicate escape of late stage enriched sulfide liquid from the Ovoid center to its surroundings. Macroscopic and microscopic textures in the ores including the occurrence of fine and coarse grained magnetite, the presence of "loops" of chalcopyrite and pentlandite interstitial to pyrrhotite, and the frequency of troilite exsolution from pyrrhotite and cubanite exsolution from chalcopyrite, were linked to the mineralogical zones. Automated image analysis using backscattered electron imaging and X-ray mapping on a scanning electron microscope verified the accuracy of the normative

calculations for a subset of samples prepared as grain mounts, and provided quantitative estimates of cubanite (up to 2 wt%) and troilite (up to 20 wt%) abundances, which could not be calculated using the algorithm. Computer-based analysis of scanned, digital optical images of polished slabs of drill core from the ore body provided inconclusive modal abundance data – in particular darker shades of pentlandite were consistently underestimated.

Systematic characterization of ore deposits through normative mineral abundance calculations that are cast in block models, verified with automated image analysis, and integrated with textural data, can provide valuable insights into ore body variations that would not be apparent otherwise.

2.2 INTRODUCTION

The origin and differentiation of massive sulfide ores is often assessed largely on the basis of bulk chemical compositions, with comparably little information about mineralogical and textural variations in the deposit. While the value of mineralogy and texture in understanding ore genesis is undoubted, it is labor intensive and time consuming to quantify mineral abundances and describe petrographic relationships in the large numbers of polished thin sections needed to characterize deposit-scale variations. In contrast, chemical assays of ore samples are routinely performed by research and commercial labs. In advanced exploration campaigns of mining companies, assays of

large numbers of samples of drill cores are routinely and systematically determined throughout an ore body.

This paper describes a method to quantify mineralogy and document textures in a systematic and consistent manner in order to evaluate spatial variations within an ore deposit. Quantitative mineralogical and textural data can then be integrated into three dimensional (3D) block models, as for any other parameter such as grade or density, and be examined in detail using computer visualization software. The method is built around an algorithm for translating large databases of whole-rock chemical assays into mineral abundances. Mineralogical domains defined by the algorithm are verified by image analysis and characterized for texture by petrographic examination of samples from each domain. An advantage of this method is that it can be used as a predictive tool to determine mineralogy from whole-rock geochemical assays utilizing thousands of samples virtually instantaneously.

The method can be used to establish mineralogical zones for evaluating the genesis of an ore deposit, to help guide exploration of economic metals, and to target additional areas with mineralization potential. Good quantitative mineralogical and textural characterization of ores is also essential for defining metallurgical domains, which may aid in improving ore recoveries during processing. "Geometallurgical" characterization of a deposit may be carried out even before mining begins to help refine mine plans and predict potential processing issues that may ensue.

In principle, this method can be applied to a variety of ore deposit types but is most well suited to massive ores. This study utilizes the Voisey's Bay Ni-Cu-Co massive

sulfide Ovoid deposit to demonstrate how the method may be applied for quantitative mineralogical ore classification. The Voisey's Bay deposits are magmatic sulfides, located in northern Labrador, and discovered in 1993. As of year end 2005, the Ovoid contained estimated proven and probable reserves of 32 million tonnes grading 2.75% nickel, 1.59% copper, and 0.14% cobalt.

Major and minor sulfide and oxide minerals in the Ovoid ore were identified in previous studies (Naldrett *et al.*, 2000a), and confirmed on the basis of petrographic observations of 37 drill core samples examined in this study. Mineral compositions were measured by electron microprobe analysis and laser ablation-inductively coupled plasma mass spectrometry. Using an algorithm developed in this study, normative modal abundances were calculated from assays of massive sulfide Ovoid samples – first, for 37 samples collected by the authors to examine the methodology in detail, and then for some 3175 samples listed in the Mine Exploration Borehole Sample (MEBS) database of Voisey's Bay Nickel Company (VBNC). The latter results were plotted in a 3D block model for the Ovoid using a mapping and visualization computer program from Datamine Corp Ltd, and mineral domains were defined on the basis of calculated mineral abundances, textural characteristics, and zonal variations within the ore body.

An important component of the method is verification of calculated mineral abundances by checking of the results against direct estimates of mineral modes for representative samples of each of the defined mineral domains. Direct modal estimates traditionally have been made by point counting using optical microscopy, which is labor intensive and prone to human error. We have thus explored two alternative techniques for

modal estimates: (1) automated image analysis on polished grain mounts using a *Mineral Liberation Analyzer*® (MLA), which is a scanning electron microscope controlled by sophisticated software developed by JKTech Pty Ltd (Gu, 2003, 2004) for mineral identification and characterization; and (2) analysis of scanned, digital optical images of drill core slabs using readily-available desktop computer software (Adobe *Photoshop*®). The requirements, advantages, and limitations of each approach are compared.

The implications of the mineralogical zonations for the genesis and crystallization history of the Ovoid deposit are discussed in a companion paper (Huminicki and Sylvester, submitted) and Chapter 3 of this thesis.

2.3 GENERAL GEOLOGY

The Voisey's Bay ore bodies are hosted by troctolites and olivine gabbros of the Voisey's Bay intrusion (Fig. 2.1), which is part of the Mesoproterozoic Nain Plutonic Suite (NPS). Emslie *et al.* (1994), Ryan (2000), and references therein summarized the regional geology of the NPS. The mineralogy and chemical composition of Voisey's Bay ores have been described by Naldrett *et al.* (2000a) and Naldrett *et al.* (2000b), respectively.

The Voisey's Bay ores are hosted by an east-west dike system intruded into Paleoproterozoic and Neoarchean gneisses (Fig. 2.1). The deposit is divided into several ore zones, which from west to east, are: the Reid Brook Zone, the Discovery Hill Zone, the Ovoid and Mini Ovoid, the Southeast Extension Zone, and the Eastern Deeps Zone.

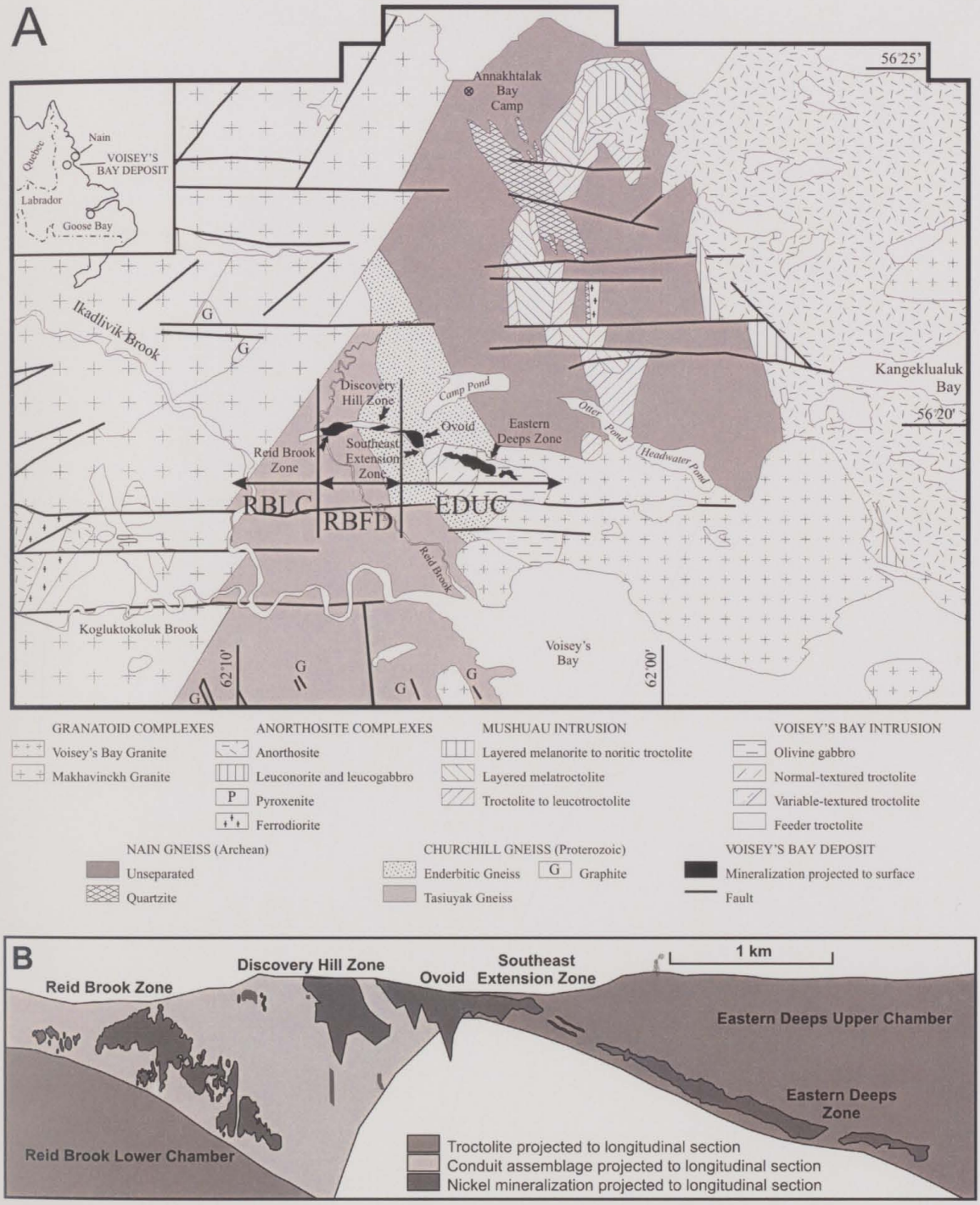

Figure 2.1. Geologic map of the Voisey's Bay area, showing the various rock types, components, and mineralized zones in: a) plan view (modified from Lightfoot, 1998 and Evans-Lamswood *et al.*, 2000), b) longitudinal north section (from Li *et al.*, 2000). Ovoid deposit is located near center of mineralized trend. RBLC = Reid Brook lower chamber, RBFD = Reid Brook feeder dyke; EDUC = Eastern Deeps upper chamber.

There are two large troctolitic bodies associated with the dike system: the "Eastern Deeps upper chamber" (EDUC) in the east and the "Reid Brook lower chamber" (RBLC) in the west (Fig. 2.1). The two chambers may be joined by the main troctolite conduit, which hosts the ores and is known as the "Reid Brook feeder dike" (RBFD). However, others believe that the conduit dyke and chambers are coincident and may not actually be physically connected (Evan-Lamswood, pers. comm., 2003). This is because the geology includes sharp contacts between the conduit and chamber troctolites in drill core indicating the magma did not continue to flow from the Reid Brook lower chamber to the conduit (Evan-Lamswood, pers. comm., 2003). Besides massive sulfide ores, there are a variety of troctolitic to gabbroic rocks in the RBFD that host semi-massive to disseminated sulfides (Li *et al.*, 2000).

2.4 SAMPLING AND SAMPLING PREPARATION

Bulk assay data for Fe, Ni, Cu, S and minor/trace elements (Co, Zn, Pb) for 3175 drill core samples (1 m half cores of massive ore) from the Ovoid were kindly provided by VBNC Ltd. In addition, a total of 37 samples of Ovoid massive sulfide ore were sampled at various locations throughout the deposit specifically for this study. Sampling aimed to provide wide spatial coverage of the ore body, as well as target specific mineralogical zones defined by the algorithm calculations. The 37 samples were examined through: (1) optical microscopy of polished thin sections to determine mineralogy and textural variability; (2) electron probe micro-analysis (EPMA) for *in situ*

major and minor element (S, O, Fe, Ni, Cu, Co) mineral chemistry; (3) laser ablation - inductively coupled plasma mass spectrometry (LA-ICP-MS) for *in situ* trace element mineral chemistry; (4) X-ray fluorescence (XRF) analyses for whole-rock major and trace geochemistry; and (5) solution nebulization (SN)-ICP-MS analyses for whole rock Zn and Pb analyses. Table 2.1 is a list of the 37 samples with borehole identification (BHID), depth (m), easting and northing, and petrographic textures (described below).

Representative lengthwise samples were taken from each core section and crushed to 1-2cm sized pieces with a steel jaw-crusher and then pulverized to <200 mesh powder in a tungsten carbide puck mill assembly for bulk XRF and SN-ICP-MS analysis. The remaining core was used for hand sample descriptions and to make polished thin sections for detailed petrography and EPMA and LA-ICP-MS analyses. All analyses were carried out at Memorial University.

For image analysis by MLA, six polished grain mounts of various size fractions were prepared from three massive sulfide Ovoid samples (VB95011, 55.25-55.55 m interval, 180-300μm, 125-180μm, 75-125μm, 45-75μm sized grains; VB95011, 70.20-70.50 m interval, 125-180μm sized grains; VB95011, 81.45-81.75 m interval, 125-180μm sized grains). Following crushing, the samples were sieved to the various size fractions, and down-sampled using a micro-rotary riffler to ensure sample homogeneity. Half of each sample was prepared as a monolayer grain mount in epoxy for the MLA and the other half was used for whole-rock XRF and SN-ICP-MS analysis.

Table 2.1. List of samples, drill holes, textures, and mineral domains from the Ovoid deposit.

BHID	FROM (m)	TO (m)	EASTING	NORTHING	MASU DOMAIN	TEXTURAL SUBCLASS
BS0209	72.65	72.85	55799	43123	TYPE III	C, G, F, I, J, K, L
BS0224	38.70	38.90	55958	43058	TYPE II	C, E, I, J, K, L
BS0224	61.10	61.30	55956	43060	TYPE II	C, E, I, J, K, L
BS0227	29.80	30.00	55968	43169	TYPE II	C, F, G, I, J, K, L
BS0227	52.80	53.00	55966	43169	TYPE III	A, B, C, E, I, J, K, L
BS0227	131.60	131.80	55961	43167	TYPE III	C, E, H, I, J, K, L
BS0232	25.50	25.70	55832	43234	TYPE III	C, F, I, J, K, L
BS0233	42.00	42.20	55833	43229	TYPE II	C, F, I, J, K, L
BS0233	73.55	73.75	55834	43220	TYPE II	B, C, J, K
BS0249	31.20	31.40	55910	43158	TYPE III	C, G, J, K
BS0249	139.65	139.85	55880	43128	TYPE III	A, C, E, I?, J, K
BS0255	56.40	56.60	55653	43280	TYPE II	C, F, I, J, K
BS0255	81.60	81.80	55662	43274	TYPE III	C, F, J, K
BS0255	92.10	92.30	55665	43272	TYPE II	C, F, I?, J, K
BS0203	54.05	54.20	55885	43185	TYPE II	C, F, J
BS0203	120.10	120.35	55885	43168	TYPE III	C, G, J, K
BS0247	51.30	51.45	55876	43114	TYPE I	D, E, I, J, K, L
BS0247	87.05	87.20	55894	43114	TYPE I	D, F, I, J, K, L
BS0248	60.20	60.35	55897	43085	TYPE I	D, E, I, J, K, L
BS0250	40.85	41.00	55806	43143	TYPE I	C, F, G, I, J, K, L
VB95011	18.70	19.00	55882	43061	TYPE III	D, G, J, K
VB95011	20.00	20.30	55882	43061	TYPE III	A, C, G, I, J, K
VB95011	27.20	27.50	55882	43061	TYPE II	D, F, I, J, K, L
VB95011	31.20	31.50	55882	43061	TYPE II	D, F, I, J, K, L
VB95011	40.30	40.60	55882	43061	TYPE II	C, F, I, J, K, L
VB95011	45.15	45.45	55882	43061	TYPE I	C, F, I, J, K, L
VB95011	55.25	55.55	55882	43061	TYPE I	D, F, I, J, K, L
VB95011	60.25	60.55	55882	43061	TYPE I	D, F, G, I, J, K, L
VB95011	65.50	65.80	55882	43061	TYPE I	D, E, I, J, K, L
VB95011	70.20	70.50	55882	43061	TYPE II	C, F, G, I, J, K, L
VB95011	75.00	75.30	55882	43061	TYPE III	C, E, H, I, J, K, L
VB95011	81.45	81.75	55882	43061	TYPE III	C, E, H, I, J, K, L
VB95012	16.50	16.75	55884	43161	TYPE III	C-D, F, H[1]
VB95012	26.95	27.20	55884	43161	TYPE II	C-D, F[1]
VB95012	66.90	67.15	55884	43161	TYPE I	A, C, F[1]
VB95012	101.70	101.95	55884	43163	TYPE III	C, F, G, H[1]
VB95012	117.10	117.35	55884	43163	TYPE III	C-D, F, G[1]

BHID = bore hole identification; MASU = massive sulfide.
MASU mineral domains defined in Table 2.5.
Textural subclasses for MASU ores defined in Table 2.2.
[1]No polished thin section available for sample; unknown whether microtextures I, J, K, L are present.

2.5 PETROGRAPHY

Ovoid massive sulfide ores contain hexagonal pyrrhotite ($Fe_{1-x}S$), troilite (FeS), pentlandite [$(Fe,Ni)_9S_8$], chalcopyrite ($CuFeS_2$), cubanite ($CuFe_2S_3$), and magnetite ($Fe^{+2}Fe_2^{+3}O_4$) as the main sulfide and oxide constituents. Trace amounts (typically <0.1 wt%) of galena (PbS), sphalerite ($Zn_{0.95}Fe^{+2}_{0.05}S$) and even rarer phases (Ag-pentlandite, ilmenite, and silicates) are also present. All massive sulfide ore contains pyrrhotite, pentlandite, chalcopyrite, and magnetite but in variable proportions. Troilite and cubanite are often present as exsolution lamellae in pyrrhotite and chalcopyrite, respectively. Macroscopic and microscopic textures of the sulfide minerals and magnetite can be divided into subclasses (Table 2.2). Examples of the macroscopic and microscopic textures are shown in Figure 2.2.

Pyrrhotite is the most abundant sulfide mineral and predominantly forms massive grains. Magnetite is commonly present in the pyrrhotite, and in places distributed in aligned bands that define a flow banding or foliation (Fig. 2.2a). Some pyrrhotite grains are surrounded by "loops" of chalcopyrite and pentlandite (Fig. 2.2b). The loops may be large, >10cm in diameter and 1cm thick. Magnetite may be fine-grained (Fig. 2.2c) or coarse-grained (Fig. 2.2d). It occurs predominantly in massive pyrrhotite as individual to aggregates of equant to amoeboid, subhedral to euhedral grains. It may be embayed and blebby. Thin rims of chalcopyrite and pentlandite have formed on some magnetite grains. Chalcopyrite occurs predominantly as irregular patches to semi-continuous loops associated with pentlandite in massive pyrrhotite (Fig. 2.2e). Pentlandite generally

occurs as coarse (0.5-1cm on average) subhedral grains to aggregates associated with irregular chalcopyrite patches (Fig. 2.2f) and aggregates in the loops in massive pyrrhotite. Some portions of the ore are completely free of chalcopyrite-pentlandite loops, and pyrrhotite takes on a massive appearance (Fig. 2.2g). A "crackle" texture consisting of pseudohexagonal fractures in pyrrhotite is prominent in some samples (Fig. 2.2h).

A variety of microscopic textures are noteworthy in the ores. Cubanite occurs as elongate and needle-like exsolution lamellae in chalcopyrite (Fig. 2.2i), and more rarely as discrete grains associated with chalcopyrite. Cubanite is thus generally more abundant where more chalcopyrite is present. Troilite occurs exclusively as exsolution lamellae in pyrrhotite (Fig. 2.2j). Troilite lamellae often exhibit a wavy appearance, reflecting crystallographic control by the host pyrrhotite. Some pentlandite forms small (<0.5mm) exsolution "flames" in pyrrhotite often associated with troilite exsolution (Fig. 2.2k). In places, chalcopyrite contains small (5-20 micron) star-shaped sphalerite inclusions formed by exsolution (Fig. 2.2l).

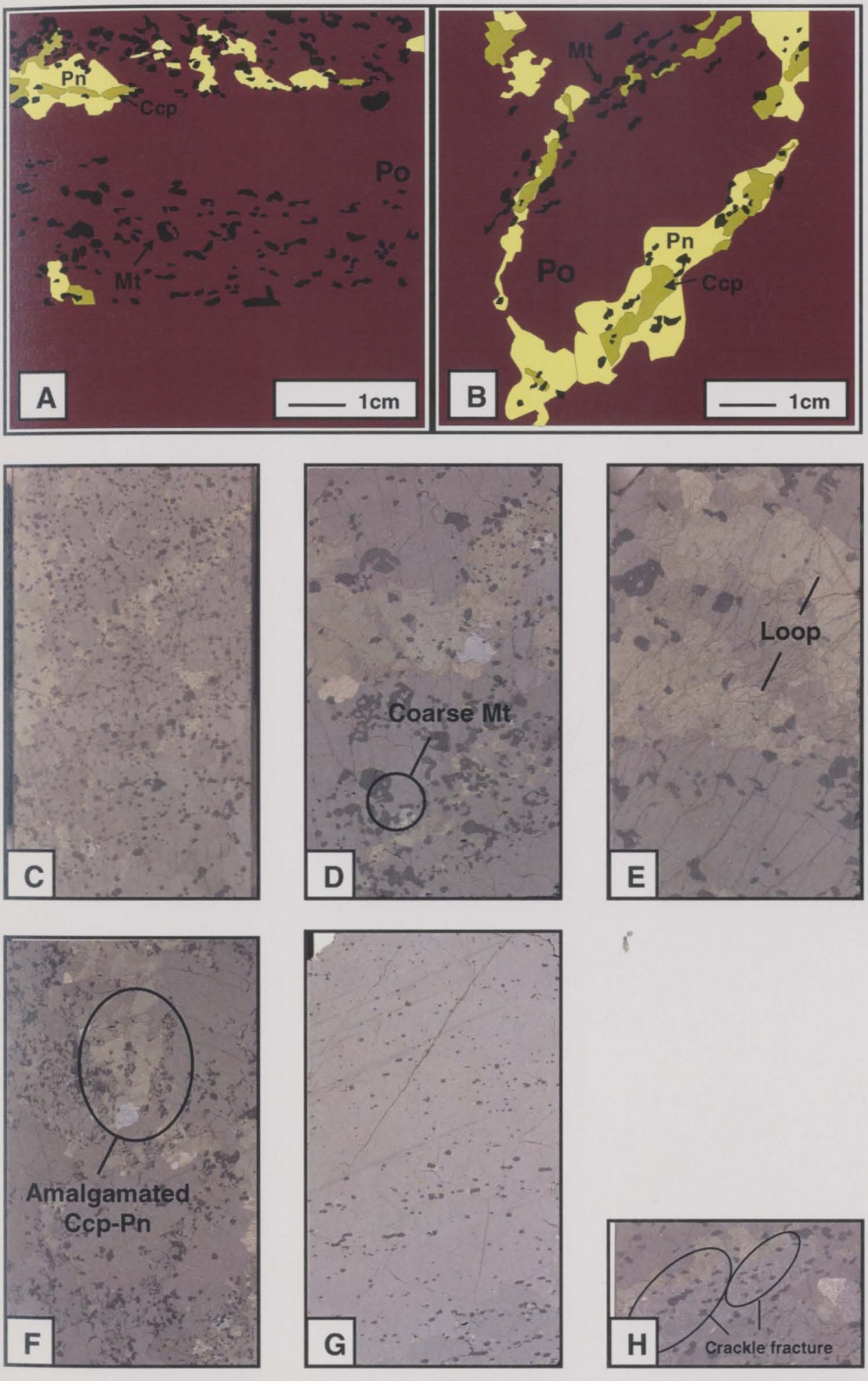
Pn
Ccp
Po
Mt
A
1cm
Mt
Pn
Po
Ccp
B
1cm
C
Coarse Mt
D
Loop
E
Amalgamated
Ccp-Pn
F
G
H
Crackle fracture

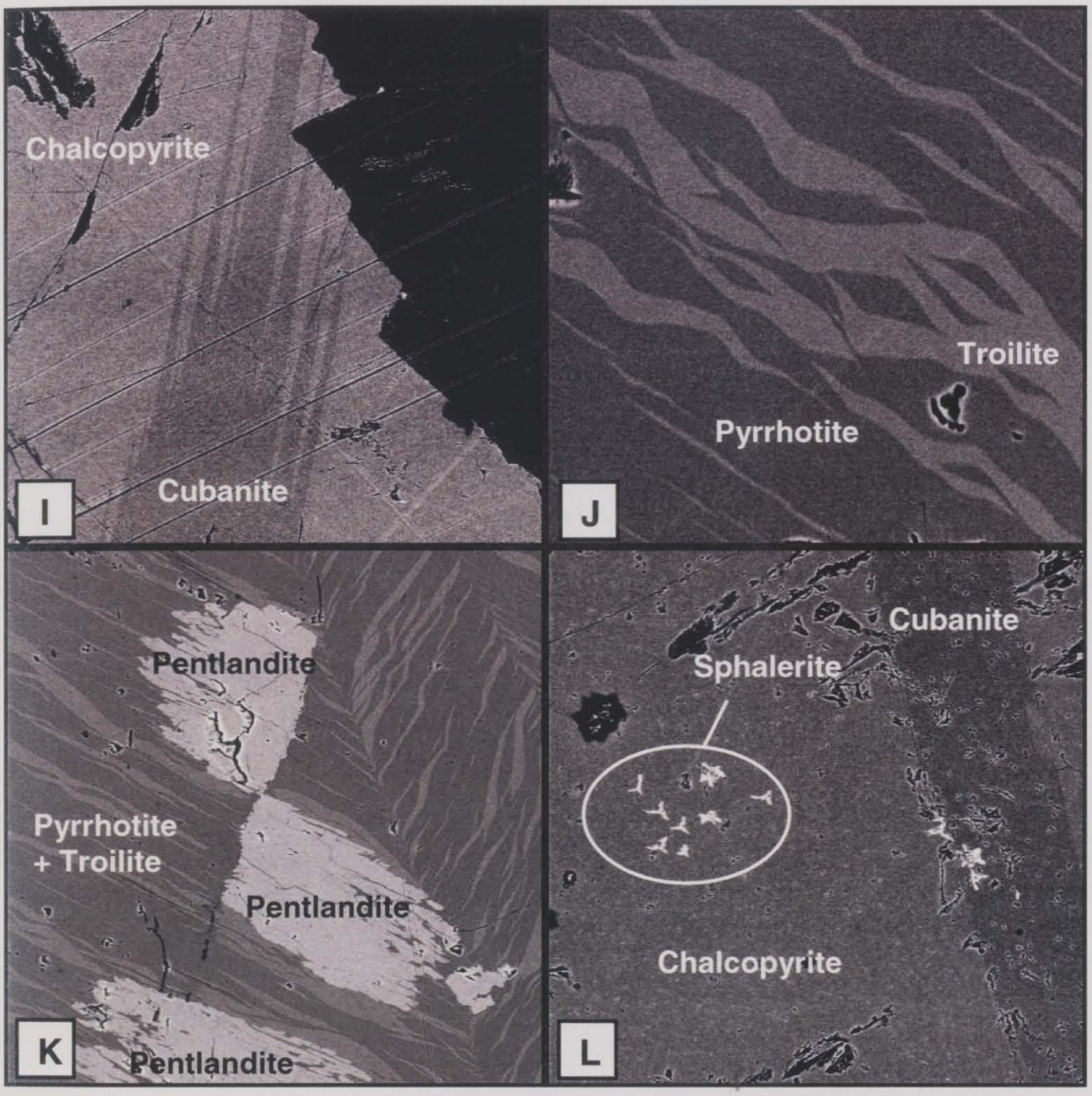

Figure 2.2. Examples of macroscopic and microscopic textural subclasses of Ovoid Deposit: a) magnetite forming aligned bands (BS0249 139.65m), b) flattened loop (BS0233 73.55m), c) fine-grained magnetite (VB95011 45.15m), d) coarse-grained magnetite (BS0248 60.2m), e) well-developed chalcopyrite-pentlandite loop in massive pyrrhotite (VB95011 52.6m), f) amalgamated chalcopyrite-pentlandite in pyrrhotite (BS0203 54.05m), g) massive pyrrhotite (BS0203 120.1m), h) crackle fracture in pyrrhotite (VB95011 81.45m). CCP = chalcopyrite; PN = pentlandite; PO = pyrrhotite. MT = magnetite, i) cubanite exsolution in chalcopyrite (BS0227 29.8m), FOV = 800*u*m, j) troilite exsolution in hexagonal pyrrhotite (BS0224 61.1m), FOV = 175*u*m, k) pentlandite flame exsolution in pyrrhotite (BS0224 38.7m), FOV = 400*u*m, l) sphalerite star exsolution in chalcopyrite (BS0224 38.7m), FOV = 800*u*m. Width of field of view (FOV) in images C, D, E, F, G, H = 9cm.

Table 2.2. Textural subclasses for Ovoid massive sulfide ore.

Textural Subclass	Description
Macroscopic textures	
A	Foliation defined by magnetite alignment
B	Foliation defined by flattened loops
C	Fine-grained magnetite
D	Coarse-grained magnetite
E	Well developed "loops" of pentlandite-chalcopyrite
F	Patchy pentlandite-chalcopyrite with poorly defined "loops"
G	Massive pyrrhotite
H	Pseudohexagonal "crackle" fractures in pyrrhotite
Microscopic textures	
I	Cubanite exsolution in chalcopyrite
J	Troilite exsolution in pyrrhotite
K	Pentlandite "flame" exsolution in pyrrhotite
L	Sphalerite "star" exsolution in chalcopyrite

2.6 ANALYTICAL TECHNIQUES AND RESULTS

2.6.1 Electron probe micro-analysis (EPMA)

Sulfide and magnetite compositions were determined using a Cameca SX-50 electron probe micro-analyzer equipped with SAMx *XMAS*® automation software. Measurements of Fe, S, Cu, Ni, and Co were performed by wavelength-dispersive X-ray analysis (WDX) using three Cameca detectors. Count times for these elements were chosen for an approximate 10% error at a concentration of 0.1 wt% and ZAF corrections were applied. Magnetite was analyzed by WDX for O, Mg, Al, Si, Ti, Mn, and Fe.

Mean and standard deviations of the measured concentrations of elements in each of pyrrhotite, troilite, chalcopyrite, cubanite, pentlandite and magnetite are reported in Table 2.3. The sulfides have similar concentrations of S. Pyrrhotite, troilite and magnetite are the most Fe-rich phases. Chalcopyrite and cubanite have Cu concentrations of ~34 and ~24 wt%, respectively. Minor amounts of Ni are present in pyrrhotite (~0.2 wt%), but Ni is negligible in troilite. There is ~1.4 wt% Co in pentlandite.

2.6.2 Laser ablation - inductively coupled plasma mass spectrometry (LA-ICP-MS)

In situ analyses of trace elements were carried out by LA-ICP-MS for pyrrhotite, troilite, chalcopyrite, cubanite, and pentlandite using an in-house built 266 nm Nd:YAG laser system attached to a VG Fisons PlasmaQuad II+"S" quadrupole mass spectrometer.

Table 2.3. Mineral compositions in massive ore in the Ovoid deposit.

	Cubanite	Chalcopyrite	Pentlandite	Pyrrhotite	Troilite	Magnetite
S (wt%)	35.13 ± 0.42	34.87 ± 0.46	33.26 ± 0.43	38.27 ± 0.67	36.38 ± 0.34	
Fe (wt%)	40.87 ± 0.44	30.68 ± 0.50	33.67 ± 0.86	61.18 ± 0.76	63.26 ± 0.55	71.03 ± 0.70
Ni (wt%)			31.45 ± 0.63	0.22 ± 0.09	0.02 ± 0.02	
Cu (wt%)	23.61 ± 0.41	34.13 ± 0.56				
Co (wt%)			1.39 ± 0.28			
O (wt%)						30.81 ± 0.37
Totals (wt%)	99.61	99.68	99.77	99.67	99.66	101.84
n_{sample}	17	34	37	37	20	5
$n_{analyses}$	126	426	741	434	82	15
Zn (ppm)	1323 ± 2245 (369)[1]	781 ± 1256 (347)[1]	106 ± 139 (55)[1]	120 ± 108 (48)[1]		
n_{sample}	9	7	8	8		
$n_{analyses}$	29	21	28	22		
Pb (ppm)	43 ± 34 (38)[1]	21 ±32 (11)[1]	49 ± 94 (6.5)[1]	2.6 ± 4.9 (0.98)[1]		
n_{sample}	17	19	19	20		
$n_{analyses}$	48	111	117	117		

Major element analyses determined by EPMA. Zn, Pb analyses by LA-ICP-MS.
Mean ± 1 standard deviation is shown. [1]Median Zn and Pb values.
n_{sample} = number of samples studied; $n_{analyses}$ = total number of analyses for all samples.

Laser spots ranged between 30 and 100μm depending on the size of the mineral grain of interest. Zn and Pb were the particular focus of this study because of the interest in evaluating the abundances of sphalerite and galena in the samples, as discussed below, but a larger suite of trace elements was also analyzed (Ge, As, Se, Mo, Ag, Cd, Sn, Sb, Te, Au, Hg, Bi, Pt, Pd, Rh, Ru, Ir, Os; Appendix 2.III).

Zn and Pb were consistently below detection limits for troilite and magnetite (Appendix 2.III). For the other minerals, the MASS-1 sulfide reference material (Wilson *et al.*, 2002) was used as the calibration standard for quantification. Concentrations of

sulfur, determined by electron microprobe, were employed as the internal standard for each mineral. Data reduction and concentration calculations were performed using the spreadsheet-based program LAMTRACE (van Achterbergh *et al.*, 2001).

The Zn and Pb data are shown in Table 2.3. Median values are included along with the mean values for each mineral because of the large variation in measured concentrations. Zinc concentrations are similar in chalcopyrite and cubanite (~350ppm) and in pentlandite and pyrrhotite (~50ppm). Lead concentrations decrease progressively from cubanite (~38ppm) to chalcopyrite (~11ppm) to pentlandite (~6ppm) to pyrrhotite (~1ppm).

2.6.3 X-ray fluorescence (XRF)

For XRF analyses, five grams of each powdered sample were mixed with 0.7 g of phenolic resin and homogenized. A Herzog press was used to compress the powders into circular pellets, which were then baked at 200°C for 20 minutes. The concentrations of major and trace elements in the whole rock pellets were obtained using an automated ARL 8420+ sequential XRF spectrometer using techniques described by Longerich (1995). Concentrations of Fe (total), Ni, Cu, S plus a variety of oxides and elements that are present in only minor concentrations in the massive ores samples (SiO_2, TiO_2, Al_2O_3, MnO, MgO, CaO, Na_2O, K_2O, P_2O_5, Cl, Sc, V, Cr, Zn, Ga, As, Rb, Sr, Y, Zr, Nb, Ba, Ce, Pb, Th, U) were determined by this technique. XRF spectra were calibrated for

concentration using a massive pyrrhotite ore standard from Sudbury (CANMET RTS-4) to account for matrix effects associated with silicate rock calibration.

Table 2.4 presents the XRF results for Fe, Ni, Cu, S and SiO_2 in the massive ores. There is typically 50 – 60 wt% Fe; 2 – 8 wt% Ni; <1 – 4 wt% Cu; and ~0.2 wt% SiO_2. Some samples are Cu-rich, containing up to 13 wt% Cu. Most of the other analytes were near or below detection limits. Some analyses have total concentrations that are less than 97 wt%, outside analytical error of up to 3% by XRF. This is because the samples contain magnetite and thus an unknown fraction of the measured iron is present as the oxide, and oxygen is not measured directly by XRF.

2.6.4 Solution nebulization - inductively coupled plasma mass spectrometry (SN-ICP-MS)

Bulk trace element concentrations of the massive sulfide samples were determined by SN-ICP-MS using a HP4500+ quadrupole mass spectrometer. Sample powders were dissolved in a hydrofluoric-nitric acid mixture in high-pressure bombs to ensure complete dissolution of sulfides and magnetite. Further details of the method are given by Diegor *et al.* (2001).

Data for Zn and Pb determined for massive ores by SN-ICP-MS are presented in Table 2.4. Zinc concentrations are quite variable but mostly <500ppm. Lead is somewhat less variable with typical concentrations of 30 – 100ppm.

Table 2.4. Whole-rock geochemical data and calculated normative mineralogy for massive sulfide samples in the Voisey's Bay Ovoid deposit.

				Whole-Rock Compositions Measured by XRF								Normative Mineralogy Calculated by Algorithm							Calculated	Recalculated	Level of
BHID	FROM (m)	TO (m)	FRACTION	Fe wt%	Ni wt%	Cu wt%	S wt%	SiO_2 wt%	Zn wt%	Pb wt%	TOTAL wt%	Chalcopyrite wt%	Pentlandite wt%	Pyrrhotite wt%	Magnetite wt%	Sphalerite wt%	Galena wt%	TOTAL wt%	Oxygen[1] wt%	XRF Total wt%	Confidence
BS0209	72.65	72.85	bulk powder	59.82	2.47	1.03	38.29	0.12	0.0111	0.0044	101.74	3.02	7.21	91.02	1.10	0.008	0.005	102.36	0.34	102.08	excellent
BS0224	38.70	38.90	bulk powder	56.27	5.04	0.39	35.26	0.18	0.0146	0.0029	97.16	1.13	15.49	77.64	4.52	0.015	0.003	98.80	1.39	98.56	excellent
BS0224	61.10	61.30	bulk powder	58.94	5.13	1.01	34.08	0.21	0.0192	0.0036	99.39	2.97	15.79	72.60	11.67	0.022	0.004	103.06	3.60	102.98	satisfactory
BS0227	29.80	30.00	bulk powder	48.59	4.29	13.28	34.42	0.17	0.0598	0.0045	100.81	38.91	13.33	42.83	8.39	0.068	0.005	103.53	2.58	103.39	satisfactory
BS0227	52.80	53.00	bulk powder	57.64	3.72	0.86	33.34	0.38	0.0217	0.0045	95.97	2.52	11.30	74.98	10.12	0.026	0.005	98.96	3.12	99.09	excellent
BS0227	131.60	131.80	bulk powder	58.06	3.11	0.59	34.02	0.29	0.0103	0.0048	96.09	1.73	9.34	79.19	8.36	0.008	0.005	98.64	2.58	98.67	excellent
BS0232	25.50	25.70	bulk powder	58.70	3.78	0.71	36.97	0.14	0.0134	0.0038	100.32	2.08	11.44	84.75	3.32	0.012	0.004	101.60	1.02	101.34	excellent
BS0233	42.00	42.20	bulk powder	57.06	6.63	0.35	35.00	0.18	0.0162	0.0033	99.23	1.02	20.58	72.61	7.59	0.018	0.004	101.82	2.34	101.57	excellent
BS0233	73.55	73.75	bulk powder	57.07	4.10	0.68	35.20	0.33	0.0097	0.0049	97.40	1.98	12.49	79.33	5.24	0.007	0.005	99.05	1.62	99.01	excellent
BS0249	31.20	31.40	bulk powder	58.11	1.73	0.11	36.09	0.14	0.0120	0.0038	96.20	0.32	4.88	89.75	2.04	0.011	0.004	97.02	0.63	96.82	satisfactory
BS0249	139.65	139.85	bulk powder	56.62	6.04	1.22	33.90	0.21	0.0144	0.0057	98.01	3.57	18.72	69.06	9.81	0.014	0.006	101.18	3.02	101.03	excellent
BS0255	56.40	56.60	bulk powder	51.75	5.13	3.59	32.97	0.17	0.0176	0.0042	93.63	10.52	15.87	62.75	6.74	0.016	0.005	95.90	2.08	95.71	satisfactory
BS0255	81.60	81.80	bulk powder	55.19	5.77	3.81	33.53	0.17	0.0165	0.0048	98.49	11.16	17.92	61.87	11.09	0.013	0.005	102.06	3.42	101.91	excellent
BS0255	92.10	92.30	bulk powder	53.31	5.94	4.71	33.91	0.21	0.0305	0.0054	98.11	13.81	18.46	59.95	8.71	0.034	0.006	100.96	2.68	100.79	excellent
BS0203	54.05	54.20	bulk powder	53.03	5.60	6.11	32.58	0.19	0.0353	0.0042	97.54	17.91	17.42	53.65	12.45	0.040	0.004	101.47	3.84	101.38	excellent
BS0203	120.10	120.35	bulk powder	58.17	3.07	0.08	37.90	0.13	0.0022	0.0043	99.34	0.22	9.12	90.90	-0.81	-0.004	0.005	99.42	-0.25	99.09	excellent[2]
BS0247	51.30	51.45	bulk powder	54.16	7.82	5.29	32.56	0.17	0.0392	0.0069	100.05	15.49	24.53	49.60	15.20	0.047	0.008	104.88	4.68	104.73	satisfactory
BS0247	87.05	87.20	bulk powder	57.18	7.62	2.12	32.14	0.19	0.0167	0.0085	99.27	6.22	23.84	57.58	16.92	0.016	0.009	104.58	5.21	104.49	satisfactory
BS0248	60.20	60.35	bulk powder	57.82	3.17	0.74	33.46	0.18	0.0078	0.0219	95.40	2.16	9.55	77.14	9.50	0.004	0.025	98.39	2.93	98.33	excellent
BS0250	40.85	41.00	bulk powder	61.17	2.83	0.60	34.67	0.12	0.0055	0.0118	99.42	1.76	8.43	81.67	11.02	0.001	0.013	102.90	3.40	102.82	satisfactory
VB95011	18.70	19.00	bulk powder	58.25	1.52	0.10	36.44	0.13	0.0050	0.0048	96.44	0.29	4.20	91.30	1.25	0.000	0.005	97.05	0.38	96.83	satisfactory
VB95011	20.00	20.30	bulk powder	55.67	5.87	1.10	35.12	0.12	0.0099	0.0045	97.90	3.22	18.16	73.05	5.45	0.007	0.005	99.89	1.68	99.58	excellent
VB95011	27.20	27.50	bulk powder	51.05	2.08	11.63	34.69	0.12	0.0760	0.0053	99.65	34.07	6.25	54.09	7.61	0.096	0.006	102.11	2.34	102.00	excellent
VB95011	31.20	31.50	bulk powder	56.44	6.08	1.69	32.77	0.15	0.0171	0.0110	97.16	4.95	18.87	64.69	12.66	0.017	0.012	101.20	3.90	101.06	excellent
VB95011	40.30	40.60	bulk powder	56.36	7.78	0.72	34.49	0.15	0.0082	0.0069	99.51	2.10	24.28	67.12	9.12	0.005	0.008	102.62	2.81	102.32	excellent
VB95011	45.15	45.45	bulk powder	54.83	3.04	5.51	33.15	0.16	0.0464	0.0090	96.76	16.15	9.24	63.83	10.86	0.058	0.010	100.14	3.34	100.10	excellent
VB95011	55.25	55.55	bulk powder	58.37	4.27	0.57	34.15	0.16	0.0067	0.0092	97.53	1.66	13.05	76.37	9.50	0.003	0.010	100.59	2.93	100.46	excellent
VB95011	60.25	60.55	bulk powder	57.69	3.38	0.57	33.64	0.16	0.0058	0.0090	95.45	1.67	10.19	77.52	8.89	0.001	0.010	98.28	2.74	98.19	excellent

VB95011	65.50	65.80	bulk powder	54.56	3.45	4.71	33.40	0.13	0.0347	0.0057	96.29	13.80	10.51	65.54	9.42	0.041	0.006	99.31	2.90	99.19	excellent
VB95011	70.20	70.50	bulk powder	49.41	5.91	8.26	34.01	0.12	0.0447	0.0038	97.76	24.20	18.45	50.74	6.67	0.051	0.004	100.10	2.05	99.81	excellent
VB95011	75.00	75.30	bulk powder	55.32	3.70	1.64	33.44	0.14	0.0124	0.0040	94.26	4.82	11.27	73.18	7.43	0.010	0.004	96.71	2.29	96.55	satisfactory
VB95011	81.45	81.75	bulk powder	56.17	3.93	0.64	35.07	0.14	0.0058	0.0038	95.97	1.88	11.93	79.56	4.09	0.001	0.004	97.47	1.26	97.23	satisfactory
VB95011	55.25	55.55	180-300*um* grains	58.10	3.49	0.37	32.84	0.14	0.0073	0.0046	94.94	1.07	10.56	75.64	11.17	0.004	0.005	98.46	3.44	98.38	excellent
VB95011	55.25	55.55	125-180*um* grains	58.15	3.68	0.38	34.38	0.17	0.0069	0.0057	96.76	1.11	11.14	79.14	7.94	0.003	0.006	99.33	2.45	99.20	excellent
VB95011	55.25	55.55	75-125*um* grains	57.74	3.95	0.42	34.31	0.15	0.0068	0.0058	96.58	1.22	12.03	78.08	7.80	0.003	0.007	99.14	2.40	98.99	excellent
VB95011	55.25	55.55	45-75*um* grains	57.78	4.19	0.45	35.38	0.22	0.0068	0.0072	98.04	1.32	12.77	80.14	5.69	0.003	0.008	99.94	1.75	99.79	excellent
VB95011	70.20	70.50	125-180*um* grains	53.13	4.33	7.43	37.78	0.28	0.0350	0.0035	103.00	21.76	13.31	67.31	1.12	0.037	0.004	103.54	0.35	103.34	satisfactory
VB95011	81.45	81.75	125-180*um* grains	58.36	4.43	0.68	38.41	0.13	0.0072	0.0039	102.02	1.99	13.47	86.86	0.10	0.003	0.004	102.42	0.03	102.05	excellent
VB95012	16.50	16.75	bulk powder	56.43	3.92	3.01	32.89	0.13	0.0228	0.0045	96.41	8.81	12.00	67.48	11.83	0.025	0.005	100.14	3.64	100.05	excellent
VB95012	26.95	27.20	bulk powder	55.43	4.75	3.47	33.76	0.13	0.0249	0.0043	97.57	10.17	14.63	66.21	9.68	0.027	0.005	100.73	2.98	100.55	excellent
VB95012	66.90	67.15	bulk powder	56.60	4.65	3.49	34.15	0.13	0.0262	0.0079	99.05	10.23	14.31	67.45	10.38	0.029	0.009	102.41	3.20	102.25	excellent
VB95012	101.70	101.95	bulk powder	56.03	4.95	1.02	35.03	0.11	0.0077	0.0022	97.15	2.99	15.21	75.59	5.27	0.003	0.002	99.06	1.62	98.77	excellent
VB95012	117.10	117.35	bulk powder	57.68	4.06	0.58	35.63	0.14	0.0064	0.0043	98.11	1.71	12.36	80.81	5.01	0.002	0.005	99.90	1.54	99.66	excellent

All elements determined by XRF except Zn and Pb measured by SN-ICP-MS.

Detection limits are Fe, Ni, Cu, S, SiO2 = 0.01 wt%; Zn = 0.0005 wt%, Pb = 0.0001 wt%.

[1]Calculated oxygen from normative magnetite.

[2]One sample has magnetite and thus oxygen contents calculated as slightly negative.

Confidence level rankings of algorithm results: excellent = 97.5 - 102.5 wt% total; satisfactory = 95 - 105 wt% total.

2.6.5 Scanning electron microscope - mineral liberation analyzer (MLA)

The instrument used for automated image analysis of grain mounts is an FEI Quanta 400 scanning electron microscope (SEM) equipped with a Roentec *XFlash*® liquid-nitrogen free, silicon-drift, energy-dispersive X-ray (EDX) detector, and integrated with JKTech *Mineral Liberation Analyzer*® software (Gu, 2003, 2004; Shaffer *et al.*, 2007). Mineral identification is performed by first distinguishing mineral phases on the basis of average atomic number determined by backscattered electron imaging, and then by matching EDX spectra to the spectra of known mineral standards. Further details of the method and MLA results are discussed in a later section of the paper.

2.7 ALGORITHM FOR CALCULATION OF NORMATIVE MINERAL ABUNDANCES

An algorithm was developed to calculate normative mineral abundances in the Ovoid based on bulk assays of massive ore samples. The approach is similar to calculations of CIPW norms for silicates (Johannsen, 1931; Philpotts, 1990) except unlike CIPW norms, which assume certain minerals are present, the algorithm requires that the actual mineral assemblage is known. Normative calculations are the preferred option for producing modal estimates for large numbers of samples because it is most efficient: once the algorithm is designed for a massive sulfide ore body, it can be applied to thousands of assayed samples virtually instantaneously as opposed to modal estimates

determined by point counting or image analysis. The latter methods are more appropriate for checking the results of the algorithm for particular samples.

Calculations of normative modal sulfide mineralogy similar to those presented here have been carried out previously by others for specific mineral assemblages (e.g., Naldrett *et al.*, 2000b; Kerr, 2003, Huminicki *et al.*, 2005). Our method calculates modes for pyrrhotite, pentlandite, chalcopyrite, galena, sphalerite and magnetite. This accounts for all major and minor sulfide and oxide minerals present in the Ovoid except for the exsolved phases, troilite and cubanite, which cannot be distinguished by the calculation. This is because troilite and cubanite have compositions that are not sufficiently distinct from those of their host phases, pyrrhotite and chalcopyrite, respectively. This limitation and other details of the algorithm are described more fully below.

2.7.1 Requirements, rationale, and limitations of normative calculations

Three types of data are required in order to calculate modal mineral abundances using an algorithm: (1) knowledge of the mineral assemblage (from detailed petrographic analysis or SEM-based examination); (2) representative mineral chemical analysis (from EPMA and LA-ICP-MS or the stoichiometric composition of each phase present); and (3) whole-rock concentrations of the chemical elements constituting the minerals. Using these data, minerals are apportioned so that their abundances provide mass balance between the chemical elements constituting the minerals and bulk sample.

The basis of the apportionment calculation is the use of the concentration of a major element concentrated solely or largely in each mineral to provide an *initial*

estimate of its abundance. The modal estimate is then refined where the same element is present as minor concentrations in other phases. Thus, in the case of the Ovoid, the *initial* normative calculations derive estimates (in a sequential manner) for the abundances of chalcopyrite, pentlandite, pyrrhotite and magnetite assuming that: (1) all Cu occurs in chalcopyrite; (2) all Ni occurs in pentlandite; (3) all S unattributed to chalcopyrite and pentlandite occurs in pyrrhotite; and (4) all Fe unattributed to chalcopyrite, pentlandite and pyrrhotite occurs in magnetite.

Potential minor errors associated with these assumptions are that minor Ni is present in pyrrhotite; some Cu is present as minor cubanite; some Fe is present as minor troilite; and abundances of the trace phases, sphalerite and galena, are ignored. The errors are addressed by revising the *initial* modal estimates for pentlandite, pyrrhotite and magnetite, after accounting for the amount of Ni attributed to pyrrhotite. The effect is modest, on average, reducing pentlandite and magnetite modes by ~0.6 and 0.2 wt%, respectively, and increasing modes for pyrrhotite by ~0.4 wt%. Modes for sphalerite and galena are determined in the revised calculations based on Zn and Pb concentrations in the ores, respectively. In the case of the Ovoid, sphalerite and galena occur in trace amounts (<0.1 wt%), and their modal estimates are thus expected to be less accurate than those for the major phases. The accuracy of the calculated modes for the major, minor and trace phases is specifically addressed for the Ovoid by comparison with the results from image analysis later in the paper. Another check on the accuracy of the method is provided by the deviation of the calculated totals of the minerals from 100 wt%.

As mentioned above, there are difficulties in distinguishing between the two Cu-bearing minerals chalcopyrite and cubanite using the algorithm, and the cubanite abundance is therefore included in the chalcopyrite value. Similarly, there are difficulties in distinguishing pyrrhotite and troilite, and the abundance of troilite is included in the pyrrhotite value. Although pyrrhotite and troilite both contain Fe and S, their stoichiometric proportions of the two metals are very similar and therefore errors in distinguishing the two iron sulfide phases do not propagate significant errors to the modal estimates of the other phases. The more problematic determination is for chalcopyrite and cubanite due to the large difference in Cu contents of the two minerals (~10 wt% absolute, Table 2.3). However, the MLA analysis presented later in the paper show that cubanite comprises only 3-8% of the sum of the chalcopyrite + cubanite mode, so these errors are minimal. Equations used for the normative calculations are presented and explained in more detail in Appendix 2.I.

2.7.2 Results of normative calculations

Table 2.4 presents the normative mineral modes calculated for the 37 massive sulfide samples listed in Table 2.1 plus the 6 additional grain-sized aliquots of the three samples (VB95011, 55.25-55.55 m interval; VB95011, 70.20-70.50 m interval; VB95011, 81.45-81.75 m interval) processed for MLA work. The calculations utilize the measured concentrations for S, Fe, Ni, Cu, Zn and Pb in each of the minerals given in Table 2.3, and the whole rock concentrations for these elements given in Table 2.4.

Stoichiometric compositions are assumed for sphalerite ($Zn_{0.95}Fe^{2+}_{0.05}S$) and galena (PbS), which were difficult to measure accurately due to their very fine grain size.

The results demonstrate that pyrrhotite is the most abundant mineral in all samples, although abundances of chalcopyrite can reach almost 40 wt%. Pentlandite abundances are up to ~25 wt%, and magnetite are 20 wt%. Sphalerite modes are less than 0.05 wt% in most samples and less than 0.1 wt% in all samples. Galena is rarer, typically less 0.01 wt%, or less.

The normative mineral modes for the samples in Table 2.4 have an average sum of 100.40 ± 2.15 wt% (1 σ), and a total range from ~96 to almost 105 wt%. Deviations of the sums from 100% are mainly a function of analytical uncertainties on the measured elemental concentrations in the bulk rock (by XRF and SN-ICP-MS) and minerals (by EPMA and LA-ICP-MS); and errors associated with the use of average, median or stoichiometric element concentrations for the minerals in all samples.

Analytical uncertainties on the XRF analyses for the major element (S, Fe, Ni, Cu) assays are on the order of 2-3% (Longerich, 1995); SN-ICP-MS errors for the Zn and Pb in the whole rocks are 3-5%. For the minerals, analytical errors on the EPMA determinations are 1-2% except for the minor Ni in pyrrhotite determinations, which may be as high as 10%. Analytical uncertainties on LA-ICP-MS analyses for Zn and Pb in sulfides are 5-10% (Wilson *et al.*, 2002). The 1 σ variance of the average elemental concentrations in the minerals is 1-3% except for Ni in pyrrhotite (~40%), and Zn and Pb in all sulfides (~80% to >100%).

Considering these uncertainties, giving most weight to those involving major elements, we can assign a confidence rating for each sample wherein the normative calculation is considered to be "excellent" for samples with sums of mineral modes of 97.5 to 102.5 wt% and "satisfactory" where equal to 95 to 105 wt%. By these criteria, the reliability of the calculated modes is excellent for 74% of the samples and satisfactory for 26% of the samples. The true measure of the accuracy of the calculations however is a sample-by-sample comparison with modes determined by image analysis, as presented later in the paper.

A demonstration of the internal consistency of the algorithm results is provided by calculating the amount of oxygen contributed to the bulk XRF assay by magnetite, and comparing the total recalculated assay (calculated O from magnetite plus measured S, Fe, Ni, Cu, Zn, Pb, SiO_2) with the sum of the normative mineral modes. For all samples in Table 2.4, the discrepancy between the total recalculated assay and sum of the normative mineral modes is very small (~0 to 0.3 wt%), and is explained by concentrations of minor analytes not considered in the normative calculations (e.g., SiO_2, Ti, Co, Ag, etc.).

2.8 MINERALOGICAL ZONATION IN THE OVOID

The algorithm was applied to 3175 sample assays for massive sulfide ores in the Ovoid in order to show how spatially controlled normative mineralogy may be used to document mineralogical zonations within an ore body. The detailed calculations for these samples are presented in Appendix 2.I. As in the calculations for the samples given

in Table 2.4, troilite is not distinguished from pyrrhotite, and cubanite is not distinguished from chalcopyrite.

The results for the 3175 samples were plotted in the block model for the Ovoid (supplied by VBNC Ltd) using the Datamine Corp Ltd *Studio2*® geological and geotechnical mapping software. Figure 2.3 is a cross sectional slice through the center of the deposit looking west. It shows variations in the abundances of normative pyrrhotite, pentlandite, chalcopyrite and magnetite as a function of lateral and vertical position throughout the deposit. Pyrrhotite ranges largely from 50-90%. It is least abundant in the center (50-65%) and increases outward (65-70%) with the highest abundance toward the base of the deposit and in the upper northern portion (70-90%). Magnetite ranges from <5-35% and is most abundant in the center of the Ovoid (15-25% and locally up to 35%) decreasing in abundance outwards (5-15%). Pentlandite, in general, is most abundant (11.5-13.5%) in a transitional portion of the body, forming a transitional zone surrounding the center, but in from the margins. There is an enriched area of pentlandite (13.5-15%) in the northern part of the deposit at its base. Chalcopyrite distribution is somewhat similar to that of pentlandite, with a higher abundance (>9%) in the transitional rind surrounding the central core.

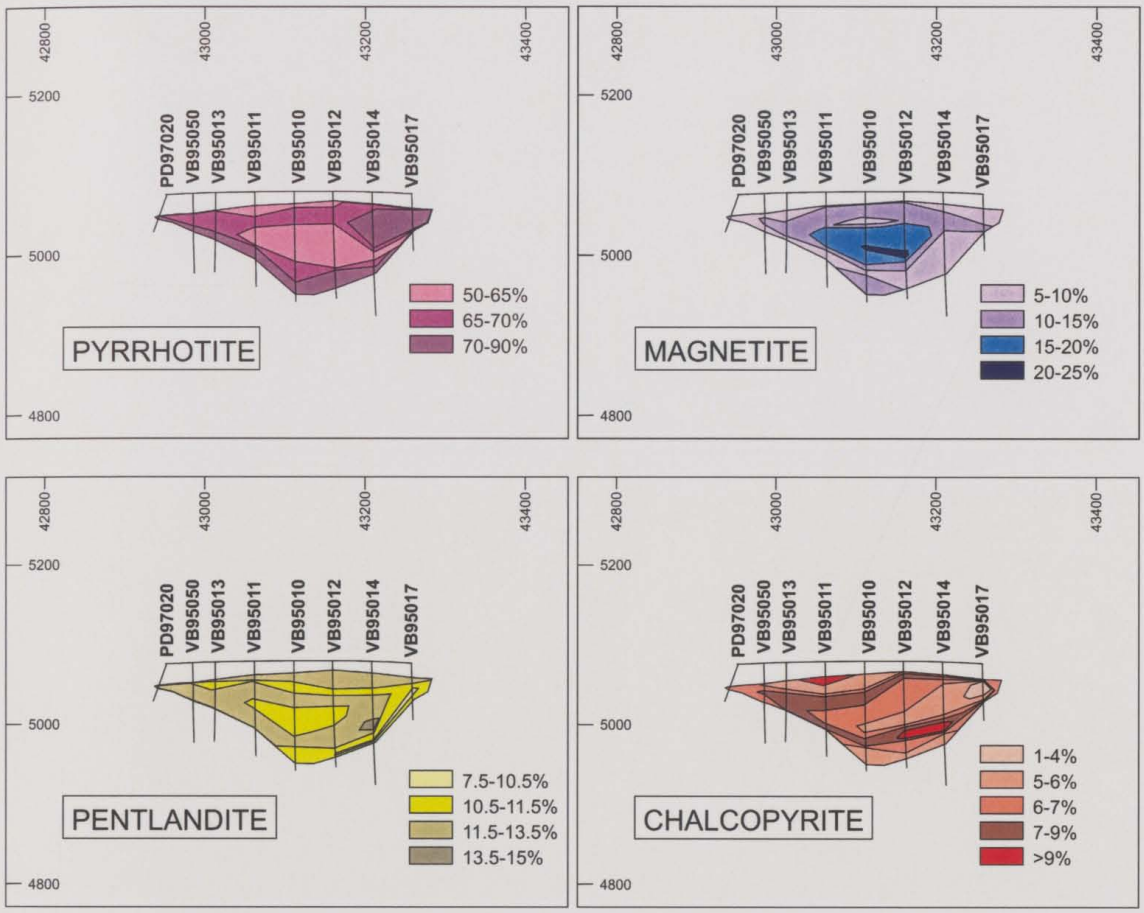

Figure 2.3. Variations in algorithm-calculated abundances (wt%) of pyrrhotite, magnetite, pentlandite, and chalcopyrite through the massive sulfide ore of the Ovoid deposit in cross section 55885E (looking west). Drillhole locations are labeled for reference. The Ovoid is approximately 800m by 350m in plan view, and about 125m thick at its thickest point (toward the center, near drill hole VB 95010).

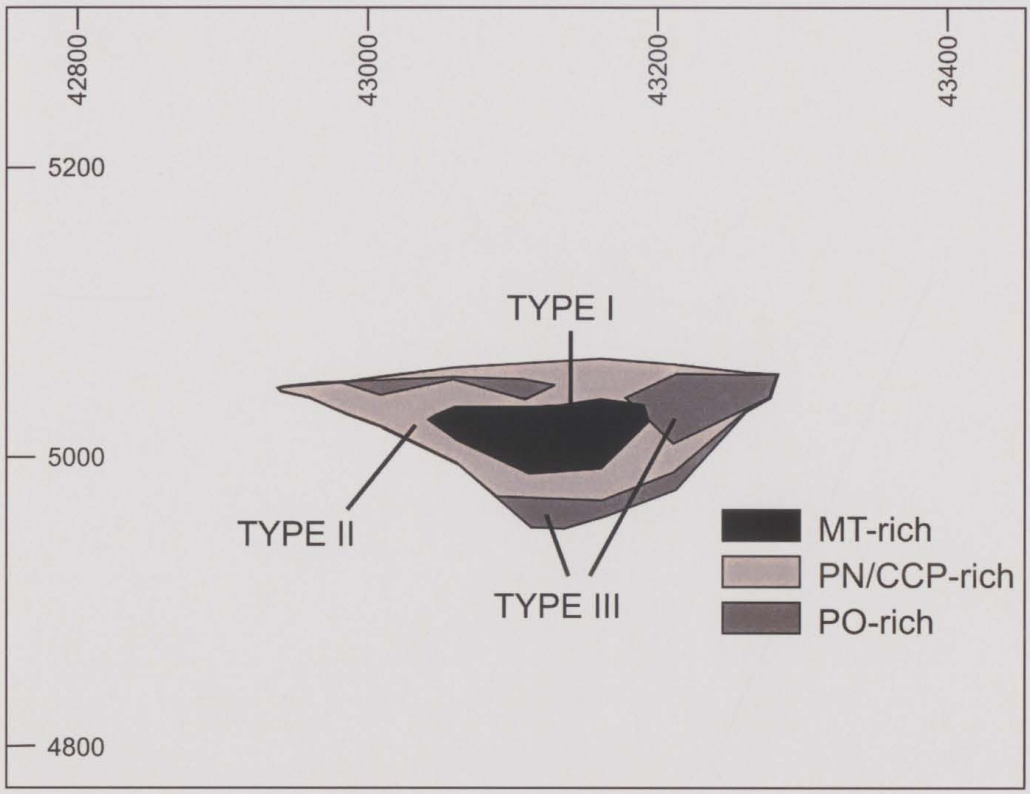

Figure 2.4. Composite of calculated mineralogical zones, showing the spatial relationships of the three mineral domains of the Ovoid deposit in cross section 55885E (looking west). CCP = chalcopyrite; PN = pentlandite; PO = pyrrhotite; MT = magnetite.

2.9 CLASSIFICATION OF MINERALOGICAL DOMAINS

Three mineral domains may be defined in the Ovoid deposit on the basis of the calculated proportions of the four major minerals in different parts of the ore body. Table 2.5 lists the ranges of typical mineralogical proportions for each mineral domain. Figure 2.4 shows the distribution of the mineral domains in the Ovoid when combined in the same cross section as is shown in Figure 2.3. Figure 2.5 is an example of the variations in normative mineralogical abundances and palladium and platinum concentrations down a drill hole (VB95010) through the center of the Ovoid deposit.

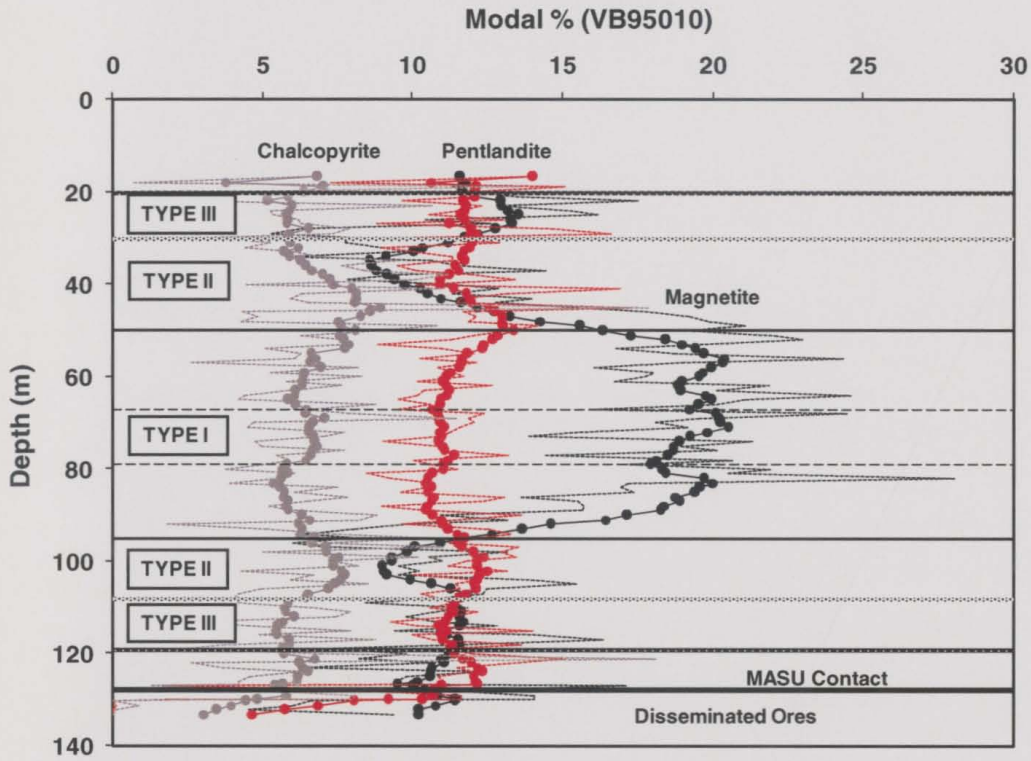
Modal % (VB95010)
0
5
10
15
20
25
30
Depth (m)
0
20
40
60
80
100
120
140
Chalcopyrite
Pentlandite
Magnetite
TYPE III
TYPE II
TYPE I
TYPE II
TYPE III
MASU Contact
Disseminated Ores

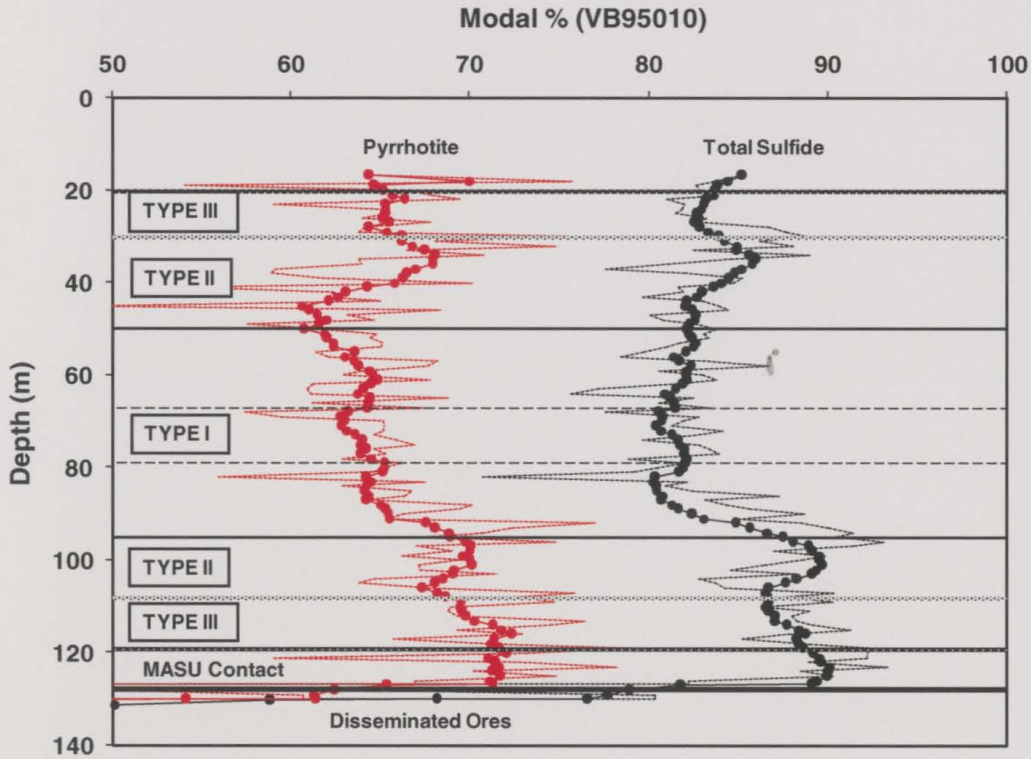
Modal % (VB95010)
50
60
70
80
90
100
Depth (m)
0
20
40
60
80
100
120
140
Pyrrhotite
Total Sulfide
TYPE III
TYPE II
TYPE I
TYPE II
TYPE III
MASU Contact
Disseminated Ores

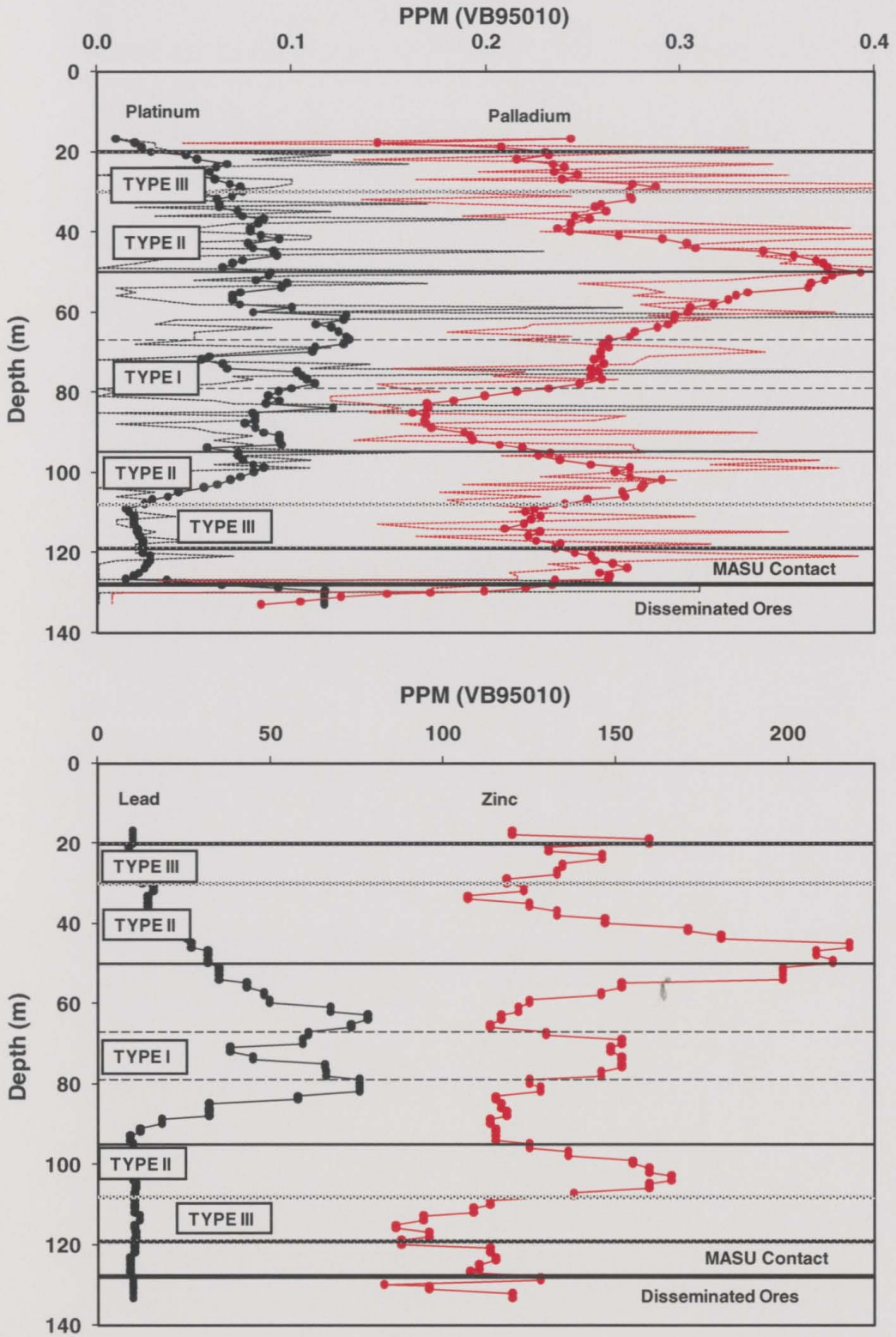
PPM (VB95010)
0.0
0.1
0.2
0.3
0.4
Platinum
Palladium
Depth (m)
0
20
40
60
80
100
120
140
TYPE III
TYPE II
TYPE I
TYPE II
TYPE III
MASU Contact
Disseminated Ores
PPM (VB95010)
0
50
100
150
200
Lead
Zinc
Depth (m)
TYPE III
TYPE II
TYPE I
TYPE II
TYPE III
MASU Contact
Disseminated Ores

Figure 2.5. Calculated mineral modes for magnetite, chalcopyrite, pentlandite, and pyrrhotite plotted for drill hole VB95010 (see Fig. 2.3 for location). Palladium, platinum, lead, and zinc abundances are also plotted for drill hole VB95010. Both the raw data (light stipple) and data smoothed with 10 point moving averages (solid lines) are shown. MASU = massive sulfide ore.

TYPE I ore occurs in the center of the Ovoid and exhibits high magnetite (15-35%), moderate chalcopyrite (± cubanite) (5-9%), moderate pentlandite (10.5-11.5%) and low pyrrhotite (± troilite) (50-65%). TYPE II ore is transitional between TYPE I and TYPE III ore and generally consists of low magnetite (5-15%), high chalcopyrite (± cubanite) (>9%), high pentlandite (11.5-13.5%), and moderate pyrrhotite (± troilite) (60-75%). TYPE III ore occurs at the base of the Ovoid and along the outer peripheries including the top of the north portion of the ore body. It typically contains low to moderate magnetite (0-15%), low chalcopyrite (± cubanite) (1-6%), moderate pentlandite (10.5-11.5%), and high pyrrhotite (± troilite) (70-90%).

Although platinum and palladium concentrations are relatively low (<0.5ppm), in the Ovoid, the distributions within each mineral domain merits discussion. Platinum is highest in TYPE I ore with the exception of the very central zone where it has a sudden decrease. TYPE II ore contains similar concentrations of Pt to TYPE I ore and gradationally decreases in TYPE III ore (Fig. 2.5). Palladium is highest in TYPE II ore, which is also enriched in chalcopyrite and pentlandite. TYPE I ore has a significant decrease in the central magnetite-rich zone. The outer pyrrhotite-rich TYPE III ore zone has moderate concentrations of palladium.

Lead is highest in TYPE I ore with the exception of the very central zone where it has a sudden decrease; TYPE II and TYPE III ores show a decrease and in lead concentrations (Fig. 2.5). Zinc is highest in TYPE II ore, which is also enriched in chalcopyrite; TYPE I ore has a significant decrease in zinc the central magnetite-rich

zone with exception of the very center which has an increase in zinc with chalcopyrite; the outer pyrrhotite-rich TYPE III ore zone also has lower relative concentrations of zinc.

The macroscopic appearance of some typical examples of polished core slabs of TYPES I, II and II ores are shown in Figure 2.6. Magnetite-rich TYPE I ores can have a variable appearance depending on whether the magnetite is fine- or coarse-grained. TYPE II ores tend to have noticeably less magnetite and more chalcopyrite than TYPE I ores, consistent with the algorithm results. TYPE III ores commonly appear the most massive because they are particularly rich in pyrrhotite, which tends to form large massive grains.

Both macroscopic and microscopic textural data can be integrated with the mineralogical domains in a more systematic fashion by determining the frequency with which the various textural subclasses defined in Table 2.2 correlate with mineral domain. Table 2.5 includes the results of such an analysis for the 37 Ovoid samples listed in Table 2.1. The results indicate that TYPE I and II ores have very similar textural characteristics with the noteworthy exception that TYPE I ores are dominated by coarse-grained magnetite whereas TYPE II ores more typically have fine-grained magnetite. In Huminicki and Sylvester (submitted) and Chapter 3 of this thesis the coarser grain size of magnetite in TYPE I ores is attributed to a slower cooling rate in the center of the Ovoid, where TYPE I ores are located. TYPE III ores differ from TYPE I and II ores by containing more massive pyrrhotite, as suggested above, but also more abundant pseudohexagonal "crackle" fractures in pyrrhotite, and rarer cubanite and sphalerite exsolution in chalcopyrite. These characteristics may be due in part to TYPE III ores

being dominated by early crystallizing cumulus monosulfide solid solution, which settled to the bottom of the Ovoid, forming a pyrrhotite-rich, chalcopyrite-poor assemblage upon cooling or crystallizing from the margins and base inward (Huminicki and Sylvester, submitted and Chapter 3 of this thesis). The correlation of Zn to chalcopyrite-rich zones is due to the presence of sphalerite exsolution "stars" in chalcopyrite. The marked Pt and Pb depletion in the very center of the Ovoid is thought to indicate escape of late stage enriched sulfide liquid from the center to its surroundings.

2.10 "GROUNDTRUTHING" THE ALGORITHM BY IMAGE ANALYSIS

It is extremely important to verify or "groundtruth" normative mineralogical calculations and the resulting mineral zonations defined in the block models. It is also useful if alternative methods can provide mineralogical and textural information that is difficult or impossible to derive from an algorithm such as the proportions of exsolved troilite in pyrrhotite, and exsolved cubanite in chalcopyrite in the Ovoid ores. The results can be applied to representative samples from specific mineral zones (defined by the algorithm results) to describe an ore deposit more completely.

Table 2.5. Classification of Ovoid massive sulfide mineral domains.

MODE (wt%)	TYPE I	TYPE II	TYPE III
Pyrrhotite	50 - 65	60 - 75	70 - 90
Magnetite	15 - 35	5 - 15	0 - 15
Chalcopyrite	5 - 9	> 9	1 - 6
Pentlandite	10.5 -11.5	11.5 - 13.5	10.5 - 11.5
FREQUENCY OF TEXTURAL SUBCLASSES[1]			
	n = 9	n = 13	n = 15
A	2%	0%	4%
B	0%	1%	1%
C	6%	16%	17%
D	11%	4%	4%
E	6%	3%	6%
F	11%	14%	7%
G	4%	3%	9%
H	0%	0%	6%
I	15%	14%	10%
J	15%	17%	15%
K	15%	16%	15%
L	15%	11%	7%

[1]Occurrence of each textural feature as a % of the total for all samples within each mineral domain. Based on 37 samples listed in Table 2.1.Textural subclasses for massive sulfide ores defined in Table 2.2. Distinctive textural variations for each mineral domain highlighted by enclosing boxes.

Error! Objects cannot be created from editing field codes. Error! Objects cannot be created from editing field codes.

Error! Objects cannot be created from editing field codes. Error! Objects cannot be created from editing field codes.

Figure 2.6. Typical examples of polished drill core slabs of TYPE I (magnetite-rich), TYPE II (chalcopyrite and pentlandite-rich), and TYPE III (pyrrhotite-rich) ores indicating the sulfide mineral phases. TYPE I ores are further subdivided into I-A (fine-grained magnetite) and I-B (coarse-grained magnetite) textural subclasses. Width of drill core = 4.5cm.

A variety of methods are available for verifying normative mineral calculations and providing additional mineralogical information. Each has advantages and disadvantages. The traditional method of determining modal abundances is by point counting using a macropoint-counter for rock slabs (Emerson, 1958; Smithson, 1963) or a Swift point-counter controller for thin sections (Schryver, 1968). The advantages of point counting are that it can be performed with inexpensive equipment and is accepted as statistically reliable. However, the identification of minerals is dependant solely on the skill of the petrographer and requires approximately 2000 points to be recorded (Hutchison, 1974) rendering it labor intensive and subject to operator bias.

X-ray diffraction analysis and mineral separation methods can also provide mineral modes, but do not give textural information and commonly produce inaccurate results for certain kinds of ores (Hutchison, 1974). More recently, X-ray computed tomography (CT) scans for modal analysis have been employed for sulfide ore samples (Godel *et al.*, 2006). The advantages of the CT method are that it is non-destructive, renders 3-dimentional images, and can be quantitative. However, the method is very expensive, not widely available, and time consuming in its off-line processing.

In this study, we have evaluated two methods of image analysis to groundtruth the results provided by the algorithm for the Ovoid: (1) automated analysis of grain mounts using the SEM-based MLA; and (2) desktop computer-based analysis of scanned digital optical images of drill core slabs. The methods and results are discussed in detail below following a brief discussion of sample selection. Our work complements that of

Castroviejo *et al.* (2002) and Pirard (2004), who have recently evaluated image analysis for polished thin sections and grain mounts using computer-aided optical microscopy.

2.10.1 Selection of sample and area for modal analysis

It is important to select or prepare a sample that has suitable representation for modal analysis, regardless of which method is used to determine mineral modes. In general, modal analysis may be carried out on a nearly flat outcrop, a flat-sawed rock surface, or a petrographic thin section and is an estimate or measure of relative area of a 2-dimensional surface. Grain mounts may be prepared from particularly heterogeneous bulk samples to provide a more representative sub-sample volume of the whole. Sample sizes or areas appropriate for different rocks will depend on the average grain size and the texture; for instance whether the sample is equigranular versus porphyritic, or massive versus banded or foliated. Modal analysis is only useful when evaluated as a representative unit cell (Hutchison, 1974). In some cases, it may be necessary to relate 2-dimentional modal analysis to a third dimension (volume) by stereological methods. For the Ovoid example, the coarse-grained nature of the ores and some banding of magnetite do not lend to the use of standard (27 x 46 mm) petrographic thin sections for modal analysis but instead to larger (4.5 x 15cm) core slabs and prepared grain mounts representing larger amounts of sample.

2.10.2 Image analysis using the MLA

An automated SEM-based, approach to modal image analysis is afforded by the use of backscattered electron imaging (BEI) to distinguish mineral phases together with X-ray mapping to determine elemental spatial distributions (Gottlieb, 1993; Lastra *et al.*, 1998; Gu, 2003). Two types of instruments are commercially available, the JKTech *Mineral Liberation Analyzer*® used here and the Intellection *QEMSCAN*™. The SEM-platform is costly, but because spectra can be acquired in as little as 20 milliseconds, and is automated, a large number of measurements can be made without human involvement once an appropriate sample has been selected and prepared, and instrument run settings have been established. Not only are the requirements for human labor lower than for many other methods of modal analysis, but the opportunities for human bias are reduced.

Depending on the application requirements and the minerals present, MLA automation offers several modes of use, and two different modes were used for the Ovoid samples: (1) backscattered electron image (BEI) determination of mineral grains, without any requirement of acquiring X-ray spectra ("BSE" mode); and (2) more detailed X-ray mapping subsequent to BEI and when the initial spectrum identified either chalcopyrite or pentlandite ("GXMAP" mode) (Gu, 2004). Detailed X-ray mapping is required for distinguishing chalcopyrite from pentlandite because BEI cannot.

The basic premise of mineral phase identification using MLA measurements is that gray levels in BEI are proportional to the average atomic number (Z) of a mineral (i.e., brighter areas of the image represent minerals of higher atomic number). The BSE

mode of the MLA simply allows the analyst to associate a mineral name with a gray level. For most other applications, a single X-ray spectrum is collected for each gray level which in turn represents each mineral phase, and each spectrum is then referenced to the spectrum of a standard reference material during post processing.

While this method suffices for most mineral mode determinations, for some minerals the average atomic numbers are very close to one another and a more rigorous method is required. For pentlandite, the stoichiometry is variable and some compositions have an atomic number identical to that of chalcopyrite, and therefore the BEI gray levels of the two phases are not distinguishable. Quantitatively distinguishing the two minerals by the MLA requires initial identification with a single X-ray spectrum, and their segmented areas to be X-ray mapped (GXMAP mode) in entirety.

Figure 2.7 is color-keyed particle image that illustrates the complementary use of the two MLA modes for Ovoid massive sulfides. In Figure 2.7a, pentlandite and chalcopyrite are distinguished from each other and from all phases except troilite in GXMAP mode. In Fig 2.7b, troilite is distinguished from pyrrhotite in BSE mode, which cannot be done on the basis of X-rays due to almost identical chemical compositions of the two minerals. To determine modes for all major (pyrrhotite, troilite, pentlandite, chalcopyrite, cubanite, and magnetite) and minor (sphalerite, galena) minerals in Ovoid massive sulfide samples, both methods are required.

Modal analyses were performed by MLA on grain mounts of six Ovoid samples – 4 samples with different grain sizes (180-300μm, 125-180μm, 75-125μm, 45-75μm) separated from a TYPE I ore (VB95011, 55.25-55.55 m interval); 1 sample of a TYPE II

ore (VB95011, 70.20-70.50 m interval, 125-180μm fraction), and 1 sample of a TYPE III (VB95011, 81.45-81.75 m interval, 125-180μm sized fraction). Quantitative results for the GXMAP and BSE modes of the MLA are presented in Tables 2.6 and 2.7, respectively, for all six samples. Figure 2.8 shows a comparison of mineral modes determined by the algorithm and by MLA for using an example from each ore zone.

The MLA software refers to "particles" in a grain mount as the number of individual mineralogical objects present, and "grains" as the number of discrete mineral phases making up all of the particles. In GXMAP mode, ~4000 to 6000 discrete "particles" containing ~5000 to 10,000 "grains" of specific mineral phases were examined for each of the six samples (Table 2.6). In BSE mode, ~1400 to more than 30,000 particles containing some 3000 to > 300,000 grains were measured in each sample (Table 2.7). The number of particle and grain measurements is set by the time allowed for the analysis and should generally be greater for finer grained and/or more mineralogical diverse samples to be statistically representative.

Modal mineralogy is obtained from GXMAP and BSE measurements in a series of off-line computations using the MLA software. The proportion of grains of each mineral phase in a sample is calculated in area percent as a function of its exposed surface area (in the portion of the mount measured by the MLA) relative to the total measured area of the grains of all mineral phases. Area percent is converted to volume percent assuming an enclosing ellipsoid for the grains of each mineral phase based on their measured x-y dimensions. Volume percent is converted to weight percent using an assumed density for the phase based on its average chemical composition.

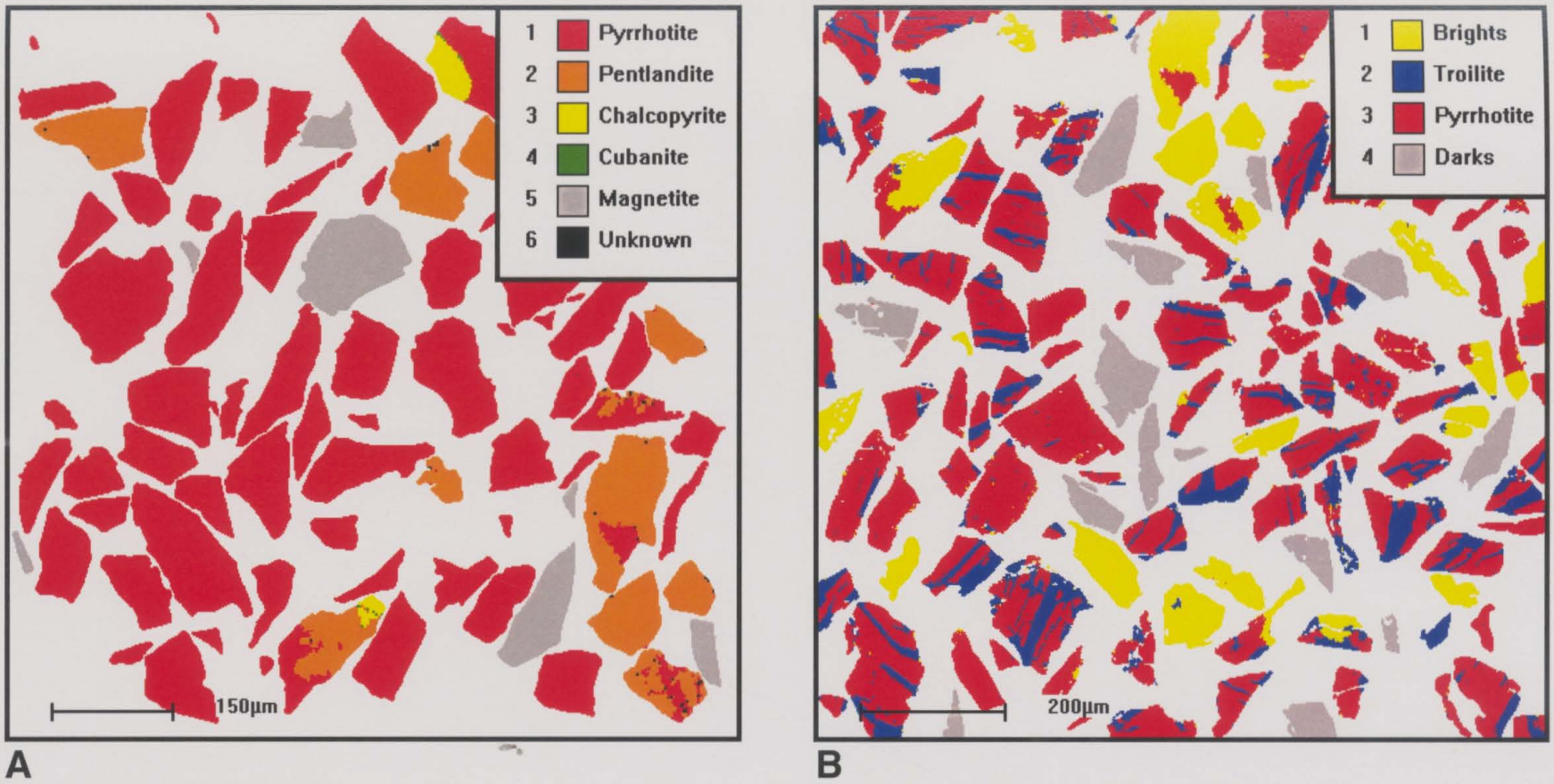

Figure 2.7. MLA-produced particle images color-keyed to mineralogy: a) X-ray mapping mode (GXMAP) to distinguish all phases (except troilite) including chalcopyrite and pentlandite, which have similar mean atomic numbers, b) backscattered electron mode (BSE) to distinguish pyrrhotite and troilite. "Brights" and "Darks" phases have average atomic numbers greater (i.e., magnetite) and less (i.e., chalcopyrite, pentlandite) than pyrrhotite-troilite, respectively.

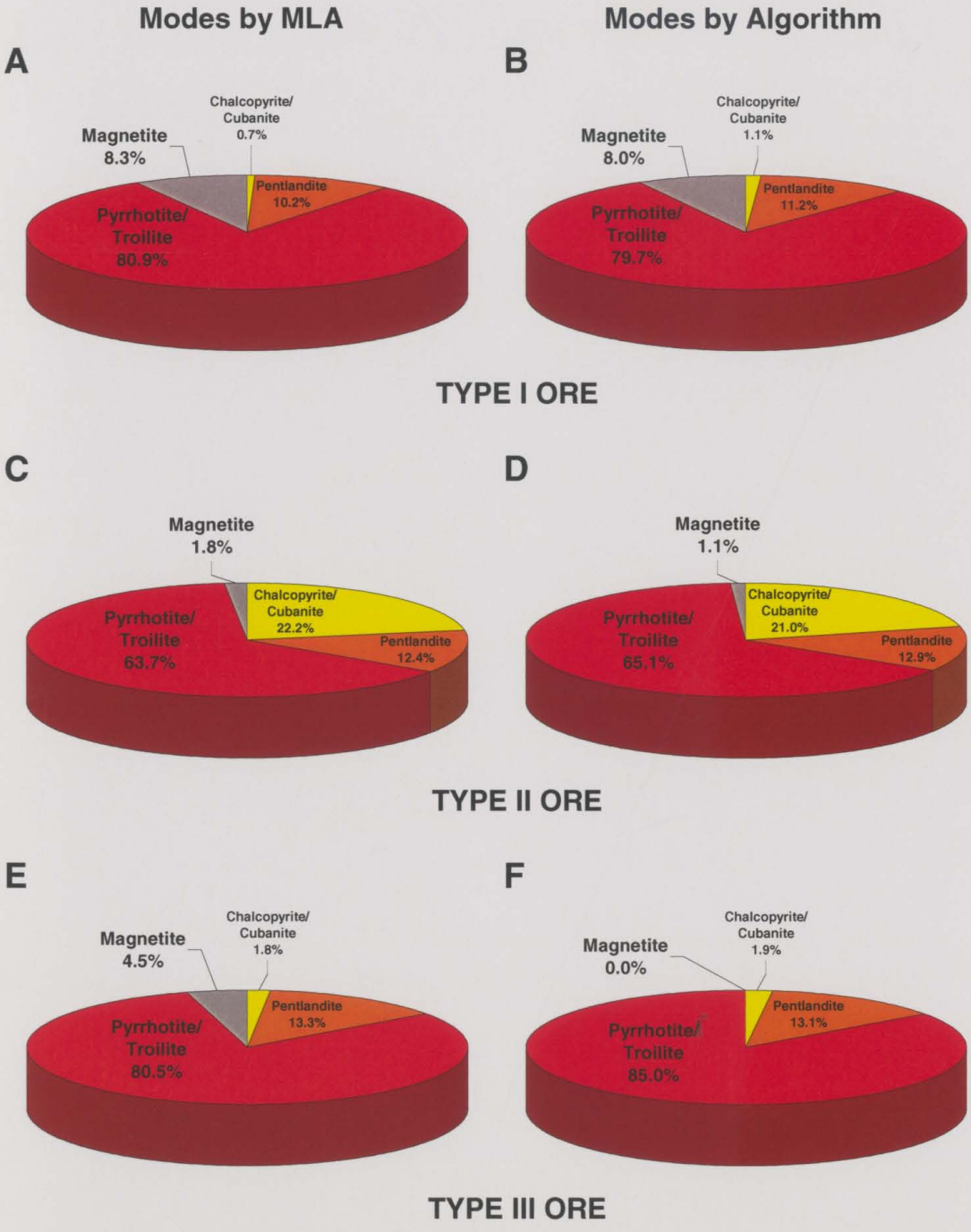

Figure 2.8. A comparison of mineral modes determined by MLA and determined by the algorithm for the three major ores types: a) and b) TYPE I ore (sample VB95011 55.25-55.55m), c) and d) TYPE II ore (sample VB95011 70.2-70.5m), e) and f) TYPE III ore (sample VB95011 81.45-81.75m). Data is from Table 2.8 and normalized to 100%.

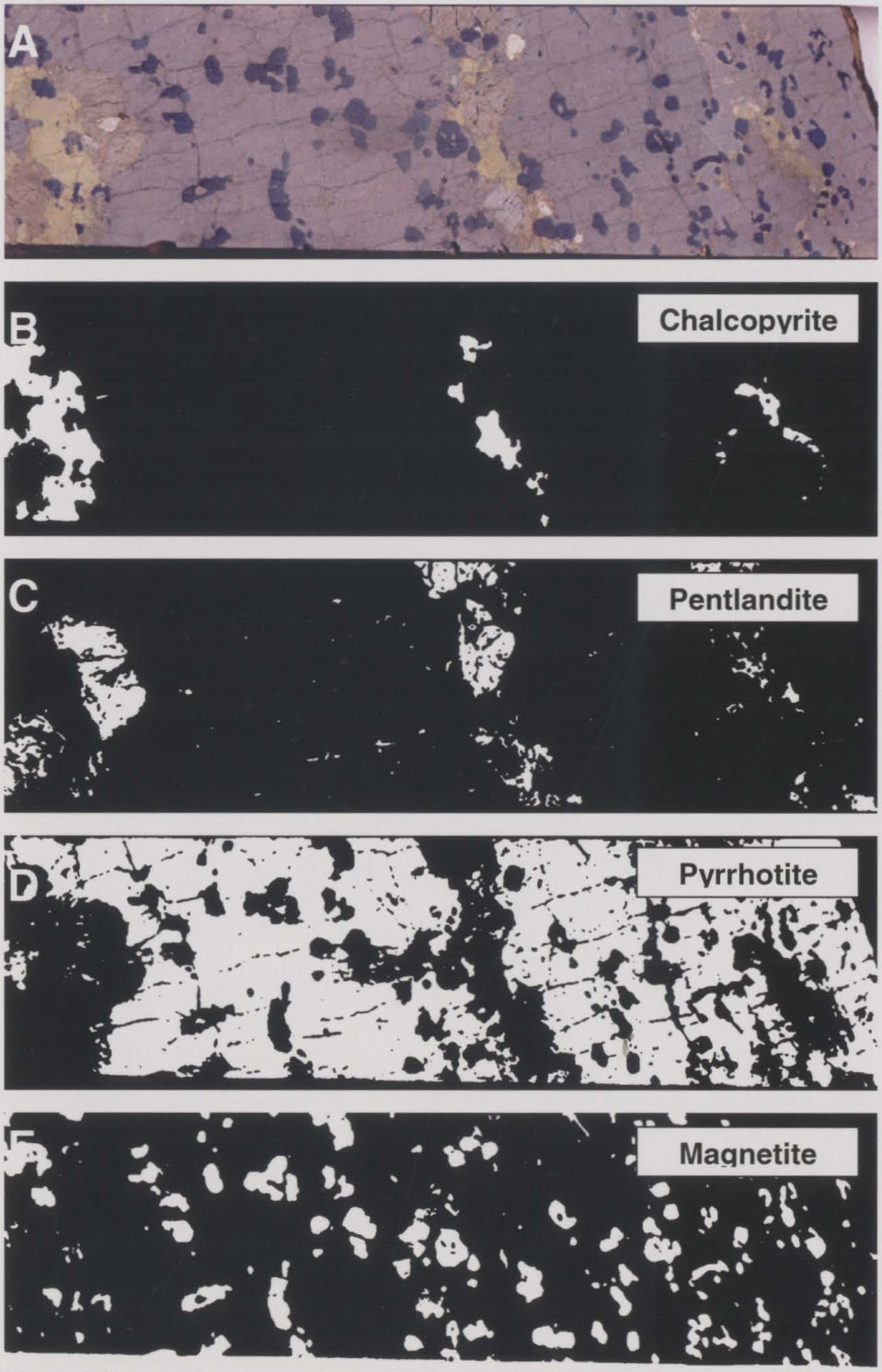

Figure 2.9. a) Original high resolution color scan of drill core, b) binary (black and white) image of chalcopyrite (white), c) binary image of pentlandite (white), d) binary image of pyrrhotite (white), e) binary image of magnetite (white). Scans are 15cm long and 4.5cm wide.

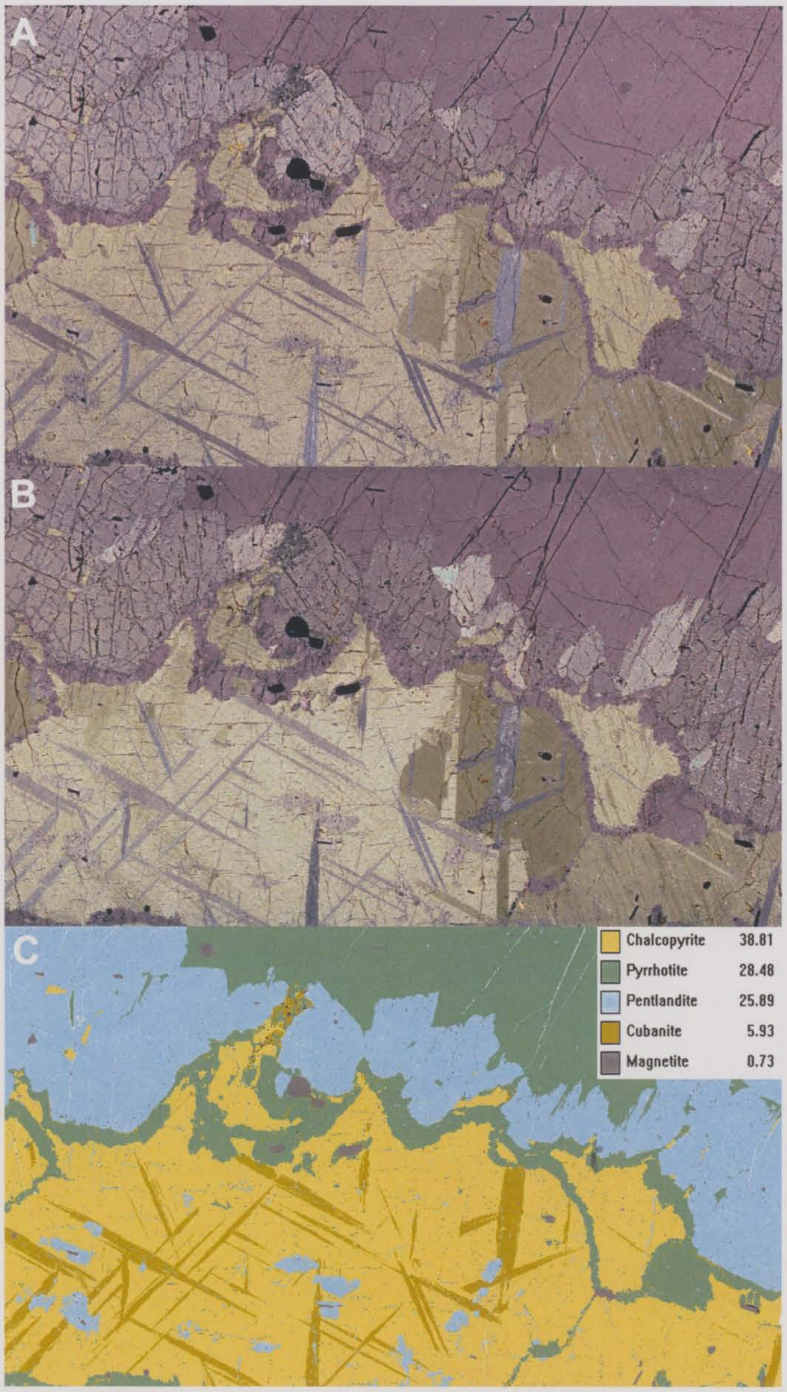

Figure 2.10. a) Digital optical image of thin section scanned in one orientation and then, b) rotated 90 degrees and scanned again (note color differences between the same minerals in different orientations, particularly for pentlandite, chalcopyrite and cubanite, as for example, where shown by arrows), c) false colored image with mineral identification determined by MLA for the same area as in a) and b). Scale of each image is 40mm in the long dimension.

Table 2.6. Mineral modes in Ovoid massive sulfide samples determined by MLA X-Ray mapping (GXMAP mode).

BHID	VB95011	VB95011	VB95011	VB95011	VB95011	VB95011
INTERVAL	55.25-55.55 m	55.25-55.55 m	55.25-55.55 m	55.25-55.55 m	70.20 - 70.50 m	81.45 - 81.75 m
FRACTION	180-300μm	125-180μm	75-125μm	45-75μm	125-180μm	125-180μm
TYPE	I	I	I	I	II	III
Pyrrhotite + Troilite						
Grain Count	4026	3525	3670	5512	3723	3962
Particle Count	3556	3395	3355	5009	3171	3786
Mineral Area (μm^2)	87735735	30676137	12929970	6240444	23248744	30183378
Mineral Area (%)	80.60	82.10	80.32	82.27	61.66	81.44
Mineral Weight (%)	79.14	80.71	78.89	81.08	62.33	80.31
TRO / PO	14.71 / 64.43	14.58 / 66.12	15.16 / 63.73	17.11 / 63.96	11.15 / 51.18	19.96 / 60.35
Pentlandite						
Grain Count	839	566	605	843	1117	899
Particle Count	529	465	448	683	748	698
Mineral Area (μm^2)	9138566	3553964	1708660	679551	4139956	4573495
Mineral Area (%)	8.40	9.51	10.61	8.96	10.98	12.34
Mineral Weight (%)	8.96	10.16	11.33	9.60	12.07	13.23
Ag-Pentlandite						
Grain Count	845	415	584	945	186	114
Particle Count	294	150	229	401	118	93
Mineral Area (μm^2)	44601	13897	9607	10610	4762	5739
Mineral Area (%)	0.0410	0.0372	0.0597	0.1399	0.0126	0.0155
Mineral Weight (%)	0.0408	0.0370	0.0594	0.1396	0.0129	0.0155
Chalcopyrite						
Grain Count	126	49	67	147	1765	190
Particle Count	85	36	51	114	1216	122
Mineral Area (μm^2)	1371919	279134	150826	90468	8858505	736422
Mineral Area (%)	1.260	0.747	0.937	1.193	23.493	1.987
Mineral Weight (%)	1.130	0.671	0.840	1.073	21.686	1.789
Cubanite						
Grain Count	383	128	187	495	2463	372
Particle Count	92	30	60	141	834	113
Mineral Area (μm^2)	76930	8235	6641	6002	813799	28805

Mineral Area (%)	0.0707	0.0220	0.0413	0.0791	2.1582	0.0777
Mineral Weight (%)	0.0634	0.0198	0.0370	0.0712	1.9922	0.0700
Magnetite						
Grain Count	646	407	433	491	901	1078
Particle Count	524	386	387	473	406	506
Mineral Area (μm^2)	10425113	2779987	1265824	527564	563274	1510901
Mineral Area (%)	9.578	7.440	7.864	6.955	1.494	4.077
Mineral Weight (%)	10.630	8.268	8.730	7.748	1.707	4.544
Ilmenite						
Grain Count	0	0	0	0	26	4
Particle Count	0	0	0	0	17	4
Mineral Area (μm^2)	0	0	0	0	49339	1262
Mineral Area (%)	0.00	0.00	0.00	0.00	0.131	0.0034
Mineral Weight (%)	0.00	0.00	0.00	0.00	0.138	0.0035
Galena						
Grain Count	3	3	2	0	0	0
Particle Count	1	3	1	0	0	0
Mineral Area (μm^2)	112	12398	15	0	0	0
Mineral Area (%)	0.0001	0.0332	0.0001	0.00	0.00	0.00
Mineral Weight (%)	0.0002	0.0532	0.0002	0.00	0.00	0.00
Sphalerite						
Grain Count	29	5	7	10	316	23
Particle Count	19	4	6	5	181	11
Mineral Area (μm^2)	2467	216	390	275	23331	1353
Mineral Area (%)	0.0023	0.0006	0.0024	0.0036	0.0619	0.0036
Mineral Weight (%)	0.0019	0.0005	0.0021	0.0031	0.0544	0.0031
Silicates						
Grain Count	395	189	304	241	19	88
Particle Count	137	93	114	160	10	44
Mineral Area (μm^2)	52522	41195	25517	30139	4853	22041
Mineral Area (%)	0.0483	0.1103	0.1585	0.3973	0.0129	0.0595
Mineral Weight (%)	0.0350	0.0801	0.1151	0.2894	0.0096	0.0433
Total						
Grain Count	7292	5287	5859	8684	10516	6730

Particle Count	4243	4040	3902	5605	4436	4448
Mineral Area (μm^2)	108847964	37365162	16097451	7585052	37706563	37063395
Mineral Area (%)	100.00	100.00	100.00	100.00	100.00	100.00
Mineral Weight (%)	100.00	100.00	100.00	100.00	100.00	100.00

"Grain Count" is the number of grains of a particular mineral phase identified by the MLA. "Particle Count" is the number of discrete particles containing the grains of a particular mineral. Particles may contain more than one mineral species thus the total number of particles in a sample is less than the sum of the particles listed for each phase. Mineral weight (%) is calculated from mineral area (%) by MLA software using assumed mineral densities. TRO/PO are the absolute abundances of troilite and pyrrhotite determined from the relative proportions of the 2 phases as measured by MLA BSE mapping (Table 2.7).

Table 2.7. Pyrrhotite and troilite modes determined by MLA backscattered electron mapping (BSE mode).

BHID	VB95011	VB95011	VB95011	VB95011	VB95011	VB95011
INTERVAL	55.25-55.55m	55.25-55.55m	55.25-55.55m	55.25-55.55m	70.20 - 70.50m	81.45 - 81.75m
FRACTION	180-300μm	125-180μm	75-125μm	45-75μm	125-180μm	125-180μm
MASU TYPE	I	I	I	I	II	III
Pyrrhotite						
Grain Count	1093	33915	46397	52674	47340	21493
Particle Count	1093	10681	20546	25488	10194	5233
Mineral Area (μm^2)	17606253	74402599	68699655	27483350	31824273	18618296
Mineral Area (%)	62.78	66.18	65.82	65.53	50.60	62.30
Mineral Weight (%)	62.44	66.10	65.90	66.10	52.34	63.24
Troilite						
Grain Count	1078	163861	160098	108842	77310	54117
Particle Count	1078	10447	20041	24072	6138	4054
Mineral Area (μm^2)	4018759	16399859	16336490	7351740	6914542	6139941
Mineral Area (%)	14.33	14.59	15.65	17.53	10.99	20.54
Mineral Weight (%)	14.25	14.57	15.67	17.68	11.37	20.85
Bright Phases						
Grain Count	1005	78544	73589	144763	171033	113921
Particle Count	1005	10499	18871	28539	10730	5531
Mineral Area (μm^2)	3162519	12324216	12207663	5941609	24134107	5121822
Mineral Area (%)	11.28	10.96	11.70	14.17	38.37	17.14
Mineral Weight (%)	10.24	10.00	10.69	13.05	36.24	15.88
Dark Phases						
Grain Count	222	1782	2764	2211	106	48
Particle Count	222	1593	2371	1550	73	38
Mineral Area (μm^2)	3257938	9296148	7134843	1166171	23759	6752
Mineral Area (%)	11.62	8.27	6.84	2.78	0.04	0.02
Mineral Weight (%)	13.06	9.34	7.74	3.17	0.04	0.03
Total						
Grain Count	3398	278102	282848	308490	295789	189579
Particle Count	1411	12849	25102	31528	10781	5560
Mineral Area (μm^2)	28045469	112422822	104378650	41942870	62896682	29886811
Mineral Area (%)	100.00	100.00	100.00	100.00	100.00	100.00

Mineral Weight (%)	100.00	100.00	100.00	100.00	100.00	100.00

"Grain Count" and "Particle Count" as defined in Table 2.6.
"Brights" and "Darks" phases have average atomic numbers greater (i.e., magnetite) and less (i.e., chalcopyrite, pentlandite) than pyrrhotite-troilite, respectively.

MLA-derived mineral modes (in wt %) are used to verify the accuracy of normative mineral calculations for the Ovoid samples in Table 2.8. The two methods compare favorably for the estimated modes of the major minerals in most cases. MLA-measured and algorithm-calculated modes differ by 15% or less for chalcopyrite (± cubanite), pentlandite, pyrrhotite (± troilite) and magnetite, except where the chalcopyrite (± cubanite) abundance (by MLA) is <1 wt%, and the magnetite abundance is < 5 wt%. Apparently, verification of algorithm results should be carried out using grain size fractions coarser than 75μm, at least in the case of the Ovoid ore.

The comparison between MLA- and algorithm-derived modal estimates for the trace abundances of galena and sphalerite in the Ovoid samples is decidedly inferior to that for the major phases, with discrepancies of 25% or more for most samples. This is not surprising, given the real possibility that the limited number measurements of trace minerals made in the MLA sample (see Table 2.6) are statistically non-representative. More measurements could be made for longer analysis times, but would not be practical for routine use of the MLA. The more important conclusion is that the abundances of the trace phases are estimated to be extremely low (typically <0.05 wt%) by both the MLA and algorithm methods. For practical use in exploration or metallurgical studies, the results in Table 2.8 suggest that an algorithm may provide useful if not precise information about the occurrence of trace minerals in an ore deposit.

A final check on the consistency of the MLA and algorithm results is shown in Table 2.9. This is a comparison of the XRF-measured assays for the samples (which is input to the algorithm) with assays calculated from the MLA-determined modal mineralogy and EMPA-measured mineral compositions (from Table 2.3). In this instance for the Ovoid, the calculated assay results from MLA are comparable (generally <16%) to the actual assay results with variance sometimes significantly greater (~20 to 60%) only for metal concentrations below 0.5 wt% (Table 2.9).

2.10.3 Digital optical image analysis: an alternative to MLA?

Image analysis by MLA requires expensive instrumentation and is time-consuming, requiring preparation of samples as polished thin sections or grain mounts, and several hours of analysis time, albeit in an automated mode. An alternative, less expensive method for directly deriving modal abundances of coarser ore samples is analysis of scanned, digital optical images of simply-prepared, polished slabs of drill core using computer software for image analysis. The distinction of minerals by digital optical image (DOI) analysis relies on the contrast in mineral colors based on their reflectance of visible light, just as in reflected light ore microscopy. We determined mineral modes for five Ovoid massive ore samples (1 TYPE I, 1 TYPE II, 3 TYPE III) by DOI analysis in order to evaluate its advantages and disadvantages compared to the MLA method.

Drill core of Ovoid ore was cut lengthwise into slabs, each 0.15 m long. The slabs were semi-polished with 1000 grit (7μm) and then scanned at high resolution (1200 pixels/inch) on a flat bed scanner (Epson P4870PH). The scan file was imported into

Adobe *Photoshop*® software and each of chalcopyrite, pyrrhotite, pentlandite, and magnetite in the image was assigned a specific identifying color. This step involves subjective judgment by the analyst, requiring knowledge of the sometimes subtle color variations of ore minerals as well as the ability to detect them visually. It is thus a significant source of error in the final modal measurements and can increase the analytical time considerably. Cubanite and troilite were included in the color defined for each of chalcopyrite and pyrrhotite, their respective hosts, because they were too fine-grained to distinguish from the host phase in many samples. Sphalerite and galena were also too small to be identified in the scans.

Once the area covered by each of the minerals was selected, separate files were created for each mineral and converted into binary black and white images, where the area of the particular mineral of interest was shown in white (8 bit grayscale value of 255) and the remainder of the image was assigned to black (value of 0). Figure 2.9 is an example of a color scan of a core slab (a) that was segmented into separate chalcopyrite (b), pentlandite (c), pyrrhotite (d) and magnetite (e) files. Once converted to black and white images, the "white" pixels were counted in each file using the image quantification software *NIH ImageJ*®, providing the total area of each mineral of interest. The same procedure was used to identify, count, and exclude areas of the scan that did not include any rock at all. The area percentage of each mineral present in the sample was calculated on the basis of its total pixel counts relative to the total pixel counts for the total rock in the scan.

Results for mineral modes determined by DOI analysis for the five Ovoid samples are reported in Table 2.10. The weight percent of each mineral was calculated from the measured area percent using assumed densities for the phases. For the calculation, area percent was assumed to be equal to volume percent due to the difficulty of establishing the volume of the grains. Comparison of the DOI-derived mineral modes in (wt%) with the normative mineral modes calculated using the algorithm indicate that the results are comparable to within 19% for pyrrhotite (+ troilite) and 26% for chalcopyrite (+ cubanite). Results for pentlandite are significantly worse, with discrepancies of 32-81% and a consistently low bias for the DOI measurements. In contrast, magnetite modes by DOI analysis are consistently higher than the calculated normative modes by 20-64%. These results are demonstrably inferior to the comparisons shown in Table 2.8 between modes determined by MLA and those calculated using the algorithm for a similar set of Ovoid samples. They illustrate that, at least in some cases, DOI on scanned cores may not be sufficiently accurate to provide verification of algorithm-calculated mineral modes for ores.

Table 2.8. Mineral modes measured by MLA compared to mineral modes calculated using the algorithm.

					Major Phases				Trace Phases		
					CCP + CB	PN	PO + TRO	MT	GN	SPH	TOTAL
BHID	INTERVAL	FRACTION	MASU TYPE	METHOD	wt %	wt %	wt %	wt %	wt %	wt %	wt%
VB95011	55.25 to 55.55m	180-300*um*	I	MLA	1.19	9.00	79.14	10.63	0.0002	0.0019	99.96
				Algorithm	1.07	10.56	75.64	11.17	0.0051	0.0042	98.46
				% Diff	11%	-15%	5%	-5%	-97%	-54%	
VB95011	55.25 to 55.55m	125-180*um*	I	MLA	0.69	10.20	80.71	8.27	0.0532	0.0005	99.92
				Algorithm	1.11	11.14	79.14	7.94	0.0064	0.0032	99.33
				% Diff	-38%	-8%	2%	4%	733%	-85%	
VB95011	55.25 to 55.55m	75-125*um*	I	MLA	0.88	11.39	78.89	8.73	0.0002	0.0021	99.88
				Algorithm	1.22	12.03	78.08	7.80	0.0065	0.0030	99.14
				% Diff	-28%	-5%	1%	12%	-98%	-32%	
VB95011	55.25 to 55.55m	45-75*um*	I	MLA	1.14	9.74	81.08	7.75	-	0.0031	99.71
				Algorithm	1.32	12.77	80.14	5.69	0.0081	0.0028	99.94
				% Diff	-13%	-24%	1%	36%	-100%	9%	
VB95011	70.20 to 70.50m	125-180*um*	II	MLA	23.68	12.08	62.33	1.85	-	0.0544	99.99
				Algorithm	21.76	13.31	67.31	1.12	0.0036	0.0367	103.54
				% Diff	9%	-9%	-7%	65%	-100%	48%	
VB95011	81.45 to 81.75m	125-180*um*	III	MLA	1.86	13.24	80.31	4.55	-	0.0031	99.96
				Algorithm	1.99	13.47	86.86	0.10	0.0042	0.0025	102.42
				% Diff	-7%	-2%	-8%	4448%	-100%	25%	

CCP = chalcopyrite; CB = cubanite; PN = pentlandite including silver pentlandite; PO = pyrrhotite; TRO = troilite; MT = magnetite including ilmenite; GN = galena; SPH = sphalerite; MASU = massive sulfide. Algorithm results from Table 2.4. MLA results from Table 2.6.

Table 2.9. Measured assays from XRF compared to calculated assays from mineral modes by MLA.

BHID	INTERVAL	FRACTION	MASU TYPE	METHOD	Fe wt%	Ni wt%	Co wt%	Cu wt%	S wt%
VB95011	55.25 to 55.55m	180-300*um*	I	XRF	58.10	3.49	0.10	0.37	32.84
				MLA	60.42	3.00	0.13	0.40	33.10
				% Diff	-4%	16%	-18%	-9%	-1%
VB95011	55.25 to 55.55m	125-180*um*	I	XRF	58.15	3.68	0.12	0.38	34.38
				MLA	59.97	3.38	0.14	0.23	33.92
				% Diff	-3%	9%	-18%	64%	1%
VB95011	55.25 to 55.55m	75-125*um*	I	XRF	57.74	3.95	0.12	0.42	34.31
				MLA	59.62	3.75	0.16	0.29	33.69
				% Diff	-3%	6%	-24%	44%	2%
VB95011	55.25 to 55.55m	45-75*um*	I	XRF	57.78	4.19	0.13	0.45	35.38
				MLA	59.84	3.22	0.13	0.39	34.06
				% Diff	-3%	30%	0%	16%	4%
VB95011	70.20 to 70.50m	125-180*um*	II	XRF	53.13	4.33	n.d.	7.43	37.78
				MLA	51.76	3.93	0.17	7.87	35.07
				% Diff	3%	10%		-6%	8%
VB95011	81.45 to 81.75m	125-180*um*	III	XRF	58.36	4.43	n.d.	0.68	38.41
				MLA	58.46	4.34	0.19	0.63	34.38
				% Diff	0%	2%		8%	12%

Measured assays by XRF in massive sulfide (MASU) ores as given in Table 2.4 (except Co determined by SN-ICP-MS on selected samples). Assays do not include measured values for oxygen, which cannot be determined by XRF. MLA-derived assays are calculated from MLA mineral modes in Table 2.6 and EPMA mineral compositions in Table 2.3.

Table 2.10. Mineral modes measured by digital optical image (DOI) analysis compared to mineral modes calculated using the algorithm.

	BHID	VB95012			VB95012			VB95012			VB95012			VB95012		
	INTERVAL	16.50 to 16.75 m			26.95 to 27.20 m			66.90 to 67.15 m			101.70 to 101.95 m			117.10 to 117.35 m		
	DOMAIN	III			II			I			III			III		
	METHOD	DOI	Algorithm	% Diff	DOI	Algorithm	% Diff	DOI	Algorithm	% Diff	DOI	Algorithm	% Diff	DOI	Algorithm	% Diff
TOTAL SCAN	pixels	40506508			49501126			40890052			47278304			35371000		
TOTAL ROCK	pixels	25234061			27331361			28158042			28208028			21755901		
NOT ROCK	pixels	15272447			22169765			12732010			19070276			13615099		
CCP + CB	pixels	1995019			2275520			2956394			1149962			360726		
	area %	7.91			8.33			10.50			4.08			1.66		
	wt %	7.13	8.81	-19%	7.54	10.17	-26%	9.49	10.23	-7%	3.69	2.99	23%	1.50	1.71	-12%
PN	pixels	1194792			744532			918949			2815697			1148128		
	area %	4.73			2.72			3.26			9.98			5.28		
	wt %	4.88	12.00	-59%	2.82	14.63	-81%	3.37	14.31	-76%	10.32	15.21	-32%	5.44	12.36	-56%
PO + TRO	pixels	18811639			21604569			20625106			22541194			18730326		
	area %	74.55			79.05			73.25			79.91			86.09		
	wt %	73.78	67.48	9%	78.58	66.21	19%	72.67	67.45	8%	79.32	75.59	5%	85.30	80.81	6%
MT	pixels	3342843			2863809			3829857			1686252			1614522		
	area %	13.25			10.48			13.60			5.98			7.42		
	wt %	14.65	11.83	24%	11.64	9.68	20%	15.08	10.38	45%	6.63	5.27	26%	8.21	5.01	64%
TOTAL	wt%	100.44	100.11		100.57	100.70		100.61	102.37		99.95	99.06		100.45	99.89	

CCP = chalcopyrite; CB = cubanite; PN = pentlandite; PO = pyrrhotite; TRO = troilite; MT = magnetite. Resolution of scanned images is 1200 pixels/inch (1 pixel = 0.0212 mm). Total pixels = sum of pixels in scanned image counted on rock + not on rock. Area % mineral = mineral pixel counts/total rock pixel counts. Wt % mineral recalculated from area % mineral (assuming equivalence to volume % mineral) using assumed densities for CCP (4.g/cc; CB = 4.7g/cc, is assumed to be minor and ignored); PN (4.8g/cc); PO + TRO (4.61g/cc); and MT (5.15g/cc). Deviation of DOI mineral totals from 100% represent errors associated with phases that are unidentified (uncounted) and ambiguous (mistakenly counted twice).

What are some of the reasons that DOI analysis gives such poor results in this example? Part of the discrepancy may be that the small area (~70cm^2) of the polished core slabs is simply not representative of the larger sample volume (~800cm^3) used for the assay that is input into the algorithm. Homogenized (riffled) grain mounts (as used for the MLA-derived modes) provide a more representative sample for image analysis but are more time-consuming to prepare than core slabs, eliminating one of the potential advantages of the DOI method. Nonetheless, it is doubtful that non-representative sampling alone is the reason for the consistently low estimates for pentlandite and high estimates for magnetite by DOI analysis relative to the abundances calculated by the algorithm.

One of the main limitations of DOI analysis is that some minerals are pleochroic (e.g., pyrrhotite, chalcopyrite, cubanite; Spry and Gedlinske, 1987 and references therein), and others may have distinct cleavage (e.g., pentlandite). Pleochroism and cleavage effects can produce distinct color variations between different grains of the same mineral in a scanned image, possibly resulting in phase misidentifications.

Figure 2.10 is an example of Ovoid massive ore scanned in one orientation (a), and then again after rotating the sample 90 degrees (b). Compare the two true-color scans (A, B) with the same area analyzed by MLA and shown in false color (c). The mineral identities are given in the MLA-derived image (c). Note the differences in shades of color for chalcopyrite and cubanite in (a) and (b). These minerals are anisotropic reflecting light differently relative to grain orientation. Pentlandite also changes shades with rotation even though it is isotropic because of reflection from fine defects at the surface

that are controlled by the preferred {111} cleavage. The effect is more severe if the sample is finely polished rather than prepared to a fine grind (e.g., 1200 grit) as it was in Figure 2.10. The cause is similar to dark field illumination which tends to enhance topography (e.g., cracks or grain boundaries). In the case of the results in Table 2.10, it is evident that some of the shades of pentlandite were mistakenly identified as other phases, producing underestimates for pentlandite abundances. The most likely explanation is that some of the darker shades of pentlandite were misidentified as magnetite, resulting in overestimates for magnetite abundances. The results imply that caution should be used in applying DOI analysis for verification of algorithm-derived modal abundances.

2.11 EXTENDING THE METHODOLOGY TO OTHER ORE DEPOSITS

The approach of ore characterization developed here for massive nickel-copper sulfide ores may, in principle, can be adapted for any other type of massive ore where the mineralogy is well characterized, recognizing that there may be practical limitations associated with normative mineral calculations that must be judged on a case-by-case basis. MLA "groundtruthing", on the other hand, should be applicable to all ore deposits and can even be used to define the detailed mineralogy of a deposit in preparation for algorithm development.

It will be easiest to develop an algorithm for an ore body where the mineral assemblage consists of phases consisting of at least one major element unique to each mineral. This is the nearly case in the Ovoid (excluding cubanite and troilite) and will be

true for many magmatic Ni sulfide ore bodies elsewhere. It will also be the case for many volcanogenic massive sulfide (VMS) ores, which consist principally of pyrite with chalcopyrite, sphalerite, galena and some magnetite. In fact, an algorithm similar to the one developed in this paper could be easily adapted for use with the foregoing VMS mineral assemblage: first the abundance of chalcopyrite would be determined by assuming it contained all of the Cu present in the whole rock; next sphalerite and galena would be calculated assuming they contained all of the Zn and Pb present, respectively; then pyrite would be calculated from the amount of S in the whole rock not taken up by chalcopyrite, sphalerite and galena; and finally magnetite would be calculated from the amount of Fe in the whole rock not taken up by pyrite, chalcopyrite and sphalerite.

Completely new algorithms could also be developed. For instance, in massive ore bodies of porphyry tungsten-molybdenum-tin deposits, the principal ore minerals commonly consist of scheelite ($CaWO_4$), wolframite [$(Fe,Mn)WO_4$], molybdenite (MoS_2), cassiterite (SnO_2), stannite (Cu_2FeSnS_4) and bismuthinite (Bi_2S_3) associated with pyrite (FeS_2), and arsenopyrite (FeAsS). An algorithm for this assemblage could involve the calculation of abundances of minerals in the following order: (1) wolframite, assuming it contains all of the Mn in the whole rock; (2) scheelite, assuming it contains all of the remaining W in the whole rock not taken up by wolframite; (3) molybdenite and stannite, assuming they contain all of the Mo and Cu, respectively, in the whole rock; (4) cassiterite, assuming it contains all of the remaining Sn in the whole rock not taken up by stannite; (5) bismuthinite and arsenopyrite, assuming they contain all of the Bi and As,

respectively, in the whole rock; and (6) pyrite, assuming it contains all of the remaining S in the whole rock not taken up by molybdenite, stannite, bismuthinite and arsenopyrite.

The development of algorithms for disseminated mineralization is more problematic than for massive ores because gangue minerals may contain some portion of one or more ore metals, and for some deposits it will be difficult to calculate the abundance of the gangue phases. In the case of disseminated mineralization associated with the Ovoid, a fraction of the Ni in the whole rock is carried by olivine and thus the amount of olivine present must be known before the pentlandite abundance is calculated from the Ni assay. Many of the silicate host rocks to the Ovoid are troctolites consisting only of olivine and plagioclase, but others are gabbros containing pyroxene as well as olivine and plagioclase (Li *et al.*, 2000). For troctolite-hosted disseminated mineralization, olivine abundances may be estimated from the Mg contents of the rocks, but this will be more difficult for gabbro-hosted mineralization where Mg is distributed between the pyroxene and olivine.

Just as for massive ores, the specific mineralogy of particular disseminated mineralization should be carefully evaluated to determine if their normative mineral abundances can be calculated using an algorithm.

2.12 SYNOPSIS

One of the most important characteristics of ore deposits is the spatial variation in mineral abundance and texture (grain size, phase alignment, exsolution relationships,

etc). If these characteristics can be determined systematically and quantitatively throughout the ore body, they can be used in a predictive manner to aid in the advanced exploration of a deposit (vectoring toward additional resources), mining (ore blending for the mill), metallurgy (improving mineral liberation and metal recoveries), and ore genesis studies (defining sulfide magma source and differentiation processes).

The most efficient method for determining mineral modes throughout a sulfide ore body is to calculate them from large numbers of spatially-controlled whole rock chemical assays using an algorithm. Representative identities and compositions of the mineral phases in a particular assemblage should be determined beforehand. With the proper assessment and reasonable assumptions, the method is quantitative and is easily applied where large geochemical databases are available, and detailed mineralogical evaluations for thousands of samples may be impractical. The advantage of working with such large databases is that the calculated mineral abundances can be linked to spatial co-ordinates and plotted in three dimensional block models similar to ore grades. More detailed textural information can then be integrated with specific mineral zones defined in the block model. Calculated normative mineral abundances should be verified on a subset of representative or random samples to ensure integrity of the results. Data presented in this paper suggest that automated image analysis on grain mounts using a MLA instrument is an eminently suitable method for algorithm verification.

We have applied this systematic and integrated approach of ore characterization to massive Ni-Cu-Co sulfide ores of the Ovoid deposit at Voisey's Bay, Labrador. The results demonstrate that the Ovoid is quantitatively zoned into three main mineral

domains (Fig. 2.5): (1) an inner zone rich in coarse-grained magnetite and poor in pyrrhotite with moderate amounts of chalcopyrite and pentlandite in addition to elevated palladium and platinum concentrations relative to the remainder of the Ovoid (with the exception of a Pt depletion in the very central portion of the Ovoid); surrounded by (2) a pentlandite- and chalcopyrite-rich transitional zone containing moderate abundances of pyrrhotite and magnetite (mainly fine-grained) in addition to moderate concentrations palladium and platinum concentrations relative to the remainder of the Ovoid; and underlain by (3) a basal zone rich in massive pyrrhotite with low chalcopyrite, moderate pentlandite, and low to moderate magnetite abundances in addition to moderate palladium and platinum concentrations relative to the reminder of the Ovoid. Sphalerite and galena are present as trace phases (commonly <0.05 wt%) in all zones. Zinc has the highest concentrations in TYPE II transitional zone and a very central peak in TYPE I ore, which correlate to chalcopyrite-rich zones; this correlation represents sphalerite exsolution "stars" in chalcopyrite. Concentrations of lead increase gradually toward the center of the Ovoid with a sharp depletion in the very center. The depletion of both Pb and Pt in the central zone of the Ovoid is thought to be due to escape of enriched and evolved sulfide liquid to the surrounding rocks. Cubanite and troilite abundances could not be calculated using the algorithm but image analysis suggests that they form up to ~2 and 20 wt%, respectively, of the massive ore. The boundaries between different ore zones are not sharp lithological contacts but consist of sharp transitions in the abundance of minerals (Fig. 2.5). Definition of ore zones in the Ovoid provides fundamental baseline

information for ore genesis and metallurgical studies. The same methodology applied to the Ovoid could easily be adapted for a wide variety of massive ores elsewhere.

2.13 ACKNOWLEDGEMENTS

This study was generously supported by grants from Inco Limited, the Atlantic Innovation Fund, and the Natural Sciences and Engineering Research Council of Canada (NSERC) to PJS, and by a NSERC postgraduate scholarship, a Northern Scientific Research Program (NSTP) scholarship, and a Society of Economic Geologist Student (SEG) Research Grant to MAEH. This project would not have been possible without the support of L. Cochrane (Inco Limited), D. Lee (Voisey's Bay Nickel Company Limited), B. Bengert (Voisey's Bay Nickel Company Limited), J. Letto (Voisey's Bay Nickel Company Limited), and K. Pittman (Voisey's Bay Nickel Company Limited).

2.14 REFERENCES

Castroviejo, R., Berrezueta, E., and Lastra, R., 2002, Microscopic digital image analysis of gold ores: a critical test of methodology, comparing reflected light and electron microscopy: Minerals & Metallurgical Processing, May 2002, v. 19, p. 102-109.

Diegor, W., Longerich, H.P., Abrajano, T., and Horn, I., 2001, Applicability of a high pressure digestion technique to the analysis of sediment and soil samples by inductively coupled plasma-mass spectrometry: Analytical Chimica Acta, v. 431, p. 195-207.

Emerson, D.O., 1958, A stage for macro point counting: American Mineralogist, v. 43, p. 1000-1003.

Emslie, R.F., Hamilton, M.A., and Theriault, R.J, 1994, Petrogenesis of a Mid-Proterozoic Anorthosite-Mangerite-Charnockite-Granite (AMCG) complex: isotopic and chemical evidence from the Nain Plutonic Suite: Geology, v. 102, p. 539-558.

Evans-Lamswood, D.M., Butt, D.P., Jackson, R.S., Lee, D.V., Muggridge, M.G., Wheeler R.I., and Wilton, D.H.C., 2000, Physical controls associated with the distribution of sulfides in the Voisey's Bay Ni-Cu-Co Deposit, Labrador: Economic Geology, v. 95, p. 749-770.

Godel, B., Barnes, S-J, and Maier, W., 2006, 3-D Distribution of sulfide minerals in the Merensky Reef (Bushveld Complex, South Africa) and the J-M Reef (Stillwater Complex, USA) and their relationship to microstructures using X-ray computed tomography: Journal of Petrology, Advanced Access Published, May 22, 2006, 20p.

Gottlieb, P., Wilkie, G.K., and Adair, B.J.I., 1993, Recent developments in the applications of QEM*SEM technology, *in* Griffin, B., Graham, J., and Linge, H.G., eds., Applied Mineralogy: Proceedings of the 4th International Congress on Applied Mineralogy, Freemantle Webley, WA, CSIRO, p. 222-224.

Gu, Y., 2003, Automated scanning electron microscope based mineral liberation analysis: Journal of Minerals and Materials Characterization and Engineering, v. 2, p. 33-41.

Gu, Y., 2004, Rapid mineral liberation analysis with X-ray and BSE image processing, *in* Pecchio *et al.*, eds., Applied Mineralogy: Proceedings of the 8th International Congress on Applied Mineralogy, Sao Paulo , p. 119-122.

Huminicki, M.A.E., Sylvester, P.J., Cabri, L.J., Lesher, C.M., and Tubrett, M., 2005, Quantitative mass balance of platinum group elements in the Kelly Lake Ni-Cu-PGE deposit, Copper Cliff Offset, Sudbury: Economic Geology, v. 100, p. 1631-1646.

Huminicki, M.A.E., and Sylvester, P.J., submitted, Genesis and crystallization history of the Voisey's Bay Ni-Cu-Co sulfide deposit: Implications from ore characterization. Journal of Petrology.

Hutchison, C.S., 1974, Laboratory handbook of petrographic techniques: NewYork, Wiley., 527p.

Johannsen, A., 1931, A descriptive petrography of igneous rocks, Vol 1. Introduction, textures, classification and glossary. Chicago, University of Chicago Press, 267p.

Kerr, A., 2003, Guidelines for the calculation and use of sulfide metal contents in research and mineral exploration: Newfoundland Department of Mines and Energy, Geological Survey, Report 03-1, p. 223-229.

Lastra, R., Petruk, W., and Wilson, J., 1998, Image analysis techniques and applications to mineral processing, in Modern Approaches to Ore and Environmental Mineralogy, eds. L.J. Cabri and D.J. Vaughan: Mineralogical Association of Cananda Short Course v. 27, p. 327-366.

Li, C., Lightfoot, P.C., Amelin, Y., and Naldrett, A.J., 2000, Contrasting Petrological and Geochemical Relationships in the Voisey's Bay and Mushuau Intrusions, Labrador, Canada: Implications for Ore Genesis: Economic Geology, v. 95, p. 771-799.

Lightfoot, P.C., 1998, Geological and geochemical relationships in the Reid Brook Intrusive Complex, Labrador: Exploration strategies for magmatic Ni-Cu-Co ores at Voisey's Bay. Inco, ITSL, Copper Cliff Exploration Office, Sudbury, Ontario, Pathways '98.

Longerich, H.P., 1995, Analysis of pressed pellets of geological samples using wavelength-dispersive X-ray fluorescence spectrometry: X-ray Spectrometry, v. 24, p. 123-136.

Naldrett, A.J., Singh, J., Krstic, S., and Li, C., 2000a, The mineralogy of the Voisey's Bay Ni-Cu-Co Deposit, Northern Labrador, Canada: influence of oxidation state on textures and mineral compositions: Economic Geology, v. 95, p. 889-900.

Naldrett, A.J., Asif, M., Krstic, S., and Li, C., 2000b, The Composition of mineralization at the Voisey's Bay Ni-Cu Sulfide Deposit, with special reference to platinum-group elements: Economic Geology, v. 95, p. 845-866.

Philpotts, A.R., 1990, Principles of igneous and metamorphic petrology: Englewood Cliffs, NJ, Prentice Hall, 497p.

Pirard, E., 2004, Multispectral imaging of ore minerals in optical microscopy: Mineralogical Magazine, v. 68, p. 323–333.

Ryan, B., 2000, The Nain-Churchill Boundary and the Nain Plutonic Suite: a regional perspective on the geologic setting of the Voisey's Bay Ni-Cu-Co Deposit: Economic Geology, v. 95, p. 703-724.

Schryver, K., 1968, Precision and components of variance in the modal analysis of coarse-grained augen gneiss: American Mineralogist, v. 53, p. 2036-2046.

Shaffer, M., Gu, Y., and Rhode, M., 2007, Practical applications for the silicon drift type X-ray detector in SEM-platformed image analysis: the Bruker-MLA in practice: 2007 SME Annual Meeting & Exhibit and 109th National Western Mining Conference, Denver, Colorado, Technical Proceedings, Paper 07-029, 6p.

Smithson, S.B., 1963, A point-counter for modal analysis of stained rock slabs: American Mineralogist, v. 48, p. 1164-1166.

Spry, P.G., and Gedlinske, B.L., 1987, Tables for determinations of common opaque minerals: Economic Geology Publishing Company, 52p.

van Achterbergh, E., Ryan, C., Jackson, S.E., and Griffin, W., 2001, Appendix III: Data reduction and software for LA-ICP-MS. *in* Sylvester, P., ed., Laser-Ablation-ICPMS in the earth sciences: principles and applications: Mineralogical Association of Canada Short Course Series, v. 29, p. 239-243.

Wilson, S.A., Ridley, W.I., and Koenig, A.E., 2002, Development of sulfide calibration standards for the laser ablation inductively-coupled plasma mass spectrometry technique: Journal of Analytical Atomic Spectrometry, v. 17, p. 406-409.

APPENDIX 2.I - EQUATIONS FOR CALCULATION OF NORMATIVE MODAL MINERALOGY

A2.1.1 Initial normative calculations

The mass fraction of chalcopyrite (X_{Ccp}) is calculated based on the concentration of Cu in the whole rock sample (Cu_{sample}), using the average concentration of Cu in chalcopyrite ($Cu_{Ccp\ (ave)}$),

$$X_{Ccp} = Cu_{sample} / Cu_{Ccp\ (ave)} \qquad (1a)$$

No other phase in the Ovoid ore contains Cu except cubanite, which cannot be calculated because its concentrations of Cu, Fe and S are similar to those in chalcopyrite (Table 2.3). Thus, the total mode of chalcopyrite + cubanite must be assumed to be equal the calculated abundance of chalcopyrite alone. In principle, where the abundance of cubanite approaches that of chalcopyrite, this assumption could produce significant errors in the calculated chalcopyrite mode because cubanite and chalcopyrite have significantly different Cu concentrations (24 and 34 wt% respectively). These potential errors would propagate to the calculated modes of all other phases, because the S, Fe and Ni attributed to the calculated chalcopyrite mode affects the calculated modes of the other phases, as shown below. In the case of the Ovoid, however, the MLA results (Table 2.6) demonstrate that cubanite comprises only 3-8% of the total chalcopyrite + cubanite mode, so the potential errors are minimal.

Once the chalcopyrite mode is determined, the abundances of S, Fe, Zn and Pb attributed to chalcopyrite are calculated by,

$$S_{Ccp} = X_{Ccp} \times S_{Ccp\ (ave)} \quad (1b)$$

$$Fe_{Ccp} = X_{Ccp} \times Fe_{Ccp\ (ave)} \quad (1c)$$

$$Zn_{Ccp} = X_{Ccp} \times Zn_{Ccp\ (median)} \quad (1d)$$

$$Pb_{Ccp} = X_{Ccp} \times Pb_{Ccp\ (median)} \quad (1e)$$

For chalcopyrite (and all of the other major sulfides in the Ovoid), the median rather than the average concentrations of Zn and Pb are used for the calculations ($Zn_{Ccp\ (median)}$, $Pb_{Ccp\ (median)}$), because the concentrations of these trace metals are highly variable in the Ovoid sulfides (Table 2.3).

Next, the mass fraction of pentlandite (X_{Pn}) is calculated based on the concentration of Ni in the whole rock sample (Ni_{sample}) using the average concentration of Ni in pentlandite ($Ni_{Pn\ (ave)}$),

$$X_{Pn} = Ni_{samp} / Ni_{Pn\ (ave)} \quad (2a)$$

The abundances of S and Fe attributed to pentlandite are then calculated by,

$$S_{Pn} = X_{Pn} \times S_{Pn\ (ave)} \quad (2b)$$

$$Fe_{Pn} = X_{Pn} \times Fe_{Pn\ (ave)} \quad (2c)$$

where $S_{Pn\ (ave)}$ and $Fe_{Pn\ (ave)}$ are the average concentrations of S and Fe in pentlandite.

The mass fraction of pyrrhotite (X_{Po}) is calculated based on the concentration of S in the whole rock sample (S_{sample}) minus the concentration of S attributed to chalcopyrite (S_{Ccp}) and pentlandite (S_{Pn}), using the average concentration of S in pyrrhotite ($S_{Po\ (ave)}$),

$$X_{Po} = (S_{sample} - S_{Ccp} - S_{Pn}) / S_{Po\ (ave)} \quad (3a)$$

The abundance of Fe attributed to pyrrhotite is calculated by,

$$Fe_{Po} = X_{Po} \times Fe_{Po\ (ave)} \quad (3b)$$

where $Fe_{Po\ (ave)}$ is the average concentration of Fe in pyrrhotite.

Troilite cannot be distinguished from pyrrhotite using the algorithm, and the total pyrrhotite + troilite mode must be assumed to be equal to pyrrhotite alone. This assumption has only a trivial affect on the calculated mode for pyrrhotite and the other phases because the Fe concentrations of troilite and pyrrhotite are so similar (63 and 61 wt% respectively).

The mass fraction of magnetite (X_{Mt}) is calculated based on the concentration of Fe in the whole rock sample (Fe_{sample}) minus the concentration of Fe attributed to chalcopyrite (Fe_{Ccp}), pentlandite (Fe_{Pn}) and pyrrhotite (Fe_{Po}), using the average concentration of Fe in magnetite ($Fe_{Mt\ (ave)}$),

$$X_{Mt} = (Fe_{sample} - Fe_{Ccp} - Fe_{Pn} - Fe_{Po}) / Fe_{Mt\ (ave)} \qquad (4)$$

A2.1.2 Refinements to normative calculations

The foregoing calculations establish the normative abundances of the major phases based only on their main constituents. Further refinements are required to account for minor and trace elements in the major phases, as well as to calculate the modes of minor phases present.

In the Ovoid deposit, Ni occurs as a trace element in hexagonal pyrrhotite with an average concentration of 0.22 ± 0.09 wt% (n = 434) (Table 2.3). Since pyrrhotite is the most abundant sulfide phase, it may contribute significant amounts of Ni to the total in the sample. If Ni in pyrrhotite is not accounted for, then all of the Ni would be assumed

to occur in pentlandite, and the pentlandite mode would be overestimated by the calculations. The abundance of Ni attributed to pyrrhotite is calculated by,

$$Ni_{Po} = X_{Po} \times Ni_{Po\ (ave)} \quad (5)$$

where $Ni_{Po\ (ave)}$ is the average concentration of Ni in pyrrhotite. The revised mass fraction of pentlandite ($*X_{Pn}$) is thus equal to,

$$*X_{Pn} = (Ni_{sample} - Ni_{Po}) / Ni_{Pn\ (ave)} \quad (6a)$$

The abundances of S, Fe, Zn and Pb attributed to pentlandite are then given by,

$$*S_{Pn} = *X_{Pn} \times S_{Pn\ (ave)} \quad (6b)$$

$$*Fe_{Pn} = *X_{Pn} \times Fe_{Pn\ (ave)} \quad (6c)$$

$$*Zn_{Pn} = *X_{Pn} \times Zn_{Pn\ (median)} \quad (6d)$$

$$*Pb_{Pn} = *X_{Pn} \times Pb_{Pn\ (median)} \quad (6e)$$

The revised mass fraction of pyrrhotite ($*X_{Po}$) is,

$$*X_{Po} = (S_{sample} - S_{Ccp} - *S_{Pn}) / S_{Po\ (ave)} \quad (7a)$$

and the abundances of S, Fe, Zn and Pb attributed to pyrrhotite are,

$$*S_{Po} = *X_{Po} \times S_{Po\ (ave)} \quad (7b)$$

$$*Fe_{Po} = *X_{Po} \times Fe_{Po\ (ave)} \quad (7c)$$

$$*Zn_{Po} = *X_{Po} \times Zn_{Po\ (median)} \quad (7d)$$

$$*Pb_{Po} = *X_{Po} \times Pb_{Po\ (median)} \quad (7e)$$

Calculation of modes for trace phases, sphalerite and galena, in the Ovoid is based on the whole rock concentrations of Zn and Pb in the massive ores, respectively. The mass fraction of sphalerite is given by,

$$X_{Sphal} = (Zn_{sample} - Zn_{Ccp} - *Zn_{Pn} - *Zn_{Po}) / Zn_{Sphal\ (stoich)} \quad (8a)$$

where $Zn_{Sphal\ (stoich)}$ is the stoichiometric concentration of Zn in sphalerite. The abundances of S and Fe attributed to sphalerite are,

$$S_{Sphal} = X_{Sphal} \times S_{Sphal\ (stoich)} \quad (8b)$$

$$Fe_{Sphal} = X_{Sphal} \times Fe_{Sphal\ (stoich)} \quad (8c)$$

where $S_{Sphal\ (stoich)}$ and $Fe_{Sphal\ (stoich)}$ are the stoichiometric concentrations of S and Fe in sphalerite, respectively. Similarly, the mass fraction of galena is,

$$X_{Gal} = (Pb_{sample} - Pb_{Ccp} - {}^{*}Pb_{Pn} - {}^{*}Pb_{Po}) / Pb_{Gal\ (stoich)} \quad (9a)$$

and the abundance of S attributed to galena is,

$$S_{Gal} = X_{Gal} \times S_{Gal\ (stoich)} \quad (9b)$$

where $Pb_{Gal\ (stoich)}$ and $S_{Gal\ (stoich)}$ are the stoichiometric concentrations of Pb and S in galena, respectively.

The final mass fraction of pyrrhotite is then,

$$**X_{Po} = (S_{sample} - S_{Ccp} - {}^{*}S_{Pn} - S_{Sphal} - S_{Gal}) / S_{Po\ (ave)} \quad (10a)$$

and the revised abundance of Fe attributed to pyrrhotite is,

$$**Fe_{Po} = **X_{Po} \times Fe_{Po\ (ave)} \quad (10b)$$

The final mass fraction of magnetite is given by,

$$*X_{Mt} = (Fe_{sample} - Fe_{Ccp} - {}^{*}Fe_{Pn} - Fe_{Sphal} - {}^{**}Fe_{Po}) / Fe_{Mt\ (ave)} \quad (11)$$

A2.1.3 Modal percentages

Calculated mass fractions of each of the minerals are converted to modal percentages using the relationships,

$$\% \text{ Chalcopyrite} = X_{Ccp} / 100 \quad (12)$$

$$\% \text{ Pentlandite} = *X_{Pn} / 100 \quad (13)$$

$$\% \text{ Sphalerite} = X_{Sphal} / 100 \quad (14)$$

$$\% \text{ Galena} = X_{Gal} / 100 \quad (15)$$

$$\% \text{ Pyrrhotite} = **X_{Po} / 100 \quad (16)$$

$$\% \text{ Magnetite} = *X_{Mt} / 100 \quad (17)$$

A2.1.4 Calculation of oxygen in bulk sample

The amount of oxygen attributable to magnetite in the bulk sample is calculated using the relationship,

$$wt\% \text{ O} = *X_{Mt} \times O_{Mt\,(ave)} \quad (18)$$

where $O_{Mt\,(ave)}$ is the average concentration of oxygen in magnetite given in Table 2.3.

CHAPTER 3: ORE GENESIS OF THE VOISEY'S BAY NI-CU-CO SULFIDE DEPOSIT: IMPLICATIONS FROM ORE CHARACTERIZATION

M. A. E. HUMINICKI and P. J. SYLVESTER

Inco Innovation Centre and Department of Earth Sciences, Memorial University of Newfoundland, St. John's, Newfoundland, Canada A1B 3X5, e-mail: g26mah@mun.ca

3.1 INTRODUCTION

The Voisey's Bay nickel-copper-cobalt (Ni-Cu-Co) deposit consists of magmatic sulfide ores (Naldrett *et al.* 2000a; 2000b; this thesis). It is located in northeastern Labrador and is currently the property of Companhia Vale do Rio Doce (CVRD). The deposit consists of several mineralized zones including the Ovoid, Mini Ovoid, Southeast Extension, Eastern Deeps, Discovery Hill, and Reid Brook Zones (Fig. 3.1). There are 32 million tonnes of proven and probable reserves consisting of 2.8% nickel, 1.6% copper, and 0.14% cobalt in the Ovoid with an additional 40 million tonnes of indicated mineral resource consisting of 1.9% nickel, 1.9% copper, and 0.12% cobalt (http://www.vbnc.com/ReservesAndResources.asp) in the associated ore zones. This paper addresses some aspects of the ore genesis of the Voisey's Bay deposit.

In evaluating the ore genesis of magmatic Ni-Cu-Co sulfide deposits some of the fundamental questions that arise are what are the metal tenors and metal distributions of the ores and what types of processes are required to produce the observed metal distributions? Simply put, what is required to produce economically viable ore deposits?

One of the main factors (and main debates) for forming a metal-rich sulfide deposit is the composition of the silicate magma that precipitated the sulfide melts. The issue is whether a magma of a particular composition can alone contribute enough metal to form an economic sulfide deposit or whether a subsequent "upgrading" mechanism is required to contribute metals to the sulfides. Another issue is the composition of the magma required to form an economic deposit. Before the discovery of Voisey's Bay,

some believed that in order to produce magmatic nickel sulfide deposits with high metal tenors, a silicate parent magma that contained high nickel concentrations such as a picrite or a komatiite, was required (Keays, 1995).

In the absence of an observed picritic or komatiitic magma at Voisey's Bay, it has been proposed that the ores formed from basaltic magmas with moderate nickel levels and an upgrading mechanism is required to explain the metal tenors (Li *et al.*, 2001 and references therein). More specifically, Li and Naldrett (1999) and Li *et al.* (2000) explained geochemical data then available for the Voisey's Bay ore deposit as the result of precipitation of sulfide melt from a low-Mg mafic (basaltic to troctolitic) magma, followed by upgrading of Ni-Cu tenors, particularly in disseminated mineralization, by reaction with new influxes of mafic magma that had not previously achieved sulfur saturation and thus was chalcophile metal enriched. With the more extensive Voisey's Bay Nickel Company Limited's Mine Exploration Borehole System (MEBS) database now available for the deposit (Table 3.1), it is useful to re-examine ore genesis at Voisey's Bay.

In light of the fact that sulfide deposits such as Voisey's Bay have been discovered and are associated with more evolved rocks (troctolites and gabbros) rather than picrites or komatiites, all possible parent magma compositions are modeled in this paper to constrain possible silicate magma sources of the sulfides in the Voisey's Bay intrusion. In particular, the purpose was to revisit the issue of whether genesis of the Voisey's Bay ores required picritic (high-Mg) rather than low-Mg basaltic compositions. The observed silicate rocks present in the ore system were also evaluated to determine

whether they may represent parental magmas or derivative magmas (that formed after sulfide precipitation). Another related issue that was evaluated is whether the massive and disseminated mineralization (including those in ultramafic rocks) formed from a common silicate magma or from multiple magmas with different compositions.

Specific methods that relate the amount of magma (whether it be a magma chamber or a volume of magma passing through a conduit) required to upgrade a sulfide liquid have been developed by previous workers and are referred to as R, N, and L factor modeling. Each of these upgrading processes was evaluated for the various deposits in the Voisey's Bay ore system.

In order to evaluate the processes involved in producing the ore deposits, a clear understanding of the metal distributions within a deposit is also required. The second portion of this paper addresses the results from a companion paper by Huminicki *et al.* (in review) and Chapter 2 of this thesis. The results of the companion paper include the quantitative classification of ore characteristics in the Ovoid deposit in terms of mineralogical zonations and textures. This paper reviews and models the quantitative mineralogical zonations in the Ovoid deposit, focusing on the genetic implications.

Besides upgrading processes, crystallization processes have also often been used to explain the metal variations within and between various ore deposits. The most commonly modeled crystallization processes in the past are fractional crystallization and equilibrium crystallization. However, partial fractional crystallization is another crystallization process that can be evaluated, which takes into account liquid that may be trapped within cumulus phases as crystallization proceeds (Lesher, 1998). In the later

portion of this paper these various crystallization processes are modeled to determine what role crystallization of sulfide melts may have had in producing the detailed variations in metal tenors within the Ovoid deposit.

3.2 GEOLOGY

The Voisey's Bay nickel-copper-cobalt magmatic sulfide ore bodies are hosted by troctolites and olivine gabbros of the Voisey's Bay intrusion, which is part of the Mesoproterozoic Nain Plutonic Suite (NPS). Emslie *et al.* (1994), Ryan (2000), and references therein summarized the regional geology of the NPS. The chemical composition and mineralogy of Voisey's Bay ores have been described by Naldrett *et al.* (2000a) and Naldrett *et al.* (2000b), respectively. The troctolitic magma system that hosts the sulfide ores has been described as two magma chambers (the Reid Brook chamber in the west and the Eastern Deeps chamber in the east) connected by a "feeder" dyke located in between (Li *et al.* 2000). An alternative model suggests however that the chambers are not actually connected by the feeder dyke and that the dyke is just co-incident with the magma chambers (Evans-Lamswood *et al.* 2000). The majority of the sulfide deposits are hosted within the feeder dyke (Fig. 3.1a) with the exception of the Eastern Deeps deposit, which is hosted at the base of the Eastern Deeps chamber (Fig. 3.1b).

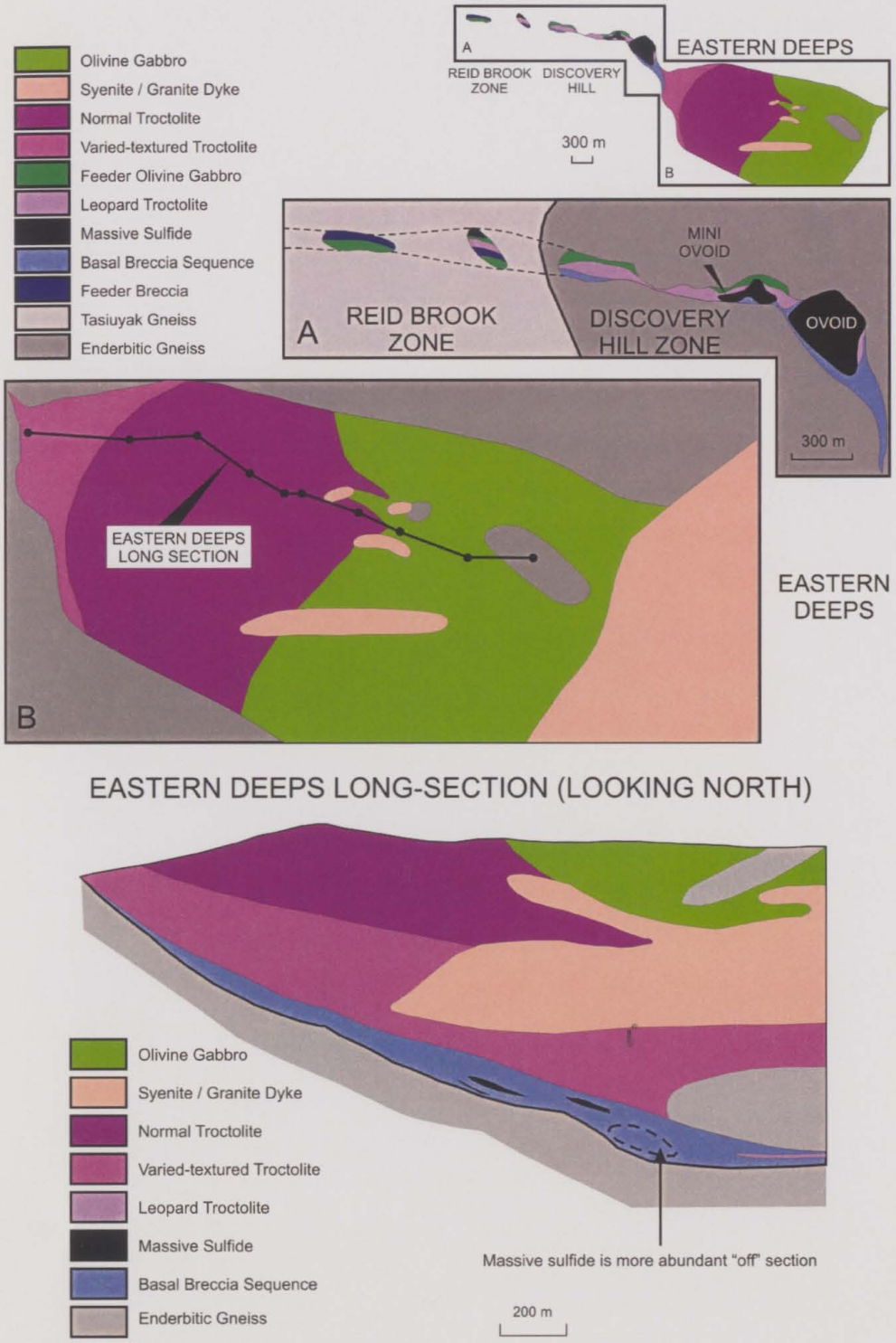

Figure 3.1. a) Plan view of the different ore zones in the Voisey's Bay deposit, b) plan and cross-sectional geology of the Eastern Deeps upper chamber (modified from Li and Naldrett, 1999).

The largest and most economic deposit at Voisey's Bay is the near surface bowl-shaped Ovoid deposit (Fig. 3.1a), which is currently being mined by open pit operations. The focus of this paper will be to model the bulk compositions of all the deposit zones but will only consider the detailed mineralogical zonations and crystallization modeling of the Ovoid deposit (both massive and disseminated mineralization).

3.3 ORIGIN OF PRIMITIVE SULFIDE MELT

The goal of the first portion of this paper is to determine the origin of the primitive sulfide melt(s) and the relationships between the sulfides and the host troctolite rocks that gave rise to the various ore deposits at Voisey's Bay. The process(es) that produced the bulk compositions of the various ore zones of the Voisey's Bay Ni-Cu-Co deposit (i.e., ore upgrading processes) are also addressed. Very generally, the two main factors governing the compositions of the sulfide melt(s) are 1) the chemical composition of the initial silicate magma that the sulfide was derived from, and 2) the principal physical processes that affected the silicate and sulfide melts. These two factors are linked because in order to calculate the parental and derivative liquid compositions, we must determine which physical model was responsible for the ore forming event and hence metal concentrations. This was approached by assessing the variation in three plausible physical models (the R, N, and L metal upgrading models of Campbell and Naldrett (1979), Brügmann *et al.* (1993) and Kerr and Leitch (2005), respectively, and described in detail below) by first assuming the parental magmas at Voisey's Bay were

basaltic in composition (a low MgO of <8.1 wt% basalt) as suggested by Li *et al.* (2000). Once we have evaluated the variations in the physical models (using an assumed basalt composition to start), we then model a large range of other possible parental silicate compositions (other than the basalt).

3.4 ORE PRECIPITATION AND UPGRADING PROCESSES

3.4.1 Upgrading models

We are attempting to explain the Ni and Cu variations in sulfide ores and therefore the data used in the modeling is the bulk Ni and Cu data normalized to 100% sulfide (Table 3.1a). It has previously been suggested that the initial sulfide liquid at Voisey's Bay contained <2.5 wt% Ni and 2 wt% Cu and was upgraded by a subsequent, chalcophile metal undepleted magma to ~6 wt% Ni and 3 wt% Cu (Li *et al.*, 2001). Models for closed-system single batch upgrading (R factor model), open-system simple multistage upgrading (N factor model), and open-system multistage dissolution upgrading (L factor model) were all evaluated.

The R and N factor models were developed to explain variations between metal compositions observed between (or within) different sulfide deposits. The models have also been used to explain the upgrade in metal tenor of some ores.

Campbell and Naldrett (1979) introduced the term R as a measure of the mass ratio of silicate magma to sulfide melt in an ore system. In using R to calculate

upgrading, they assume a situation such as in a magma chamber, where all of the magma is in equilibrium with the sulfide melt and the system is always just at sulfur saturation.

N, a term similar to R (Brügmann *et al.*, 1993) is the mass of silicate magma to mass of sulfide where the silicate magma is continually being replenished by new pulses (such as in a lava flow or magma conduit). The model assumes the system is always just at sulfur saturation. R factor generally pertains to closed-system conditions, whereas N factor generally pertains to open-system conditions. R refers to a simple single batch upgrading process, whereas N refers to a simple multistage upgrading process.

The equations relating sulfide metal content to R and N factor, respectively, are as follows:

$$Y_i = [D_i * X_{io} * (R+1)]/(R+D_i) \ldots\ldots\ldots (1)$$

$$Y_i = X_{io} * \{D_i - [(D_i - 1) * e^{-(N/Di)}]\} \ldots\ldots\ldots (2)$$

Where i = metal; R = ratio of mass of silicate magma to mass of sulfide magma, N = ratio of cumulative amount of magma passing through a system and reacting with the sulfide to the amount of sulfide in the system, Y_i = final concentration of metal in sulfide melt, X_{io} = initial concentration of metal in the original silicate magma, and D_i = Nernst partition coefficient for the metal in sulfide relative to silicate magma (Campbell and Naldrett, 1979; Naldrett, 2004).

One of the main criticisms of multistage upgrading (N factor) is that it is likely that the new influxes of magma would be S-undersaturated and would therefore redissolve pre-existing sulfide (Kerr and Leitch, 2005). Thus, Kerr and Leitch (2005)

have expanded the idea of upgrading by modeling a more complex situation in which the sulfide liquid is progressively redissolved as it is enriched in metals; they have termed this process "multistage-dissolution upgrading" (L factor model). The equations relating sulfide metal content to cumulative R factor, R_L, for multistage dissolution upgrading are as follows:

$$Y_i \approx X_{io}*[(R'_{inc}*D_i)/(R'_{inc}-L*D_i)]*\{1-[D_i/(D_i+R'_{inc}-L*D_i)]^n\} \ldots\ldots\ldots (3)$$

$$R_L \approx R'_{inc}/L[(1/1-L)^n-1] \ldots\ldots\ldots (4)$$

Where R'_{inc} = the incremental R factor for each batch of magma, L = fraction of sulfide that dissolves into each batch of magma, n = number of batches and R_L = the mass ratio of the total mass of silicate magma that has passed through the system to the mass of sulfide liquid.

The premise here is that upgrading is not simply dependant on the amount of available metal from the original silicate magma but also on metal available from dissolving pre-existing sulfide released back to the magma. The additional variables to consider are the amount of sulfide that gets dissolved back into the magma (L the "loss" factor) and the number of batches of magma (n), both of which will govern how much metal will be available.

Alternative explanations (other than R, N, and L factor) for variations in metal compositions of sulfide mineralization may include variations in initial magma compositions, fractional crystallization processes, or redistribution of metals by alteration

processes (Campbell and Naldrett, 1979). These processes are also addressed in this paper.

3.4.2 Assumptions for modeling upgrading processes

The bulk of the mineralization at Voisey's Bay is contained within the feeder dyke with lesser mineralization occurring in the Reid Brook and Eastern Deeps chambers. As such, mineralization in the feeder dyke was probably formed in a dynamic open system where the N factor or L factor would likely be more appropriate than R factor, accounting for multiple magma injections using multistage upgrading. However, mineralization in the chambers may have formed in a more closed-system manner, whereby an R factor may be more appropriate. R, N, and R_L deviate from each other in the situation where R, N, or R_L approaches D (Kerr and Leitch, 2005). For the case here R, N, and R_L approach D for Cu and Ni (see below) and therefore all three models were evaluated. Massive ores were normalized to 100% sulfide plus magnetite, whereas disseminated mineralization was normalized to sulfide only, by methods outlined in Huminicki *et al.* (in review) and Chapter 2 of this thesis. Values in the literature for D_{Ni} (between sulfide and silicate) range from 300-1050 and for D_{Cu} range from 800-1400 (Barnes and Maier, 1999). A range of D_{Ni} and D_{Cu} values were evaluated and a Here the values of D_{Ni} = 800 and D_{Cu} = 1400 from Naldrett (2004) were used. Initial starting compositions of Cu and Ni in a typical basaltic magma, X_{oCu} = 100ppm and X_{oNi} = 250ppm were assumed (Foster, 2006).

For modeling multistage dissolution upgrading we must also assume an L value and R'_{inc} value. Here the proportion of sulfide dissolved into any given new batch of magma was L = 0.03 and the incremental R value was $R'_{inc} = 50$. If we were to increase L it would result in an effective decrease in R_L.

3.4.3 Modeling R, N, and L

R, N, and L processes were modeled to address the questions relevant to Voisey's Bay including: 1) whether the ores been have upgraded as suggested previously (Li *et al.*, 2001) and whether R, N, or L processes more closely describe the ore tenors, 2) whether a single, common magma composition could be responsible for the metal tenor variations of different sulfides, 3) whether other processes modified the ore tenors (i.e., fractional crystallization or subsolidus redistribution of metals), and 4) what were the composition of the parent and derivative silicate magma(s).

Unfortunately, over the range of ore tenors observed at Voisey's Bay, model curves for each of the three processes (R, N, and L) are very similar making it virtually impossible to distinguish the processes by modeling alone (Fig. 3.2a). The curve for R factor diverges slightly from the N and L factor curves only at R >300, whereas the Voisey's Bay massive ores formed at lower R factors. This divergence infers that multistage upgrading (N factor) and multistage dissolution upgrading (L factor) require slightly lower ratios of silicate magma to sulfide melt. For $D_{Ni} = 800$, $D_{Cu} = 1400$, X_{oNi} = 250ppm, and X_{oCu} = 100ppm, the model curves are consistent with data from the massive

sulfide ores hosted by troctolitic rocks and from disseminated sulfide hosted by the ultramafic rocks (Fig. 3.2a). Because the samples plot along a single curve, this implies that at D_{Ni} = 800 and D_{Cu} = 1400 the troctolite-hosted massive sulfide and the ultramafic-hosted disseminated inclusions can be related by any one of the three processes (R, N, or L factor) with slightly only different values (i.e., ~150 for massive ores and ~300-500 for ultramafic hosted disseminated sulfide).

Although at the metal tenors observed at Voisey's Bay the R, N, and L models cannot be distinguished, an interesting result of the modeling in general is that due to the divergence of the curves at higher metal tenors, the amount of silicate magma required to interact with the sulfide is less for multistage upgrading (N factor) and multistage dissolution upgrading (L factor) than for single batch upgrading (R factor).

Under reasonable X_o and D values, Ni and Cu tenors in the disseminated sulfides from ultramafic inclusions and the massive sulfides in the troctolites can be related by one common magma and either an R, N, or L process. Semi-massive and disseminated sulfides hosted by troctolite are spatially related to the massive sulfides. They define a trend in Ni and Cu tenors that increase away from the values for the massive sulfides in each deposit. The trend cannot be explained by variations in R, N, or L factors (Fig. 3.2b). In order to fit a model upgrading curve to the data using X_{oNi} = 250ppm and X_{oCu} = 100ppm, a very large difference between D_{Ni} and D_{Cu} would be required, which is unrealistic based on literature values. If the D_{Ni} was the minimum literature value (300) and D_{Cu} was the maximum literature value (1400), it would require a X_{oNi} ~130-140 and X_{oCu} ~40 and R between ~400-3700 to fit the data. Although it is possible to fit the data,

these D values are extreme and the initial compositions are much lower than any picrite, komatiite, or basalt magma compositions. Under these circumstances, it is thought that an alternate explanation other than R, N, or L variations is required to explain the composition of the ores. The trend of increasing Cu from massive to disseminated sulfide is best explained by partial fractional crystallization, which accounts for trapped liquid (Fig. 3.2b). This is modeled later in the paper using the Ovoid as an example. Another possibility is that massive ore has lost Cu-rich sulfide and the disseminated mineralization has a composition closer to the original composition.

3.4.4 Parent silicate magma source of the sulfides

Several potential parent magma compositions (X_{io}) were modeled as the source of sulfides in the Voisey's Bay intrusion (Figure 3.2b). These include some hypothetical compositions - picrite, komatiite, komatiitic basalt, basalt, and some compositions of rocks actually present in the deposit - normal troctolite, variable troctolite, ultramafic inclusions, and olivine gabbro (Table 3.2). The compositions of rocks from the deposit and used in the modeling were filtered to exclude mineralized samples (>0.5 wt% S).

Table 3.1a. Bulk compositions of the massive and disseminated sulfides in the various ore zones in the Voisey's Bay intrusion derived from the MEBS database.

Zone	Rock Type	Number	Ni[100] wt%	Cu[100] wt%	Ni/Cu
Ovoid	Massive + Disseminated	n = 4196	4.03	2.62	1.54
	Massive	n = 2671	3.89	2.24	1.74
	Disseminated (Total)	n = 1525	4.28	3.29	1.30
	Olivine Gabbro	n = 22	4.86	4.11	1.18
	Leopard Troctolite	n = 118	4.35	2.76	1.58
	Variable Troctolite	n = 47	4.33	3.35	1.29
	Troctolite	n = 1333	4.25	3.32	1.28
	Ultramafic Inclusions	n = 5	6.81	5.03	1.35
Mini Ovoid	Massive	n = 509	3.56	2.10	1.70
	Disseminated (Total)	n = 666	3.58	3.97	0.90
	Leopard Troctolite	n = 30	4.02	2.65	1.52
	Variable Troctolite	n = 8	3.34	3.95	0.85
	Troctolite	n = 628	3.50	4.24	0.83
SE Extension	Massive	n = 58	3.85	1.96	1.96
	Disseminated (Total)	n = 1792	4.31	3.55	1.21
	Olivine Gabbro	n = 17	3.63	4.35	0.83
	Leopard Troctolite	n = 16	3.98	2.66	1.49
	Variable Troctolite	n = 1110	4.54	3.32	1.37
	Troctolite	n = 649	3.93	3.92	1.00
Reid Brook Zone	Massive	n = 1982	3.16	1.42	2.23
	Disseminated (Total)	n = 8844	3.64	4.77	0.76
	Olivine Gabbro	n = 31	0.27	3.27	0.08
	Leopard Troctolite	n = 772	3.98	3.39	1.17
	Variable Troctolite	n = 2663	3.46	4.15	0.83
	Troctolite	n = 5089	3.52	5.39	0.65
	Ultramafic Inclusions	n = 289	6.90	3.52	1.96
Discovery Hill Zone	Massive	n = 90	3.76	2.31	1.63
	Disseminated (Total)	n = 6119	3.84	5.45	0.70
	Olivine Gabbro	n = 23	2.69	2.68	1.00
	Leopard Troctolite	n = 609	4.15	3.76	1.10
	Variable Troctolite	n = 1501	3.63	5.28	0.69
	Troctolite	n = 3734	3.64	5.93	0.61
	Ultramafic Inclusions	n = 252	7.44	3.74	1.99
Eastern Deeps	Massive	n = 457	3.53	1.41	2.50
	Disseminated (Total)	n = 2296	4.71	3.31	1.42
	Olivine Gabbro	n = 76	4.99	3.44	1.45
	Leopard Troctolite	n = 316	3.84	1.78	2.16
	Variable Troctolite	n = 1750	4.77	3.61	1.32
	Troctolite	n = 63	4.73	2.40	1.97
	Normal Troctolite	n = 83	6.34	3.01	2.11
	Ultramafic Inclusions	n = 7	6.22	2.45	2.54

Table 3.1b. Bulk compositions of the sulfides from the MUN database.

Zone	Rock Type	Metal	Ni[100] wt%	Cu[100] wt%	Ni/Cu
Ovoid	Massive	n = 37	4.46	2.56	1.74
	Disseminated	n = 12	4.86	3.39	1.43
	Massive + Disseminated	n = 49	4.56	2.77	1.65

[100] denotes metal is normalized to 100% sulfide; for massive ores metal is normalized to sulfide plus magnetite. Disseminated samples are filtered for S >0.5 wt%.

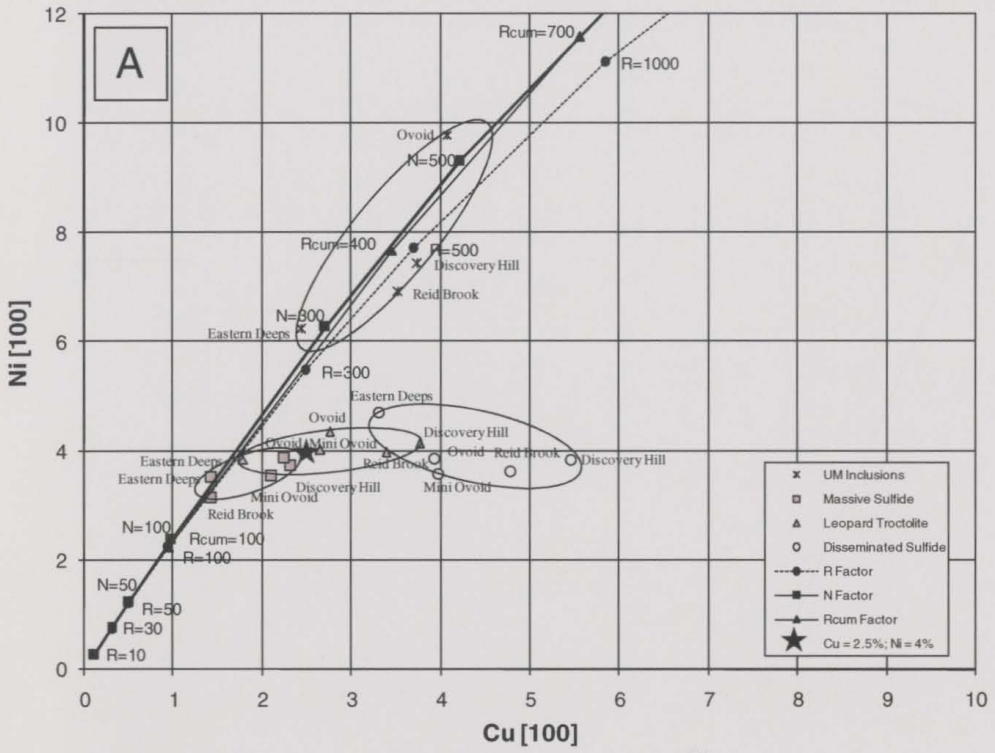
A
Rcum=700
R=1000
Ovoid
N=500
Rcum=400
R=500
Discovery Hill
Reid Brook
N=300
Eastern Deeps
R=300
Eastern Deeps
Ovoid
Discovery Hill
Ovoid
Mini Ovoid
Reid Brook
Ovoid
Reid Brook
Discovery Hill
Eastern Deeps
Eastern Deeps
Discovery Hill
Mini Ovoid
Mini Ovoid
Reid Brook
N=100
Rcum=100
R=100
N=50
R=50
R=30
R=10
UM Inclusions
Massive Sulfide
Leopard Troctolite
Disseminated Sulfide
R Factor
N Factor
Rcum Factor
Cu = 2.5%; Ni = 4%
Ni [100]
Cu [100]
0
1
2
3
4
5
6
7
8
9
10
12

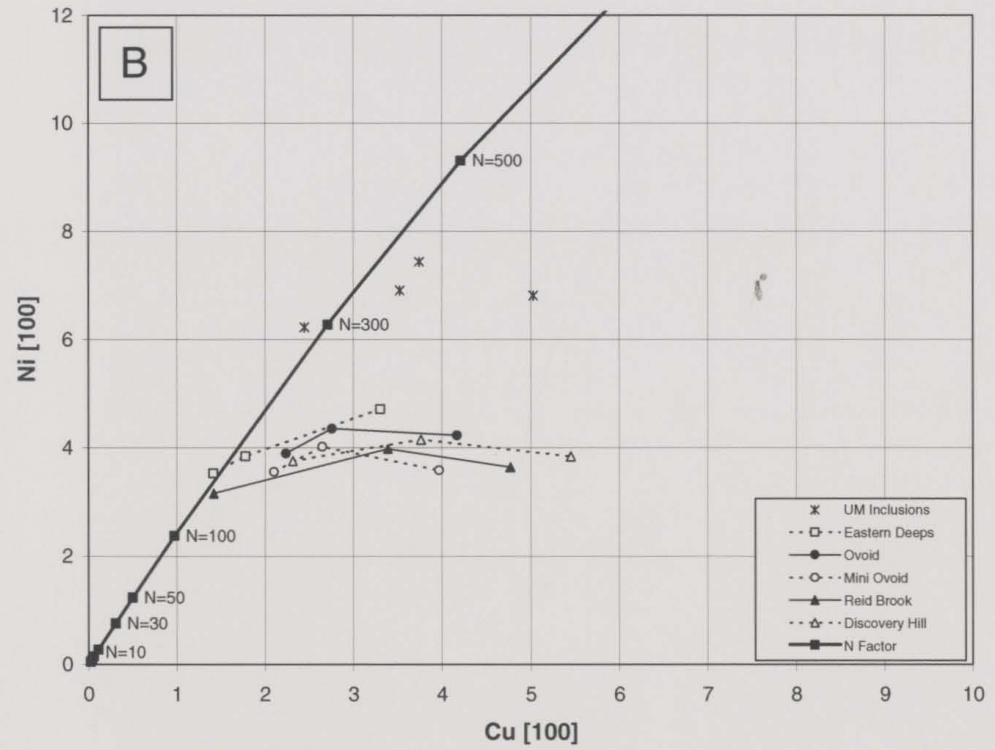
B
N=500
N=300
N=100
N=50
N=30
N=10
UM Inclusions
Eastern Deeps
Ovoid
Mini Ovoid
Reid Brook
Discovery Hill
N Factor
Ni [100]
Cu [100]
0
1
2
3
4
5
6
7
8
9
10
12

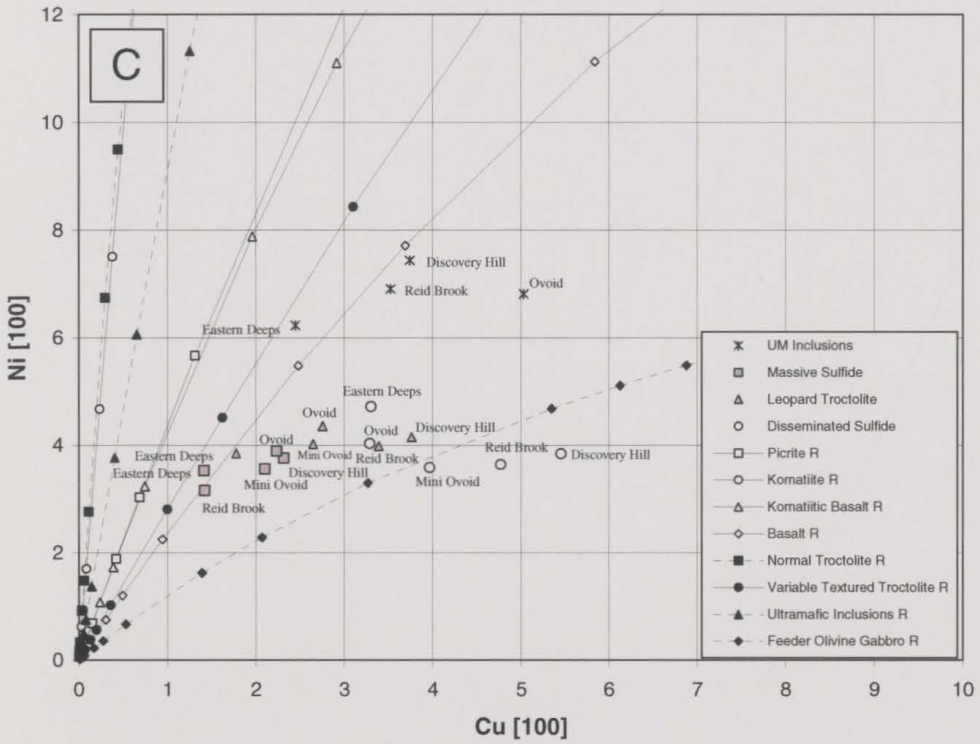

Figure 3.2. a) Average Cu versus Ni concentrations (wt% normalized to 100% sulfide) separated into disseminated, semi-massive, and massive sulfides hosted by the troctolitic rocks, and disseminated sulfide hosted by ultramafic rocks for each deposit (Eastern Deeps, Ovoid, Mini Ovoid, Reid Brook, and Discovery Hill Zones). Disseminated sulfides hosted by the ultramafic inclusions and the massive ores lie on one model curve indicating that the sulfide compositions could have been produced by the same initial magma at slightly different R, N, or R_L factors. No R, N, or R_L curve fits the trend of the massive to disseminated mineralization hosted by the troctolites. This indicates some other process is likely responsible for the compositional variability of these sulfides. b) same data as a) but with curves through massive to disseminated mineralization in each deposit. This shows at least qualitatively that the ores may be related by fractional crystallization trends (i.e., increasing Cu in the disseminated mineralization). c) same data as a) and b) showing model R factor curves for picrite, komatiite, komatiitic basalt, basalt, normal troctolite, variable textured troctolite, ultramafic inclusions, and feeder olivine gabbro. Note that the basalt and variable textured troctolite curves are the only curves that are consistent with the data. Data are from Table 3.1 and 3.2 where $D_{Ni} = 800$, $D_{Cu} = 1400$, $D_{Co} = 40$, $X_{oNi} = 250$ppm, $X_{oCu} = 100$ppm, $X_{oCo} = 50$ppm for model curves of R, N, and R_L.

The parent magma of the Voisey's Bay intrusion has been thought to be broadly basaltic with a low MgO of <8.1 wt% (Li *et al.*, 2000). The low-Mg basalt has been modeled as a product of crustal contamination of a high-Mg magma with a composition similar to Noril'sk and West Greenland uncontaminated picritic basalts (Li *et al.* 2000).

Table 3.2. Possible parent magmas (X_{io}) for the Voisey's Bay intrusion.

Reference	Rock	Co (ppm)	Ni (ppm)	Cu (ppm)	Ni/Cu
Lightfoot *et al.* (1997)	Picrite	97	631	139	4.5
Barnes and Maier (1999)	Komatiite		1563	77	28.3
Barnes and Maier (1999)	Komatiitic Basalt		360	79	10.0
Foster (2006)	Basalt	50	250	100	2.0
Table 6.1; Naldrett (2004)	Normal Troctolite (n = 7; S = 0.03%)	48	308	12	25.7
Table 6.1; Naldrett (2004)	Variable Troctolite (n = 57; S = 0.43%)	75	939	329	2.9
Table 6.1; Naldrett (2004)	Ultramafic Inclusions (n = 8; S = 0.16%)	101	1261	133	9.5
Table 6.1; Naldrett (2004)	Feeder Olivine Gabbro (n = 6; S = 0.12%)	50	74	56	1.3

3.4.4.1 Picrite or komatiite as the source of sulfide mineralization

Based on whole-rock major and trace element geochemistry, the primitive magma of the Voisey's Bay intrusion has been suggested to be a mantle-derived picritic basalt similar in composition to Noril'sk and West Greenland uncontaminated picrites (Li *et al.*, 2000). In this case an average value from West Greenland picrites was used (Lightfoot *et al.*, 1997) as suggested by Li *et al.* (2000). Using the final ore compositions and published D values of D_{Ni} = 800 and D_{Cu} = 1400 (Naldrett, 2004), we attempted to model the initial magma compositions required to produce the observed ores (Fig. 3.2b). The curves modeled for starting compositions of a picrite, komatiite, and komatiitic basalt

have Ni/Cu ratios that are too high to fit the sulfide data (Table 3.2). It should be noted that a Ni/Cu ratio of ~1 to 2.5 best fit the data. This indicates that the sulfides did not precipitate from the high-Mg magmas that were modeled from literature values, which produce higher Ni/Cu ratios. This is because any values with greater than ~250ppm Ni and less than ~100ppm Cu would produce Ni/Cu ratios that are greater than 2.5.

3.4.4.2 Basalt as the source of sulfide mineralization

Unlike the curves modeled for picrite and komatiite parent magmas, a model assuming a parent composition of a basalt (i.e., X_{oNi} = 250ppm and X_{oCu} = 100ppm) fits the sulfide data using the published D values (Naldrett, 2004). This implies that a single magma of basaltic composition could have formed the massive ores that are hosted by troctolite and disseminated sulfide hosted by ultramafic inclusions related by R, N, or L factor processes alone. There is no need to invoke another process to explain the sulfide compositions. The semi-massive (leopard troctolite) and disseminated sulfide now hosted in the variable troctolite and the normal troctolite form a trend with the massive sulfide ores that cannot be modeled by R, N, or L upgrading processes alone and another process is required to explain this variation. As mentioned above, we suggest fractional crystallization further modified the ore compositions (Fig. 3.2b).

3.4.4.3 Rocks that are actually observed as potential parents

Another scenario that was tested is the whether any of the magmatic rocks present in the Voisey's Bay Intrusion (olivine gabbro, normal troctolite, variable troctolite, leopard troctolite, or ultramafic inclusions) have the compositions that may be the parent magma to the Voisey's Bay ores. Based on the modeled values, the variable troctolite is the only rock present that could have been capable of producing ores with compositions of both the massive ores and the disseminated sulfides that are now hosted by the ultramafic inclusions and massive ores. The variable troctolite has higher absolute Ni and Cu concentrations than the basalt modeled above (Table 3.2) but does have similar Ni/Cu ratios near that which will produce a curve that fits the sulfide data (i.e., Ni/Cu = 2.9). This would, however, require an R, N, or R_L factor of ~35 for massive sulfides and ~75-200 for disseminated sulfide hosted by ultramafic inclusions. According to the modeling, the normal troctolite, leopard troctolite, or ultramafic inclusions were not the parent magma compositions that produced ores. Another consideration is that the variable troctolite, normal troctolite, and leopard troctolite are likely cumulus rocks and are therefore not likely candidates for initial bulk magma compositions.

3.4.5 Derivative silicate rocks after sulfide removal

The amount of metal that would remain in the silicate magma after sulfide segregation can be calculated from the final composition of metal (Y_i) in the sulfide and

the known D values for metal partitioning between sulfide and silicate. Contents of Ni, Cu and Co in this derivative liquid (magma) was calculated as $X_i = Y_i/D_i$; where X_i = final concentration of metal (i) in silicate magma, Y_i = final concentration of metal in sulfide melt, and D_i = is the Nernst partition coefficient for the metal in sulfide to silicate magma.

From modeling, it is seen that the Ni, Cu, and Co compositions of the resultant magmas that were produced after separation of the massive sulfide ores most closely resembles the compositions of the feeder olivine gabbro (compare Tables 3.2 and 3.3). The feeder olivine gabbro is evaluated as potential derivative magma from which sulfides were removed in more detail below, particularly in terms of geological associations and mineral compositions (i.e., An and Fo contents of plagioclase and olivine, respectively).

3.4.5.1 Feeder olivine gabbro as the derivative after sulfide formation

The feeder olivine gabbro is more closely associated with the mineralized leopard troctolite and the underlying massive sulfides than is the normal troctolite (Fig. 3.1a). Also, the feeder olivine gabbro has the lowest An and Fo contents of plagioclase and olivine, respectively, indicating that it is the most evolved rock present (Li and Naldrett, 1999). This is consistent with the feeder olivine gabbro being the derivative liquid since sulfide would have had a chance to segregate sulfide and form the ores at some stage earlier in the silicate crystallization sequence.

Absolute Ni (34-86ppm) and Cu (16-30ppm) contents and Ni/Cu (1.2-3.0) ratios of the feeder olivine gabbro from Table 3.3 are consistent with it being a derivative of the magma that formed the ores (compare Table 3.1). The geology and mineral chemistry of olivine and plagioclase indicate that the feeder olivine gabbro is consistent as a derivative from a magma that had sulfide removed (i.e., not the composition that would produce the ores but a composition that would be left after the ores were produced).

3.4.6 Comparison of other R factor values determined for Voisey's Bay

R factor values calculated in this study are ~150 for massive ores from the Ovoid, Mini Ovoid, Discovery Hill, Eastern Deeps, and Reid Brook. The results are based on averages of tens of thousands of samples from the MEBS database, in contrast to previous estimates based on much more limited datasets. R factor values range from 400-700 in disseminated sulfides in ultramafic inclusions from all deposits at Voisey's Bay. These are the first R factor estimates for sulfides in the ultramafic inclusions.

R factor values of 50-500 were estimated by Lambert *et al.* (2000) for the Voisey's Bay deposit based on Re-Os isotopic data and a model that calls for an immiscible sulfide liquid forming from one silicate magma and then interacting with a second chalcophile-metal undepleted magma. Their model gives R factors for the Ovoid massive ore closer to 50, whereas disseminated mineralization is associated with normal troctolite or variable troctolite have values closer to 500. The values determined in this study span a similar range; however, this study relates disseminated sulfides to massive

sulfides hosted by troctolitic rocks by fractional crystallization (Fig 3.2b and discussed more extensively below) rather than to R factor processes alone.

Naldrett *et al.* (2000a) attempted to estimate R factors using concentrations of Rh and Cu. They found however that the Rh distributions in ore from most deposits could not be explained by either R factor processes or fractional crystallization of sulfides alone. They suggested that Rh in these deposits was redistributed following ore formation. However, in disseminated to semimassive sulfide samples from the variable textured troctolite from the Eastern Deeps, the original Rh concentrations appear to be preserved. There they estimated R factor processes ranging from 280 to 1000. Again, we interpret the compositions of disseminated to semimassive samples to have been modified by fractional crystallization. Nonetheless, the R values inferred by Naldrett *et al.* (2000a) using Rh and Cu are only slightly higher than values determined in this study, which are based on Ni and Cu concentrations.

Kerr (2000) modeled Voisey's Bay ores assuming they contained 4% Ni on average, which is typical of the Ovoid. For D_{Ni} values from Kerr (2000) of 300-600 and magma with a starting composition of 150ppm Ni, calculated R factors are 500-2000. These R factor values are somewhat higher than what was determined in this study. However, with the slightly higher D_{Ni} and X_{oNi} values used in this study, the R factors would be similar to those calculated here.

Foster (2006) calculated R factors using Ni and Cu data from Naldrett *et al.* (2000a) and assuming $D_{Ni} = 500$, $D_{Cu} = 750$, $X_{oCu} = 100$ppm and $X_{oNi} = 200$ppm. The results indicate R factors from about 200-600 with the Ovoid at about 300.

Table 3.3. Derivative silicate magma compositions (X_i) of the massive and disseminated sulfides in the various ore zones in the Voisey's Bay intrusion (i.e., metal in silicate after removal of the sulfide ores).

Zone	Rock Type	Metal	Ni	Cu	Ni/Cu
		D value	800	1400	
		Unit	ppm	ppm	
Ovoid	Massive	n = 2671	43	16	2.7
	Disseminated (Total)	n = 1525	44	30	1.5
	Olivine Gabbro	n = 22	86	29	3.0
	Leopard Troctolite	n = 118	47	20	2.4
	Variable Troctolite	n = 47	48	25	1.9
	Troctolite	n = 1333	34	29	1.2
	Ultramafic Inclusions	n = 5	52	29	1.8
Mini Ovoid	Massive	n = 509	45	15	3.0
	Disseminated (Total)	n = 863	46	28	1.6
	Leopard Troctolite	n = 30	93	19	4.9
	Variable Troctolite	n = 8	44	28	1.6
	Troctolite	n = 628	66	30	2.2
SE Extension	Massive	n = 58	62	14	4.4
	Disseminated (Total)	n = 3076	48	36	1.3
	Olivine Gabbro	n = 17	60	31	1.9
	Leopard Troctolite	n = 16	59	19	3.1
	Variable Troctolite	n = 1110	79	24	3.3
	Troctolite	n = 649	78	28	2.8
Reid Brook Zone	Massive	n = 1982	49	10	4.9
	Disseminated (Total)	n = 8844	53	34	1.6
	Olivine Gabbro	n = 31	61	23	2.7
	Leopard Troctolite	n = 772	54	24	2.3
	Variable Troctolite	n = 2663	52	30	1.7
	Troctolite	n = 5089	47	38	1.2
	Ultramafic Inclusions	n = 289	122	25	4.9
Discovery Hill Zone	Massive	n = 90	45	17	2.6
	Disseminated (Total)	n = 6119	46	39	1.2
	Olivine Gabbro	n = 23	50	19	2.6
	Leopard Troctolite	n = 609	42	27	1.6
	Variable Troctolite	n = 1501	44	38	1.2
	Troctolite	n = 3734	48	42	1.1
	Ultramafic Inclusions	n = 252	52	27	1.9
Eastern Deeps	Massive	n = 457	45	10	4.5
	Disseminated (Total)	n = 3633	50	27	1.9
	Olivine Gabbro	n = 76	57	25	2.3
	Leopard Troctolite	n = 316	49	13	3.8
	Variable Troctolite	n = 1750	40	26	1.5
	Troctolite	n = 63	46	17	2.7
	Normal Troctolite	n = 83	3	21	0.1
	Ultramafic Inclusions	n = 7	50	17	2.9

3.4.7 Ni in olivine in disseminated sulfide

It is thought that a discussion of the whole rock Ni concentrations due to Ni in olivine deserves consideration as olivine can substitute significant Ni in its structure. It should be noted that this only effects disseminated sulfide containing olivine and not massive sulfide, where all Ni will be contained in the sulfide.

Here, the effect of Ni in olivine on the whole rock composition is demonstrated for 60% olivine in a rock with 500ppm Ni in olivine with 0.5% S (1.5% sulfide), where the sulfide contains 4% Ni. For this calculation, 4% Ni in 100% sulfide is equivalent to 0.06% Ni in the total rock and olivine would contribute 0.03% Ni for a total of 0.09% Ni. This example indicates that up to one third of the Ni can be contributed by the Ni in olivine. Although, this is an important point it is difficult to ascertain the actually contribution of Ni in olivine to individual samples because the olivine content and Ni content in olivine is very variable. However, previous estimates of the olivine content is generally less with a maximum of 30-40% olivine (Table 4.2; Chapter 4 of this thesis) reducing the maximum contribution of Ni in olivine to 25%.

3.5 DIFFERENTIATION OF SULFIDE MELTS

3.5.1 Zonation and crystallization of magmatic sulfide deposits

It has been generally observed that magmatic Cu-Ni-(PGE), which have cooled slowly in intrusive bodies are commonly zoned into Fe-(Ni)-rich, Cu-poor and Fe-(Ni)-poor, Cu-rich portions (Naldrett, 1989; Fleet and Pan, 1994). Examples include Sudbury (Hawley, 1965) and Noril'sk (Distler *et al.*, 1977). Czamanske *et al.* (1992) described Noril'sk ores as concentrically zoned with pyrrhotite-rich (Fe-rich) ore at the base and at the margins and Cu-rich ore at the top and in the center. The quantitative mineralogical characterization of the Ovoid deposit is described in this paper as well as in Huminicki *et al.* (in review) and Chapter 2 of this thesis and indicates that the Ovoid is also zoned into more Fe-rich portion at the margins and toward the base and a Cu-rich portion toward the center and the top, similar to Noril'sk (Figs. 3.3 and 3.4).

One of the main questions in ore deposit research is how and why a deposit is compositionally (or mineralogically) variable (i.e., zoned). Determining whether a deposit is zoned is important in ore genesis studies but mining and metallurgical research can also benefit from predictive mineral zonation models for cost-effective mineral extraction. Determining models for deposit zonation can also aid in developing exploration models where we can predict whether Cu-rich ores that often contain precious metals will occur and where they may be located (Barnes *et al.*, 1997). In terms of ore genesis, the careful three dimensional characterization of the mineralogy at

Voisey's Bay has allowed us to test various crystallization models in more detail to see which one (if any) is responsible for the spatial compositional zonation within the deposit.

Based on experimental work of Craig and Kullerud (1969) and Kullerud *et al.* (1969) for the Cu-Fe-Ni-S system, this type of compositional zoning of sulfide deposits into Fe-rich assemblages and Cu-rich portions in general has most often been attributed to fractional crystallization. It has been proposed that large magmatic Fe-Ni-Cu-(PGE) sulfide deposits form from a sulfide liquid that fractionates high temperature monosulfide solid solution (MSS) producing a Cu-rich residual liquid, where the Fe-rich assemblages are MSS cumulates that may have settled out due to gravity, and Cu-rich portions of the ore are residual liquids capable of crystallizing intermediate solid solution (ISS) (Naldrett *et al.*, 1982; Barnes and Naldrett, 1986; Li *et al.*, 1993; Naldrett *et al.*, 1994; Li and Barnes, 1996; Ebel and Naldrett, 1997; Barnes *et al.*, 1997; and many others).

In the initial stages of formation of magmatic Fe-Ni-Cu-PGE sulfide deposits, an immiscible sulfide liquid will separate from the silicate magma (Naldrett, 1981). The sulfide droplets are denser than the silicate liquid and are thought to sink and coalesce into a homogenous sulfide pool (Barnes *et al.*, 1997). The Ni, Cu, and PGE are chalcophile and will partition strongly into the sulfide rather than the silicate melt (Naldrett, 2004). The degree of partitioning of metals from the silicate to sulfide melt will depend on R factor and original composition of the silicate magma as discussed in previous sections. The following sections will discuss the paragenetic sequence and

sulfide mineral zonations in the Ovoid deposit with respect to various crystallization models (including fractional, equilibrium, and partial fractional crystallization).

3.5.2 Sulfide Mineralogy and Paragenetic Sequence of the Ovoid

3.5.2.1 Sulfide ore mineralogy and textures in the Ovoid

The main ore minerals present in the Voisey's Bay Ovoid deposit are hexagonal pyrrhotite (± troilite), magnetite, chalcopyrite (± cubanite), and pentlandite. In terms of evaluating crystallization processes, it is important to distinguish which minerals actually crystallize as liquidus phases or as subsolidus phases. Textures of the massive sulfide can indicate ore forming processes and are described in more detail in Chapter 2 (Huminicki *et al*, in review). However, here we want to particularly emphasize the Cu-rich "loop" texture in the massive ores of the Ovoid (Figs. 3.5a-c). The Cu-rich "loop" texture is important in the ore genesis interpretation because it is thought that the Cu-rich "loops" that occur interstitial to large pyrrhotite grains in the Ovoid formed as a result of ISS crystallization from residual Cu-rich trapped liquid. Another texture that should be emphasized for genetic interpretation is the fine-grained and coarse-grained nature of the magnetite (Figs. 3.5a-b). The fine-grained magnetite occurs predominantly at the margins of the Ovoid indicating quicker cooling due to heat loss at the margins. Coarse-grained magnetite occurs predominantly in the center of the Ovoid indicating slower cooling rates as a consequence of slower heat dissipation from the core of the sulfide body.

The temperature at which the sulfide ore starts to crystallize and final solidification is also important when considering how far the sulfide can move as a magma away from the host intrusion (Naldrett, 2004).

3.5.2.2 Paragenetic sequence

The Ovoid has been considered to have crystallized as a closed system from the base up and margins inward from a relatively reduced and metal-rich sulfide liquid (Naldrett, 2000b). Naldrett (2004) and references therein discussed the phase relations in the Fe-Ni-S system. In terms of phase relations, at Voisey's Bay all phases in the Ovoid would be liquid at 1200°C. Upon cooling, monosulfide solid solution [$Fe_{(1-x)}S$ to $Ni_{(1-x)}S$] begins to crystallize Fe-rich compositions followed by Ni-rich compositions at lower temperatures. The solidus is between 1010°C and 1050°C for the Ni, Cu poor system; Ni does not change the solidus significantly; however, Cu may lower the solidus to 850°C (Naldrett, 2004). Crystallization of MSS concentrates oxygen in the fractionated liquid causing magnetite to start crystallizing as a liquidus phase likely above ~900°C (Naldrett, 2000b, 2004). Naldrett (2000b) interprets the center zone of the Ovoid with pyrrhotite and high magnetite to be a zone of cotectic crystallization of monosulfide solid solution and magnetite. There may be evidence in natural ores (Distler and Genkin pers. comm. in Naldrett, 2004) and experimental work (Ballhaus, 1999) that there is a miscibility gap in the Fe-Cu-Ni-S system giving rise to co-existing Cu-rich and MSS-rich liquids. Copper is incompatible in MSS so as the MSS crystallizes, the liquid becomes enriched in Cu with

respect to the MSS. Nickel starts out incompatible in MSS, so initially the liquid also becomes enriched in Ni with respect to MSS, however, at lower temperatures Ni is thought to behave compatibly in MSS and therefore the residual liquid becomes increasingly Cu-rich but not as Ni-rich.

Since Cu is insoluble in MSS, eventually, down temperature, a Cu-rich sulfide melt or ISS is produced at a liquidus temperature somewhere between ~880-970°C (Cabri and Laflamme, 1976) or 900-950°C (Fleet and Pan, 1994). Further down temperature at subsolidus conditions the ISS is thought to break down into chalcopyrite, pyrrhotite, and cubanite (Cabri, 1973; Craig and Scott, 1974; Naldrett, 1989; Naldrett, 2004). Pentlandite is mostly known to exsolve from MSS at subsolidus condition (i.e., MSS + liquid react to form pentlandite at 610°C; Kullerud, 1963). However, the upper stability of pentlandite is ~865°C according to Sugaki and Kitakaze (1998), so it is possible pentlandite can crystallize as a liquidus phase in the presence of Cu-rich sulfide liquids since the Cu may lower the solidus to 850°C.

Pentlandite has not previously been considered a liquidus phase at Voisey's Bay because according to the pure Fe-Ni-S system the pentlandite would form at 500°C in the Ovoid, which is below the solidus temperature (Naldrett, 2000b). However, the Ovoid does contain significant Cu, which according to Sugaki and Kitakaze (1998) may drive the solidus to significantly higher temperatures and may form pentlandite as a liquidus phase. The evidence for this early form of pentlandite is coarse grains associated with ISS or the Cu-rich "loops" (Fig. 3.5c). The lower temperature subsolidus pentlandite usually occurs as exsolved "flames" in pyrrhotite. Troilite forms as a subsolidus exsolution from

hexagonal pyrrhotite at 142°C (Naldrett 2000b). The paragenetic sequence for the Ovoid is summarized in Table 3.4.

Table 3.4. Crystallization sequence of the Voisey's Bay massive sulfide Ovoid deposit.

Temperature	Mineral	Reference
1200°C	Phases all liquid	Naldrett (2004)
1010-1050°C (solidus for Ni, Cu poor system)	Liquidus MSS	Naldrett (2004)
>900°C? (depends on pyrrhotite composition and fO_2)	Liquidus magnetite	Naldrett (1969); Naldrett (2000b); Naldrett (2004)
880-960°C or 900-950°C	Liquidus ISS	Cabri and Laflamme (1976); Fleet and Pan (1994)
865°C	Liquidus pentlandite	Sugaki and Kitakaze (1998); Naldrett (2000b)
<550°C	Subsolidus chalcopyrite and cubanite exsolve from ISS	Cabri and Laflamme (1976)
500-610°C	Subsolidus reaction of heazlewoodite and MSS to form pentlandite	Naldrett (2000b); Kullerud (1963)
142°C	Subsolidus troilite exsolves from MSS	Naldrett (2004)

3.5.2.3 Mechanical processes

There are also physical constraints on crystallization of sulfides. The sulfide melt will either crystallize *in situ* or be transported before crystallization (e.g., injected into faults or breccias or weaknesses in the footwall). Sulfides can also be transported or disrupted during various stages of crystallization by new influxes of magma in a dynamic system, by gravity settling in chambers, or by capillary filtration.

During early stages of MSS crystallization, the MSS cumulates are denser than the liquid and may sink (Czamanske *et al.*, 1992; Ebel and Naldrett, 1997). However, as fractionated sulfide liquids become more Cu-rich the viscosities and surface tensions

decrease and densities and metal diffusivities increase (Ebel and Naldrett, 1997). This enrichment of metal in the liquid has caused some to propose that at some point the liquid is denser than the MSS and that the MSS may float (Ebel and Naldrett, 1997). As the metal-rich liquids sink by percolating through the MSS, remelting or zone refining of the sulfide can occur (Lesher and Golightly, 2001a and 2001b).

Another result of lower viscosities of more Cu-rich liquids is the ability to infiltrate smaller cracks (Ebel and Naldrett, 1997). Mungall *et al.* (2005) indicated that there may be a critical point where Cu-rich residual liquid is lost from MSS cumulates. It has been proposed that at this stage in some deposits the dense Cu-(PPGE) liquid can be drawn into fractured, less dense footwall rocks (i.e., SE Extension Dyke; Chapter 4 and Huminicki *et al.*, 2008).

It has also been shown in Chapter 2 (Fig. 2.5) that Pt and Pb correlate with each other increasing toward the center (as would be expected with fractionation from the margins inward). However, both Pt and Pb are significantly depleted in the very central portion relative to the remainder of the Ovoid (possibly due to escape of this fractionated liquid).

Others have invoked other possibilities than primary crystallization processes (equilibrium, fractional, and partial fractional crystallization) and R factor (Campbell and Naldrett, 1979) for explaining the zonation of sulfide deposits such as separation of sulfide into two immiscible liquids (Ballhaus, 1999; Golightly and Lesher, 1999; Ballhaus *et al.*, 2001; Lesher and Golightly, 2001a and 2001b; Beswick, 2002); filtration mechanisms (Lesher and Golightly, 2001a); zone refining (Lesher and Golightly, 2001a

and 2001b); hydrothermal deposition of sulfides (Fleet, 1977); and metamorphic replacement (Fleet *et al.*, 1993; Fleet, 1996). It should be noted that all of these processes are not mutually exclusive and all may have occurred at some scale or to some degree but the question is what is considered the primary process that caused the metal zonation or metal distributions. Although the authors are aware of these other processes, evidence discussed below (see Section 3.5.5.5 - Preferred Model, for a summary) suggests that primary crystallization processes and R factor processes are of the most significant importance in explaining metal distribution at Voisey's Bay and are the main focus of this paper.

3.5.3 Spatial variations in sulfide mineralogy in the Ovoid

All massive ore in the Ovoid deposit consists of pyrrhotite (± troilite), pentlandite, chalcopyrite (± cubanite), and magnetite and how these minerals are distributed will effect the metal zonation within a deposit. The abundance of these major phases varies both laterally and vertically throughout the Ovoid deposit resulting in mineralogical zonations based on the proportions of minerals present. A method for the determinations of the mineral abundances using whole rock data is explained in detail in Huminicki *et al.*, (in review) and Chapter 2 of this thesis. Verification of the mineral modes by Mineral Liberation Analysis (MLA was subsequently carried out and is also discussed in detail in Huminicki *et al.* (in review) and Chapter 2.

The distributions of pyrrhotite (± troilite), magnetite, chalcopyrite (± cubanite), and pentlandite are rendered in three dimensions in plan view cross sections of the Ovoid and Mini Ovoid (Figs. 3.3a-d). The sections start near the surface of the Ovoid and Mini Ovoid and go to the base at 20m intervals.

Pyrrhotite ranges in the Ovoid massive sulfide from 50-90%. In general, the Ovoid is zoned in pyrrhotite with the margins (particularly the north margin) and the base being most pyrrhotite-rich (70-90%) with the center (to south of center) containing the least pyrrhotite (50-65%). Toward the top of the Ovoid, the low pyrrhotite center shifts to the south. The Mini Ovoid is generally higher in pyrrhotite (65-90%).

Magnetite ranges from <5% to 35% with its highest concentration (>20%) in the center and lowest concentration (5-10% and <5%) at the peripheries and at depth at the expense of pyrrhotite mostly. At further depth the high magnetite zone (15-20%) trends NW-SE across the deposit and at the base of the Ovoid, there is overall lower magnetite (5-10%). The Mini Ovoid is generally low in magnetite (5-10%).

Chalcopyrite for the most part coincides with increasing magnetite in the south center and center (9-17%) and decreases (<5% to 5-6%) at the margins (particularly the north margin). The Ovoid has two chalcopyrite-rich lobes one to the south center and one in the northeast center. Higher up sequence in the Ovoid, higher chalcopyrite zones correspond to higher magnetite zones. The Mini Ovoid is generally 7-9% in the center and 6-7% at the peripheries.

Pentlandite in the Ovoid is less variable than other minerals and is generally between 10.5-13.5%. Pentlandite coincides with increased pyrrhotite at the peripheries

higher up in section but decreases with depth. The Mini Ovoid contains 7.5-11.5% pentlandite and is generally more abundant in the center.

The spatial distributions of the minerals are consistent with the fractional crystallization of MSS (i.e., pyrrhotite) then magnetite followed by ISS (i.e., chalcopyrite) with cooling and crystallization from the margins inward (i.e., pyrrhotite-rich at the margins and the base increasing to magnetite- and chalcopyrite-rich toward the center). The spatial distributions are consistent with magnetite coming on the liquidus after MSS and either proceeding or coinciding with ISS crystallization. As discussed above, pentlandite can form as a liquidus phase after ISS or pentlandite can exsolve later from MSS as a subsolidus phase.

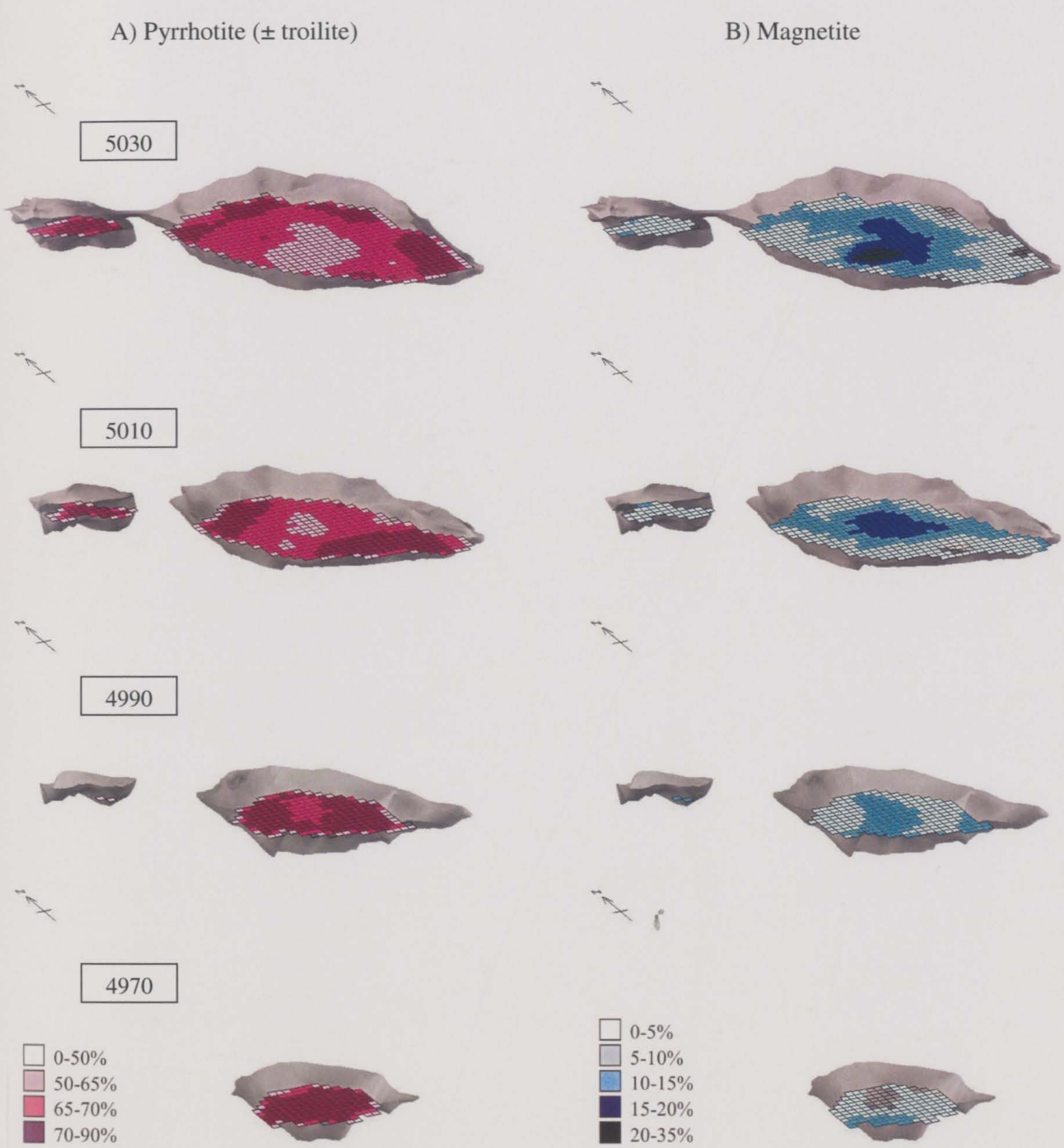
A) Pyrrhotite (± troilite)
B) Magnetite
5030
5010
4990
4970
0-50%
50-65%
65-70%
70-90%
0-5%
5-10%
10-15%
15-20%
20-35%

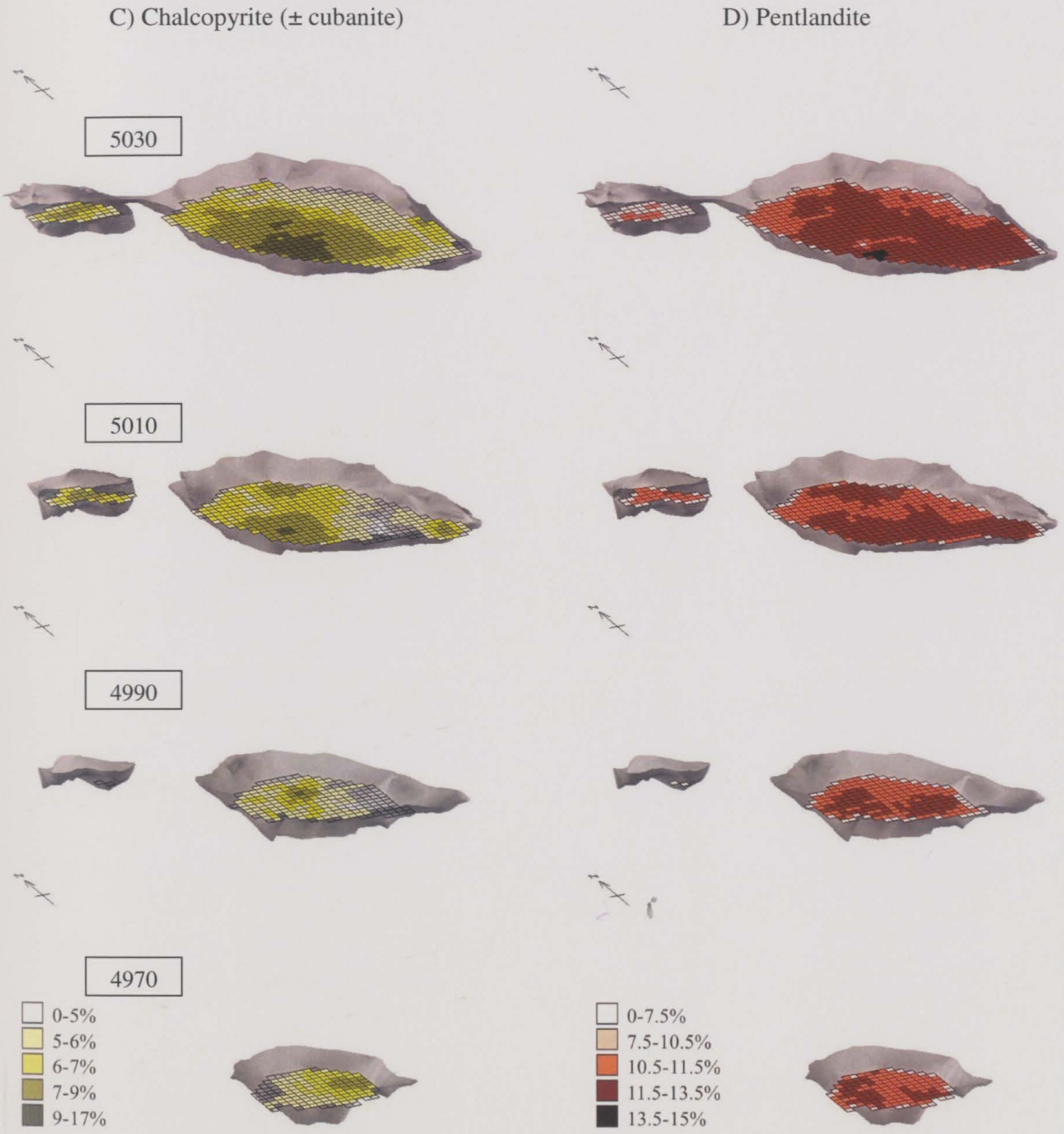

Figure 3.3. Three-dimensional mineralogical zonations of: a) pyrrhotite (± troilite), b) magnetite, c) chalcopyrite (± cubanite), and d) pentlandite in the Ovoid and Mini Ovoid shown at 20m intervals indicated by section number in the top left; this number refers to a local datum in meters. The grey shading indicates the envelope of massive sulfide.

3.5.4 Mineral Domains in the Ovoid

Ore classifications are primarily based on mineralogical abundances (Table 3.5). The abundances of the four major minerals (pyrrhotite ± troilite, pentlandite, chalcopyrite ± cubanite, and magnetite) define three different mineral domains (Huminicki *et al.*, (in review) and Chapter 2 of this thesis), which are outlined in Table 3.5. All ore zones contain trace (<0.05 wt%) amounts of sphalerite and galena. Concentrations of Zn correlate to chalcopyrite-rich zones and Pt and Pb show a marked decrease in the very central zone of the Ovoid. The correlation of Zn and chalcopyrite is due to the presence of sphalerite exsolution "stars" in the chalcopyrite. The Pt and Pb depletion is thought to indicate escape of late stage enriched sulfide liquid from the Ovoid center to its surroundings.

Table 3.5. Mineral domains based on mineral abundances (Ovoid and Mini Ovoid).

Mineral	TYPE I	TYPE II	TYPE III
Pyrrhotite	50-65%	60-75%	70-90%
Magnetite	15-35%	5-15%	0-15%
Chalcopyrite	5-9%	>9%	1-6%
Pentlandite	10.5-11.5%	11.5-13.5%	10.5-11.5%

Figure 3.4 shows the distribution of the three mineral domains in a cross sectional view through the center portion of the Ovoid. TYPE I ore generally occurs in the center of the Ovoid deposit and decreases with depth, TYPE II ore generally occurs between TYPE I and III ores, and TYPE III ore occurs at the outer peripheries (mostly the north and southeast margins) and at the base of the Ovoid. The Mini Ovoid mostly consists of TYPE II (at the peripheries) and TYPE III ore (in the center).

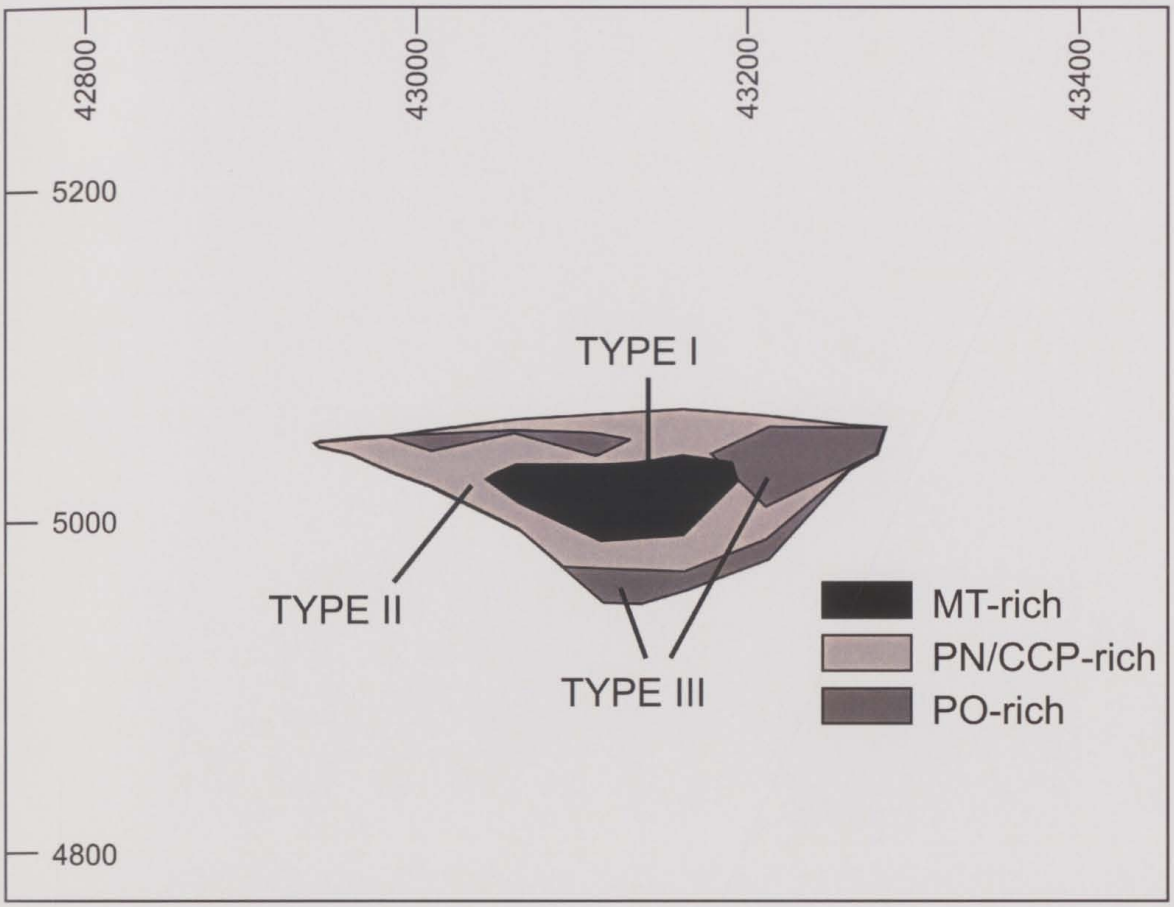

Figure 3.4. Composite of three mineral domains in west-facing cross sectional view (55885) of the Ovoid.

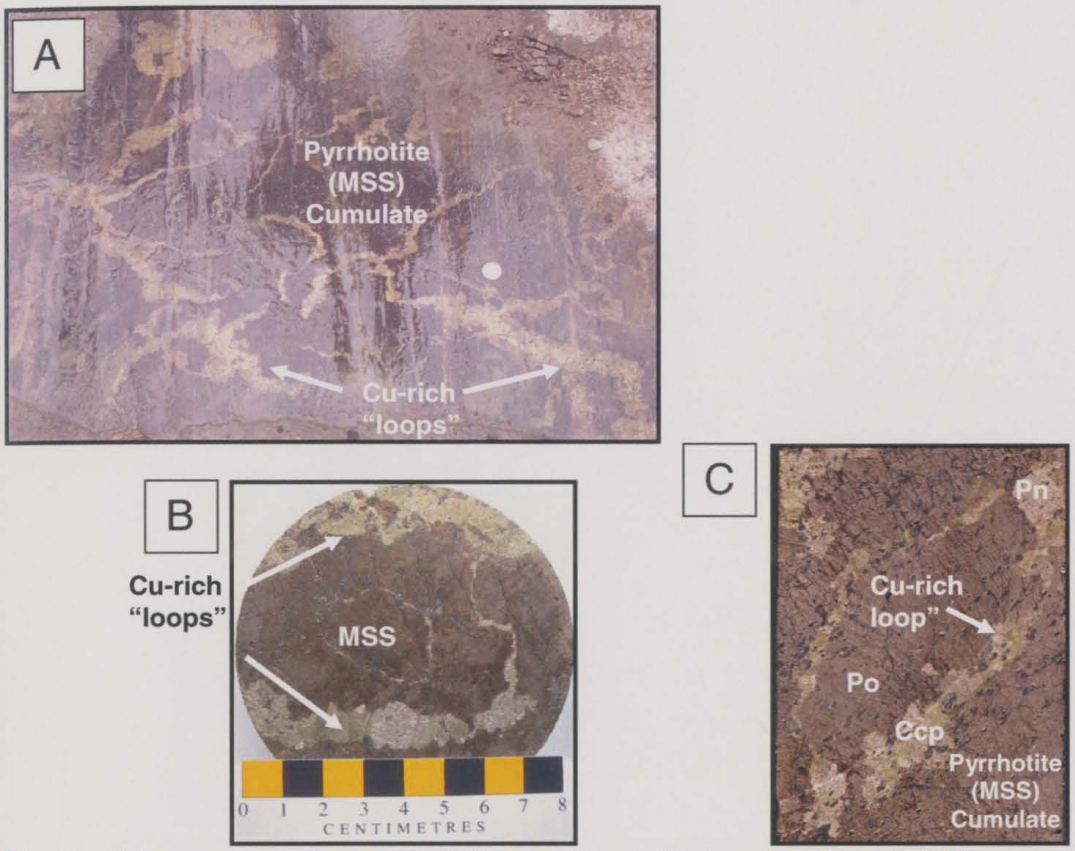

Error! Objects cannot be created from editing field codes. Error! Objects cannot be created from editing field codes.

Figure 3.5. a) Surface of the Voisey's Bay Ovoid deposit after overburden was removed prior to open-pit mining. The darker portions consist primarily of pyrrhotite (i.e., MSS cu te) and the lighter portions consist primarily of chalcopyrite (± pentlandite) as in ial "loops" (i.e., ISS liquid); looney for scale. b) "loops" in drill core sample BS0256 36.0m illustrating that the interstitial ISS liquid forms closed loops and in three-dimensions can actually form an interstitial network to MSS analogous to soap bubbles. c) "loops" in drill core sample BS0233 73.55m; width of core = 8cm. d) fine-grained magnetite in drill core sample VB95011 20. (margins of deposit). e) coarse-grained magnetite in drill core sample VB95011 55.2 (center of deposit). Po = pyrrhotite; Ccp = chalcopyrite; Pn = pentlandite.

3.5.5 Quantitative Modeling and Differentiation of the Ovoid

3.5.5.1 Significance of sampling in interpreting compositional variations of ores

Before any assumptions can be made about crystallization processes, there must be a clear understanding of what the whole-rock data represent. The following illustrates the point that knowing what the bulk data represent is crucial in interpreting the validity of any crystallization models. Here, the effects of the sampling scale and the material sampled are discussed. In the Voisey's Bay Ovoid, the deposit is sampled at 1-m intervals in the Mine Exploration Borehole System (MEBS) database. However, a smaller subset of samples were analyzed at MUN which represent samples that are <30cm. The effect of these two sampling scales is shown in Figure 3.6a. The MEBS 1-m interval samples have a much more limited compositional range (i.e., Ni[100] from 2.0-7.2 wt% and Cu[100] from 0.23-10.36 wt%) than the smaller (<30cm) MUN sample scale (i.e., Ni[100] from 1.57-7.58 wt% and Cu[100] from 0.08-12.83 wt%). This is thought to be due to the fact that the majority of the Ovoid contains cumulates and trapped liquid (Fig. 3.5a-c). The more limited range in compositional data in the Ovoid MEBS data versus MUN data (Figs. 3.6a) is the result of sampling at a larger scale where a combination of the compositions of liquids (Cu-rich "loops") and cumulates (pyrrhotite) are more representative of averages than of end member phase compositions. At a larger sample scale, both cumulates and liquids are sampled together effectively homogenizing the composition, whereas a smaller sample scale will sample cumulates and liquids separately effectively increasing the compositional range. Therefore a finer sample scale may be required to represent the liquid (i.e., Cu-rich "loops") and the cumulates separately and thus observe the entire range in compositions. Therefore, the lack of spread in the MEBS data may be a sampling artifact and at the 1-m sampling scale the

Cu-rich "loops" are being averaged into the MSS cumulates (Fig. 3.5a-c). Compositional data of Voisey's Bay massive sulfide at the MEBS 1-m sample interval has a much more limited compositional range than the full compositional range relevant to magmatic sulfide ores of Cu[100] from 0-32 wt% and Ni[100] from 0-15 wt% (Ebel and Naldrett, 1996). But when sampled at a smaller scale (MUN <30cm samples), the data are closer to the full range of magmatic sulfides. However, one should note that sampling at too fine of a scale may have the opposite effect, that is of unmixing cumulates or liquids into the constituent minerals that crystallized from each. Thus the sample may represent only portions of the cumulate or only portions of the liquid. In light of this argument the most appropriate liquid and cumulate model curves may be those that fall in between the MEBS and MUN data sets.

The point about sampling scale can also be illustrated (and is important to recognize) when comparing different deposits. Figure 3.6b compares the Ovoid deposit data to the Lindsley and Craig deposits of Sudbury. If one was to use the larger sample scale (MEBS 1m data) for the Ovoid, one would conclude that the Ovoid is much more restricted in its compositional range than deposits from Sudbury. However, if one were to use the smaller sample scale (MUN <30cm data) for the Ovoid, one would conclude that the compositional range of the Ovoid is more comparable to deposits of Sudbury. For example, the Lindsley deposit (Sudbury) ranges from 0.24-25.9% Cu and 2.15-11.1% Ni and the Craig deposit (Sudbury) ranges from 0.7-22.0% Cu and 1.24-5.45% Ni, whereas the Ovoid deposit ranges only from 0.23-10.36% Cu and 2.0-7.2% Ni in the MEBS data. However, the MUN data exhibits a larger range in compositional data of 0.08-12.83% Cu

and 1.57-7.58% Ni. Note that the Sudbury deposits use a smaller sampling scale (<15cm) similar to the MUN data; the length of core sample was assumed using the volume of sample (0.5-1kg) reported for Lindsley and Craig deposits in Naldrett *et al.*, 1999).

The other important issue is not only what scale is being sampled but what material is being sampled. This is illustrated by Figure 3.6c, which shows the effect of sampling disseminated sulfide versus massive sulfide material. Although both are normalized to 100% sulfide, it is clear that the disseminated mineralization has higher metal tenors than massive ores. This should be considered when modeling crystallization processes and interpreting the results.

Another example of recognizing what material is being sampled is illustrated in Figure 3.6d. The three mineral domains in the Ovoid deposit are broken out on the compositional diagram and we can clearly see that the samples plot in different locations based on whether they are TYPE I, II, or III ores. Again, this should be considered when modeling crystallization processes and interpreting the results.

3.5.5.2 Crystallization models

Fractional crystallization is commonly used to model sulfide crystallization (e.g., Naldrett *et al.*, 1994). Perfect fractional crystallization or *Raleigh fractionation* (Fig.

3.7b) is an end-member process, where the crystallizing phases are continuously and completely removed from the magma, resulting in significant depletion of compatible elements, moderate enrichment of incompatible elements, and continuously zoned cumulus phases (Philpotts, 1990). Fractional crystallization can be described by the equations:

$$C_L = C_O F^{(D-1)} \ldots\ldots\ldots (1)$$

$$C_S = C_O DF^{(D-1)} \ldots\ldots\ldots (2)$$

However, it has been proposed that equilibrium crystallization is more realistic than FC, especially for sulfides, which re-equilibrate rapidly at magmatic temperatures (Mungall *et al.*, 2005). Equilibrium crystallization is also an end-member process in which equilibrium is maintained for an element between the crystallizing phase and the liquid (Fig. 3.7a), resulting in moderate depletion of compatible elements, moderate enrichment of incompatible elements, and unzoned cumulus phases (Philpotts, 1990). Equilibrium crystallization can be described by the equations:

$$C_L = C_O/[F+D(1-F)] \ldots\ldots\ldots (3)$$

$$C_S = C_O*D/[F+D(1-F)] \ldots\ldots\ldots (4)$$

Although fractional and equilibrium crystallization have been used to model sulfide deposits, it has been proposed that fractional crystallization is not physically realistic in most systems, as residual liquids are commonly trapped in the cumulates (Lesher, 1998). Fractional and equilibrium crystallization are also end member models,

where a model somewhere in between may be more appropriate. A model that addresses trapped liquid is partial fractional crystallization (PFC).

Partial fractional crystallization involves removal of crystallizing phases but invokes some trapped liquid from the magma with the cumulates (Fig. 3.7c), resulting in less depletion of compatible elements, less enrichment of incompatible elements, and less-zoned cumulus phases relative to FC (Lesher, 1998). Partial fractional crystallization can be described by the equations:

$$C_L = C_O F^{(D-1)(1-p)} \quad \text{.....(5)}$$

$$C_S = C_O D F^{(D-1)(1-p)} \quad \text{.....(6)}$$

C_O = initial liquid concentrations, C_L = final liquid concentrations, C_S = final solid concentrations, D = solid-liquid partition coefficient, F = fraction of liquid remaining, p = fraction of trapped liquid.

The numerical modeling of crystallization processes can be carried out using experimental partition coefficients (D values) for the metals and initial sulfide liquid starting compositions. In order to model the various crystallization processes we must first assume appropriate metal partition coefficients and initial starting compositions. It is felt a discussion is warranted here on choice of D values and initial starting compositions since these two assumptions will affect the outcome of the modeling scenarios.

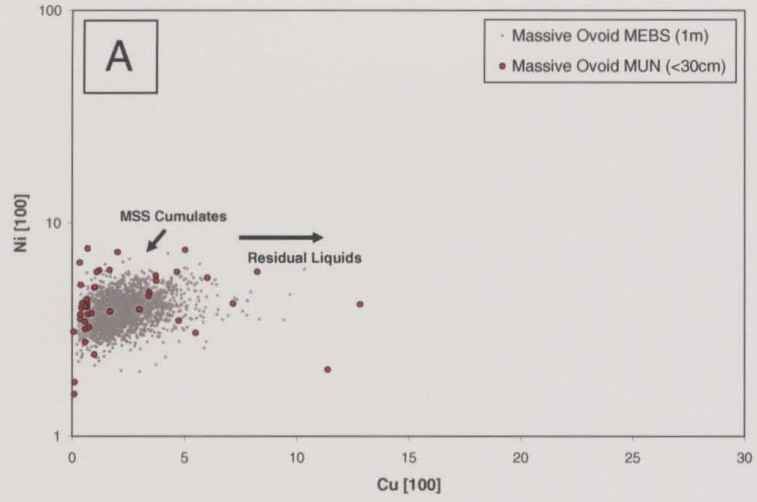
A
Massive Ovoid MEBS (1m)
Massive Ovoid MUN (<30cm)
MSS Cumulates
Residual Liquids
Ni [100]
Cu [100]
100
10
1
0
5
10
15
20
25
30

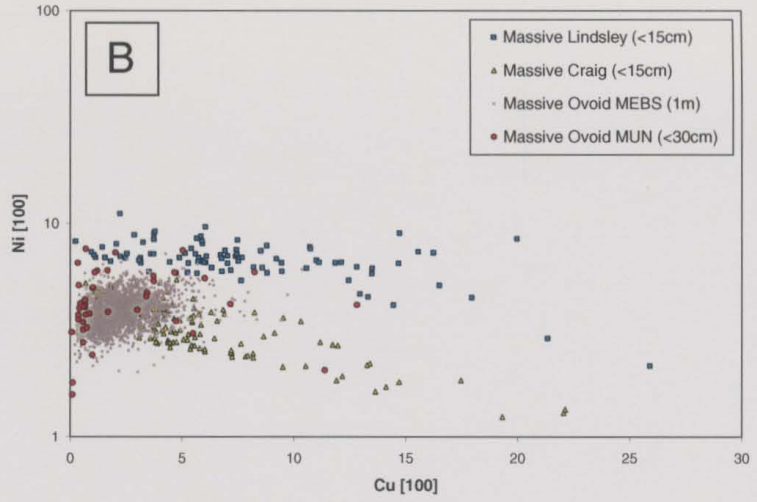
B
Massive Lindsley (<15cm)
Massive Craig (<15cm)
Massive Ovoid MEBS (1m)
Massive Ovoid MUN (<30cm)
Ni [100]
Cu [100]
100
10
1
0
5
10
15
20
25
30

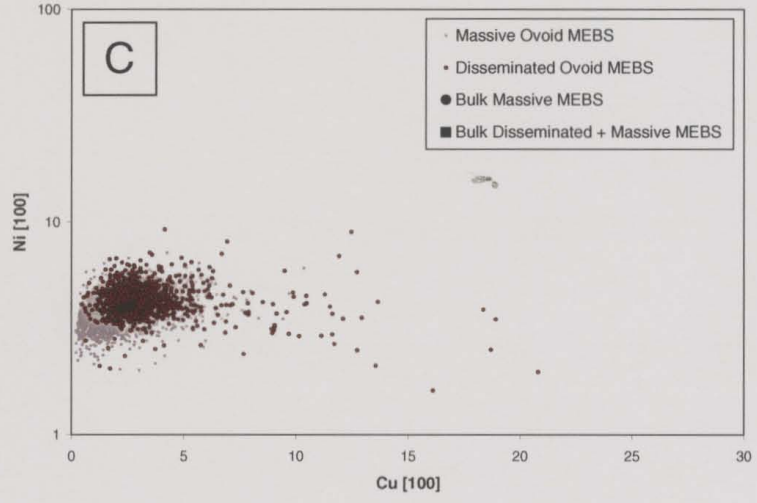
C
Massive Ovoid MEBS
Disseminated Ovoid MEBS
Bulk Massive MEBS
Bulk Disseminated + Massive MEBS
Ni [100]
Cu [100]
100
10
1
0
5
10
15
20
25
30

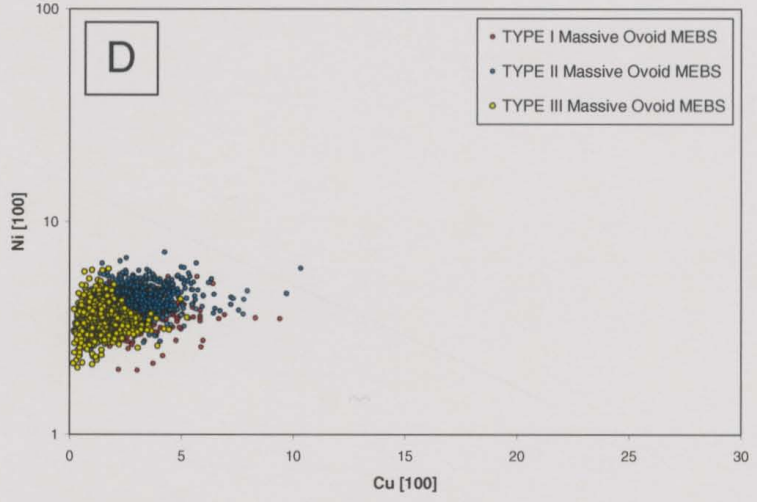
D
TYPE I Massive Ovoid MEBS
TYPE II Massive Ovoid MEBS
TYPE III Massive Ovoid MEBS
Ni [100]
Cu [100]
100
10
1
0
5
10
15
20
25
30

Figure 3.6. Cu[100] versus Ni[100] showing: a) data from massive Ovoid samples using 1m sample scale (MEBS database) and using <30cm sample scale (MUN data). Note that the finer sample scale (<30cm) exhibits a greater range in composition, whereas the coarser sample scale (1m) exhibits a more restricted range in compositions. The finer (MUN) samples are thought to be a result of sampling cumulates and liquid separately, whereas the coarser sample scale (MEBS) is thought to be sampling a mixture of both cumulates and liquids together. Using a smaller sampling scale, produces a larger compositional range for the Ovoid massive sulfide, b) data from the Lindsley and Craig massive deposits from Sudbury, Ontario for comparison to the massive Ovoid samples indicating a larger range in compositions than the MEBS data but a similar range to the MUN data range for the Ovoid (sample scale is <15cm for Lindsley and Craig calculated from Naldrett *et al.*, 1999), c) data for massive and disseminated Ovoid samples from the MEBS database (1m) indicating the bulk composition of the massive sulfide and the bulk composition of the disseminated plus massive sulfide. Note that disseminated samples are shifted to higher Cu[100] values than massive samples, which shifts the bulk composition to higher Cu[100] concentrations, d) data from the massive sulfide Ovoid deposit dividing the ores into three mineral domains using MEBS data (1m). MUN = Memorial University of Newfoundland; MEBS = Mine Exploration Borehole System (data courtesy of Voisey's Bay Nickel Company Limited).

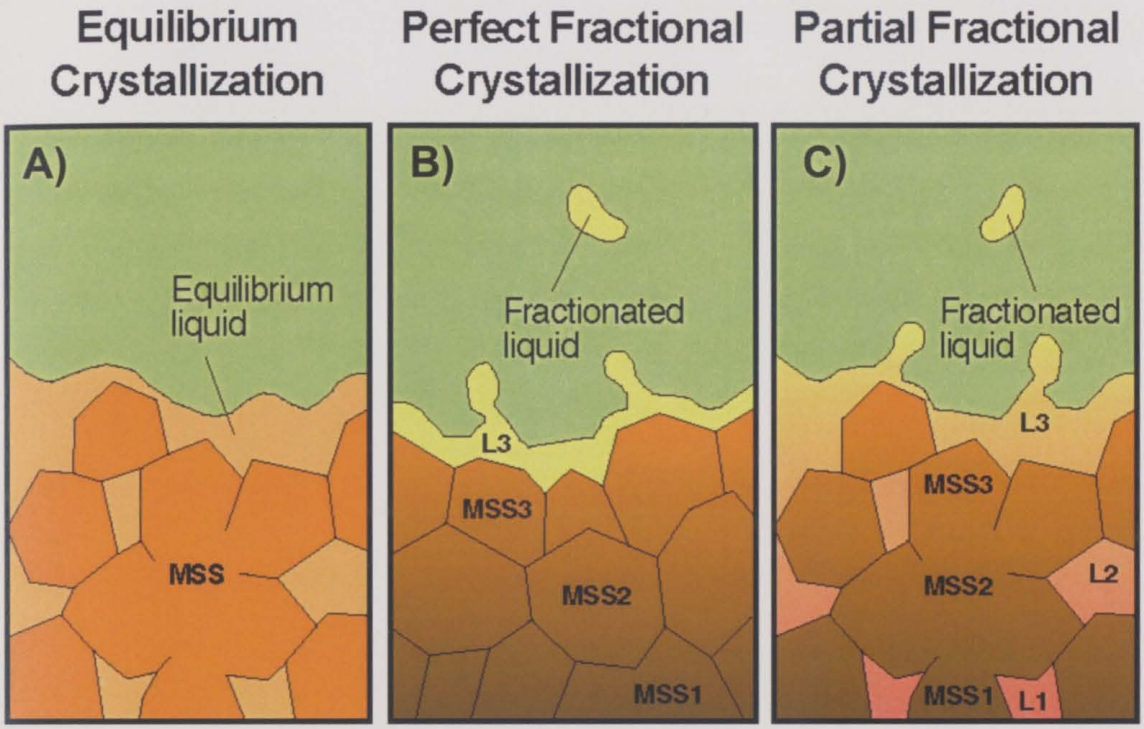

Figure 3.7. Schematic diagram illustrating components of: a) equilibrium crystallization, b) perfect fractional crystallization, and c) partial fractional crystallization. MSS = monosulfide solid solution and L = liquid. From Lesher and Golightly (in prep).

3.5.5.3 Assumptions for modeling

D values

The partition co-efficient ($D_{i(MSS\text{-}liquid)}$) is the concentration of element (i) in monosulfide solid solution (MSS) divided by the concentration in co-existing sulfide liquid. Where D is >1 for a given element, the element is compatible in the solid MSS phase upon crystallization. Where D is <1 for a given element, the element is incompatible and therefore concentrated in the liquid.

It has been shown that D_{Ni} and D_{Cu} are sensitive to temperature, sulfur fugacity, oxygen fugacity, the Cu content of the liquid, and metal/S ratio (Fleet and Pan, 1994; Ebel and Naldrett, 1996; Ebel and Naldrett, 1997; Barnes *et al.*, 1997; Ballhaus *et al.*, 2001; Naldrett, 2004; Mungall *et al.*, 2005). Table 3.6 lists the range of D_{Ni} and D_{Cu} values at various conditions. Nickel behaves mostly incompatibly in crystallizing MSS but also has strong fS_2 and temperature dependence becoming increasingly compatible to the point that D_{Ni} >1 at very high S-contents and very low temperatures close to the solidus of natural sulfide magmas (Ballhaus *et al.*, 2001; Mungall *et al.*, 2005 and references therein). However, the exact point at which D_{Ni} becomes compatible and how high D_{Ni} reaches is still debatable. D_{Ni} increases with decreasing temperature, decreasing sulfur fugacity, increasing oxygen fugacity, increasing Cu content in the liquid, and decreasing metal/S (Ebel and Naldrett, 1996; 1997).

The attractive thing about the Mungall *et al.* (2005) data is that the study has equilibrated oxygen-bearing sulfide liquid with MSS at known fO_2 and fS_2 (their experiments use Fe-Ni-Cu-S-O-PGE) and the results are comparable to previous studies. The significance of using the system with oxygen is that oxygen is a major element in natural sulfide liquids some of which contain several weight percent oxygen and most of which magnetite can crystallize as a liquidus phase (Mungall, 2005). This is thought to be the case at Voisey's Bay (Naldrett, 2000b). Fleet and Pan (1994) also implied that oxide minerals can hypothetically be interpreted as representing oxygen dissolved in the sulfide melt as opposed to alteration products.

In this study, we assumed that D_{Ni} increases incrementally from 0.6 at the start of crystallization to 1.0 at 65% crystallization, and to 1.2 in the final stages of crystallization. These D_{Ni} values are intermediate between those of the "MS-11" experiment of Ballhaus *et al.* (2001), which had a metal/S ratio (1.03, Table 3.7) similar that calculated here for the massive sulfide Ovoid deposit (1.06), and the D_{Ni} values of Naldrett (2004), which are based on a large range in Cu content in the liquid (<2 to 20 wt%), similar to what is observed in the Ovoid. The D_{Ni} values used here are also consistent with Barnes *et al.* (1997) for a S-oversaturated system and are consistent with the extrapolation of Mungall *et al.* (2005) data to slightly higher and lower temperatures. In summary, the values chosen here are consistent with the data for an oxidized system (Mungall *et al.*, 2005), the metal/S ratios (Ballhaus *et al.*, 2001), and Cu content (Naldrett, 2004) appropriate for the Ovoid.

One of the discrepancies with D_{Cu} is whether it varies and this point is less clear in the literature than for D_{Ni}. Many use D_{Cu} as a constant (Ballhaus *et al.*, 2001; Mungall *et al.*, 2005), however, it has been shown that D_{Cu} decreases with decreasing temperature, decreasing sulfur fugacity, and increasing Cu content in the liquid (Ebel and Naldrett, 1996 and 1997). The main point though, is that Cu may have a range in D values but unlike Ni, D values for Cu are always <1 (i.e., incompatible in the MSS solid). Here, we model crystallization using a range in D_{Cu} from ~0.28 to ~0.16 based on a range in Cu content in the liquid from <2 to 20 wt% (Naldrett, 2004). Extrapolating D_{Cu} data from Mungall *et al.* (2005) to slightly higher and slightly lower temperatures produce values that are virtually identical values to those of Naldrett (2004).

Table 3.6. Experimental partition coefficients (D) for Ni and Cu in MSS-sulfide liquid.

D_{Ni}	D_{Cu}	Conditions	Reference
0.23		S-undersaturated	Fleet and Stone (1991)
0.84	0.27	S-saturation	Fleet *et al.* (1993)
0.19-1.17	0.27-0.17	54-50.5 atomic % S	Li *et al.* (1996)
0.18-0.36	0.2-0.17	S-undersaturated	Barnes *et al.* (1997)
0.36-0.8	0.25-0.2	S-saturation	Barnes *et al.* (1997)
0.7-1.2	0.27-0.22	S-oversaturated	Barnes *et al.* (1997)
0.6-1.4	0.2	1100-900°C; metal/S = 1.03	MS-11 from Ballhaus *et al.* (2001)
0.66-0.94	0.22-0.15	1050-950°C; Pt-PtS; FMQ	Mungall *et al.* (2005)
0.2-2.0	0.2	Values used for modeling	Mungall *et al.* (2005) and pers. comm.
0.6-1.0	0.28-0.16	<2 to 20% Cu in liquid	Naldrett (2004)*

*Naldrett (2004) contains data compiled from Ebel and Naldrett (1996), Ebel and Naldrett (1997), and Fleet and Pan (1994).

Table 3.7. Parameters used for the Voisey's Bay sulfide ore.

Parameter		Reference
Average atomic metal/S	1.06	This study
Average atomic % S of Ovoid	48.5%	This study
Average bulk composition of massive Ovoid; Cu and Ni are normalized to 100% sulfide plus magnetite	Fe = 55.38 wt%, S = 32.98 wt%, Cu[100] = 2.24 wt%, Ni[100] = 3.89 wt%	This study
Average bulk composition of disseminated plus massive Ovoid; Cu and Ni are normalized to 100% sulfide	Cu[100] = 2.62 wt%, Ni[100] = 34.03 wt%	This study
Approximate liquidus (based on metal/S of the ore)	1110 ± 10°C	MS-11 from Ballhaus *et al.* (2001)
Approximate solidus (based on metal/S of the ore)	890 ± 20°C	MS-11 from Ballhaus *et al.* (2001)
D values	D_{Ni} = 0.6-1.2; D_{Cu} = 0.28-0.16	Ballhaus *et al.* (2001); Naldrett (2004)

Initial compositions (open versus closed system and missing material)

The simplest assumption is that the observed bulk sulfide composition represents the initial starting composition for modeling. This would assume that the final and initial bulk compositions are the same. This would require a closed system where no material

has been gained or lost. However, it is a topic of much discussion in modeling sulfide systems if material has been lost, whether due to an open system during crystallization or possibly by late hydrothermal/metamorphic remobilization or perhaps even erosion (i.e., in the case of the Ovoid where glacial striations are present at the top surface of the ore body) and therefore it is difficult to ascertain the initial starting composition.

We started by using two different observed, initial starting compositions for the sulfides: 1) the bulk composition of the massive Ovoid (i.e., Cu[100] = 2.24 wt% and Ni[100] = 3.89 wt%; Table 3.1) (MODEL I), and 2) the bulk composition of the massive plus the disseminated sulfide in the Ovoid deposit (i.e., Cu[100] = 2.62 wt% and Ni[100] = 4.03 wt%; Table 3.1) (MODEL II). If the first assumption is correct then the massive sulfide would have formed as a closed system cut off and unrelated to the disseminated sulfides. If the second assumption is correct then the massive sulfide would be related to the disseminated sulfide, where the system was "open" enough to infiltrate the surrounding silicate producing disseminated sulfide but would infer that no material moved beyond that to other areas of the system not yet identified by advanced exploration. Figure 3.6c illustrates that initial starting composition using bulk massive ore has a different initial starting composition than using bulk massive plus disseminated compositions.

The Ovoid is a near surface body and significant amounts of the deposit may be missing due to erosion. Therefore, we also attempt to model the crystallization history of a pre-erosion deposit (MODEL III) assuming a hypothetical initial composition (see below).

3.5.5.4 Modeling crystallization processes

Each type of crystallization (equilibrium, fractional, and partial fractional crystallization) were modeled for Cu and Ni compositions using incremental amounts of crystallized liquids and compared to data from the Voisey's Bay Ovoid deposit (Figs.3.8-3.10). Each increment on the model curves represent 10% crystallization (from right to left as shown in Fig. 3.9a). For partial fractional crystallization, the fractions of trapped liquid (p) modeled were 0.3 and 0.4 or 30% and 40%, respectively. The model curves are compared to both MUN (<30cm) samples and MEBS (1m) samples as it is thought that a combination of these data represent cumulates and liquids best.

The modal compositions were calculated using the batch equilibrium equation of Campbell and Naldrett (1979). The various crystallization processes were tested using the chosen D values from above sections. It should be noted that if D_{Ni} is constant and close to 1, there is not much variation in the Ni, if D_{Ni} is constant and <1 the model curve for the liquid will continue to increase in Ni since Ni is incompatible in the MSS at these conditions, and if D_{Ni} is constant and >1 the model curve for the liquid will continue to decrease in Ni since Ni is compatible in the MSS at these conditions. As discussed in earlier sections, it is thought that D_{Ni} crosses over from <1 to >1 at 65% crystallization. This will produce an inflection in the model curve where the range in Ni will depend on the range in D_{Ni} (i.e., increase in D_{Ni} range will increase the range in Ni compositions) and the point and degree of inflection of Ni concentrations depends on the cross over when Ni becomes compatible in MSS (i.e., when D_{Ni} >1). D_{Cu} does not go above 1 (i.e.,

it is always incompatible in the MSS and remains in the liquid) and therefore Cu concentration will only increase in the liquid during crystallization.

In modeling of crystallization processes, the D_{Cu} will affect the extent of the residual liquid model curve along the Cu[100] axis, which represents the degree of crystallization that has taken place. A lower D_{Cu} value will produce a curve that has more Cu enrichment in the residual liquid and varying D_{Cu} during crystallization will vary the length of the liquid curve. If the model curve extends past the data this suggests that some of the material is missing from the system. If the model curve falls short of fitting the sample data for more enriched Cu compositions, this indicates that the model is not likely to be correct.

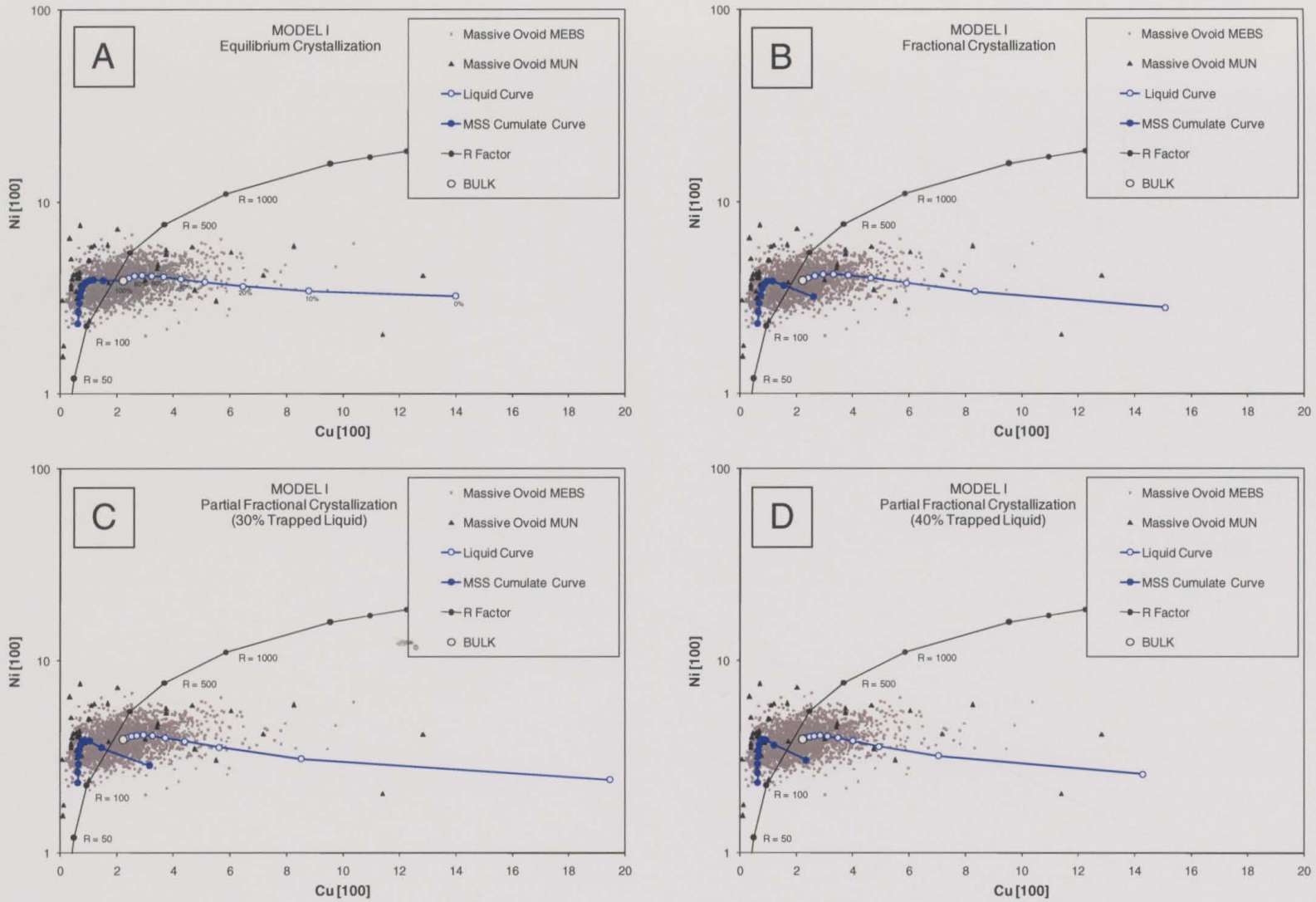

Figure 3.8. a) Equilibrium, b) fractional, c) 30% partial fractional, d) 40% partial fractional crystallization for MODEL I.

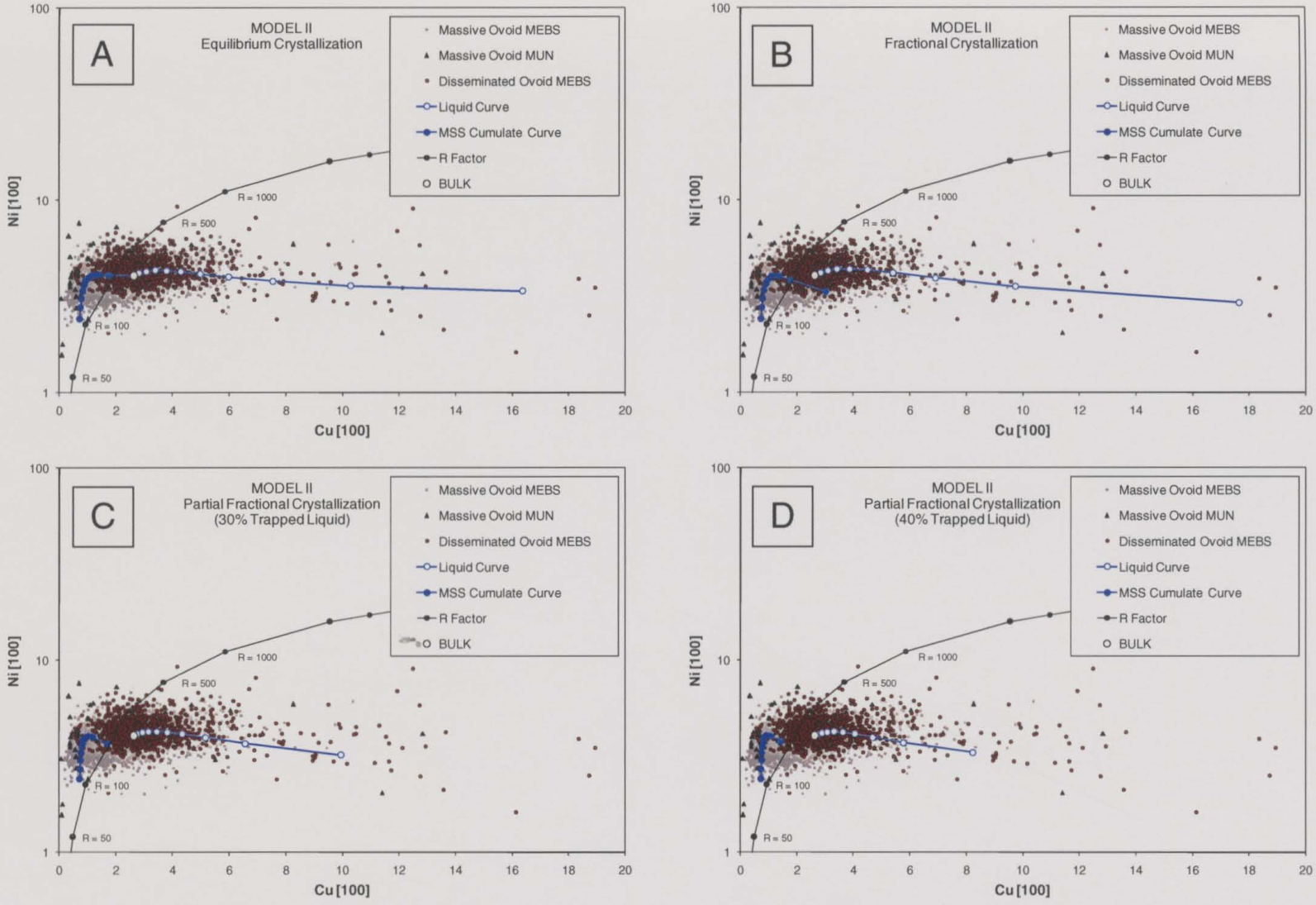

Figure 3.9. a) Equilibrium, b) fractional, c) 30% partial fractional, d) 10% partial fractional crystallization for MODEL II.

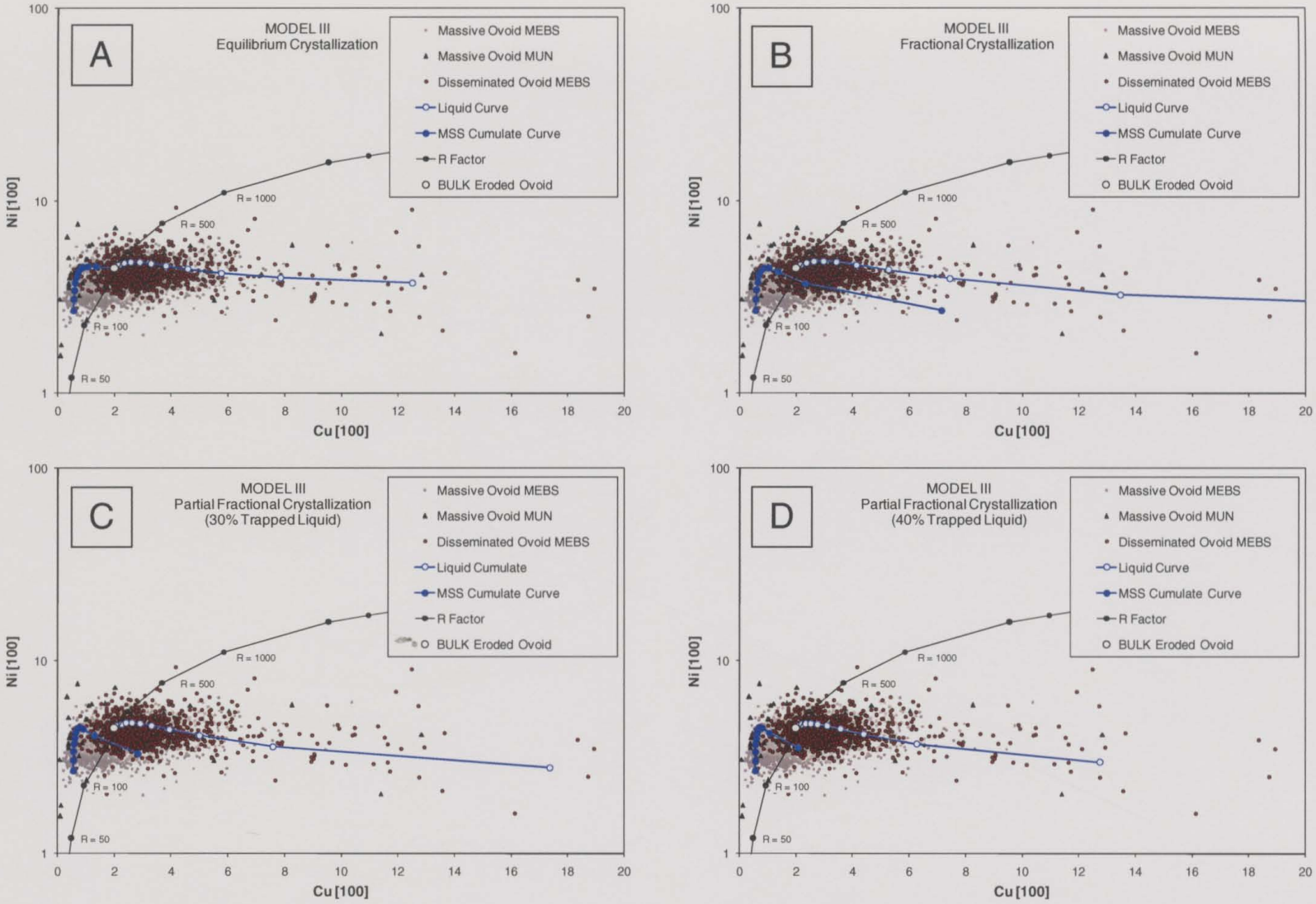

Figure 3.10. a) Equilibrium, b) fractional, c) 30% partial fractional, d) 40% partial fractional crystallization for MODEL III.

MODEL I: Massive sulfide (closed system)

MODEL I starts by accounting for massive sulfide only and does not include disseminated sulfide for the system. This model uses the bulk MEBS for massive sulfide as the initial starting composition, which assumes that there was no material gained or lost (i.e., closed system). Equilibrium, fractional, and partial fractional crystallization model curves for MODEL I are shown in Figure 3.8. The model curves are compared to massive sulfide data from both the MUN (<30cm) sample set and the MEBS (1m) sample set.

The residual liquid model curve for equilibrium crystallization (Fig. 3.8a) extends through the majority of the data in the x-direction (i.e., Cu[100]). However, there are very few data points that correspond to model liquids that formed between 85 to 100% crystallization (15 to 0% residual liquid), suggesting that such liquids are largely missing from the system. This is inconsistent with the closed-system assumption of the model since the system would have to be open to lose material. The same problem exists for the model curves for fractional crystallization (Fig. 3.8b) and partial fractional crystallization (Figs. 3.8c,d). Another issue with these models is that the curves for both cumulates and residual liquids tend to plot at lower Ni tenors than do many of the observed compositions.

MODEL II: Massive and disseminated sulfide (partially open system)

MODEL II is invoked to take into account the disseminated sulfide that surrounds the Ovoid massive sulfide. This assumes that the massive and disseminated sulfides are

related genetically and part of the same system; in this case, residual liquids in the massive ores would have escaped to the surrounding silicates. This model requires that the initial bulk composition includes the disseminated mineralization, which makes it slightly more Cu-rich compared to MODEL I (compare compositions in Fig. 3.6c). Equilibrium, fractional, and partial fractional crystallization model curves for MODEL II are shown in Figure 3.9.

The model curve for equilibrium crystallization is plotted in Figure 3.9a. However, if we are to consider the disseminated sulfide in the silicates to represent escaped liquids from the cumulates in the massive ore, there could not be complete chemical communication between crystal and liquids, which is the definition of equilibrium crystallization. Thus this model need not be considered.

The model curves for fractional crystallization and partial fractional crystallization are shown in Figs. 3.8b,c,d. Model curves for the residual liquid do not have the problem seen with MODEL I with regard to the paucity of observed Cu-compositions that could have formed after 85 to 100% crystallization. There are many disseminated ores that possess such Cu-rich compositions. In fact, for partial fractional crystallization, there cannot be more than about 10% trapped liquid or else many of the observed Cu-rich compositions are not accounted for by the model curves (compare Fig. 3.9c with Fig. 3.9d).

The problem with the MODEL II results is that, like MODEL I, the curves for compositions of residual liquids and cumulates tend to be Ni-poor compared to many observed Ovoid ores. For this reason, it is likely that the starting composition of the Ovoid sulfide was more Ni-rich than assumed in MODEL I and II. This could be explained by

missing material with slightly higher Ni[100] values, which would drive the initial starting composition to higher values. This is a plausible scenario as we know that the Ovoid deposit occurs near surface and some of must be missing due to erosion. This scenario is addressed in MODEL III below.

MODEL III: Massive and disseminated sulfide (eroded system)

The two previous models considered the observed bulk compositions of the massive ore (MODEL I) and the massive plus disseminated mineralization (MODEL II) as the starting compositions for modeling. Both models assumed no sulfide was lost from either the massive or disseminated systems. However, in order for a model curve to fit the data better we require a slightly higher initial composition for Ni than in the bulk compositions. Because of erosion some fraction of the original top of the Ovoid must have been removed from the system; the only question is whether what was removed was Ni-rich compared to what has remained.

One indication that what was lost may have been Ni-rich comes from the observed mineral zonation patterns of pentlandite in the Ovoid (Fig. 3.3d). This diagram indicates that the material closest to the present erosional surface is somewhat richer in pentlandite than what lies at depth (compare the pentlandite distribution for the 5030 level with those below in Fig. 3.3d). If we were to extrapolate these trends, at least qualitatively, we could assume that indeed the material missing was more Ni rich, thereby justifying using a higher initial Ni starting composition for modeling.

For MODEL III, we have assumed that the initial composition of the bulk sulfide was Ni[100] = 4.5 wt% and Cu[100] = 2 wt%. We have chosen this composition based on the trends of the modeled R-factor curves for the Voisey's ore system presented earlier in this paper; the composition is shown by a star in Fig. 3.2a. The rationale for this particular composition is that the observed sulfide compositions for the Ovoid and many of the other mineralized zones trend off to the high Cu side of the R-factor curves. We have argued here that this trend is the result of crystallization processes. The implication is that the initial composition of the Ovoid may have fallen on the R-factor curve, near its intersection with the low Cu end of the trend of the sulfide compositions (Fig. 3.2a). Assuming this starting composition and 50% of the Ovoid missing due to erosion, we can calculate the composition of the eroded ore must have been Ni[100] = 5.1 wt% and Cu[100] = 1.1 wt%.

The MODEL III curves for equilibrium crystallization are plotted in Figure 3.10a. As before however, if we are to consider the disseminated sulfide in the silicates to be part of the system, the definition of equilibrium crystallization does not allow for this model.

The MODEL III curves for fractional crystallization are shown in Fig. 3.10b. The fractional crystallization model for the MODEL III does not fit the data very well in two important ways. First there are very few compositions that match model residual liquids formed after 90% crystallization (10% residual liquid). Second, the corresponding cumulates formed between 90 and 100% crystallization are not well represented by the observed ore compositions.

In the case of partial fractional crystallization for MODEL III, the model curves for both cumulates and residual liquids fit the data fairly well, and this is the preferred model

(Fig. 3.10c and d). The model predicts between 30% and 40% trapped liquid in the massive Ovoid ores.

3.5.5.5 Discussion of crystallization models

Fractional crystallization can be achieved in: (a) an open system where crystals are physically separated from the liquid and removed from the system entirely, (b) a closed system where the crystals are physically removed from the liquid and transported to some other portion of the system (i.e., crystals settling in a magma chamber) or the liquid is removed (i.e., concentrates in the center or expelled from the system), or (c) a closed system where the crystals remain *in situ* but are chemically "cut off" from reacting with the liquid (i.e., rapid crystallization or slow diffusion impeding equilibration between the crystal and liquid) (Philpotts, 1990).

Mungall *et al.* (2005) invoked equilibrium crystallization, which is essentially a closed system process, as a more realistic model than fractional crystallization.

Equilibrium and fractional crystallization are end member models and a scenario that might be more realistic is likely somewhere in between them, such as partial fractional crystallization. Partial fractional crystallization could occur in similar scenarios as fractional crystallization except some liquid would be trapped with the cumulates. Partial fractional crystallization is not only physically more realistic but it can also explain a wider range of ore compositions if different proportions of liquid are trapped in different parts of the system.

Scatter and remobilization

Mungall *et al.* (2005) considered a crystallization model successful if the Ni[100] and Cu[100] data are within 0.5 log units of a model trend (i.e., closely follows the trend line) and unsuccessful if not. The data for the Ovoid scatter significantly more than 0.5 log units for any of the crystallization models (Figs. 3.8-3.10). The significant scatter in the data may indicate that a single simple magmatic process alone is not responsible for the observed compositions of the ores. Often it is suggested that significant scatter in the data is the result of late deuteric Cu remobilization or post-crystallization metamorphic remobilization where either process will scatter the data away from the primary magmatic trends (Mungall *et al.*, 2005). However, it is not clear that there is significant evidence for large scale hydrothermal or metamorphic remobilization in the Ovoid deposit (Naldrett, 2000a).

The dispersion of data is alternatively thought to suggest that variable amounts of liquid were trapped in the cumulates, resulting in variable compositions of the ores (Mungall *et al.*, 2005). This is consistent with the scenario at Voisey's Bay where the Cu-rich "loops", which are distributed interstitial to massive pyrrhotite, are considered to represent the trapped liquid (or ISS) (Fig. 3.5a-c). This is interpreted to be an example where complete separation of the cumulate and residual liquid did not occur. And in this case the 1-m sampling scale of the MEBS database would be sampling both cumulates and liquids in random proportions. Therefore, the scatter in the data represents this random mixture of both cumulates and liquids.

R factor

Although the composition of the Ovoid ores has been modified by fractional crystallization it is important to remember that R-factor processes also played a role in defining their compositions. Earlier in this paper there is a discussion of R factor and it is thought here that the composition of bulk disseminated and massive ore resulted from a sulfide liquid that had an initial composition that is consistent with an R factor of ~150, which was subsequently followed by partial fractional crystallization. The individual data have a range of composition from Ni = 2.0-7.2% and Cu = 0.23-10.36%, which would require a range in R factor values of 20-750. However, it is not likely that such a large range in R factor values would occur in a single sulfide body. More significantly, the data does not follow the R factor trend indicating that R factor alone is not responsible for the ore compositions (Fig. 3.2 and 3.8). The scatter in the data is thought to be due to sampling scale and the overall trend in the data is due to partial fractional crystallization.

Preferred model

In deciding on the best model for the crystallization of the Ovoid, there are several important observations and interpretations that must be considered. The model should include disseminated samples as part of the system, where the disseminated sulfide in part represents expelled liquid and the "loops" represent trapped liquid. This is illustrated in Fig. 3.11a and c. This would imply that the system was partially open (at least in the sense

that some liquid was expelled to the surrounding silicates). Another consideration of the Ovoid model is that it should take into account the pre-erosion composition since the Ovoid sits at the surface and it is clear that the Ovoid has been glacially eroded.

MODEL III is self-consistent model that adheres to these requirements. MODEL III is partial fractional crystallization with 30-40% trapped liquid. This is consistent with the erosion of the Ovoid, the visual estimate of 30% "loops" (Fig. 3.5a-c), and the disseminated sulfide representing some expelled liquid. The majority of the Ovoid behaved initially as closed system with some expulsion of sulfide to the surrounding magma during silicate crystallization.

Naldrett *et al.* (2000a) found that the covariation of Cu, Au, Pd, and Pt in the Ovoid is what would be expected from the fractional crystallization of MSS from a sulfide liquid. They suggested that the Ovoid body fractionally crystallized from the margins inward and base upward. This is a closed system fractional crystallization model where fractionated material remains in the system and the bulk composition is represented by the initial bulk sulfide liquid, in contrast to open systems where all fractionated material is lost to the surroundings (Naldrett *et al.*, 2000a).

Naldrett *et al.* (2000a) presented Pt/Os versus Pd/Ir data for the Ovoid deposit, which has relatively high Pt/Os and Pt/Ir ratios indicating the Ovoid retained considerable fractionated liquid. This is consistent with a predominantly closed system where Cu-rich "loops" indicate the residual liquid which was retained.

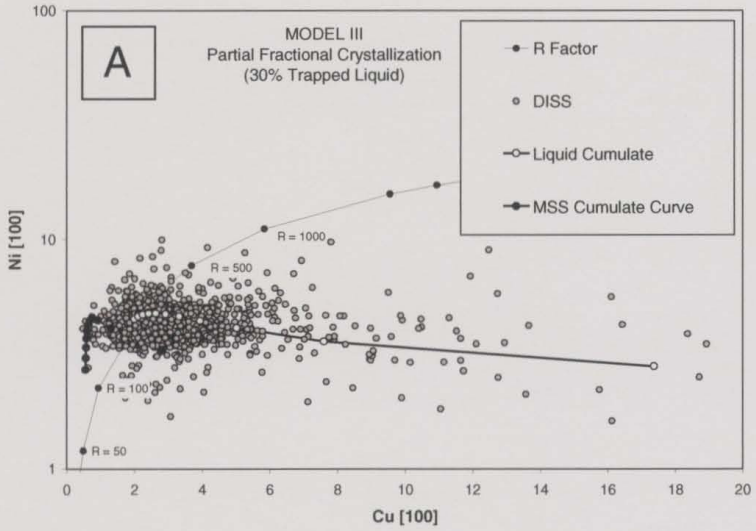
A
MODEL III
Partial Fractional Crystallization
(30% Trapped Liquid)
R Factor
DISS
Liquid Cumulate
MSS Cumulate Curve
R = 1000
R = 500
R = 100
R = 50
Ni [100]
Cu [100]

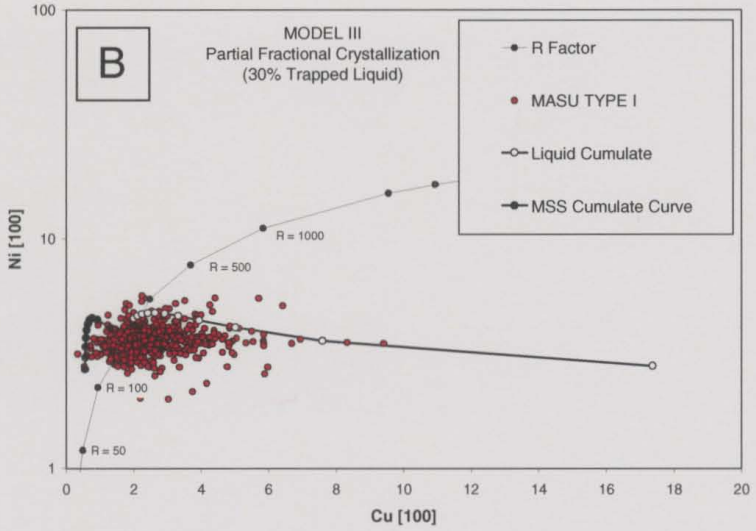
B
MODEL III
Partial Fractional Crystallization
(30% Trapped Liquid)
R Factor
MASU TYPE I
Liquid Cumulate
MSS Cumulate Curve
R = 1000
R = 500
R = 100
R = 50
Ni [100]
Cu [100]

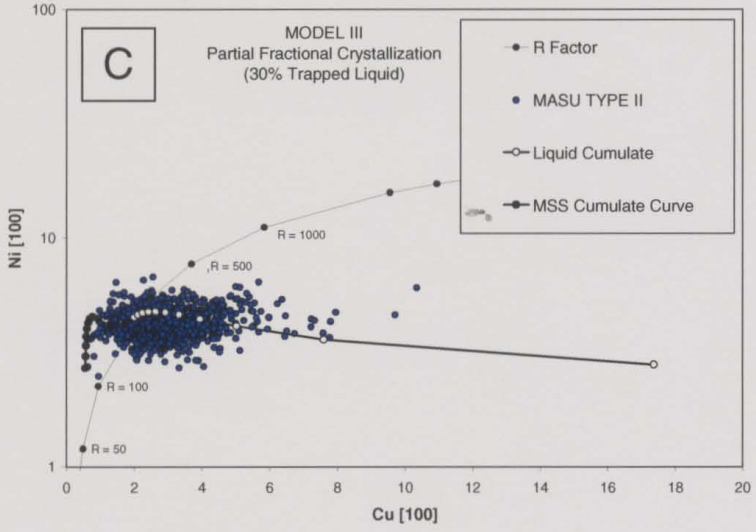
C
MODEL III
Partial Fractional Crystallization
(30% Trapped Liquid)
R Factor
MASU TYPE II
Liquid Cumulate
MSS Cumulate Curve
R = 1000
R = 500
R = 100
R = 50
Ni [100]
Cu [100]

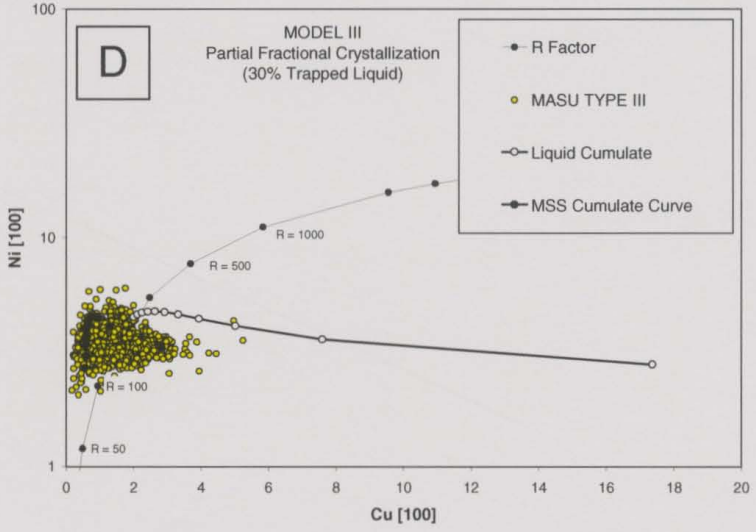
D
MODEL III
Partial Fractional Crystallization
(30% Trapped Liquid)
R Factor
MASU TYPE III
Liquid Cumulate
MSS Cumulate Curve
R = 1000
R = 500
R = 100
R = 50
Ni [100]
Cu [100]

Figure 3.11. Preferred crystallization model of partial fractional crystallization with 30% trapped liquid showing the compositional distributions of: a) disseminated mineralization, b) TYPE I massive ore, c) TYPE II massive ore, and d) TYPE III massive ore.

Crystallization summary of the Ovoid deposit

Figure 3.12 is an atomic ratio diagram (see Beswick, 2002 for a more extensive review of atomic ratio diagrams), which plots atomic S/Cu versus atomic (Fe+Ni)/Cu for the three different mineral domains in the Ovoid. This diagram was chosen to illustrate the relationship between the crystallization history of the Ovoid deposit and the spatial distributions of the different mineral domains. The main control line on this diagram is the MSS fractionation line. We start at the top right of the diagram and as we crystallize predominantly MSS cumulate type rocks (TYPE III), we drive the composition of remaining liquid to more Cu-rich compositions. This MSS-rich TYPE III ore crystallizes at the margins and base of the Ovoid deposit. As we increase Cu in the residual liquid, we begin to form ISS as trapped Cu-rich "loops" and we increase the amount of trapped liquid and decreases the amount of MSS cumulate. This can be seen in our TYPE II image, where there is more chalcopyrite than magnetite or pyrrhotite (MSS cumulate). The TYPE II ore increases toward the center of the Ovoid deposit. This ratio diagram also indicates the direction the samples will plot if we begin to have magnetite accumulation. We know from detailed ore characterization that the magnetite is concentrated in the center of the Ovoid. This accumulation is thought to be due to MSS crystallization first at the margins followed by the crystallization of magnetite which subsequently moves toward the center as it crystallizes. Figure 3.12 illustrates the direction that samples would plot if there was any magnetite accumulation. The TYPE I ores begin to plot in the direction of magnetite accumulation and the samples do indeed

contain more magnetite (Fig. 3.12). Another indication that the Ovoid cooled from the margins inward is that the magnetite is finer grained at the margins (Fig. 3.6d) indicating quicker cooling and is coarser grained in the center (Fig. 3.6e) indicating slower cooling.

The Pt and Pb correlate and increase toward the center of the Ovoid with the exception of the very central zone which has a decrease in Pt and Pb (Chapter 2; Fig. 2.5). This would be consistent with Pt and Pb being enriched as the deposit fractionated from the margins toward the center with the last bit of enriched fractionated material escaping (leaving a Pt-Pb depleted central zone).

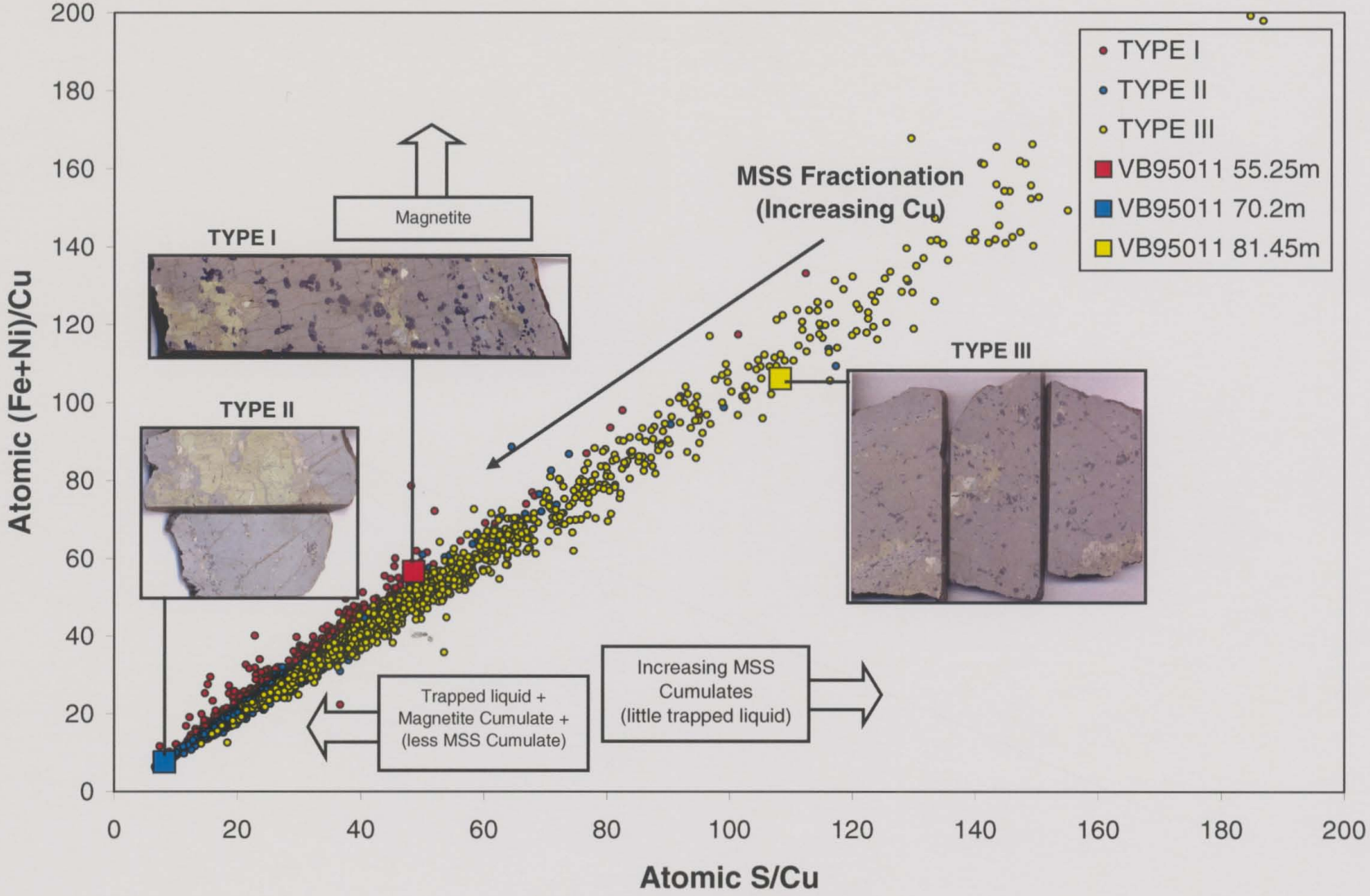
Atomic (Fe+Ni)/Cu
Atomic S/Cu
0
20
40
60
80
100
120
140
160
180
200
TYPE I
TYPE II
TYPE III
Magnetite
MSS Fractionation
(Increasing Cu)
Trapped liquid +
Magnetite Cumulate +
(less MSS Cumulate)
Increasing MSS
Cumulates
(little trapped liquid)
TYPE I
TYPE II
TYPE III
VB95011 55.25m
VB95011 70.2m
VB95011 81.45m

Figure 3.12. Atomic ratio diagram of atomic S/Cu versus atomic (Fe+Ni)/Cu. This diagram illustrates that TYPE I ores are a combination of magnetite cumulates (with lesser trapped liquid and MSS cumulates), TYPE II ores have a high degree of trapped liquid (with lesser magnetite and MSS cumulates), and TYPE III ores contain predominantly MSS cumulates (with lesser magnetite cumulates and trapped liquid).

3.6 CONCLUSIONS

1) The Ni/Cu ratios of the Voisey's Bay ores are too high to account for the ores being produced directly from a picrite of suggested composition of West Greenland and would have formed from initial magmas of more broadly basaltic compositions, as suggested previously by Li *et al.* (2000).

2) R, N, or L processes cannot be distinguished based on the observed Ni and Cu ore tenors. All the models give very similar trends through the data using reasonable D and X_o parameters.

3) The compositions of disseminated sulfide hosted by the ultramafic inclusions and the massive sulfide hosted by troctolite at Voisey's Bay can be explained by a single basaltic parent magma with X_{oNi} ~250ppm and X_{oCu} ~100ppm.

4) All massive ores from the different deposits at Voisey's Bay could have formed from the same magma.

5) The massive sulfide hosted by troctolite rocks and the disseminated sulfide hosted by the ultramafic inclusions can be related by a single process (R, N, or L) with values of ~150 and ~300-500, respectively (i.e., the sulfides formed from the same magma). However, the sulfides in the ultramafic inclusions have been upgraded in metal tenor

due to slightly higher R, N, or L factors indicating they reacted with more silicate magma than the massive sulfides. This is consistent with the ultramafic inclusions forming earlier (most primitive magma) and being in contact with the silicate magma longer.

6) The trend from massive sulfides to semi-massive sulfides to disseminated sulfides (Fig. 3.2b) cannot be explained by R, N, or L processes alone (under any reasonable D and X_o values) and requires an alternate explanation. The increasing Cu-content from massive to semi-massive to disseminated mineralization is consistent with fractionation.

7) Modeled R factor processes do not fully account for the trend of the detailed Ovoid sulfide data. However, it is likely that R factor processes played a role in the initial sulfide compositions (~150), which were subsequently further affected by crystallization processes.

8) The Ovoid is zoned in mineral abundances (pyrrhotite, pentlandite, chalcopyrite, and magnetite), which define three zones (TYPE I, II, and III). Higher pyrrhotite (MSS cumulate) occurs at the base and at the margins with increasing chalcopyrite (residual liquid) and magnetite being concentrated toward the center with finer grained magnetite at the margins and coarser grained magnetite in the center. This indicates that crystallization occurred from the margins inward.

9) The paragenetic sequence for the Ovoid is the crystallization of MSS at 1010-1050°C, crystallization of magnetite, crystallization of ISS between 880-960°C or 900-950°C, crystallization of high temperature pentlandite at 865°C, exsolution chalcopyrite and cubanite from ISS below 550°C, subsolidus reaction of heazlewoodite and MSS to form pentlandite at 500-610°C, and exsolution of troilite from MSS at 142°C.

10) Copper-rich "loops" are interpreted to represent trapped liquid interstitial to MSS cumulates. Therefore, large scale sampling will include random mixtures of cumulates and liquids in any given sample. A finer sampling scale would sample cumulates and liquids separately, which is required to model crystallization processes more accurately. However, sampling at too fine a scale may have the opposite effect and may represent only a portion of the cumulate or liquid. Therefore, some intermediate sampling scale would be most appropriate.

11) Using a smaller sampling scale for the Ovoid produces whole-rock Cu[100] and Ni[100] compositional ranges that are much more similar to other deposits (i.e., Sudbury) than using a coarser sampling scale.

12) Disseminated sulfides are thought to represent more evolved liquid that has been expelled during crystallization and should be included in the crystallization models; some of this expelled disseminated sulfide is thought to contain the missing Pt and Pb

from the central portion of the Ovoid (i.e., the PGE mineralized gabbro dyke in the Southeast Extension Zone; Chapter 4 of this thesis and Huminicki *et al.*, 2008).

13) Plotting the composition of samples by mineral domain indicates that the three different mineral domains plot at different compositions based on the varying proportions of MSS cumulates and trapped liquid.

14) The correct partition coefficients (D values) are critical in determining accurate crystallization models. This can sometimes be difficult to determine for specific deposits because it will change as a function of temperature, fS_2, fO_2, Cu-content of the liquid, and metal/S ratio, which are not always well constrained for some deposits. Where these conditions are well-constrained for deposits, experimental data on partition coefficients are available to make reasonable estimates for more accurate modeling as is the case for Voisey's Bay (i.e., used D_{Ni} of 0.6-1.4 and used D_{Cu} of 0.16-0.28).

15) The initial starting Ni[100] composition that fit the data best is slightly higher than the bulk composition for the preferred crystallization model. The assumption was that the slightly higher Ni tenor material was been removed during glaciation of the Ovoid. This is consistent with the mineralogical zonations and compositions indicated on the R factor diagram (Fig. 3.2a).

16) The fact that the Ovoid is at surface and some material is lost due to erosion was taken into account in the models.

17) The favored model for the Ovoid deposit is partial fractional crystallization with approximately 30% trapped liquid. The Cu-rich "loops" represent this trapped liquid, whereas the remainder of the liquid is thought to have been expelled as the surrounding disseminated sulfide.

18) It is possible that the increase in Pt-Pb toward the center of the Ovoid represents the enrichment of a fractionated liquid and the depleted Pt-Pb at the very center indicates the escape of Pt-Pb enriched fractionated material.

3.7 ACKNOWLEDGEMENTS

This study was generously supported by grants from Inco Limited, the Atlantic Innovation Fund, and the Natural Sciences and Engineering Research Council of Canada (NSERC) to PJS, and by a NSERC postgraduate scholarship, a Northern Scientific Research Program (NSTP) scholarship, and a Society of Economic Geologist Student (SEG) Research Grant to MAEH. This project would not have been possible without the support of D. Wilton (Memorial University of Newfoundland), L. Cabri (Memorial University of Newfoundland), L. Cochrane (Inco Limited), D. Evans-Lamswood (Voisey's Bay Nickel Company Limited), R. Wheeler (Voisey's Bay Nickel Company Limited), and D. Lee (Voisey's Bay Nickel Company Limited).

3.8 REFERENCES

Ballhaus, 1999, A liquid miscibility gap in the system Fe-Ni-Cu-S?: Geological Association of Canada - Mineralogical Association of Canada Joint Annual Meeting, Program Abstract 24, p. 5.

Ballhaus, C., Tredoux, M., and Spath, A., 2001, Phase relations in the Fe-Ni-Cu-PGE-S system at magmatic temperature and application to massive sulfide ores of the Sudbury Igneous Complex: Journal of Petrology, v. 42, p. 1911-1926.

Barnes, S-J., and Naldrett, A.J., 1986, Variations in platinum-group elements in the Brava intrusion, Cape Smith fold belt, Northern Quebec: Canadian Mineralogist, v. 28, p. 431-449.

Barnes, S-J., and Maier, W.D.,1999, The fractionation of Ni, Cu and the noble metals in silicate and sulfide liquids, *in* Keays, R.R., Lesher, C.M., Lightfoot, P.C., and Farrow, C.E.G., eds., Dynamic processes in magmatic ore deposits and their application to mineral exploration, Geological Association of Canada Short Course Notes Volume 13, p. 69-106.

Barnes, S-J, Makovicky, E., Makovicky, M., Rose-Hansen, J., and Karup-Moller, S., 1997, Partition coefficients for Ni, Cu, Pd, Pt, Rh, and Ir between monosulfide solid

solution and sulfide liquid and the formation of compositionally zoned Ni-Cu sulfide bodies by fractional crystallization of sulfide liquid: Canadian Journal of Earth Science, v. 34, p. 366-374.

Beswick, A.E., 2002, An analysis of compositional variations and spatial relationships within Fe-Ni-Cu sulfide deposits on the North Range of the Sudbury Igneous Complex: Economic Geology, v. 97, p. 1487-1508.

Brügmann, E., Naldrett A.J., Lightfoot P.S., Gorbachev N.S., and Fedorenko, V.A., 1993, Siderophile and chalcophile metals tracers of the evolution of the Siberian Trap in the Noril'sk region, Russia: Geochimica et Cosmochimica Acta, v. 57, p. 2001-2018.

Cabri, L.J., 1973, New data on phase relations in the Cu-Fe-S system: Economic Geology, v. 68, p. 443-454.

Cabri, L.J., and Laflamme, J.H.G., 1976, The mineralogy of platinum-group elements from some copper-nickel deposits of the Sudbury area, Ontario: Economic Geology, v. 71, p. 1159-1195

Campbell, I.H., and Naldrett, A.J., 1979, The influence of silicate:sulfide ratios on the geochemistry of magmatic sulfides: Economic. Geology, v. 74, p. 1503-1505.

Craig, J.R., and Kullerud, G., 1969, Phase relations in the Cu-Fe-Ni-S system and their application to magmatic ore deposits: Economic Geology Monograph 4, p. 344-358.

Craig, J.R., and Scott, S.D., 1974, Sulfide phase equilibria, *in* Ribbe P.II., ed., Sulfide mineralogy, Mineralogical Society of America Short Course Notes Volume 1, p. CS1-S110.

Czamanske, G.K., Kunilov, V.E., Zientek, M.L., Cabri, L.J., Likhachev, A.P., Calk, L.C., and Oscarson, R.L., 1992, A proton-microprobe study of magmatic sulfide ores from the Noril'sk-Talnakh district, Siberia: Canadian Mineralogist, v. 30, p. 249-287.

Distler, V.V., Malesvsky, A.Y., and Laputina, I.P., 1977, Distribution of platinoids between pyrrhotite and pentlandite in crystallization of a sulfide melt: Geochemica International, v. 14, p. 30-40.

Ebel, D. S. and Naldrett, A. J., 1996, Fractional crystallization of sulfide ore liquids at high temperature: Economic Geology, v. 91, p. 607-621.

Ebel, D. S. and Naldrett, A. J., 1997, Crystallization of sulfide liquids and the interpretation of ore composition: Canadian Journal of Earth Sciences, v. 34, p. 352-365.

Emslie, R.F., Hamilton, M.A., and Theriault, R.J, 1994, Petrogenesis of a Mid-Proterozoic Anorthosite-Mangerite-Charnockite-Granite (AMCG) Complex: Isotopic and Chemical Evidence from the Nain Plutonic Suite: Geology, v. 102, p. 539-558.

Fleet, M.E., 1977, Origin of disseminated copper-nickel sulfide ore at Frood, Sudbury, Ontario: Economic Geology, v. 72, p. 1449-1456.

Fleet, M.E., 1996, Partitioning of platinum-group elements and Au in the Fe-Ni-Cu-S system: experiments on the fractional crystallization of sulfide melt – reply: Contributions to Mineralogy and Petrology, v. 123, p. 438-440.

Fleet, M.E., and Stone, W.E., 1991, Partitioning of platinum-group elements in the Fe-Ni-S system and fractionation in nature: Geochimica and Cosmochimica Acta, v. 55, p. 245-253.

Fleet, M.E., and Pan, Y., 1994, Fractional crystallization of anhydrous sulfide liquid in the system Fe-Ni-S with application to magmatic sulfide deposits: Geochimica and Cosmochimica Acta, v. 58, p. 3369-3377.

Fleet, M.E., Chryssoulis, S.L., Stone, W.E., and Weisner, C.G., 1993, Partitioning of platinum-group elements and Au in the Fe-Ni-Cu-S system: experiments on the fractional

crystallization of sulfide melt: Contributions to Mineralogy and Petrology, v. 115, p.36-44.

Foster, J., 2006, Voisey's Bay: Geology, Geochemistry, and Genesis: Australian Earth Science Conference, July, 2006, Melbourne.

Golightly, J.P., and Lesher, C.M., 1999, MSS Fractionation, volatile-enhanced partitioning, and sulfide liquid immiscibility in magmatic Fe-Ni-Cu-(PGE) deposits: Geological Associations of Canada – Mineralogical Association of Canada Joint Annual Meeting, Program Abstract 24, p. 46.

Hawley, J.E., 1962, The Sudbury ores: Their mineralogy and origin: Canadian Mineralogist, v. 7, p. 207.

Hawley, J.E., 1965, Upside-down zoning at Frood, Sudbury, Ontario: Economic Geology, v. 60, p. 529-575.

Hawley, J.E., and Stanton, R.L., 1962, The facts, the ores, their minerals, metals and distribution: Canadian Mineralogist, v. 7, p. 30-145.

Huminicki, M.A.E., Sylvester, P.J., Lastra, R., Cabri, L.J., Evans-Lamswood, D., Wilton, D.H.C., 2008, First report of platinum-group minerals from a hornblende gabbro dyke in

the vicinity of the Southeast Extension Zone of the Voisey's Bay Ni-Cu-Co deposit, Labrador: Mineralogy and Petrology, v. 92, p. 129-164.

Huminicki, M.A.E., Sylvester, P.J., Shaffer, M., Wilton, D.H.C., Evans-Lamswood, D., and Wheeler, R. (in review), Systematic and Integrative Ore Characterization of Massive Sulfide Deposits: An Example from the Voisey's Bay Ovoid Deposit, Labrador: Economic Geology.

Kerr, A., 2000, Magmatic sulphide mineralization in the Pants Lake Intrusion, Labrador: implications for geological exploration models for Voisey's Bay-style deposits: Geological Association of Canada 2000 Annual Technical Meeting Newfoundland Section, Atlantic Geoscience Society, 171p.

Kerr, A., 2003, Guidelines for the calculation and use of sulfide metal contents in research and mineral exploration: Newfoundland Department of Mines and Energy, Geological Survey, Report 03-1, p. 223-229.

Kerr, A., and Leitch, A.M., 2005, Self-destructive sulfide segregation systems and the formation of high-grade magmatic ore deposits: Economic Geology, v. 100, p. 311-332.

Kullerud, G., 1963, Thermal stability of pentlandite: Canadian Mineralogist, v. 7, p. 353-343.

Kullerud, G., Yund, R.A., and Moh, G.H., 1969, Phase relations in the Cu-Fe-S, Cu-Ni-S, and Fe-Ni-S systems: Economic Geology Monograph 4, p. 323-343.

Lambert, D.D., Frick, L.R., Foster, J.G., Li, C., and Naldrett, A.J., 2000, Re-Os isotope systematics of the Voisey's Bay Ni-Cu-Co magmatic sulfide system, Labrador, Canada: II. Implications for parental magma chemistry, ore genesis, and metal redistribution: Economic Geology, v. 95, p. 867-888.

Langmuir, C.H., 1989, Geochemical consequences of in situ crystallization: Nature, v. 340, p. 199-205.

Lesher, C.M., 1998, Partial fractional crystallization of MSS from sulfide liquid in magmatic Fe-Ni- (Cu)-PGE sulfide deposits: Geological Association of Canada - Mineralogical Association of Canada Joint Annual Meeting, Program Abstract 23, p. 108.

Lesher, C.M., and Burnham, M.O., 2001, Multicomponent elemental and isotopic mixing in Ni-Cu-(PGE) ores at Kambalda: Canadian. Mineralogist, v. 39, 421-446.

Lesher, C.M., and Golightly, J.P., 2001a, Fractionation of PGEs in the Sudbury Igneous Complex: LU-SEG Student Chapter and Mineral Exploration Research Centre PGE Workshop, Sudbury.

Lesher, C.M., and Golightly, J.P., 2001b, Geochemistry of magmatic Ni-Cu-(PGE) sulfide ores: Eleventh annual Goldschmidt Conference, Abstract 3122.

Li, C. and Barnes, S-J., 1996, Partitioning of platinum-group elements and Au in the Fe-Ni-Cu-S system: experiments on the fractional crystallization of sulfide melt – a discussion: Contributions to Mineralogy and Petrology, v. 123, p. 435-437.

Li, C., and Naldrett, A.J., 1999, Geology and petrology of the Voisey's Bay intrusion: reaction of olivine with sulfide and silicate liquids: Lithos 47, p. 1-31

Li, C., Naldrett, A.J., Rucklidge, J.C., Kilius, L.R., 1993, Concentrations of platinum-group elements and gold in sulfides from the Strathcona deposit, Sudbury, Ontario: Canadian Mineralogist, v. 30, p. 523-531.

Li, C., Barnes, S-J., Makovicky, E., Rose-Hansen, J.R., and Makovicky, M., 1996, Partitioning of Ni, Cu, Ir, Rh, Pt, and Pd between monosulfide solid solution and sulfide liquid: effects of composition and temperature: Geochimica and Cosmochimica Acta, v. 60, p. 1231-1238.

Li, C., Lightfoot, P.C., Amelin, Y., and Naldrett, A.J., 2000, Contrasting Petrological and Geochemical Relationships in the Voisey's Bay and Mushuau Intrusions, Labrador, Canada: Implications for Ore Genesis: Economic Geology, v. 95, p. 771-799.

Li, C., Naldrett, A.J., and Ripley, E.M, 2001, Critical factors for the formation of a nickel-copper deposit in an evolved magma system: lessons from a comparison of the Pants Lake and Voisey's Bay sulfide occurrences in Labrador, Canada: Mineralium Deposita, v. 36, p. 85-92.

Lightfoot, P.C., Hawkesworth, C.J., Olshefsky, K.O., Green, T., Doherty, W., and Keays, R.R., 1997, Geochemistry of Tertiary tholeiites and picrites form Qeqertarssuaq (Disko Island) and Nuussuaq, West Greenland with implications for the mineral potential of comagmatic intrusions: Contributions to Mineralogy and Petrology, v. 128, p. 139-163.

Mungall, J.E., 2002, Late-stage sulfide liquid mobility in the Main Mass of the Sudbury Igneous Complex: Examples from the Victor Deep, McCreedy East and Trillabelle Deposits: Economic Geology, v. 97, p. 1563-1576.

Mungall, J.E., Andrews, D.R.A., Cabri, L.J., Sylvester, P.J., and Tubrett, M., 2005, Partitioning of Cu, Ni, Au, and platinum-group elements between monosulfide solid solution and sulfide melt under controlled oxygen and sulfur fugacities: Geochimica and Cosmochimica Acta, v. 69, p. 4349-4360.

Naldrett, A.J., 1969, Discussion of papers concerned with sulfide deposits. Economic Geology Monograph 4, p. 359-365.

Naldrett, A.J., 1981, Nickel sulfide deposits: Classification, composition and genesis: Economic Geology, v. 75, p. 628-685.

Naldrett., A.J., 1989, Magmatic sulfide deposits: N.Y.-Oxford, Clarendon Press-Oxford University Press, 186p.

Naldrett, A.J., 2004, Magmatic Sulfide Deposits: Geology, Geochemistry, and Exploration: Springer, 727p.

Naldrett, A. J., Craig, J. R., and Kullerud, G., 1967, The central portion of the Fe-Ni-S system and its bearing on pentlandite exsolution in iron-nickel sulfide ores: Economic Geology, v. 62, p. 826-847.

Naldrett, A.J., Hoffman, E.L., Green, A.H., Chou, C.L, Naldrett, F.R., and Alcock, R.A., 1979, The compositions of Ni-sulfide ores, with particular reference to their content of PGE and Au: Canadian Mineralogist, v. 17, p. 403-415.

Naldrett, A.J., Innes, D.G., Sowa, J., and Gorton, M.P., 1982, Compositional variations within and between five Sudbury ore deposits: Economic Geology, v.77, p. 1519-1534.

Naldrett, A.J., Pessaran, R., Asif, M., and Li, C., 1994, Compositional variation in the Sudbury ores and prediction of the proximity of footwall copper-PGE orebodies: Ontario Geological Survey Special Volume 5, p. 133-143.

Naldrett, A.J., Asif, M., Schandl, E., Searcy, T., Morrison, G.G., Binney, W.P., and Moore, C., 1999, Platinum-group elements in the Sudbury ores: significance with respect to the origin of different ore zones and to the exploration for footwall orebodies: Economic Geology, v. 94, p. 185-210.

Naldrett, A.J., Asif, M., Krstic, S., and Li, C., 2000a, The Composition of Mineralization at the Voisey's Bay Ni-Cu Sulfide Deposit, with Special Reference to Platinum-Group Elements: Economic Geology, v. 95, p. 845-866.

Naldrett, A.J., Singh, J., Krstic, S., and Li, C., 2000b, The Mineralogy of the Voisey's Bay Ni-Cu-Co Deposit, Northern Labrador, Canada: Influence of Oxidation State on Textures and Mineral Compositions: Economic Geology, v. 95, p. 889-900.

Philpotts, A.R., 1990, Igneous and Metamorphic Petrology: Prentice Hall, 497p.

Prichard, H.M., Hutchinson, D., and Fisher, P.C., 2004, Petrology and crystallization history of multiphase sulfide droplets in a mafic dike from Uruguay: Implications for the origin of Cu-Ni-PGE sulfide deposits: Economic Geology, v. 99, p. 365-376

Ryan, B., 2000, The Nain-Churchill Boundary and the Nain Plutonic Suite: A Regional Perspective on the Geologic Setting of the Voisey's Bay Ni-Cu-Co Deposit: Economic Geology, v. 95, p. 703-724.

CHAPTER 4: FIRST REPORT OF PLATINUM-GROUP MINERALS AND IN SITU PLATINUM-GROUP ELEMENT ANALYSES IN SULFIDE FROM A HORNBLENDE GABBRO DYKE IN THE VICINITY OF THE SOUTHEAST EXTENSION ZONE OF THE VOISEY'S BAY NI-CU-CO DEPOSIT, LABRADOR: A PROPOSED MODEL FOR THE FORMATION OF PGE MINERALIZATION

M. A. E. HUMINICKI, P. J. SYLVESTER,

Inco Innovation Centre and Department of Earth Sciences, Memorial University of Newfoundland, St. John's, Newfoundland, Canada A1B 3X5, e-mail: g26mah@mun.ca

R. LASTRA,

CANMET Mining and Mineral Sciences Laboratories, Natural Resources Canada, 555 Booth Street, Ottawa, ON, Canada K1A 0G1

L.J. CABRI,

Cabri Consulting Inc., 99 Fifth Avenue, Suite 122, Ottawa, ON, Canada, K1S 5P5 and Memorial University of Newfoundland, Department of Earth Sciences, St. John's, NL, Canada A1B 3X5

D. EVANS-LAMSWOOD,

Voisey's Bay Nickel Company Limited, Suite 700, Baine Johnston Centre, 10 Fort William Place, St. John's, NL Canada A1C 1K4

D.H.C. WILTON,

Inco Innovation Centre and Department of Earth Sciences, Memorial University of Newfoundland, St. John's, Newfoundland, Canada A1B 3X5, e-mail: g26mah@mun.ca

4.1 SUMMARY

This study reports the first documented occurrence of platinum group-minerals (PGM) in the vicinity of the Voisey's Bay magmatic sulfide ore deposit. The PGM are present in a sulfide poor, hornblende gabbro dyke in the Southeast Extension Zone of the massive sulfide Ovoid deposit. The dyke has somewhat elevated concentrations of platinum-group elements (PGE) and gold (up to 1.95g/t Pt, 1.41g/t Pd, and 6.59g/t Au), as well as Cu, Pb, Ag, Sn, Te, Bi and Sb. The dyke consists of an inner PGE-elevated zone and an outer PGE-poor zone, which corresponds to disseminated sulfide mineralization consisting of typical disseminated magmatic pyrrhotite, pentlandite, and chalcopyrite in the outer zone with bornite and galena associated with the inner zone. The PGM formed by magmatic processes and were little disturbed by subsequent infiltration of an externally-supplied hydrothermal fluid. To date, no similar PGM occurrences have been discovered within the Ovoid deposit itself.

Whole rock REE patterns indicate that the dyke is geochemically related to the main conduit troctolites, which carry the bulk of the massive sulfide mineralization at Voisey's Bay. The PGE mineralization is Pt- and Pd-rich, where the Pt and Pd occur predominantly as discrete PGM with minor Pd in solid solution in galena (ave = 1.9ppm) and pentlandite (ave = 2ppm). The discrete PGM are predominantly hosted by disseminated base-metal sulfides (bornite, chalcopyrite, and galena) (56 vol%) and are associated with other precious metal minerals (13 vol%) with only ~3 vol% of the PGM hosted by silicate minerals. In whole rock samples, the PPGE (Pt, Pd, and Rh) correlate

with abundances of chalcopyrite, bornite, galena, and other precious metal minerals (PMM), whereas the IPGE (Ir, Ru, and Rh) correlate with pyrrhotite and pentlandite. There are no correlations of the PGE with chlorine. Lead isotope compositions of galena associated with the PGE mineralization in the Southeast Extension Zone are broadly similar to those for galena in the Ovoid. The lead isotope compositions are much different from those in the Voisey's Bay Syenite, which is a potential external hydrothermal fluid source.

The observed Cu-rich, Pb-rich sulfide compositions and associated Pt-Pd-Au-Ag-Sn-Te-Bi-Sb assemblage in the dyke indicate that the PGM are magmatic in origin and related to a highly differentiated intermediate solid solution (ISS) that was derived from crystallization of monosulfide solid solution (MSS) of a typical sulfide deposit (i.e., the Ovoid deposit). Melting temperatures of the PGM are also consistent with a magmatic origin. It is proposed that the MSS was injected as the first pulse of a late syn-magmatic dyke producing the outer zone of the dyke, whereas the ISS differentiate concentrated the PGE and was subsequently injected as a second pulse forming the inner zone of the dyke.

The significant abundance of amphibole in the dyke suggests fluids were present. However, the amphibole is secondary, produced from an external REE-enriched hydrothermal fluid that post dates the mineralization. There is only evidence for local remobilization of Pb and Sn but not the PGE from the sulfides that host the PGM.

4.2 INTRODUCTION

The 1.3 Ga Voisey's Bay Ni-Cu-Co magmatic sulfide deposit, located in northern Labrador, Canada was discovered in 1993. As of 2005 the deposit was estimated to contain 32 million tonnes of proven and probable reserves consisting of 2.8% nickel, 1.6% copper, and 0.14% cobalt in the Ovoid with an additional 40 million tonnes of indicated mineral resource consisting of 1.9% nickel, 1.9% copper, and 0.12% cobalt (http://www.vbnc.com/ReservesAndResources.asp) in the associated ore zones.

During a diamond drilling program in 2003 by Voisey's Bay Nickel Company Limited, somewhat elevated levels of platinum-group elements (PGE) and Au (up to 1.95g/t Pt, 1.41g/t Pd, and 6.59g/t Au) were intersected within a sulfide-poor, hornblende gabbro dyke in the vicinity of the Southeast Extension Zone of the Voisey's Bay massive sulfide Ovoid deposit. Generally, PGE deposits occur as either: 1) low sulfur PGE deposits (i.e., Bushveld and Stillwater; Naldrett, 2004), or 2) a by-product associated with high sulfur base-metal deposits (i.e., Noril'sk and Sudbury; Naldrett, 2004). Previous analyses of both massive and disseminated base-metal sulfide ores at Voisey's Bay indicated generally poor PGE grades (Table 4.1). Thus, this occurrence is of particular interest as a newly documented type of mineralization associated with the Voisey's Bay deposit that is distinct in PGE content and style of sulfide mineralization.

This report presents detailed data on the mineralogy and geochemistry of a PGE occurrence at Voisey's Bay much of which has been published in Huminicki *et al.* (2008). The data are used to assess magmatic and hydrothermal origins for the precious

metal mineralogy. Some geological and geochemical evidence (whole rock REE patterns and lead isotope data) present possible links of the PGE mineralization to the major Ni-Cu-Co sulfide mineralization at Voisey's Bay.

4.3 OVERVIEW OF APPROACH

The PGE occurrence in the dyke in the Southeast Extension is described in geological context of the Voisey's Bay intrusion. The PGE are hosted in hornblende gabbros that are geologically similar to the troctolite rocks that host the massive sulfide Ovoid deposit, and the dyke is in close spatial proximity to the Ovoid.

The identity, composition, abundance, association, and trace element abundances of the PGM and host sulfides were evaluated using a combination of hydroseparation, rare phase searches, electron probe microanalysis, and laser ablation – inductively coupled plasma – mass spectrometry in order to characterize the occurrence and determine whether it was produced magmatically or hydrothermally.

Whole rock lithogeochemistry was evaluated in the Southeast Extension Zone to determine: 1) how the hornblende gabbro dyke compares compositionally to the main Voisey's Bay host troctolite (whole rock REE patterns), 2) inter-element correlations indicating crystallization mechanisms (correlation coefficients), and 3) how the PGE are fractionated from one another (chondrite normalized PGE patterns).

The composition of the silicates was evaluated to determine whether the amphibole is magmatic or hydrothermal and whether the PGE are related to amphibole formation.

Lead isotopes were evaluated to determine source of the PGE mineralization (magmatic versus hydrothermal) and whether there was an external influence on the magmas such as country rock contamination.

4.4 GENERAL GEOLOGY

The Voisey's Bay ore bodies are hosted by troctolites and olivine gabbros of the Voisey's Bay intrusion, which is part of the Mesoproterozoic Nain Plutonic Suite. Most of the deposit intrudes Paleoproterozoic enderbitic orthogneiss (Rawlings-Hinchey *et al.*, 2003) except in the west where the country rock is Paleoproterozoic Tasiuyak paragneiss of the Churchill Province. Tonalitic gneisses of the Archean Nain Province are present to the east of the deposit. The Voisey's Bay intrusion, and more generally, the entire Nain Plutonic Suite is thought to have been emplaced along a suture between the Nain and Churchill Provinces (Ryan, 2000). Emslie *et al.* (1994), Ryan (2000), and references therein summarized the regional geology of the Nain Plutonic Suite. The composition and mineralogy of Voisey's Bay ores have been described by Naldrett *et al.* (2000a) and Naldrett *et al.* (2000b), respectively.

There are two large troctolitic bodies associated with the dyke system: the "Eastern Deeps upper chamber" in the east and the "Reid Brook lower chamber" in the

west (Figs. 4.1 and 4.2). The two chambers may be joined by the main conduit host of the ores, which is known as the "Reid Brook feeder dyke". The dyke dips steeply south and may widen at depth into the lower Reid Brook chamber. The Reid Brook feeder dyke is exposed in the Discovery Hill Zone. The base of the Eastern Deeps upper chamber is thought to be represented by the Ovoid, which is located between the Eastern Deeps and Discovery Hill Zone. The Mini Ovoid is separate from and lies to the west of the Ovoid. Besides massive sulfide ores, the Voisey's Bay conduit dyke system includes a variety of troctolitic to gabbroic rocks that host semi-massive to disseminated sulfides.

The PGE occurrence, which is the subject of this study, is located in the vicinity of the Southeast Extension Zone of the Ovoid (Fig. 4.3). At this location the main troctolite feeder dyke that hosts the majority of the sulfide deposits opens up and bends into the Eastern Deeps upper chamber to the east (Fig. 4.3b). The Ovoid deposit occurs at this inflection point in the dyke. The PGE occurrence is hosted by a hornblende gabbro (to troctolitic) dyke located below the main feeder dyke between the Ovoid and Eastern Deeps ore zones in the area termed the Southeast Extension Zone occurring as a splay off the main troctolite dyke (Figs. 4.3c).

Table 4.1. Average metal contents in 100% sulfide (after Naldrett, 2000a).

Rock Types and Zones	Ni	StDev	Cu	StDev	Pt	StDev	Pd	StDev	Rh	StDev	Ru	StDev	Ir	StDev	Os	StDev	Au	StDev
Units	wt%		wt%		ppb		ppb		ppb		ppb		ppb		ppb		ppb	
Varied troctolite																		
Eastern Deeps > 10% sulfide (21)	4.72	1.03	2.91	1.38	360	309	354	264	19	9	31	34	6.4	3.8	10	8	355	349
Eastern Deeps < 10% sulfide (25)	6.08	1.04	3.22	0.93	447	251	354	347	19	10	60	88	5.1	2.7	4	7	546	387
Leopard troctolite																		
Eastern Deeps (9)	3.41	0.23	1.87	0.5	107	75	154	126	16	3	23	20	6	1.4	13	4	93	49
Mini Ovoid (7)	3.94	0.242	2.77	0.94	145	71	228	60	12	6	25	16	2.9	0.91	7	2	224	80
Discovery Hill Zone (12)	3.79	0.27	2.23	0.47	377	197	345	129	9	1	35	24	2	0.8	3	1	337	73
Reid Brook Zone (20)	3.29	0.58	1.98	1.32	162	119	143	76	10	1	30	12	2.5	0.5	4	2	189	119
Basal Breccia Sequence																		
Eastern Deeps (44)	4.4	0.88	2.47	1.09	242	220	264	180	13	6	37	26	4.6	2.5	9	6	245	176
Ovoid (4)	4.14	1.1	3.44	1.31	430	159	521	136	23	5	70	16	9.1	1.9	13	4	469	178
Mini Ovoid (6)	4.11	0.85	3.83	1.68	489	255	307	181	10	2	56	43	3.6	2.3	11	8	360	452
Discovery Hill Zone (18)	4.06	0.41	2.2	0.78	266	154	346	163	11	4	31	17	2.7	1.7	5	3	278	168
Reid Brook Zone (26)	3.75	0.72	1.69	0.72	203	136	258	171	14	10	82	60	4.1	4.2	7	5	200	143
Massive Sulfide																		
Eastern Deeps (12)	3.32	0.99	1.15	1.55	34	30	144	106	18	6	26	17	6.6	2.4	15	6	18	17
Ovoid (52)	4.61	1.08	2.84	1.4	123	111	252	115	8	3	17	10	2	1.1	4	1.5	93	130
Mini Ovoid (11)	3.96	1.23	2.3	2.41	178	85	221	127	9	3	17	5	2.5	0.6	5	2	116	48
Reid Brook Zone (16)	2.95	0.43	1.17	0.86	42	33	102	36	10	1	19	6	2.8	0.8	4	3	60	67

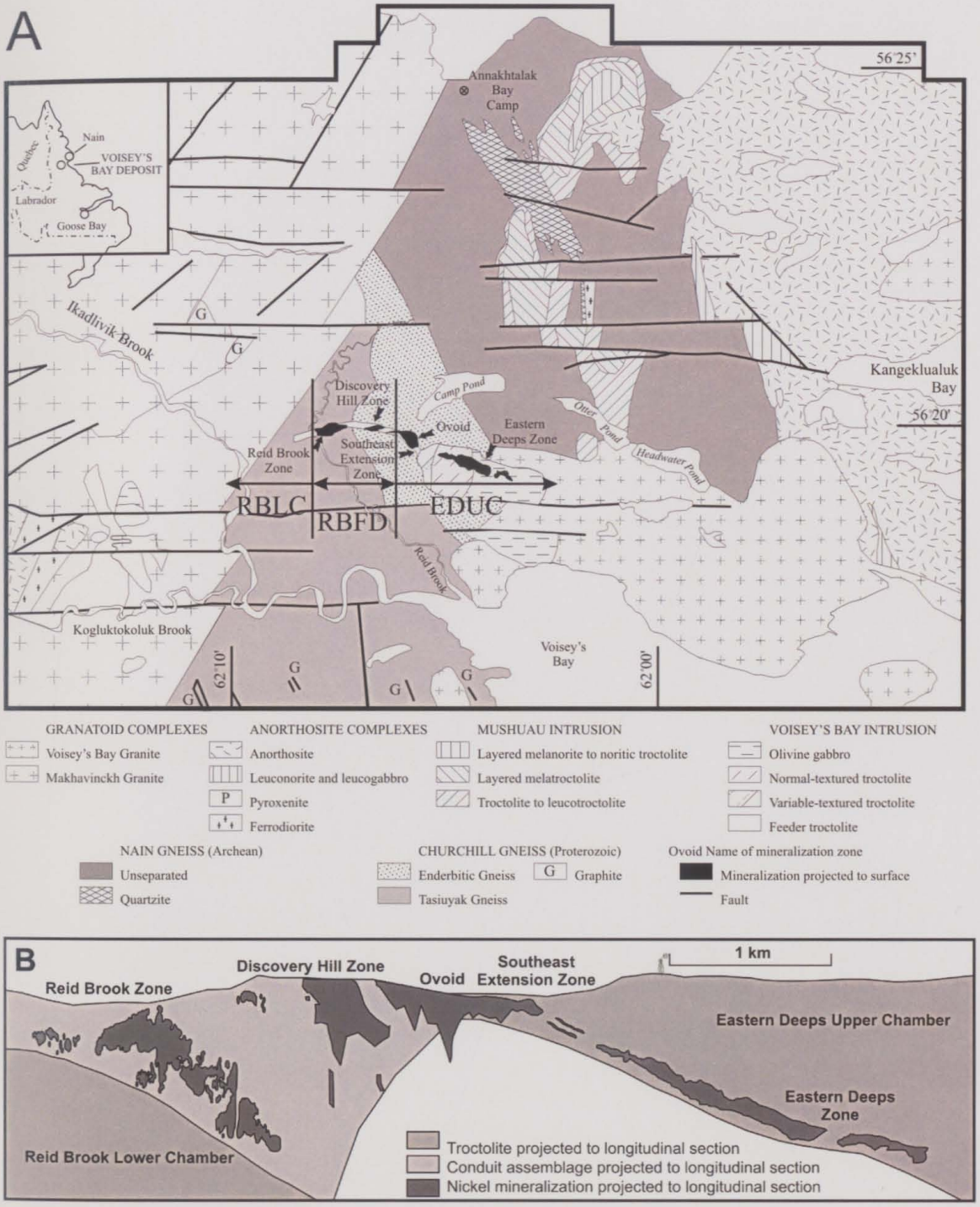

Figure 4.1. Geologic map of the Voisey's Bay area, showing the various rock types, components, and mineralized zones in a) plan view (modified from Lightfoot, 1998 and Evans-Lamswood *et al.*, 2000), and b) longitudinal section looking north showing various components and mineralized zones (modified from Li *et al.*, 2000).

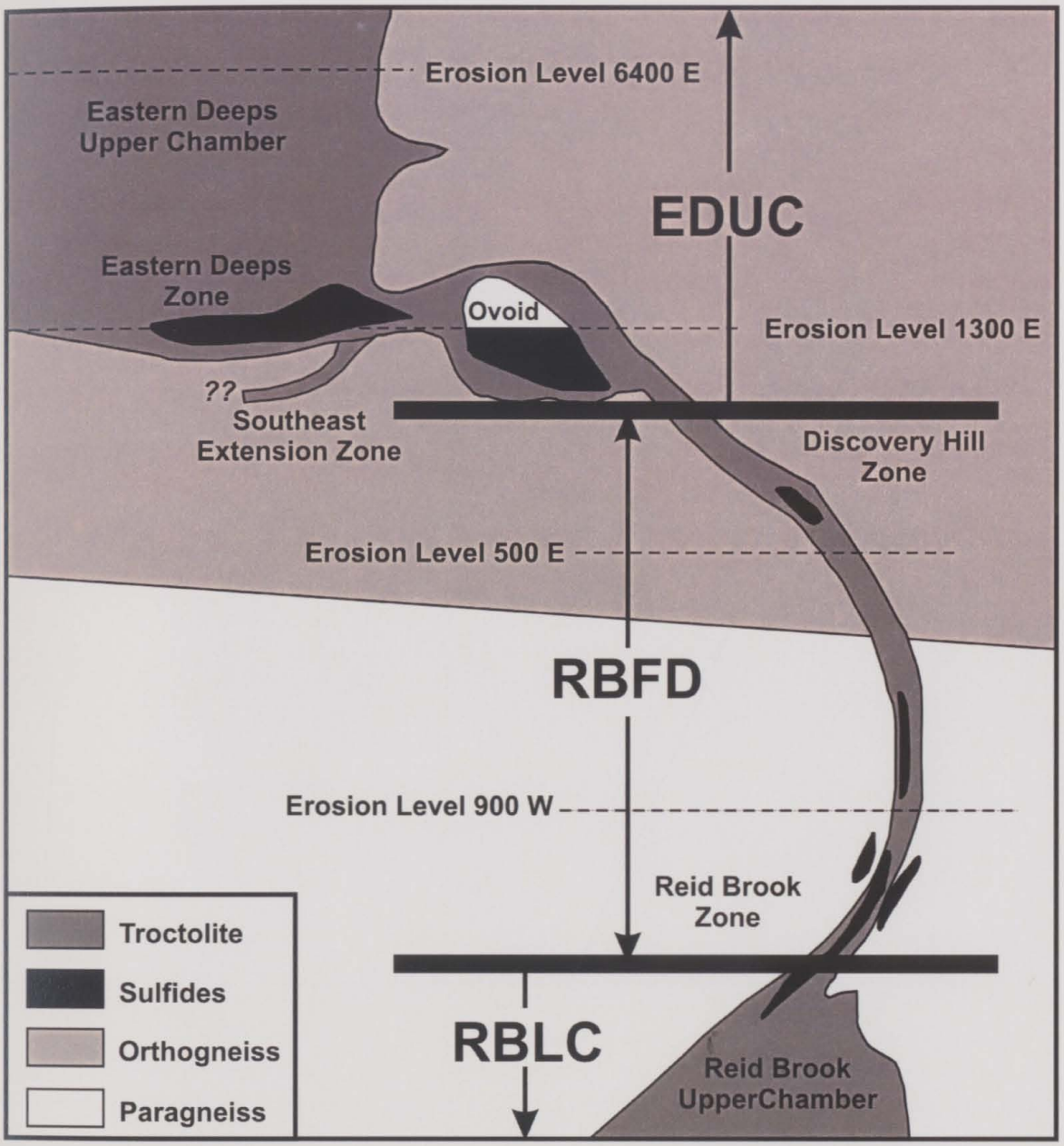

Figure 4.2. West-facing conceptual section with the Eastern Deeps upper chamber (EDUC) projected from the east and the Reid Brook lower chamber (RBLC) projected from the west joined by the Reid Brook feeder dyke (RBFD). The location of the Southeast Extension Zone has been added and is only an approximation for conceptual purposes. After Lightfoot and Naldrett (1999).

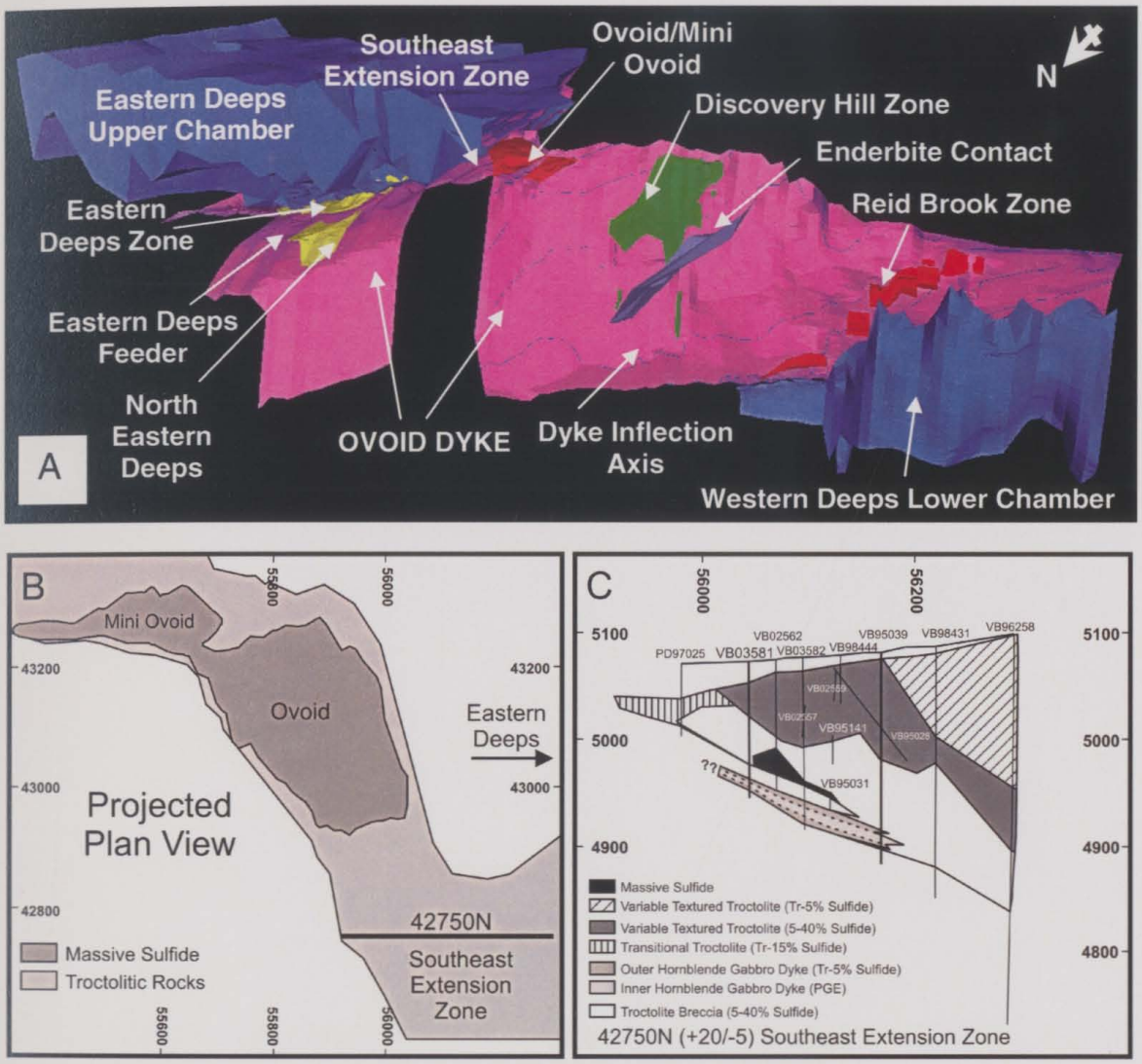

Figure 4.3. a) Longitudinal section of the Voisey's Bay deposits looking south (courtesy Voisey's Bay Nickel Company Ltd), b) plan view of the Ovoid, Mini Ovoid, and Southeast Extension Zone massive sulfides and associated troctolites projected to surface, and c) north-facing (42750N) cross-section through the Southeast Extension Zone indicating the lithological division in the overlying Voisey's Bay troctolites and the spatial relationship to the hornblende gabbro to troctolite dyke that hosts the PGE mineralization in this study.

4.5 UNITS AND ROCK TYPES OF THE SOUTHEAST EXTENSION ZONE

Samples for this study were collected from drill holes VB95039 and VB03581 located in the Southeast Extension Zone of the main Ovoid deposit; these holes are approximately 120 m apart. Figure 4.3c demonstrates the main geometry and distribution of troctolitic units in the Southeast Extension Zone and the hornblende gabbro dyke in relation to Ovoid and the troctolites of the main conduit in longitudinal section looking north (42750N; 20 m to the south and 5 m to the north projected to the plane); this was compiled using Voisey's Bay Nickel Company Limited's Mine Exploration Borehole System database. Locations of each sample collected for this study are labeled in lithostratigraphic profiles through drill core VB03581 and VB95039 in Figure 4.4. The hornblende gabbro dyke (labeled 1) with elevated PGE and Au is approximately 10-20 m thick. It is overlain by troctolite breccia and variable-textured troctolite of the main Voisey's Bay feeder dyke and is underlain by enderbitic gneiss (Fig. 4.4). The dyke exploits the contact between the troctolite rocks of the main Voisey's Bay feeder dyke and the enderbitic gneiss in drill hole VB95039 and solely intrudes the enderbitic gneiss in drill hole VB03581. The dyke has a chill margin with the enderbitic gneiss in drill hole VB03581. However, the full dimensions and geometry of the dyke are not well-constrained.

The troctolite rocks of the Voisey's Bay intrusion have been described in general by Li and Naldrett (1999) and are summarized in Table 4.2. The mineralogy of the hornblende gabbro dyke in both drill cores differs from the main troctolite rocks in the

Voisey's Bay intrusion in that it tends to contain more hornblende (generally 20-45%) as opposed to 0-10% in the typical troctolite rocks and is more commonly foliated and recrystallized. Almost no primary textures are preserved within the dyke as it has a granoblastic texture with varying degrees of fabric development. The dyke consists of an outer PGE-poor zone and an inner "PGE-elevated" zone, which corresponds in each case to disseminated sulfide mineralization (<5% sulfide) consisting of magmatic pyrrhotite, pentlandite, and chalcopyrite in the outer zone, and bornite and galena associated with the inner zone.

Another hornblende gabbro dyke (labeled 2) with similar characteristics was intersected higher up in the section between the troctolite breccia and the variable-textured troctolite (Fig. 4.4). This dyke does not contain elevated PGE at this location.

4.5.1 Rock classifications and descriptions

Modal mineral estimates were made in thin section for each of the main silicate phases through each drill hole from the Southeast Extension Zone (Table 4.3a). These modal estimates were normalized to: 1) 100% plagioclase-pyroxene-hornblende for the dyke rocks, or 2) 100% plagioclase-pyroxene-olivine for the main conduit troctolitic rocks and then plotted on simple IUGS classification diagrams (Fig. 4.5). A detailed list of rock type based on the IUGS classifications for each sample is summarized in Table 4.3b. Representative drill core photos of each unit are shown in Figure 4.6 and a brief description of each unit is described below:

Table 4.2. Major rock types in the Voisey's Bay Complex (Li and Naldrett, 1999).

Rock Types
1. Olivine gabbro: Olivine-plagioclase cumulate with 50-70% modal plagioclase (tabular, 5-20mm), 15-30% modal olivine (elliptical, 5-10mm), 10-20% modal augite (oikocrysts), and less than 20% interstitial hornblende-biotite-oxide-sulfide.
2. Feeder Olivine Gabbro: Plagioclase ± olivine cumulate with 40-50% modal plagioclase (tabular, framework, 2-10mm), and 30-50% interstitial pyroxene-hornblende-biotite-oxide-plagioclase.
3. Normal Troctolite: Medium-grained olivine-plagioclase cumulate with uniform texture consisting of 20-40% modal olivine and 40-65% modal plagioclase with some interstitial orthopyroxene-hornblende-biotite-oxide.
4. Variable Textured Troctolite: Similar to normal troctolite with variable range in plagioclase grain size, contains up to 25% gneissic fragments, and contains <25% blebby sulfide.
5. Leopard Troctolite: Olivine-plagioclase with 40-60% modal cumulus plagioclase, 20-30% modal cumulus olivine, 10% modal augite oikocrysts giving the appearance of leopard spots against a matrix of up to 50% interstitial yellow sulfide.
6. Basal Breccia Sequence and Feeder Breccia: Consists of abundant gneissic inclusions and lesser other types of inclusions, small lenses and blotches of massive sulfide, and veins of leopard troctolite in a matrix of equal amounts plagioclase and olivine.
7. Ferrodiorite: Fine-grained, generally massive (can contain flow-banding), noncumulate rock containing <10% modal granular pyroxene, 25-40% modal hornblende, 30-40% modal plagioclase, and 5-10% modal oxides.

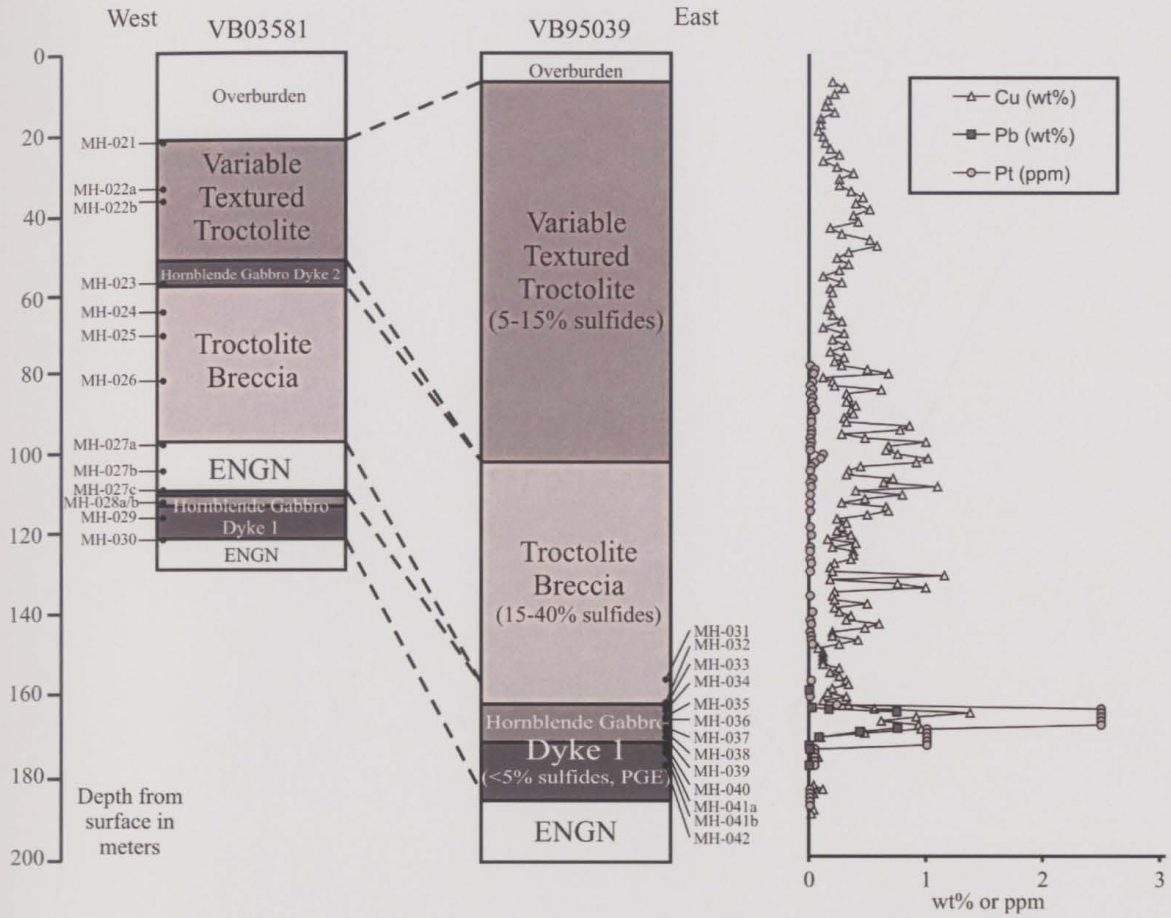

Figure 4.4. Lithostratigraphic and chemostratigraphic profiles through drill holes VB03581 and VB95039 with sample locations. ENGN = enderbitic gneiss.

A) Dyke rocks (≥20% hornblende)

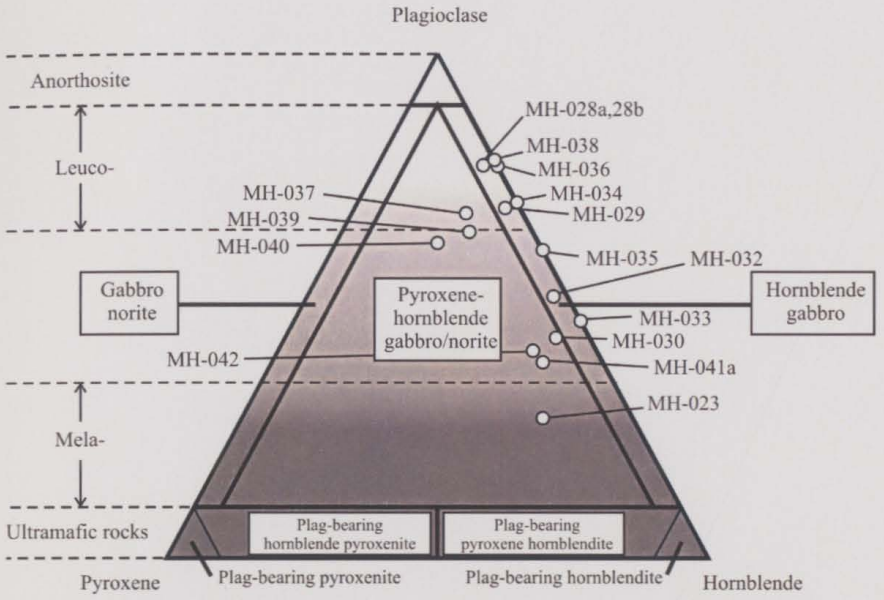

B) Main conduit troctolite rocks (≤15% hornblende)

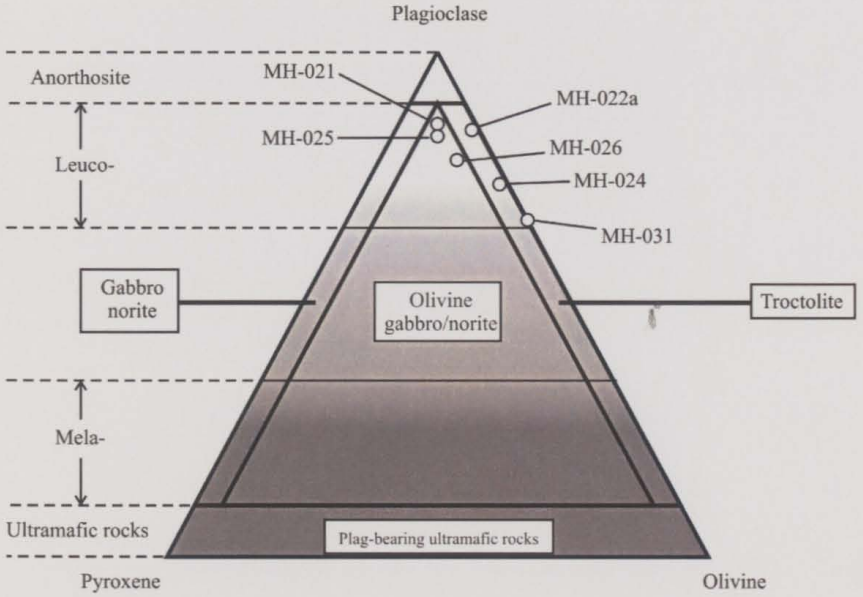

Figure 4.5. IUGS rock classification diagrams for samples from the Southeast Extension Zone based on normalization of a) 100% plagioclase-pyroxene-hornblende for dyke rocks (≥20% hornblende), and b) 100% plagioclase-pyroxene-olivine for main conduit troctolite rocks (≤15% hornblende).

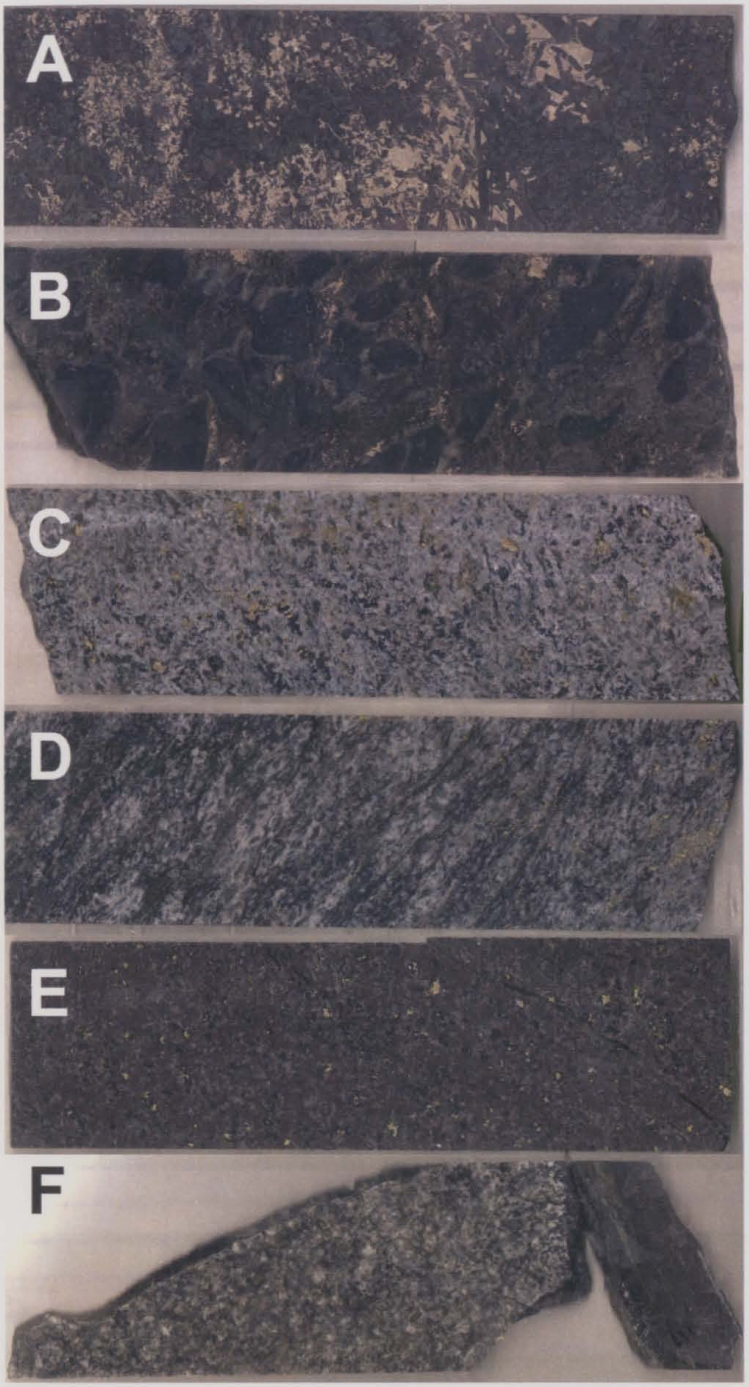

Figure 4.6. a) Variable textured troctolite MH-022a VB03581, b) troctolite breccia MH-031 VB95039, c) coarse-grained leucocratic inner hornblende gabbro dyke MH-034 VB95039, d) coarse-grained foliated inner hornblende gabbro dyke MH-038 VB95039, e) medium-grained melanocratic inner hornblende gabbro dyke MH-028 VB03581, and f) chill contact between enderbitic gneiss and fine-grained outer hornblende gabbro dyke MH-027c VB03581. Width of core = 4.5cm.

Table 4.3a. Silicate assemblages through drill holes VB95039 and VB03581.

No.	Depth	Rock	Minerals	Texture
VB03581				
21	22.00	VTT	60fPL ~ gPL, 5OL, 5PX, 10HN, 5-10BT, 10S	fine-med grained
22a	33.50	VTT	60fPL, 15OL, 1PX, 5HN, 5BT, 15S	med-coarse grained
22b-1	36.65	HGD	80fPL < gPL, 15S, carbonate-amphibole altered	granoblastic, framework
22b-2	37.71	HGD	70gPL, 20HN, 15S, altered	fabric, med, granoblastic
23	56.80	HGD	20-30gPL, 15PX, 50HN, 30S, altered	med-grained granoblastic
24-1	63.84	TBX	40-50fPL > gPL, 15OL, <5HN, 5BT, 10HI, 20S	coarse intergranular, bx
24-2	63.96	TBX	40-50fPL > gPL, 15OL, 15-20HN, 5-10BT, 20S	coarse intergranular, bx
25-1	69.60	TBX	50fPL ~ gPL, 5OL, 5PX, 10HN, 5-10BT, 15S	v. coarse intergranular, bx
25-2	69.64	TBX	50fPL ~ gPL, 5OL, 5PX, 5-10HN, 5BT, 5-10HI, 15S	coarse intergranular, bx
26-1	80.84	TBX	55-60fPL > gPL, 10OL, 5PX, <5HN, 5-10BT, 15HI, 15S	coarse intergranular, bx
26-2	80.90	TBX	55-60fPL > gPL, 10OL, 5PX, <5HN, 5BT, 5HI, 15S	coarse intergranular, bx
27a	96.80	ENGN	30gPL-interlobate, 10OPX, 10BT, 50S	fine-grained granoblastic
27b	103.40	ENGN	5aP, 60gPL-interlobate, 10OPX, 10BT, 10S	fine-grained granoblastic
27c-1	109.60	ENGN	70gPL-interlobate, 20OPX, <5BT	fine-grained granoblastic
27c-2	109.65	CONT	20gPL, 10OPX, 60BT	fine-grained granoblastic
28-1	112.25	IHGD	70fPL < gPL (alt), 2PX, <2OL, 15HN, 5-10BT, 5S	coarse intergranular
28-2	112.27	IHGD	60fPL > gPL, 10-15OL, 2PX, 15HN, 10BT, 5S	coarse intergranular
28-3	112.29	IHGD	60fPL > gPL, 10-15OL, 2PX, 15HN, 5-10BT, 5S	coarse intergranular
28-4	112.47	IHGD	60fPL > gPL (alt), 2PX, 10HN, 15HN, 15BT, 2HI, 5S	coarse intergranular
28-5	112.34	IHGD	60fPL, 10OL, 2PX, 15HN, 5BT, 5S	coarse intergranular
29-2	114.60	IHGD	60fPL (alt), 1OL, 2PX, 20HN, 5BT, HI?, <1S	coarse intergranular
29-1	114.75	OHGD	40fPL (alt), 5OL, 2PX, 40HN, 5-10BT, HI?, <1S	med-grained intergranular
30	120.60	ENGN	35fPL, 5OPX, 40HN, 15BT, <1S	fine-grained granoblastic
VB95039				
31	157.30	TBX	30fPL > gPL, 15OL, 15BT, ACT, 15HN, 10S	intergranular, bx
32	161.70	OHGD	40gPL (ser), 2-5PX, 35HN, 10BT, 5-10CHL, 5S	granoblastic, med-grained
33-1	162.16	IHGD	40gPL (ser), <2PX, 45HN, 5BT, 5-10CHL, 5S	weak fabric, med-grained
33-2	162.35	IHGD	40gPL (ser), 45HN, 5BT, 5-10CHL, 5S, altered	weak fabric, med-grained
33-3	162.25	IHGD	40gPL (ser), 45HN, <5BT, 5-10CHL, 5S, altered	weak fabric, med-grained
33-4	162.32	IHGD	40gPL (ser), 45HN, <5BT, 5-10CHL, 5S, altered	weak fabric, med-grained
34-1	162.74	IHGD	60gPL (ser), 20-30HN, 2BT, 5CHL, 5S	med-coarse grained
34-2	162.76	IHGD	60gPL (ser), 20-30HN, 2BT, 5-10CHL, 5S	med-coarse grained
34-3	162.70	IHGD	60gPL (ser), 20-30HN, 2-5BT, 5CHL, 5S	med-coarse grained
34-4	162.79	IHGD	60gPL (ser), 20-30HN, 2-5BT, 5CHL, 5S	med-coarse grained
35	164.05	IHGD	55gPL (ser), 35HN, 10BT, >5CHL, 5S	fabric, med-coarse grained
36	164.80	IHGD	70gPL (ser), 20HN, 10-15BT, 5CHL, 5S	fabric, fine-med grained
37	166.80	IHGD	60-70gPL, 10PX, 20HN, 15-20BT, 5S	fabric, fine-grained
38	167.70	IHGD	75gPL, 20HN, <5BT, 5S	fabric, med-grained
39	169.10	IHGD	50-60gPL, 10-15PX, 20HN, 20-30BT, 1S	strong fabric, fine-grained
40	171.10	OHGD	50gPL, 15PX, 15-20HN, 5BT	fabric, fine-grained
41a	172.00	OHGD	30-40gPL, 10PX, 40-50HN, 10-15BT	fabric, fine-med grained
42	176.05	OHGD	30-40gPL, 10PX, 35-45HN, 10BT	med-coarse grained

gPL = granoblastic plagioclase; fPL = framework plagioclase; aP = antiperthite; ser = sericite; HN = hornblende; BT = biotite; CL = chlorite; ACT = actinolite; OL = olivine; PX = pyroxene; OPX = orthopyroxene; CPX = clinopyroxene; S = sulfide; HI = hercynite inclusions; TR = trace; VTT = variable textured troctolite; TBX = troctolite breccias; HGD = hornblende gabbro dyke; OHGD = outer hornblende gabbro dyke; IHGD = inner hornblende gabbro dyke; ENGN = enderbitic gneiss; CONT = contact.

Table 4.3b. IUGS rock classification for samples in Southeast Extension Zone.

No.	Unit	Plagioclase-Pyroxene-Hornblende	Plagioclase-Pyroxene-Olivine
VB03581			
21	VTT		Leuco-olivine gabbronorite
22a	VTT		Leuco-troctolite
23	HGD	Mela-pyroxene hornblende gabbronorite	
24	TBX		Leuco-troctolite
25	TBX		Leuco-olivine gabbronorite
26	TBX		Leuco-olivine gabbronorite
28a	IHGD	Leuco-hornblende gabbro	
28b	IHGD	Leuco-hornblende gabbro	
29	OHGD	Leuco-hornblende gabbro	
30	OHGD	Pyroxene-hornblende gabbronorite	
VB95039			
31	TBX		Leuco-troctolite
32	OHGD	Hornblende gabbro	
33	IHGD	Hornblende gabbro	
34	IHGD	Leuco-hornblende gabbro	
35	IHGD	Hornblende gabbro	
36	IHGD	Leuco-hornblende gabbro	
37	IHGD	Leuco-pyroxene hornblende gabbronorite	
38	IHGD	Leuco-hornblende gabbro	
39	IHGD	Pyroxene-hornblende gabbronorite	
40	OHGD	Pyroxene-hornblende gabbronorite	
41a	OHGD	Pyroxene-hornblende gabbronorite	
42	OHGD	Pyroxene-hornblende gabbronorite	

VTT = variable textured troctolite; TBX = troctolite breccias; HGD = hornblende gabbro dyke; OHGD = outer hornblende gabbro dyke; IHGD = inner hornblende gabbro dyke; ENGN = enderbitic gneiss.

4.5.1.1 Variable textured troctolite

The variable textured troctolite (Fig. 4.6a) is a fine to very coarse-grained intergranular to ophitic textured leuco-troctolite to leuco-olivine gabbronorite. Plagioclase (~60%) occurs mostly as large resorbed (0.25-5mm) tabular grains (with aspect ratios of 2:1 up to 5:1) that define a framework within which other minerals occur interstitially. Fine-grained equigranular granoblastic plagioclase (ave = 0.05mm) forms 5-30% of the rock. It appears that the larger framework plagioclase has recrystallized to a granoblastic to interlobate texture at grain boundaries. The variable textured troctolite contains about 5-15% subhedral olivine (0.05-1.5mm; ave = 0.25mm) interstitial to framework plagioclase where the olivine contains rims of amphibole and biotite. The variable textured troctolite also contains <5% recrystallized patches of pyroxene and 5-10% hornblende. Biotite (5-10%) occurs as rims on sulfide and olivine. Sulfide (10-15%) occurs as interstitial blotches and disseminations of pyrrhotite-pentlandite-chalcopyrite (Fig. 4.6a). Trace magnetite (~1%) occurs interstitial to silicate minerals and is often associated with sulfides.

4.5.1.2 Troctolite breccia

The troctolite breccia (Fig. 4.6b) is a fine to coarse-grained intergranular to ophitic leuco-troctolite to olivine leuco-gabbronorite (Fig. 4.7a) with up to 20% hercynitic-bearing gneissic inclusions (Fig. 4.7b). The matrix to the breccia is a fine to

coarse-grained intergranular to ophitic textured troctolite with 30-60% plagioclase. The plagioclase occurs mostly as large resorbed (0.25-5mm) tabular grains (Fig. 4.7a) and to a lesser extent occurs as fine-grained equigranular granoblastic plagioclase similar to the variable textured troctolite (Fig. 4.7b). The troctolite breccia contains olivine (0.05-1.5mm; ave = 0.25mm), pyroxene, hornblende, biotite, and magnetite similar in texture and abundance to the variable textured troctolite. There is 15-20% sulfide that, as in the variable textured troctolite, occurs as interstitial blotches and disseminations of pyrrhotite-pentlandite-chalcopyrite (Fig. 4.6b).

4.5.1.3 Inner hornblende gabbro dyke

The mineralized dyke in this study may be subdivided into inner and outer domains based mainly on differences in sulfide mineralogy and PGE content. The inner hornblende gabbro dyke is a leucocratic to melanocratic, fine to locally coarse-grained granoblastic hornblende gabbro to leuco-hornblende gabbro/gabbronorite with a weak to strong fabric (Figs. 4.6c-e). It consists of 40-70% granoblastic (Fig. 4.7e) plagioclase (0.15-1.5mm, ave = 0.5mm) with 15-70% sericite in VB95039. There is 60-70% tabular plagioclase in VB03581 with >50% alteration. The inner hornblende gabbro dyke contains 15-45% euhedral (to locally subhedral) greenish-brown hornblende (0.1-1.5mm, ave = 0.5mm) in granoblastic patches and strings (Fig. 4.7d and f). Biotite (5-15%) commonly forms tabular grains (0.25-0.3mm) with ragged edges associated with either hornblende or chlorite and is foliated in places (Fig. 4.7h). Chlorite (5-10%) is generally

0.15mm (up to 2-3mm) and is associated with hornblende and is either greenish and feathery (Fig. 4.7g), or forms fibrous bundles, or forms irregular patches often associated with flecks of sulfide and oxide. Chlorite only occurs in the inner hornblende gabbro dyke in drill hole VB95039. Magnetite tends to be associated with hornblende exhibiting a similar polygonal shape as hornblende and also as small flecks within chlorite patches. The PGE and sulfide mineralization in the inner and outer domains of the dyke is described separately below.

4.5.1.4 Outer hornblende gabbro dyke

The outer hornblende gabbro dyke (Fig. 4.6f) is a medium-grained equigranular granoblastic leuco-hornblende gabbro to pyroxene-hornblende gabbronorite consisting predominantly of plagioclase (30-60%) and hornblende (15-50%). Plagioclase occurs in two forms: as equigranular granoblastic (Fig. 4.7i) grains (0.25-0.5mm; ave = 0.4mm) in VB95039, and as tabular grains defining a framework in VB03581 (Fig. 4.7j). Hornblende (15-50%) is euhedral (to locally subhedral), greenish-brown and occurs as chains or granoblastic patches (Fig. 4.7k) of individual grains (0.025-0.3mm; ave 0.25mm). It is associated with relict olivine (Fig. 4.7l) and pyroxene patches in VB03581. In VB95039, the lower outer hornblende gabbro dyke is foliated and overall the mineralogy and textures are better preserved in VB03581. Sulfide occurs as irregular to cuspate pyrrhotite-pentlandite (with minor chalcopyrite) blebs and disseminations (1.5-5mm; ave = 3mm). Sulfide is associated with euhedral to subhedral magnetite that

contains ilmenite exsolution lamellae rimmed by biotite and hornblende. In places, sulfides exhibit the granoblastic habit of hornblende and plagioclase (Fig. 4.7k). Olivine and plagioclase locally contain small (<0.025mm) sulfide grains (Fig. 4.7j).

4.5.1.5 Enderbitic gneiss

The enderbitic gneiss (Fig. 4.6f) consists of medium-grained plagioclase, orthopyroxene, and biotite and has a granoblastic to interlobate texture. Plagioclase (ave = 0.25mm) ranges from 30-70%; up to 15% antiperthite occurs as large (ave = 2-3mm) irregular grains. Orthopyroxene (10-20%) ranges in texture from recrystallized (ave = 0.1mm) to large equant grains (0.25mm up to 2-3mm). The enderbitic gneiss contains 10-15% weakly foliated biotite and up to 50% "invasive" sulfide (pyrrhotite). Magnetite (5%) occurs as small equigranular grains.

4.6 SULFIDE MINERALIZATION IN THE DYKE

Sulfides are a minor constituent (trace-5%) of the hornblende gabbro dyke. They range from a typical magmatic pyrrhotite ($Fe_{1-x}S$), pentlandite $(Fe,Ni)_9S_8$, chalcopyrite ($CuFeS_2$) assemblage (Figs. 4.8a-c) in the outer zone of the dyke to a predominantly chalcopyrite, bornite (Cu_5FeS_4), and galena (PbS) (Figs. 4.8d-f) with trace pyrite (FeS_2), sphalerite (ZnS), millerite (NiS), mackinawite $(Fe,Ni)S_{0.9}$, parkerite? ($Ni_3Bi_2S_2$), and volfsonite? ($Cu^{+}{}_{10}Cu^{+2}Fe^{+2}Fe^{+3}{}_2Sn^{+4}{}_3S_{16}$) assemblage in the "PGE-elevated" inner zone

of the dyke. The sulfides occur as blebs (Figs. 4.8a and b) and irregular and cuspate disseminations (0.1-5mm) interstitial to plagioclase and hornblende (Figs. 4.8c-e). Trace sulfides also occur along cleavage planes of biotite and hornblende in the inner hornblende gabbro dyke. Framework plagioclase can also contain "trains" of small sulfide inclusions (black inclusions in plagioclase in Fig. 4.7j) in the outer hornblende gabbro dyke. The sulfide assemblages for the dyke rocks and the main conduit troctolitic rocks are summarized in Table 4.4.

4.7 LITHOGEOCHEMISTRY

Whole rock major, trace, REE, and PGE concentrations for 20 samples (MH-021 to 041) from the two drill holes VB03581 and VB95039 in the hornblende gabbro dyke and surrounding host rocks were analyzed and evaluated to determine processes that may control the crystallization of the sulfides and PGM as well as the host silicates. Analytical details are outlined in Appendix 4.I and complete results are reported in Appendix 4.II.

Table 4.4. Sulfide assemblages through drill holes VB95039 and VB03581.

No.	Depth	Rock	Minerals	% Sulfide
VB03581				
21	22.0	VTT	po > ccp – pn	6.11
22a	33.5	VTT	po > ccp – pn	14.4
23	56.8	HGD	po > ccp – pn	28.5
24	63.8	TBX	po > ccp – pn	18.2
25	69.6	TBX	po > ccp – pn	13.3
26	80.8	TBX	po > ccp – pn	14.5
27a	96.8	ENGN	po > ccp – pn	46.2
28a	112.3	IHGD	ccp – gn – bn (tr py – ml – mk – park – volf)	4.39
28b	112.5	IHGD	ccp – gn – bn (tr po – py)	1.44
29	114.6	OHGD	po > ccp – pn	0.82
30	120.6	OHGD	tr ccp – gn	0.51
VB95039				
31	157.3	TBX	po – pn – ccp	7.38
32	161.7	OHGD	po > pn – ccp (vein)	51.9
33	162.1	IHGD	po ~ ccp > pn (tr gn – py – sph)	5.16
34	162.7	IHGD	po – pn – ccp (tr gn – bn – py – sph)	7.62
35	164.1	IHGD	ccp >> po – pn (tr gn – py – ml)	~5
36	164.8	IHGD	ccp > gn (tr po – pn – py – ml)	~5
37	166.7	IHGD	ccp > gn ~ bn	4.76
38	167.7	IHGD	ccp > gn – po	3.44
39	169.1	IHGD	tr ccp	1.06
40	171.1	OHGD	no sulfide	0.03
41a	172.0	OHGD	no sulfide	0.09
42	176.1	OHGD	tr ccp	0.33

Tr = trace; po = pyrrhotite; pn = pentlandite; ccp = chalcopyrite; gn = galena; py = pyrite, bn = bornite; ml = millerite; sph = sphalerite; mk = mackinawite; park = parkerite; volf = volfsonite; VTT = variable textured troctolite; TBX = troctolite breccias; HGD = hornblende gabbro dyke; OHGD = outer hornblende gabbro dyke; IHGD = inner hornblende gabbro dyke; ENGN = enderbitic gneiss.

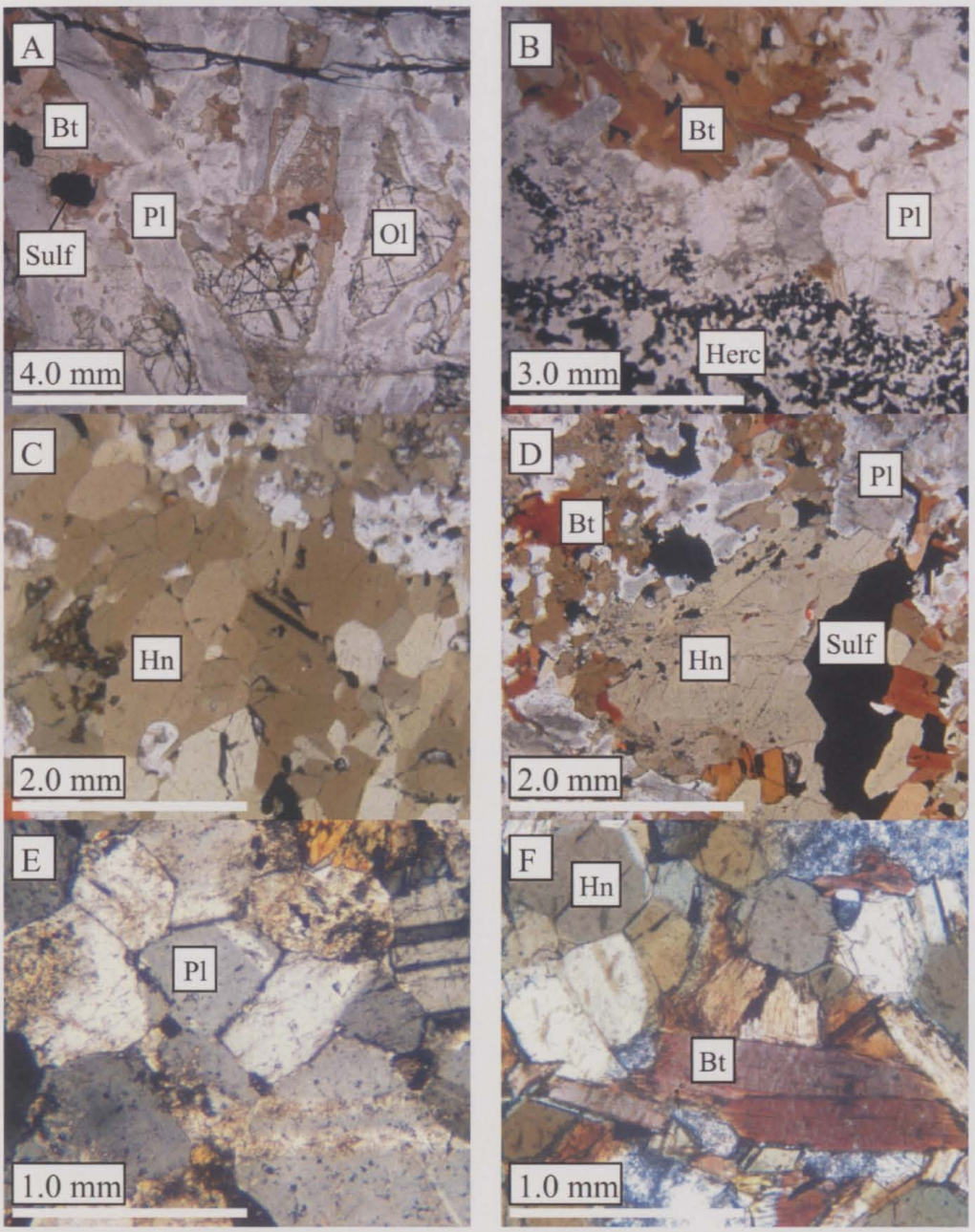

Figure 4.7. a) Framework plagioclase (pl) and olivine (ol) in the troctolite breccia (ppl) MH-024-2 VB03581, b) hercynite (herc) inclusion with granoblastic plagioclase (pl) and biotite (bt) in the troctolite breccia (ppl) MH-031-1 VB95039, c) hornblende (hn) in the hornblende gabbro dyke (ppl) MH-023 VB03581, d) hornblende (hn), plagioclase (pl), and biotite (bt) with sulfide (sulf) bleb in the inner hornblende gabbro dyke (ppl) MH-028-4 VB03581, e) granoblastic plagioclase (pl) in the inner hornblende gabbro dyke (xpl) MH-033-4 VB95039, f) granoblastic hornblende (hn) with biotite (bt) in the inner hornblende gabbro dyke (ppl) MH-033-4 VB95039.

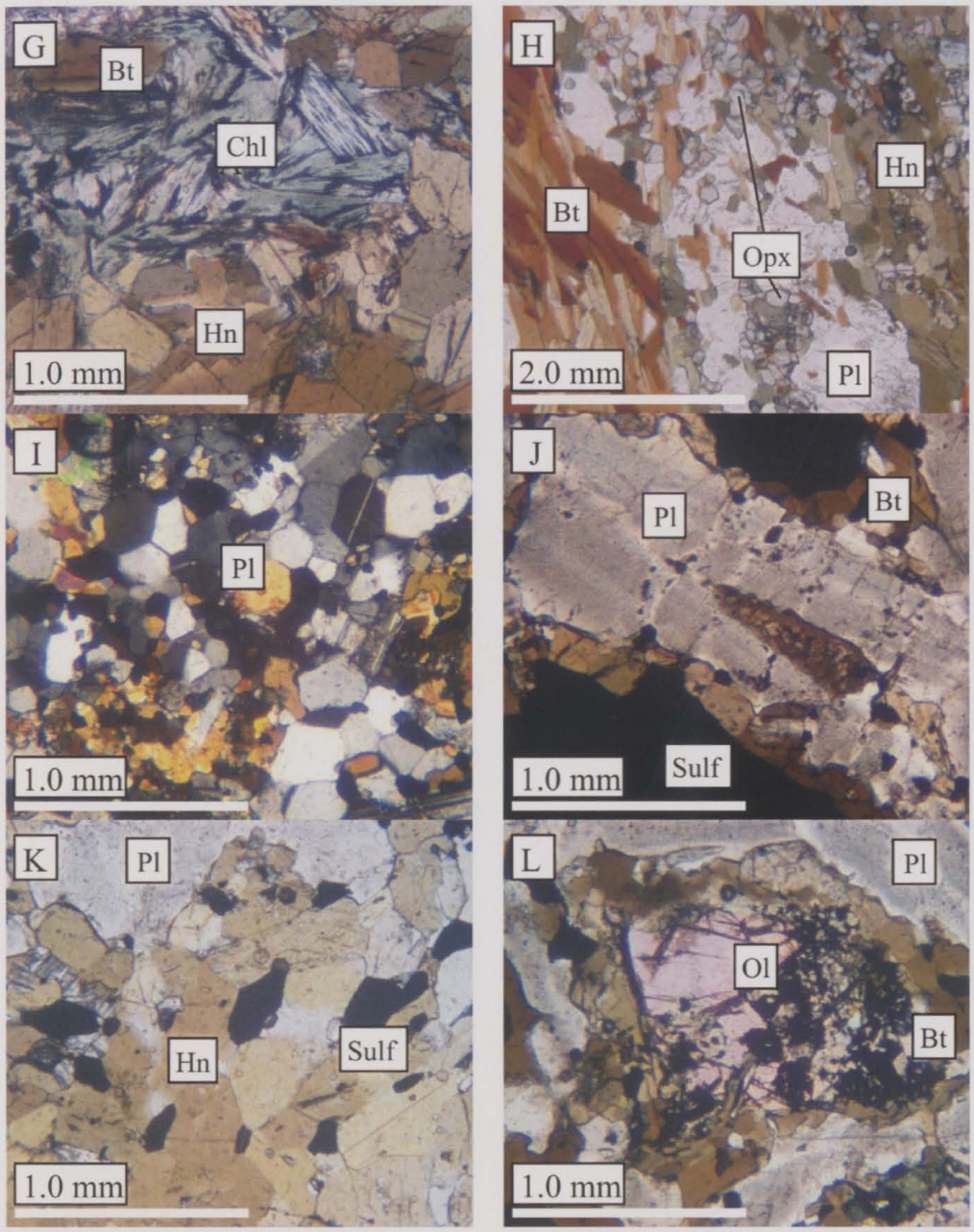

Figure 4.7. (*continued*). g) hornblende (hn), biotite (bt), and chlorite (chl) in the inner hornblende gabbro dyke (ppl) MH-033-4 VB95039, h) foliated hornblende (hn), plagioclase (pl), and biotite (bt) in the inner hornblende gabbro dyke (ppl) MH-039 VB95039, i) granoblastic plagioclase (pl) in the outer hornblende gabbro dyke (xpl) MH-029-1 VB03581, j) framework plagioclase (pl) in the outer hornblende gabbro dyke (xpl) MH-029-1 VB03581, k) granoblastic hornblende (hn) and plagioclase (pl) in the outer hornblende gabbro dyke (ppl) MH-029-1 VB03581, and l) olivine (ol) surrounded by hornblende (hn) in the outer hornblende gabbro dyke (xpl) MH-029-1 VB03581. Ppl = plane polarized light; xpl = cross polarized light.

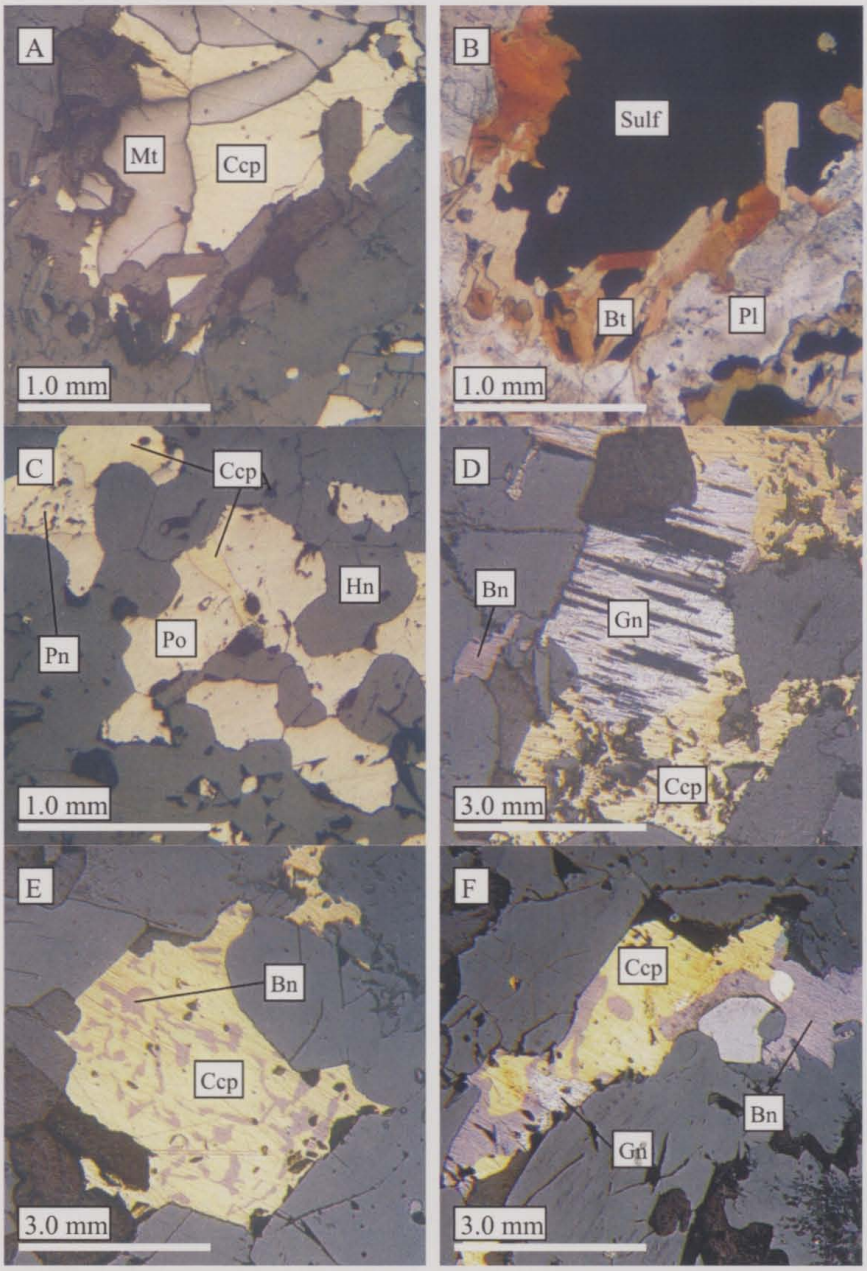

Figure 4.8. a) Magnetite (mt) and chalcopyrite (ccp) bleb with a biotite (bt) rim typical of the outer hornblende gabbro dyke (rl) MH-029-1 VB03581, b) same as a) in ppl, c) typical pyrrhotite-pentlandite-chalcopyrite (po-pn-ccp) assemblage interstitial to silicates in the outer hornblende gabbro dyke (rl) MH-029-1 VB03581, d) typical chalcopyrite-bornite-galena (ccp-bn-gn) assemblage in the inner hornblende gabbro dyke (rl) MH-028-5 VB03581, e) bornite (bn) exsolution in chalcopyrite (ccp) in the inner hornblende gabbro dyke (rl) MH-028-5 VB03581, and f) typical chalcopyrite-bornite-galena (ccp-bn-gn) assemblage in the inner hornblende gabbro dyke (rl) MH-028-5 VB03581. Rl = reflected light; ppl = plane polarized light.

4.7.1 Whole rock inter-element correlations

Whole rock inter-element correlation coefficients (R values) indicate that different groups of elements correlate with each other in the inner hornblende gabbro dyke and outer hornblende gabbro dyke (Table 4.5). A positive correlation between two elements approaches R = +1 with increasing degree of positive correlation, whereas a negative correlation approaches R = -1 with increasing degree of negative correlation.

The first group of elements that are highly correlated are Cu, Pb, Sn, Ga, Pt, Pd, Au, Ag, Bi, and Sb (Table 4.5). The second group of elements that have positive correlations is Rh, Ru, Ir, S, Fe, Ni, and Co (Table 4.5). There are no positive or negative correlations of the first group of elements with the second group of elements. Correlation coefficients are plotted in Figure 4.9.

Table 4.5. Correlation coefficient matrix using whole-rock data for dyke samples in the Southeast Extension Zone.

	n = 15 Pd	n = 15 Pt	n = 13 Au	n = 15 Cu	n = 15 Pb	n = 15 Ga	n = 6 Ru	n = 4 Ir	n = 4 Rh	n = 15 S	n = 15 Fe	n = 15 Ni	n = 11 Co	n = 12 As	n = 8 Se	n = 11 Ag	n = 11 Cd	n = 11 Sn	n = 7 Sb	n = 9 Te	n = 11 Bi	n = 15 Cl
Pd	**1.0000**																					
Pt	**0.8561**	**1.0000**																				
Au	**0.8800**	*0.7845*	**1.0000**																			
Cu	*0.6566*	*0.7038*	*0.7477*	**1.0000**																		
Pb	*0.6703*	*0.5996*	*0.7875*	**0.8900**	**1.0000**																	
Ga	*0.5858*	*0.5374*	*0.6922*	**0.8058**	**0.9490**	**1.0000**																
Ru	-0.0005	-0.0410	0.0114	-0.0365	0.0886	-0.3112	**1.0000**															
Ir	-0.0293	-0.1184	-0.1107	-0.1568	-0.2736	-0.5502	**0.9150**	**1.0000**														
Rh	-0.0563	-0.2151	-0.1054	-0.2910	-0.3064	-0.4967	**0.9977**	**1.0000**	**1.0000**													
S	0.0004	-0.0073	-0.0032	0.0000	-0.0041	-0.0475	**0.9400**	**0.9940**	**0.9973**	**1.0000**												
Fe	-0.0238	-0.0842	-0.0529	-0.0687	-0.1066	-0.2023	**0.9062**	**0.9830**	**0.9778**	**0.8686**	**1.0000**											
Ni	-0.0020	-0.0285	-0.0116	-0.0085	-0.0219	-0.0910	**0.9397**	**0.9990**	**0.9982**	**0.9866**	**0.9173**	**1.0000**										
Co	0.0000	-0.0223	-0.0196	-0.0028	-0.0295	-0.1468	**0.9207**	**0.9995**	**1.0000**	**0.9844**	**0.9095**	**0.9978**	**1.0000**									
As	0.1841	0.2585	0.1959	0.4188	0.3542	0.2651	0.1689	0.2075	1.0000	0.2052	0.0554	0.1453	0.1308	**1.0000**								
Se	0.0162	0.0271	0.0457	0.0662	0.0735	0.0326	-0.0150	**1.0000**	NA	0.0191	-0.4295	-0.0020	-0.0527	0.0000	**1.0000**							
Ag	*0.6962*	*0.7056*	*0.7640*	**0.9116**	**0.8745**	**0.8015**	-0.2011	-0.2559	**-1.0000**	-0.0049	-0.1142	-0.0243	-0.0322	0.2670	0.0895	**1.0000**						
Cd	0.4588	*0.5021*	*0.5765*	**0.9683**	**0.9895**	**0.8941**	-0.0852	-0.2868	**-1.0000**	-0.0044	-0.1355	-0.0237	-0.0330	0.3126	0.1062	**0.9083**	**1.0000**					
Sn	*0.6641*	**0.8353**	*0.7771*	**0.8670**	**0.8166**	*0.7376*	-0.1829	-0.2583	**-1.0000**	-0.0063	-0.1251	-0.0286	-0.0349	0.3869	0.0451	**0.8835**	**0.8261**	**1.0000**				
Sb	*0.7036*	**0.8601**	**0.8207**	0.4014	0.3320	0.2333	0.2877	**1.0000**	NA	-0.0678	-0.1431	-0.0814	-0.0973	0.1541	0.2706	*0.5164*	0.4169	*0.6577*	**1.0000**			
Te	0.2085	0.2919	0.3179	0.3470	0.3465	0.2659	-0.1298	*-0.5438*	**-1.0000**	-0.0189	-0.1219	-0.0372	-0.0191	0.0387	**0.8334**	0.4139	0.4057	0.3605	*0.5578*	**1.0000**		
Bi	0.3448	0.4274	0.4597	**0.9433**	**0.9758**	**0.8787**	-0.1272	-0.3052	**-1.0000**	-0.0026	-0.1452	-0.0203	-0.0280	0.3329	0.1702	**0.8476**	**0.9700**	*0.7845*	0.3439	0.4773	**1.0000**	
Cl	-0.0531	-0.0478	-0.2400	-0.1327	-0.1226	-0.0841	-0.4827	-0.1144	NA	-0.1125	-0.0478	-0.0903	-0.1543	-0.0130	-0.0639	-0.0144	-0.0459	-0.0333	-0.2566	-0.0850	-0.0594	**1.0000**

Values in bold = correlation coefficients >0.8000.

Values in italics = correlation coefficients from 0.5000-0.8000.

Negative values are negative correlations, positive values are positive correlations.

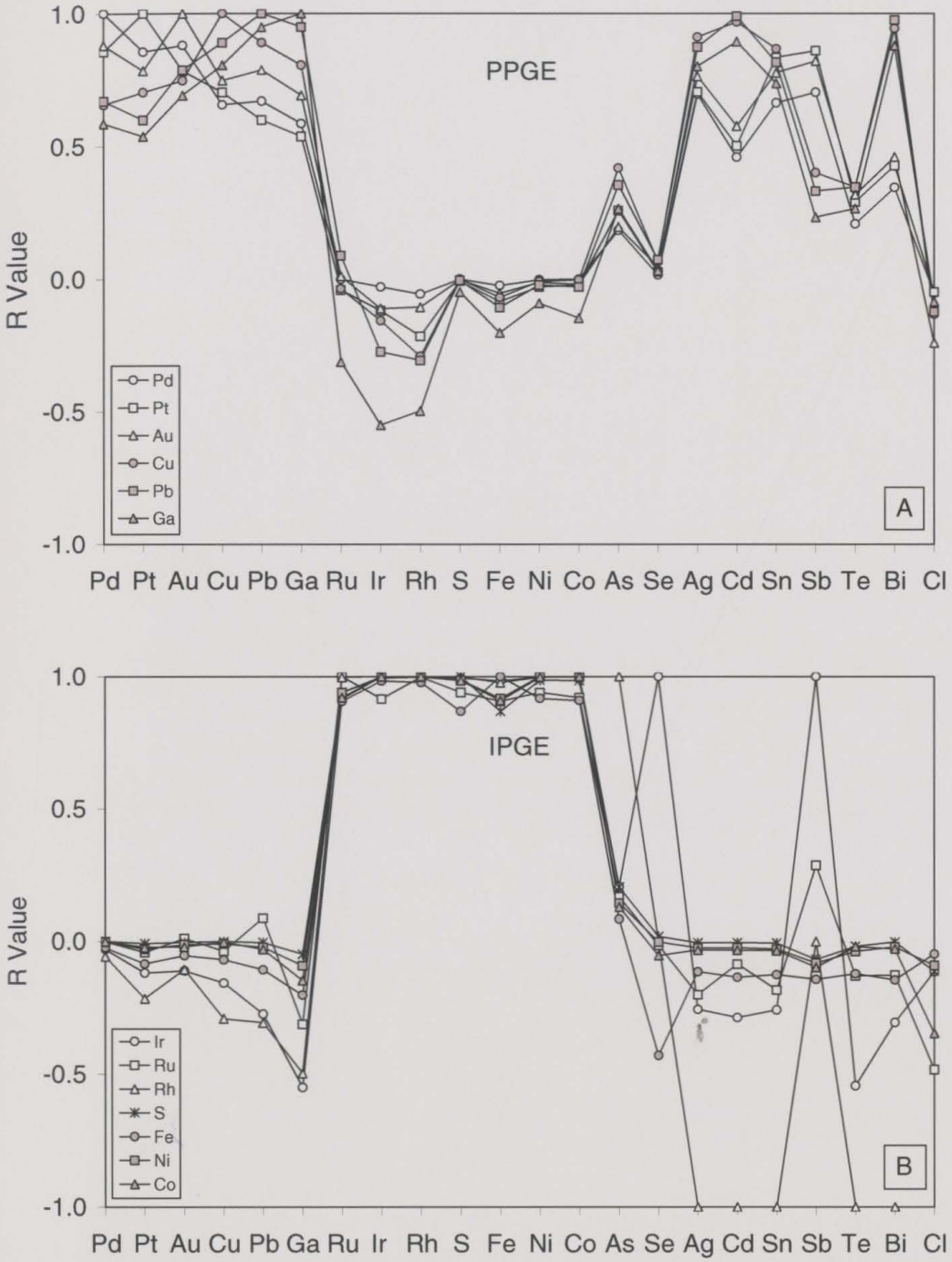

Figure 4.9. Correlation coefficients (R) plotted for a) PPGE, Au, Cu, Pb, and Ga, and b) IPGE, S, Fe, Ni, and Co against other elements. A positive correlation between two elements is denoted as positive and approaches R = +1 with increasing degree of positive correlation, whereas a negative correlation is denoted as negative and approaches R = -1 with increasing degree negative of correlation.

4.7.1.1 PPGE

Palladium and Pt have a strong positive correlation with each other exhibit a strong to moderately strong correlation with Cu, Pb, Ga, Au, Ag, Cd, Sn, and Sb (Fig. 4.9a). Copper, Pb, and Ga also have strong positive correlations with Au, Ag, Cd, Sn, and Bi.

4.7.1.2 IPGE

Rhodium, Ru, and Ir have a strong positive correlation with each other and exhibit a strong positive correlation with the base metals S, Fe, Ni, and Co (Fig. 4.9b).

Several correlation coefficient values are 1.0000 due to the fact that only analyses 1-2 samples are available of the particular elements being compared and should be interpreted with caution. However, these apparent perfect correlations do not effect the interpretations of the PPGE and IPGE correlations discussed above.

4.7.2 Chalcophile element chemostratigraphy

Chemostratigraphy through drill holes VB03581 and VB95039 for base metals (S, Ni, Cu, and Pb), the PGE (Pt and Pd), and various ratios (Cu/Ni, Cu/S, Ni/S, Pt/Pd, Pt/S, and Pd/S) from the different units are summarized in Figure 4.10. Data plotted in Figure

4.10 are from the Voisey's Bay Nickel Company Limited Mine Exploration Borehole System database.

The chalcophile element chemostratigraphy for each lithology relative to the other units (Fig. 4.10) is: 1) variable textured troctolite: moderate sulfide, constant and moderate Cu, constant and moderate Ni, low Pb, low PGE and Au, low Cu/Ni, and low Pt/Pd. 2) troctolite breccia: high sulfide, slightly increasing Cu down hole, slightly increasing Ni down hole, low Pb, low PGE, low Cu/Ni, and very low Pt/Pd, 3) unmineralized hornblende gabbro dyke: moderate sulfide, moderate Cu, moderate Ni, low Pb, low PGE, low Cu/Ni, and low Pt/Pd, 4) enderbitic gneiss: low sulfide, low Cu, depleted in Ni, low Pb, no PGE, moderate Cu/Ni, and moderate Pt/Pd, 5) inner hornblende gabbro dyke: low sulfide, strongly enriched in Cu, low Ni, enriched in Pb, strongly enriched in PGE and Au, high Cu/Ni, and high Pt/Pd, and 6) outer hornblende gabbro dyke: low sulfide, low Cu, low Ni, low Pb, low PGE and Au, low to moderate Cu/Ni, and low to moderate Pt/Pd.

4.7.3 PGE patterns

Whole rock PGE patterns (normalized to 100% sulfide and then normalized against chondrite values (McDonough and Sun, 1995; Appendix 4.I - Table A4.1b) were plotted to evaluate the fractionation and enrichment processes affecting the PGE distribution in the Southeast Extension Zone (Fig. 4.11).

The PGE patterns for the variable textured troctolite (5-15% sulfide) and troctolite breccia (5-15% sulfide) are moderately fractionated and are highly depleted in IPGE (Figs. 4.11a and b); the Pt/Pd ratio ranges from 0.05-0.35. The PGE patterns for the outer hornblende gabbro dyke are fractionated with moderately depleted IPGE (Figs. 4.11c and d); the Pt/Pd ratios range from 0.22-0.67. The PGE patterns for the inner hornblende gabbro dyke rocks (trace-5% sulfide) show an extreme fractionation between the IPGE and the PPGE with highly enriched PPGE and depleted IPGE (Figs. 4.11e and f); the Pt/Pd ratios range from 0.45-2.82. The PGE pattern for the enderbitic gneiss (30-40% sulfide in this example) is unfractionated and slightly depleted relative to chondrite (Fig. 4.11g); the Pt/Pd ratio is 0.20.

4.7.4 Rare earth element (REE) patterns

The whole rock REE of 20 samples from the variable troctolite, troctolite breccia, inner hornblende gabbro dyke, outer hornblende gabbro dyke, and the enderbitic gneiss from drill holes VB03581 and VB95039 in the Southeast Extension Zone were normalized to primitive mantle values (McDonough and Sun, 1995; Appendix 4.I - Table A4.1a) and compared to values of some typical Voisey's Bay rock types from Li *et al.* (2000) in Figure 4.12 (i.e., conduit rocks with Ce <50 (n = 11), conduit rocks with Ce >50 (n = 20), variable textured troctolite with Ce <50 (n = 48), variable textured troctolite with Ce >50 (n = 7), and normal troctolite (n = 102)). The whole rock REE patterns for the dyke and main conduit troctolite rocks in the Southeast Extension Zone are similar to

those of other typical Voisey's Bay troctolite rocks in other portions of the intrusion. Similar to the main conduit rocks, the hornblende gabbro dyke rocks can be grouped into two types based on their whole rock REE patterns. Although, there are two distinct REE patterns in the dyke rocks, these do not correlate with inner and outer dyke rocks; both the inner and outer dyke rocks contain both type I and type II REE patterns. Type I rocks have overall lower whole rock REE patterns, LREE enrichment, and a positive Eu anomaly and are represented by troctolites and breccias of typical conduit rocks (Fig. 4.12a) and by some of the hornblende gabbro dyke rocks (Fig. 4.12b). Type II rocks have overall higher whole rock REE contents, LREE enrichment, and little or no Eu anomaly and are represented by the remaining hornblende gabbro dyke rocks (Fig. 4.12c). All troctolite conduit rocks exhibit similarly fractionated heavy and light REE patterns but vary in their overall abundances and the size of the Eu anomalies.

The lower REE pattern with a positive Eu anomaly is attributed to a cumulate rock that has crystallized and accumulated plagioclase. The higher REE pattern with little or no Eu anomaly is attributed to a melt-dominated rock that did not accumulate plagioclase. The host enderbitic gneiss exhibits the largest LREE/HREE fractionation but no Eu anomaly deviating from the trend of the Voisey's Bay rocks (Fig. 4.12d). The fact that the two REE patterns exist in the main conduit rocks and the hornblende gabbro dyke rocks implies that both cumulate and melt material are present in the system.

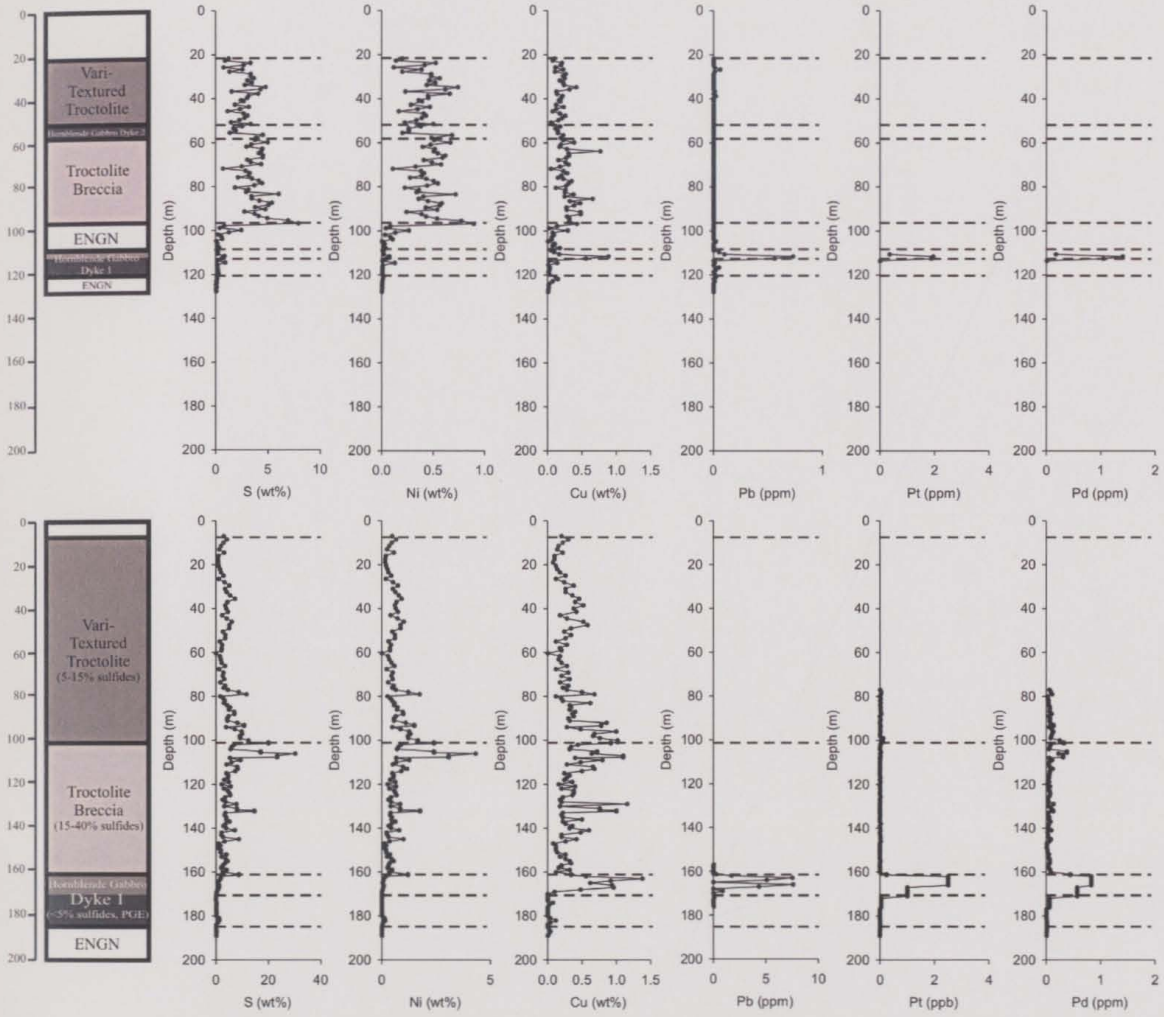

Figure 4.10. a) Downhole chemostratigraphy through drill holes VB03581 and VB95039 for chalcophile elements (S, Ni, Cu, Pb, Pt, and Pd). Data from Voisey's Bay Nickel Company Limited Mine Exploration Borehole System database.

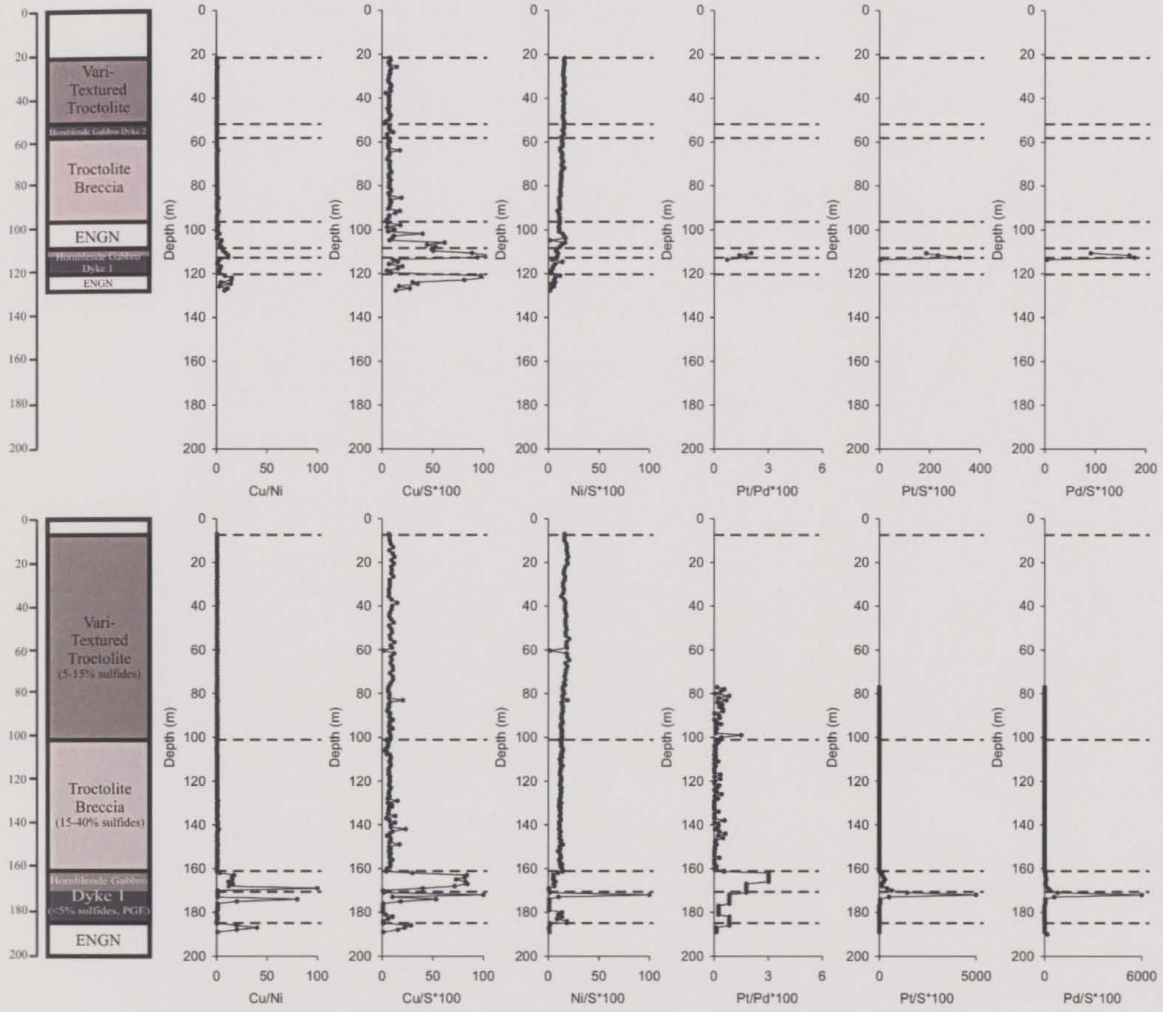

Figure 4.10. *continued.* b) Downhole chemostratigraphy through drill holes VB03581 and VB95039 for chalcophile element ratios (Cu/Ni, Cu/S*100, Ni/S*100, Pt/Pd*100, Pt/S*100, and Pd/S*100). Data from Voisey's Bay Nickel Company Limited Mine Exploration Borehole System database.

4.8 PRECIOUS METAL MINERALS (PMM) IN THE DYKE

Platinum-group minerals (PGM) and other precious metal minerals (PMM) were separated from the dyke in order to determine their identity and associations. Discrete PMM were concentrated from three samples (MH-028, MH-035, and MH-036) that contained elevated PGE values in the inner hornblende gabbro dyke. The samples were initially carefully crushed in a shatter box and sieved to different size fractions and then passed through a hydroseparator (model HS-02) to concentrate the PMM (Rudashevsky *et al.,* 2002 used model HS-01). Monolayer grain-mounts were made from the concentrates and automated PMM searches were preformed at CANMET (see Appendix 4.I for details of analytical method).

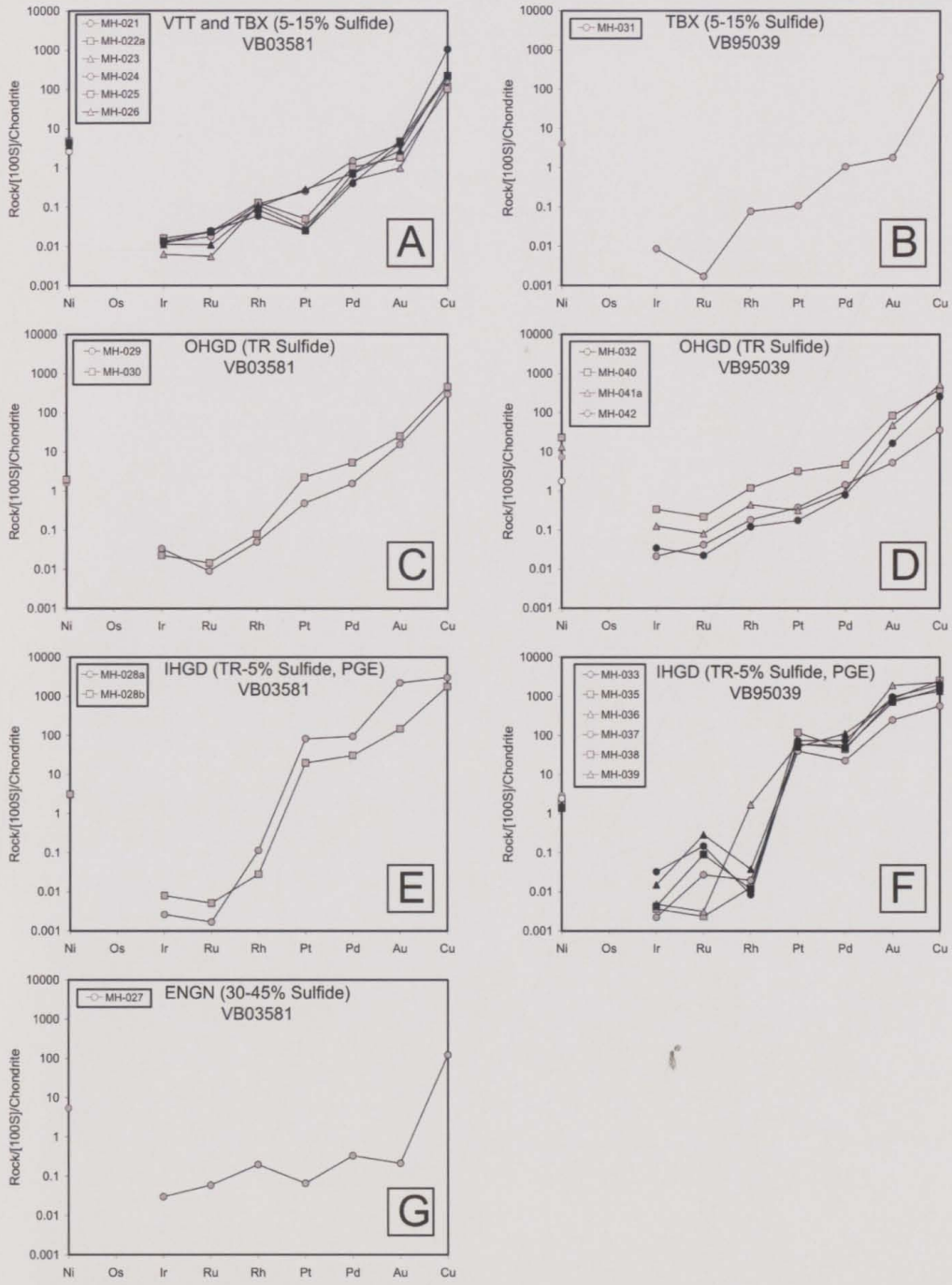

Figure 4.11. Sulfide and chondrite-normalized PGE patterns for: a) variable textured troctolite (VTT) and troctolite breccia (TBX), b) troctolite breccia (TBX), c) outer hornblende gabbro dyke (OHGD), d) outer hornblende gabbro dyke (OHGD), e) inner hornblende gabbro dyke (IHGD), f) inner hornblende gabbro dyke (IHGD), and g) enderbitic gneiss (ENGN). [100S] = 100% sulfides. Chondrite values are from McDonough and Sun (1995).

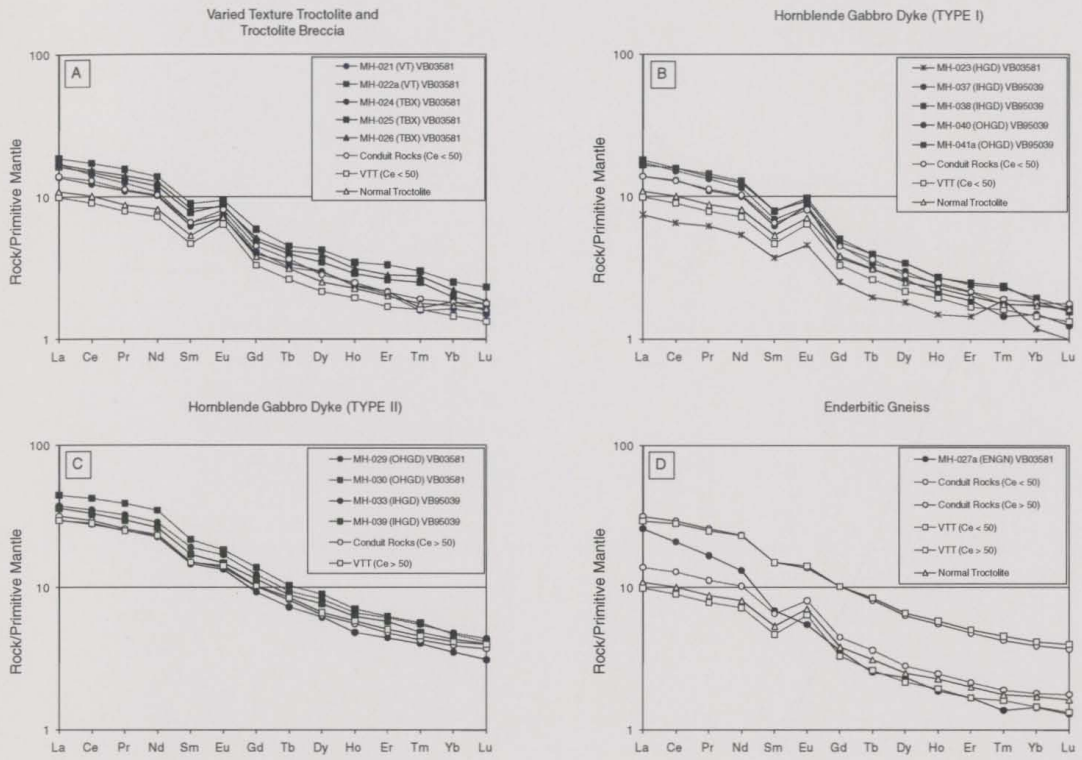

Figure 4.12. Whole rock REE patterns for: a) variable textured troctolite (VTT) and troctolite breccia (TBX) from the main conduit in Southeast Extension Zone, b) hornblende gabbro dyke (type I), c) hornblende gabbro dyke (type II), and d) enderbitic gneiss (ENGN) normalized to primitive mantle values (McDonough and Sun (1995); Appendix 4.I – Table A4.1a) and compared to other main conduit and troctolite rocks of the Voisey's Bay intrusion from Li *et al.* (2000). IHGD = inner hornblende gabbro dyke, OHGD = outer hornblende gabbro dyke.

4.8.1 PMM identities

The searches located 186 discrete PGM grains and 295 other PMM (Table 4.6). In order of decreasing volume percent abundance the PGM are sperrylite ($PtAs_2$), paolovite (Pd_2Sn), froodite (PdBiTe), Sn-stibiopalladinite [$Pd_{5-x}(Sb,Sn)_{2-x}$], sobolevskite or polarite

(PdBi), maslovite (PtBiTe), and unnamed (Pd-Bi-Sb-Te) (Figs. 4.13a and b). The identifications of the PGM were subsequently confirmed by electron probe microanalysis carried out on the Cameca SX-50 in the Memorial University of Newfoundland Department of Earth Sciences laboratories. Details of analytical methods are outlined in Appendix 4.I; electron probe microanalysis results are reported in Appendix 4.IIIa. Further work is required to confirm the identification of the unnamed Pd-Bi-Sb-Te mineral. Approximately 30 of the 186 PGM grains were too small (1-5 μm) to analyze by electron probe microanalysis or had low totals when analyzed. The energy dispersive X-ray spectra of these phases suggest they include geversite ($PtSb_2$), niggliite (PtSn), "vincentite" $(Pd,Pt)_3(As,Sb,Te)$, insizwaite $Pt(Bi,Sb)_2$, rustenburgite $(Pt,Pd)_3Sn$, and two undefined PGM. The discrete PGM are predominantly Pt and Pd bismuth tellurides, antimonides, and Sn-PGM with Pt minerals being dominant. This is consistent with the whole rock having high Pt/Pd ratios (Fig. 4.10b). Representative images of the dominant PGM are located in Figure 4.14. The PGM and other PMM, their associations, and abundances are outlined in Table 4.6.

The other precious metal minerals (n = 295) associated with the PGM in order of decreasing volume percent abundance include native Ag, stützite ($Ag_{5-x}Te_3$), electrum, matildite ($AgBiS_2$), and three undefined Ag-minerals (Figs. 4.13a and b). Several grains of tsumoite (BiTe) and sulphotsumoite? (Bi_3Te_2S) were also identified and are associated with the PGM (Appendix 4.IIIa).

4.8.2 PMM associations

The PGM and other PMM were most often completely liberated (27.7% of the total number of grains) or hosted by and/or associated with base-metal sulfides (55.9% of the grains) and other PMM (13.0% of the grains). Only 3.35% of the total number of PMM grains are associated with silicate minerals (Figs. 4.13c and d).

It can be seen that the most important base-metal sulfides associated with the PMM are galena (16.1% of the total number of grains), chalcopyrite (15.5% of the total number of grains), and bornite (15.3% of the total number of grains). Approximately 18 grains of 481 PMM are associated with silicate minerals (hornblende, chlorite, pyroxene, and plagioclase), 150 are liberated, and the remaining 313 grains are associated with and/or hosted by one or more of the following: galena (86) > chalcopyrite (83) > bornite (82) > other PMM (67) > pentlandite (31) > stützite (21) > parkerite (9) > millerite (6) > native Ag (6) > electrum (4) > volfsonite? (1). No PMM were found to be associated with pyrrhotite.

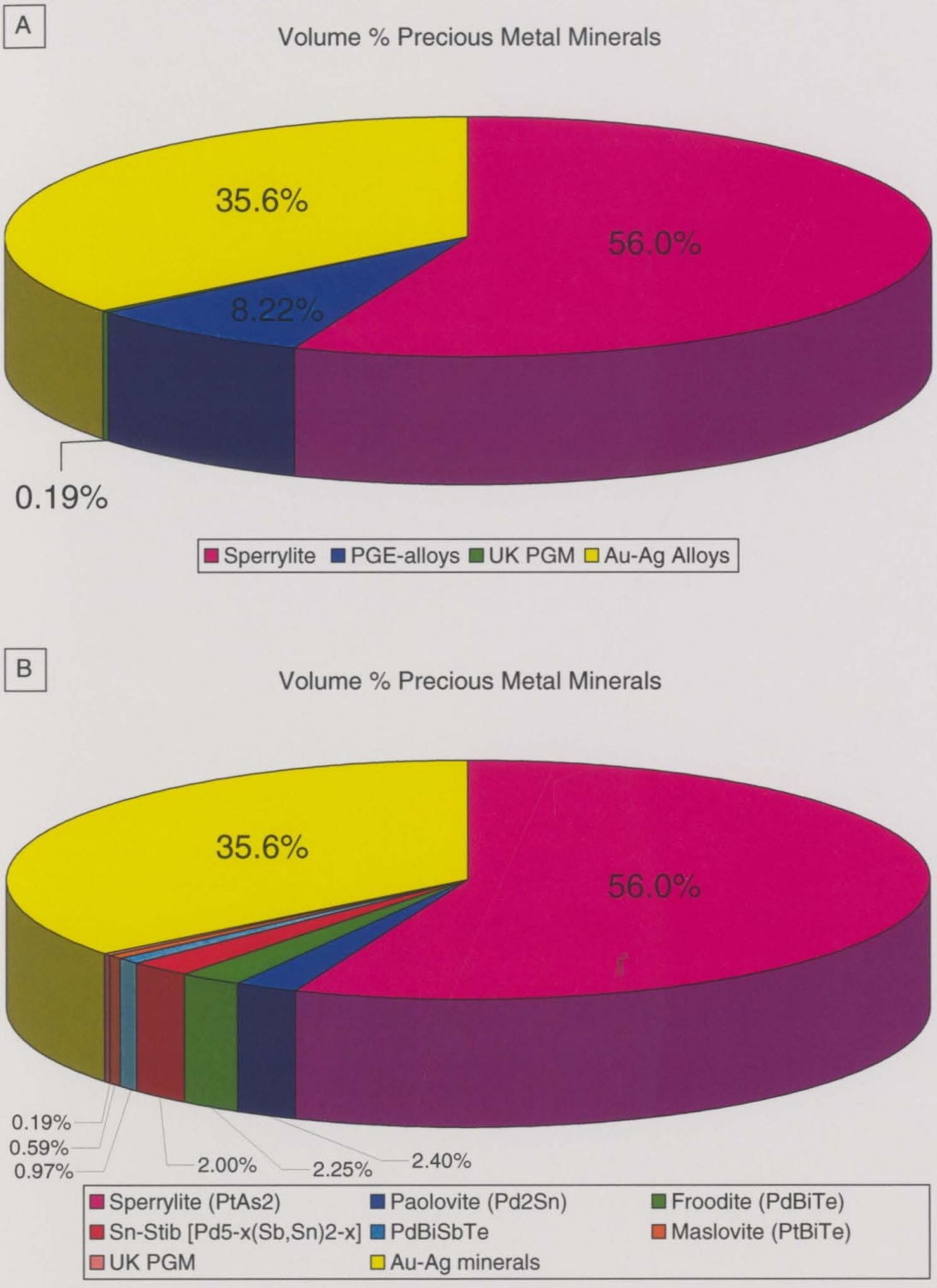

Figure 4.13. a) Relative volume % abundance of precious metal minerals, b) relative volume % abundance of precious metal minerals indicating the individual PGE-alloys.

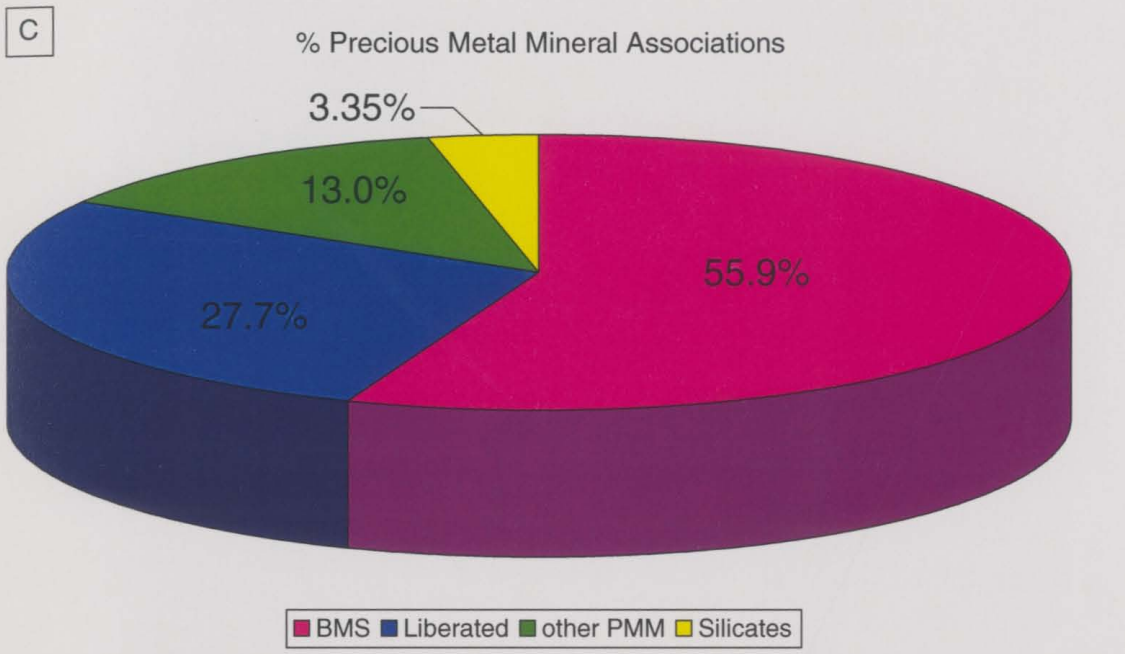

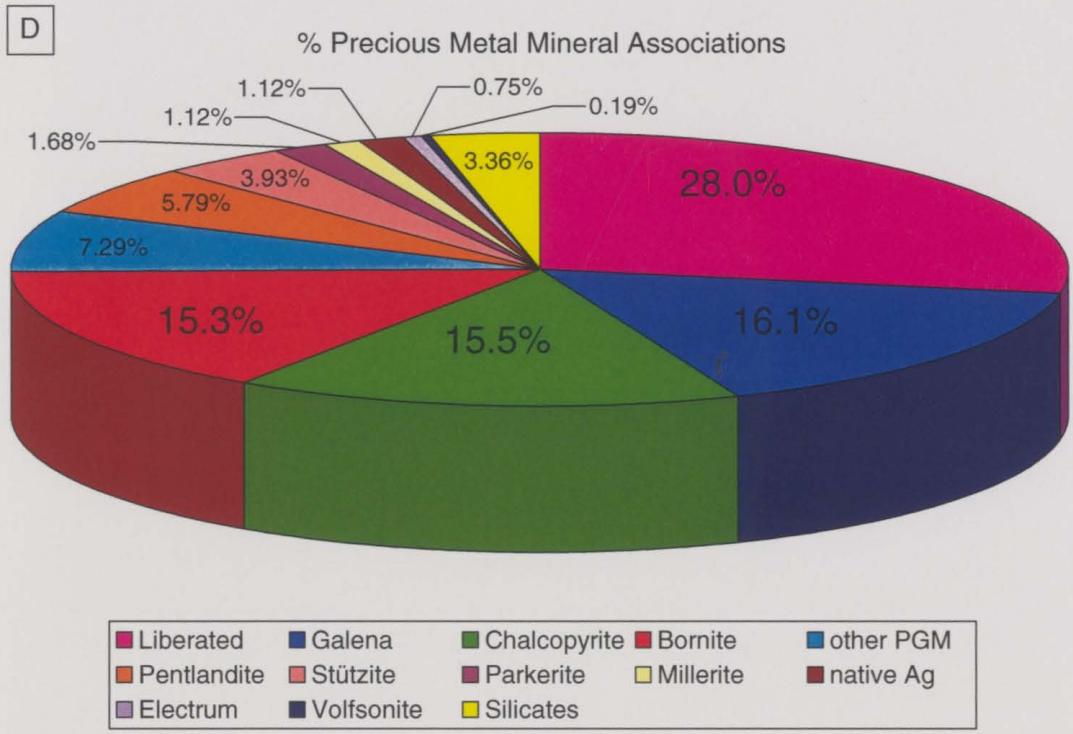

Figure 4.13. (*continued*). c) % precious metal mineral associations, and d) % precious metal mineral associations with each BMS and PMM phase indicated.

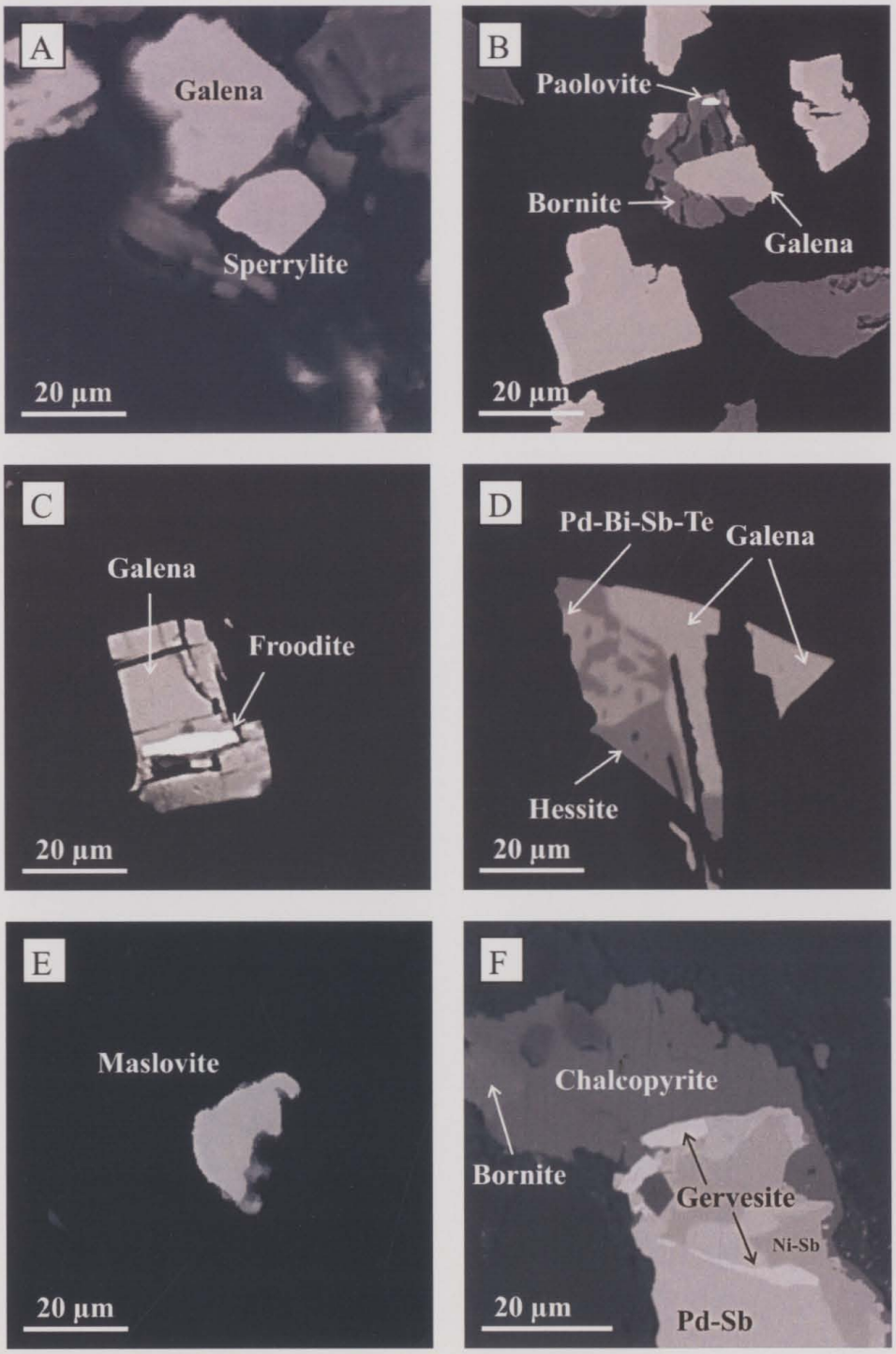

Figure 4.14. Photomicrographs of: a) sperrylite (MH-035/36), b) paolovite (MH-028a), c) froodite (MH-028a), d) Pd-Bi-Sb-Te (MH-035/36), e) maslovite (MH-035/36), and f) geversite (MH-028a).

Table 4.6. Precious metal minerals, associated phases, and abundances.

PGM	Associations (based on number of grains)	No.	Volume (μm^3)	Volume %
Sperrylite	ccp (25) > liberated (20) > bn (17) > sz (14) > gn (6) = pn (6) > elec (4) > park (3) = Ag (3) > px (3) > PGM (1) = pl (1)	88	901285	55.9
Paolovite	PGM (9) > ccp (5) = bn (5) > liberated (4) > pn (2) > pl (2) > sz (1) = volf (1) = hn (1) = chl (1)	29	38658	2.40
Froodite	gn (7) > liberated (4) = PGM (2) > ccp (1) = px (1)	15	36208	2.24
Sn-Stibiopalladinite	PGM (2) > liberated (1) = ccp (1) = sz (1) = Ag (1) = px (1)	5	32251	2.00
Pd-Bi-Sb-Te	PGM (9) > gn (5) > sz (3) > liberated (2) > ccp (1) > Ag (1)	17	15607	0.97
Maslovite	liberated (5)	5	9462	0.59
Platarsite*	liberated (1) = ccp (1) = gn (1)	3	4459	0.28
Geversite*	PGM (16) > bn (1) = sz (1) = px (1)	11	1888	0.12
Soblolevskite/Polarite*	PGM (2) > hn (1)	3	1067	0.07
Niggliite*	bn (1)	1	37	0.002
Vincentite?*	pn (1)	1	21	0.001
Insizwaite*	bn (1)	1	13	0.0008
Rustenburgite*	bn (5)	5	9	0.0006
Unknown 1*	ccp (1) = pn (1) = PGM (1) = chl (1) = px (1)	4	52	0.003
Unknown 2*	ccp (1) = pn (1)	1	2	0.0001
Ag-Au Minerals				
Native Ag	liberated (72) > bn (43) > gn (33) > ccp (29) > pn (17) > ml (4) > park (3) = pl (3) > PGM (2) > sz (1) = chl (1) = hn (1)	188	388348	24.1
Stützite	gn (32) > ccp (15) > PGM (12) > liberated (10) > bn (4) > park (3) > Ag (1)	61	121808	7.55
Electrum	liberated (30) > ccp (3) > bn (1) = hn (1)	35	43196	2.68
Matildite	gn (4)	4	1947	0.12
Unknown 1*	liberated (1)	1	14160	0.88
Unknown 2*	gn (1) = ccp (1)	1	1563	0.10
Unknown 3*	pn (3) > ml (2)	5	1342	0.08

*Identities of these minerals are not confirmed but abundance and associations were determined. Ccp = chalcopyrite; bn = bornite; sz = stützite; gn = galena; pn = pentlandite; elec = electrum; ml = millerite; park = parkerite; px = pyroxene; pl = plagioclase; volf = volfsonite; chl = chlorite; hn = hornblende.

4.9 CHEMISTRY OF SULFIDE MINERALS

4.9.1 Major and minor elements in sulfide phases by EPMA

The sulfide minerals pyrrhotite, pentlandite, chalcopyrite, bornite, galena, pyrite, millerite, mackinawite, parkerite, and volfsonite were analyzed by electron probe microanalysis (see Appendix 4.I for analytical details) for their major and trace elements (S, Pb, Fe, Cu, Zn, Ni, Co, As, Se, Sb, Te, Cd, Bi, and Sn). Depending on the mineral, these elements can vary from a major constituent to a trace element and not all elements were measured in all phases. Analytical totals for parkerite and volfsonite may be slightly low since not all elements may have been analyzed. Complete data for individual analyses are reported in Appendix 4.IIIa and average values for each sulfide mineral are reported in Table 4.7.

A notable result from the electron probe microanalysis data is that in addition to the major Ni-bearing sulfides (pentlandite, millerite, and mackinawite), pyrrhotite and pyrite also contain measurable amounts of Ni (average of 0.68 ± 0.17 wt% in pyrrhotite and up to 0.8 wt% in pyrite) and Co (up to 2.9 wt% in millerite, 2.2 wt% in mackinawite, and 3.6 wt% in pyrite), however, these elements are not main constituents of the platinum-group minerals (PGM) and these minerals are not spatially associated with the PGM. The Cu-rich minerals chalcopyrite and bornite can contain measurable amounts of Pb (0.68-0.99 wt%), Sb (0.13-0.59 wt%), Te (0.19-0.28 wt%), and Bi (1.03-1.5 wt%); galena can contain measurable Te (0.1-0.4 wt%) and Bi (0.2-1.5 wt%); and parkerite can

contain measurable Sb (0.1-0.5 wt%) where detected. Antimony, Te, and Bi are main constituents of the PGM and the Cu-rich minerals and galena are spatially associated with the PGM.

4.9.2 PGE in solid solution in sulfide phases by LA-ICP-MS

In situ trace-element PGE (Pt, Pd, Rh, Ru, Ir, and Os) analyses were carried out on pyrrhotite (n = 32), pentlandite (n = 37), chalcopyrite (n = 74), cubanite (n = 4), bornite (n = 5), galena (n = 17), and pyrite (n = 2) in 13 samples from the two drill holes (VB03581: MH-021, 022a, 022b, 023, 024, 025, 026, 028, 209; VB95039: MH-033, 034, 036, 038) in the Southeast Extension Zone using laser ablation – inductively coupled plasma – mass spectrometry at Memorial University of Newfoundland Department of Earth Sciences laboratories (see analytical methods section for operating conditions and interpretation of data; Appendix 4.I). Complete laser ablation – inductively coupled plasma – mass spectrometry results are listed in Appendix 4.IVa and summarized in Table 4.8 and below. Where values were below the detection, the detection limit value was used and is an upper limit of the element concentration. The PGE are listed in order of decreasing abundance for each sulfide mineral in Table 4.9a and for each element the order of abundance in the minerals is listed in Table 4.9b.

The most significant result is that Pd occurs in pentlandite (ave = 2ppm) and galena (ave = 1.9ppm). This may be the first documented occurrence of PGE in solid solution in galena. Figure 4.15 shows representative laser ablation – inductively coupled

plasma – mass spectrometry spectra of these analyses. The continuous signals for Pd during ablation indicate that the metal is present in solid solution in both pentlandite and galena (Fig. 4.15).

Palladium was also found in chalcopyrite (ave = 0.15ppm), cubanite (ave = 0.13ppm), and bornite (ave = 0.10ppm). The Pd values reported for chalcopyrite, cubanite, and bornite required large corrections (up to a 95% correction for chalcopyrite) due to interferences with $^{40}Ar\,^{65}Cu$, ^{106}Cd and/or $^{40}Ar\,^{66}Zn$, ^{108}Cd and/or $^{40}Ar\,^{68}Zn$, and ^{110}Cd on ^{105}Pd, ^{106}Pd, ^{108}Pd, and ^{110}Pd, respectively. Platinum is only slightly above detection in pyrrhotite (ave = 0.038ppm), chalcopyrite (ave = 0.034ppm), pentlandite (ave = 0.055ppm), galena (ave = 0.057ppm), and bornite (ave = 0.154ppm). Rhodium occurs in solid solution in pyrrhotite (ave = 0.23ppm) and pentlandite (ave = 0.76ppm) but was not determined in chalcopyrite, cubanite, and bornite due to interferences from $^{40}Ar^{63}Cu$ on ^{103}Rh; and it was not determined in galena due to interferences from doubly-charged ^{206}Pb. Ruthenium occurs in solid solution in pyrrhotite (ave = 0.07ppm), pentlandite (ave = 0.79), and pyrite (ave = 0.09ppm). The values reported for Ru in pyrrhotite and pentlandite required large corrections (up to 90% correction for pentlandite) from isotope interferences of $^{40}Ar^{59}Co$, $^{40}Ar^{61}Ni$, $^{40}Ar^{62}Ni$ on ^{99}Ru, ^{101}Ru, and ^{102}Ru, respectively. Osmium is only slightly above detection in pyrrhotite (ave = 0.023ppm) and pentlandite (ave = 0.23ppm). Iridium is only slightly above detection for pentlandite (ave = 0.08ppm), galena (ave = 0.033ppm), and bornite (ave = 0.019ppm).

Table 4.7. Average major element compositions of sulfide minerals determined by electron probe microanalysis.

Label	S	Pb	Fe	Cu	Ni	Bi	Sn	Totals
Unit	wt%	wt%	wt%	wt%	wt%	wt%	wt%	
Pyrrhotite (n = 21)	39.42		60.29		0.68			100.4
	± 0.35		± 0.29		± 0.17			
Pentlandite (n = 5)	32.87		29.78		36.07			98.7
	± 0.23		± 0.18		± 0.26			
Chalcopyrite (n = 40)	34.56		30.53	34.05				99.1
	± 0.93		± 0.54	± 0.50				
Bornite (n = 4)	25.46		11.54	61.44				98.4
	± 1.15		± 0.26	± 0.31				
Galena (n = 13)	13.26	85.84						99.1
	± 0.16	± 1.25						
Pyrite (n = 6)	54.10		45.45		0.25			99.8
	± 0.28		± 1.50		± 0.31			
Millerite (n = 3)	34.65				61.48			96.1
	± 1.72				± 2.16			
Mackinawite (n = 9)	33.28		21.49		43.10			97.9
	± 0.35		± 1.06		± 0.81			
Parkerite (n = 4)	10.11				25.47	59.91		95.5
	± 0.10				± 0.31	± 0.57		
Volfsonite (n = 2)	29.58		10.04	39.28			17.28	96.2
	± 0.04		± 0.10	± 0.19			± 0.01	

4.10 MINERAL CHEMISTRY OF SILICATES

Plagioclase, olivine, pyroxene, amphibole, biotite, and chlorite major element and Cl compositions were determined by electron probe microanalysis. Analytical details are outlined in Appendix 4.I; results are reported in Appendix 4.IIIb.

Results indicate that plagioclase from the inner and outer hornblende gabbro dyke rocks tend to be more sodic (An <50) (Fig. 4.16) than plagioclase from troctolites and olivine gabbros of the Voisey's Bay intrusion (An >50) published in Li *et al.* (2000).

able 4.8. Average in situ PGE and trace element analysis of pyrrhotite, chalcopyrite, pentlandite, galena, cubanite, bornite, and pyrite.

	Element	SO_2	Pd	Rh	Ru	Os	Ir	Pt	Ga	Zn	Se	Mo	Ag	Cd	Sn	Sb	Te	Au	Hg	Pb	Bi
	Isotope	34	105-108	103	101-102	188-189	191-193	194-195	69	70	77	95	107-109	111	118	121	125	197	202	208	209
	Unit	wt%	ppm	ppm	ppm	ppm	ppm	ppm	ppm	ppm	ppm	ppm	ppm	ppm	ppm	ppm	ppm	ppm	ppm	ppm	ppm
	Detection Limit	0.100	0.010	0.050	0.020	0.010	0.010	0.010	0.020	0.500	1.500	0.020	0.100	0.050	0.030	0.010	0.100	0.010	0.050	0.100	0.010
YRRHOTITE																					
	Median	38.630	0.026	0.144	0.068	0.018		0.036	0.099	11.091	68.187	0.428	0.847	0.216	0.331	0.067	0.939	0.017	0.854	1.133	0.213
	Average	38.630	0.030	0.235	0.071	0.023		0.038	0.509	45.586	69.396	0.591	1.046	0.269	0.412	0.086	1.253	0.101	1.078	2.065	0.354
	Min	38.630	0.023	0.050	0.047	0.012		0.013	0.022	0.786	26.429	0.111	0.157	0.075	0.044	0.010	0.150	0.000	0.152	0.130	0.068
	Max	38.630	0.046	0.813	0.110	0.056		0.068	3.020	214.683	128.068	2.034	3.853	1.277	1.762	0.325	4.767	0.696	4.668	9.874	2.550
	n = 32	32	3	14	9	7	0	4	17	20	32	29	31	21	31	24	31	24	32	32	32
HALCOPYRITE																					
	Median	34.830	0.079		0.153	0.012		0.036	0.215	463.159	48.370	0.173	17.434	34.605	8.091	0.041	5.310	0.043	2.059	6.260	0.322
	Average	34.933	0.150		0.153	0.012		0.034	0.351	516.551	48.131	0.296	47.061	45.676	60.203	0.104	6.829	0.082	2.048	13.081	0.583
	Min	34.830	0.016		0.153	0.010		0.010	0.036	25.029	13.069	0.024	2.067	1.521	0.435	0.014	0.181	0.003	0.115	0.959	0.035
	Max	38.630	1.178		0.153	0.013		0.058	2.238	1656.120	154.813	1.803	267.627	382.281	298.097	0.817	24.304	0.367	4.456	100.745	4.773
	n = 74	74	45	0	1	2	0	9	51	74	74	48	74	74	74	50	72	69	74	72	74
ENTLANDITE																					
	Median	33.210	0.772	0.269	0.194	0.232	0.028	0.032	0.543	23.650	54.358	0.439	1.326	0.382	0.455	0.091	1.979	0.032	0.746	8.857	0.419
	Average	33.210	2.025	0.763	0.793	0.232	0.080	0.055	0.793	89.047	53.325	0.663	5.477	2.952	0.766	0.165	4.137	0.099	1.249	18.064	0.819
	Min	33.210	0.117	0.079	0.029	0.232	0.011	0.011	0.040	1.135	20.114	0.055	0.179	0.090	0.050	0.015	0.282	0.000	0.142	1.131	0.022
	Max	33.210	15.500	3.925	7.506	0.232	0.252	0.185	2.794	922.528	96.865	3.620	56.371	35.660	4.413	0.718	22.089	0.713	8.936	63.294	4.125
	n = 37	37	37	13	14	1	4	5	33	31	37	25	35	24	37	33	37	35	37	36	37
GALENA																					
	Median	13.080	0.246				0.033	0.040	0.509	9.535	1413.411	0.152	933.879	95.760	5.465	0.667	105.621	0.023	0.141		36.139
	Average	13.080	1.949				0.033	0.057	0.510	558.394	1306.318	0.245	3109.386	108.628	10.956	0.955	484.636	0.338	0.470		47.845
	Min	13.080	0.019				0.026	0.011	0.035	2.034	10.403	0.022	3.788	0.120	0.039	0.025	9.261	0.000	0.070		24.068
	Max	13.080	7.055				0.040	0.122	1.133	5919.090	3135.267	0.847	7092.047	398.700	51.315	3.834	2708.174	2.548	3.071		107.338
	n = 17	17	10	0	0	0	2	5	11	11	17	11	17	17	17	14	17	15	10	0	6
CUBANITE																					
	Median	35.160	0.130						0.333	634.267	56.480	1.059	23.003	50.280	2.687	0.082	5.477	0.084	1.465	7.828	0.121
	Average	35.160	0.133						0.478	611.413	57.161	1.059	28.115	47.732	3.020	0.075	6.030	0.061	1.524	8.262	0.105
	Min	35.160	0.057						0.036	482.220	47.559	1.059	13.969	37.071	1.833	0.022	3.921	0.003	0.911	6.504	0.036
	Max	35.160	0.217						1.065	694.899	68.124	1.059	52.486	53.296	4.873	0.121	9.246	0.096	2.254	10.888	0.157
	n = 4	4	4	0	0	0	0	0	3	4	4	1	4	4	4	3	4	3	4	4	3

BORNITE																					
	Median	23.790	0.095				0.019	0.154		52.434	11.679	1.144	527.796	3.295	2.459	0.279	1.408	0.086	3.011		5.168
	Average	23.790	0.099				0.019	0.154		79.177	10.315	1.408	2477.573	4.778	16.846	0.279	1.216	0.086	2.793		6.311
	Min	23.790	0.013				0.019	0.154		35.402	2.999	1.034	28.915	3.210	0.138	0.279	0.111	0.028	1.219		3.668
	Max	23.790	0.190				0.019	0.154		176.436	16.268	2.046	7148.352	7.829	68.918	0.279	1.939	0.144	3.933		11.543
	n = 5	5	3	0	0	0	1	1	0	4	3	3	5	3	5	1	4	2	4	0	5
PYRITE																					
	Median	53.450			0.086				0.328	41.300	10.030		15.643	12.875	5.519	0.126	0.425		0.525	4.202	0.365
	Average	53.450			0.086				0.328	41.300	10.030		15.643	12.875	5.519	0.126	0.425		0.525	4.202	0.365
	Min	53.450			0.086				0.328	0.949	3.221		0.596	12.875	5.519	0.080	0.185		0.525	1.695	0.162
	Max	53.450			0.086				0.328	81.650	16.838		30.691	12.875	5.519	0.171	0.664		0.525	6.708	0.568
	n = 2	2	0	0	1	0	0	0	1	2	2	0	2	1	1	2	2	0	1	2	2

n values are the number of analyses that had concentrations above detection.

4.9a. Summary of PGE detected in sulfide phases.

Mineral	Elements	<Detection	Not Determined
Pyrrhotite	Rh >> Ru	Pd, Os, Ir, Pt	
Pentlandite	Pd >> Rh > Ru	Os, Ir, Pt	
Chalcopyrite	Pd	Ru, Os, Ir, Pt	Rh
Cubanite	Pd	Ru, Os, Ir, Pt	Rh
Bornite	Pd > Pt	Ru, Os, Ir,	Rh
Galena	Pd >> Pt	Ru, Os, Ir	Rh
Pyrite	Ru	Pd, Rh, Os, Ir, Pt	

Table 4.9b. PGE in decreasing abundance in sulfide phases.

Element	Minerals	<Detection	Not Determined
Pd	Pn > Gn > Cb > Ccp > Bn > Po	Py	
Rh	Pn > Po	Py	Ccp, Cb, Bn, Gn
Ru	Pn > Py > Po	Ccp, Cb, Bn, Gn	
Os		Po, Pn, Ccp, Cb, Bn, Gn, Py	
Ir		Po, Pn, Ccp, Cb, Bn, Gn, Py	
Pt	Bn > Gn	Po, Pn, Cb, Py	

Py = pyrite; ccp = chalcopyrite; cb = cubanite; bn = bornite; gn = galena; po = pyrrhotite; pn = pentlandite.

Table 4.10. Chlorine, Sn, and Pb in hydrous silicate minerals.

Sample	Rock	n (Cl)	Cl (wt%)	St Dev	n	Sn (ppm)	St Dev	Pb (ppm)	St Dev
HORNBLENDE									
MH-028-4	IHGD	11	0.05	0.01	7	729	169	461	690
MH-034-2	IHGD				5	300	24	207	21
MH-029	OHGD				10	141	9	145	11
MH-039	IHGD-OHGD	16	0.14	0.03	15	20	7	84	13
MH-024-2	TBX	11	0.12	0.06	11	12	5	15	6
MH-023	HGD	10	0.29	0.02	11	9	1	13	2
MH-027c-1	ENGN				4	5	1	5	2
BIOTITE									
MH-028-4	IHGD	6	0.07	0.03	2	169	27	291	44
MH-029	IHGD				9	35	5	208	58
MH-039	IHGD-OHGD	13	0.20	0.02	11	6	1	145	13
MH-024-2	TBX	7	0.10	0.05	5	2	1	49	24
MH-027c-1	ENGN				10	16	3	18	5
MH-027c-2	ENGN				7	10	2	65	68
CHLORITE									
MH-034-2	IHGD				5	4	3	141	167

IHGD = inner hornblende gabbro dyke; OHGD = outer hornblende gabbro dyke; TBX = troctolite breccias; HGD = hornblende gabbro dyke; ENGN = enderbitic gneiss.

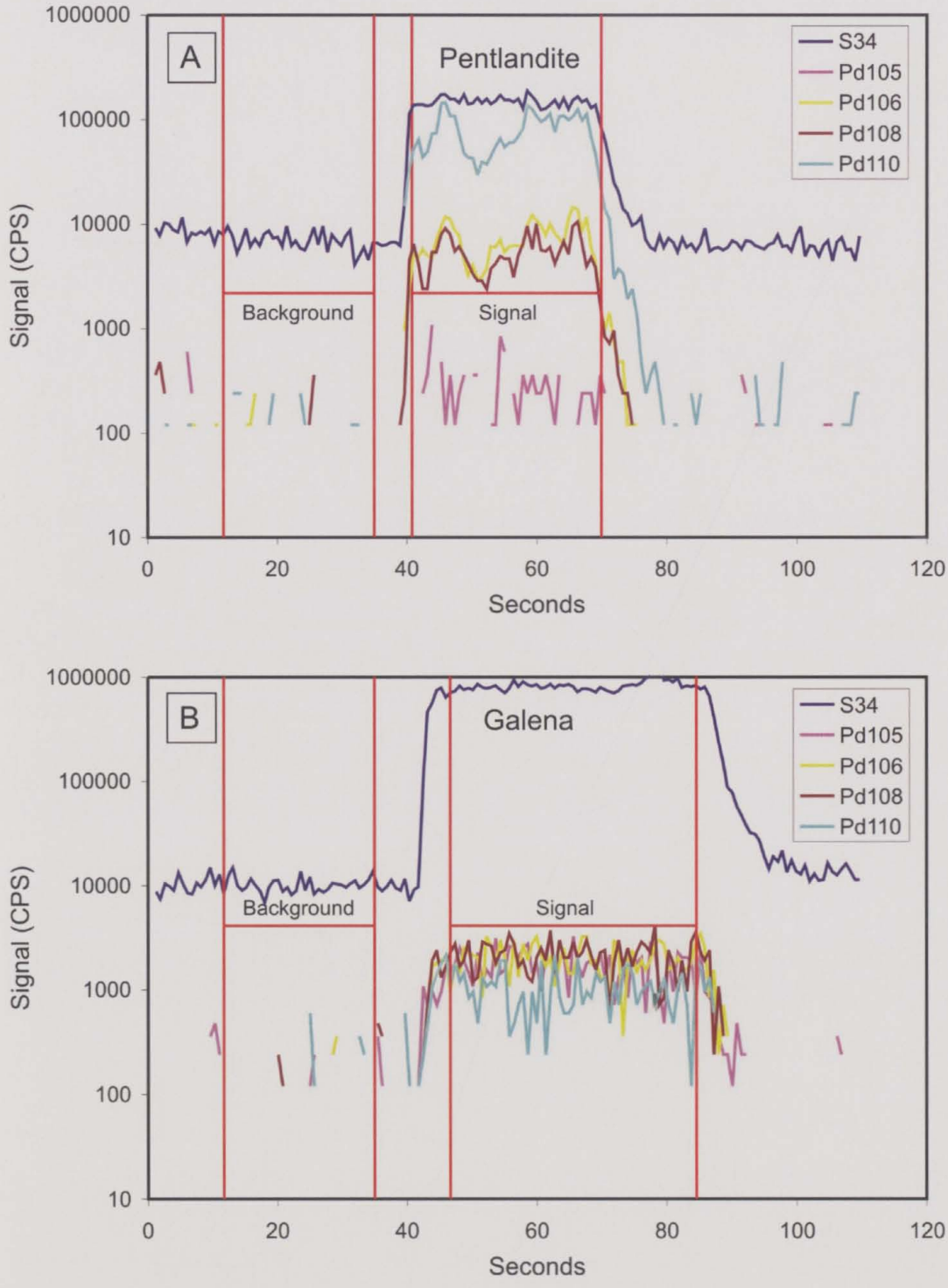

Figure 4.15. a) Palladium in solid solution in pentlandite, and b) palladium in solid solution in galena determined by laser ablation – inductively coupled plasma – mass spectrometry.

Amphibole compositions are plotted with respect to Si and Mg/(Mg+Fe*) on the classification diagram of Hawthorne (1981) in Figure 4.17. Results show that the amphibole all plot at high Mg/(Mg+Fe*) (>0.5) and range in composition from magnesio-hornblende to tschermakite in composition. There is a slight trend from higher Mg/(Mg+Fe*) and lower Si to lower Mg/(Mg+Fe*) and higher Si with troctolite breccia rocks having the most primitive values, the outer hornblende gabbro dyke rocks have moderate values, and the inner hornblende gabbro dyke rocks having the most evolved values.

4.10.1 Rare earth elements (REE) in silicate minerals

In situ trace-element analyses of the REE were carried out on olivine (n = 11), orthopyroxene (n = 5), clinopyroxene (n = 10), amphibole (n = 63), biotite (n = 44), chlorite (n = 5), and plagioclase (n = 23) from both PGE mineralized and non-mineralized samples in the dyke by laser ablation – inductively coupled plasma – mass spectrometry (see Appendix 4.I for details on analytical method and a discussion of interferences; results are reported in Appendix 4.IVb).

Rare earth element patterns for hornblende, biotite, chlorite, olivine, pyroxene, and plagioclase are shown in Figure 4.18. The results indicate that chlorite and biotite have relatively flat and near chondrite REE values similar to those of pyroxene, olivine, and plagioclase in the mineralized dyke. Hornblende, on the other hand, is much more enriched in REE. Interferences result in slight overestimates of Ho and Yb in plagioclase

(due to Rb and Ba, respectively) and of La and Ce in olivine and pyroxene (due to Co and Ni, respectively) (see Appendix 4.I)

Although, there may be slight overestimates in these element concentrations in these silicate minerals due to interferences (Appendix 4.I), it does not effect the overall interpretation. It is still clear that these minerals could not have contributed to the high amphibole REE concentrations through breakdown during alteration processes, especially if these are overestimates (see Section 4.12.2.3).

4.10.2 Chlorine, Sn, and Pb in hydrous minerals

There is a common spatial association of Cl-rich hydrothermal minerals with PGE mineralization in many deposits (Sudbury, Stillwater, Rathburn Lake, New Rambler, Salt Chuck, and others; Hanley (2005) and references therein). From this association, it has been suggested that PGE can form Cl-complexes and be transported in hydrothermal fluids that precipitate PGE deposits. Chlorine was analyzed by electron probe microanalysis and Pt, Pd, Sn, Sb, Bi, Te and Pb were analyzed by laser ablation – inductively coupled plasma – mass spectrometry at Memorial University of Newfoundland Department of Earth Sciences laboratories in hornblende, biotite, and chlorite from the dyke in this study in order to assess the role of fluid transport on PGE. (analytical details are outlined in Appendix 4.I; results are reported in Appendix 4.IVb)

The Pt and Pd were below detection in amphibole, so a direct correlation between PGE and Cl in the hydrous phases could not be made, however, there are some other

important general observations. The chlorine contents of amphibole (0.05 ± 0.01 wt%; n = 11) and biotite (0.07 ± 0.03 wt%; n = 6) in the dyke are low relative to some other PGE deposits. For example, secondary Al-rich amphibole contains up to 2.5 wt% Cl and biotite contains up to 0.55 wt% Cl associated with the PGE mineralization in the Lukkalaisvaara Intrusion, Northern Karelia (Glebovitsky *et al.*, 2001). At Sudbury, amphibole ranges from 0.01 wt% Cl (distal to ores) to 1.36 wt% Cl (proximal to ores) and biotite ranges from 0.09 wt% Cl (distal to ores) to 1.77 wt% Cl (proximal to ores) (Hanley *et al.*, 2003).

Not only are the Cl contents low in the hydrous minerals in Southeast Extension Zone, but some of the lowest Cl contents in amphibole are from samples containing the highest PGE mineralization (sample MH-028-4; Table 4.10), which is opposite to the Sudbury example. There is also no correlation between Cl and PGE or Pb in the whole rock data (Table 4.5).

The amphiboles are elevated in Pb and Sn in samples containing the Pb-Sn-PGM mineralization (inner hornblende gabbro dyke; Table 4.10). However, amphiboles not associated with Pb-Sn-PGM mineralization do not contain elevated Pb and Sn.

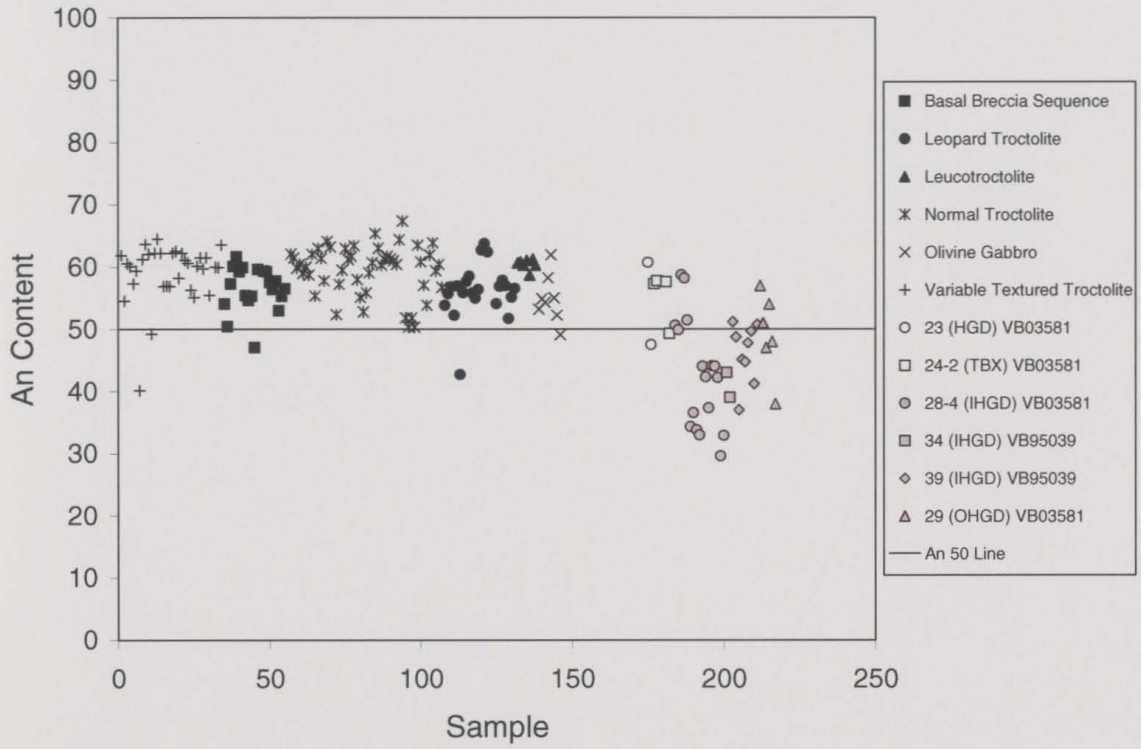

Figure 4.16. Anorthite (An) compositions of plagioclase in Southeast Extension Zone rocks compared to other Voisey's Bay troctolite rocks from Li and Naldrett (1999). TBX = troctolite breccias; HGD = hornblende gabbro dyke; IHGD = inner hornblende gabbro dyke; OHGD = outer hornblende gabbro dyke.

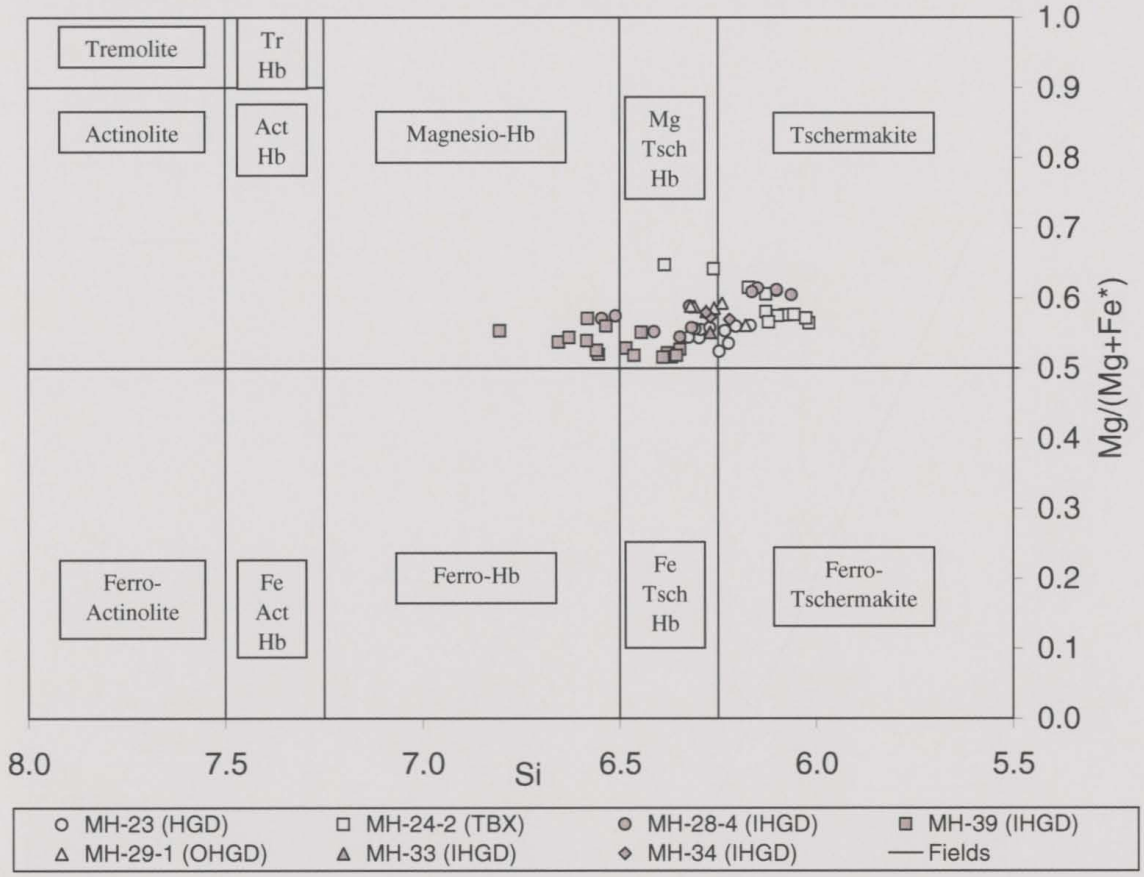

Figure 4.17. Amphibole compositions plotted on Si versus Mg/(Mg+Fe*) discrimination diagram for rocks in the Southeast Extension Zone (classification after Hawthorne, 1981). TBX = troctolite breccias; HGD = hornblende gabbro dyke; IHGD = inner hornblende gabbro dyke; OHGD = outer hornblende gabbro dyke.

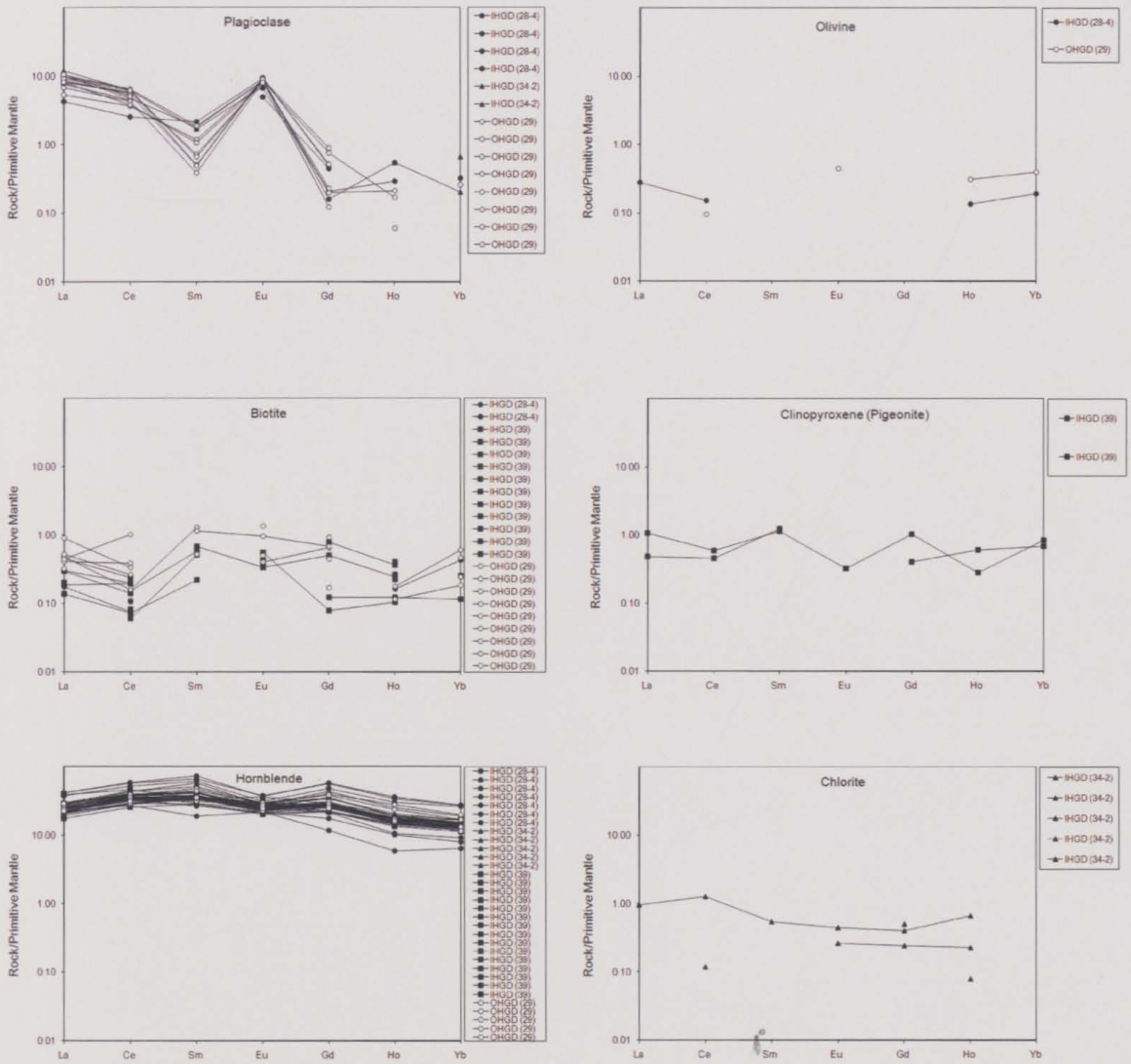

Figure 4.18. REE patterns for plagioclase, olivine, biotite, pyroxene, hornblende, and chlorite in the inner hornblende gabbro dyke (IHGD) and outer hornblende gabbro dyke (OHGD) rocks.

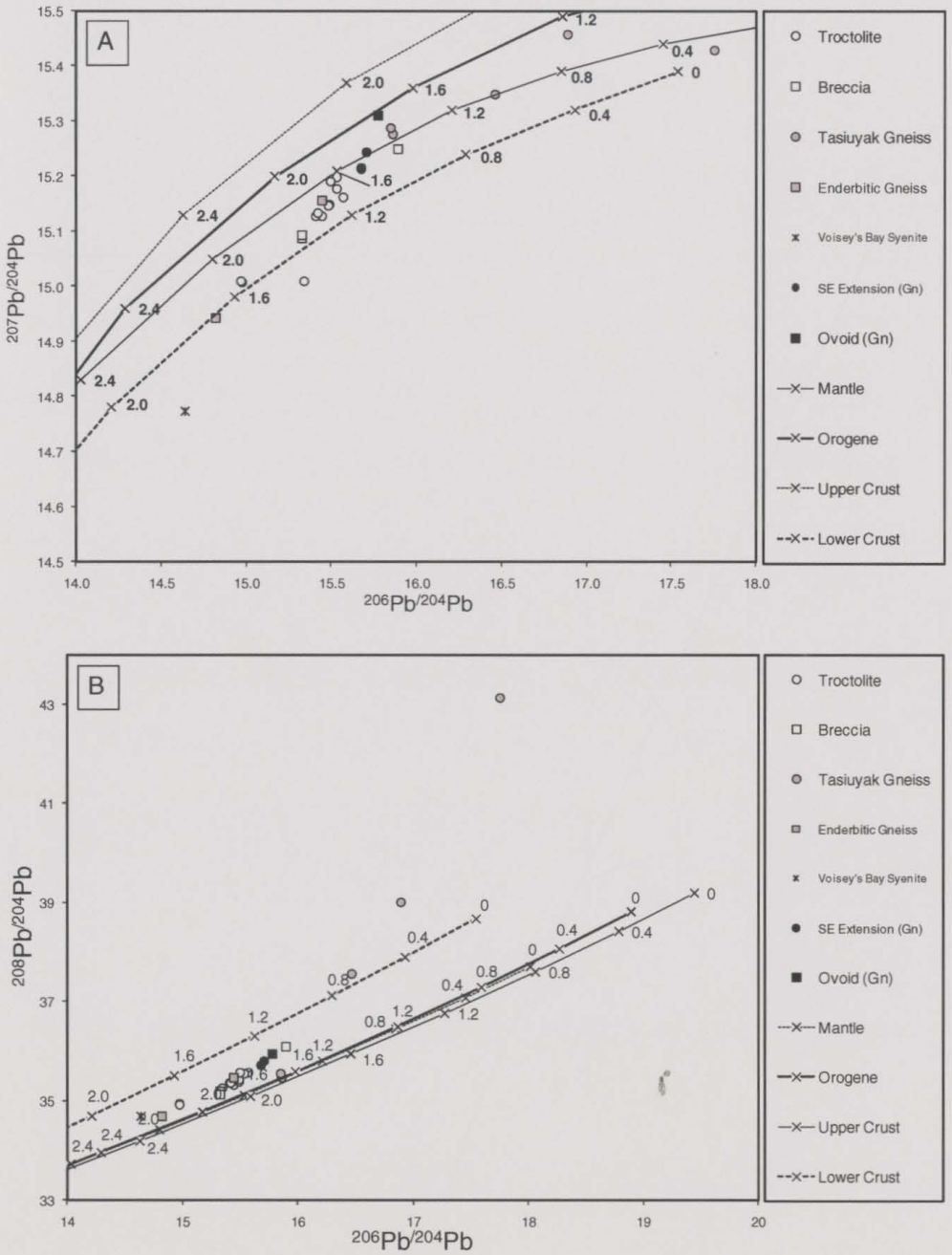

Figure 4.19. a) $^{206}Pb/^{204}Pb$-$^{207}Pb/^{204}Pb$ data, and b) $^{206}Pb/^{204}Pb$-$^{208}Pb/^{204}Pb$ data for the Voisey's Bay intrusion and related rocks. Data for the Voisey's Bay troctolite rocks, breccia, Tasiuyak gneiss, enderbitic gneiss, and Voisey's Bay syenite are from silicate minerals (Amelin *et al.*, 2000), whereas the hornblende gabbro dyke (Southeast Extension Zone) and Ovoid data are from galena (Gn) grains (this study). Mantle, orogene, upper crust, and lower crust reference lines are from Zartman and Doe (1981) with ages in Ga.

4.11 LEAD ISOTOPES

Lead isotope data was collected for galena associated with the PGE mineralization in the disseminated sulfides in the hornblende gabbro dyke in the Southeast Extension Zone and from galena from the massive sulfide in the Ovoid deposit using a Finnigan Neptune multicollector ICP-MS at the Inco Innovation Centre, Memorial University of Newfoundland and using an IsoProbe multicollector at GEOTOP laboratories, Université du Québec á Montréal (see Appendix 4.I for details of analytical details). The Pb isotopes from the galena grains were compared to published data for feldspars (Amelin *et al.*, 2000) from the Voisey's Bay Intrusion, Breccias, Tasiuyak Gneiss, Enderbitic Gneiss, and the Voisey's Bay Syenite on plots of $^{206}Pb/^{204}Pb$ vs. $^{207}Pb/^{204}Pb$ and $^{206}Pb/^{204}Pb$ vs. $^{208}Pb/^{204}Pb$ (Zartman and Doe, 1981). The purpose of the comparison is to determine whether the source of the galena in the hornblende gabbro dyke in the Southeast Extension Zone is related to the main Voisey's Bay mineralization event or a later hydrothermal event (i.e., granitic/syenitic intrusions). Data are shown in Table 4.11 and plotted in Figure. 4.19.

The galena in the hornblende gabbro dyke (Southeast Extension Zone) and the galena in the Ovoid both have Pb isotope ratios that are similar to each other but not identical (within the limited data set available). The most significant result of the lead isotope data collected from galena associated with the PGE mineralization in the hornblende gabbro dyke (Southeast Extension Zone) is that the compositions plot on a potential mixing line between the Voisey's Bay troctolites and the Ovoid magmatic

sulfides (Fig. 4.19). The galena from the dyke is also much more radiogenic than the Voisey's Bay granite/syenite (Fig. 4.19). The galena in the Ovoid and the galena in Southeast Extension Zone also fall along a linear array between the magmatic troctolite rocks and at least some samples of the heterogeneous Tasiuyak Gneiss country rock; the galena being skewed toward the Tasiuyak Gneiss (Fig. 4.19).

Although, not analyzed in this study, the Eastern Deeps and other sulfide deposits at Voisey's Bay are thought to have lead isotope values similar to the Ovoid.

4.12 DISCUSSION OF THE ORIGIN OF THE PGE

With the discovery of this PGE occurrence in the Southeast Extension Zone hornblende gabbro dyke in the vicinity of the Voisey's Bay massive magmatic sulfide Ni-Cu-Co deposit several key questions arise: 1) is the Voisey's Bay deposit prospective for PGE? 2) is the PGE mineralization magmatic or hydrothermal? and 3) if the PGE mineralization is magmatic, is it related to the other magmatic sulfide deposits at Voisey's Bay?

4.12.1 Paucity of PGE in the Voisey's Bay Intrusion

Magmatic associated PGE deposits can be classified into two main groups: 1) sulfide-poor PGE associated deposits, and 2) sulfide-rich base-metal associated deposits. Generally, sulfide-poor magmatic PGE deposits contain PGE as the primary commodity,

whereas the sulfide-rich base-metal deposits may contain PGE as by product. The Voisey's Bay Ni-Cu-Co deposit consists primarily of massive and disseminated magmatic sulfide ores, i.e., it is of the sulfide-rich base-metal type. It has been noted that the deposit contains very low abundances of PGE (Table 4.1) so has not been considered prospective for PGE. However, because some primarily high sulfur base-metal deposits are producers of significant PGE (i.e., Sudbury and Noril'sk; Naldrett, 2004), the paucity of known PGE in the Voisey's Bay deposit does not preclude that that PGE exist elsewhere in the deposit. It is stressed that discrete PGM have been found only in the hornblende dyke as of this time. Although relatively low levels of PGE have been determined in the principal deposits to date (Table 4.1), the full extent of how much PGE could be associated with the entire Voisey's Bay deposit (i.e., in dykes similar to the Southeast Extension) is not well established. Therefore, further exploration for PGE occurrences such as that in the Southeast Extension Zone may be warranted.

4.12.2 Magmatic versus Hydrothermal PGE

There are at least three possible mechanisms for formation of the PGE occurrence in the Southeast Extension Zone of the Voisey's Bay deposit: (1) direct crystallization of PGM from a magmatic sulfide melt, (2) precipitation of PGM from low-temperature hydrothermal (<500°C) fluids derived from an external source, or (3) precipitation of PGM from high-temperature fluids (~500-800°C) exsolved during the magmatic-hydrothermal transition in the troctolitic host rocks. The presence of a fluid is indicated

by the significant abundance of hydrous mineral phases (amphibole and biotite). However, the evidence outlined in this study suggests that the PGM crystallized directly from an evolved sulfide melt possibly related to the Voisey's Ni-Cu-Co ores. Only limited indirect evidence suggests minor post mineralization modification of the dyke occurred by low-temperature hydrothermal fluids (possibly derived from late granitic magmas of the Nain Plutonic Suite).

4.12.2.1 Crystallization of PGM from magmas

Both empirical and theoretical studies of magmatic Fe-Ni-Cu-PGE sulfide deposits suggest that, under certain conditions, an immiscible sulfide liquid will separate from a silicate magma at suprasolidus temperatures (Naldrett, 1981). The PGE are chalcophile and will partition strongly into the sulfide over the silicate melt (Naldrett, 2004). Upon cooling, the sulfide liquid will first crystallize an Fe-Ni-rich monosulfide solid solution (MSS) at ~1100°C, followed by magnetite at a temperature that depends on the pyrrhotite composition and fO_2 (Naldrett, 1969). Copper is insoluble in MSS, and eventually, down temperature, a Cu-rich sulfide melt or intermediate solid solution (ISS) is produced at a liquidus temperature somewhere between ~880-970°C (Cabri and Laflamme, 1976). During subsolidus cooling, pyrrhotite and pentlandite exsolve from the MSS (Naldrett *et al.*, 1967) and chalcopyrite and cubanite exsolve from the ISS (Cabri, 1973; Craig and Scott, 1974; Naldrett, 1989). At these conditions pyrite crystallizes below ~700°C, chalcopyrite below ~550°C, and pentlandite below ~300°C (Cabri and

Laflamme, 1976). PGE in the sulfide melt will further partition between MSS and ISS with the IPGE (Ir, Os, Ru, and Rh) partitioning into the MSS and the PPGE (Pt and Pd) partitioning into the ISS (Hawley and Stanton, 1962; Naldrett *et al.*, 1979; Fleet *et al.*, 1993; Naldrett *et al.*, 1994; Ebel and Naldrett, 1996; Barnes *et al.*, 1997).

There are at least five lines of evidence that support the model for PGM crystallization from a highly differentiated Cu-rich sulfide melt (close to ISS in composition) in the Voisey's Bay ore system: (1) petrographic associations, (2) elemental correlations, (3) palladium concentrations in sulfides, (4) melting temperatures of the PGM, and (5) lead isotope compositions of galena.

Petrographically, the PGM and other PMM are not spatially related to hydrous minerals but are hosted by the sulfides. Sulfide minerals that host the PGE mineralization in the mafic dyke in the Southeast Extension Zone consist of the Cu-rich sulfides chalcopyrite and bornite, Pb-sulfides such as galena, and Sn-sulfides such as volfsonite. The PGM are the Pt-PGM (sperrylite [$PtAs_2$], maslovite [PtBiTe], and geversite [$PtSb_2$]), the Pd-PGM (paolovite [Pd_2Sn], froodite [PdBiTe], unnamed [Pd-Bi-Sb-Te], and the Sn-bearing stibiopalladinite [$Pd_{5-x}(Sb,Sn)_{2-x}$]). Other PMM are the Au-Ag minerals matildite ($AgBiS_2$), stützite ($Ag_{5-x}Te_3$), electrum (AuAg), and native Ag. Only 3.35% of the total number of PMM grains investigated in this study were associated with silicates and of those only two were amphibole (representing only ~1% of the total number of PMM grains); 68.9% of the total number of PMM grains were associated with other precious metal minerals and/or sulfides (Fig. 4.13). This suggests that the amphibole-forming fluids were not likely the dominant agent of PGE mineralization. The close spatial

association of PGM with sulfides of these compositions suggests that the PGM formed from a sulfide melt enriched in Cu, Pb, Sn, Pt, Pd, Au, Ag, As, Bi, Te, and Sb. No PGM grains were found to be hosted by pyrrhotite, which may indicate that the PGM formed late in the crystallization sequence, with Pt and Pd partitioning preferentially into a Cu-rich sulfide liquid (close to ISS in composition), following the crystallization of MSS. It is suggested that Cu-rich sulfide melts in the dyke became highly enriched in these metals and upon cooling precipitated the observed suite of PGM.

The PGM in the Southeast Extension Zone have strong spatial associations with the disseminated sulfides, in particular the Cu- and Pb-rich assemblage consisting of chalcopyrite, bornite, and galena as well as silver tellurides (i.e., stützite). Whole-rock inter-element correlation results indicate that different groups of elements correlate with each. The first group of elements that are highly correlated are Cu-Pb-Sn-Ga-Pt-Pd-Au-Ag-Bi-Sb (Table 4.5). Since Cu is present as chalcopyrite and bornite and Pb is present as galena, the simplest explanation for the Cu-Pb correlation is that chalcopyrite, bornite, and galena crystallization are genetically related. The correlations of Pt and Pd with Au and Ag are confirmed by the strong association of Ag-tellurides and electrum with the PGM. The correlations of Pt and Pd with Sn, Bi, and Sb can be explained because the PGM are Sn-, Bi-, and Sb-bearing. These elemental correlations are consistent with what is observed in the mineral distributions (i.e., Pt and Pd form Sn-, Sb- and Bi-bearing PGM that are spatially associated with and hosted by chalcopyrite, bornite, and galena).The second group of elements that have positive correlations is Rh-Ru-Ir-S-Fe-Ni-Co. Since Fe, S, Ni, and Co are present as pyrrhotite and pentlandite, the simplest

explanation for the S-Fe-Ni-Co correlations is that pyrrhotite and pentlandite crystallization and IPGE distribution are genetically related, which would be consistent with derivation of the IPGE from MSS. The lack of correlation of whole rock Rh-Ru-Ir-S-Fe-Ni-Co with PPGE, Cu, and Pb likely indicates that the distributions of these elements were not controlled by the formation of Cu and Pb minerals (chalcopyrite, bornite, and galena).

The PGE distributions within the sulfides from the dyke are also consistent with what would be observed in magmatic sulfide liquid fractionating from MSS to ISS, where IPGE (e.g., Ru) are more compatible in earlier phases (pyrrhotite) and PPGE (e.g., Pd) are more compatible in intermediate (pentlandite) and later crystallizing phases (chalcopyrite, bornite, and galena). Data are sparse in the literature for galena. However, trace element distributions in the dyke indicate that the Pd has similar distributions in galena as in chalcopyrite and bornite (Table 4.9a). The spatial association of chalcopyrite and bornite with galena and PGM also supports a model in which galena and PGM are related to direct crystallization from a Cu-rich sulfide melt close to ISS composition. The fractionation of the PGE (Fig. 4.11) and the enrichment of PPGE could also be accomplished by this fractional crystallization of MSS and enrichment of PPGE into ISS.

Experimentally-determined melting temperatures for the PGM as identified in the Southeast Extension Zone in order of decreasing temperature are: sperrylite ($PtAs_2$) >1400°C (Hansen and Anderko, 1958; Bennett and Heyding, 1966), geversite ($PtSb_2$) 1225°C (Shunk, 1969; Moffatt, 1979), paolovite (Pd_2Sn) 820°C (Elliott, 1965), polarite (PdBi) 620°C (Hansen and Anderko, 1958; Elliott, 1965; Shunk, 1969), and froodite

($PdBi_2$) 380°C (Hansen and Anderko, 1958). For maslovite (PtBiTe) and Sn-stibiopalladinite [$Pd_{5-x}(Sb,Sn)_{2-x}$] the reaction temperature and/or compositional range has not been determined (Belincourt *et al.,* 1981). The melting temperatures of paolovite, polarite, and froodite are consistent with crystallization from ISS below ~970°C (Cabri and Laflamme, 1976). Sperrylite and geversite may have crystallized at similar temperatures because As and Sb were not yet sufficiently concentrated in the sulfide melt to this point. However, there is no sperrylite or geversite associated with pyrrhotite indicating that the melt was not sufficiently concentrated in Pt, As, and Sb to produce these minerals at the time of MSS crystallization. Thus the PGE would have still been dissolved in the ISS and could have been transported along in Cu-Pb-Sn-Au-Ag-As-Bi-Te-Sb rich sulfide drops in the silicate melt to the site of emplacement of the dyke.

The most significant result of the lead isotope data collected from galena associated with the PGE mineralization in the Southeast Extension Zone is that the compositions plot on a potential mixing line between the Voisey's Bay troctolites and the magmatic sulfides (i.e., the Ovoid) (Fig. 4.19). The galena from the dyke is also much more radiogenic than the Voisey's Bay granite/syenite. This is significant because it links the evolved Cu-rich (and Pb-rich) sulfide in the Southeast Extension Zone to the sulfides and host troctolites through magmatic processes. The data are inconsistent with a hydrothermal fluid from the Voisey's Bay Syenite being the source of the Pb in the Southeast Extension Zone. The Ovoid and Southeast Extension Zone galena data are skewed toward the Tasiuyak Gneiss, which would be consistent with the Pb source being

the mantle-derived troctolites with some interaction from the country rock Tasiuyak Gneiss (Fig. 4.19).

Although the lead data available is for the Ovoid magmatic sulfide, it should be noted that other sulfide zones in the Voisey's Bay deposit (i.e., the Eastern Deeps) are also potential sources for the evolved SE Extension mineralization. It has been suggested that the Eastern Deeps is depleted in concentrations of Pb, due to the loss of a fractionated material or escape of low temperature re-melting products (Naldrett, 2000a) and could be a potential source to the SE Extension mineralization providing the lead isotopes are similar. Regardless of which is the actual source sulfide, an important factor is that the SE Extension lead isotope data is related to a magmatic not hydrothermal source.

Table 4.11. Lead isotope data.

Sample No	Zone	Rock	Fraction	U (ppm)	Pb (ppm)	$^{238}U/^{204}Pb$	$^{206}Pb/^{204}Pb$	$^{207}Pb/^{204}Pb$	$^{208}Pb/^{204}Pb$
VOISEY'S BAY									
VB189/120	Eastern Deeps Zone	Normal Troctolite	Pl-1	0.0053	1.06	0.288	15.341 ± 37	15.009 ± 41	35.244 ± 104
VB231/78	Eastern Deeps Zone	Normal Troctolite	Pl-1	0.0035	1.57	0.129	15.535 ± 52	15.199 ± 54	35.556 ± 132
VB231/78	Eastern Deeps Zone	Normal Troctolite	Pl-2	0.0185	2.12	0.509	15.569 ± 21	15.162 ± 25	35.569 ± 77
VB201/292.3	Eastern Deeps Zone	Variable Textured Troctolite	Pl-1	0.0138	4.86	0.164	15.443 ± 17	15.128 ± 22	35.306 ± 69
VB231/731	Eastern Deeps Zone	Variable Textured Troctolite	Pl-1	0.0046	4.18	0.063	15.409 ± 15	15.128 ± 21	35.358 ± 67
VB291/15	Eastern Deeps Zone	Leucotroctolite	Pl-1	0.0054	1.68	0.188	15.530 ± 22	15.178 ± 27	35.542 ± 74
VB315/780.8	Eastern Deeps Zone	Feeder Olivine Gabbro	Pl-1	0.0065	19.4	0.019	14.974 ± 15	15.008 ± 21	34.940 ± 65
VB315/780.8	Eastern Deeps Zone	Feeder Olivine Gabbro	Pl-2	0.0068	17.1	0.023	14.970 ± 22	15.009 ± 32	34.923 ± 100
VB329/684.3	Eastern Deeps Zone	Feeder Olivine Gabbro	Pl-1	0.0072	6.84	0.061	15.420 ± 16	15.133 ± 22	35.367 ± 66
VB247/925	Eastern Deeps Zone	Ultramafic Inclusions	Pl-1	0.0030	3.81	0.073	15.492 ± 19	15.148 ± 24	35.386 ± 90
VB98/43.7	Discovery Hill Zone	Feeder Olivine Gabbro	Pl-1	0.0084	7.98	0.061	15.486 ± 16	15.147 ± 22	35.425 ± 67
VB368/992.5	Reid Brook Zone	Leucotroctolite	Pl-1	0.0047	1.97	0.14	15.494 ± 37	15.190 ± 39	35.561 ± 134
VB257/232.5	Red Dog	Normal Troctolite	Pl-1	0.0031	0.88	0.2	15.443 ± 20	15.129 ± 24	35.375 ± 71
MUSHUAU									
AS1/370.5	Asini	Leucotroctolite	Pl-1	0.0016	0.87	0.102	14.208 ± 18	14.631 ± 23	34.363 ± 68
AS1/591.5	Asini	Leucotroctolite	Pl-1	0.0014	0.62	0.13	14.461 ± 18	14.740 ± 25	34.571 ± 77
S7/90	Sarah	Melatroctolite	Pl-1	0.0058	2.27	0.143	14.357 ± 16	14.689 ± 22	34.489 ± 68
VB356/245	Second Pond	Gabbro	Pl-2	0.0033	2.2	0.083	14.552 ± 41	14.767 ± 49	34.596 ± 132
VB252/900	Otter Pond	Leucotroctolite	Pl-1	0.0107	1.73	0.348	14.491 ± 14	14.725 ± 21	34.654 ± 63
BRECCIA									
VB54/65 Fsp	Discovery Hill Zone		Fsp-1	0.1956	131	0.086	15.328 ± 15	15.087 ± 21	35.187 ± 70
VB54/65 Fsp	Discovery Hill Zone		Fsp-2	0.0108	16.8	0.037	15.326 ± 23	15.093 ± 33	35.133 ± 100
VB216/112.6	Reid Brook Zone		Pl-1	0.0071	6.67	0.063	15.894 ± 48	15.250 ± 52	36.090 ± 140
VB192/357.5	Reid Brook Zone	Tasiuyak Gneiss	Pl-2	0.1681	25	0.393	15.860 ± 24	15.277 ± 33	35.455 ± 101
VB192/357.5	Reid Brook Zone	Tasiuyak Gneiss	Pl-1	0.1172	15.4	0.445	15.847 ± 15	15.287 ± 21	35.546 ± 65
VB223/99.7	Reid Brook Zone	Tasiuyak Gneiss	WR-1	0.8861	28.4	2.056	16.463 ± 18	15.349 ± 24	37.548 ± 75
VB223/99.7	Reid Brook Zone	Tasiuyak Gneiss	Kfsp-1	0.0692	1.02	4.242	16.888 ± 39	15.458 ± 39	38.998 ± 109
VB213/159.5	Reid Brook Zone	Tasiuyak Gneiss	Pl-1	0.4463	3.26	9.143	17.753 ± 29	15.429 ± 30	43.134 ± 172
ENDERBITIC GNEISS									
VB108/483.6	Discovery Hill Zone	Enderbitic Gneiss	Pl-1	0.0025	2.96	0.048	14.823 ± 22	14.943 ± 29	34.690 ± 87

VB231/863	Eastern Deeps Zone	Enderbitic Gneiss	Pl-1	0.0266	22.6	0.068	15.443 ± 28	15.157 ± 37	35.455 ± 149
NAIN GNEISS									
VB263/870	Eastern Deeps Zone	Mafic Nain Gneiss	WR-1	0.2102	7.15	1.698	15.431 ± 25	15.008 ± 29	35.390 ± 80
VB263/870	Eastern Deeps Zone	Mafic Nain Gneiss	Kfsp-1	0.0182	9.42	0.11	14.948 ± 14	14.957 ± 20	34.968 ± 63
VB264/655	Eastern Deeps Zone	Felsic Nain Gneiss	Pl-1	0.0382	6.04	0.362	15.098 ± 29	15.006 ± 33	35.000 ± 88
VB263/840.5	Eastern Deeps Zone	Felsic Nain Gneiss	Pl-1	0.0154	6.23	0.141	14.828 ± 28	14.926 ± 36	35.056 ± 86
S2/75.5	Mushuau	Mafic Nain Gneiss	Pl-1	0.0282	7.06	0.22	14.226 ± 29	14.573 ± 38	33.996 ± 110
VOISEY'S BAY GRANITE									
VB173/485	Voisey's Bay	Syenite	Fsp-1	0.0047	8.71	0.03	14.642 ± 25	14.774 ± 35	34.695 ± 103
SOUTHEAST EXTENSION ZONE/OVOID*									
VB03581/112.25/28a	Southeast Extension	Disseminated Sulfide	Galena-1	Neptune			15.6769 ± 0.0084	15.2157 ± 0.0079	35.7075 ± 0.0188
VB03581/112.25/28a	Southeast Extension	Disseminated Sulfide	Galena-2	Neptune			15.6746 ± 0.0029	15.2141 ± 0.0031	35.7045 ± 0.0071
VB03581/112.25/28a	Southeast Extension	Disseminated Sulfide	Galena-3	IsoProbe			15.708 ± 0.003	15.243 ± 0.003	35.788 ± 0.006
VBGALENA	Ovoid Zone	Massive Sulfide	Galena-4	IsoProbe			15.774 ± 0.002	15.310 ± 0.002	35.939 ± 0.005
SRM 981 as unknown for galena 1 and 2			Standard	Neptune			16.9347 ± 0.0036	15.4880 ± 0.0034	36.6921 ± 0.0078

*Data from this study (other data from Amelin *et al.*, 2000)

SRM 981 Accepted values (Todt *et al.*, 1996): $^{206}Pb/^{204}Pb = 16.9356$; $^{207}Pb/^{204}Pb = 15.4891$; $^{208}Pb/^{204}Pb = 36.7006$

4.12.2.2 Role of fluids in the transport of PGE

The ability of a fluid to entrain, transport, and deposit PGE depends on: i) solubility of the PGE in the fluid, ii) the PGE source (pre-existing PGM, silicate/sulfide melt), iii) the mass flux, and iv) the efficiency of the final precipitation method. The pH, fO_2, T, salinity, and S content of the fluid will determine the amount of PGE dissolved and the nature of the PGE complexes in solution. Hanley (2005) reviewed, from experiments and theoretical sources, the ability of the PGE to form complexes under various conditions in different environments. The ability of the PGE to complex with other ions or ligands (i.e., Cl) is important in PGE transport as the dissolved metal alone, in equilibrium with ore minerals, does not commonly have high enough concentrations in solution to allow significant metal transport (Hanley, 2005 and references therein).

Low-temperature hydrothermal fluids

In a low temperature hydrothermal environment (<500°C) defined by post-magmatic hydrothermal alteration by low temperature fluids, it has been observed that there is a strong spatial association between PGE occurrences and Cl-rich phases and fluid inclusions in some deposits (i.e., Sudbury, Stillwater, Rathburn Lake, New Rambler, Salt Chuck and others; Hanley, 2005). This association has been attributed to high salinity Cl-rich fluids transporting PGE complexes with cooling and alteration of magmatic Ni-Cu-PGE deposits. However, Hanley (2005) pointed out that Pd and Pt in

low temperature hydrothermal environments will only dissolve as chloride complexes under highly oxidizing (log fO_2 > -25 atm) or acidic (pH < 2) conditions, whereas, in magmatic Ni-Cu-PGE environments, near neutral, reducing conditions are typical (i.e., lack of high fO_2, low pH alteration assemblages).

High-temperature hydrothermal fluids

In the high-temperature late magmatic-hydrothermal environment (~500-800°C), Cl-rich volatiles or fluids may be able to transport and distribute PGE (Hanley, 2005; Mungall, 2005). If considering transport alone, the favorable conditions for the PGE to be stable in Cl-rich fluids are even more favorable for the transport of Fe, Ni, and Cu (Hanley, 2005) so low PGE to base metal ratios are expected in the ores formed by this process as opposed to high PGE concentrations if transport alone is considered. However, in principle, when also considering precipitation, PGE to base metal ratios could be high in ore deposits formed form such fluids if PGE precipitation was enhanced relative to the base metals under certain pH, fO_2, or salinity conditions or the presence of As, Te, Sb, and Bi but experimental evidence for such processes is lacking.

4.12.2.3 Evidence for late hydrothermal fluids modifying the mineralization

Although hydrous phases indicate that a fluid was present in the Southeast Extension Zone, their presence does not necessitate that the PGE mineralization was introduced with this fluid. There are several lines of evidence that indicate the amphibole, and hence the fluids, were introduced by later granitic intrusions after PGE mineralization and that the PGM did not form directly from hydrothermal fluids but may have been modified by these fluids. The relevant observations include: (1) the significant abundance of hydrous phases associated with the PGE mineralization, (2) the petrographic relationships and elevated REE abundances in amphibole, (3) the lack of Cl content of hydrous phases, (4) Pb and Sn in amphibole, and (5) metal associations.

The presence of a fluid is indicated by the significant abundance of hydrous mineral phases in the dyke and country rocks of the Southeast Extension Zone. The hydrous mineral phases are amphibole, biotite, and chlorite. They are most abundant in the hornblende gabbro dyke, which hosts the PGE mineralization. The host variable textured troctolite and troctolite breccia rocks contain 5-15% amphibole, 5-10% biotite, and no chlorite, whereas the dyke contains 15-45% amphibole, 5-15% biotite, and 5-10% chlorite.

There are at least three possible sources for the fluids that formed the hydrous phases including: (a) high-temperature magmatic-hydrothermal fluids derived from crystallizing troctolites in the Southeast Extension Zone, (b) a secondary low-temperature REE-poor hydrothermal source, or (c) a secondary REE-enriched external hydrothermal

source. Petrographic observations indicate that the amphiboles in the Southeast Extension Zone are of secondary hydrothermal origin. They are fibrous green amphibole, rather than the euhedral brown interstitial amphibole commonly formed by late magmatic processes. Although some mafic rocks contain abundant primary amphibole, the majority contain <5% in the rock. There, the significant abundance of amphibole (up to 45%) may be more consistent with a secondary source. The observed REE data indicate that the amphibole are too enriched in REE (especially with the overestimates due to interferences; see Appendix 4.I) to be produced from the simple secondary breakdown of pyroxene (± olivine) and plagioclase in the dyke rocks (Fig. 4.18). Therefore, if the amphibole are secondary, they would require an external REE-enriched source. If they formed from late magmatic fluids, they would require extensive crystallization of the troctolitic parent magma to enrich the REEs. The whole rock REE compositions of a basalt magma in equilibrium with the observed amphibole compositions may be calculated using partition coefficients (K_d = concentration of element in amphibole/concentration of element in magma) for a basalt (McKenzie and O'Nions, 1991). The expected basalt magma whole rock REE composition is plotted in Figure 4.20a along with the actual REE compositions of the troctolitic rocks from the Voisey's Bay conduit and intrusion. However, the results indicate that the magma expected to be in equilibrium with the observed amphibole should contain much higher REE than what is observed in the troctolite whole-rock data (Fig. 4.20a). If the elevated REE in amphibole were derived from a secondary REE enriched external hydrothermal source, the two most probable sources would be the Voisey's Bay granite/syenite or the Makhavinekh Lake

Pluton. The Voisey's Bay granite/syenite is younger (1305Ma; Amelin *et al.*, 2000) than the troctolitic rocks and is in close proximity to the Voisey's Bay intrusion (Fig. 4.1a) intruding portions of the Eastern Deeps (Fig. 4; Li *et al.*, 2000). The Makhavinekh granite is also younger (1322 ± 1Ma) than the troctolitic rocks and, although it is more distal to the Southeast Extension Zone than the Voisey's Bay granite/syenite, it is a large batholith (Fig. 4.1a). The REE compositions of a granitic magma required to produce the observed REE compositions in the amphiboles were calculated using partition coefficients (K_d) for a rhyolite (Bacon and Druitt, 1988). The expected granitic magma REE composition is plotted in Figure 4.20b along with the actual REE compositions of the Makhavinekh Lake Pluton and Voisey's Bay granite/syenite. The results indicate that both granitic intrusives have sufficient REE to have produced the observed amphibole REE compositions in the dyke rocks (Fig. 4.20b). Therefore, the REE patterns of the amphibole are consistent with an external REE enriched granitic source such as either the Makhavinekh Lake Pluton or the Voisey's Bay granite/syenite.

The chlorine contents of amphibole (0.05 ± 0.01 wt%; n = 11) and biotite (0.07 ± 0.03 wt%; n = 6) in the dyke are low relative to some other PGE deposits. For example, secondary Al-rich amphibole contains up to 2.5 wt% Cl and biotite contains up to 0.55 wt% Cl associated with the PGE mineralization in the Lukkalaisvaara Intrusion, Northern Karelia (Glebovitsky *et al.*, 2001). At Sudbury, amphibole ranges from 0.01 wt% Cl (distal to ores) to 1.36 wt% Cl (proximal to ores) and biotite ranges from 0.09 wt% Cl (distal to ores) to 1.77 wt% Cl (proximal to ores) (Hanley *et al.*, 2003)). Not only are the Cl contents low in the hydrous minerals in Southeast Extension Zone, but some of the

lowest Cl contents in amphibole are from samples containing the highest PGE mineralization (sample MH-028-4; Table 4.10), which is opposite to the Sudbury example. Therefore, the low Cl fluid that formed the amphibole and biotite in the Southeast Extension Zone likely did not have the potential to transport the PGE in the form of Cl-PGE complexes. There is also no correlation between Cl and PGE or Pb in the whole-rock data (Table 4.5) indicating that the PGM and galena formation are not directly correlated to the Cl content of the rock. These observations suggest that the Cl did not act as a complexing ligand for the transport of the PGE in the fluids that formed the amphibole in the Southeast Extension Zone.

The amphiboles also have elevated Pb and Sn in samples containing the Pb-Sn-PGM mineralization. If the fluid that formed the amphibole also formed the mineralization, all the amphibole should be elevated in Pb and Sn. However, amphiboles not associated with Pb-Sn-PGM mineralization do not contain elevated Pb and Sn. This implies that the secondary fluids forming the amphiboles did not carry the Pb and Sn because not all amphiboles contain elevated Pb and Sn. It suggests that the Pb-Sn-PGM mineralization was already present and when the fluids were introduced later, the fluids only locally leached the Pb and Sn in areas of pre-existing sulfide mineralization and reprecipitated it during later amphibole formation. Amphibole formation as well as Pb and Sn mobilization by fluids post dates the mineralization. There is no direct evidence that the PGE were even affected by hydrothermal fluids although Pb and Sn were shown to be remobilized from the sulfides that host the PGE mineralization.

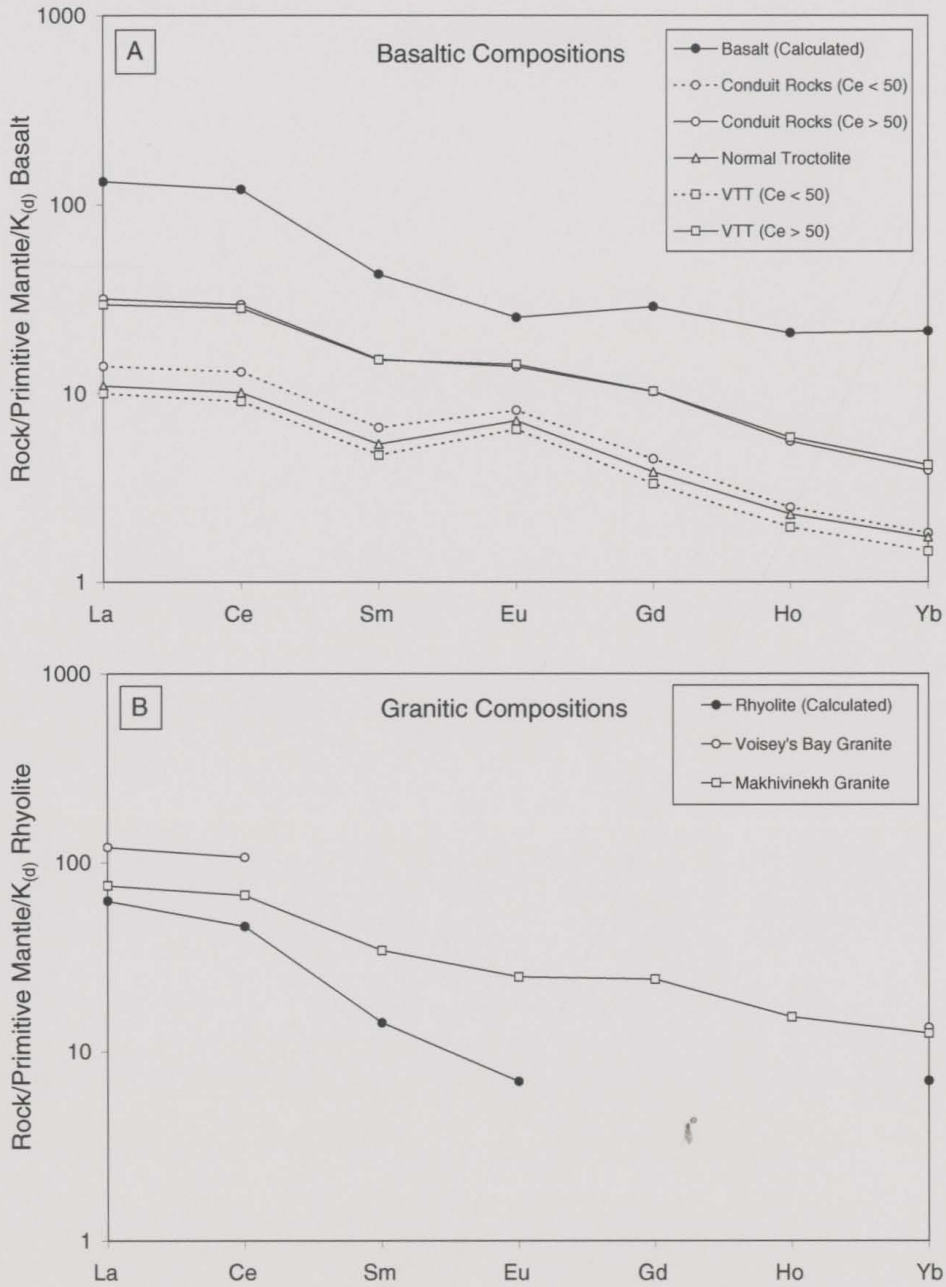

Figure 4.20. Calculated average REE composition required for: a) a basaltic magma to produce the observed REE compositions in amphibole compared with the host conduit, normal troctolite, and variable texture troctolite (VTT) rocks of Li *et al.* (2000), and b) for a granitic magma to produce the observed REE compositions in amphibole compared with the Voisey's Bay granite (Ryan, 2002 open file report) and the Makhavinekh granite (Lightfoot unpublished data). Primitive mantle values from McDonough and Sun (1995); basalt K_d values from McKenzie and O'Nions (1991); and rhyolite K_d values from Bacon and Druitt (1998).

Another factor limiting the solubility of PGE may be that, as tellurides and arsenides, the PGE have low solubilities and the presence of elements such as S, Fe, Te, Se, As, Sn, Sb, Cu, Bi, and Ag may promote precipitation and not transport of PGE in solution (Hanley, 2005; Wood, 2002). Therefore, the Cu-Pb-Sn-Au-Ag-As-Te-Bi-Sb metal associations in the inner hornblende gabbro dyke of the Southeast Extension Zone implies that there would be limited solubility and transport capacity of fluids for the PGE.

4.13 PROPOSED EMPLACEMENT MODEL AND PARAGENETIC SEQUENCE FOR THE FORMATION OF PGE MINERALIZATION IN THE SOUTHEAST EXTENSION ZONE

4.13.1 Key factors in the model

Evidence presented in this paper indicates that the PGE occurrence in a hornblende gabbro dyke near the Southeast Extension Zone of the Voisey's Bay Ovoid deposit likely has a primary magmatic origin. Geological relationships indicate that the dyke is spatially connected as a splay off the main troctolite conduit dyke (Fig. 4.3), which hosts the Ovoid massive sulfide deposit. The PGE are hosted by rocks that are similar in geochemical (whole rock REE) composition to the troctolitic rocks that host the Ovoid deposit. The PGE-bearing dyke formed from a mafic silicate magma (troctolite to hornblende gabbro) and can by divided into an "outer" portion containing MSS compositions (Po-Pn-Ccp) and an "inner" portion containing "extreme" ISS compositions (Ccp-Bn-Gn-PGM). The similarity in rock types that host the PGE and Voisey's Bay massive Ovoid deposit and the close proximity of the PGE to the Ovoid deposit indicate

they may be related by a similar mafic silicate magma source. The very center of the Ovoid is depleted in Pt and Pb and the hornblende gabbro dyke is enriched in Pt and Pb, which may imply that the Pt and Pb of the dyke were sourced from an evolved enriched sulfide liquid that "escaped" from the Ovoid (Chapter 2 of this thesis; Huminicki *et al.*, in review). The PGE mineralization is Pt- and Pd-rich (Appendix 4.II), where the Pt and Pd occur predominantly as discrete platinum-group minerals (PGM) although palladium does occur in minor amounts in solid solution in galena (ave = 1.9ppm) and pentlandite (ave = 2ppm). The PGM are predominantly hosted by base-metal sulfides (bornite, chalcopyrite, and galena) and are associated with other precious metal minerals (PMM). Less than 4% (by volume) of all the PMM are associated with or hosted by silicate minerals (Fig. 4.13). The geochemical correlations (Table 4.5) also indicate that the PGE are strongly associated with base-metals. More specifically, the PPGE (Pt and Pd) are correlated with Cu, Pb, Sn, Au, Ag, and Sb, which are major constituents of the ISS minerals chalcopyrite, bornite, and galena as well as other PMM, whereas the IPGE (Ir, Ru, and Rh) are strongly correlated with S, Fe, Ni, and Co, which are the main constituents of the MSS minerals pyrrhotite and pentlandite. There are no correlations of the PGE or base-metals with chlorine. The Cu-rich, Pb-rich sulfides and associated Pt-Pd-Au-Ag-Sn-Te-Bi-Sb assemblage can be produced magmatically as late ISS differentiates (Prichard *et al.*, 2004). If the sulfide compositions can be produced magmatically then the spatial association of sulfides with PGM, Pd in galena and pentlandite, and the base-metal and PGE correlations in the whole rock indicate similar magmatic processes may have formed the PGM. Melting temperatures of the PGM are also consistent with a

magmatic origin. An alternate model suggested by Naldrett (2000a) that might produce a liquid very similar to that formed by extreme fractionation is partial melting of pre-existing sulfides due to subsequent influxes of new magma.

If the PGE mineralization is indeed magmatic and is a late differentiate, the most probable sources would be the nearby Ovoid or Eastern Deeps sulfide deposits. Although there are minimal data, the similar Pb isotope ratios for the Ovoid galena and the Southeast Extension Zone galena indicates that they were produced through similar processes. The fact that the galena from the Ovoid and Southeast Extension Zone plot on a mixing line is significant because it links the evolved Cu-rich (and Pb-rich) ISS sulfide in the Southeast Extension Zone to the Ovoid sulfides and host troctolites through magmatic processes. Although there is no current data available, it is thought that from other magmatic sulfide zones (i.e., Eastern Deeps) may have similar isotope signatures to the Ovoid. The radiogenic nature of the galena (Fig. 4.19) is inconsistent with a hydrothermal fluid from the Voisey's Bay Syenite being the source of the Pb in the Southeast Extension Zone. The galena plotting between the magmatic troctolite rocks and the Tasiuyak Gneiss is consistent with the Pb source being the mantle-derived troctolites with some interaction from the country rock Tasiuyak Gneiss (Fig. 4.19).

It has also been shown in Chapter 2 (Fig. 2.5) that Pt and Pb correlate with each other increasing toward the center (as would be expected with fractionation from the margins inward). However, both Pt and Pb are significantly depleted in the very central portion relative to the remainder of the Ovoid (possibly due to escape to the surrounding troctolitic rocks).

The parent magma of the dyke was probably more evolved than the main troctolite-Ovoid system at Voisey's Bay. Not only are the sulfides more evolved in the dyke but the REE patterns are enriched in some of the dyke rocks indicating the silicates are also more evolved. Lower An contents (<50) in plagioclase and lower Mg # in the amphiboles in the dyke (Fig. 4.16) are also consistent with the dyke silicates being more evolved, although still spatially related to the main conduit rocks.

Prichard *et al.* (2004) described petrographic evidence from magmatic sulfide droplets in a mafic dyke from Uruguay and outlined a paragenetic sequence which indicates that the sulfides and related PGM formed through primary magmatic processes. Since the sulfide blebs are isolated from external influences with little alteration of the surrounding silicates, it is believed that the evolved Cu-rich liquid was produced by crystallization processes as opposed to later hydrothermal processes and that the Pd, Bi, Te, and Sb are related to the crystallization of the immiscible sulfide liquid. The similar compositions of the sulfides and PGM in the inner dyke at Voisey's Bay to the sulfide blebs of Prichard *et al.* (2004) are consistent with a magmatic origin.

4.13.2 Compositional zonation of sulfide and PGE mineralization

The "zonation" of magmatic sulfides into Fe-Ni-rich and Cu-rich portions not only occurs on the scale of individual sulfide blebs (as in the mafic dyke in Uruguay; Prichard *et al.*, 2004) but can occur on the ore deposit scale (i.e., Sudbury; Naldrett, 1989). The sulfide blebs in the mafic dyke from Uruguay represent a static isolated

closed system, which preserve a whole continuum from MSS to ISS to the late stage veinlets of extreme fractionated ISS + PGM. In contrast, the blebs in the inner hornblende gabbro dyke at Voisey's Bay consist predominantly of only an evolved Cu-Pb rich (gn-bn-ccp)-PGM composition. Other examples in the literature may represent "open" systems that have been affected by the removal of different portions of MSS or ISS material.

Because the inner dyke in the Voisey's Bay example only contains the evolved ISS portion of sulfide (ccp-bn-gn-PGM) and the outer dyke only contains MSS compositions, it is suggested that the sulfide was removed and transported from its source in the Ovoid in at least two pulses. This suggests the system was "open" and allowed the first pulse to entrain and transport MSS material (outer dyke) and the second pulse to entrain and transport ISS material (inner dyke). A mechanism for this segregation, removal, and transport of the evolved sulfide material may be that the some of the sulfide was still liquid and could be drawn away by lithostatic differences during injection of the dyke. The resulting compositions of any given sulfide blebs will likely depend on the timing and efficiency of the removal of ISS from the MSS.

4.13.3 Proposed Model

Initial studies of the Voisey's Bay deposit supposed that the massive sulfides of the Ovoid deposit were accumulated at the base of a magma chamber through gravity settling (Naldrett *et al.*, 1996). Drilling and modeling of the geology indicated that there

is a conduit dyke below the chamber (Eastern Deeps) that contained sulfide (Naldrett *et al.*, 1996; Evans-Lamswood, 1999). It was later thought that the conduit was the likely supply of sulfide to the Ovoid and evidence indicates that the sulfide was brought up from below and deposited at the base of the Eastern Deeps Chamber (Evans-Lamswood, 1999). This model also indicates that the Ovoid formed as a rather open system in its initial stages. Following emplacement in a "dynamic" environment there appears to have been some period of static activity whereby the sulfides crystallized and were relatively undisturbed to form an ore body broadly zoned in mineralogy. The data presented here suggest that later in the sequence of events, the system was once again open, which allowed transport and removal of magmatic material to the Southeast Extension Zone.

The paragenetic sequence proposed to explain the formation of the PGE and associated sulfide mineralization in the mafic dyke in the Southeast Extension Zone is outlined in more detail in Figure 4.21:

STAGE 1:

(a) Separation of a sulfide melt from a silicate melt;

(b) Onset of MSS crystallization possibly represented by the Ovoid sulfides (Fe and Ni removal and fractionation to more Cu-rich compositions in the liquid);

(c) Some residual Cu-rich fractionated ISS liquid is retained in the Ovoid trapped as chalcopyrite "loops";

(d) The remaining ISS liquid in the Ovoid becomes extremely differentiated and enriched in Cu, Pb, Sn, Ag, Au, Pd, Pt, Bi, and Te as indicated by the formation of bornite, galena, Pd-Pt-Sn-Bi-Te-bearing PGM, Ag-tellurides, and electrum;

STAGE 2:

(e) At some point during crystallization of the system structural readjustment of the country rocks resulted in injection of the remaining evolved silicate magma or new pulses of more evolved magma into the structural weakness in two episodes;

(f) The observed pyrrhotite-pentlandite-chalcopyrite compositions of the sulfides in the outer hornblende gabbro dyke indicate that the first pulse sampled a sulfide liquid of MSS composition and transported it to the Southeast Extension Zone;

(g) Following this initial injection, the evolved Cu-Pb-PGE rich ISS liquid was entrained and transported into the Southeast Extension Zone by a second pulse, forming the inner hornblende gabbro dyke; and

(h) Pyrrhotite and pentlandite exsolve from MSS during subsolidus cooling and chalcopyrite, bornite, galena, minor pyrite, and the PGM exsolved from ISS.

The dyke is divided into "inner" and "outer" portions based on the difference in sulfide and PGE mineralization. However, the silicate portion of both the inner and outer dyke are similar in their REE contents both containing patterns indicative of evolved melts and cumulates. There is no inner chill contact within the dyke. For these reasons, the two episodes of dyke emplacement would have occurred relatively close in time to each other with the main difference being the composition of the sulfide liquid entrained

(i.e., MSS in the outer dyke producing pyrrhotite-pentlandite-chalcopyrite and "extreme" ISS in the inner dyke producing chalcopyrite-bornite-galena-PGM).

Following crystallization of the PGM from magmatic sulfide (STAGE 2), an external REE-enriched hydrothermal fluid was introduced to the system and was likely focused along the dyke. The source of the fluids is thought to be the Voisey's Bay granite/syenite, which produced secondary amphibole and locally remobilized the Pb and Sn from the sulfides that host the PGE mineralization. However, no direct evidence was found that the PGE were disturbed by this later hydrothermal fluid.

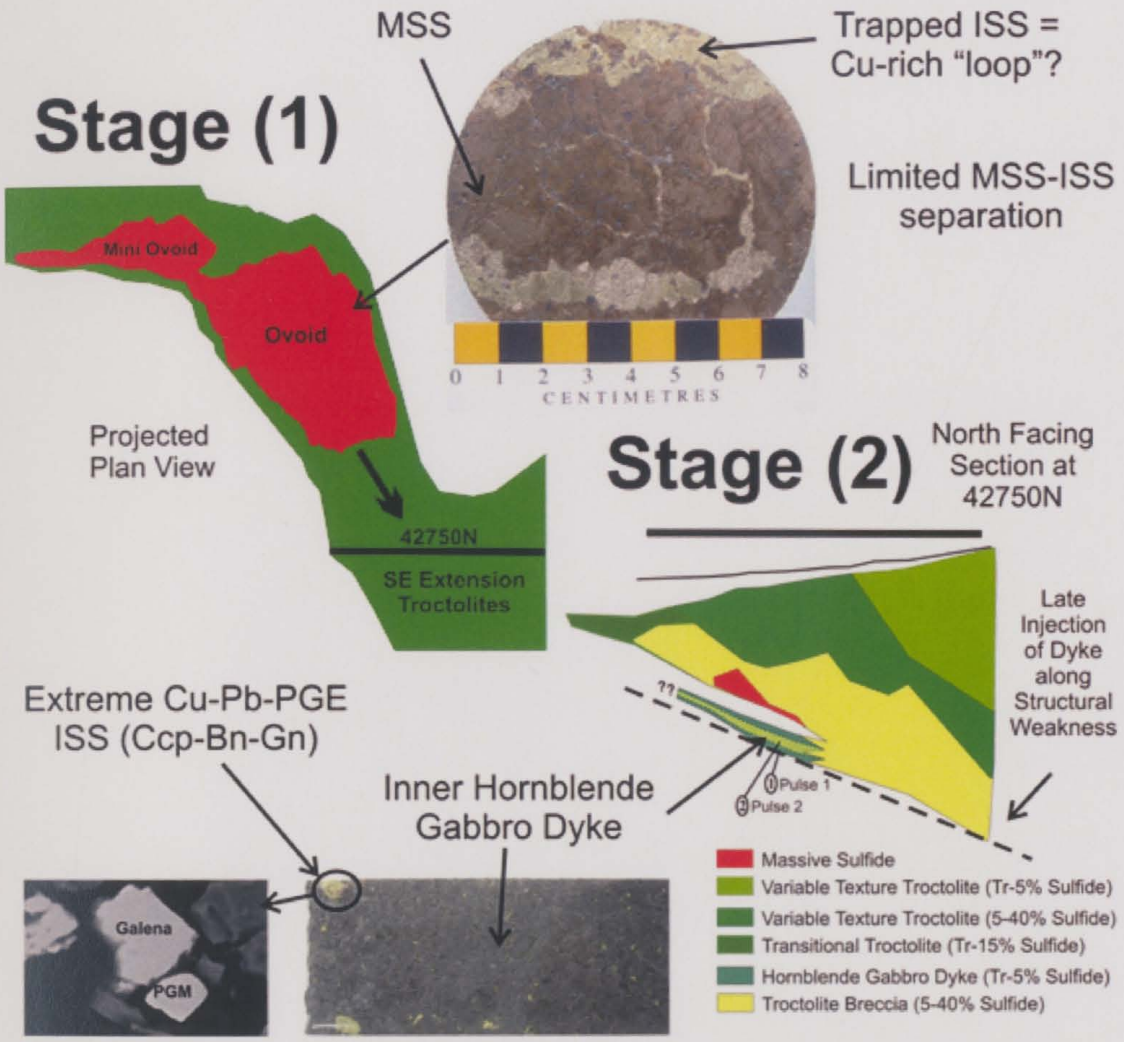

Figure 4.21. Simplified conceptual diagram of PGM formation where STAGE 1 is the crystallization of early magmatic sulfide (MSS and some ISS). At some time during crystallization of the system, it is proposed that there is structural readjustment of the country rocks surrounding the crystallizing system and STAGE 2 is the injection of a late dyke (in two pulses) along the structural weakness carrying with it in the second pulse, the most evolved sulfide as Pb-Cu-PGE enriched ISS.

4.14 ACKNOWLEDGEMENTS

This study was generously supported by grants from Inco Limited, the Atlantic Innovation Fund, and the Natural Sciences and Engineering Research Council of Canada (NSERC) to PJS, and by a NSERC postgraduate scholarship, a Northern Scientific Research Program (NSTP) scholarship, and a Society of Economic Geologist Student Research Grant to MAEH. Electron probe microanalytical work was carried out with the assistance of M. Shaffer and laser ablation – inductively coupled plasma – mass spectrometry analytical work was carried out with the assistance of M. Tubrett at Memorial University of Newfoundland Department of Earth Sciences laboratories, which is supported by a NSERC Major Facilities Access award. M. Poujol carried out the lead isotope measurements at the Inco Innovation Center – Memorial University of Newfoundland. This project would not have been possible without the support of L. Cochrane (Inco Limited), R. Wheeler, D. Lee, B. Bengert, and J. Letto (Voisey's Bay Nickel Company Limited).

4.15 REFERENCES

Amelin, Y., Li, C., Valayev, O., and Naldrett, A.J., 2000, Nd-Pb-Sr Isotope Systematics of Crustal Assimilation in the Voisey's Bay and Mushuau Intrusions, Labrador, Canada: Economic Geology, v. 95, p. 815-830.

Bacon, C.R., and Druitt, T.H., 1988, Compositional Evolution of the Zoned Calcalkaline Magma Chamber of Mount-Mazama, Crater Lake, Oregon: Contributions to Mineralogy and Petrology, v. 98, p. 224-256.

Barnes, S-J, Makovicky, E., Makovicky, M., Rose-Hansen, J., and Karup-Moller, S., 1997, Partition coefficients for Ni, Cu, Pd, Pt, Rh, and Ir between monosulfide solid solution and sulfide liquid and the formation of compositionally zoned Ni-Cu sulfide bodies by fractional crystallization of sulfide liquid: Canadian Journal of Earth Sciences, v. 34, p. 366-374.

Belincourt, L.E., Hummel, H.H., and Skinner, B.J., 1981, Phases and phase relations of the platinum-group elements, *in* Cabri, L.J., ed., Platinum-group elements: Mineralogy, Geology, Recovery: Canadian Institute of Mining and Metallurgy, Special Volume 23, p. 19-46.

Bennett, S.L., and Heyding, R.D., 1966, Arsenides of the transition metals. VIII. Some binary and ternary Group VIII diarsenides and their magnetic and electric properties: Canadian Journal of Chemistry, v. 44, p. 3017-3030.

Bowman, W., 1990, RTS-1, RTS-2, RTS-3, and RTS-4 sulfide ore mill tailings reference materials: Certificate of Analysis, Mining and Mineral Sciences Laboratories, CANMET.

Cabri, L.J., 1973, New data on phase relations in the Cu-Fe-S system: Economic Geology, v. 68, p. 443-454.

Cabri, L.J., and Laflamme, J.H.G., 1976, The mineralogy of platinum-group elements from some copper-nickel deposits of the Sudbury area, Ontario: Economic Geology, v. 71, p. 1159-1195.

Cabri, L.J., Sylvester, P.J., Tubrett, M.N., Peregoedova, A., and Laflamme, G.J.H., 2003, Comparison of LAM-ICP-MS and MICRO-PIXE results for palladium and rhodium in selected samples of Noril'sk and Talnakh sulfides: Canadian Mineralogist, v. 41, p. 321-329.

Craig, J.R., and Scott, S.D., 1974, Sulfide phase equilibria, *in* Ribbe, P.II., ed., Sulfide mineralogy: Mineralogical Society of America Short Course Notes Volume 1, p. CS1-S110.

Ebel, D. S. and Naldrett, A. J., 1996, Fractional crystallization of sulfide ore liquids at high temperature: Economic Geology, v. 91, p. 607-621.

Elliott, R.P., 1965, Constitution of Binary Alloys, 1st supplement: Materials Science and Engineering Series, McGraw-Hill Book Co, New York, 877p.

Emslie, R.F., Hamilton, M.A., and Theriault, R.J, 1994, Petrogenesis of a Mid-Proterozoic Anorthosite-Mangerite-Charnockite-Granite (AMCG) Complex: Isotopic and Chemical Evidence from the Nain Plutonic Suite: Journal of Geology, v. 102, p. 539-558.

Evans-Lamswood, D.M., 1999, Physical and geometric controls on the distribution of magmatic and sulfide-bearing phases within the Voisey's Bay Nickel-Copper-Cobalt Deposit, Voisey's Bay, Labrador: Unpublished M.Sc. thesis, St. John's, Newfoundland, Memorial University of Newfoundland, 265p.

Evans-Lamswood, D.M., Butt, D.P., Jackson, R.S., Lee, D.V., Muggridge, M.G., Wheeler R.I., and Wilton, D.H.C., 2000, Physical Controls Associated with the Distribution of Sulfides in the Voisey's Bay Ni-Cu-Co Deposit, Labrador: Economic Geology, v. 95, p. 749-770.

Fleet, M.E., Chryssoulis, S.L., Stone, W.E., and Weisner, C.G., 1993, Partitioning of platinum-group elements and Au in the Fe-Ni-Cu-S system: experiments on the fractional

crystallization of sulfide melt: Contributions to Mineralogy and Petrology, v. 115, p. 36-44.

Glebovitsky, V.A., Semenov, V.S., Belyatsky, B.V., Koptev-Dvornikov, E.V., Pchelintseva, N.F., Kireev, B.S., and Koltsov, A.B., 2001, The Structure of the Lukkulaisvaara Intrusion, Oulanka Group, Northern Karelia: Petrological Implications: Canadian Mineralogist, v. 39, p. 607-637.

Govindaraju, K., 1989, Compilation of working standards and sample descriptions for 272 geostandards: Geostandards Newsletter Special Issue 13, 114p.

Hanley, J.J., 2005, The Aqueous Geochemistry of the Platinum-Group Elements (PGE) in Surficial, Low-T Hydrothermal and High-T Magmatic-Hydrothermal Environments, *in* Mungall, J.E., ed., Exploration for Platinum-Group Element Deposits: Mineralogical Association of Canada Short Course Series Volume 34, p. 35-56.

Hanley, J.J., and Mungall, J.E., 2003, Chlorine Enrichment and Hydrous Alteration of the Sudbury Breccia Hosting Footwall Cu-Ni-PGE Mineralization at the Fraser Mine, Sudbury, Ontario, Canada: Canadian Mineralogist, v. 41, p. 857-881.

Hansen, M., and Anderko, K., 1958, Constitution of Binary Alloys, 2nd edition: Metallurgy and Metallurgical Engineering Series, McGraw-Hill Book Co, New York, 1305p.

Hawley, J.E., and Stanton, R.L., 1962, The Sudbury ores, their mineralogy and origin, Part 2: The facts, the ores, their minerals, metals and distribution: Canadian Mineralogist, v. 7, p. 30-145.

Hawthorne, F.C., 1981, Crystal Chemistry of the Amphiboles: Reviews in Mineralogy v. 9A, p. 1-102.

Huminicki, M.A.E., Sylvester, P.J., Lastra, R., Cabri, L.J., Evans-Lamswood, D., Wilton, D.H.C., 2008, First report of platinum-group minerals from a hornblende gabbro dyke in the vicinity of the Southeast Extension Zone of the Voisey's Bay Ni-Cu-Co deposit, Labrador: Mineralogy and Petrology, v. 92, p. 129-164.

Huminicki, M.A.E., Sylvester, P.J., Shaffer, M., Wilton, D.H.C., Evans-Lamswood, D., and Wheeler, R. (in review), Systematic and Integrative Ore Characterization of Massive Sulfide Deposits: An Example from the Voisey's Bay Ovoid Deposit, Labrador: Economic Geology.

Lastra, R., Wilson, J.M.D., and Cabri, L.J., 1999, Automated gold search and applications in process mineralogy: Transactions Institute of Mining and Metallurgy Section C Volume 108, p. 75-84.

Li, C., and Naldrett, A.J., 1999, Geology and petrology of the Voisey's Bay intrusion: reaction of olivine with sulfide and silicate liquids: Lithos, v. 47, p. 1-31.

Li, C., Lightfoot, P.C., Amelin, Y., and Naldrett, A.J., 2000, Contrasting Petrological and Geochemical Relationships in the Voisey's Bay and Mushuau Intrusions, Labrador, Canada: Implications for Ore Genesis: Economic Geology, v. 95, p. 771-799.

Lightfoot, P.C., 1998, Geological and geochemical relationships in the Reid Brook Intrusive Complex, Labrador: Exploration strategies for magmatic Ni-Cu-Co ores at Voisey's Bay. Inco, ITSL, Copper Cliff Exploration Office, Sudbury, Ontario, Pathways '98.

Lightfoot, P.C., and Naldrett, A.J., 1999, Geological and geochemical relationships in the Voisey's Bay intrusion, Nain Plutonic Suite, Labrador, Canada: Geological Association of Canada Short Course Notes Volume 13, p. 1-30.

Longerich, H.P., 1995, Analysis of Pressed Pellets of Geological Samples Using Wavelength-Dispersive X-Ray Fluorescence Spectrometry: X-Ray Spectrometry, v. 24, p. 123-136.

McDonough, W.F., and Sun S-S., 1995, The composition of the Earth: Chemical Geology, v.120, p. 223-253.

McKenzie, D., and O'Nions, R.K., 1991, Partial melt distributions from inversion of rare Earth element concentrations: Journal of Petrology, v. 32, p. 1021-1091.

Moffatt, W.G., 1979, The Handbook of Binary Phase Diagrams, 3rd volume, and The Index to Binary Phase Collections, 1st edition, General Electric Company, Schenectady, New York.

Mungall, J.E., 2005, Magmatic Geochemistry of the Platinum-Group Elements, *in* Mungall, J.E., ed., Exploration for Platinum-Group Element Deposits: Mineralogical Association of Canada Short Course Series Volume 34, p. 1-34.

Naldrett, A.J., 1969, Discussion of papers concerned with sulfide deposits. Economic Geology Monograph 4, p. 359-365.

Naldrett, A.J., 1981, Nickel sulfide deposits: Classification, composition and genesis: Economic Geology, v. 75, p. 628-685.

Naldrett., A.J., 1989, Magmatic sulfide deposits: N.Y.-Oxford, Clarendon Press-Oxford University Press, 186p.

Naldrett, A.J., 2004, Magmatic Sulfide Deposits: Geology, Geochemistry, and Exploration: Springer, 727p.

Naldrett, A. J., Craig, J. R., and Kullerud, G., 1967, The central portion of the Fe-Ni-S system and its bearing on pentlandite exsolution in iron-nickel sulfide ores: Economic Geology, v. 62, p. 826-847.

Naldrett, A.J., Hoffman, E.L., Green, A.H., Chou, C.L, Naldrett, F.R., and Alcock, R.A., 1979, The compositions of Ni-sulfide ores, with particular reference to their content of PGE and Au: Canadian Mineralogist, v. 17, p. 403-415.

Naldrett, A.J., Pessaran, R., Asif, M., and Li, C., 1994, Compositional variation in the Sudbury ores and prediction of the proximity of footwall copper-PGE orebodies: Ontario Geological Survey Special Volume 5, p. 133-143.

Naldrett, A.J., Keats, H., Sparkes, K., and Moore, R., 1996, Geology of the Voisey's Bay Ni-Cu-Co Deposit, Labrador, Canada: Exploration and Mining Geology, v. 5, p. 169-179.

Naldrett, A.J., Asif, M., Krstic, S., and Li, C., 2000a, The Composition of Mineralization at the Voisey's Bay Ni-Cu Sulfide Deposit, with Special Reference to Platinum-Group Elements: Economic Geology, v. 95, p. 845-866.

Naldrett, A.J., Singh, J., Krstic, S., and Li, C., 2000b, The Mineralogy of the Voisey's Bay Ni-Cu-Co Deposit, Northern Labrador, Canada: Influence of Oxidation State on Textures and Mineral Compositions: Economic Geology, v. 95, p. 889-900.

Pearce, N.J.G., Perkins, W.T., Westgate, J.A., Gorton, M.P., Jackson, S.E., Neal, C.R., and Chenery, S.P., 1997, A compilation of new and published major and trace element data for NIST SRM 610 and NIST SRM 612 glass reference materials: Geostandards Newsletter, Journal of Geostandards and Geoanalysis, v. 21, p. 115-144.

Prichard, H.M., Hutchinson, D., and Fisher, P.C., 2004, Petrology and crystallization history of multiphase sulfide droplets in a mafic dike from Uruguay: Implications for the origin of Cu-Ni-PGE sulfide deposits: Economic Geology, v. 99, p. 365-376.

Rawlings-Hinchey, A.M., Sylvester, P.J., Myers, J.S., Dunning, G.R., Kosler, J., 2003, Paleoproterozoic crustal genesis: calc-alkaline magmatism of the Torngat Orogen, Voisey's Bay area, Labrador: Precambrian Research, v. 125, p. 55-85.

Rudashevsky, N.S., Garuti, G., Andersen, J.C.Ø., Kretser, Y.L., Rudashevsky, V.N., and Zaccarini, F., 2002, Separation of accessory minerals from rocks and ores by hydroseparation (HS) technology: method and application to CHR-2 chromitite, Niquelandia, Brazil: Transactions Institute of Mining and Metallurgy Section B, Applied Journal of Earth Sciences, v. 11, p. B87-B94.

Ryan, B., 2000, The Nain-Churchill Boundary and the Nain Plutonic Suite: A Regional Perspective on the Geologic Setting of the Voisey's Bay Ni-Cu-Co Deposit: Economic Geology, v. 95, p. 703-724.

Ryan, B., 2002, Whole-rock analyses and assays of rock samples from the Mesoproterozoic Nain Plutonic Suite and the enclosing Archean and Paleoproterozoic gneisses from the Voisey's Bay – Konrad Brook area of north-central, Labrador: Geological Survey of Newfoundland and Labrador Open File 014D/0283.

Shunk, F.A., 1969, Constitution of Binary Alloys, 2nd supplement: Materials Science and Engineering Series, McGraw-Hill Book Co, New York, 720p.

Sylvester, P.J., 2001, A practical guide to Platinum-Group Element analysis of sulphides by Laser-Ablation-ICP-MS: Mineralogical Association of Canada Short Course Series Volume 29, p. 203-211.

Todt, W., Cliff, R.A., Hanser, A., and Hofmann, A.W., 1996, Evaluation of a 202Pb–205Pb double spike for high precision lead isotope analysis, *in* Basu, A., and Hart, S., eds., Earth processes: reading the isotopic code: Geophysical Monograph 95, American Geophysical Union, Washington, DC, p. 429-437.

van Achterbergh, E., Ryan, C., Jackson, S.E., and Griffin, W., 2001, Appendix III: Data reduction and software for laser ablation – inductively coupled plasma – mass spectrometry, *in* Sylvester, P., ed., Laser-Ablation-ICPMS in the Earth Sciences: Principles and Applications: Mineralogical Series Volume 29, p. 239-243.

Wilson, S.A., Ridley, W.I., and Koenig, A.E., 2002, Development of sulfide calibration standards for the laser ablation inductively-coupled plasma mass spectrometry technique: Journal Anal At Spectrum, v. 17, p. 406-409.

Wood, S.E., 2002, The aqueous geochemistry of the platinum-group elements with applications to ore deposits, *in* Cabri, L.J., ed., The Geology, Geochemistry, Mineralogy, and Mineral Beneficiation of Platinum-Group Elements: Canadian Institute of Mining, Metallurgy, and Petroleum, Special Volume 54, p. 211-250.

Zartman, R.E., Doe, B.R., 1981, Plumbotectonics: the model: Tectonophysics, v. 75, p. 135-162.

APPENDIX 4.I – ANALYTICAL METHODS

A4.1.1 Whole rock major and trace element X-ray fluorescence

Samples were crushed to 1-2cm sized pieces with a steel jaw-crusher and then pulverized to a 50-35 mesh size (300-500 μm) powder in a tungsten carbide puck mill assembly at the Memorial University of Newfoundland Department of Earth Sciences laboratories. A portion of this powder was set aside to maintain coarser mineral fractions for further sieving and hydroseparation (see below for method). The remainder was further pulverized to a >200 mesh (<75μm) powder for whole rock NiS fire assay (see below) and X-ray fluorescence. For X-ray fluorescence, five grams of each powdered sample were mixed with 0.7 gm of phenolic resin and homogenized. A Herzog press was then used to compress these powders into circular pellets, which were then baked at 200°C for 20 minutes. The concentrations of major and trace elements in the whole rock pellets were obtained by X-ray fluorescence using the automated ARL 8420+ sequential spectrometer at Memorial University of Newfoundland Department of Earth Sciences laboratories (after techniques described by Longerich, 1995). Concentrations of Fe_2O_3T, Fe, Ni, Cu, S, SiO_2, TiO_2, Al_2O_3, MnO, MgO, CaO, Na_2O, P_2O_5, K_2O, Cl, Sc, V, Cr, Zn, Ga, As, Rb, Sr, Y, Zr, Nb, Ba, Ce, Pb, Th and U were determined by this technique. Samples were calibrated for sulfides using RTS-4 (CANMET; Bowman, 1990), a high pyrrhotite (unoxidized) material from Sudbury provided by Falconbridge Limited and

RTS-2 (CANMET; Bowman, 1990), a low pyrrhotite (oxidized) material from Sudbury provided by Inco Limited. Results and detection limits are reported in Appendix 4.II.

A4.1.2 Whole rock trace element ICP-MS

The trace elements Co, Se, Ag, Cd, Sn, Sb, Te, Bi, Li, Rb, Sr, Y, Zr, Nb, Mo, Cs, Ba, La, Ce, Pr, Nd, Sm, Eu, Gd, Tb, Dy, Ho, Er, Tm, Yb, and Lu were analyzed by solution ICP-MS in the Memorial University of Newfoundland Department of Earth Sciences laboratories. For dissolution, 8N HNO_3 and HF acid are added to 0.1000g of sample and refluxed overnight to dissolve the sample (longer if sample is not dissolved). Once dissolved, samples are rinsed with 8N HNO_3 and evaporated at 80-100°C until dry. Once dry, HF and 8N HNO_3 are added and the sample is refluxed for several days to insure complete dissolution of all minerals. Boric acid and 8N HNO_3 are added to the sample and evaporated in several stages. Finally, 8N HNO_3 is added to the sample such that the entire sample is in solution and oxalic acid and a boric acid-HF acid mix are added with nanopure water to a 60g weight. Samples are "spiked" with a known solution before running on the ICP-MS. Two runs are done for each sample, a "spiked" and an "unspiked" run. The spiked sample contains 5g of spike solution plus 4.5g of 0.2N HNO_3 with 0.5g of unknown sample solution; the unspiked sample contains 4.5g of 0.2N HNO_3 and 0.5g of sample solution. Each run on the ICP-MS consists of 1 acid blank, standards BR688 and MRG-1, 3 procedure duplicates and 18 samples (Govindaraju, 1989). Results and detection limits are reported in Appendix 4.II.

The REE (La, Ce, Pr, Nd, Sm, Eu, Gd, Tb, Dy, Ho, Er, Tm, Yb, and Lu) were normalized to chondrite using values from Table A4.1a. Partition coefficients (K_d) used in calculating melt compositions in equilibrium with amphibole are listed in Table A4.2.

Table A4.1a. Primitive mantle normalizing values for REE (McDonough and Sun, 1995).

Element	Primitive Mantle (ppm)	Element	Primitive Mantle (ppm)
La	0.648	Tb	0.099
Ce	1.675	Dy	0.674
Pr	0.254	Ho	0.149
Nd	1.25	Er	0.438
Sm	0.406	Tm	0.068
Eu	0.154	Yb	0.441
Gd	0.544	Lu	0.0675

Table A4.1b. Normalizing values for PGE and base metals (McDonough and Sun, 1995).

Element	Primitive Mantle	CI Chondrite	Element	Primitive Mantle	CI Chondrite
Bi	2.5 ppb	110 ppb	Pt	7.1 ppb	1010 ppb
S	250 ppm	5.40 %	Rh	0.9 ppb	130 ppb
Te	12 ppb	2330 ppb	Ru	5 ppb	710 ppb
Se	0.075 ppm	21 ppm	Ni	1960 ppm	10500 ppm
As	0.05 ppm	1.85 ppm	Ir	3.2 ppb	455 ppb
Sb	5.5 ppb	140 ppb	Co	105 ppm	500 ppm
Pb	250 ppb	2470 ppb	Fe	62600 ppm	181000 ppm
Au	1 ppb	140 ppb	Zn	55 ppm	310 ppm
Pd	3.9 ppb	550 ppb	Cr	2625 ppm	2650 ppm
Cu	30 ppm	120 ppm	Ag	8 ppb	200 ppb

A4.1.3 Whole rock NiS fire assay

Samples were sent to Actlabs (Ancaster, Ontario) for whole rock analysis of 5 of the PGE (Pt, Pd, Rh, Ru, and Ir) as well as Au by NiS fire assay followed by a HR-ICP-MS finish (Code 1B3). Results and detection limits are reported in Appendix 4.II. The PGE (Pt, Pd, Rh, Ru, and Ir), Au, Cu, and Ni were normalized to chondrite using values from Table A4.1b.

Table A4.2. Partition coefficients for amphibole in basalt (McKenzie and O'Nions, 1991) and in rhyolite (Bacon and Druitt, 1988).

Rock	Element	K_d	Rock	K_d
Basalt	Ce	0.26	Rhyolite	0.68
Basalt	Dy	0.78	Rhyolite	
Basalt	Er	0.68	Rhyolite	
Basalt	Eu	0.88	Rhyolite	3.2
Basalt	Gd	0.86	Rhyolite	
Basalt	Ho	0.73	Rhyolite	
Basalt	La	0.17	Rhyolite	0.36
Basalt	Lu	0.51	Rhyolite	1.8
Basalt	Nb	0.8	Rhyolite	1.6
Basalt	Nd	0.44	Rhyolite	1.6
Basalt	Pb	0.1	Rhyolite	
Basalt	Pr	0.35	Rhyolite	
Basalt	Sm	0.76	Rhyolite	2.3
Basalt	Sr	0.12	Rhyolite	0.01
Basalt	Ta	0.38	Rhyolite	0.43
Basalt	Tb	0.83	Rhyolite	2.4
Basalt	Ti	0.69	Rhyolite	
Basalt	Tm	0.64	Rhyolite	
Basalt	Yb	0.59	Rhyolite	1.8

A4.1.4 Hydroseparation

Several PGE elevated samples were selected for concentration of heavy minerals (sulfides and platinum-group minerals) by hydroseparation at Memorial University of Newfoundland Department of Earth Sciences laboratories in order to maximize chances of finding discrete platinum-group minerals (PGM) and other precious metal minerals (PMM) since they are small and rare. Care was taken not to over crush the sample with a shatter box in order to maintain coarser size fractions. The samples were sieved to several size fractions (>325 mesh or <45 μm, 325-200 mesh or 45-75 μm, 200-120 mesh or 75-125 μm, 120-80 or 125-180 μm, and 80-50 mesh or 180-300 μm) before hydroseparation.

The hydroseparation technique is a new technique that concentrates the minerals based on density using water (Rudashevsky *et al.*, 2002). It is a preferred method as it eliminates the use of harsh chemicals used in other types of mineral separation, it is simple to use, and efficient in producing a representative concentrate of heavier minerals. Sieving samples to different size fractions before hydroseparating the material results in particles separating out based on density alone and not due to the varying sizes of particles. Initially the lightest particles will be removed as tailings (i.e., silicates), leaving a concentrate of heavier minerals (i.e., sulfides and platinum-group minerals). The densest sulfide mineral in the sample is galena (SG = 7.4), which tends to remain in the concentrate. If liberated PGM phases are present they will also remain in the concentrate because of their high specific gravity (i.e., for sperrylite SG = 10.58). This technique can be repeated until optimal concentrates are obtained. Following the HS process, samples were subsequently sent to CANMET for mounting as monolayer polished sections and automated precious metal mineral (PMM) searches.

A4.1.5 Automated precious metal mineral (PMM) searches

Monolayer epoxy-mounted 25 to 32mm round polished sections were made using each size fraction of the hydroseparator concentrates and were automatically searched using an image analyzer (KS400, ZEISS) interfaced to an electron microprobe (JEOL 733) by R. Lastra at CANMET. The search was set up to determine precious metal minerals (PMM) including platinum-group minerals (PGM) and Ag- and Au-bearing

phases. The information obtained about each particle included a semi-quantitative energy discriminating X-ray spectrometry spectra for mineral identification, the particle MDL size, any associated minerals, and a back scattered electron image. The automated search is beneficial in that it is more efficient and representative of all the discrete PGM and other PMM than manual searches.

The image analysis program was based on one developed for PMM searches (gold minerals). Detailed information concerning the automated gold search by electron microscopy is published elsewhere (Lastra *et al.*, 1999). Briefly, the image analysis program for automated PMM search consists of three main parts: 1) location of grains with high brightness in BSE images at 400x magnification, 2) a check for the presence of PMM using the X-ray signals from a drift chamber detector capable of a yielding a high count rate of 1,000,000 counts per second, and 3) if a PMM mineral is found, then the image and stage location are recorded for subsequent retrieval.

It is simplest to program searches to follow a square meander. To accommodate this, a square template was used to mount the specimen in the polished section. The automated PMM search on the polished sections was performed at a magnification of 400x. A total of ~10,000 fields were scanned on each polished section. On average, it took approximately 15 hours to complete the scan of one polished section. A lower magnification would decrease the required run time. However, search tests using gold grains (Lastra *et al.*, 1999), indicated that grains as small as one micrometer cannot be consistently detected at magnifications lower than 400x magnification. Thus, for the automated PMM search, it was assumed that a 400x magnification would also allow

proper detection of grains as small as one micrometer. After the 10,000 field automated PMM scan was finished, the stage positions for located grains were retrieved for further identification of the PMM and to determine its association with other minerals. Quantitative mineral chemistry was then obtained by electron probe microanalysis for each representative PMM that was detected by the automated search (see below).

A4.1.6 Electron probe microanalysis

Analyses were carried out on the Cameca SX-50 electron probe microanalyzer in the Memorial University of Newfoundland Department of Earth Sciences laboratories for major element mineral compositions. The automation software is SamX's "Xmas" for combined wave discriminating X-ray spectrometry (Cameca) & energy discriminating X-ray spectrometry (Oxford/Link). The intention of the electron probe microanalysis is to quantify the silicate, sulfide, and the precious metal mineral (PMM) compositions.

The sulfides, platinum-group minerals, tellurides, bismuthides, native Ag, and electrum were analyzed by a combination of wave discriminating X-ray spectrometry and energy discriminating X-ray spectrometry for the following elements: S, Pb, Fe, Cu, Zn, Ni, Co, As, Se, Ag, Sb, Te, Pt, Au, Pd, Rh, Cd, Bi, and Sn. For the sulfides (pyrrhotite, pentlandite, chalcopyrite, bornite, pyrite, millerite, mackinawite, parkerite?, and volfsonite?), measurements of S, Fe, Cu, Ni, and Co are the most precise, utilizing wave discriminating X-ray spectrometry with special attention to background measurement. Count times for these elements were chosen for an approximate 10% error at a

concentration of 0.1 wt% and ZAF corrections were applied. Zinc was measured with an otherwise idle TAP wave discriminating X-ray spectrometer. Elements also measured in the sulfide by energy discriminating X-ray spectrometry were Pb, As, Se, Sb, Te, Bi, and Sn. For galena, Pb and S were measured by wave discriminating X-ray spectrometry. For the PGM (sperrylite, paolovite, froodite, Pd-Bi-Sb-Te, Sn-stibiopalladinite, maslovite, geversite?, polarite/sobolevskite?, insizwaite?, and niggliite?), measurements of As, Se, Ag, Sb, Te, Pt, Au, Pd, Bi, and Sn are most precise using wave discriminating X-ray spectrometry; elements also measured in the PGM were S, Fe, Cu, Ni, Co, and Cd by energy discriminating X-ray spectrometry. For the Ag- and Bi-tellurides (stützite, matildite, tsumoite, and sulphotsumoite?), measurements were most precise for Ag, Te, Au, and Bi using wave discriminating X-ray spectrometry; elements also measured by energy discriminating X-ray spectrometry were S, Fe, Cu, Ni, Co, As, Se, Sb, Pt, Pd, Cd, and Sn. For electrum and native Ag, measurements for Au and Ag were the most precise using wave discriminating X-ray spectrometry. Results and detection limits are reported in Appendix 4.IIIa

Olivine was measured for SiO_2, TiO_2, Al_2O_3, Cr_2O_3, FeO, MnO, MgO, CaO, and NiO, pyroxenes were measured for SiO_2, TiO_2, Al_2O_3, Cr_2O_3, Fe_2O_3(c), FeO(c), MnO, MgO, CaO, Na_2O, and K_2O, amphiboles were measured for SiO_2, TiO_2, Al_2O_3, Cr_2O_3, Fe_2O_3(c), FeO(c), MnO, MgO, CaO, Na_2O, K_2O, NiO, F, Cl, and H_2O(c), biotite was measured for SiO_2, TiO_2, Al_2O_3, Cr_2O_3, FeO, MnO, MgO, CaO, Na_2O, K_2O, NiO, F, Cl, and H_2O(c), and chlorite was measured for SiO_2, TiO_2, Al_2O_3, FeO, MnO, MgO, CaO, Na_2O, and K_2O. Results and detection limits are reported in Appendix 4.IIIb.

A4.1.7 Laser ablation - inductively coupled plasma - mass spectrometry

In situ trace-element analyses were carried out for sulfide minerals in the Memorial University of Newfoundland Department of Earth Sciences laboratories using an in-house built 266 nm Nd:YAG laser system attached to a VG Fisons PlasmaQuad II+"S" quadrupole mass spectrometer and the silicate minerals using a HP4500+ mass spectrometer.

A4.1.7.1 Sulfides

Isotopic masses of elements in the sulfide minerals (pyrrhotite, pentlandite, chalcopyrite, bornite, galena, and pyrite) were analyzed using sulfur as an internal calibration. Analyses of the standards and sulfide grains were run with laser energies between 0.08 and 0.50 mJ/p using raster widths between 30 and 100μm, respectively, and ablation times of 120 seconds.

The PGE (Pt, Pd, Rh, Ru, Ir, and Os) were standardized using the PO-31 sulfide reference material (unpublished Memorial University of Newfoundland data) and all other elements (S, Ga, Zn, Ge, As, Se, Mo, Ag, Cd, Sn, Sb, Te, Au, Hg, Pb, and, Bi) were standardized using the MASS-1 sulfide reference material (Wilson *et al.*, 2002), which were each run four and two times, respectively, during each block of data. The fused pyrrhotite standard (PO-31), containing all six PGE, was synthesized by A. Perogoedova at McGill University using a method similar to that described by Cabri *et al.* (2003);

MASS-1 and PO-31 were calibrated by solution ICP-MS at Memorial University of Newfoundland Department of Earth Sciences laboratories. Calibration values employed for the synthetic sulfides are given in Table A4.3.

Raw counts were processed off line using the spreadsheet based program CONVERT to integrate signals from each sequential set of 3 sweeps. Data reduction and concentration calculations were then performed on the raw data using spreadsheet based program LAMTRACE (van Achterbergh *et al.*, 2001). For calibration purposes S, determined by electron microprobe, was used as an internal standard for each mineral (average S from Voisey's Bay sulfides were used for pyrrhotite = 38.63 wt% (n = 315), pentlandite = 33.21 wt% (n = 297), chalcopyrite = 34.83 wt% (n = 290), cubanite = 35.16 wt% (n = 68), and bornite = 23.79 wt% (n = 5); stoichiometric S was used for galena = 13.08 wt% and pyrite = 53.45 wt%). Use of an internal standard enables the laser ablation – inductively coupled plasma – mass spectrometry technique to deal with different ablation yields in different minerals. Differences between the measured and expected values in PO-31 are <15% for each of the PGE when standardized against MASS-1 (Table A4.4a) and the differences between measured and expected values in MASS-1 are <10% for all other trace elements when standardized against PO-31 (Table A.4.4b).

Table A4.3. Element concentrations in synthetic standards used as calibration values for the laser ablation – inductively coupled plasma – mass spectrometry. All values are in ppm unless otherwise noted.

Element	MASS-1	PO-31	NIST SRM 612	USGS BCR-2G
SiO_2			72.72 (wt%)	54.06 (wt%)
CaO			11.85 (wt%)	6.82 (wt%)
TiO_2			48.11	2.68 (wt%)
S	27.6 (wt%)	37.15 (wt%)		
Sc			41.05	34.8
V	63		39.22	400
Cr	37		39.88	16.9
Mn	260			
Co	67		35.26	35.4
Ni	*94		38.44	11
Rb			31.63	44.5
Sr			76.15	329
Y			38.25	31.3
Zr			35.99	162
Nb			38.06	12.3
Ba			37.74	655
Ga	50			
Ge	50			
As	65			
Se	53			
Mo	61			
Ag	67			
Cd	70			
Sn	55		37.96	
Sb	55		38.44	
La			35.77	24.4
Ce			38.35	51.0
Sm			36.72	6.20
Eu			34.44	1.85
Gd			36.95	6.03
Ho			37.87	1.19
Yb			39.95	3.23
Hf			34.77	4.57
Ta			39.77	0.78
Te	*14			
W	*45			
Au	47			
Hg	57			
Pb	*67		38.96	10.2
Bi	45		29.84	
Th			37.23	5.72
U			37.15	1.58
Zn	21 (wt%)			
Ru		19.3		
Rh		77.9		
Pd		10.3		
Os		10.2		
Ir	*68.5	19		
Pt	*72.8	75.6		
Au	47			

MASS-1 values are from Wilson *et al.* (2002) except * are unpublished Memorial University of Newfoundland solution ICP-MS values; PO-31 values are from unpublished Memorial University of Newfoundland data except S was done using wave discriminating X-ray spectrometry electron probe microanalysis by J.H.G. Laflamme; NIST SRM 612 values are from Pearce *et al.* (1997); USGS BCR-2G values are from solution ICP-MS at Memorial University of Newfoundland, which were calibrated with NIST SRM 612 using values from Pearce *et al.* (1997).

Table A4.4a. Measured and expected values for PO-31 standard.

Element	SO2	Ru	Ru	Ru	Rh	Pd	Pd	Pd	Pd	Os	Os	Ir	Ir	Pt	Pt
Isotopic mass	33	99	101	102	103	105	106	108	110	188	189	191	193	194	195
Units	wt%	ppm	ppm	ppm	ppm	ppm	ppm	ppm	ppm	ppm	ppm	ppm	ppm	ppm	ppm
Mean (ppm) n = 64	38.7	20.1	20.1	20.1	81.0	10.7	10.7	10.7	10.7	10.6	10.6	19.8	19.8	78.8	78.8
St Dev (ppm)	1.57	2.78	2.76	2.71	8.25	0.81	0.82	0.80	0.88	1.44	1.41	2.96	2.85	9.46	9.31
Rel St Dev (%)	4.06	13.86	13.77	13.50	10.18	7.57	7.67	7.46	8.26	13.51	13.27	14.92	14.40	12.01	11.83
*Expected value (ppm)	38.7	19.3	19.3	19.3	77.9	10.3	10.3	10.3	10.3	10.2	10.2	19.0	19.0	75.6	75.6
Mean/Expected value	1.00	1.04	1.04	1.04	1.04	1.04	1.04	1.04	1.04	1.04	1.04	1.04	1.04	1.04	1.04

Table A4.4b. Measured and expected values for MASS-1 standard.

Element	SO2	Ga	Zn	Ge	Se	Mo	Ag	Cd	Sn	Sb	Te	Au	Hg	Pb	Bi
Isotopic Mass	33	69	70	72	77	95	107	111	118	121	125	197	202	208	209
Units	wt%	ppm	ppm	ppm	ppm	ppm	ppm	ppm	ppm	ppm	ppm	ppm	ppm	ppm	ppm
Mean (ppm) n = 64	28.3	51.3	168733	51.3	54.1	62.5	68.7	71.8	56.4	56.4	14.4	48.2	58.4	68.7	46.1
St Dev (ppm)	2.70	4.90	1740	4.90	5.26	5.98	6.57	6.90	5.39	5.39	1.37	4.62	5.62	6.59	4.42
Rel St Dev (%)	9.53	9.56	1.03	9.55	9.72	9.56	9.57	9.62	9.57	9.56	9.56	9.60	9.61	9.59	9.58
*Expected value (ppm)	27.6	50.0	210000	50.0	53.0	61.0	67.0	70.0	55.0	55.0	14.0	47.0	57.0	67.0	45.0
Mean/Expected value	1.03	1.03	0.80	1.03	1.02	1.03	1.03	1.03	1.03	1.03	1.03	1.03	1.03	1.03	1.03

A4.1.7.2 Corrections for Spectral Interferences on Pd, Rh, and Ru

Measured isotopes of the PGE were ^{99}Ru, ^{101}Ru, ^{102}Ru, ^{103}Rh, ^{105}Pd, ^{106}Pd, ^{108}Pd, ^{188}Os, ^{189}Os, ^{191}Ir, ^{193}Ir, ^{194}Pt, and ^{195}Pt. ^{63}Copper and ^{65}Cu were periodically measured to check for isobaric spectral interferences of ^{40}Ar^{63}Cu on ^{103}Rh and ^{40}Ar^{65}Cu on ^{105}Pd; if Cu is not present then there will be no argide interferences on Pd from Cu. The ^{70}Zn isotope was monitored for isobaric spectral interferences of ^{40}Ar^{66}Zn on ^{106}Pd and ^{40}Ar^{68}Zn on ^{108}Pd; if Zn is not present then there will be no argide interferences on Pd from Zn. ^{111}Cadmium was monitored to check for interferences of ^{106}Cd on ^{106}Pd and ^{108}Cd on ^{108}Pd. Corrections were done on all light PGE (Pd, Rh, and Ru) in all sulfide minerals analyzed (pyrrhotite, pentlandite, chalcopyrite, cubanite, bornite, galena, and

pyrite) and were calculated and subtracted using the mathematical algorithms of Sylvester (2001). A low percent of correction is desired. The heavy PGE isotopes (Pt, Ir, and Os) do not have interferences and are therefore not corrected. The light PGE (Pd, Rh, and Ru) all require corrections and the percent that an isotope is corrected for will vary for the different minerals. Some corrections are greater in different minerals, however, if the isotopes are within 10% of each other and are above detection, analyses requiring larger corrections were still used. The maximum percent correction used for each element in each mineral are outlined in Table A4.5.

Three of the palladium isotopes were measured (^{105}Pd, ^{106}Pd, and^{108}Pd). The relative concentration of the 106 isotope was found to be much higher and dissimilar to the 105 and 108 isotopes of palladium, which is likely due to some other interference, therefore the 105 and 108 isotopes of palladium were used for all minerals. If the 105 and 108 isotopes agree within 10% of each other, the average of the two isotopes was used, if the isotopes do not agree within 10% of each other the lower isotope (105) was used. At least one isotope was corrected for <10% for pyrrhotite, <40% for pentlandite, <95% for chalcopyrite, <85% for cubanite, <20% for bornite, and <65% for galena. Only two grains of pyrite were analyzed and values could not be determined. Detection limit for Pd is 0.01ppm.

Three of the ruthenium isotopes were measured (^{99}Ru, ^{101}Ru, and^{102}Ru) The 99 isotope was not corrected for and is dissimilar to the 101and 102 isotopes of ruthenium, which is likely due to some other interference, therefore the 101 and 102 isotopes of ruthenium were used for all minerals. If the 101 and 102 isotopes agree within 10% of

each other, the average of the two isotopes was taken, if the isotopes do not agree within 10% of each other the lower isotope (102) was taken. At least one isotope was corrected <25% for pyrrhotite, <90% for pentlandite, and <10% for pyrite. Both Ru isotopes were below detection in chalcopyrite, cubanite, bornite, and galena. Detection limit for Ru is 0.02ppm.

Rhodium only has one isotope, 103, and it will have an interference from the $^{40}Ar^{63}Cu$ in Cu-rich minerals. Corrections are greater than 90% for ^{103}Rh in the Cu-bearing minerals chalcopyrite, cubanite, and bornite and since only one isotope is measured (nothing to check with), the ^{103}Rh data cannot be relied upon for these minerals. Rhodium cannot be measured satisfactorily in galena either because of the double-charging effects of the ^{206}Pb. For pyrrhotite and pentlandite, values are used where Rh is <50% corrected and above a detection limit of 0.05ppm.

For other elements where more than one isotope was measured (Os, Ir, Pt, Mo, and Ag) and if two isotopes agree within 10% of each other, the average of the two isotopes was taken. ^{72}Germanium and ^{73}Ge were analyzed but not reported due to potential interferences from $^{40}Ar^{32}S$ and $^{40}Ar^{33}S$, respectively from the sulfides. ^{75}Arsenic and ^{77}Se were analyzed but not reported due to potential interferences with $^{40}Ar^{35}Cl$ and $^{40}Ar^{37}Cl$, respectively, which may represent ablate through in the sample and composition of the epoxy. For all other elements (Ga, Zn, Cd, Sn, Sb, Te, Au, Hg, Pb, and Bi) only one isotope was measured and they are not expected to have any interferences. Results and detection limits are reported in Appendix 4.IVa.

Table A4.5. Maximum percent correction for light PGE isotopes in each sulfide mineral.

Mineral	^{105}Pd-^{108}Pd	^{103}Rh	^{101}Ru-^{102}Ru
Pyrrhotite	<10%	<50%	<25%
Pentlandite	<40%	<50%	<90%
Chalcopyrite	<95%	nd	<det
Cubanite	<85%	nd	<det
Bornite	<20%	nd	<det
Galena	<65%	nd	<det
Pyrite	nd	<50%	<10%

nd = not determined; <det = below detection

A4.1.7.3 Silicates

Isotopic masses of elements were analyzed using silica as an internal calibration for the silicate minerals (olivine, pyroxene, amphibole, biotite, chlorite, and plagioclase). Analyses of the standards and samples were run with average laser energies of 0.065 mJ/p and raster width of 30μm with ablation times of 80 seconds.

The 29 elements SiO_2, CaO, Sc, TiO2, V, Cr, Co, Ni, Rb, Sr, Y, Zr, Nb, Sn, Sb, Ba, La, Ce, Sm, Eu, Gd, Ho, Yb, Hf, Ta, Pb, Bi, Th, and U were calibrated against the NIST SRM 612 silicate glass reference material (Pearce *et al.*, 1997) and the USGS BCR-2G was used as an unknown reference and were run four and two times, respectively, during each block of data. Calibration values employed for the synthetic standards are given in Table A4.3. Platinum, Pd, and Te were also analyzed but no counts were measured above detection in any silicate minerals and therefore were not standardized.

Raw counts were processed the same as the sulfides (above) but for calibration purposes SiO_2, determined by electron microprobe was used as the internal standard.

Where SiO_2 was unavailable for the individual mineral, values used were: olivine = 34.15 wt%, pyroxene = 50.5 wt%, amphibole = 43.0 wt%, biotite = 36.0 wt%, chlorite = 26.45 wt%, and plagioclase = 57.5 wt%. Results and detection limits are reported in Appendix 4.IVb.

A4.1.7.4 Corrections for Spectral Interferences on REE in Silicates

In terms of these potential interferences of other elements with the REE in the silicates, the argide $^{40}Ar^{40}Ar^{85}Rb$ would interfere with ^{165}Ho and $^{40}Ar^{132}Ba$ would interfere with ^{172}Yb. This would be due to small amounts of Rb and Ba that is often found in plagioclase. It is possible that there may be small amounts of interference from $^{40}Ar^{40}Ar\,^{59}Co$ and $^{40}Ar^{40}Ar^{60}Ni$ on ^{139}La and ^{140}Ce, respectively, in olivine and pyroxene. All other elements that could potentially cause interferences with the REE are not determined to occur in plagioclase, olivine, biotite, pyroxene, hornblende, and chlorite and therefore are not considered.

A4.1.8 Lead isotope data

The lead isotope data were collected by M. Poujol at the Inco Innovation Centre on the Memorial University of Newfoundland campus using a Finnigan Neptune multicollector ICP-MS. Two galena grains were analyzed and reported in Table 4.11 from 125-180μm separates of sample MH-028a (galena 1 and 2). The galena grains were

fully dissolved in a mixture of HF + HNO_3 + HCl in a Teflon beaker on a hot plate at 130°C overnight. The samples were then allowed to dry in an open beaker and collected with a drop of 8N HNO_3, placed in an ultrasonic bath, and diluted to 200ppb Pb with double distilled water.

Galena samples were run on the Neptune using 5 blocks of 15 cycles each (1 integration of 16.77 seconds per cycle). First a blank was measured. The SRM 981 Pb standard was measured before and after the samples. The samples were first corrected for the blank contribution. Then, the samples were normalized (for the mass bias and drift) using the standards measured before and after the samples by averaging the two standards before normalization. The same standard SRM 981 was measured as a sample for quality control. Published values for SRM 981 used are from Todt *et al.* (1996): $^{206}Pb/^{204}Pb$ = 16.9356; $^{207}Pb/^{204}Pb$ = 15.4891; $^{208}Pb/^{204}Pb$ = 36.7006. Sample MH-028a (galena 3) and galena from the massive Ovoid (galena 4) were also analyzed for lead isotope data using an IsoProbe multi-collector ICP-MS at the GEOTOP Laboratory, Université du Québec á Montréal. The galena grains were leached with 6N HCl for several days. Following this, a small aliquot of the solution was diluted with ~0.6ml of a 2% HNO_3 solution spiked with the NBS 997 Tl standard. The Pb and Tl isotopes as well as the ^{202}Hg ion signal were measured in the multi-collector using 7 Faraday collectors. The $^{205}Tl/^{203}Tl$ ratio was measured to correct for instrumental mass bias. Prior to sample introduction, collector baselines were measured with the line of sight valve closed for 50 seconds followed by an "on-peak-zero" baseline measurement (i.e., gas and acid blank) for 50 seconds. Upon sample introduction, data acquisition consisted of 2 half-mass unit baseline

measurements and one block of 50 scans (10 seconds integration each) for isotope ratio analysis. Standards used were the NBS 981 Pb standard spiked with the NBS 997 Tl standard.

APPENDIX 4.II Major and trace element concentrations in whole rock by XRF, solution ICP-MS, and NiS fire assay.

Sample No.				MH-021	MH-022a	MH-023	MH-024	MH-025	MH-026	MH-027a	MH-028a	MH-028b	MH-029	MH-030	MH-031	MH-032	MH-033	MH-034	MH-035	MH-036	MH-037	MH-038	MH-039	MH-040	MH-041a	MH-042
Rock				VTT	VTT	HGD	TBX	TBX	TBX	ENGN	IHGD	IHGD	OHGD	OHGD	TBX	OHGD	IHGD	IHGD	IHGD	IHGD	IHGD	IHGD	IHGD	OHGD	OHGD	OHGD
Element	Method	Unit	Detection																							
Fe_2O_3T	XRF	wt%	0.01	12.88	18.65	28.02	19.83	17.41	18.75	31.89	9.73	13.88	12.90	14.87	13.98	38.68	13.25	9.60	11.45	10.40	11.81	8.43	13.14	10.97	9.95	13.30
FeOT	XRF	wt%	0.01	11.59	16.78	25.21	17.85	15.66	16.87	28.70	8.76	12.49	11.61	13.38	12.58	34.81	11.93	8.64	10.30	9.36	10.63	7.59	11.82	9.87	8.95	11.97
Ni	XRF	ppm	6.0	3125.87	7032.59	13628.81	4766.06	5797.55	5468.52	24731.15	1272.00	451.00	130.92	99.76	2962.48	37635.95	1473.80	2521.85	926.00	475.00	1153.33	473.05	164.94	78.17	121.34	58.75
Co	ICP-MS	ppm	3.50	172.02	283.23	519.29	279.55	294.75	276.62	917.44			86.02	74.33	173.22	1181.45	153.55	144.47			93.83	101.62	97.03	110.23	88.51	99.02
Cu	XRF	ppm	5.0	1304.17	1671.68	5367.79	21566.81	3330.49	4117.13	6455.72	15042.00	2915.00	278.65	264.79	1782.76	2129.35	3325.54	9314.56	12307.00	6090.00	10792.08	6146.04	1648.53	15.08	54.55	98.12
S	XRF	ppm	29.0	21827.53	51439.43	101763.23	65001.84	47639.28	51739.06	164904.46	15675.00	5153.00	2923.53	1815.83	26334.06	185200.45	18418.28	27214.27	18492.00	10338.00	17005.83	12280.58	3792.77	121.29	325.76	1186.69
SiO_2	XRF	wt%	0.01	37.69	35.74	28.79	32.76	35.30	32.64	21.70	40.07	44.70	41.24	39.85	36.13	16.60	42.52	41.14	41.60	42.21	39.22	41.56	43.04	40.42	41.69	41.62
TiO_2	XRF	wt%		1.84	1.55	1.15	1.21	1.11	1.81	0.63	1.08	4.11	3.08	3.69	2.12	1.20	2.21	1.44	1.64	1.36	3.35	1.28	3.19	3.83	1.47	3.36
Al_2O_3	XRF	wt%	0.02	17.60	14.88	9.23	13.00	15.66	15.81	6.89	16.50	15.17	14.91	13.01	17.76	4.86	15.57	17.20	15.01	15.64	13.93	18.15	14.62	15.26	15.57	14.10
MnO	XRF	wt%		0.09	0.11	0.14	0.12	0.10	0.10	0.06	0.09	0.17	0.15	0.17	0.11	0.06	0.11	0.06	0.10	0.10	0.10	0.08	0.14	0.12	0.11	0.15
MgO	XRF	wt%	0.01	5.68	5.86	6.86	6.65	6.00	4.76	1.76	8.23	6.56	6.65	7.63	6.06	2.67	6.01	3.27	9.33	9.70	9.51	6.07	7.26	9.20	10.43	7.24
CaO	XRF	wt%		7.33	7.29	6.44	7.09	7.71	7.24	2.86	7.59	7.78	7.63	7.96	7.01	2.73	7.95	7.26	7.15	7.21	6.53	8.51	7.78	6.87	7.68	7.84
Na_2O	XRF	wt%	0.01	2.84	2.64	1.47	1.83	2.37	2.25	1.54	2.67	3.46	3.16	2.70	2.60	0.87	3.20	3.48	2.64	2.60	2.37	3.08	3.04	2.84	2.85	3.00
P_2O_5	XRF	wt%		0.31	0.42	0.16	0.32	0.37	0.37	0.24	0.36	1.18	1.08	1.42	0.67	0.29	0.75	0.51	0.49	0.43	0.39	0.43	0.98	0.35	0.47	1.01
K_2O	XRF	wt%		0.62	0.59	0.42	0.52	0.62	0.57	1.20	0.59	0.93	1.13	1.69	0.86	0.28	0.68	0.81	0.51	0.69	0.73	0.75	1.08	0.79	0.71	0.78
Cl	XRF	ppm	44	93.40	180.53	1344.86	440.74	329.64	250.03	582.89	361.00	333.00	164.43	1016.97	841.86	392.75	933.20	631.38	813.00	761.00	821.72	855.60	1638.95	1160.48	1101.02	1807.39
Sc	XRF	ppm	`12	<det	<det	<det	12.26	<det	16.15	<det	12.62	22.40	19.72	20.34	15.43	<det	23.67	15.39	<det	14.00	16.76	6.18	23.49	<det	15.13	21.59
V	XRF	ppm	7.5	135.05	58.57	88.19	54.13	86.35	156.43	54.94	48.23	158.27	128.81	141.72	180.21	78.91	100.63	60.65	66.00	64.00	119.17	53.72	133.89	126.03	65.88	130.99
Cr	XRF	ppm	8.5	205.70	52.52	307.80	63.84	169.79	203.38	87.61	44.69	69.19	56.07	62.02	252.38	105.11	44.13	17.67	113.00	48.00	108.58	29.35	59.79	69.53	195.12	66.09
Zn	XRF	ppm	2.2	62.64	42.38	59.22	84.10	43.97	72.24	51.64	50.98	57.04	55.41	72.59	99.98	28.84	46.75	94.79	74.00	55.00	67.01	50.45	67.81	44.58	42.52	67.20
Ga	XRF	ppm	4.5	25.80	19.57	9.57	10.52	21.45	23.18	13.14	68.32	24.25	21.96	21.78	31.84	10.18	27.60	51.39	35.00	31.00	49.74	33.19	24.29	15.71	16.36	20.98
As	XRF	ppm	21	<det	<det	<det	<det	<det	<det	<det	<det	<det	<det	<det	<det	<det	<det	<det	<det	<det	13.07	7.60	0.23	0.37	0.51	<det
Rb	XRF	ppm	1.5	6.53	6.31	10.67	8.59	7.69	6.56	40.09	7.79	12.40	10.15	30.31	14.99	10.19	18.29	24.71	11.80	14.10	16.45	18.36	28.14	14.25	12.46	10.89
Sr	XRF	ppm	2	540.74	524.27	251.84	550.57	579.23	535.36	553.96	696.64	491.55	535.71	503.76	491.98	203.33	660.86	854.74	621.00	626.10	571.86	832.99	496.58	571.51	665.44	513.72
Y	XRF	ppm	1.1	9.04	13.10	5.75	9.42	10.66	12.21	7.60	5.72	30.87	26.63	27.82	16.94	8.49	19.31	15.24	11.90	10.00	7.94	9.71	25.39	7.05	9.81	27.02
Zr	XRF	ppm	2	77.09	103.21	37.60	74.19	78.02	95.51	118.57	51.33	237.67	197.92	236.97	150.86	62.39	132.01	131.63	90.60	75.50	72.72	71.01	193.86	66.31	74.58	190.18
Nb	XRF	ppm	1.2	5.16	6.96	3.59	5.05	4.38	6.59	7.24	1.56	16.16	13.22	16.40	10.35	6.18	8.50	6.89	5.20	4.80	4.78	3.36	12.19	6.01	4.81	13.66
Ba	XRF	ppm	30	347.06	289.16	61.07	190.11	318.83	244.19	327.71	278.85	502.50	623.55	673.44	448.09	77.29	287.94	340.36	232.00	386.00	306.61	362.89	493.66	320.27	348.53	439.05
Ce	XRF	ppm	47.5	<det	<det	<det	<det	<det	60.17	<det	390.43	152.27	103.21	110.80	61.67	<det	106.33	269.23	221.00	178.00	201.55	170.33	107.12	<det	62.37	105.93
Pb	XRF	ppm	6.5	46.90	78.87	33.43	50.56	46.87	39.32	43.54	13444.97	1251.22	24.18	281.25	43.59	268.58	1721.62	7533.44	5109.00	3524.00	7599.17	4355.39	874.02	49.47	79.78	34.72
Th	XRF	ppm	5	<det	<det	<det	<det	<det	<det	<det	61.24	6.87	<det	<det	<det	<det	12.78	59.74	30.00	22.00	51.25	32.70	<det	<det	<det	<det
U	XRF	ppm	6	<det	<det	<det	<det	<det	<det	<det			<det	<det	<det	<det	<det	<det			<det	<det	<det	<det	<det	<det
Se	ICP-MS	ppm	1.00	4.19	6.33	17.45	8.49	5.00	4.32	16.75			<det	<det	<det	<det	2.12	14.21			5.36	41.96	10.53	10.07	3.99	7.07
Ag	ICP-MS	ppm	0.10	1.25	1.11	3.21	12.37	1.76	2.00	2.75			0.78	2.82	1.26	4.43	18.11	35.49			55.22	34.36	20.89	0.50	0.88	0.53
Cd	ICP-MS	ppm	0.10	0.83	0.81	2.60	6.69	1.13	1.33	1.11			0.35	1.27	0.41	1.41	6.46	33.62			38.08	23.60	5.74	0.87	0.85	0.63
Sn	ICP-MS	ppm	0.10	1.77	4.89	3.82	2.97	1.78	1.68	0.79			1.59	9.32	1.00	10.30	78.91	81.98			141.66	87.06	15.94	11.92	9.08	7.71
Sb	ICP-MS	ppm	0.10	<det	<det	<det	<det	<det	<det	<det			<det	<det	<det	<det	<det	0.14			0.44	0.42	0.13	0.19	0.13	0.14
Te	ICP-MS	ppm	1.00	<det	4.49	1.32	<det	<det	<det	<det			<det	<det	<det	6.81	14.71	46.86			47.58	138.68	18.32	2.75	1.18	3.24
Bi	ICP-MS	ppm	0.01	0.35	0.58	0.72	0.33	0.38	0.49	1.03			0.09	0.69	0.38	4.99	29.51	131.91			114.15	93.61	15.21	0.33	0.47	0.34
Li	ICP-MS	ppm	0.39	7.24	6.62	7.48	9.52	7.95	6.47	9.68			15.32	11.88	15.66	5.53	9.22	7.43			20.14	15.88	13.38	18.22	16.65	21.09
Rb	ICP-MS	ppm	0.10	6.63	6.35	10.05	7.32	6.83	5.88	35.35			9.22	27.37	14.72	7.08	20.07	22.35			16.81	18.26	25.96	15.85	12.82	10.51
Sr	ICP-MS	ppm	0.31	539.80	474.99	221.16	502.34	526.88	454.73	431.16			481.32	456.78	439.07	137.19	706.30	762.74			505.49	771.27	447.33	605.03	622.09	452.29
Y	ICP-MS	ppm	0.01	8.51	12.56	5.66	8.73	10.50	10.79	6.73			24.58	24.93	16.90	6.76	21.83	15.28			8.45	9.32	22.37	8.16	10.27	23.41
Zr	ICP-MS	ppm	0.28	25.49	30.55	35.86	36.14	32.04	24.73	31.23			60.38	48.92	31.78	12.62	49.09	42.32			40.02	43.43	41.61	53.78	54.71	49.54
Nb	ICP-MS	ppm	0.02	6.74	7.29	3.09	4.51	4.99	7.73	6.32			14.30	16.68	12.80	5.44	11.04	9.77			7.50	5.28	13.03	6.62	5.77	14.77
Mo	ICP-MS	ppm	0.19	0.60	1.03	1.51	0.64	0.99	1.03	3.04			1.39	2.13	0.92	3.36	1.55	1.61			1.21	1.84	1.74	1.27	0.69	1.62
Cs	ICP-MS	ppm	0.04	0.08	0.09	0.31	0.09	0.11	0.08	0.36			0.12	0.30	0.31	0.11	0.08	0.08			0.26	0.24	0.47	0.49	0.26	0.27
Ba	ICP-MS	ppm	0.38	349.15	346.62	172.02	250.61	371.82	301.04	536.36			604.71	636.22	437.09	143.90	393.79	417.06			369.67	417.70	497.59	423.90	416.07	519.25
La	ICP-MS	ppm	0.07	11.06	12.05	4.84	8.87	10.58	11.01	16.94			24.25	28.94	21.83	8.12	19.40	20.27			11.35	11.75	23.48	9.05	10.85	23.37
Ce	ICP-MS	ppm	0.02	23.90	28.84	11.01	20.57	24.99	25.63	35.28			59.26	71.10	50.88	19.27	46.78	45.71			25.47	26.67	55.37	21.87	26.66	58.75
Pr	ICP-MS	ppm	0.06	3.18	3.97	1.59	2.79	3.38	3.60	4.28			8.26	9.91	6.73	2.55	6.46	5.92			3.38	3.66	7.57	2.80	3.52	7.98
Nd	ICP-MS	ppm	0.08	13.56	17.34	6.77	12.71	14.87	15.90	16.59			35.86	43.58	28.42	10.69	28.43	24.99			14.42	16.10	33.17	12.60	15.61	35.33
Sm	ICP-MS	ppm	0.05	2.67	3.63	1.51	2.53	3.14	3.35	2.81			7.76	8.85	5.89	2.14	5.94	4.97			2.84	3.25	7.00	2.54	3.22	7.52
Eu	ICP-MS	ppm	0.02	1.16	1.46	0.70	1.09	1.34	1.31	0.85			2.63	2.84	1.84	0.62	2.06	1.92			1.32	1.51	2.28	1.33	1.45	2.46
Gd	ICP-MS	ppm	0.03	2.26	3.21	1.37	2.15	2.65	2.80	1.96			6.68	7.52	4.73	1.64	5.04	4.17			2.46	2.76	6.24	2.02	2.62	6.34
Tb	ICP-MS	ppm	0.01	0.32	0.44	0.19	0.34	0.39	0.41	0.25			0.93	1.03	0.67	0.24	0.72	0.59			0.34	0.39	0.88	0.31	0.39	0.98
Dy	ICP-MS	ppm	0.03	2.00	2.86	1.22	1.99	2.35	2.64	1.57			5.58	6.06	4.13	1.54	4.17	3.58			2.02	2.31	5.19	1.77	2.31	5.58
Ho	ICP-MS	ppm	0.01	0.35	0.52	0.22	0.35	0.43	0.46	0.28			1.00	1.05	0.69	0.26	0.72	0.64			0.36	0.41	0.93	0.32	0.40	1.02
Er	ICP-MS	ppm	0.03	0.90	1.46	0.63	0.94	1.15	1.23	0.74			2.68	2.73	1.84	0.72	1.94	1.75			0.93	1.06	2.53	0.82	1.09	2.69
Tm	ICP-MS	ppm	0.04	0.11	0.20	0.13	0.11	0.17	0.19	0.09			0.37	0.38	0.23	0.12	0.27	0.26			0.12	0.16	0.33	0.10	0.16	0.36
Yb	ICP-MS	ppm	0.03	0.72	1.11	0.52	0.81	0.87	0.97	0.63			2.12	2.08	1.38	0.56	1.55	1.38			0.77	0.85	1.91	0.66	0.81	2.18
Lu	ICP-MS	ppm	0.02	0.10	0.16	0.07	0.11	0.12	0.12	0.09			0.29	0.28	0.19	0.07	0.21	0.19			0.11	0.11	0.27	0.08	0.11	0.27
Pt	NiS fire assay	ppb	0.05	14.89	6.91	8.94	4.35	3.22	39.31	29.08	3430.00	272.00	3.81	10.93	7.64	188.42	1980.00	364.44			3330.00	1980.00	516.47	1.03	0.28	0.56
Pd	NiS fire assay	ppb	0.05	48.05	77.74	71.16	37.88	50.01	52.92	79.71	2150.00	231.00	6.61	14.07	41.64	393.44	610.36	70.40			1850.00	870.41	620.04	0.84	0.46	1.38
Rh	NiS fire assay	ppb	0.05	0.90	2.31	3.89	1.33	1.43	1.80	11.15	0.62	<det	<det	<det	0.71	11.70	0.13	<det			<det	<det	<det	<det	<det	<det
Ru	NiS fire assay	ppb	0.05	0.73	2.28	1.06	3.05	2.09	1.08	18.32	<det	<det	<det	<det	0.09	14.82	0.95	<det			4.75	2.09	2.07	<det	<det	<det
Ir	NiS fire assay	ppb	0.05	0.34	1.01	0.78	0.92	0.78	0.70	5.98	<det	<det	0.12	<det	0.27	4.80	<det	<det			0.06	0.07	<det	<det	<det	<det
Au	NiS fire assay	ppb	0.05	32.04	34.55	37.54	102.45	83.88	53.19	13.03	12900.00	281.00	16.78	17.09	18.01	365.02	1700.00	479.24			6070.00	3250.00	1140.00	3.83	5.85	7.34

<det = below detection

VTT = variable textured troctolite, HGD = hornblende gabbro dyke, TBX = troctolite breccia, ENGN = enderbitic gneiss, IHGD = inner hornblende gabbro dyke, OHGD = outer hornblende gabbro dyke

APPENDIX 4.IIIa. Compositions of sulfide minerals, PGM, Ag- and Bi-tellurides, electrum, and native Ag determined by electron probe miroanalysis (EPMA).

Label	S	Pb	Fe	Cu	Zn	Ni	Co	As	Se	Ag	Sb	Te	Pt	Au	Pd	Cd	Bi	Sn	Totals	Mineral
Unit	wt%	wt%	wt%	wt%	wt%	wt%	wt%	wt%	wt%	wt%	wt%	wt%	wt%	wt%	wt%	wt%	wt%	wt%	wt%	
Detection Limit	0.10	0.10	0.10	0.10	0.10	0.10	0.10	0.10	0.10	0.10	0.10	0.10	0.10	0.10	0.10	0.10	0.10	0.10		
SULFIDE MINERALS																				
MH-009-14Po-a	39.42	<det	60.03	<det	<det	0.37	na	<det	<det	na	<det	<det	na	na	na	<det	<det	<det	99.8	Pyrrhotite
MH-033-1-7Po-a	39.34	<det	60.05	<det	<det	0.53	na	<det	<det	na	<det	<det	na	na	na	<det	<det	<det	99.9	Pyrrhotite
MH-009-16Po-c	38.86	<det	60.65	<det	<det	0.36	na	<det	<det	na	<det	<det	na	na	na	<det	<det	<det	99.9	Pyrrhotite
MH-009-18Po-a	39.03	<det	60.20	<det	<det	0.71	na	<det	<det	na	<det	<det	na	na	na	<det	<det	<det	99.9	Pyrrhotite
MH-009-36Po-a	39.53	<det	59.93	<det	<det	0.60	na	<det	<det	na	<det	<det	na	na	na	<det	<det	<det	100.1	Pyrrhotite
MH-009-22Po-a	39.01	<det	60.34	<det	<det	0.68	na	<det	<det	na	<det	<det	na	na	na	<det	<det	<det	100.0	Pyrrhotite
MH-009-24Po-a	39.00	<det	60.43	<det	<det	0.79	na	<det	<det	na	<det	<det	na	na	na	<det	<det	<det	100.2	Pyrrhotite
MH-009-8Po-f	38.72	<det	61.12	<det	<det	0.33	na	<det	<det	na	<det	<det	na	na	na	<det	<det	<det	100.2	Pyrrhotite
MH-034-1-4Po-a	39.49	<det	60.06	<det	na	0.74	na	<det	<det	na	<det	<det	na	na	na	na	<det	<det	100.3	Pyrrhotite
MH-034-1-4Po-a	39.49	<det	60.06	<det	na	0.74	na	<det	<det	na	<det	<det	na	na	na	na	<det	<det	100.3	Pyrrhotite
MH-034-1-10Po-c	39.44	<det	60.04	<det	na	0.89	na	<det	<det	na	<det	<det	na	na	na	na	<det	<det	100.4	Pyrrhotite
MH-034-1-5Po-b	39.47	<det	60.16	<det	na	0.72	na	<det	<det	na	<det	<det	na	na	na	na	<det	<det	100.4	Pyrrhotite
MH-009-25Po-b	39.12	<det	60.52	<det	<det	0.73	na	<det	<det	na	<det	<det	na	na	na	<det	<det	<det	100.4	Pyrrhotite
MH-033-2-9Po-b	39.52	<det	60.13	<det	<det	0.76	na	<det	<det	na	<det	<det	na	na	na	<det	<det	<det	100.4	Pyrrhotite
MH-034-1-7Po-b	39.57	<det	60.21	<det	na	0.82	na	<det	<det	na	<det	<det	na	na	na	na	<det	<det	100.6	Pyrrhotite
MH-034-1-8Po-b	39.76	<det	60.31	<det	na	0.68	na	<det	<det	na	<det	<det	na	na	na	na	<det	<det	100.8	Pyrrhotite
MH-034-2-11Po-b	40.03	<det	59.88	<det	na	0.86	na	<det	<det	na	<det	<det	na	na	na	na	<det	<det	100.8	Pyrrhotite
MH-009-26Po-a	39.69	<det	60.51	<det	<det	0.55	na	<det	<det	na	<det	<det	na	na	na	<det	<det	<det	100.8	Pyrrhotite
MH-034-1-9Po-a	39.60	<det	60.34	<det	na	0.88	na	<det	<det	na	<det	<det	na	na	na	na	<det	<det	100.8	Pyrrhotite
MH-034-1-6Po-a	39.63	<det	60.55	<det	na	0.81	na	<det	<det	na	<det	<det	na	na	na	na	<det	<det	101.0	Pyrrhotite
MH-033-2-12Po-b	40.00	<det	60.53	<det	<det	0.68	na	<det	<det	na	<det	<det	na	na	na	<det	<det	<det	101.2	Pyrrhotite
MH-034-1-4Pn-c	32.66	<det	29.97	<det	na	35.87	na	<det	<det	na	<det	<det	na	na	na	na	<det	<det	98.5	Pentlandite
MH-034-1-4Pn-c	32.66	<det	29.97	<det	na	35.87	na	<det	<det	na	<det	<det	na	na	na	na	<det	<det	98.5	Pentlandite
MH-034-1-6Pn-b	32.91	<det	29.75	<det	na	36.01	na	<det	<det	na	<det	<det	na	na	na	na	<det	<det	98.7	Pentlandite
MH-034-2-11Pn-c	33.23	<det	29.65	<det	na	36.08	na	<det	<det	na	<det	<det	na	na	na	na	<det	<det	99.0	Pentlandite
MH-034-1-10Pn-d	32.87	<det	29.57	<det	na	36.51	na	<det	<det	na	<det	<det	na	na	na	na	<det	<det	99.0	Pentlandite
35/36 45-125 (CM) #CCP-R7	35.15	na	30.47	32.76	<det	<det	<det	na	na	na	na	na	na	na	na	na	na	na	98.4	Chalcopyrite
28a <45 #228CCP-c	34.69	na	29.68	34.08	<det	<det	<det	na	na	na	na	na	na	na	na	na	na	na	98.5	Chalcopyrite
MH-0028-1-4CCP	32.12	0.68	29.24	33.95	na	na	na	<det	<det	na	0.25	<det	na	na	na	na	1.03	na	97.3	Chalcopyrite
35/36 45-125 (CM) #23PN-b	34.89	na	30.86	33.00	<det	<det	<det	na	na	na	na	na	na	na	na	na	na	na	98.7	Chalcopyrite
35/36 45-125 (CM) #53SP-a	34.24	na	28.96	32.81	na	<det	<det	<det	<det	na	<det	<det	na	na	na	<det	<det	<det	96.0	Chalcopyrite
MH-034-2-2Ccp-b	34.66	<det	30.52	33.73	na	<det	na	<det	<det	na	<det	<det	na	na	na	na	<det	<det	98.9	Chalcopyrite
35/36 45-125 (CM) #CCP-R1	35.16	na	30.81	33.11	<det	<det	<det	na	na	na	na	na	na	na	na	na	na	na	99.1	Chalcopyrite
MH-009-36Ccp-b	34.52	<det	30.59	33.74	<det	<det	na	<det	<det	na	<det	<det	na	na	na	<det	<det	<det	98.9	Chalcopyrite
28a <45 #CCP-R8	34.71	na	30.04	34.25	<det	<det	<det	na	na	na	na	na	na	na	na	na	na	na	99.0	Chalcopyrite
28a 45-75 #56CCP-f	35.08	na	30.13	33.87	<det	<det	<det	na	na	na	na	na	na	na	na	na	na	na	99.1	Chalcopyrite
MH-0028-1-15CCP	31.91	0.75	29.74	33.74	na	na	na	<det	<det	na	0.32	0.28	na	na	na	na	1.21	na	98.0	Chalcopyrite
MH-009-26Ccp-b	34.41	<det	30.70	33.92	<det	<det	na	<det	<det	na	<det	<det	na	na	na	<det	<det	<det	99.0	Chalcopyrite
MH-009-22Ccp-b	34.75	<det	30.44	34.03	<det	<det	na	<det	<det	na	<det	<det	na	na	na	<det	<det	<det	99.2	Chalcopyrite
MH-0028-1-33CCP	32.13	0.85	29.53	33.21	na	na	na	<det	<det	na	0.59	<det	na	na	na	na	1.50	na	97.8	Chalcopyrite
28a 45-75 #56CCP-g	34.96	na	30.01	34.65	<det	<det	<det	na	na	na	na	na	na	na	na	na	na	na	99.6	Chalcopyrite
MH-034-2-2Ccp-a	34.86	<det	30.78	33.96	na	<det	na	<det	<det	na	<det	<det	na	na	na	na	<det	<det	99.6	Chalcopyrite
28a <45 #CCP-R9	35.02	na	30.54	34.16	<det	<det	<det	na	na	na	na	na	na	na	na	na	na	na	99.7	Chalcopyrite
28a <45 #131CCP-c	34.70	na	30.39	34.68	<det	<det	<det	na	na	na	na	na	na	na	na	na	na	na	99.8	Chalcopyrite
MH-034-1-3Ccp-d	34.71	<det	31.00	33.95	na	<det	na	<det	<det	na	<det	<det	na	na	na	na	<det	<det	99.7	Chalcopyrite
MH-034-1-3Ccp-d	34.71	<det	31.00	33.95	na	<det	na	<det	<det	na	<det	<det	na	na	na	na	<det	<det	99.7	Chalcopyrite
MH-034-1-3Ccp-c	34.84	<det	30.67	34.19	na	<det	na	<det	<det	na	<det	<det	na	na	na	na	<det	<det	99.7	Chalcopyrite
MH-034-1-3Ccp-c	34.84	<det	30.67	34.19	na	<det	na	<det	<det	na	<det	<det	na	na	na	na	<det	<det	99.7	Chalcopyrite

28a 45-75 #67CCP-d	34.90	na	30.65	34.44	<det	<det	<det	na	na	na	na	na	na	na	na	na	na	na	100.0	Chalcopyrite
MH-034-1-4Ccp-b	34.66	<det	30.84	34.40	na	<det	na	<det	<det	na	<det	<det	na	na	na	na	<det	<det	99.9	Chalcopyrite
MH-034-1-4Ccp-b	34.66	<det	30.84	34.40	na	<det	na	<det	<det	na	<det	<det	na	na	na	na	<det	<det	99.9	Chalcopyrite
MH-034-2-11Ccp-a	34.75	<det	31.05	34.34	na	<det	na	<det	<det	na	<det	<det	na	na	na	na	<det	<det	100.1	Chalcopyrite
35/36 45-125 3T RCcp9	35.64	na	30.39	34.15	<det	<det	<det	na	na	na	na	na	na	na	na	na	na	na	100.2	Chalcopyrite
MH-0028-1-20CCP	32.76	0.81	29.66	34.02	na	na	na	<det	<det	na	0.13	<det	na	na	na	na	1.32	na	98.7	Chalcopyrite
MH-034-1-10Ccp-e	34.76	<det	30.98	34.45	na	<det	na	<det	<det	na	<det	<det	na	na	na	na	<det	<det	100.2	Chalcopyrite
MH-009-25Ccp-a	35.17	<det	30.94	34.21	<det	<det	na	<det	<det	na	<det	<det	na	na	na	<det	<det	<det	100.3	Chalcopyrite
MH-034-1-7Ccp-a	34.74	<det	31.10	34.53	na	<det	na	<det	<det	na	<det	<det	na	na	na	na	<det	<det	100.4	Chalcopyrite
MH-033-2-5Po-c	35.07	<det	31.16	34.18	<det	<det	na	<det	<det	na	<det	<det	na	na	na	<det	<det	<det	100.4	Chalcopyrite
MH-034-1-8Ccp-a	35.12	<det	30.78	34.55	na	<det	na	<det	<det	na	<det	<det	na	na	na	na	<det	<det	100.5	Chalcopyrite
MH-034-1-9Ccp-b	35.02	<det	30.98	34.50	na	<det	na	<det	<det	na	<det	<det	na	na	na	na	<det	<det	100.5	Chalcopyrite
MH-034-1-6Ccp-c	35.05	<det	31.00	34.40	na	<det	na	<det	<det	na	<det	<det	na	na	na	na	<det	<det	100.5	Chalcopyrite
MH-034-1-5Ccp-a	34.68	<det	31.08	34.59	na	<det	na	<det	<det	na	<det	<det	na	na	na	na	<det	<det	100.4	Chalcopyrite
35/36 45-125 3T RCcp7	35.67	na	30.71	34.26	<det	<det	<det	na	na	na	na	na	na	na	na	na	na	na	100.6	Chalcopyrite
MH-033-2-2Ccp-a	35.12	<det	30.73	34.64	<det	<det	na	<det	<det	na	<det	<det	na	na	na	<det	<det	<det	100.5	Chalcopyrite
MH-033-2-9Ccp-a	35.06	<det	30.86	34.53	<det	<det	na	<det	<det	na	<det	<det	na	na	na	<det	<det	<det	100.5	Chalcopyrite
MH-0028-1-12CCP	32.32	0.99	30.53	33.66	na	na	na	<det	<det	na	0.23	0.19	na	na	na	na	1.44	na	99.4	Chalcopyrite
28a 45-75 #56BN-e	26.07	na	11.70	61.24	<det	<det	<det	na	na	na	na	na	na	na	na	na	na	na	99.0	Bornite
28a 75-125 #BN-R11	26.13	na	11.76	61.18	<det	<det	<det	na	na	na	na	na	na	na	na	na	na	na	99.1	Bornite
28a 45-75 #56BN-d	25.90	na	11.53	61.86	<det	<det	<det	na	na	na	na	na	na	na	na	na	na	na	99.3	Bornite
MH-0028-1-28BN	23.74	0.84	11.19	61.49	na	na	na	<det	<det	na	0.50	0.27	na	na	na	na	1.18	na	99.2	Bornite
28a 75-125 #20GN-c	13.18	84.72	na	na	<det	na	<det	na	na	na	na	na	na	na	na	na	<det	0.62	na	98.5	Galena
28a <45 #126GN-b	13.17	85.23	na	na	<det	na	<det	na	na	na	na	na	na	na	na	na	<det	0.23	na	98.6	Galena
28A <45 #87 GN-R1	12.96	85.79	na	na	<det	na	<det	na	na	na	na	na	na	na	na	na	<det	<det	na	98.8	Galena
28a <45 #74GN-c	13.39	85.57	na	na	<det	na	<det	na	na	na	na	na	na	na	na	na	<det	0.21	na	99.2	Galena
28a <45 #150GN-b	13.31	86.27	na	na	<det	na	<det	na	na	na	na	na	na	na	na	na	<det	<det	na	99.6	Galena
MH-033-1-rGn-4	13.26	84.14	<det	<det	<det	<det	na	<det	0.45	na	<det	0.38	na	na	na	na	<det	1.30	<det	99.5	Galena
MH-034-1-5Gn-d	13.26	85.06	<det	<det	na	<det	na	<det	0.20	na	<det	0.11	na	na	na	na	na	0.91	<det	99.5	Galena
MH-009-RGn-1	13.26	85.49	<det	<det	<det	<det	na	<det	0.18	na	<det	0.25	na	na	na	na	<det	0.47	<det	99.7	Galena
MH-034-1-10Gn-a	13.58	84.27	<det	<det	na	<det	na	<det	0.22	na	<det	0.10	na	na	na	na	na	1.48	<det	99.7	Galena
28a 45-75 #56GN-c	13.24	87.07	na	na	<det	na	<det	na	na	na	na	na	na	na	na	na	<det	<det	na	100.3	Galena
28A <45 #87 GN-R2(+Cd,Zn)	13.40	86.49	na	na	<det	na	<det	na	na	na	na	na	na	na	na	na	<det	0.65	na	100.5	Galena
28a 45-75 #67GN-c	13.32	87.62	na	na	<det	na	<det	na	na	na	na	na	na	na	na	na	<det	<det	na	100.9	Galena
28a 45-75 #56GN-b	13.06	88.21	na	na	<det	na	<det	na	na	na	na	na	na	na	na	na	<det	<det	na	101.3	Galena
35/36 45-125 (CM) #PO-R3	53.96	na	42.96	<det	<det	<det	3.68	na	na	na	na	na	na	na	na	na	na	na	na	100.6	Pyrite
35/36 45-125 (CM) #PO-R4	53.92	na	46.78	<det	<det	<det	<det	na	na	na	na	na	na	na	na	na	na	na	na	100.7	Pyrite
35/36 45-125 (CM) #PO-R5	53.97	na	45.84	<det	<det	0.41	0.68	na	na	na	na	na	na	na	na	na	na	na	na	100.9	Pyrite
35/36 45-125 (CM) #PO-R8	53.95	na	46.29	<det	<det	0.81	<det	na	na	na	na	na	na	na	na	na	na	na	na	101.1	Pyrite
35/36 45-125 (CM) #PO-R2	54.14	na	44.30	<det	<det	0.13	2.58	na	na	na	na	na	na	na	na	na	na	na	na	101.2	Pyrite
35/35 <45 2T 15Ccp	54.64	na	46.52	<det	<det	<det	<det	na	na	na	na	na	na	na	na	na	na	na	na	101.2	Pyrite
35/36 45-125 (CM) #46HZ-b	36.05	na	1.30	<det	<det	59.11	2.86	na	na	na	na	na	na	na	na	na	na	na	na	99.3	Millerite
28a <45 #107CCP-f	32.73	na	3.24	<det	<det	63.33	0.23	na	na	na	na	na	na	na	na	na	na	na	na	99.5	Millerite
28a <45 #MK?-R4	35.19	na	0.80	<det	<det	61.99	1.88	na	na	na	na	na	na	na	na	na	na	na	na	99.9	Millerite
28a 75-125 #MIL-R15	33.45	na	22.04	<det	<det	42.09	1.18	na	na	na	na	na	na	na	na	na	na	na	na	98.8	Mackinawite
28a <45 #221PN-b	32.85	na	20.05	<det	<det	43.71	2.24	na	na	na	na	na	na	na	na	na	na	na	na	98.8	Mackinawite
28a 75-125 #MIL-R16	33.81	na	21.24	<det	<det	42.93	1.05	na	na	na	na	na	na	na	na	na	na	na	na	99.0	Mackinawite
28a <45 #PN-R3	32.84	na	21.57	<det	<det	43.90	1.02	na	na	na	na	na	na	na	na	na	na	na	na	99.3	Mackinawite
28a <45 #PN-R5	32.93	na	23.92	<det	<det	41.47	0.94	na	na	na	na	na	na	na	na	na	na	na	na	99.3	Mackinawite
28a 75-125 #MIL-R17	33.37	na	20.85	<det	<det	43.33	1.83	na	na	na	na	na	na	na	na	na	na	na	na	99.4	Mackinawite
28a <45 #PN-R7	33.39	na	21.40	<det	<det	43.25	1.65	na	na	na	na	na	na	na	na	na	na	na	na	99.7	Mackinawite
28a <45 #PN-R6	33.28	na	21.05	<det	<det	43.67	1.69	na	na	na	na	na	na	na	na	na	na	na	na	99.7	Mackinawite
28a 75-125 #6PN-R12	33.64	na	21.33	<det	<det	43.50	1.53	na	na	na	na	na	na	na	na	na	na	na	na	100.0	Mackinawite

28a 75-125 #2BISMAUCH-d	9.98	na	<det	<det	na	25.00	<det	<det	<det	na	0.18	<det	na	na	na	<det	59.37	<det	94.5	Parkerite
28a 75-125 #12BINI-R13-b	10.19	na	<det	<det	na	25.66	<det	<det	<det	na	0.53	<det	na	na	na	<det	59.52	<det	95.9	Parkerite
28a 75-125 #2BISMAUCH-e	10.10	na	<det	<det	na	25.64	<det	<det	<det	na	0.11	0.14	na	na	na	<det	60.12	<det	96.1	Parkerite
28a 75-125 #12BINI-R13	10.18	na	<det	<det	na	25.59	<det	<det	<det	na	0.35	<det	na	na	na	<det	60.62	<det	96.7	Parkerite
28a 75-125 #12STAN-d	29.55	na	10.11	39.15	na	<det	<det	<det	<det	na	<det	<det	na	na	na	<det	<det	17.27	96.1	Volfsonite?
28a 75-125 #12STAN-c	29.60	na	9.97	39.42	na	<det	<det	<det	<det	na	<det	<det	na	na	na	<det	<det	17.29	96.3	Volfsonite?
PLATINUM-GROUP MINERALS																				
28a 45-75 #24SP-d	0.08	na	0.16	<det	na	<det	<det	43.42	0.13	<det	0.76	<det	53.85	<det	<det	<det	<det	<det	98.4	Sperrylite
28a <45 #131SP-a	0.22	na	0.29	<det	na	<det	<det	43.60	0.14	<det	<det	<det	54.23	<det	<det	<det	<det	<det	98.5	Sperrylite
28a 75-125 #11SP-c	0.85	na	0.14	<det	na	<det	<det	43.29	0.13	<det	<det	0.11	53.28	<det	<det	<det	<det	1.37	99.2	Sperrylite
28a 75-125 #3SP-a	0.05	na	<det	<det	na	<det	<det	45.35	0.14	<det	<det	<det	53.85	<det	<det	<det	<det	<det	99.4	Sperrylite
MH-0028-1-14PTb**	0.00	0.95	1.89	3.41	na	na	na	44.71	3.64	0.44	0.45	0.18	42.33	0.49	0.21	na	<det	na	98.7	Sperrylite
MH35-36 [45]_#1	0.21	na	1.46	0.46	na	na	na	43.08	na	na	0.39	1.45	48.24	na	na	na	4.43	na	99.7	Sperrylite
MH35-36 [45]_#11c	0.16	na	0.34	0.37	na	na	na	40.59	na	na	1.36	<det	54.50	na	na	na	2.64	na	99.9	Sperrylite
MH35-36 [45]_#16	1.29	na	0.40	0.34	na	na	na	40.14	na	na	<det	<det	54.58	na	na	na	3.30	na	100.0	Sperrylite
MH35-36 [45]_#15c	0.19	na	0.54	0.86	na	na	na	41.30	na	na	0.96	2.07	51.54	na	na	na	2.88	na	100.3	Sperrylite
MH35-36 [45]_#27	0.29	na	0.24	0.40	na	na	na	42.86	na	na	<det	<det	53.43	na	na	na	3.06	na	100.3	Sperrylite
MH35-36 [45]_#4b	0.36	na	0.70	0.26	na	na	na	43.76	na	na	<det	<det	52.53	na	na	na	2.99	na	100.6	Sperrylite
MH35-36 [45]_#11	0.38	na	0.49	0.50	na	na	na	40.46	na	na	2.42	<det	53.13	na	na	na	3.40	na	100.8	Sperrylite
28a 75-125 #2SP-a	1.40	na	0.21	<det	na	<det	<det	40.37	0.13	<det	<det	<det	55.65	0.19	<det	<det	<det	3.12	101.1	Sperrylite
28a <45 #78AT-a	0.03	na	0.31	<det	na	<det	<det	<det	<det	<det	<det	<det	0.18	<det	65.19	<det	<det	32.68	98.4	Paolovite
28a <45 #235STIB-d	0.00	na	0.18	0.14	na	<det	<det	<det	<det	<det	<det	<det	<det	<det	65.40	<det	0.18	32.74	98.6	Paolovite
28a 45-75 #38AT-a	0.02	na	0.12	<det	na	<det	<det	<det	<det	<det	<det	<det	1.98	<det	64.56	<det	0.21	31.83	98.7	Paolovite
28a 45-75 #1AT-a	0.01	na	<det	<det	na	<det	<det	<det	<det	<det	<det	<det	0.46	<det	64.64	<det	<det	34.18	99.3	Paolovite
28a 75-125 #12AT-b	0.03	na	0.39	0.86	na	<det	<det	<det	<det	<det	<det	<det	0.62	<det	64.56	<det	<det	33.03	99.5	Paolovite
28a <45 #78AT-b	0.00	na	0.32	<det	na	<det	<det	<det	<det	<det	<det	<det	0.26	<det	65.26	<det	<det	33.88	99.7	Paolovite
28a 75-125 #20FRO-a	0.31	na	<det	<det	na	<det	<det	<det	<det	1.45	<det	<det	1.31	<det	21.67	<det	73.44	<det	98.2	Froodite
28a <45 #233FRO-a	0.00	na	0.33	<det	na	<det	<det	<det	<det	<det	<det	0.56	1.78	<det	21.78	<det	75.26	<det	99.7	Froodite
28a <45 #233FRO-b	0.03	na	0.33	<det	na	<det	0.10	<det	<det	<det	<det	0.46	1.91	<det	21.67	0.11	75.26	<det	99.9	Froodite
28a 45-75 #11FRO-b	0.04	na	<det	<det	na	<det	<det	<det	<det	<det	<det	<det	1.95	<det	21.70	<det	77.48	<det	101.2	Froodite
35/36 45-125 (CM) #68MI-a	0.03	na	0.29	<det	na	<det	<det	<det	<det	<det	8.81	9.36	0.66	<det	38.06	<det	41.78	<det	99.0	Pd-Bi-Sb-Te
28a <45 MI-a	0.00	na	0.20	2.09	na	<det	<det	<det	<det	<det	7.77	6.61	1.28	<det	32.47	<det	48.34	0.48	99.2	Pd-Bi-Sb-Te
28a <45 #38MI-a	0.01	na	0.23	2.12	na	<det	<det	<det	<det	<det	7.58	6.80	1.12	<det	32.19	<det	48.98	0.45	99.5	Pd-Bi-Sb-Te
28a 45-75 #49UK-b	0.04	na	0.25	<det	na	<det	0.12	<det	<det	<det	17.40	0.68	0.85	<det	39.75	<det	40.44	0.28	99.8	Pd-Bi-Sb-Te
MH35-36_#67cMI	0.68	na	0.61	0.38	na	na	na	na	na	na	14.72	13.77	0.68	na	37.10	na	32.51	na	100.4	Pd-Bi-Sb-Te
28a <45 #228UK-a	0.02	na	0.28	<det	na	<det	<det	<det	<det	<det	8.89	6.45	1.22	<det	38.96	<det	44.75	0.17	100.7	Pd-Bi-Sb-Te
28a 75-125 #20UK-b	0.26	na	0.11	<det	na	<det	<det	<det	<det	2.70	14.66	1.42	0.87	<det	38.17	<det	42.40	0.34	100.9	Pd-Bi-Sb-Te
MH35-36_#67MI	1.38	na	0.58	0.36	na	na	na	na	na	na	10.31	22.70	0.74	na	36.19	na	28.96	na	101.2	Pd-Bi-Sb-Te
28a <45 #228UK-b	0.02	na	0.28	<det	na	<det	<det	<det	<det	<det	9.08	6.36	1.09	<det	38.98	<det	45.14	0.22	101.2	Pd-Bi-Sb-Te
28a 45-75 #56UK-j	0.02	na	0.40	<det	na	0.12	<det	<det	<det	3.26	38.98	0.17	0.16	<det	44.29	<det	12.80	0.76	101.0	Pd-Bi-Sb-Te
28a <45 #235STIB-a	0.01	na	0.23	0.12	na	<det	0.10	<det	<det	<det	10.43	<det	<det	<det	66.27	<det	0.15	17.64	95.0	Sn-Stibiopalladinite
28a 45-75 #56STIB-i	0.02	na	0.13	0.11	na	<det	<det	<det	<det	5.07	15.67	<det	<det	<det	66.54	<det	<det	13.89	101.4	Sn-Stibiopalladinite
28a 45-75 #56STIB-h	0.01	na	0.12	0.13	na	<det	<det	<det	<det	5.08	17.36	<det	<det	<det	67.18	<det	0.12	12.51	102.5	Sn-Stibiopalladinite
MH35-36 [45]_#39b	0.07	na	0.15	0.30	na	na	na	<det	na	na	0.55	29.51	35.70	na	na	na	33.79	na	100.1	Maslovite
28a 45-75 #32UK-b	0.04	na	0.26	<det	na	<det	<det	0.74	<det	<det	46.16	2.12	39.06	<det	0.11	<det	2.57	0.49	91.6	Geversite
28a <45 #127GER-a	0.04	na	0.68	<det	na	<det	<det	0.89	<det	<det	46.74	3.61	39.73	<det	0.12	<det	1.15	0.77	93.7	Geversite
28a <45 #127GER-b	0.06	na	0.48	<det	na	<det	<det	0.83	<det	<det	46.71	3.29	40.25	<det	0.26	<det	1.18	0.78	93.8	Geversite
28a 45-75 #52STUMP-a	0.55	na	1.03	0.19	na	<det	<det	0.78	<det	<det	48.54	2.17	38.66	<det	0.63	<det	0.97	0.47	94.0	Geversite
MH-0028-1-29PT**	0.00	0.66	1.11	1.49	na	na	na	0.36	0.43	0.54	54.62	0.87	34.72	<det	0.12	na	<det	na	94.9	Geversite
MH-0028-1-32PT	0.00	0.67	0.26	0.33	na	na	na	0.23	0.21	<det	55.11	0.49	36.52	0.36	0.28	na	1.60	na	96.1	Geversite
28A <45 #127C	0.06	na	0.48	<det	na	<det	<det	0.83	<det	<det	46.69	3.21	42.34	0.15	0.13	<det	2.44	0.81	97.1	Geversite
28a 45-75 #11POL-d	0.02	na	0.15	<det	na	<det	<det	<det	<det	<det	0.29	1.53	1.52	<det	36.50	<det	63.14	<det	103.1	Polarite/Sobolevskite
28a 45-75 #11POL-c	0.01	na	<det	<det	na	<det	<det	<det	<det	<det	0.33	2.03	1.82	<det	36.55	<det	63.05	<det	103.8	Polarite/Sobolevskite

28a <45 #224INZ-a	0.91	na	1.34	2.09	na	<det	<det	0.18	<det	<det	12.99	4.30	29.33	<det	5.39	<det	39.64	0.61	96.8	Insizwaite
28A <45 #107UK-D	0.08	na	0.68	0.14	na	<det	<det	<det	<det	1.06	<det	0.46	53.59	<det	3.72	<det	<det	36.28	96.0	Niggliite
28a <45 #107UK-a	0.09	na	0.73	<det	na	<det	<det	<det	<det	<det	<det	9.76	50.08	<det	1.27	<det	<det	33.35	95.3	Niggliite
AG- AND BI-TELLURIDES																				
28a 75-125 #11HESS-b	0.00	na	<det	<det	na	<det	0.18	<det	<det	57.12	0.24	40.67	0.22	<det	<det	0.49	<det	<det	98.9	Stützite
28a 75-125 #3HESS-b	0.04	na	<det	<det	na	<det	0.25	<det	<det	55.93	0.21	41.25	0.59	<det	<det	0.57	<det	<det	98.8	Stützite
MH35-36 [45]_#13c	0.01	na	na	na	na	na	na	na	na	58.08	na	41.15	na	<det	na	na	<det	na	99.2	Stützite
28a 75-125 #2HESS-f	0.05	na	<det	0.12	na	<det	0.15	<det	<det	56.19	0.27	41.45	0.13	<det	<det	0.51	0.41	<det	99.3	Stützite
35/36 45-125 (CM) #71HESS-a	0.07	na	0.50	0.45	na	<det	0.11	<det	<det	60.34	0.29	37.21	<det	<det	<det	0.47	<det	<det	99.4	Stützite
35/36 45-125 (CM) #68HESS-b	0.17	na	0.26	<det	na	<det	0.14	<det	0.14	57.91	0.27	40.19	<det	<det	<det	0.47	<det	<det	99.5	Stützite
MH35-36 [45]_#30d	0.17	na	na	na	na	na	na	na	na	58.97	na	40.70	na	<det	na	na	<det	na	99.8	Stützite
MH35-36 [45]_#14c	0.00	na	na	na	na	na	na	na	na	58.75	na	41.81	na	<det	na	na	<det	na	100.6	Stützite
MH35-36 [45]_#38c	0.02	na	na	na	na	na	na	na	na	58.95	na	41.79	na	<det	na	na	<det	na	100.8	Stützite
35/36 45-125 (CM) #48UK-a	0.10	na	0.27	0.17	na	<det	0.14	<det	<det	57.55	0.19	41.45	<det	<det	<det	0.58	0.76	<det	101.2	Stützite
MH35-36 [45]_#42b	0.02	na	na	na	na	na	na	na	na	59.58	na	41.71	na	<det	na	na	<det	na	101.3	Stützite
MH35-36_#28b	0.08	na	na	na	na	na	na	na	na	62.31	na	38.97	na	<det	na	na	<det	na	101.4	Stützite
MH35-36 [45]_#13	0.00	na	na	na	na	na	na	na	na	60.36	na	41.00	na	<det	na	na	<det	na	101.4	Stützite
28a 45-75 #56UK-k	0.02	na	0.16	<det	na	<det	<det	<det	<det	61.39	0.25	36.78	<det	<det	0.11	0.48	<det	<det	99.2	Stützite
35/36 45-125 (CM) #46UK-b	17.95	na	0.49	0.57	na	2.07	0.11	<det	<det	25.19	<det	<det	1.00	<det	<det	0.34	52.95	<det	100.7	Matildite
35/36 45-125 (CM) #48UK-c	2.93	na	0.47	0.13	na	<det	<det	<det	0.18	<det	<det	22.72	0.86	<det	<det	<det	71.24	<det	98.5	Sulphotsumoite?
MH-033-1-rPbTe-5	0.06	2.04	0.54	0.47	0.10	0.16	na	<det	0.18	<det	0.26	33.32	1.16	<det	<det	<det	62.76	na	101.1	Tsumoite
ELECTRUM AND NATIVE AG																				
MH35-36 [45]_#35d	na	na	na	na	na	na	na	na	na	53.58	na	na	na	44.97	na	na	na	na	98.5	Electrum
35/36 <45 2T 14AuAg	0.00	0.77	0.62	0.68	na	na	na	0.43	0.90	43.91	<det	<det	<det	48.30	1.74	na	0.93	na	98.3	Electrum
MH35-36 [45]_#29c	na	na	na	na	na	na	na	na	na	30.93	na	na	na	68.11	na	na	na	na	99.0	Electrum
35/36 45-125 (CM) #1ELE-a	0.15	na	<det	<det	na	<det	<det	<det	<det	25.85	<det	<det	<det	73.05	<det	0.24	0.35	<det	99.6	Electrum
MH35-36 [45]_#9	na	na	na	na	na	na	na	na	na	36.47	na	na	na	63.41	na	na	na	na	99.9	Electrum
MH35-36 [45]_#10b	na	na	na	na	na	na	na	na	na	31.16	na	na	na	69.21	na	na	na	na	100.4	Electrum
MH35-36 [45]_#9c	na	na	na	na	na	na	na	na	na	35.10	na	na	na	66.02	na	na	na	na	101.1	Electrum
28a <45 #126AG-a	na	na	na	na	na	na	0.14	na	na	92.43	na	na	na	<det	na	na	na	na	92.6	native Ag
28a <45 #206AG-a	na	na	na	na	na	na	0.12	na	na	92.70	na	na	na	2.96	na	na	na	na	95.8	native Ag
28a <45 #52AG-b	na	na	na	na	na	na	0.15	na	na	89.59	na	na	na	6.37	na	na	na	na	96.1	native Ag
28a <45 #52AG-a	na	na	na	na	na	na	0.13	na	na	90.40	na	na	na	6.15	na	na	na	na	96.7	native Ag

na = not analyzed

<det = below detection

APPENDIX 4.IIIb. Compositions of olivine, pyroxene, hornblende, biotite, chlorite, and plagioclase determined by electron probe microanalysis (EPMA).

Label	SiO2	TiO2	Al2O3	Cr2O3	Fe2O3	FeO	MnO	MgO	CaO	Na2O	K2O	NiO	F	Cl	H2O	Total	Fo	An	Mineral
Unit	wt%	wt%	wt%	wt%	wt%	wt%	wt%	wt%	wt%	wt%	wt%	wt%	wt%	wt%	wt%	wt%			
Detection Limit	0.01	0.01	0.01	0.01	0.01	0.01	0.01	0.01	0.01	0.01	0.01	0.01	0.01	0.01	0.01				
OLIVINE (n = 14)																			
28-4 (6) OL-e	34.64	<det	<det	0.03	na	39.85	0.55	23.68	0.02	na	na	0.12	na	na	na	98.9	51		Olivine
24-2 (6) OL-c	33.28	na	na	<det	na	42.09	0.53	22.87	na	na	na	0.14	na	na	na	98.9	49		Olivine
24-2 (6) OL-d	33.71	na	na	<det	na	42.88	0.52	22.51	na	na	na	0.14	na	na	na	99.8	48		Olivine
24-2 (6) OL-e	34.63	na	na	<det	na	43.22	0.51	22.65	na	na	na	0.11	na	na	na	101.1	48		Olivine
24-2 (7) OL-g	34.44	na	na	<det	na	41.30	0.50	23.87	na	na	na	0.15	na	na	na	100.3	51		Olivine
24-2 (7) OL-h	34.22	na	na	0.03	na	41.47	0.50	23.64	na	na	na	0.15	na	na	na	100.0	50		Olivine
24-2 (8) OL-a	34.57	na	na	<det	na	40.04	0.48	24.92	na	na	na	0.17	na	na	na	100.2	53		Olivine
24-2 (8) OL-b	34.69	na	na	<det	na	39.74	0.48	25.08	na	na	na	0.15	na	na	na	100.1	53		Olivine
24-2 (8) OL-d	34.29	na	na	0.01	na	37.20	0.42	27.43	na	na	na	0.15	na	na	na	99.5	57		Olivine
24-2 (8) OL-e	35.03	na	na	<det	na	37.16	0.44	27.59	na	na	na	0.15	na	na	na	100.4	57		Olivine
24-2 (8) or 5 OL-f	35.26	na	na	<det	na	37.55	0.45	27.22	na	na	na	0.14	na	na	na	100.6	56		Olivine
24-2 (8) or 5 OL-g	34.95	na	na	<det	na	37.81	0.41	27.42	na	na	na	0.16	na	na	na	100.8	56		Olivine
MH-029-8Sil-b	35.96	<det	<det	na	na	38.88	0.77	24.74	0.03	<det	<det	na	na	na	na	100.4	53		Olivine
MH-029-8Sil-a	36.06	0.03	<det	na	na	38.67	0.77	24.81	0.01	<det	0.01	na	na	na	na	100.4	53		Olivine
CLINOPYROXENE (n = 20)																			
39 (3) OL-d	51.98	0.10	0.58	<det	<det	28.04	0.68	18.17	0.68	0.04	<det	na	na	na	na	100.3			Pigeonite
39 (4) PX-a	51.88	0.08	0.61	<det	0.76	27.43	0.70	18.46	0.64	0.05	0.01	na	na	na	na	100.6			Pigeonite
39 (4) PX-b	51.70	0.11	0.67	0.01	<det	27.53	0.64	18.39	0.63	0.01	<det	na	na	na	na	99.7			Pigeonite
39 (4) PX-d	51.75	0.11	0.44	<det	<det	27.95	0.63	18.07	0.57	0.01	0.01	na	na	na	na	99.5			Pigeonite
24-2 (8) PX-j	52.35	0.15	0.71	<det	1.52	21.47	0.45	22.53	0.51	na	na	na	na	na	na	99.7			Pigeonite
23 (6) PX-a	50.77	0.08	0.84	0.03	2.01	25.08	0.46	19.25	0.73	na	na	na	na	na	na	99.3			Pigeonite
23 (6) PX-b	50.54	0.07	0.83	0.03	2.77	24.05	0.49	19.62	0.76	na	na	na	na	na	na	99.2			Pigeonite
27c-2 (1) PX-a	51.02	0.11	0.49	<det	1.00	11.13	0.28	11.77	22.41	na	na	na	na	na	na	98.21			Augite
27c-2 (1) PX-b	50.24	0.18	0.88	<det	0.87	11.90	0.34	11.50	21.47	na	na	na	na	na	na	97.38			Augite
27c-2 (4) PX-a	51.13	0.11	0.55	<det	<det	12.01	0.26	11.41	21.82	na	na	na	na	na	na	97.29			Augite
27c-2 (4) PX-a-2	51.10	0.11	0.50	0.03	<det	12.25	0.25	11.42	21.99	na	na	na	na	na	na	97.65			Augite
27c-2 (5) PX-b-1	50.92	0.16	0.70	0.02	0.10	12.40	0.29	11.40	21.87	na	na	na	na	na	na	97.86			Augite
27c-2 (5) PX-b-2	51.17	0.24	0.68	<det	<det	12.82	0.24	11.25	21.36	na	na	na	na	na	na	97.76			Augite
27c-2 (5) PX-c-1	50.93	0.15	0.72	0.04	<det	14.38	0.27	11.64	19.91	na	na	na	na	na	na	98.04			Augite
27c-1 (1) PX-a-1	50.12	0.57	4.07	0.01	<det	15.94	0.22	12.91	11.81	na	na	na	na	na	na	95.65			Augite
27c-1 (1) PX-a-2	51.50	0.08	0.49	0.02	0.02	11.26	0.21	12.22	22.17	na	na	na	na	na	na	97.97			Augite
27c-1 (1) PX-b-1	51.51	0.20	0.70	0.04	<det	12.28	0.19	11.73	21.17	na	na	na	na	na	na	97.82			Augite
27c-1 (3) PX-a-1	51.30	0.09	0.55	<det	<det	11.85	0.23	11.99	21.79	na	na	na	na	na	na	97.80			Augite
27c-1 (3) PX-b-1	51.07	0.10	0.64	0.03	<det	11.94	0.29	11.72	21.81	na	na	na	na	na	na	97.60			Augite
27c-1 (5) PX-a-1	50.95	0.13	0.64	0.03	<det	12.30	0.20	11.80	21.42	na	na	na	na	na	na	97.47			Augite
HORNBLENDE (n = 58)																			
28-4 (3) HN-a	41.75	2.23	13.51	0.03	8.28	6.70	0.18	12.16	10.57	2.79	0.48	0.04	0.40	0.05	1.86	101.0			Hornblende
28-4 (3) HN-b	42.07	2.01	12.66	<det	8.29	6.48	0.14	12.48	10.48	2.81	0.47	0.08	<det	0.04	2.04	100.1			Hornblende
28-4 (3) HN-f	41.38	2.38	11.49	<det	4.70	9.62	0.20	11.12	10.15	2.71	0.38	0.06	0.13	0.05	1.89	96.3			Hornblende
28-4 (6) HN-a	41.10	2.12	12.88	<det	6.37	7.66	0.16	11.71	10.22	2.90	0.38	0.06	0.00	0.04	1.99	97.6			Hornblende

28-4 (6) HN-b	41.34	2.40	13.25	<det	6.99	7.28	0.17	11.95	10.34	2.95	0.40	0.06	0.10	0.04	1.97	99.2	Hornblende
28-4 (6) HN-c	41.39	2.51	13.03	<det	7.52	6.86	0.17	12.06	10.39	2.78	0.37	0.08	<det	0.05	2.02	99.2	Hornblende
28-4 (2) HN-a	41.71	2.71	10.96	<det	3.77	12.14	0.20	10.42	10.55	2.53	0.53	0.10	<det	0.07	1.95	97.6	Hornblende
28-4 (2) HN-b	41.46	2.87	10.17	0.04	2.70	12.65	0.18	10.45	10.38	2.62	0.55	0.10	<det	0.06	1.92	96.2	Hornblende
28-4 (2) HN-c	42.48	2.40	10.97	0.03	5.98	10.44	0.18	11.21	10.74	2.41	0.61	0.11	<det	0.06	2.00	99.6	Hornblende
28-4 (2) HN-d	42.96	2.80	9.66	<det	1.13	13.69	0.16	10.98	11.10	2.19	0.66	0.08	<det	0.06	1.95	97.4	Hornblende
28-4 (2) HN-e	42.66	2.55	9.56	0.02	2.87	12.22	0.17	11.21	10.81	2.30	0.64	0.10	0.06	0.06	1.92	97.2	Hornblende
39 (3) HN-a	42.60	2.16	10.58	<det	8.02	10.17	0.25	10.39	10.31	2.08	0.53	0.02	0.14	0.15	1.90	99.3	Hornblende
39 (3) HN-e	42.87	2.03	10.54	0.02	8.43	9.76	0.22	10.63	10.35	2.04	0.54	<det	<det	0.15	1.98	99.6	Hornblende
39 (3) HN-f	42.91	1.88	11.09	<det	8.26	9.70	0.22	10.71	10.55	2.07	0.52	0.02	0.25	0.13	1.88	100.2	Hornblende
39 (5) PX oik-a	44.81	1.30	9.98	0.04	8.84	8.53	0.22	11.78	10.77	1.84	0.36	0.02	<det	0.12	2.02	100.6	Hornblende
39 (5) PX oik-b	47.22	0.85	6.63	0.05	20.74	0.00	0.37	12.98	7.11	1.27	0.29	<det	0.12	0.10	2.00	99.7	Hornblende
39 (5) PX oik-c	45.44	1.08	9.95	0.02	9.83	7.35	0.21	12.09	10.63	1.66	0.34	0.01	0.04	0.12	2.02	100.8	Hornblende
39 (5) PX oik-d	43.28	1.64	9.86	0.03	6.39	11.17	0.27	10.27	10.37	1.99	0.40	<det	0.14	0.13	1.88	97.8	Hornblende
39 (5) PX oik-e	43.68	2.15	9.90	<det	7.75	10.17	0.21	10.79	10.34	1.97	0.52	0.01	0.06	0.13	1.96	99.6	Hornblende
39 (5) HN-f	43.29	1.99	9.39	0.02	7.21	10.39	0.22	10.48	10.08	1.93	0.46	0.02	<det	0.14	1.94	97.6	Hornblende
39 (5) HN-g	44.40	1.93	8.73	0.02	8.09	9.53	0.22	10.96	10.02	1.71	0.43	0.00	<det	0.13	1.97	98.1	Hornblende
39 (5) HN-h	44.87	2.07	10.09	<det	9.86	8.29	0.22	11.83	10.63	1.90	0.48	0.02	0.01	0.13	2.05	102.5	Hornblende
39 (5) HN-i	44.36	2.05	8.68	0.03	8.17	9.37	0.22	11.19	10.15	1.72	0.44	<det	<det	0.11	1.98	98.5	Hornblende
39 (5) HN-j	43.95	1.95	9.11	0.01	7.57	9.96	0.24	11.00	10.24	1.91	0.46	0.01	<det	0.10	1.98	98.5	Hornblende
39 (4) HN-e	42.25	2.05	10.19	0.01	6.00	11.29	0.23	10.07	10.24	2.07	0.52	0.01	<det	0.17	1.92	97.0	Hornblende
39 (2) HN-c	42.86	1.91	10.84	0.07	7.39	10.65	0.19	10.34	10.48	2.08	0.53	0.03	0.03	0.19	1.95	99.5	Hornblende
39 (2) HN-d	42.66	2.14	10.76	0.05	7.95	10.15	0.21	10.46	10.45	2.03	0.51	0.03	0.10	0.17	1.92	99.6	Hornblende
s4-2 (6) BT-g	41.15	2.34	13.09	0.06	9.73	6.14	0.20	11.37	9.78	2.80	0.32	0.07	<det	0.15	1.99	99.2	Hornblende
s4-2 (6) HN-h	41.20	2.23	13.37	0.09	10.33	5.64	0.18	11.41	9.87	2.66	0.30	0.09	0.05	0.17	1.98	99.6	Hornblende
s4-2 (6) HN-i	40.98	2.25	12.88	0.05	9.38	6.01	0.24	11.22	9.52	2.77	0.28	0.06	0.21	0.14	1.87	97.9	Hornblende
s4-2 (7) BT-c	42.18	1.93	13.43	0.01	10.75	5.72	0.17	11.67	10.02	2.79	0.23	0.06	0.13	0.15	1.97	101.2	Hornblende
s4-2 (7) BT-d	41.82	1.94	13.33	0.03	9.47	6.84	0.18	11.24	10.05	2.76	0.28	0.06	<det	0.16	2.01	100.2	Hornblende
s4-2 (7) HN-k	41.49	2.14	14.02	0.02	9.93	6.56	0.18	11.29	10.13	2.89	0.28	0.04	<det	0.19	2.02	101.2	Hornblende
s4-2 (7) HN-l	41.49	2.12	13.90	0.04	10.29	5.99	0.21	11.41	10.05	2.83	0.28	0.08	<det	0.16	2.02	100.9	Hornblende
s4-2 (8) BT-e	41.78	1.97	12.79	0.06	11.19	4.07	0.22	12.21	9.66	2.72	0.24	0.04	0.07	0.09	1.99	99.1	Hornblende
s4-2 (8) BT-f	41.89	1.95	12.87	0.03	9.76	4.77	0.22	12.16	9.77	2.75	0.19	0.07	0.10	0.07	1.97	98.6	Hornblende
s4-2 (5) BT-c	42.47	2.43	12.17	0.02	6.09	7.08	0.15	12.63	10.41	2.76	0.36	0.06	<det	0.03	2.03	98.7	Hornblende
s4-2 (8) or 5 alt-h	43.53	2.21	11.27	0.00	6.04	7.17	0.20	13.01	10.65	2.53	0.29	0.05	0.24	0.03	1.92	99.1	Hornblende
23 (4) HN-c	42.66	1.96	12.11	0.09	9.31	8.52	0.20	10.92	10.42	2.39	0.43	0.10	<det	0.27	1.99	101.4	Hornblende
23 (4) HN-d	42.55	1.83	12.15	0.11	8.63	9.33	0.15	10.56	10.51	2.27	0.43	0.07	<det	0.29	1.97	100.9	Hornblende
23 (4) HN-e	43.29	1.88	11.64	0.08	8.83	8.79	0.17	11.18	10.54	2.33	0.42	0.07	0.15	0.26	1.92	101.6	Hornblende
23 (5) HN-a	43.08	1.92	12.64	0.10	8.92	8.04	0.18	11.47	10.72	2.37	0.44	0.09	<det	0.28	2.01	102.3	Hornblende
23 (5) HN-b	42.73	1.93	12.27	0.09	8.31	8.64	0.16	11.22	10.56	2.44	0.46	0.09	<det	0.31	1.98	101.2	Hornblende
23 (5) HN-c	42.35	1.71	11.82	0.06	7.79	8.75	0.14	11.04	10.38	2.39	0.44	0.10	0.12	0.29	1.89	99.3	Hornblende
23 (5) HN-d	42.25	1.72	11.73	0.13	7.82	8.55	0.17	10.96	10.24	2.33	0.44	0.07	0.08	0.29	1.90	98.7	Hornblende
23 (6) HN-c	42.12	1.60	11.65	0.06	6.97	9.70	0.14	10.69	10.31	2.47	0.49	0.08	<det	0.31	1.92	98.5	Hornblende
23 (6) HN-d	42.89	1.60	12.08	0.06	8.62	8.27	0.20	11.35	10.64	2.29	0.46	0.05	0.05	0.29	1.95	100.8	Hornblende
23 (7) HN-a	42.46	1.81	12.71	0.03	8.49	8.35	0.17	11.46	10.81	2.47	0.53	0.08	<det	0.32	1.98	101.7	Hornblende
MH-029-25Sil-c	42.25	2.76	10.59	na	na	16.01	0.24	11.49	10.30	2.61	0.50	na	na	na	na	96.8	Hornblende

MH-029-8Sil-c	42.63	2.35	11.61	na	na	14.66	0.21	11.97	10.35	2.83	0.44	na	na	na	na	97.1	Hornblende
MH-029-36Sil-d	42.75	2.58	11.27	na	na	15.00	0.23	11.90	10.28	2.70	0.48	na	na	na	na	97.2	Hornblende
MH-029-18Sil-c	42.88	2.73	11.25	na	na	14.82	0.23	11.53	10.65	2.77	0.51	na	na	na	na	97.4	Hornblende
MH-029-22Sil-d	43.08	2.75	11.07	na	na	14.65	0.26	11.74	10.46	2.69	0.49	na	na	na	na	97.2	Hornblende
MH-029-36Sil-c	43.16	2.57	11.33	na	na	14.77	0.20	11.87	10.52	2.81	0.48	na	na	na	na	97.7	Hornblende
MH-033-2-2Sil-b	42.83	1.98	12.42	na	na	16.78	0.25	11.57	9.53	2.58	0.25	na	na	na	na	98.2	Hornblende
MH-034-1-7Sil-d	42.49	2.24	11.30	na	na	15.69	0.21	11.65	10.63	2.33	0.41	na	na	na	na	97.0	Hornblende
MH-034-2-1Hn-b	42.81	2.29	11.57	na	na	15.69	0.23	11.81	10.45	2.36	0.32	na	na	na	na	97.5	Hornblende
MH-034-2-1Hn-a	42.89	2.24	11.31	na	na	15.47	0.21	11.98	10.46	2.25	0.34	na	na	na	na	97.1	Hornblende
BIOTITE (n = 35)																	
28-4 (3) BT-c	36.77	3.55	16.01	0.03	na	13.78	0.04	15.14	0.02	0.99	7.86	0.20	0.15	0.04	3.94	98.5	Biotite
28-4 (3) BT-d	36.11	3.78	15.58	<det	na	13.59	0.03	14.62	0.04	1.03	7.64	0.16	0.07	0.06	3.89	96.6	Biotite
28-4 (3) BT-e	37.32	3.84	16.19	0.01	na	14.17	0.06	15.25	0.08	0.94	7.88	0.18	<det	0.06	4.07	100.1	Biotite
28-4 (3) BT-g	36.83	3.75	16.06	<det	na	13.80	0.03	15.04	0.05	0.98	8.04	0.15	0.11	0.07	3.96	98.9	Biotite
28-4 (1) BT-a	35.24	3.69	15.00	0.01	na	13.62	0.02	13.94	<det	0.83	7.90	0.32	<det	0.11	3.81	94.5	Biotite
28-4 (1) BT-b	35.89	4.15	15.19	<det	na	14.18	0.04	13.71	<det	1.00	7.79	0.23	<det	0.10	3.88	96.2	Biotite
39 (3) BT-g	35.65	3.44	14.44	0.01	na	17.07	0.07	12.42	<det	0.58	8.42	0.01	0.28	0.17	3.66	96.2	Biotite
39 (3) BT-h	36.22	3.47	15.07	0.01	na	17.29	0.05	13.04	<det	0.52	8.50	0.02	0.19	0.17	3.80	98.4	Biotite
39 (3) HN-i	36.44	3.40	14.49	0.02	na	17.16	0.07	12.87	<det	0.60	8.59	0.02	0.12	0.17	3.80	97.8	Biotite
39 (3) BT-j	36.41	3.38	14.96	<det	na	17.07	0.10	12.94	<det	0.55	8.36	0.03	0.08	0.17	3.84	97.9	Biotite
39 (4) BT-f	35.69	3.58	14.58	<det	na	17.01	0.05	12.40	<det	0.51	8.35	0.05	0.15	0.18	3.73	96.3	Biotite
39 (4) BT-g	36.44	3.39	15.14	0.04	na	17.52	0.06	13.04	0.04	0.55	8.26	0.03	0.01	0.20	3.89	98.6	Biotite
39 (4) BT-h	36.40	3.63	14.83	0.01	na	17.75	0.05	12.70	0.02	0.51	8.37	0.04	0.25	0.19	3.77	98.5	Biotite
39 (4) BT-i	35.96	3.41	14.81	0.06	na	17.45	0.05	12.63	<det	0.49	8.49	0.04	0.24	0.22	3.72	97.6	Biotite
39 (4) BT-j	36.56	3.60	15.19	0.02	na	18.12	0.06	12.89	0.04	0.54	8.45	0.04	0.24	0.20	3.81	99.8	Biotite
39 (2) BT-e	36.33	3.11	15.13	0.03	na	16.49	0.05	13.49	0.03	0.47	8.58	0.03	0.07	0.21	3.84	97.9	Biotite
39 (2) BT-f	36.28	3.50	15.01	0.07	na	17.19	0.05	13.04	0.06	0.53	8.43	0.04	0.33	0.22	3.72	98.5	Biotite
39 (2) BT-g	36.01	3.50	15.01	0.07	na	16.48	0.07	13.24	0.04	0.54	8.34	0.03	0.11	0.23	3.80	97.5	Biotite
39 (2) BT-h	36.60	3.53	15.34	0.06	na	17.28	0.07	13.33	0.04	0.50	8.53	0.04	0.06	0.21	3.90	99.5	Biotite
24-2 (6) BT-f	35.78	2.80	16.39	0.03	na	12.68	0.03	15.16	0.16	1.36	6.69	0.09	0.06	0.14	3.85	95.2	Biotite
24-2 (7) BT-i	37.08	3.57	17.13	0.02	na	14.65	0.04	15.20	0.04	1.34	7.32	0.12	<det	0.14	4.08	100.7	Biotite
24-2 (7) BT-j	36.47	3.57	16.72	0.01	na	15.16	0.04	14.97	0.07	1.20	7.12	0.12	0.16	0.13	3.95	99.7	Biotite
24-2 (8) BT-g	36.04	3.07	16.31	0.05	na	13.78	0.01	15.10	0.04	1.37	7.11	0.10	0.07	0.08	3.91	97.0	Biotite
24-2 (8) BT-h	36.39	2.89	16.20	0.07	na	13.32	0.02	15.05	<det	1.36	6.95	0.10	<det	0.10	3.93	96.4	Biotite
24-2 (5) BT-a	36.85	3.05	16.20	0.26	na	11.29	0.03	16.73	<det	1.21	7.46	0.11	0.18	0.02	3.93	97.3	Biotite
24-2 (5) BT-b	34.36	3.03	14.99	0.21	na	10.92	0.04	15.50	0.05	1.26	6.99	0.07	0.07	0.06	3.71	91.3	Biotite
MH-029-33Sil-c	35.87	3.82	14.53	na	na	11.93	0.05	14.28	0.03	0.86	7.30	na	na	na	na	88.7	Biotite
MH-029-33Sil-d	36.98	3.68	14.31	na	na	12.94	0.06	14.47	<det	0.85	7.60	na	na	na	na	90.9	Biotite
MH-029-24Sil-c	37.19	4.14	14.49	na	na	15.33	0.10	14.48	<det	0.82	8.10	na	na	na	na	94.7	Biotite
MH-029-26Sil-d	37.20	4.11	14.91	na	na	14.11	0.04	14.97	<det	0.93	8.23	na	na	na	na	94.5	Biotite
MH-029-24Sil-d	37.57	3.96	14.52	na	na	14.76	0.05	14.70	0.01	0.78	8.28	na	na	na	na	94.6	Biotite
MH-029-4Sil-c	37.63	3.83	14.89	na	na	12.34	0.03	15.12	0.01	0.87	8.21	na	na	na	na	92.9	Biotite
MH-029-26Sil-e	38.01	3.70	14.85	na	na	13.26	<det	15.28	<det	0.91	8.17	na	na	na	na	94.2	Biotite
MH-033-2-7Sil-b	36.69	3.28	15.53	na	na	15.89	0.07	13.71	<det	0.61	8.25	na	na	na	na	94.0	Biotite
MH-033-2-7Sil-a	37.14	3.36	15.78	na	na	16.29	0.04	13.73	<det	0.87	7.57	na	na	na	na	94.8	Biotite

CHLORITE (n = 5)																	
MH-034-2-2Pl-c	25.74	0.09	20.00	na	na	24.72	0.09	15.76	0.04	<det	0.01	na	na	na	na	86.4		Mg-Fe chlorite
MH-034-1-3Chl-e	26.08	0.05	19.84	na	na	25.14	0.11	15.73	0.01	<det	<det	na	na	na	na	87.0		Mg-Fe chlorite
MH-034-2-2Chl-b	26.44	0.08	19.87	na	na	24.49	0.08	16.06	0.04	<det	0.02	na	na	na	na	87.1		Mg-Fe chlorite
MH-034-2-2Chl-a	26.45	0.07	19.84	na	na	24.95	0.10	15.48	0.01	<det	<det	na	na	na	na	86.9		Mg-Fe chlorite
MH-033-2-5Sil-b	26.46	0.06	19.02	na	na	28.96	0.12	12.94	0.06	0.02	0.02	na	na	na	na	87.7		Mg-Fe chlorite
PLAGIOCLASE (n = 25)																		
28-4 (5) PL-c	55.93	0.02	29.58	na	0.21	na	na	<det	10.24	5.51	0.02	na	na	na	na	101.5	51	Labradorite
28-4 (5) PL-d	55.90	<det	29.48	na	0.15	na	na	<det	10.19	5.65	0.01	na	na	na	na	101.4	50	Labradorite
28-4 (6) PL-f	53.21	0.11	30.31	na	0.22	na	na	<det	11.60	4.58	0.04	na	na	na	na	100.1	58	Labradorite
28-4 (6) PL-g	54.19	<det	28.63	na	0.44	na	na	0.21	10.11	5.26	0.03	na	na	na	na	98.9	52	Labradorite
28-4 (1) PL-d	58.48	0.02	26.60	na	0.07	na	na	<det	7.43	7.06	0.12	na	na	na	na	99.8	37	Andesine
28-4 (1) PL-f	60.52	0.01	26.32	na	0.15	na	na	<det	6.68	7.46	0.07	na	na	na	na	101.2	33	Andesine
28-4 (2) PL-g	56.79	0.06	28.21	na	0.12	na	na	<det	8.98	6.21	0.15	na	na	na	na	100.5	44	Andesine
28-4 (2) PL-i	58.80	0.08	27.15	na	0.17	na	na	<det	7.72	7.08	0.12	na	na	na	na	101.1	38	Andesine
28-4 (4) PL-c	57.97	0.01	28.06	na	0.13	na	na	<det	8.56	6.36	0.19	na	na	na	na	101.3	43	Andesine
28-4 (4) PL-d	61.32	<det	25.62	na	0.25	na	na	<det	6.10	7.92	0.16	na	na	na	na	101.4	30	Andesine
28-4 (4) PL-e	59.73	0.13	25.70	na	0.16	na	na	<det	6.57	7.32	0.15	na	na	na	na	99.8	33	Andesine
39 (4) BT-k	57.12	0.03	28.50	na	0.14	na	na	<det	9.20	6.14	0.07	na	na	na	na	101.2	45	Andesine
24-2 (6) PL-j	53.94	na	30.04	na	0.45	na	na	na	11.52	4.74	0.01	na	na	na	na	100.7	57	Labradorite
24-2 (6) PL-k	53.11	na	30.55	na	0.28	na	na	na	11.61	4.68	0.02	na	na	na	na	100.3	58	Labradorite
24-2 (7) PL-a	52.86	na	30.16	na	1.00	na	na	na	11.47	4.65	0.03	na	na	na	na	100.2	58	Labradorite
24-2 (7) PL-b	55.05	na	29.17	na	0.13	na	na	na	10.10	5.72	0.02	na	na	na	na	100.2	49	Andesine
24-2 (7) PL-c	54.78	na	28.24	na	0.09	na	na	na	9.36	6.10	0.04	na	na	na	na	98.6	46	Andesine
MH-029-8Sil-d	53.81	0.49	28.07	na	na	0.69	0.00	0.01	11.64	4.87	0.05	na	na	na	na	99.6	57	Labradorite
MH-029-16Sil-a	55.15	0.04	27.70	na	na	0.17	0.01	0.01	10.94	5.24	0.05	na	na	na	na	99.3	54	Labradorite
MH-029-16Sil-b	55.52	0.12	27.53	na	na	0.23	0.00	0.01	10.46	5.55	0.06	na	na	na	na	99.5	51	Labradorite
MH-029-8Sil-e	57.98	0.01	24.94	na	na	1.75	0.04	0.64	7.51	6.72	0.06	na	na	na	na	99.7	38	Andesine
MH-029-RSil-3	58.01	0.01	26.09	na	na	0.17	0.01	<det	8.99	6.48	0.02	na	na	na	na	99.8	43	Andesine
MH-029-25Sil-d	58.70	0.06	25.66	na	na	0.15	0.02	0.01	8.10	6.87	0.05	na	na	na	na	99.6	40	Andesine
MH-034-1-5Sil-e	55.05	<det	27.38	na	na	0.18	0.03	0.02	9.84	6.01	0.04	na	na	na	na	98.6	48	Andesine
MH-034-2-4Pl-a	55.58	<det	26.86	na	na	0.08	0.00	<det	10.08	5.95	0.05	na	na	na	na	98.6	48	Andesine
MH-034-2-4Pl-b	64.42	<det	18.04	na	na	0.06	0.00	0.02	<det	0.28	15.87	na	na	na	na	98.7		Orthoclase

na = not analyzed

<det = below detection

APPENDIX 4.IVa. *In situ* platinum-group element (PGE) and other trace element analysis compositions of pyrrhotite, chalcopyrite, pentlandite, galena, cubanite, bornite, and pyrite determined by LA-ICP-MS.

	Element	SO2	SO2	Pd	Rh	Ru	Os	Ir	Pt	Ga	Zn	As	Se	Mo	Ag	Cd	Sn	Sb	Te	Au	Hg	Pb	Bi	Mineral
	Isotope	33	34	105-108	103	101-102	188-189	191-193	194-195	69	70	75	77	95	107-109	111	118	121	125	197	202	208	209	
	Unit	wt%	wt%	ppm	ppm	ppm	ppm	ppm	ppm	ppm	ppm	ppm	ppm	ppm	ppm	ppm	ppm	ppm	ppm	ppm	ppm	ppm	ppm	
Sample No.	Detection Limit	0.100	0.100	0.010	0.050	0.020	0.010	0.010	0.010	0.020	0.500	0.100	1.500	0.020	0.100	0.050	0.030	0.010	0.100	0.010	0.050	0.100	0.010	
PYRRHOTITE (n = 32)																								
21 PO 3D	nv25d07	24.896	38.630	<det	<det	<det	<det	<det	<det	1.831	<det	283.604	100.393	<det	0.327	<det	0.512	0.226	0.201	0.089	1.287	3.577	0.582	Pyrrhotite
21 PO 4C	nv25d10	41.028	38.630	<det	0.051	<det	<det	<det	<det	0.801	<det	13.087	93.406	1.038	0.961	0.223	0.331	0.044	0.961	0.058	1.078	1.873	0.308	Pyrrhotite
21 PO 1C	nv25d14	37.062	38.630	<det	<det	<det	<det	<det	<det	3.020	214.683	172.048	89.267	0.901	0.770	0.216	0.532	0.103	0.286	0.042	1.223	4.620	0.513	Pyrrhotite
21 PO 1D	nv25d15	34.714	38.630	<det	<det	<det	<det	<det	<det	<det	<det	40.133	77.051	1.078	0.780	0.430	0.366	0.021	1.504	0.003	0.842	1.416	0.146	Pyrrhotite
22A PO 3A	nv25e10	50.195	38.630	<det	<det	<det	0.024	<det	<det	<det	<det	<det	93.747	0.299	0.575	0.267	<det	0.085	<det	<det	3.006	0.580	0.238	Pyrrhotite
22A 30 3D	nv25e13	28.721	38.630	<det	<det	<det	<det	<det	<det	1.418	192.057	<det	68.731	<det	<det	<det	0.291	0.013	0.610	0.013	2.668	0.487	0.252	Pyrrhotite
22A PO 4A	nv25e14	37.640	38.630	<det	0.195	<det	<det	<det	0.0130	<det	143.667	4.147	94.909	0.548	2.121	0.361	1.762	0.325	1.697	0.288	1.312	9.507	0.148	Pyrrhotite
22A PO 4B	nv25e15	39.617	38.630	0.046	<det	<det	<det	<det	<det	<det	114.182	1.723	128.068	2.034	0.563	<det	0.525	0.188	0.444	0.696	1.165	2.246	0.179	Pyrrhotite
22B-1 PO 4A	nv29a12	39.058	38.630	<det	0.408	0.0930	0.028	<det	<det	<det	9.856	1.343	54.699	0.400	3.853	<det	0.110	0.038	0.857	0.025	0.438	0.500	0.138	Pyrrhotite
22B-1 PO 4B	nv29a13	40.619	38.630	0.0260	0.295	<det	0.0160	<det	<det	0.055	<det	1.249	57.358	0.373	0.696	<det	0.159	<det	0.594	<det	0.611	0.910	0.218	Pyrrhotite
22B-1 PO 5A	nv29a16	38.577	38.630	0.023	0.124	0.110	0.0560	<det	0.068	0.022	98.101	0.449	52.770	0.241	0.422	0.075	0.247	0.045	1.516	0.007	1.611	0.195	0.068	Pyrrhotite
22B-2 PO 1A	nv29b04	37.338	38.630	<det	0.642	<det	<det	<det	<det	<det	<det	1.533	66.019	0.314	1.761	1.277	0.969	0.149	3.424	0.418	4.668	3.954	1.413	Pyrrhotite
22B-2 PO 2C	nv29b14	37.562	38.630	<det	0.150	<det	<det	<det	<det	<det	3.798	0.472	26.429	0.132	0.233	0.075	0.044	<det	0.189	0.001	0.152	0.130	0.072	Pyrrhotite
22B-2 PO 3C	nv29b17	36.197	38.630	<det	0.138	<det	<det	<det	<det	<det	7.308	0.371	27.642	0.111	0.157	0.129	0.070	<det	0.150	0.011	0.204	0.228	0.082	Pyrrhotite
23 PO 2B	nv29c08	39.342	38.630	<det	0.050	<det	<det	<det	<det	0.099	8.001	1.276	66.890	0.595	3.078	0.183	0.253	0.198	4.767	0.017	1.055	0.846	2.550	Pyrrhotite
23 PO 2F	nv29c12	38.364	38.630	<det	0.113	<det	<det	<det	<det	0.167	13.946	0.664	81.369	0.356	0.840	0.238	0.252	0.087	0.939	<det	0.585	0.925	0.312	Pyrrhotite
23 PO 3E	nv29c17	39.391	38.630	<det	<det	0.047	<det	<det	<det	0.095	11.372	4.641	76.143	0.599	1.182	0.122	0.516	0.092	1.695	0.648	0.571	5.227	0.469	Pyrrhotite
25-1 PO 2D	nv29e11	39.549	38.630	<det	<det	0.0650	<det	<det	<det	<det	0.786	0.840	55.786	0.490	0.847	0.357	0.209	0.012	0.874	<det	0.729	1.080	0.296	Pyrrhotite
25-1 PO 2E	nv29e12	40.261	38.630	<det	<det	0.068	<det	<det	<det	<det	22.518	0.787	66.322	1.409	0.921	0.285	0.143	0.070	1.725	0.018	0.603	1.078	0.193	Pyrrhotite
25-1 PO 4C	nv29e17	39.700	38.630	<det	<det	0.071	0.012	<det	<det	0.095	4.951	1.445	68.335	1.367	1.753	0.162	0.156	<det	2.313	0.004	0.817	1.483	0.253	Pyrrhotite
26-1 PO 1A	nv29f04	36.946	38.630	<det	<det	0.079	<det	<det	<det	0.048	<det	1.030	67.497	0.428	0.542	0.164	0.498	0.076	2.472	0.102	0.694	1.288	0.193	Pyrrhotite
26-1 PO 2C	nv29f10	39.648	38.630	<det	<det	<det	0.018	<det	<det	0.086	<det	1.756	77.943	1.042	0.941	0.115	0.655	<det	1.501	0.006	0.657	1.280	0.262	Pyrrhotite
26-1 PO 3C	nv29f13	37.171	38.630	<det	<det	<det	<det	<det	<det	0.039	17.426	1.079	76.133	0.634	1.692	<det	0.291	<det	2.193	0.017	0.866	0.643	0.165	Pyrrhotite
26-1 PO 3D	nv29f14	39.378	38.630	<det	<det	<det	0.014	<det	<det	<det	57.705	0.851	80.500	0.510	0.746	0.259	0.334	0.050	2.310	<det	0.834	0.604	0.184	Pyrrhotite
26-1 PO 4C	nv29f17	41.761	38.630	<det	<det	0.057	<det	<det	<det	0.073	2.260	1.108	85.141	0.769	1.099	0.517	0.293	0.037	1.513	<det	0.898	0.765	0.341	Pyrrhotite
29-2 PO 1A	nv30b04	40.489	38.630	<det	0.239	<det	<det	<det	<det	<det	<det	0.549	62.472	0.235	1.119	<det	0.819	0.036	0.607	0.011	0.816	1.186	0.180	Pyrrhotite
29-2 PO 2C	nv30b09	36.786	38.630	<det	0.813	<det	<det	<det	0.0400	0.519	8.293	0.458	68.242	0.326	0.617	<det	0.545	0.010	0.271	0.016	0.626	3.025	0.164	Pyrrhotite
29-2 PO 3A	nv30b10	38.160	38.630	<det	0.092	0.056	<det	<det	<det	0.414	10.810	0.322	59.439	0.325	0.703	<det	0.754	<det	0.193	0.015	0.889	0.753	0.158	Pyrrhotite
29-2 PO 4A	nv30b14	38.357	38.630	<det	0.066	<det	<det	<det	0.032	<det	4.487	0.762	60.004	0.253	0.491	<det	0.452	<det	0.366	<det	1.268	0.641	0.158	Pyrrhotite
33-3 PO-1D	nv30c07	39.616	38.630	<det	<det	<det	<det	<det	<det	<det	<det	0.435	40.346	0.138	1.024	<det	0.223	<det	1.543	0.003	1.039	9.874	0.526	Pyrrhotite
34-3 PO 3D	nv30e07	40.911	38.630	<det	<det	<det	<det	<det	<det	<det	<det	0.528	68.132	0.347	0.924	0.083	0.336	0.067	0.828	0.000	0.942	3.756	0.505	Pyrrhotite
34-3 PO 5A	nv30e10	39.107	38.630	<det	<det	<det	<det	<det	<det	0.277	<det	0.613	30.695	<det	0.898	0.162	0.192	0.016	0.608	<det	0.558	2.334	0.208	Pyrrhotite
CHALCOPYRITE (n = 74)																								
21 CCP 4D	nv25d11	24.510	34.830	<det	nd	<det	<det	<det	<det	<det	306.242	39.641	58.770	<det	3.150	17.699	7.049	0.130	5.043	0.004	0.509	4.730	0.467	Chalcopyrite
21 CCP 1A	nv25d12	28.323	34.830	<det	nd	<det	<det	<det	<det	<det	859.435	115.621	29.929	0.038	10.388	18.833	4.721	0.058	11.260	0.202	1.721	6.410	0.179	Chalcopyrite
21 CCP 1B	nv25d13	58.744	34.830	<det	nd	<det	<det	<det	<det	<det	1656.120	344.556	46.999	<det	8.65	22.412	6.946	0.365	14.560	0.064	2.321	10.509	0.412	Chalcopyrite
21 CCP 2A	nv25d16	42.273	38.630	na	na	na	na	na	na	<det	290.234	32.762	126.629	0.555	7.193	19.877	7.641	0.015	7.873	<det	2.270	9.220	1.051	Chalcopyrite
22A CCP 3B	nv25e11	36.853	34.830	0.116	nd	<det	<det	<det	<det	<det	569.877	2.894	154.813	1.328	2.946	22.221	2.815	0.039	8.901	0.015	3.894	1.464	0.293	Chalcopyrite
22A CCP 3C	nv25e12	22.191	34.830	<det	nd	<det	<det	<det	<det	<det	128.206	<det	45.315	0.612	101.527	20.283	2.815	<det	8.845	<det	2.814	1.457	0.241	Chalcopyrite
22B-1 CCP 1A	nv29a04	35.312	34.830	0.552	nd	0.1530	<det	<det	<det	0.218	472.547	0.513	50.967	0.178	6.420	29.354	8.611	<det	7.817	0.008	3.563	8.922	0.174	Chalcopyrite
22B-1 CCP 1B	nv29a05	36.033	34.830	<det	nd	<det	<det	<det	<det	0.077	450.275	0.232	40.700	0.054	5.247	31.698	6.257	0.020	5.768	0.008	1.820	5.187	0.152	Chalcopyrite
22B-1 CCP2A	nv29a06	34.124	34.830	0.079	nd	<det	<det	<det	<det	0.216	409.147	0.638	49.577	0.099	4.286	29.811	8.057	0.036	5.388	0.012	1.567	3.880	0.111	Chalcopyrite
22B-1 CCP 2B	nv29a07	34.835	34.830	0.067	nd	<det	0.0130	<det	0.0580	0.297	474.132	0.216	43.608	<det	5.592	31.728	6.263	<det	5.985	0.005	1.299	4.531	0.121	Chalcopyrite
22B-1 CCP 3A	nv29a08	34.848	34.830	0.139	nd	<det	<det	<det	<det	0.036	349.248	0.751	45.617	0.077	2.067	20.373	6.244	0.017	3.406	0.005	1.415	1.960	0.115	Chalcopyrite
22B-1 CCP 3B	nv29a09	38.140	34.830	0.093	nd	<det	<det	<det	<det	0.175	366.396	0.155	43.447	0.041	2.683	29.591	6.189	<det	3.510	0.010	1.409	4.750	0.204	Chalcopyrite
22B-1 CCP 3C	nv29a10	33.889	34.830	0.108	nd	<det	0.0100	<det	<det	0.172	383.327	0.534	47.164	0.056	3.778	35.952	8.767	0.033	4.310	0.018	0.953	5.273	0.194	Chalcopyrite
22B-2 CCP 3A	nv29b15	33.498	34.830	<det	nd	<det	<det	<det	0.0200	0.094	375.790	0.571	21.568	0.061	9.527	42.231	2.400	0.027	1.757	0.226	0.201	8.411	0.162	Chalcopyrite
23 CCP 1C	nv29c06	34.399	34.830	0.128	nd	<det	<det	<det	<det	0.303	327.763	3.225	60.883	0.200	5.247	35.668	1.322	0.817	5.406	0.272	1.498	28.270	0.690	Chalcopyrite
23 CCP 2C	nv29c09	34.514	34.830	0.050	nd	<det	<det	<det	<det	0.219	1046.687	0.832	57.389	0.122	19.381	63.347	0.581	0.102	10.806	0.032	1.971	12.544	0.951	Chalcopyrite
23 CCP 2D	nv29c10	35.546	34.830	0.047	nd	<det	<det	<det	0.010	0.484	591.046	0.797	58.348	0.244	22.974	70.154	0.491	0.062	8.919	0.010	1.734	8.608	0.622	Chalcopyrite
23 CCP 2E	nv29c11	35.450	34.830	0.142	nd	<det	<det	<det	<det	0.194	651.852	0.578	61.386	0.167	51.856	46.244	0.435	0.272	13.193	0.023	1.869	6.826	0.904	Chalcopyrite
23 CCP 3D	nv29c16	36.000	34.830	0.069	nd	<det	<det	<det	<det	0.096	428.047	2.767	58.081	0.242	14.633	45.605	0.734	0.137	12.533	0.026	3.696	11.129	0.612	Chalcopyrite
24-2 CCP 1A	nv29d04	34.693	34.830	0.051	nd	<det	<det	<det	<det	0.118	631.150	0.584	52.765	0.184	3.997	40.683	2.819	<det	4.733	<det	3.708	1.585	0.061	Chalcopyrite
24-2 CCP 1B	nv29d05	32.981	34.830	<det	nd	<det	<det	<det	<det	0.253	583.399	0.897	72.995	0.164	4.120	38.938	3.012	0.048	5.443	0.008	3.213	0.959	0.052	Chalcopyrite
24-2 CCP 1C	nv29d06	34.269	34.830	0.035	nd	<det	<det	<det	<det	<det	485.118	1.017	58.023	0.156	4.881	36.854	3.816	0.015	5.206	0.030	2.420	3.159	0.067	Chalcopyrite
24-2 CCP 2A	nv29d07	32.931	34.830	0.250	nd	<det	<det	<det	<det	0.242	544.364	0.170	55.112	<det	3.182	34.398	2.513	<det	4.588	0.010	1.864	1.153	0.050	Chalcopyrite
24-2 CCP 2B	nv29d08	35.018	34.830	<det	nd	<det	<det	<det	0.0550	0.178	558.374	0.638	61.867	<det	4.407	32.348	2.934	0.015	5.812	0.003	2.048	3.860	0.079	Chalcopyrite
24-2 CCP 2D	nv29d10	39.079	34.830	<det	nd	<det	<det	<det	<det	0.110	575.860	0.633	57.866	0.051	5.926	45.834	3.445	<det	5.823	0.016	2.433	5.301	0.285	Chalcopyrite

24-2 CCP 3D	nv29d14	36.182	34.830	<det	nd	<det	<det	<det	<det	0.149	687.772	0.487	48.061	0.134	4.140	41.260	2.818	0.015	5.547	0.017	2.123	1.310	0.063	Chalcopyrite
24-2 CCP 3E	nv29d15	36.589	34.830	0.043	nd	<det	<det	<det	<det	0.176	615.740	0.427	63.743	0.030	3.642	34.811	2.983	0.028	6.410	0.007	1.316	1.510	0.042	Chalcopyrite
24-2 CCP 4A	nv29d16	35.204	34.830	0.041	nd	<det	<det	<det	<det	0.288	485.889	0.875	53.301	<det	9.858	32.239	2.602	<det	5.119	0.004	2.112	3.994	0.091	Chalcopyrite
24-2 CCP 4B	nv29d17	36.339	34.830	0.026	nd	<det	<det	<det	<det	0.691	622.001	0.789	54.561	0.167	26.244	38.185	2.859	0.031	5.557	0.028	2.084	1.785	0.035	Chalcopyrite
25-1 CCP 1A	nv29e04	36.534	34.830	0.114	nd	<det	<det	<det	<det	0.243	702.140	0.784	60.792	0.259	30.928	33.320	3.558	<det	10.907	0.079	1.399	8.330	1.924	Chalcopyrite
25-1 CCP 2A	nv29e08	33.967	34.830	0.067	nd	<det	<det	<det	0.0360	0.088	671.856	0.907	54.255	<det	11.658	37.516	2.446	0.039	14.735	0.020	1.945	2.617	0.358	Chalcopyrite
25-1 CCP 2B	nv29e09	35.851	34.830	0.031	nd	<det	<det	<det	<det	0.349	657.358	0.696	51.702	0.048	11.365	39.195	2.124	<det	14.170	0.005	1.993	1.831	0.305	Chalcopyrite
25-1 CCP 2C	nv29e10	36.314	34.830	0.195	nd	<det	<det	<det	<det	1.906	1236.924	0.516	48.539	<det	33.917	75.732	1.057	0.045	10.231	0.012	1.629	6.157	0.411	Chalcopyrite
25-1 CCP 3A	nv29e13	33.521	34.830	0.136	nd	<det	<det	<det	0.0210	1.004	879.938	0.834	52.100	0.225	14.428	68.107	1.242	0.039	14.104	0.011	2.372	5.019	0.276	Chalcopyrite
25-1 CCP 3B	nv29e14	34.459	34.830	0.032	nd	<det	<det	<det	<det	2.238	528.329	0.270	53.135	0.507	30.095	40.288	1.488	0.044	8.297	0.017	1.643	4.540	0.284	Chalcopyrite
26-1 CCP 1B	nv29f05	33.508	34.830	<det	nd	<det	<det	<det	<det	0.746	443.776	2.704	76.243	0.981	50.914	56.026	8.125	0.181	24.304	0.169	2.700	12.080	1.261	Chalcopyrite
26-1 CCP 1C	nv29f06	33.429	34.830	1.178	nd	<det	<det	<det	<det	0.735	1039.210	1.694	72.121	0.230	249.869	284.361	11.216	<det	23.283	0.106	3.283	11.062	1.536	Chalcopyrite
26-1 CCP 2B	nv29f09	34.180	34.830	<det	nd	<det	<det	<det	<det	0.215	384.425	1.931	68.918	0.439	9.780	26.695	5.290	0.046	21.597	0.057	2.238	2.749	0.525	Chalcopyrite
26-1 CCP 3B	nv29f12	33.884	34.830	0.092	nd	<det	<det	<det	<det	0.649	777.680	2.058	68.559	0.736	5.012	53.436	9.910	0.165	17.178	0.055	2.151	14.220	0.496	Chalcopyrite
26-1 CCP 4A	nv29f15	35.415	34.830	<det	nd	<det	<det	<det	<det	0.218	322.922	1.901	70.332	0.034	11.687	38.935	7.850	0.106	22.406	0.051	2.165	6.204	0.754	Chalcopyrite
26-1 CCP 4B	nv29f16	35.846	34.830	0.104	nd	<det	<det	<det	<det	0.556	432.817	2.775	65.480	0.046	8.06	41.120	5.326	<det	19.028	0.004	2.772	1.757	0.685	Chalcopyrite
28-5 CCP 2C	nv29g08	36.140	34.830	<det	nd	<det	<det	<det	<det	<det	88.436	2.488	18.502	1.803	18.047	16.328	34.668	0.505	1.796	<det	0.200	na	0.787	Chalcopyrite
28-5 CCP 4A	nv29g12	34.863	34.830	<det	nd	<det	<det	<det	<det	0.384	25.029	0.378	20.420	0.252	32.624	1.521	78.198	0.161	15.325	0.008	2.622	na	0.223	Chalcopyrite
29-2 CCP 1B	nv30b05	36.221	34.830	0.076	nd	<det	<det	<det	<det	0.250	436.210	0.336	46.636	0.024	76.479	46.665	59.719	0.083	2.902	0.048	2.324	30.465	0.226	Chalcopyrite
29-2 CCP 2A	nv30b07	35.112	34.830	0.066	nd	<det	<det	<det	<det	0.124	333.604	0.482	50.127	<det	28.693	27.661	68.552	<det	3.206	0.078	3.040	6.768	0.213	Chalcopyrite
29-2 CCP 2B	nv30b08	36.905	34.830	0.733	nd	<det	<det	<det	<det	0.100	773.875	0.605	49.052	<det	44.669	382.281	132.129	<det	1.859	0.074	2.286	11.323	0.427	Chalcopyrite
29-2 CCP 3B	nv30b11	36.021	34.830	<det	nd	<det	<det	<det	<det	0.188	410.861	0.324	48.201	<det	23.756	38.414	58.321	0.014	3.511	0.043	3.387	9.244	0.219	Chalcopyrite
29-2 CCP 4B	nv30b15	35.024	34.830	<det	nd	<det	<det	<det	<det	0.822	309.993	0.423	34.715	<det	37.515	28.117	45.896	<det	1.512	0.009	1.494	3.999	0.071	Chalcopyrite
33-3 CCP 3A	nv30c11	35.593	34.830	0.112	nd	<det	<det	<det	<det	<det	473.318	0.627	62.424	0.071	18.939	65.274	86.659	0.028	5.230	0.366	2.440	42.169	1.951	Chalcopyrite
33-3 CCP 3B	nv30c12	34.920	34.830	0.047	nd	<det	<det	<det	<det	<det	444.762	1.424	59.669	0.034	22.179	38.692	86.552	0.027	5.231	0.364	2.087	30.537	2.449	Chalcopyrite
33-3 CCP 3C	nv30c13	31.728	34.830	<det	nd	<det	<det	<det	<det	<det	453.770	0.572	60.138	<det	17.551	35.781	96.094	0.031	3.169	0.116	1.956	17.898	0.902	Chalcopyrite
33-3 CCP 4A?	nv30c15	36.756	34.830	<det	nd	<det	<det	<det	<det	<det	283.539	0.399	58.015	0.252	44.261	26.311	8.015	0.362	0.694	0.358	2.195	85.129	1.041	Chalcopyrite
33-3 CCP 4B	nv30c16	33.607	34.830	0.065	nd	<det	<det	<det	<det	<det	411.221	0.289	45.725	<det	19.568	36.690	41.285	<det	3.405	0.181	3.072	17.057	1.259	Chalcopyrite
34-3 CCP 1B	nv30d05	35.119	34.830	<det	nd	<det	<det	<det	<det	<det	496.728	1.111	44.127	<det	66.028	84.403	190.340	<det	7.011	0.367	1.718	100.745	4.773	Chalcopyrite
34-3 CCP 1C	nv30d06	35.510	34.830	<det	nd	<det	<det	<det	<det	<det	526.547	1.057	34.265	<det	178.663	81.132	255.548	0.393	7.133	0.121	0.115	11.272	0.926	Chalcopyrite
34-3 CCP 2B	nv30d08	34.067	38.630	na	na	na	na	na	na	0.937	891.958	2.107	13.069	<det	19.248	76.783	115.416	<det	1.673	0.282	1.891	6.315	1.447	Chalcopyrite
34-3 CCP 4A	nv30e08	34.986	34.830	<det	nd	<det	<det	<det	0.0170	0.142	692.418	0.345	38.897	0.185	72.396	76.349	249.249	0.072	5.183	0.206	2.316	15.605	1.139	Chalcopyrite
34-3 CCP 4B	nv30e09	34.848	34.830	0.326	nd	<det	<det	<det	<det	0.119	826.430	0.701	44.145	<det	56.969	80.337	224.192	0.199	7.260	0.202	2.732	16.617	1.142	Chalcopyrite
34-3 CCP 5C	nv30e12	38.675	34.830	0.035	nd	<det	<det	<det	<det	0.127	571.019	0.645	27.106	0.640	17.318	87.139	173.877	0.018	2.228	0.193	1.469	77.082	1.579	Chalcopyrite
36 CCP 1A	nv30f04	31.861	34.830	0.076	nd	<det	<det	<det	<det	0.095	385.389	1.028	21.412	<det	253.435	16.948	298.097	0.023	<det	0.043	4.456	4.345	0.173	Chalcopyrite
36 CCP 1B	nv30f05	35.035	34.830	0.115	nd	<det	<det	<det	<det	0.178	183.111	<det	30.294	<det	227.056	13.223	84.130	<det	0.301	0.069	2.234	2.423	0.635	Chalcopyrite
36 CCP 1C	nv30f06	34.482	34.830	0.044	nd	<det	<det	<det	0.053	<det	311.283	0.940	17.716	<det	258.682	14.375	137.525	0.023	0.181	0.069	2.059	5.565	0.206	Chalcopyrite
36 CCP 2A	nv30f07	33.319	34.830	0.083	nd	<det	<det	<det	<det	0.116	379.353	0.598	30.389	0.137	248.694	19.266	229.189	0.014	4.072	0.032	2.328	4.535	0.166	Chalcopyrite
36 CCP 2B	nv30f08	33.918	34.830	<det	nd	<det	<det	<det	<det	0.315	430.998	0.625	28.808	0.053	248.202	22.624	222.883	<det	0.648	<det	1.731	1.608	0.511	Chalcopyrite
36 CCP 2C	nv30f09	32.211	34.830	<det	nd	<det	<det	<det	<det	<det	381.938	0.111	25.700	<det	226.823	22.101	162.068	<det	<det	0.021	1.754	1.086	0.281	Chalcopyrite
36 CCP 2D	nv30f10	35.088	34.830	0.046	nd	<det	<det	<det	<det	<det	425.242	0.491	25.919	0.031	267.627	25.940	279.230	<det	0.292	0.032	1.847	2.065	0.339	Chalcopyrite
38 CCP 1A	nv30g04	35.024	34.830	0.545	nd	<det	<det	<det	<det	0.058	413.950	0.378	22.786	0.218	5.001	19.524	70.869	<det	0.490	0.051	2.059	21.387	0.134	Chalcopyrite
38 CCP 1B	nv30g05	35.058	34.830	0.253	nd	<det	<det	<det	<det	0.125	270.131	1.310	15.422	1.191	58.354	25.290	77.206	0.042	0.468	0.050	0.134	53.257	0.090	Chalcopyrite
38 CCP 2A	nv30g08	34.316	34.830	0.037	nd	<det	<det	<det	<det	<det	487.315	0.736	31.488	0.510	22.441	32.642	193.175	0.072	1.055	0.145	1.681	17.950	0.413	Chalcopyrite
38 CCP 2B	nv30g09	33.841	34.830	<det	nd	<det	<det	<det	<det	<det	519.876	<det	27.293	<det	18.956	34.349	141.524	0.022	0.422	0.064	2.182	5.171	0.340	Chalcopyrite
38 CCP 3A	nv30g10	34.137	34.830	<det	nd	<det	<det	<det	<det	<det	344.237	0.878	27.851	<det	8.905	19.629	62.276	0.022	2.126	0.319	1.195	18.566	1.104	Chalcopyrite
38 CCP 4A	nv30g12	36.749	34.830	<det	nd	<det	<det	<det	<det	<det	329.367	0.681	25.317	<det	2.737	23.626	74.125	0.085	0.935	0.020	2.687	61.245	0.371	Chalcopyrite
38 CCP 5A	nv30g13	34.535	34.830	0.079	nd	<det	<det	<det	0.038	0.089	428.998	<det	29.816	0.327	10.790	32.952	168.434	<det	2.059	0.043	0.915	7.067	0.221	Chalcopyrite
38 CCP 5B	nv30g14	36.562	34.830	0.016	nd	<det	<det	<det	<det	<det	480.473	<det	24.572	<det	4.288	24.259	71.810	0.039	0.568	0.047	0.789	8.086	0.095	Chalcopyrite
PENTLANDITE (n = 37)																								
21 PN 3A	nv25d04	35.293	33.210	0.802	<det	0.846	<det	<det	<det	0.214	419.761	207.846	96.865	0.310	<det	0.413	0.506	0.142	3.785	0.070	1.288	4.522	0.409	Pentlandite
21 PN 3B	nv25d05	23.563	33.210	0.664	<det	<det	<det	<det	<det	<det	922.528	36.223	75.660	<det	0.79	7.346	0.566	<det	9.011	0.040	1.355	2.773	0.539	Pentlandite
21 PN 4A	nv25d08	30.041	33.210	0.829	<det	<det	<det	<det	<det	0.633	<det	111.139	64.147	<det	0.647	<det	0.455	0.068	0.744	0.154	1.589	8.080	0.376	Pentlandite
21 PN 4B	nv25d09	37.437	33.210	1.134	0.216	<det	<det	<det	<det	2.139	<det	<det	91.973	<det	0.786	<det	0.612	0.054	11.178	<det	1.748	2.583	0.369	Pentlandite
21 PN 2B	nv25d17	44.750	33.210	0.5720	0.114	0.029	<det	<det	<det	2.794	<det	6.477	20.114	0.915	0.179	<det	0.327	0.084	3.232	0.012	0.936	2.009	0.060	Pentlandite
22A PN 1A	nv25e04	40.572	33.210	0.538	<det	0.186	<det	<det	<det	2.654	<det	249.294	45.450	0.496	<det	0.698	0.878	0.062	0.495	0.417	1.211	6.026	0.480	Pentlandite
22A PN 1B	nv25e05	34.753	33.210	0.4230	0.328	0.202	<det	<det	<det	0.595	39.155	611.406	39.807	0.439	2.613	0.694	1.393	0.506	8.143	0.493	0.633	29.138	0.488	Pentlandite
22A PN 1C	nv25e06	41.561	33.210	0.7000	0.124	<det	<det	<det	0.0330	0.580	24.243	67.370	52.082	3.620	1.044	1.097	0.679	0.150	6.920	0.057	0.557	16.188	0.370	Pentlandite
22A PN 2A	nv25e07	35.448	33.210	1.5140	0.153	0.154	<det	<det	<det	0.542	49.511	9.866	50.839	0.120	2.103	<det	0.225	0.091	4.379	0.036	0.718	2.029	0.172	Pentlandite
22A PN 2B	nv25e08	28.574	33.210	1.594	<det	<det	<det	<det	0.0120	<det	146.445	94.102	64.364	<det	1.326	0.098	0.283	0.070	0.825	0.029	1.033	1.131	0.030	Pentlandite
22B-1 PN 4C	nv29a14	34.140	33.210	2.0320	1.473	<det	<det	0.0200	<det	0.346	41.466	16.728	64.359	0.234	15.256	0.477	0.452	0.103	22.089	0.015	0.572	36.287	1.338	Pentlandite
22B-1 PN 4D	nv29a15	32.610	33.210	3.856	1.860	<det	<det	<det	<det	<det	3.170	8.794	57.688	<det	18.721	0.099	0.294	0.039	12.750	0.023	0.708	26.358	0.559	Pentlandite
22B-1 PN 5B	nv29a17	32.213	33.210	0.218	0.195	0.049	<det	0.0110	0.1850	0.197	23.056	1.445	56.514	0.190	31.233	0.117	0.274	0.079	0.970	0.022	0.894	44.890	0.419	Pentlandite
22B-2 PN 1C	nv29b06	34.569	33.210	13.753	<det	7.506	0.2320	0.2520	<det	0.458	131.368	<det	39.327	1.507	9.135	<det	1.722	0.488	3.368	0.713	8.936	62.184	4.125	Pentlandite

22B-2 PN 1D	nv29b07	33.528	33.210	15.500	<det	<det	<det	<det	<det	0.040	<det	2.141	49.700	<det	7.714	0.840	4.413	0.198	6.425	<det	6.592	63.294	3.646	Pentlandite
22B-2 PN 2A	nv29b12	30.560	33.210	0.851	<det	0.069	<det	<det	<det	0.102	<det	0.662	20.217	<det	0.704	<det	0.088	0.015	0.822	0.000	0.206	2.812	0.093	Pentlandite
22B-2 PN 2B	nv29b13	32.300	33.210	0.772	nd	<det	<det	<det	<det	0.041	3.278	0.361	21.576	<det	0.237	<det	0.050	<det	0.287	0.001	0.142	1.978	0.022	Pentlandite
23 PN 1A	nv29c04	29.941	33.210	0.182	<det	<det	<det	<det	<det	1.517	435.554	4.347	56.347	0.798	0.715	0.198	3.196	0.693	3.597	0.489	1.993	50.075	0.342	Pentlandite
23 PN 1B	nv29c05	33.230	33.210	0.117	<det	0.469	<det	<det	<det	0.280	20.974	1.149	57.220	0.671	0.807	0.196	0.732	0.246	0.885	0.188	1.049	13.977	1.752	Pentlandite
23 PN 2A	nv29c07	38.835	33.210	0.127	0.841	0.132	<det	<det	<det	1.242	44.856	1.075	51.893	0.094	7.857	7.447	0.953	0.199	7.306	0.001	2.146	5.902	0.726	Pentlandite
23 PN 3A	nv29c13	33.334	33.210	0.173	<det	<det	<det	<det	<det	0.543	7.555	3.634	55.149	0.256	1.243	<det	0.370	0.150	1.284	0.063	0.627	9.634	0.731	Pentlandite
23 PN 3B	nv29c14	33.301	33.210	0.207	<det	0.337	<det	<det	<det	0.174	1.202	1.500	58.570	0.055	1.581	0.090	0.240	0.718	2.847	0.082	0.858	7.446	0.733	Pentlandite
25-1 PN 1B	nv29e05	33.713	33.210	0.661	0.337	<det	<det	<det	<det	0.655	27.507	4.895	53.991	<det	0.271	0.300	0.171	0.049	1.979	0.008	0.785	3.725	0.106	Pentlandite
25-1 PN 1C	nv29e06	35.050	33.210	0.613	<det	<det	<det	<det	<det	1.758	33.573	0.997	54.358	2.218	0.440	0.113	0.193	<det	7.909	0.003	0.792	47.697	0.067	Pentlandite
25-1 PN 1D	nv29e07	33.241	33.210	0.319	nd	<det	<det	<det	<det	2.325	41.339	0.648	56.787	0.551	0.537	0.229	0.243	0.040	7.631	0.028	0.699	7.157	0.156	Pentlandite
25-1 PN 4A	nv29e15	33.077	33.210	0.476	0.079	<det	<det	<det	<det	0.054	3.697	2.350	52.521	0.069	1.438	<det	0.193	0.036	0.732	0.003	0.569	1.498	0.069	Pentlandite
25-1 PN 4B	nv29e16	35.746	33.210	0.526	<det	<det	<det	<det	0.032	0.231	18.675	0.656	57.557	0.370	1.458	0.337	0.458	0.035	1.008	0.030	0.923	2.601	0.386	Pentlandite
26-1 PN 1D	nv29f07	30.673	33.210	0.415	0.269	<det	<det	<det	<det	0.422	1.135	1.011	51.803	0.746	9.888	<det	0.272	0.027	1.030	0.068	0.726	10.026	2.032	Pentlandite
26-1 PN 2A	nv29f08	34.152	33.210	1.949	<det	<det	<det	<det	<det	<det	<det	0.713	75.507	0.242	0.668	<det	0.268	0.040	12.144	0.004	0.945	3.021	0.248	Pentlandite
26-1 PN 3A	nv29f11	33.340	33.210	1.288	<det	0.239	<det	<det	<det	0.880	18.463	4.005	59.984	0.599	0.976	<det	0.926	0.260	3.211	0.149	0.746	12.458	0.651	Pentlandite
29-2 PN 1C	nv30b06	33.970	33.210	4.258	3.925	<det	<det	0.035	<det	1.690	63.203	1.262	55.787	<det	2.780	0.398	1.024	0.324	0.989	0.048	0.460	10.188	0.951	Pentlandite
29-2 PN 3C	nv30b12	34.877	33.210	7.294	<det	<det	<det	<det	<det	0.343	8.264	0.392	50.780	<det	0.422	<det	0.449	0.097	0.343	0.002	0.733	4.492	0.302	Pentlandite
29-2 PN 3D	nv30b13	34.047	33.210	6.328	<det	<det	<det	<det	0.0110	0.563	15.256	0.545	46.991	1.086	1.078	0.365	0.151	0.112	0.282	0.023	0.692	na	0.376	Pentlandite
29-2 PN 4C	nv30b16	32.462	33.210	1.054	<det	<det	<det	<det	<det	0.656	92.480	1.392	35.696	<det	3.666	35.660	1.937	0.063	1.347	0.010	0.663	43.246	1.046	Pentlandite
29-2 PN 4D	nv30b17	34.570	33.210	1.676	<det	<det	<det	<det	<det	0.417	22.650	1.281	45.403	0.128	3.402	12.947	1.961	0.128	1.302	0.032	0.485	26.687	1.467	Pentlandite
34-3 PN 3B	nv30e05	32.284	33.210	0.332	<det	0.711	<det	<det	<det	0.140	6.228	6.882	61.460	0.407	3.616	0.449	0.688	0.070	0.935	0.106	0.596	57.161	2.014	Pentlandite
34-3 PN 5B	nv30e11	34.219	33.210	1.180	<det	0.179	<det	<det	<det	0.946	4.826	0.165	24.532	0.449	56.371	0.244	0.686	<det	0.894	0.058	0.606	21.038	2.637	Pentlandite
GALENA (n = 17)																								
28-5 GN 1A	nv29g04	13.389	13.080	1.900	nd	<det	<det	0.0400	0.1220	0.926	5919.090	3.376	1000.144	0.214	479.213	101.675	34.036	0.774	136.038	0.249	3.071	na	51.729	Galena
28-5 GN 2A	nv29g06	12.902	13.080	5.813	nd	<det	<det	<det	<det	0.043	8.670	<det	1321.090	0.847	307.046	69.580	8.049	<det	60.385	<det	0.644	na	31.657	Galena
28-5 GN 4D	nv30a08	12.887	13.080	0.034	nd	<det	<det	<det	0.0890	1.133	<det	51.372	1536.316	<det	459.008	94.195	11.341	<det	105.621	0.008	<det	na	33.213	Galena
28-5 GN 4D	nv30a10	13.384	13.080	4.092	nd	<det	<det	<det	<det	<det	2.034	1.923	1697.721	<det	750.186	162.267	51.315	0.042	170.337	0.026	<det	na	107.338	Galena
28-5 GN 6A	nv30a11	13.454	13.080	0.019	nd	<det	<det	<det	<det	<det	<det	0.173	1536.808	0.565	809.962	95.760	14.449	0.025	241.824	0.012	0.130	na	39.065	Galena
28-5 GN 6B	nv30a12	13.457	13.080	<det	nd	<det	<det	<det	<det	<det	4.884	0.329	1581.647	<det	933.879	96.874	11.913	0.124	302.487	0.003	<det	na	24.068	Galena
33-3 GN 1A	nv30c04	13.172	13.080	0.182	nd	<det	<det	<det	<det	0.192	<det	0.106	1731.359	0.152	5822.823	398.700	19.081	2.699	2708.174	<det	<det	na	na	Galena
33-3 GN 1B	nv30c05	13.251	13.080	0.311	nd	<det	<det	<det	<det	0.329	116.973	0.124	1873.956	<det	5819.413	152.486	16.410	1.128	1762.854	0.118	0.167	na	na	Galena
34-3 GN 1A	nv30d04	18.352	13.080	7.055	nd	<det	<det	0.0260	<det	<det	<det	0.488	3135.267	0.552	7092.047	263.856	5.004	1.820	2055.657	1.826	<det	na	na	Galena
36 GN R1	nv30f14	15.620	13.080	nd	nd	<det	<det	<det	0.0110	0.509	33.963	0.228	1269.607	0.065	4997.433	45.103	1.355	<det	50.516	0.000	0.134	na	na	Galena
36 GN R2A	nv30f15	13.718	13.080	<det	nd	<det	<det	<det	<det	0.115	<det	11.754	1246.890	<det	5874.584	54.573	2.657	0.227	61.788	0.005	0.089	na	na	Galena
36 GN R2B	nv30f16	12.969	13.080	nd	nd	<det	<det	<det	0.0400	0.658	22.682	0.226	1392.229	0.190	7084.014	115.703	5.465	0.879	75.962	0.007	0.091	na	na	Galena
36 GN R2C	nv30f17	14.538	13.080	0.0200	nd	<det	<det	<det	<det	0.887	13.019	0.150	1430.921	<det	6343.111	79.116	4.784	0.559	68.778	0.020	0.070	na	na	Galena
38 GN 1C	nv30g06	13.910	13.080	0.069	nd	<det	<det	<det	<det	<det	2.189	16.969	16.606	0.022	70.945	1.375	0.118	0.234	24.384	2.548	<det	na	na	Galena
38 GN 1D	nv30g07	13.373	13.080	<det	nd	<det	<det	<det	<det	0.035	<det	107.841	10.403	0.033	18.710	3.689	0.053	0.130	9.261	0.091	<det	na	na	Galena
38 GN/PO 5D	nv30g16	13.610	13.080							0.779	9.535	82.800	13.038	0.029	3.788	0.120	0.039	0.889	27.684	0.140	0.153	na	na	Galena
38 GN R1	nv30g17	13.532	13.080	nd	nd	<det	<det	<det	0.0250	<det	9.294	0.199	1413.411	0.030	5993.401	111.596	0.176	3.834	377.057	0.023	0.148	na	na	Galena
CUBANITE (n = 4)																								
24-2 CB 2C	nv29d09	40.085	35.160	0.217	nd	<det	<det	<det	<det	1.065	694.899	<det	54.466	<det	13.969	48.710	1.927	0.082	4.858	0.084	0.911	6.504	<det	Cubanite
24-2 CB 3A	nv29d11	36.037	35.160	0.153	nd	<det	<det	<det	<det	0.333	614.333	0.186	47.559	<det	23.465	53.296	4.873	0.022	9.246	<det	2.254	10.888	0.157	Cubanite
24-2 CB 3B	nv29d12	34.158	35.160	0.107	nd	<det	<det	<det	<det	0.036	654.201	0.186	68.124	<det	22.541	51.850	3.447	<det	6.095	0.003	1.788	9.022	0.121	Cubanite
24-2 CB 3C	nv29d13	31.696	35.160	0.057	nd	<det	<det	<det	<det	<det	482.220	2.878	58.493	1.059	52.486	37.071	1.833	0.121	3.921	0.096	1.142	6.634	0.036	Cubanite
BORNITE (n = 5)																								
28-5 BN 2B	nv29g07	21.651	23.790	0.095	nd	<det	<det	<det	<det	<det	176.436	<det	<det	1.144	28.915	7.829	0.138	<det	1.938	<det	1.219	na	6.590	Bornite
28-5 BN 2D	nv29g09	28.330	23.790	<det	nd	<det	<det	<det	<det	<det	62.846	1.397	2.999	<det	527.796	3.210	2.459	<det	0.111	0.144	2.973	na	5.168	Bornite
28-5 BN 7B	nv30a14	25.818	23.790	<det	nd	<det	<det	<det	<det	<det	35.402	1.241	11.679	1.034	4483.337	3.295	1.047	<det	0.877	<det	<det	na	11.543	Bornite
28-5 BN 8A	nv30a16	23.545	23.790	0.013	nd	<det	<det	<det	0.1540	<det	42.022	0.316	16.268	<det	199.465	<det	11.668	0.279	1.939	<det	3.048	na	4.587	Bornite
28-5 BN 8B	nv30a17	27.590	23.790	0.190	nd	<det	<det	0.0190	<det	<det	<det	<det	<det	2.046	7148.352	<det	68.918	<det	<det	0.028	3.933	na	3.668	Bornite
PYRITE (n = 2)																								
36 PY 3A	nv30f11	52.600	53.450	<det	nd	0.086	<det	<det	<det	<det	0.949	0.548	16.838	<det	0.596	<det	<det	0.171	0.664	<det	0.525	1.695	0.568	Pyrite
36 PY 3B	nv30f12	50.819	53.450	<det	nd	<det	<det	<det	<det	0.328	81.650	1.346	3.221	<det	30.691	12.875	5.519	0.080	0.185	<det	<det	6.708	0.162	Pyrite

nd = not determined (where both isotopes were greater than the correction value)

na = not analyzed

<det = below detection

APPENDIX 4.IVb. *In situ* rare earth element (REE) and other trace element analysis compositions of olivine, pyroxene, hornblende, biotite, chlorite, and plagioclase determined by LA-ICP-MS.

	Element	SiO2	CaO	Sc	TiO2	V	Cr	Co	Ni	Rb	Sr	Y	Zr	Nb	Sn	Sb	Ba	La	Ce	Sm	Eu	Gd	Ho	Yb	Hf	Ta	Pb	Bi	Th	U	Mineral
	Isotopic Mass	29	43	45	49	51	53	59	60	85	86	89	90	93	118	121	137	139	140	147	151	157	165	172	178	181	208	209	232	238	
	Unit	wt%	wt%	ppm	wt%	ppm	ppm	ppm	ppm	ppm	ppm	ppm	ppm	ppm	ppm	ppm	ppm	ppm	ppm	ppm	ppm	ppm	ppm	ppm	ppm	ppm	ppm	ppm	ppm	ppm	
Sample No.	Detection Limit	0.100	0.050	0.500	0.003	0.500	10.000	0.500	3.000	0.100	0.500	0.100	0.100	0.100	0.100	0.100	0.500	0.100	0.100	0.100	0.050	0.050	0.010	0.050	0.050	0.010	0.100	0.010	0.010	0.010	
OLIVINE (n = 11)																															
24-2 (5) OL-d	au24c04	34.150	<det	4.035	<det	<det	<det	226.433	837.907	0.618	1.225	0.284	1.265	<det	0.742	<det	4.261	0.155	<det	<det	0.118	0.158	<det	<det	<det	<det	0.275	0.061	<det	<det	Olivine
24-2 (5) OL-f	au24c05	35.260	<det	0.935	<det	<det	<det	229.783	859.661	<det	<det	<det	0.605	<det	<det	0.515	<det	<det	<det	0.194	0.171	<det	0.016	<det	0.142	<det	0.545	<det	<det	0.019	Olivine
24-2 (5) OL-g	au24c06	34.950	0.090	1.798	<det	<det	<det	223.184	888.196	0.175	2.941	<det	<det	0.120	<det	<det	<det	0.116	0.211	<det	<det	0.055	0.013	<det	<det	<det	0.357	0.048	<det	0.016	Olivine
24-2 (6) OL	au24c14	34.150	0.050	2.061	0.007	1.111	<det	141.032	815.616	1.079	3.888	0.145	1.728	<det	0.770	0.280	14.697	0.109	0.100	<det	<det	0.301	<det	0.084	0.096	0.020	2.974	0.038	<det	<det	Olivine
24-2 (6) OL-b	au24c15	32.820	<det	1.629	0.006	0.555	<det	216.123	1064.616	0.297	1.991	<det	0.233	<det	<det	0.466	8.849	0.446	0.842	<det	<det	<det	<det	0.101	<det	0.026	1.128	0.023	0.044	0.020	Olivine
24-2 (6) OL-e	au24c16	34.630	0.134	3.279	0.016	3.101	<det	227.297	1133.539	<det	<det	<det	0.819	0.214	<det	<det	16.571	<det	0.360	<det	0.100	0.552	0.037	0.196	0.060	<det	2.339	<det	0.023	<det	Olivine
24-2 (7) OL-g	au25a04	34.440	0.140	3.021	0.015	1.588	14.733	244.079	1134.679	0.278	<det	<det	<det	<det	0.708	0.229	<det	0.111	0.126	0.489	<det	<det	<det	<det	0.045	1.249	0.027	<det	<det	Olivine
24-2 (8) OL-a	au25a12	34.570	0.083	3.839	0.022	<det	<det	236.631	1111.014	0.382	3.476	<det	3.434	<det	2.167	0.348	23.705	0.159	<det	0.189	<det	0.561	0.013	<det	0.054	<det	1.392	0.018	0.013	0.010	Olivine
24-2 (8) OL-c	au25a13	33.520	<det	2.916	<det	0.764	15.819	216.537	1023.748	0.305	<det	0.403	2.080	<det	0.501	<det	24.521	<det	0.488	<det	<det	<det	<det	0.084	<det	1.355	<det	0.039	<det	Olivine
28-4 (6) OL-d	au25c17	34.360	0.165	2.102	0.009	0.669	781.091	206.660	832.067	0.176	8.717	0.316	2.383	<det	3.041	0.917	6.839	0.199	0.281	<det	<det	<det	0.022	0.092	<det	0.011	11.221	0.033	0.022	0.018	Olivine
29 (8) Ol-a-b	au31a10	36.060	<det	3.161	0.004	<det	12.281	221.708	1307.507	<det	<det	<det	5.459	0.167	2.943	<det	18.644	<det	0.175	<det	0.076	<det	0.051	0.191	0.244	0.020	9.872	0.038	<det	<det	Olivine
ORTHOPYROXENE (n = 5)																															
39 (4) PX-c	au24b10	50.730	0.700	7.366	0.186	19.770	42.844	71.886	80.101	<det	2.648	0.854	1.282	0.208	0.536	0.221	0.664	0.765	1.093	0.504	0.054	0.616	0.046	0.403	<det	<det	4.744	<det	0.076	0.032	Orthopyroxene
39 (4) PX-b	au24b11	51.700	0.712	8.180	0.108	16.591	46.052	79.390	65.765	<det	<det	0.853	2.677	<det	1.195	<det	0.923	0.343	0.837	0.548	<det	0.242	0.100	0.329	0.054	<det	0.951	<det	0.036	<det	Orthopyroxene
23 (6) PX-a	au25b14	50.770	0.715	8.147	0.059	26.960	53.469	87.169	333.565	<det	1.299	0.520	1.288	0.273	0.299	0.567	3.405	<det	<det	<det	<det	0.169	<det	<det	<det	<det	0.316	0.070	0.013	0.028	Orthopyroxene
23 (6) PX-b	au25b15	50.540	0.546	10.458	0.049	28.938	74.308	92.235	346.368	0.520	0.557	0.445	3.008	0.153	<det	<det	2.194	<det	<det	0.190	<det	<det	0.032	0.219	<det	<det	<det	<det	<det	0.037	Orthopyroxene
27c-1 (1) CPX-OL?	se01a06	50.500	0.763	21.804	0.116	89.316	100.175	87.744	153.787	0.220	3.532	7.504	1.263	1.947	1.438	0.512	1.343	0.873	2.849	<det	0.096	0.485	0.360	3.047	<det	0.147	15.070	0.116	0.110	0.076	Orthopyroxene
HORNBLENDE (n = 63)																															
39 (2) HN-d	au24a08	42.660	10.994	46.648	2.593	304.654	369.493	64.004	130.331	0.785	89.918	78.402	176.194	4.798	25.132	0.357	68.595	17.015	63.502	17.164	4.111	17.030	2.879	7.415	6.387	0.193	87.743	0.183	0.425	0.070	Hornblende
39 (2) HN	au24a09	43.000	10.656	47.909	2.455	285.784	281.380	65.589	130.160	0.943	84.505	73.706	169.406	6.716	25.813	<det	62.543	18.416	64.409	15.218	4.578	16.346	2.969	6.877	6.613	0.288	89.288	0.214	0.366	0.042	Hornblende
39 (2) HN	au24a10	43.000	10.517	52.219	2.472	307.402	280.094	62.422	136.292	1.108	94.789	77.452	170.569	7.691	29.765	0.286	72.713	18.661	65.853	16.079	4.115	16.065	2.814	7.298	6.547	0.298	95.749	0.236	0.426	0.061	Hornblende
39 (3) HN-c	au24a14	42.870	10.876	53.196	2.229	194.856	137.265	59.948	114.567	<det	124.945	71.874	156.227	8.873	20.379	0.449	52.123	19.437	70.040	16.669	4.261	16.296	2.591	6.776	6.479	0.507	107.917	0.233	0.477	0.052	Hornblende
39 (3) HN-a	au24a15	42.600	10.704	46.283	2.431	187.797	52.458	64.344	114.687	0.818	88.828	66.928	170.939	11.146	18.589	0.521	48.273	17.027	63.415	15.151	4.494	14.761	2.397	6.176	5.291	0.564	84.239	0.191	0.454	0.073	Hornblende
39 (3) HN-f	au24a16	42.910	11.220	39.952	2.275	193.274	72.595	62.071	120.997	0.913	90.591	72.206	185.451	9.237	24.596	0.300	59.361	20.606	75.320	15.567	6.092	17.389	2.579	8.268	6.071	0.588	89.434	0.465	0.503	0.046	Hornblende
39 (3) HN	au24a17	43.000	10.990	51.903	2.416	194.631	129.455	60.797	113.938	0.861	122.390	70.034	172.608	10.825	20.732	<det	74.637	27.864	84.422	15.681	5.001	16.158	2.732	6.290	6.672	0.667	96.895	0.212	0.659	0.120	Hornblende
39 (4) HN	au24b07	43.000	10.485	48.366	2.482	153.737	47.346	58.958	117.527	1.240	88.116	62.031	163.047	12.702	25.293	<det	56.857	18.601	63.847	14.865	4.888	13.201	2.408	6.109	5.694	0.804	85.897	0.245	0.446	0.054	Hornblende
39 (4) HN-e	au24b08	42.250	10.537	41.986	2.411	146.253	87.257	62.074	103.229	1.009	82.811	59.532	155.819	13.078	24.360	<det	54.763	17.510	61.598	14.487	4.304	13.248	2.371	5.848	5.626	0.933	85.847	0.318	0.439	0.047	Hornblende
39 (4) HN	au24b12	43.000	11.387	52.965	2.567	248.143	71.663	62.765	104.521	1.224	90.084	66.512	163.782	11.066	26.222	<det	64.176	16.931	59.018	15.512	4.035	17.509	2.460	6.140	6.585	0.795	94.433	0.191	0.506	0.061	Hornblende
39 (5) HNoik-e	au24b13	43.680	9.579	139.853	2.345	497.996	62.482	68.975	96.123	0.912	65.841	73.026	115.861	6.704	12.967	<det	72.471	14.561	53.524	15.358	3.859	16.735	2.750	7.015	5.926	0.314	72.816	0.199	0.339	0.055	Hornblende
39 (5) HN-h+i	au24b14	44.870	10.440	94.727	2.348	358.494	114.036	70.820	97.128	0.521	53.710	57.259	116.836	3.790	11.773	<det	68.205	12.366	47.034	12.635	3.569	12.977	2.171	5.362	4.343	0.186	61.867	0.222	0.263	0.021	Hornblende
39 (5) HN-j	au24b15	44.360	11.186	129.780	2.232	447.236	92.331	68.367	98.914	1.254	62.284	72.728	124.217	6.346	11.674	<det	68.511	17.055	59.253	15.778	3.746	16.252	2.837	6.751	5.336	0.299	66.885	0.213	0.585	0.112	Hornblende
39 (5) HN	au24b16	43.000	9.994	128.699	2.194	464.602	82.287	71.040	104.508	1.339	53.257	60.402	117.810	4.954	10.923	<det	58.001	14.683	54.494	12.656	3.400	12.933	2.298	5.742	5.136	0.311	65.805	0.245	0.542	0.049	Hornblende
39 (5) HN	au24b17	43.000	10.048	136.167	2.362	497.165	92.395	72.646	100.880	0.584	61.835	67.116	133.394	5.891	12.058	<det	71.484	13.787	51.673	15.338	3.556	14.807	2.714	6.327	5.521	0.321	75.181	0.161	0.238	0.051	Hornblende
24-2 (5) BT-c	au24c09	42.470	10.268	82.792	2.020	593.249	71.594	67.735	370.374	3.209	84.032	76.115	198.050	4.436	6.100	<det	102.904	13.300	47.213	14.737	3.399	19.903	3.076	6.112	8.692	0.314	8.815	<det	0.307	0.076	Hornblende
24-2 (5) HN	au24c10	43.000	10.782	107.006	1.926	823.400	1284.744	64.504	312.451	1.144	81.963	61.962	163.871	6.732	5.786	<det	106.287	13.682	52.900	13.392	3.603	13.920	2.466	6.800	10.724	0.314	7.009	<det	0.240	0.024	Hornblende
24-2 (5) ALT-h	au24c11	43.530	10.290	130.059	1.890	379.890	13.190	68.943	405.084	0.300	58.108	64.207	163.839	3.134	6.388	<det	78.532	9.821	39.426	13.265	2.540	15.215	2.646	5.712	8.705	0.136	6.252	<det	0.159	0.053	Hornblende
24-2 (6) BT-g	au24c13	41.150	9.309	32.353	1.882	321.684	513.075	59.994	448.873	0.540	84.829	42.524	203.009	8.039	16.394	<det	43.164	9.530	40.267	10.549	3.071	8.920	1.755	4.415	5.072	0.721	17.267	0.102	0.510	0.052	Hornblende
24-2 (6) HN-i	au24c17	40.980	9.836	35.895	2.075	308.697	364.283	66.347	601.343	0.312	86.955	41.847	208.574	8.733	16.845	<det	78.414	10.482	42.122	10.137	2.738	10.123	1.652	4.262	4.746	0.639	18.357	0.074	0.581	0.083	Hornblende
24-2 (7) HN	au25a05	43.000	9.987	59.616	2.927	359.762	518.615	83.454	723.442	0.695	78.515	55.991	233.863	8.267	19.232	0.816	73.821	11.613	49.347	13.194	3.646	10.805	2.360	6.779	3.751	0.382	24.748	0.073	0.613	0.129	Hornblende
24-2 (7) HN-l	au25a08	41.490	12.431	65.583	2.636	299.109	295.184	61.820	472.106	2.464	98.953	79.558	256.587	10.085	15.135	<det	121.401	46.666	135.625	21.493	4.138	17.963	2.666	7.691	8.046	0.804	23.175	0.099	3.830	0.516	Hornblende
24-2 (7) BT-c	au25a09	42.180	10.196	151.289	2.472	305.172	134.741	73.574	505.099	0.586	65.625	71.725	1119.957	6.802	16.786	<det	51.577	9.724	43.578	15.449	3.392	19.200	3.311	6.970	32.815	0.481	17.596	0.052	0.711	0.129	Hornblende
24-2 (7) PX-e	au25a11	41.910	8.097	104.233	1.613	230.316	107.657	68.904	403.696	<det	55.670	38.508	128.676	4.176	9.742	<det	32.587	6.081	24.689	8.063	1.923	7.740	1.541	3.675	5.436	0.257	11.844	0.024	0.502	0.033	Hornblende
24-2 (8) BT-f	au25a16	41.890	10.899	66.065	2.488	367.461	388.301	66.877	426.877	0.475	80.856	57.908	227.587	9.325	10.553	<det	87.610	12.022	45.701	12.803	3.099	12.573	2.095	5.435	6.779	0.584	13.341	0.062	0.447	0.036	Hornblende
24-2 (8) BT-e	au25a17	41.780	9.659	59.361	2.601	358.899	403.328	82.017	571.534	1.055	69.157	46.256	180.946	7.598	9.004	<det	70.968	9.916	37.367	11.502	2.544	8.617	1.806	5.036	5.891	0.274	11.237	0.079	0.456	0.041	Hornblende
23 (4) HN-d	au25b04	42.550	10.528	53.277	1.862	317.398	709.469	73.110	560.312	0.971	60.101	21.854	113.923	5.251	7.879	<det	84.672	7.751	23.709	4.187	1.569	3.666	0.812	2.371	2.875	0.382	13.187	0.047	0.268	0.109	Hornblende
23 (4) HN-e	au25b05	43.290	10.656	49.688	1.838	311.868	706.977	80.568	581.976	1.274	55.993	20.921	107.655	6.268	8.589	0.307	101.314	8.147	26.335	3.993	1.354	4.671	0.747	1.992	2.853	0.320	12.281	<det	0.327	0.023	Hornblende
23 (4) HN-c	au25b06	42.660	10.857	55.642	1.929	331.831	764.992	81.638	590.233	0.785	71.822	24.778	127.793	6.223	9.504	0.366	80.503	8.153	26.709	5.240	1.784	5.522	0.853	2.572	3.155	0.375	13.865	0.014	0.351	0.105	Hornblende
23 (5) HN-b	au25b07	42.730	11.688	60.199	1.860	296.527	820.956	90.700	634.229	1.923	80.729	31.398	163.573	6.351	9.655	<det	125.034	10.143	32.426	6.113	2.209	7.031	1.177	3.070	4.378	0.484	14.805	0.127	0.480	0.132	Hornblende
23 (5) HN-a	au25b08	43.080	11.884	57.829	2.070	302.642	553.651	89.541	666.888	1.593	92.576	29.458	158.246	6.412	9.264	<det	142.474	11.675	35.741	5.698	1.970	6.133	1.093	3.307	4.128	0.574	16.245	0.149	0.648	0.151	Hornblende
23 (5) HN-d	au25b09	42.250	11.103	63.046	1.632	299.867	567.742	82.814	557.339	1.397	75.994	28.551	158.790	6.262	8.889	0.561	115.062	8.897	29.462	6.431	1.639	7.066	1.149	2.943	4.444	0.507	13.038	0.125	0.477	0.123	Hornblende
23 (5) HN-c	au25b10	42.350	11.025	64.762	1.533	296.124	662.852	90.245	805.201	1.077	69.096	25.597	154.833	6.331	8.274	0.403	116.348	10.663	31.679	5.364	1.964	5.328	1.020	2.935	4.207	0.528	13.207	0.081	0.524	0.161	Hornblende
23 (5) HN	au25b11	43.000	12.203	57.061	1.852	304.336	589.535	84.646	612.091	1.212	87.217	28.149	148.748	7.458	9.424	<det	125.740	10.896	32.437	7.775	2.198	5.628	1.242	2.845	4.591	0.598	14.113	0.077	0.489	0.118	Hornblende
23 (5) HN	au25b12	43.000	11.881	58.179	1.969	310.285	862.377	89.131	571.447	2.126	79.688	27.511	138.927	6.640	9.576	0.198	129.021	11.098	29.905	6.628	1.681	5.645	1.127	2.710	3.484	0.496	13.572	0.107	0.405	0.123	Hornblende
23 (6) HN-c	au25b16	42.120	10.855	60.738	1.300	266.940	550.630	77.331	575.779	0.857	51.281	33.421	151.895	6.524	8.488	0.193	79.942	10.120	31.824	7.452	2.038	8.079	1.247	3.654	4.300	0.308	10.417	0.156	0.477	0.054	Hornblende
23 (6) HN	au25b17	43.000	11.468	63.215	1.408	296.425	675.861	85.560	753.891	1.056	74.814	38.715	182.336	8.130	9.363	<det	102.157	10.604	34.509	10.207	2.044	9.150	1.573	3.792	6.087	0.514	12.203	0.066	0.419	0.104	Hornblende
28-4 (2) HN-a	au25c04	41.710	11.491	107.587	3.112	434.179	134.539	52.460	639.686	1.077	87.346	130.552	151.166	21.763	808.304	0.372	197.086	26.861	96.180	27.199	5.298	28.668	4.946	12.560	6.277	1.004	1989.284	93.743	0.170	0.045	Hornblende
28-4 (2) HN-b	au25c05	41.460	11.808	124.222	3.507	486.809	175.806	54.555	693.070	1.160	87.468	145.954	192.920	24.011	991.202	<det	357.054	29.695	107.901	32.304	6.226	33.827	5.882	13.190	7.907	1.087	147.024	<det	0.283	0.049	Hornblende
28-4 (2) HN-c	au25c06	42.480	12.694	132.561	3.032	484.440	141.335	54.665	728.921	1.102	88.123	142.601	145.012	22.821	867.175	0.214	265.633	29.325	104.676	29.081	6.374	33.052	5.572	13.214	6.793	1.085	533.809	0.249	0.273	0.036	Hornblende
28-4 (3) HN-b	au25c09	42.070	11.164	35.377	2.429	284.739	62.017	63.675	429.835	0.428	86.230	84.928	88.148	21.797	673.502	<det	63.743	20.906	82.135	22.718	4.998	20.580	3.137	7.019	3.698	1.534	93.664	0.125	0.203	0.023	Hornblende
28-4 (3) HN	au25c12	43.000	11.529	29.695	2.985	148.678	85.433	58.120	483.420	0.932	97.382	46.669	193.212	20.357	618.399	<det	68.245	20.791	73.616	12.786	4.099	12.829	1.699	4.362	5.480	1.183	144.638	0.114	0.325	0.055	Hornblende
28-4 (6) HN-a	au25c14	41.100	10.873	26.645	2.636	206.300	106.068	59.015	411.869	0.725	104.435	46.288	124.298	16.513	490.769	<det	37.593	16.884	61.019	11.934	3.575	10.466	1.659	3.802	3.925	0.957	153.155	0.069	0.267	0.056	Hornblende
28-4 (6) HN-c	au25c15	41.390	11.378	22.097	2.958	145.804	84.557	59.691	422.116	<det	103.311	26.084	150.790	9.326	651.465	0.744	28.147	15.232	49.582	8.411	3.623	6.992	0.961	3.050	2.508	0.509	163.979	0.097	0.389	0.044	Hornblende
29 (8) HN-c	au31a12	42.630	12.433	83.570	2.639	133.911	120.127	61.112	527.004	0.941	102.375	108.167	263.310	27.266	138.659	0.204	83.748	18.215	70.056	21.297	4.797	23.605	4.501	9.421	11.057	1.874	130.864	0.205	0.276	0.011	Hornblende
29 (8) HN	au31a13	43.000	12.573	87.921	2.967	224.848	96.642	57.514	535.617	0.720	99.403	94.873	278.532	17.189	158.966	0.888	90.462	20.573	72.768	19.820	5.144	23.175	3.914	8.108	10.476	1.095	161.676	0.181	0.246	0.083	Hornblende
29 (22) HN-d	au31a14	43.080	12.151	55.644	2.755	220.772	101.633	54.661	499.989	0.169	110.641	70.863	232.536	11.462	137.588	0.166	85.281	14.991	52.635	15.468	3.854	17.363	2.775	6.120	7.569	0.500	134.023	0.092	0.234	0.022	Hornblende
29 (22) HN	au31a15	43.000	12.245	56.787	2.734	233.096	83.125	56.193	495.269	0.668	106.342	72.657	234.439	11.488	142.175	0.624	111.475	14.645	53.617	16.077	4.298	18.409	2.650	6.029	7.956	0.563	135.989	0.142	0.235	0.034	Hornblende
29 (36) HN-d	au31b08	42.750	11.234	43.932	2.755	188.289	80.303	55.398	824.095	0.370	103.634	70.345	253.225	17.081	142.435	0.930	86.281	16.064	64.057	16.303	4.848	14.620	2.641	6.629	8.222	1.035	145.048	0.118	0.252	0.026	Hornblende
29 (36) HN-c	au31b09	43.160	11.337	48.645	2.666	214.617	85.729	53.912	483.674	0.916	85.948	64.299	239.255	14.015	133.130	<det	72.352	15.504	58.505	13.831	4.567	14.964	2.472	6.078	6.937	0.816	140.414	0.252	0.244	0.044	Hornblende
29 (36) HN	au31b10	43.000	12.560	45.421	2.574	222.117	96.245	53.817	469.042	0.542	95.577	67.437	248.744	13.853	136.144	0.157	77.752	15.516	59.772	15.365	4.600	15.169	2.695	6.286	6.877	0.700	148.015	0.098	0.253	0.030	Hornblende
29 (36) HN	au31b11	43.000	12.058	52.943	2.414	241.176	103.223	49.281	439.975	1.265	105.456	72.501	206.323	13.144	152.816	1.129	110.210	16.766	66.087	16.511	4.997	16.936	2.778	6.319	7.932	0.792	159.500	0.144	0.250	<det	Hornblende
29 (24) HN	au31b15	43.000	11.513	33.356	2.189	235.949	110.100	54.216	455.743	0.973	101.355	67.298	248.229	13.374	132.811	<det	86.835	15.963	58.440	16.089	4.605	15.550	2.520	6.367	7.814	0.819	152.372	0.084	0.226	<det	Hornblende
29 (24) HN	au31b16	43.000	12.524	28.317	2.074	232.186	137.951	51.714	454.193	1.052	95.901	62.960	225.445	12.706	134.696	<det	90.282	16.085	57.996	15.752	4.194	14.679	2.638	5.548	7.046	0.783	137.754	0.182	0.328	0.023	Hornblende
34-2 (1) HN-a	au31c04	42.890	11.665	53.284	1.921	364.188	88.036	59.010	472.617	1.180	98.531	82.977	144.390	20.611	279.252	<det	97.252	19.294	71.319	18.551	4.666	20.097	3.318	7.851	4.038	1.496	190.644	0.242	0.849	0.145	Hornblende
34-2 (1) HN-b	au31c05	42.810	11.417	56.097	1.954	357.718	105.664	59.281	470.569	0.986	85.310	77.427	186.789	16.214	285.767	<det	98.828	17.916	69.306	19.001	4.001	17.707	3.207	7.345	4.758	1.281	224.432	1.537	0.690	0.085	Hornblende
34-2 (3) HN	au31c12	43.000	11.228	55.427	2.363	366.151	137.083	61.633	438.772	0.692	85.665	81.344	209.676	10.860	284.866	0.790	233.142	14.789	70.979	18.200	4.353	21.075	3.066	6.859	6.475	0.497	229.900	0.254	0.628	0.087	Hornblende

34-2 (3) HN	au31c13	43.000	11.156	53.867	2.259	360.571	169.775	59.723	469.172	0.675	90.642	75.264	203.391	12.338	311.823	0.621	214.130	17.718	68.407	19.410	3.727	17.714	3.171	8.043	5.771	0.476	206.659	0.108	0.693	0.132	Hornblende
34-2 rCHL	au31c16	43.000	11.831	63.141	2.669	364.903	145.716	60.412	470.726	1.026	84.093	107.421	204.627	17.438	335.793	<det	141.142	19.689	79.341	25.562	4.676	26.081	4.129	9.173	6.785	1.745	181.888	0.194	0.864	0.148	Hornblende
27c-1 (2) BT-HN?	se01a11	43.000	5.112	36.091	2.303	321.916	394.042	60.402	180.294	71.088	42.207	10.636	4.110	50.119	5.036	<det	176.650	14.518	43.367	3.851	0.472	2.107	0.395	2.869	0.280	1.966	2.337	0.079	0.260	0.145	Hornblende
27c-1 (2) HN	se01a12	43.000	9.925	59.710	0.360	286.594	208.412	59.355	120.972	0.799	28.379	50.105	10.399	9.725	5.450	<det	8.107	17.463	71.119	12.892	1.038	10.812	1.819	4.609	0.567	0.278	5.545	0.062	0.023	0.024	Hornblende
27c-1 (3) HN	se01a16	43.000	10.349	65.918	0.324	183.239	152.147	58.800	133.760	<det	21.917	89.345	6.911	8.768	6.066	<det	38.035	18.934	99.713	23.759	1.305	19.203	3.055	8.448	0.646	0.348	4.948	0.100	0.025	0.055	Hornblende
27c-1 (3) OPX-HN?	se01a17	43.000	18.556	102.932	0.294	289.235	198.105	52.204	161.195	5.880	36.872	64.002	10.619	5.080	3.411	0.162	34.171	17.536	66.564	16.771	0.668	14.055	2.439	6.491	0.799	0.170	6.779	0.083	0.035	0.032	Hornblende
BIOTITE (n = 44)																															
39 (2) BT-e	au24a04	36.330	0.083	4.385	3.896	293.138	579.200	108.221	301.745	190.088	1.853	<det	2.550	7.215	7.272	<det	3447.144	<det	0.112	0.230	<det	<det	<det	0.122	0.064	0.263	152.672	0.019	<det	<det	Biotite
39 (2) BT-g	au24a05	36.010	0.065	5.563	4.489	278.509	454.365	104.469	297.353	193.655	6.962	0.355	3.758	8.456	7.836	0.176	3310.705	<det	0.285	0.261	<det	<det	0.043	<det	0.141	0.269	162.621	0.019	0.024	<det	Biotite
39 (2) BT-h	au24a06	36.600	0.066	4.883	4.563	269.026	478.297	107.407	295.256	205.122	7.623	<det	5.361	7.475	7.032	0.545	3224.669	<det	<det	<det	<det	<det	<det	<det	0.171	0.288	162.104	0.060	<det	<det	Biotite
39 (2) BT	au24a07	36.000	0.116	6.193	4.241	272.313	474.693	106.932	293.679	189.441	8.606	0.117	5.774	7.083	6.242	<det	3327.271	<det	0.134	<det	<det	0.469	0.060	<det	0.134	0.292	147.393	<det	<det	0.017	Biotite
39 (3) BT-g	au24a11	35.650	<det	3.993	4.042	97.854	89.510	94.002	194.295	174.519	12.893	<det	4.610	11.776	5.282	0.230	2954.664	0.214	0.261	<det	0.073	<det	0.067	<det	<det	0.652	144.909	0.065	0.023	<det	Biotite
39 (3) BT-j	au24a12	36.410	0.095	5.221	4.181	96.076	84.245	99.212	252.270	175.370	4.675	0.155	4.662	12.727	5.763	<det	3069.051	<det	0.152	<det	<det	<det	<det	<det	0.118	0.624	145.236	0.023	0.023	0.016	Biotite
39 (3) BT	au24a13	36.000	<det	4.854	4.075	92.263	79.928	100.494	225.946	174.711	10.674	<det	6.562	11.678	4.478	<det	2924.127	0.324	0.443	<det	<det	<det	<det	<det	0.216	0.639	133.470	0.025	<det	<det	Biotite
39 (4) BT-j	au24b04	36.560	<det	5.155	4.858	265.197	231.914	104.899	236.900	209.727	6.973	<det	4.566	9.860	6.128	<det	3519.823	0.144	<det	0.306	0.057	0.302	0.040	<det	0.251	0.458	155.319	0.043	0.014	<det	Biotite
39 (4) BT-i	au24b05	35.960	<det	5.638	4.245	259.421	294.743	94.840	228.123	187.582	8.450	<det	21.665	8.457	7.003	0.154	3065.825	0.217	0.368	<det	0.064	<det	0.037	<det	0.458	0.402	121.068	0.020	0.039	0.018	Biotite
39 (4) BT-h	au24b06	36.400	<det	5.037	4.432	201.388	197.686	99.731	244.800	181.880	9.541	<det	3.112	9.802	5.970	0.259	2922.501	<det	<det	<det	<det	0.074	0.020	0.056	<det	0.587	146.568	0.075	0.011	<det	Biotite
39 (4) BT	au24b09	36.000	0.057	5.337	4.184	252.057	344.543	94.846	231.752	197.299	6.657	0.102	3.588	7.859	6.058	0.279	3046.763	0.133	0.358	<det	0.095	<det	0.017	<det	0.099	0.397	128.108	<det	0.015	<det	Biotite
24-2 (5) BT-b	au24c07	34.360	0.077	8.370	2.470	518.994	1232.240	75.101	560.197	104.573	26.350	0.155	4.194	7.446	1.553	<det	3824.225	<det	0.135	<det	<det	0.225	0.033	<det	0.167	0.327	28.649	<det	0.047	0.030	Biotite
24-2 (5) BT-a	au24c08	36.850	0.110	8.479	2.598	572.079	1381.290	91.203	627.096	83.029	23.704	<det	2.258	4.413	0.647	0.972	4901.352	0.149	0.368	0.622	<det	<det	<det	<det	<det	0.110	19.792	<det	0.010	<det	Biotite
24-2 (7) BT-i	au25a06	37.080	<det	6.158	4.572	174.866	98.954	90.193	881.909	81.521	19.301	<det	9.701	7.348	2.623	<det	4843.357	<det	<det	0.853	<det	<det	0.062	0.415	0.078	0.577	72.435	<det	0.039	<det	Biotite
24-2 (8) BT-h	au25a14	36.390	<det	2.690	3.386	281.091	535.779	70.559	797.858	61.258	28.517	<det	2.778	7.101	1.297	0.317	3039.479	0.264	<det	<det	<det	0.282	0.050	<det	0.391	0.314	59.422	0.037	<det	<det	Biotite
24-2 (8) BT-g	au25a15	36.040	<det	6.466	3.510	288.411	629.036	66.265	749.535	70.857	43.180	0.178	4.714	5.867	3.039	<det	3414.019	<det	<det	<det	<det	<det	<det	<det	0.276	0.297	66.933	0.081	0.033	0.010	Biotite
28-4 (3) BT-e	au25c10	37.320	<det	5.866	4.903	107.862	206.388	87.279	1220.352	115.216	20.045	0.194	5.947	11.495	149.780	0.320	2468.081	0.127	0.140	<det	<det	<det	0.027	0.208	0.135	0.839	321.860	0.137	0.022	0.027	Biotite
28-4 (3) BT-c	au25c11	36.770	<det	3.424	3.821	84.281	82.494	75.660	1587.639	88.473	11.270	<det	1.528	9.369	187.532	0.651	2172.404	<det	0.195	<det	<det	<det	<det	<det	0.080	0.502	259.604	0.054	<det	<det	Biotite
29 (4) BT-c	au31a04	37.630	<det	9.067	4.609	250.078	114.440	49.024	726.863	92.338	13.813	<det	7.983	6.288	28.959	0.846	3598.221	0.343	0.295	0.583	<det	0.101	<det	<det	0.337	0.305	153.088	0.023	<det	<det	Biotite
29 (4) BT	au31a05	36.000	0.190	6.628	4.017	231.694	110.920	46.893	676.328	89.251	6.034	0.462	3.565	5.728	182.224	<det	3171.556	0.296	0.715	<det	<det	<det	0.019	<det	0.119	0.330	133.408	0.044	0.020	<det	Biotite
29 (33) BT-c	au31a08	35.870	0.189	6.443	4.820	161.859	87.742	59.690	779.889	98.764	14.759	<det	16.289	8.313	39.581	1.417	4098.257	0.376	0.489	<det	<det	0.269	<det	<det	0.488	0.370	284.239	0.380	0.034	<det	Biotite
29 (33) BT-d	au31a09	36.980	0.259	6.954	4.670	141.830	100.799	58.474	860.373	93.306	5.777	<det	9.177	7.608	32.779	1.013	3973.850	<det	0.209	<det	0.068	0.396	<det	<det	0.444	0.322	174.805	0.100	<det	<det	Biotite
29 (26) BT-d	au31a16	37.200	<det	5.542	4.189	133.359	71.958	56.352	791.242	88.766	16.537	0.326	6.701	10.950	35.850	0.640	3734.863	0.230	<det	0.236	<det	0.553	<det	0.224	0.371	0.592	287.741	0.016	<det	<det	Biotite
29 (26) BT-e	au31a17	38.010	0.058	5.755	3.728	124.030	89.955	52.468	843.472	87.157	16.005	<det	6.108	7.624	43.844	0.604	3729.043	0.640	0.620	<det	<det	<det	<det	0.117	0.355	0.400	150.967	0.040	0.023	0.035	Biotite
29 (24) BT-c	au31b12	37.190	<det	4.321	3.707	180.515	117.929	54.578	836.227	95.333	2.549	<det	7.268	9.790	31.034	1.483	3937.072	<det	<det	0.514	0.163	0.411	<det	<det	<det	0.314	238.466	0.069	0.055	<det	Biotite
29 (24) BT-d	au31b13	37.570	<det	5.317	3.478	188.376	120.112	118.264	2285.986	96.053	11.419	<det	3.044	9.862	28.387	<det	4077.945	<det	<det	<det	0.086	<det	0.029	0.293	<det	0.454	205.844	0.035	<det	<det	Biotite
29 (24) HN?	au31b17	36.000	0.283	5.602	3.202	175.825	114.995	62.698	764.319	106.248	13.943	0.638	12.237	7.901	37.728	0.613	3737.521	0.317	1.891	<det	0.232	<det	0.019	0.089	0.272	0.465	241.230	0.039	0.037	<det	Biotite
27c-1 (1) BT	se01a04	36.000	0.315	20.437	3.603	1271.572	1493.209	121.022	500.603	483.882	19.374	0.291	8.881	59.463	15.643	0.800	1597.294	<det	0.369	<det	0.100	<det	<det	<det	0.362	1.575	19.957	0.046	0.023	0.021	Biotite
27c-1 (1) BT	se01a05	36.000	0.190	16.554	3.662	1291.025	1517.494	121.598	480.946	495.028	5.982	0.422	4.663	59.199	16.180	0.505	1550.839	0.382	0.972	<det	<det	0.062	<det	<det	0.398	1.413	14.678	0.088	<det	<det	Biotite
27c-1 (2) BT	se01a10	36.000	0.242	19.872	4.816	1425.945	2157.167	146.017	541.637	465.555	10.559	0.303	2.282	102.491	21.316	0.573	1443.889	1.119	1.922	0.685	<det	0.078	0.079	<det	0.326	3.752	12.146	0.043	0.031	0.023	Biotite
27c-1 (3) BT-HN?	se01a15	36.000	1.383	8.901	2.126	581.521	838.655	72.735	321.884	258.870	246.124	0.671	1.234	32.900	9.484	<det	780.237	7.100	10.519	0.988	0.400	<det	0.020	0.188	0.263	0.799	27.891	0.020	<det	0.021	Biotite
27c-1 (4-1) BT	se01b07	36.000	<det	16.669	6.574	1566.182	1717.845	126.113	538.490	473.735	8.490	0.182	0.716	56.397	17.052	<det	1599.232	<det	0.177	0.251	<det	0.145	<det	0.203	0.142	1.464	20.463	<det	0.041	0.023	Biotite
27c-1 (4-1) BT	se01b09	36.000	0.108	13.333	6.766	1237.514	1247.043	116.736	534.387	460.663	24.068	<det	1.068	51.492	16.413	0.999	1424.333	11.538	26.347	0.325	0.106	<det	0.020	0.209	0.115	1.101	21.848	0.039	0.625	<det	Biotite
27c-1 (4-2) BT	se01b10	36.000	<det	13.392	6.234	1670.135	1568.219	127.057	527.480	425.991	7.102	0.303	1.384	51.445	17.889	<det	1508.454	0.237	0.129	<det	0.061	<det	0.088	0.211	<det	1.231	14.558	<det	<det	<det	Biotite
27c-1 (5) PX?	se01b11	36.000	<det	17.905	7.371	1460.111	2098.647	123.667	556.899	449.125	7.531	<det	1.537	53.722	15.588	0.665	1596.245	0.958	2.422	<det	<det	0.784	<det	<det	0.162	1.422	16.557	0.035	<det	0.029	Biotite
27c-1 (5) BT	se01b12	36.000	0.160	15.637	7.299	1383.712	1916.902	132.538	532.943	445.540	2.557	0.257	0.665	51.404	16.139	<det	1511.905	0.216	0.865	0.426	<det	0.241	0.017	<det	<det	1.289	13.979	<det	0.063	<det	Biotite
27c-1 (5) BT	se01b13	36.000	<det	18.556	7.288	1565.155	2159.256	124.142	555.656	471.070	6.289	<det	1.205	56.923	16.658	<det	1693.527	<det	<det	<det	<det	<det	0.101	<det	0.099	1.479	17.834	<det	<det	<det	Biotite
27c-2 (1) BT	se01c04	36.000	0.099	19.411	2.874	302.992	151.218	94.118	53.968	293.074	8.142	<det	1.172	11.002	9.834	0.387	1191.067	<det	<det	0.280	<det	<det	<det	0.112	0.341	0.539	48.379	0.024	<det	<det	Biotite
27c-2 (2) BT	se01c06	36.000	<det	21.804	2.968	274.316	130.927	99.188	75.924	286.124	6.946	<det	4.155	12.874	9.137	1.143	1461.141	0.559	0.929	<det	<det	0.874	<det	<det	0.094	0.535	51.886	0.074	<det	<det	Biotite
27c-2 (2) BT-HN?	se01c07	36.000	0.224	22.952	3.244	293.143	159.569	98.054	75.097	303.154	3.023	1.111	3.484	10.851	10.709	<det	1457.796	1.047	2.838	0.382	0.063	<det	0.047	<det	0.147	0.571	46.739	<det	0.022	0.032	Biotite
27c-2 (3) BT	se01c08	36.000	1.185	23.627	3.755	332.284	104.205	95.304	68.393	289.669	8.854	3.007	1.391	14.860	12.006	0.668	1235.878	3.076	6.034	2.061	0.284	<det	0.013	<det	0.151	0.715	47.522	<det	<det	0.018	Biotite
27c-2 (3) BT	se01c09	36.000	0.271	18.103	3.131	270.291	135.370	91.238	79.008	257.317	26.513	0.246	1.884	11.986	10.573	0.277	1023.634	0.543	0.958	<det	0.216	0.299	<det	<det	0.190	0.522	215.036	0.323	0.012	0.023	Biotite
27c-2 (5) BT	se01c10	36.000	0.304	4.979	3.176	430.044	137.803	105.611	71.767	39.009	7.645	<det	0.680	29.969	8.063	<det	226.681	0.153	0.173	<det	<det	<det	0.015	<det	0.180	1.315	21.326	0.074	<det	0.020	Biotite
22c-2 (5) BT	se01c15	36.000	0.299	5.774	3.845	392.123	155.486	94.018	113.027	43.357	8.565	<det	0.211	28.309	7.227	<det	153.496	0.278	0.552	0.762	0.122	0.669	<det	<det	<det	1.391	21.567	0.025	0.018	<det	Biotite
CHLORITE (n = 5)																															
34-2 (1-1) ?	au31c06	26.450	0.505	4.266	0.106	230.809	174.360	80.179	1375.968	<det	5.188	1.912	6.163	0.759	9.106	<det	10.260	0.674	2.315	0.241	0.075	0.239	0.109	<det	0.467	0.048	56.865	0.175	0.027	<det	Chlorite
34-2 (1-2) ?	au31c07	26.450	0.069	3.175	0.057	239.373	181.027	86.454	1475.039	0.568	2.079	0.498	3.494	0.159	5.591	0.347	2.698	<det	<det	<det	<det	<det	<det	<det	0.087	<det	30.800	0.049	<det	0.011	Chlorite
34-2 (2) CHL-a-b	au31c08	26.450	<det	2.537	0.060	256.797	170.339	81.523	1456.119	0.529	<det	0.147	2.548	<det	1.903	0.411	5.297	<det	0.218	<det	<det	<det	0.013	<det	0.115	<det	114.392	0.144	<det	<det	Chlorite
34-2 (2) CHL-a-b	au31c09	26.450	<det	3.199	0.056	246.189	177.892	82.101	1438.257	0.240	1.167	<det	0.921	0.239	2.019	<det	2.038	<det	<det	<det	<det	0.297	<det	<det	0.094	0.016	434.762	7.177	<det	<det	Chlorite
34-2 (2) CHL-a-b	au31c17	26.450	0.055	3.091	0.079	263.991	170.286	87.384	1511.579	<det	2.470	<det	0.602	0.291	1.617	<det	4.042	<det	<det	<det	<det	0.144	0.037	<det	<det	0.041	67.019	0.293	<det	<det	Chlorite
PLAGIOCLASE (n = 23)																															
23 (5) PL	au25b13	57.500	14.000	1.931	0.020	<det	60.080	<det	<det	0.153	942.701	0.155	<det	<det	0.779	<det	128.885	4.202	4.064	0.875	0.793	<det	0.032	0.498	<det	<det	56.710	<det	0.032	<det	Plagioclase
28-4 (2) PL	au25c07	57.500	6.333	2.753	0.207	3.488	12.118	0.694	5.457	0.687	773.892	1.269	1.137	0.479	7.087	0.500	424.317	7.517	11.916	0.226	1.598	0.298	<det	0.155	0.121	<det	515.032	0.049	0.116	0.227	Plagioclase
28-4 (2) PL-h	au25c08	57.640	9.079	2.889	0.241	2.586	<det	1.516	<det	0.251	905.350	<det	1.421	0.332	5.450	0.929	438.474	3.035	4.670	0.972	1.573	0.095	0.090	<det	0.095	0.055	342.101	0.071	<det	0.027	Plagioclase
28-4 (3) PL	au25c13	57.500	11.151	3.128	0.231	2.680	29.263	<det	4.636	1.157	1106.597	0.160	1.877	0.429	6.106	<det	74.938	5.839	10.736	<det	1.141	0.125	0.048	<det	<det	<det	729.017	<det	0.067	<det	Plagioclase
28-4 (6) PL-f	au25c16	53.210	10.554	2.711	0.255	2.219	939.940	1.097	4.475	<det	1091.279	<det	2.165	<det	2.880	0.678	62.452	5.523	8.315	<det	0.843	0.267	<det	<det	<det	<det	580.869	0.031	0.063	<det	Plagioclase
29 (6) PL	au31a06	57.500	10.640	3.207	0.329	4.541	<det	1.308	10.833	0.159	1117.371	0.156	3.714	<det	3.291	<det	171.052	4.900	8.005	0.172	1.402	0.137	<det	0.125	0.086	0.022	679.133	0.275	0.123	0.022	Plagioclase
29 (6) PL	au31a07	57.500	12.313	4.240	0.287	3.752	<det	0.589	10.093	0.447	1209.810	0.049	2.279	0.271	2.809	<det	207.523	3.859	6.717	0.525	1.440	0.073	<det	<det	0.137	0.043	649.953	<det	0.048	0.126	Plagioclase
29 (8) PL-d-e	au31a11	53.810	11.014	4.474	0.262	2.173	<det	<det	5.104	0.942	1077.522	<det	6.516	0.654	3.775	<det	138.377	6.998	11.846	0.831	1.452	0.452	0.028	<det	<det	0.038	666.704	0.036	0.047	0.290	Plagioclase
29 (16) PL	au31b04	57.500	11.062	4.321	0.248	3.451	28.487	2.901	4.671	0.928	1119.051	0.120	3.136	0.353	3.986	0.293	132.777	5.879	10.751	0.322	1.410	0.119	0.035	<det	<det	0.074	810.182	0.455	<det	0.042	Plagioclase
29 (16) PL-a	au31b05	55.150	9.428	2.558	0.269	3.068	<det	1.195	5.208	0.217	990.697	<det	1.910	0.692	2.115	<det	131.170	6.195	10.070	0.223	1.564	0.310	<det	<det	0.068	0.042	672.067	0.143	0.038	<det	Plagioclase
29 (16) PL-b	au31b06	55.520	10.342	4.763	0.317	2.987	<det	<det	<det	0.462	1095.278	<det	1.617	1.073	0.885	<det	207.099	6.622	11.477	0.299	1.425	<det	0.010	<det	<det	<det	653.978	<det	0.100	0.028	Plagioclase
29 (16) PL	au31b07	57.500	10.016	3.056	0.208	2.524	19.052	1.272	31.467	2.269	1131.332	<det	3.829	<det	2.522	<det	149.208	7.598	9.365	<det	1.500	0.533	<det	<det	<det	0.056	643.128	0.073	0.069	<det	Plagioclase
29 (24) PL	au31b14	57.500	8.812	3.379	0.013	3.147	<det	1.221	21.854	0.973	1064.975	0.195	3.806	0.404	7.096	<det	148.499	5.814	6.984	0.472	1.355	<det	<det	<det	<det	<det	693.481	0.141	<det	0.095	Plagioclase
34-2 (5) PL	au31c14	57.500	9.535	0.800	0.017	<det	<det	<det	<det	0.446	1042.743	0.217	0.867	0.348	1.133	<det	245.468	7.086	8.821	0.806	1.432	<det	0.090	0.099	0.223	0.070	880.958	0.032	<det	0.073	Plagioclase
34-2 (5) PL	au31c15	57.500	10.316	2.159	0.015	0.860	<det	<det	<det	0.545	1129.103	<det	0.687	<det	1.353	<det	183.322	8.630	11.478	0.760	1.187	<det	<det	0.325	<det	<det	823.687	<det	0.022	0.036	Plagioclase
27c-1 (1) PL	se01a09	57.500	4.244	1.631	0.006	<det	31.376	<det	<det	1.528	1003.756	0.103	1.061	0.300	0.692	<det	162.553	25.231	29.376	0.193	1.183	0.180	<det	<det	<det	0.045	79.684	<det	0.203	0.027	Plagioclase
27c-1 (2) PL	se01a14	57.500	4.214	2.525	0.012	1.941	<det	0.596	<det	0.608	962.558	0.327	0.835	<det	0.545	<det	140.018	21.220	25.396	<det	1.629	0.815	<det	<det	<det	0.081	113.671	<det	0.052	<det	Plagioclase
27c-1 (3) PL	se01b06	57.500	4.566	4.651	0.010	<det	<det	<det	<det	0.687	969.119	0.247	<det	0.187	<det	<det	157.558	54.273	64.315	0.358	1.206	0.502	0.087	0.098	<det	<det	99.895	0.121	0.549	0.045	Plagioclase
27c-1 (5) PL	se01b15	57.500	0.213	3.537	0.023	0.689	<det	<det	<det	163.279	1045.845	<det	<det	0.369	0.969	<det	3306.145	4.043	2.745	<det	1.734	<det	0.013	0.109	0.082	<det	400.703	<det	<det	0.017	Plagioclase
27c-1 (6) PL	se01b17	57.500	0.237	2.094	0.020	<det	69.017	<det	<det	153.062	1073.104	<det	0.405	<det	0.975	0.286	3625.376	4.720	5.040	<det	1.811	0.633	0.040	<det	<det	<det	371.618	0.077	0.064	0.099	Plagioclase
22c-2 (5) PL	se01c12	57.500	0.399	1.725	0.003	1.040	<det	<det	<det	0.274	156.877	<det	0.406	<det	0.408	<det	14.319	0.990	2.987	<det	0.050	0.161	0.045	0.051	0.147	0.015	21.884	0.055	<det	0.218	Plagioclase
22c-2 (6) PL	se01c13	57.500	0.347	2.501	0.017	1.114	574.548	<det	<det	1.027	229.450	1.547	<det	0.119	0.229	0.235	32.606	7.481	15.201	1.031	0.167	0.823	0.057	0.082	<det	<det	28.092	0.384	0.079	0.050	Plagioclase
22c-2 (4) PL	se01c16	57.500	0.330	2.622	<det	<det	<det	0.654	<det	0.801	169.408	<det	0.114	<det	0.271	0.283	12.153	0.620	1.424	0.210	<det	0.444	0.047	<det	<det	<det	1.956	0.141	0.031	0.057	Plagioclase

CLINOPYROXENE (n =10)																												
27c-2 (1) PX	se01c05	51.02	22.99	65.82	0.10	81.56	25.51	40.52	12.92	<det	28.62	66.97	26.12	<det	2.84	0.33	1.67	9.71	32.22	11.42	1.57	13.02	2.53	8.77	1.98	0.02	15.88	0.23	0.14	0.36	Clinopyroxene
27c-2 (5) CPX-OL?	se01c11	50.93	21.83	67.60	0.12	187.01	221.07	48.06	36.14	<det	27.04	44.23	19.85	0.59	2.52	<det	4.02	13.69	51.29	12.06	0.85	9.91	1.54	5.32	1.07	0.01	12.34	0.21	0.05	0.02	Clinopyroxene
27c-2 (5) CPX?	se01c14	51.17	22.73	56.89	0.14	241.55	174.42	53.10	49.91	<det	28.84	45.63	26.37	0.14	3.20	0.16	26.42	14.60	52.56	11.94	1.01	11.56	1.93	4.72	1.50	0.03	12.97	0.11	0.08	0.02	Clinopyroxene
27c-2 (4) CPX-OL?	se01c17	51.13	21.56	53.74	0.11	263.32	167.60	53.40	74.86	<det	33.93	42.80	18.04	0.32	2.04	<det	17.04	17.72	57.50	10.60	0.98	10.39	1.77	5.08	1.21	0.02	13.84	0.25	0.06	<det	Clinopyroxene
27c-1 (1) OPX-HN?	se01a07	51.51	20.856	114.975	0.123	301.675	441.637	50.568	101.859	1.9	77.528	71.03	16.274	1.178	3.34	<det	7.983	20.721	79.882	19.676	0.743	14.919	2.711	7.334	1.333	0.089	9.515	0.028	0.107	0.028	Clinopyroxene
27c-1 (1) OPX-HN?	se01a08	50.12	18.715	122.85	0.225	331.214	137.62	52.122	90.735	2.61	25.799	73.03	9.952	7.047	7.827	<det	10.533	25.657	83.32	19.13	1.262	14.413	2.768	7.887	0.896	0.359	5.239	0.049	0.655	0.029	Clinopyroxene
27c-1 (3) OPX-HN?	se01b04	51.3	20.451	81.612	0.24	196.224	321.222	48.063	111.381	4.09	47.244	77.246	27.135	0.901	4.49	<det	8.089	22.939	94.834	23.235	0.78	20.274	2.938	7.332	1.858	0.056	8.672	0.064	0.077	<det	Clinopyroxene
27c-1 (3) OPX-HN?	se01b05	51.07	20.675	111.149	0.237	323.317	245.199	48.61	129.78	5.891	22.691	75.964	16.67	0.866	4.573	0.118	51.426	18.171	79.786	20.66	0.594	19.124	2.795	7.971	1.188	<det	8.408	0.055	0.074	0.06	Clinopyroxene
27c-1 (5) OPX-HN?	se01b14	50.95	19.663	99.009	0.496	238.184	224.162	47.919	134.883	1.115	38.402	94.356	35.93	5.33	5.721	<det	20.215	33.28	133.506	29.142	0.956	23.947	3.612	9.66	2.754	0.32	9.009	0.077	0.087	0.036	Clinopyroxene
27c-1 (6) OPX-HN?	se01b16	51	20.74	109.33	0.657	362.15	207.242	49.594	129.053	5.825	52.37	69.546	15.566	4.752	4.779	<det	92.302	20.133	80.359	22.175	0.792	16.9	2.513	6.808	1.468	0.195	8.25	0.049	0.211	0.069	Clinopyroxene

<det = below detection

CHAPTER 5: SUMMARY

This PhD thesis is a synthesis of three manuscripts that are all related to topics on the Voisey's Bay magmatic nickel-copper-cobalt sulfide deposit of northern Labrador. The thesis itself is entitled "A comprehensive geological, petrological, and geochemical evaluation of the Voisey's Bay Ni-Cu-Co sulfide deposit: an integration of empirical data and process mechanics". The title is significant in that it describes the overview of the thesis.

Chapter 1 introduces the subject of magmatic ore genesis and platinum-group element mineralogy and provides a comprehensive review of literature. It sets out the objectives of the thesis, and attempts to place the research in a larger context, providing a cohesive framework for the three research manuscripts that follow. The research work is related in that the first manuscript (Chapter 2) lays the foundation for the interpretations of the second manuscript (Chapter 3). Although, the manuscripts are stand alone papers there is a general progression of themes.

The first manuscript (Chapter 2) develops a systematic and integrative geological, petrological, and geochemical method for detailed ore characterization and applies it the Voisey's Bay magmatic sulfide deposit. The natural progression from describing an ore deposit in detail is to develop ore genesis models based on the detailed ore characterization and these models are emphasized in the second manuscript (Chapter 3).

The final manuscript (Chapter 4) characterizes a newly discovered platinum-group element mineralization style in the Voisey's Bay deposit and describes how it is related to the main sulfide mineralization both spatially and in its formation.

The main results of the thesis are:

(1) The Ovoid deposit at Voisey's Bay is strongly zoned from pyrrhotite-rich margins to a chalcopyrite- and pentlandite-rich core. Both cumulates and residual liquids are present in the Ovoid. Cumulates are present as large pyrrhotite grains, many containing magnetite. Residual liquids are present as chalcopyrite and pentlandite "loops" that surround the pyrrhotite grains.

(2) The Ovoid formed by segregation of magmatic sulfide melts at an R-factor of ~150 from common basalt parent magmas. The parent sulfide melt was differentiated by partial fractional crystallization, trapping 30-40% residual liquid, mainly in the core of the Ovoid body. Some of the residual liquid escaped to form disseminated ores surrounding the Ovoid.

(3) Discrete platinum group-minerals (PGM) are hosted by disseminated base-metal sulfides in a hornblende gabbro dyke near the Southeast Extension Zone at Voisey's Bay. The grades of the occurrence are 1.95g/t Pt, 1.41g/t Pd, and 6.59g/t Au. The PGM have a primary magmatic origin. Geological and geochemical relationships suggest that the dyke is associated with the main troctolite rocks that host the Ovoid, indicating a similar magma source. The PGM are related to a highly differentiated sulfide liquid that formed intermediate solid solution (ISS) and was

derived by crystallization of monosulfide solid solution (MSS) from a sulfide melt of the type that formed the Ovoid.